Vol. 142, October 1, 1982
Complete in one issue

ISSN 0003-2670

ANALYTICA CHIMICA ACTA

International journal devoted to all branches of analytical chemistry

ELSEVIER SCIENTIFIC PUBLISHING COMPANY

ANALYTICA CHIMICA ACTA

International journal devoted to all branches of analytical chemistry
Revue internationale consacrée à tous les domaines de la chimie analytique
Internationale Zeitschrift für alle Gebiete der analytischen Chemie

PUBLICATION SCHEDULE FOR 1982

	J	F	M	A	M	J	J	A	S	O	N	D
Analytica Chimica Acta	134	135/1	135/2	136	137	138	139	140/1 140/2	141	142	143	144

Scope. *Analytica Chimica Acta* publishes original papers, short communications, and reviews dealing with eve aspect of modern chemical analysis, both fundamental and applied.

Submission of Papers. Manuscripts (three copies) should be submitted as designated below for rapid and efficie handling:

Papers from the Americas to: Professor Harry L. Pardue, Department of Chemistry, Purdue University, West Lafayet IN 47907, U.S.A.

Papers from all other countries to: Dr. A. M. G. Macdonald, Department of Chemistry, The University, P.O. Box 3(Birmingham B15 2TT, England. Papers dealing particularly with computer techniques to: Professor J. T. Cle Universität Bern, Pharmazeutisches Institut, Sahlistrasse 10, CH-3012 Bern, Switzerland.

Submission of an article is understood to imply that the article is original and unpublished and is not being consider for publication elsewhere. Upon acceptance of an article by the journal, authors resident in the U.S.A. will be asked transfer the copyright of the article to the publisher. This transfer will ensure the widest dissemination of informati under the U.S. Copyright Law.

Information for Authors. Papers in English, French and German are published. There are no page charg Manuscripts should conform in layout and style to the papers published in this Volume. Authors should cons Vol. 132, p. 239 for detailed information. Reprints of this information are available from the Editors or from: Elsev Editorial Services Ltd., Mayfield House, 256 Banbury Road, Oxford OX2 7DH (Great Britain).

Reprints. Fifty reprints will be supplied free of charge. Additional reprints (minimum 100) can be ordered. An or form containing price quotations will be sent to the authors together with the proofs of their article.

Advertisements. Advertisement rates are available from the publisher.

Subscriptions. Subscriptions should be sent to: Elsevier Scientific Publishing Company, P.O. Box 211, 1000 Amsterdam, The Netherlands.

Publication. *Analytica Chimica Acta* appears in 11 volumes in 1982. The subscription for 1982 (Vols. 134–144) Dfl. 1815.00 plus Dfl. 220.00 (postage) (total approx. U.S. $814.00). Journals are sent automatically by airmail to U.S.A. and Canada at no extra cost and to Japan, Australia and New Zealand for a small additional postal charge. earlier volumes (Vols. 1–133) except Vols. 23 and 28 are available at Dfl. 182.00 (U.S. $72.80), plus Dfl. 14.00 (U $5.60) postage and handling, per volume.

Claims for issues not received should be made within three months of publication of the issue, otherwise they can be honoured free of charge.

Customers in the U.S.A. and Canada who wish to obtain additional bibliographic information on this and ot Elsevier journals should contact Elsevier Science Publishing Company Inc., Journal Information Center, 52 Vande Avenue, New York, NY 10017. Tel: (212) 867-9040.

Neutral Ionophores for Ion-Selective Electrodes

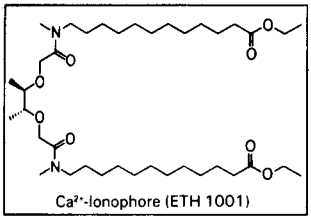
Ca²⁺-Ionophore (ETH 1001)

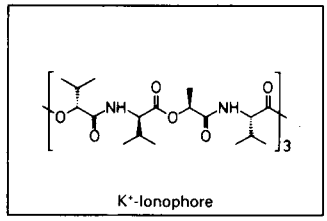
K⁺-Ionophore

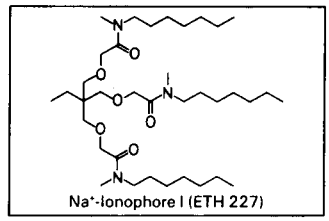
Na⁺-Ionophore I (ETH 227)

Certain natural and synthetic lipophilic ligands for cations (ion-carriers, ionophores) are used as carriers in a wide range of ion-selective electrodes (ISEs)[1),2)]. The development of electrically neutral ionophores lead to clear improvements in selectivities and detection limits. K^+, Na^+ and Ca^{2+} play a central role in biological systems. The advantageous selectivity characteristics of liquid membrane ion-selective microelectrodes based on neutral ionophores[3)] for these cations make such microelectrodes especially attractive for medical and biological applications[4)].

References

1) M.E. Meyerhoff, Y.M. Fraticelli, Anal. Chem. **(1982)** *54*, 27R–44R

2) Please note that the commercial use of synthetic ionophores for ion-selective electrodes is protected by the following patents: CH 605661; GB 1432807; IT 987080; US 3957607; DT-OS 2319365; FR 73.14839; JPN (Pend.) 50-073017

3) D. Ammann, F. Lanter, R. Steiner, D. Erne, W. Simon, "New Ion-selective Liquid Membrane Microelectrodes" in "Ion-selective Microelectrodes and their Use in Excitable Tissues", E. Syková, P. Hnik, L. Vyklický, Eds., Planum Publ. Corp., New York **(1981)** 13–23

4) W. Simon, D. Ammann, W. Bussmann, P.C. Meier, "Ion-selective Electrodes in Biology and Medicine" in IUPAC "Frontiers of Chemistry", K.J. Laidler, Ed., Pergamon Press, Oxford and New York **(1982)** 217–226

FLUKA now offers ready-to-use cocktails for ion-selective liquid membranes in microelectrodes; as well as ionophores, auxiliary compounds and additives for mini- and macroelectrodes.

			sFr.		sFr.
Ionophores					
	Ammonium-Ionophore see 74155 ***Nonactin***				
21192	**Calcium²⁺-Ionophore** (ETH 1001)		50 mg 190.–	250 mg	790.–
62557	**Lithium⁺-Ionophore** (ETH 149)		50 mg 150.–	250 mg	600.–
63082	**Magnesium²⁺-Ionophore** (ETH 1117)		50 mg 35.–	250 mg	125.–
74155	**Nonactin puriss.**		100 mg 50.–	1 g	400.–
	Potassium⁺-Ionophore see 94675 ***Valinomycin***				
	Proton-Ionophore see 91660 ***Tridodecylamine***				
71732	**Sodium⁺-Ionophore I** (ETH 227)		50 mg 400.–		
71733	**Sodium⁺-Ionophore II** (ETH 157)		50 mg 120.–	250 mg	495.–
91660	**Tridodecylamine puriss.**		1 ml 200.–		
94675	**Valinomycin purum**	10 mg 20.–	100 mg 160.–	500 mg	610.–
Cocktails for ion-selective liquid membranes in microelectrodes					
21048	**Calcium²⁺-Cocktail**		0.1 ml 90.–		
62380	**Lithium⁺-Cocktail**		0.1 ml 100.–		
63048	**Magnesium²⁺-Cocktail**		0.1 ml 85.–		
60031	**Potassium⁺-Cocktail**		0.1 ml 90.–		
82500	**Proton-Cocktail**		0.1 ml 65.–		
71176	**Sodium⁺-Cocktail**		0.1 ml 130.–		
Auxiliary components and additives for ion-selective membrane electrodes					
02150	**Bis(1-butylpentyl) adipate purum** p.a. for ion-selective electrodes		5 ml 25.–	25 ml	105.–
84818	**Bis(2-ethylhexyl) sebacate purum** p.a. for ion-selective electrodes, DOS		5 ml 15.–	25 ml	55.–
84838	**Dibutyl sebacate purum** p.a. for ion-selective electrodes, DBS		5 ml 15.–	25 ml	55.–
40870	**1,2-Dimethyl-3-nitrobenzene purum** p.a. for ion-selective electrodes		25 ml 16.–	100 ml	50.–
73732	**2-Nitrophenyl octyl ether puriss.** p.a. for ion-selective electrodes, o-NPOE		25 ml 55.–	100 ml	200.–
81392	**Polyvinyl chloride high molecular weight,** for ion-selective electrodes		10 g 16.–	50 g	60.–
60591	**Potassium tetrakis(4-chlorophenyl)borate purum** p.a.		1 g 25.–	5 g	105.–
82227	**Propylene carbonate puriss.** p.a. for ion-selective electrodes		5 ml 20.–	25 ml	85.–
85417	**Siloprene K 1000** for ion-selective electrodes		5 ml 12.–	25 ml	50.–
85418	**Siloprene Crosslinker KA 1,** for ion-selective electrodes		5 ml 12.	25 ml	50.–
72020	**Sodium tetraphenylborate puriss.** p.a.	10 g 28.–	50 g 105.–	250 g	350.–
87369	**Tetrahydrofuran puriss.** p.a. for ion-selective electrodes		500 ml 50.–		
93299	**Tris(2-ethylhexyl) phosphate puriss.** p.a. for ion-selective electrodes		5 ml 12.–	25 ml	50.–
Silanizing agents					
40140	**Dimethyldichlorosilane puriss.**		100 ml 10.–	500 ml	37.–
41720	**N-Trimethylsilyldimethylamine purum**		10 ml 15.–	50 ml	63.–
90796	**Tributylchlorosilane purum**		5 ml 16.–	25 ml	67.–

For more detailed information ask for the FLUKA-Brochure "Neutral Ionophores for Ion-selective Electrodes".

Fluka Chemical Corp., 255 Oser Avenue, Hauppauge, New York 11787, Telephone (516) 273-0110, Telex 96-7807
Fluka Feinchemikalien GmbH, Messerschmittstraße 17, D-7910 Neu-Ulm, Telephone (0731) 740 88-89, Telex 712316

FLUKA AG, CH-9470 BUCHS, SWITZERLAND, TELEPHONE (085) 602 75, TELEX 855 282

Electrodes of Conductive Metal Oxides

edited by SERGIO TRASATTI, *Laboratory of Electrochemistry, University of Milan, Italy.*

STUDIES IN PHYSICAL AND THEORETICAL CHEMISTRY 11.

This two-part work provides a general unifying introduction plus a state-of-the-art review of the physicochemical properties and electrochemical behaviour of conductive oxide electrodes (DSA). The text has been divided into two volumes – Part A dealing mainly with structural and thermodynamic properties and Part B dealing with kinetic and electrocatalytic aspects. This division came about due to the large amount of material to be treated and also because, in a rapidly developing field, difficulties arise in collecting all relevant material at one given moment.

The editor approaches the subject from a multidisciplinary angle, for example, the electrochemical behaviour of oxide electrodes is presented and discussed in the context of a variety of physicochemical properties – electronic structure, nonstoichiometry, crystal structure, surface structure, morphology and adsorption properties. For the first time the different groups of oxides are treated together in order to emphasise their similarities and differences.

This major reference work is mainly directed to electrochemists and those working on catalysis. It will also be useful to those in the fields of materials science, physical chemistry, surface and colloid chemistry and in areas where oxide surfaces may play a major role as in chromatography and photochemistry.

CONTENTS: Chapters. 1. Electronic Band Structure of Oxides with Metallic or Semiconducting Characteristics *(J. M. Honig)*. 2. Chemisorption and Catalysis on Metal Oxides *(A. Cimino and S. Carrà)*. 3. Oxide Growth and Oxygen Evolution on Noble Metals *(L. D. Burke)*. 4. Electrochemistry of Lead Dioxide *(J. P. Pohl and H. Rickert)*. 5. Properties of Spinel-Type Oxide Electrodes *(M. R. Tarasevich and B. N. Efremov)*. 6. Physicochemical and Electrochemical Properties of Perovskite Oxides *(H. Tamura, Y. Yoneyama and Y. Matsumoto)*. 7. Properties of Conductive Transition Metal Oxides with Rutile-Type Structure *(S. Trasatti and G. Lodi)*. 8. Fundamental Properties of the Oxide/Aqueous Solution Interface *(D. N. Furlong, D. E. Yates and T. W. Healy)*. 9. Reactions of Hydrogen and Organic Substances with and at Anodic Oxide Films at Electrodes *(B. E. Conway)*. 10. Oxygen and Chlorine Evolution at Conductive Metallic Oxide Anodes *(S. Trasatti and G. Lodi)*. 11. Technological Impact of Metallic Oxides as Anodes *(A. Nidola)*.

Part A:
1980 xvi + 366 pages.
US $72.25/Dfl. 170.00.
ISBN 0-444-41912-8.

Part B:
1981 xiv + 336 pages.
US $72.25/Dfl. 170.00.
ISBN 0-444-41988-8.

ELSEVIER

P.O. Box 211
1000 AE Amsterdam
The Netherlands

52 Vanderbilt Avenue,
New York, N.Y. 10017

The Dutch guilder price is definitive. US $ prices are subject to exchange rate fluctuations.

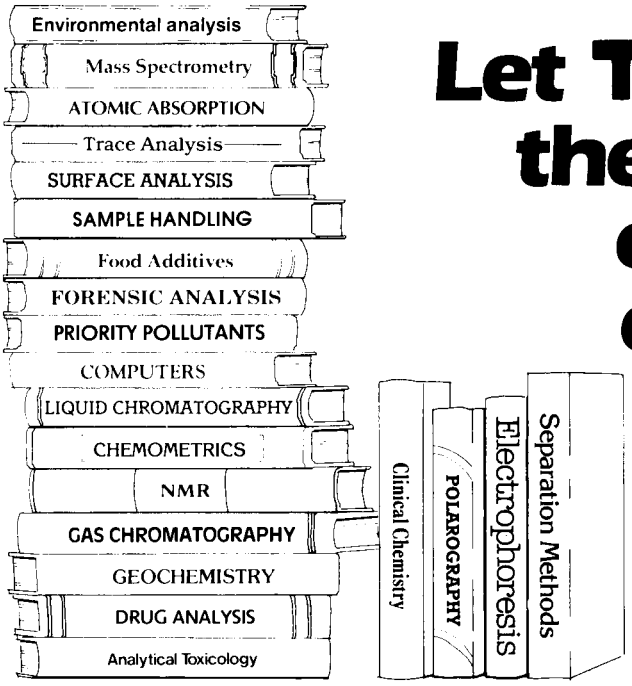

Let TrAC cover the whole of analytical chemistry for you!

TrAC trends in analytical chemistry

TrAC - Trends in Analytical Chemistry is a topical monthly which provides you with an easy-to-read interdisciplinary digest of current developments and new ideas in the analytical sciences.

TrAC's authors are leading scientists, its articles practically oriented, its coverage international.

TrAC covers the broader issues which affect those who develop and use analytical methods, such as the impact of computers on the analytical laboratory and the implications of new governmental regulations.

TrAC comes from the publishers of the **Journal of Chromatography** and **Analytica Chimica Acta.**

Subscription Information
Personal edition: 12 issues -
U.K. £ 20.00,
USA and Canada US$ 42.50,
Europe 91.50 Dutch guilders,
Japan Yen 12400,
Rest of World 95.50 Dutch guilders

Library edition: Vol. 1
(16 issues + Compendium) -
US$ 133.25 or 260 Dutch guilders.

Prices include air delivery worldwide.

Send now for a free sample copy to

Elsevier Scientific Publishing Company

P.O. Box 330
1000 AH Amsterdam
The Netherlands

52 Vanderbilt Avenue
New York, NY 10017
U.S.A.

Elite-Inn Yushima IF
3-28-1 Yushima, Bunkyo-ku,
Tokyo 113, Japan

7242

Electron Capture – Theory and Practice in Chromatography

edited by A. ZLATKIS, *Houston, TX, USA and* C.F. POOLE, *Detroit, MI, USA*

JOURNAL OF CHROMATOGRAPHY LIBRARY – Volume 20

Sept. 1981 xii + 418 pages
Price: US $76.50/ Dfl. 180.00
ISBN 0-444-41954-3

This book provides the first comprehensive coverage of all aspects of the theory, design, operation and applications of the electron capture detector (ECD) from the chromatographer's point of view. In addition, an up-to-date look at the ancillary techniques of selective electron-capture sensitization, atmospheric pressure ionization and plasma chromatography has been included. ECD users will find the solutions to instrumental and technical problems which arise during practice particularly valuable. These have been derived from the experiences of the internationally distinguished team of authors.

Each chapter has been prepared by experts in their field and provides an in-depth coverage of its topic. The basic theory of the mechanisms of electron capture detection is included. Practical sections form the bulk of the book and are devoted to such topics as the construction and operating principles of the detector, including the establishment of instrument design criteria, and the different methods of derivatization. A more personal touch is provided by the inventor of the ECD, J.E. Lovelock, in his review of the development of the technique. Other chapters illustrate the importance of ECD in trace analysis in environmental and biomedical research. A unique feature is the extensive tabulation of all the pertinent data concerning the use of ECD in gas and liquid chromatography.

For those analytical chemists who use chromatography in their research, this book should become a standard text.

CONTENTS: Chapter 1. The electron-capture detector – A pe sonal odyssey *(J.E. Lovelock)*. 2. The design and operation of the electron-capture detector *(C.F. Poole and A. Zlatkis)*. 3. Theory of electron capture *(W.E. Wentworth and E.C.M. Chen)*. 4. Selective electron-capture sensitization *(F.C. Fehsenfeld, P.D. Goldan, M.P. Phillips and R.E. Sievers)*. 5. Oxygen-doping of the carrier gas in electron-capture detectio *(E.P. Grimsrud)*. 6. Wide-range calibration of electron-capture detectors *(R.E. Kaiser and R.I. Rieder)*. 7. Response of the electron-capture detector to compounds with natural electro phores *(J. Vessman)*. 8. Sensitiv derivatives for the determinatio of organic compounds by electron-capture gas chromatography *(C.F. Poole and A. Zlatkis)*. 9. The detection of inorganic and organometallic compounds by electron-capture gas chromatography *(C.F. Pool and A. Zlatkis)*. 10. Environment applications of the electron-capture detector – pesticides *(W.P. Cochrane and R.B. Maybury)*. 11. Environment applications of the electron-capture detector – dioxins *(F. Bruner)*. 12. The electron-capture detector as a monitor o halocarbons in the atmosphere *(P.G. Simmonds)*. 13. Biomedica applications of the electron-capture detector *(J. Vessman)*. 14. Negative ion atmospheric pressure ionization mass spectr metry and the electron-capture detector *(E.C. Horning, D.I. Carroll, I. Dzidic and R.N. Stillwell)*. 15. Electron-capture process and ion mobilit spectra in plasma chromatography *(F.W. Karasek and G.E. Spangler)*. 16. The electron capture detector as a detector i liquid chromatography *(U.A. Th Brinkman)*. Subject index.

ELSEVIER

P.O. Box 211, 1000 AE Amsterdam The Netherlands

52 Vanderbilt Ave. New York, N.Y. 10017

The Dutch guilder price is definitive. US $ prices are subject to exchange rate fluctuations.

ANALYTICA CHIMICA ACTA
VOL. 142 (1982)

ANALYTICA CHIMICA ACTA

International journal devoted to all branches of analytical chemistry

ELSEVIER SCIENTIFIC PUBLISHING COMPANY

Anal. Chim. Acta, Vol. 142 (1982)

Analytica Chimica Acta, 142 (1982) 1—12
Elsevier Scientific Publishing Company, Amsterdam — Printed in The Netherlands

TIME-RESOLVED FLUORIMETRY WITH A SUB-NANOSECOND DYE LASER SOURCE FOR THE DETERMINATION OF POLYNUCLEAR AROMATIC HYDROCARBONS AFTER SEPARATION BY HIGH-PERFORMANCE LIQUID CHROMATOGRAPHY

TOTARO IMASAKA, KOUICHI ISHIBASHI and NOBUHIKO ISHIBASHI*
Faculty of Engineering, Kyushu University, Hakozaki, Fukuoka 812 (Japan)
(Received 12th May 1982)

SUMMARY

A sub-nanosecond tunable dye laser pumped by a transversely-excited atmospheric-pressure nitrogen laser is combined with a time-resolved fluorescence detection system, consisting of a microchannel plate photomultiplier, a sampling oscilloscope, and micro-computer data-processing equipment. This system has a time resolution of 1.4 ns, and is used for determinations of traces of polynuclear aromatic hydrocarbons, in conjunction with high-performance liquid chromatography. The advantages of time-resolved detection are illustrated. Benzo(a)pyrene is determined in samples obtained from airborne particulates.

Polynuclear aromatic hydrocarbons (PAHs) are emitted into the atmosphere mainly by combustion of fossil fuel from electric power-generating plants and automobiles. At least some of the PAHs are carcinogenic and their levels in the atmosphere and water should be regulated. In particular, benzo(a)pyrene [B(a)py] has strong carcinogenicity and has been used for years as an indicator of PAH content. As a result, there have been extensive efforts to develop sensitive and selective methods for the determination of B(a)py. Samples from the environment include many PAHs, so that either a very selective spectrometric technique or a sensitive detection system combined with a separation technique such as thin-layer or column chromatography is essential [1, 2]. The most reliable and sensitive method currently used seems to be a combination of gas chromatography and mass spectrometry [3—6]. Most of the PAHs are strongly fluorescent, so that fluorimetry can be used advantageously for determining traces of these compounds. A synchronous luminescence technique is capable of resolving mixtures of PAHs on a spectrum, because the PAHs have relatively sharp bands in comparison with other fluorescent compounds [7, 8]. Recently, a room-temperature phosphorescence technique has been proposed [9, 10] and the phosphorescence enhancement effect of micelles has also been discussed [11].

For the determination of PAHs at trace levels, laser fluorimetry may be very attractive because of its high sensitivity and selectivity. Geel and

0003-2670/82/0000-0000/$02.75

Winefordner [12] have pointed out that pyrene can be selectively detected in the presence of anthracene by means of time-resolved fluorimetry. Richardson and Ando [13] have investigated ultratrace determinations of PAHs and have reported that the detection limits of benzene, naphthalene, anthracene, fluoranthene, and pyrene in an aqueous solution are 19 $\mu g\ l^{-1}$, 1.3 ng l^{-1}, <4.4 ng l^{-1}, 1.0 ng l^{-1}, and 0.5 ng l^{-1}, respectively. Kunitake et al. [14] have discussed the advantages of time-resolved detection and fluorescence isolation by a monochromator and have achieved the determination of pyrene down to 0.5 ng l^{-1} even in an organic solvent such as methanol, in which the background problem from Raman scattering and impurity fluorescence is usually serious. These investigations verified the advantage of laser fluorimetry with respect to sensitivity in the determination of PAHs at ultratrace levels. However, additional selectivity may be necessary for the practical application of laser fluorimetry to environmental samples.

Recently, intensive efforts have been directed toward the determination of mixtures of PAHs based on low-temperature fluorimetry combined with laser excitation and a Shpol'skii effect or matrix isolation [15]. At low temperature, the structures in the excitation and fluorescence spectra are very sharp, which makes selective determinations possible even for real samples with complex compositions [16—22]. It is noted that Maple et al. [17] obtained a well-resolved fluorescence spectrum of B(a)py from real samples using a *n*-heptane matrix.

Many investigations based on separation with high-performance liquid chromatography (h.p.l.c.) have been reported for the selective determination of PAHs [23—28]. The application of laser fluorimetry in conjunction with h.p.l.c. is very attractive because of the sensitivity conferred by laser fluorimetry and the selectivity of h.p.l.c. [29]. CW laser sources are currently used for ultratrace determinations of toxic substances [30, 31] and hormones [32, 33]. A time-resolved laser-induced fluorimetric system has the ability to resolve components on the time scale as well as the wavelength scale. Richardson et al. [34] have described the determination of PAHs, using a nitrogen-laser-pumped dye laser and a CW krypton laser, with detection limits of the order of 1—10 pg. They resolved several structures in the chromatogram for real samples obtained from coal gasification and assigned the fluoranthene peak. Some PAHs such as B(a)py have long fluorescence lifetimes of the order of 20—100 ns, but some of the other PAHs, such as anthracene, have relatively short fluorescence lifetimes of the order of several nanoseconds. The conventional nitrogen-laser-pumped dye lasers have pulse widths of 10 ns; therefore, the time resolution of the instrument is not necessarily sufficient for the time-resolved determination of all the PAHs molecules. It seems that laser fluorimetry with a nanosecond time resolution should be useful for the sensitive and selective determination of PAHs.

In this study, a transversely-excited atmospheric-pressure (TEA) nitrogen laser was developed and used as the pumping source of a dye laser. By using a generated sub-nanosecond tunable dye laser as light source, a sub-

nanosecond response photomultiplier, a sampling oscilloscope with a bandwidth of 1 GHz, it became possible to achieve time-resolved laser fluorimetry with nanosecond time-resolution. The use of a monochromator for isolation of fluorescence from the PAHs and microcomputer data-processing equipment provided further selectivity and convenience in the determination of B(a)py.

EXPERIMENTAL

Apparatus

A schematic diagram of the apparatus is shown in Fig. 1. The pumping source of the dye laser is a TEA nitrogen laser, consisting of a parallel-plate transmission line of the Blumlein type. The output power and the pulse width of the laser were 0.1 mJ/pulse and 700 ps, respectively. It was operated at a repetition rate of 20—30 Hz. A Hänsch-type dye laser system is used for obtaining the tunable dye laser emission. Details of the laser system are available [35, 36]. The laser dye used in this study was 4,4‴-bis(butyloctyloxy)-*p*-quaterphenyl (BBQ) and the oscillating wavelength was adjusted to 386 nm by tilting the angle of the grating for excitation of B(a)py. The pulse width of the dye laser was 140—400 ps. The dye laser beam is split by a quartz plate, and the reflected laser pulse is detected by a photodiode (NEC, LSD-39A, 1 GHz) to provide a trigger pulse for a sampling oscilloscope (Iwatsu, SS601B, 6 GHz). The transmitted laser beam is tightly focused by a lens (Asahi, focal length 40 cm) and introduced into a sample cell from a bottom window which is made of non-fluorescent quartz glass. The flowing sample cell is shown schematically in Fig. 2; the body is made of stainless steel (2 mm diameter, 10 mm long) with a window made of quartz glass.

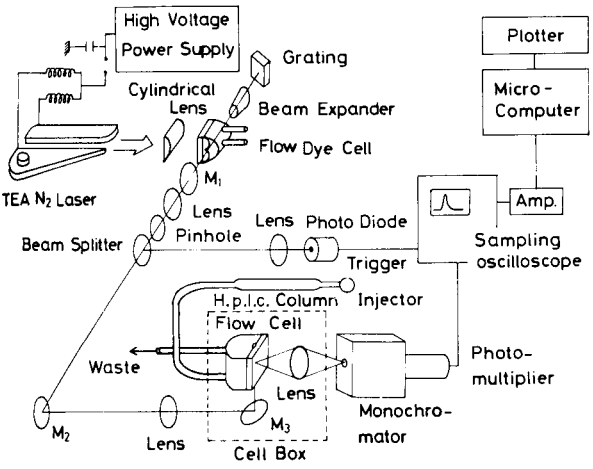

Fig. 1. Block diagram of apparatus.

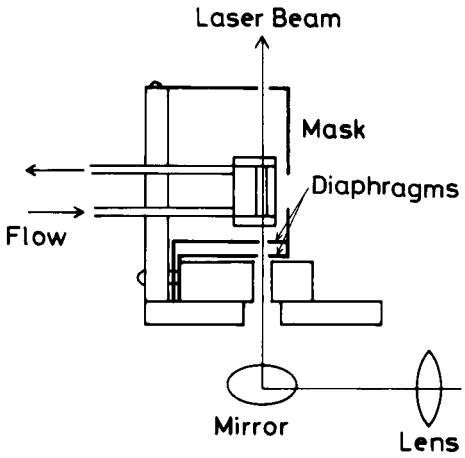

Fig. 2. Flow cell for h.p.l.c.

The dye laser beam passes through two diaphragms to reduce scattered emission and fluorescence from window materials. Optical masks are also placed in front of the sample cell window. The active volume of the flow cell is 10 μl. When the fluorescence lifetime of a sample was measured in a batch system, a conventional 1 cm-quartz cuvette was used. Fluorescence from the sample is focused by a glass lens (focal length 35 cm, diameter 4 cm) onto the entrance slit of a monochromator (Jasco CT-10, dispersion 8 nm mm^{-1}, 500 nm blaze) equipped with a microchannel plate photomultiplier (HTV R1294U-01) or a conventional head-on photomultiplier (HTV R1332). The signal is introduced into the SH-3B head of the sampling oscilloscope. The output analog signal from the oscilloscope is amplified ten times by a home-made amplifier and introduced into an analog input—output interface of a microcomputer (Sord, M223 Mark III) for data aquisition and processing. The chromatogram is drawn by a plotter (Watanabe, WX4671) controlled by the microcomputer.

Components for h.p.l.c. were obtained from Kyowa Co., consisting of a high-pressure pump (KA-90U), a sample injector (KLS-3F), and a column (ODS-6013 1Z). Samples were injected by a microsyringe (Terumo, MS-NT10, 10 μl).

Reagents and procedure

Benzo(a)pyrene (Wako Chemicals) and benzo(ghi)perylene (Aldrich) were used without further purification. Anthracene (Wako Chemicals) was purified by recrystallization. The PAH sample from airborne particulates was a gift. The collection procedure and the method of pretreatment have been described in detail elsewhere [37]. Stock solutions of standard samples (10^{-3} M) were prepared in benzene. The methanol solvent (Kishida Chemical Co.), specified for use in h.p.l.c., was used as received. Cyclohexane, benzene,

and acetonitrile were of guaranteed grade (Kishida Chemical Co.). The water was doubly-distilled and deionized.

Oxygen dissolved in the methanol used for elution was removed by bubbling with nitrogen for 15 min. It was further treated by ultrasonic agitation (Yamato, Brasonic 12) for 10 min, and the atmosphere of the solvent bottle was saturated with the flowing nitrogen during measurements. The sample solution was also treated for 30 s by ultrasonic agitation just before being injected into the h.p.l.c. system. This procedure caused no errors in the peak heights of the chromatograms and reduced fluorescence quenching by dissolved oxygen.

RESULTS AND DISCUSSION

Time resolution

The time profile of the scattered exciting pulse was measured by using the present laser fluorimeter with the microchannel plate photomultiplier at an applied voltage of 2.7 kV. The result is shown in Fig. 3; the full width at half maximum (FWHM) is 1.4 ns. The rise and fall times of the photomultiplier were specified by the manufacturer as 300 ps and 700 ps, respectively. The use of a delay cable degrades the response time of the sampling oscilloscope down to 1 GHz. The observed response time of the overall system is consistent with the estimated value of the FWHM from the pulse width of the laser, the response time of the photomultiplier, and the bandwidth of the oscilloscope. A similar fluorimetric system using a static crossfield photomultiplier has been reported [38, 39]. When the conventional head-on photomultiplier (R1332) was used, the observed response time was 4 ns at an applied voltage of 1.8 kV.

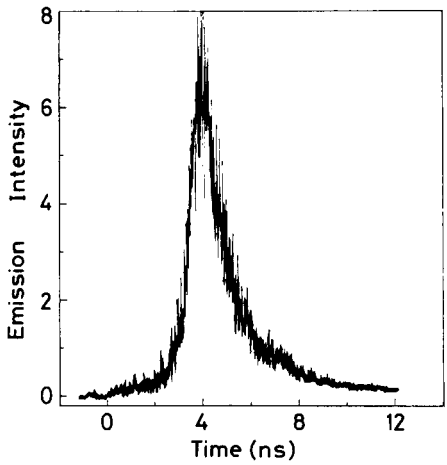

Fig. 3. Time resolution of laser fluorimeter with microchannel plate photomultiplier.

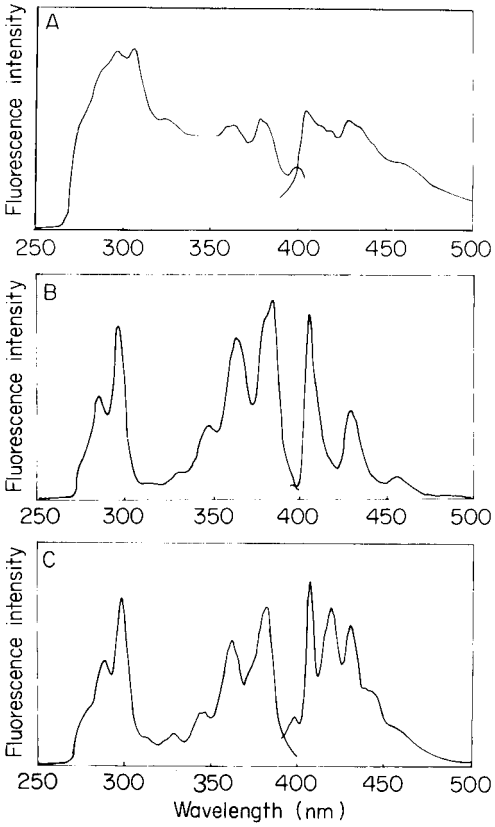

Fig. 4. Excitation and fluorescence spectra. (A) Sample extracted from airborne particulates, λ_{ex} = 378 nm, λ_{em} = 408 nm; (B) 1 × 10^{-7} M benzo(a)pyrene, λ_{ex} = 383 nm, λ_{em} = 404 nm; (C) 1 × 10^{-7} M benzo(ghi)perylene, λ_{ex} = 382 nm, λ_{em} = 419 nm.

Spectrum

Figure 4A shows the excitation and fluorescence spectra of the sample extracted from airborne particulates. There are several structures, but they are not well resolved in the spectra. As seen in the excitation spectrum, the sample can be efficiently excited at 378 nm. It is known that the PAHs of B(a)py and benzo(ghi)perylene [B(ghi)per] have absorption maxima at this wavelength. The fluorescence spectra of these molecules are shown in Fig. 4B and C. The bands observed in Fig. 4A are apparently different from the bands for either of the fluorescence spectra shown in Fig. 4B and C. It seems that many components are present in this sample and it is difficult to separate their contributions to the spectrum. Therefore, chromatographic separation is necessary for identification of the samples. The measurements were repeated for the sample in benzene; there was no appreciable change from the result obtained with the methanol solution.

Fluorescence decay

The fluorescence decay curve of anthracene in methanol is shown in Fig. 5A. The excitation wavelength was shifted slightly from 386 nm to shorter wavelengths to adjust to the absorption maximum of anthracene. The semi-log plot of the decay curve in Fig. 5A was not an exact straight line, and it was found that a short-lived component was superimposed on the decay curve for 0—1 ns after excitation (4—5 ns for the time scale of the figure). This component may be scattered emission or a short-lived impurity fluorescence from the solvent. The lifetime of anthracene was calculated to be 7 ns, using the data from 1 ns to 10 ns after excitation. This value agrees reasonably with the reference value of 4.9 ns for a cyclohexane solution [40]. A conventional nitrogen-laser-pumped dye laser has pulse widths of 10 ns and suffers from the poor time resolution in the measurement of such short-lived fluorescence decay. In the present laser fluorimetric system, no deconvolution procedure is necessary, and it is apparent that this system

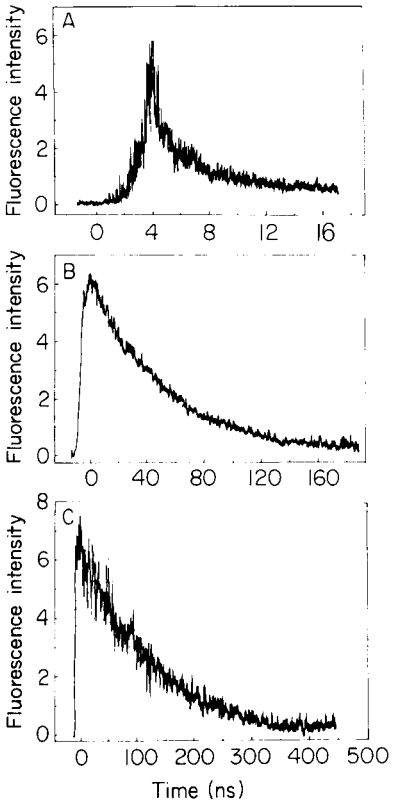

Fig. 5. Fluorescence decay curves with λ_{ex} = 386 nm: (A) 1 × 10^{-7} M anthracene, λ_{em} = 405 nm; (B) 1 × 10^{-7} M B(a)py, λ_{em} = 405 nm; (C) 1 × 10^{-7} M B(ghi)per, λ_{em} = 419 nm.

with a better time resolution has a distinct advantage for the determination of PAHs with short-lived fluorescence.

Figure 5B and C are fluorescence decay curves of B(a)py and B(ghi)per in methanol measured with a head-on photomultiplier. The calculated lifetimes were 53 ns and 110 ns, respectively. The fluorescence lifetime of B(ghi)per agrees well with the reference value of 107 ns for a benzene solution [40]. The noise in the decay curve originates mainly from instability of the repetition rate and the output power of the nitrogen laser, because it was operated in the free-running condition; it should be noted that the signal level of the sampling oscilloscope decreased with decreasing repetition rate of the trigger pulse. The radiofrequency interference from the nitrogen laser seems to be also a source of noise in the decay curve. The fluorescence decay curves were measured in various solvents such as cyclohexane, benzene and methanol—water (9 + 1), under air-saturated and degassed conditions. The fluorescence lifetimes of B(a)py were 17—24 ns for the air-saturated samples and 38—61 ns for the degassed samples, and no drastic changes were observed for these different solvents. The lifetimes of B(ghi)per were 21—32 ns and 90—134 ns for the air-saturated and degassed samples, respectively. Because the lifetimes for the air-saturated samples are similar for B(a)py and B(ghi)per, the removal of oxygen from the sample solution is essential for selective determination of these compounds by time-resolved fluorimetry. The sample was sealed by Parafilm during its measurement, but this was not very successful. The fluorescence lifetime of B(ghi)per decreased to half the original intensity in a few minutes and to one third in 10 min. The present results show that the fluorescence of the PAHs is strongly quenched by oxygen dissolved from the air and the observed lifetime depends strongly on the conditions under which measurements are made.

Emission decay for a blank solution was also measured by using the present instrument. Most of the background emission came from Raman scattering of the methanol used as solvent. The decay had a small tail which corresponded to a lifetime of 2.5 ns and seemed to be fluorescence from impurities in the solvent.

High-performance liquid chromatography

A typical chromatogram of a mixture of B(a)py and B(ghi)per is shown in Fig. 6. The exciting laser beam was intercepted during the measurement of the first 2 or 3 min to clarify the baseline levels of the chromatograms. When the delay time was adjusted to 0 ns, the background signal was large. This background signal was almost completely removed for the chromatogram measured with a delay time of 20 ns. It is obvious that time-resolved fluorimetry has a distinct advantage for discrimination against Raman scattering and short-lived fluorescence from the eluting solvent in h.p.l.c. Emission decay of the background is very short, therefore a fluorimeter with good time-resolution is useful for efficient reduction of the background emission, especially for the determination of substances with relatively short

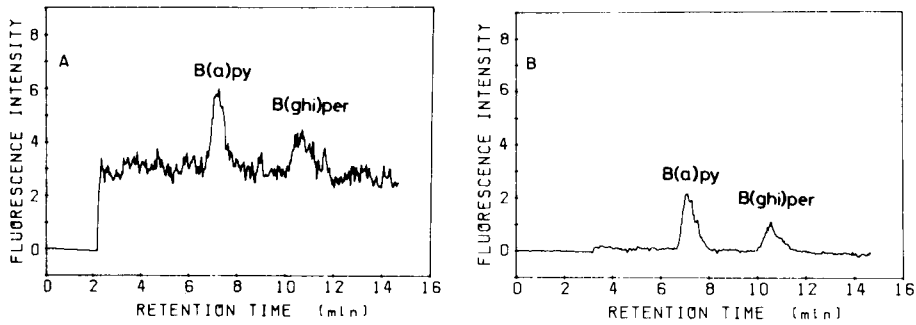

Fig. 6. Chromatograms for a mixture of B(a)py (2×10^{-6} M) and B(ghi)per (8×10^{-6} M) based on time-resolved fluorescence detection. Delay time: (A) 0 ns; (B) 20 ns, λ_{em} = 405 nm, flow rate 1.8 ml min^{-1}.

fluorescence lifetimes. In h.p.l.c., the elution times are sometimes too long for routine analyses when single eluents are used. Gradient elution is then useful, but the baseline of the chromatogram sometimes increases with increasing methanol content in the aqueous mobile phase [22]. This background may originate from the Raman scattering of methanol and impurity fluorescence, as in the present study. The present system can remove such background problems by means of its time-resolved fluorescence detection.

Figure 7 is a three-dimensional chromatogram of the mixture. The calculated lifetimes of B(a)py and B(ghi)per from these results were 42 ns and 97 ns, respectively; these values agree with the data obtained in measurements by the batch system. The signal-to-noise (*S/N*) ratios for the B(a)py and B(ghi)per peaks were calculated from these data for different delay times and are plotted against the delay time in Fig. 8. Just after excitation, the strong baseline drift in the chromatogram originates from background emission and instability of the output power of the dye laser, therefore the *S/N* ratio at 0 ns is quite small. After 40 ns, the baseline drift becomes

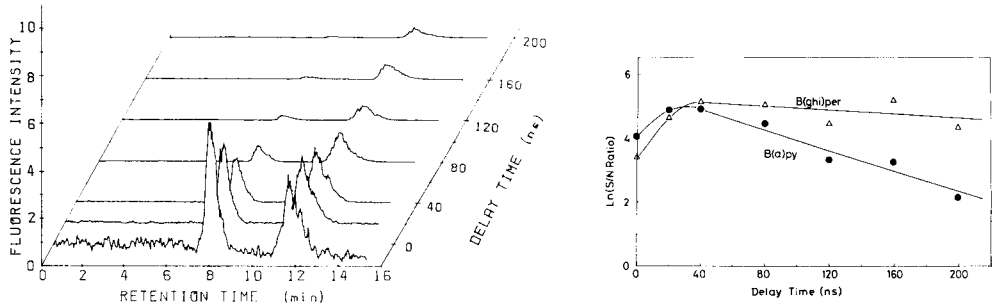

Fig. 7. Three-dimensional chromatogram for the mixture of B(a)py and B(ghi)per based on time-resolved fluorescence detection.

Fig. 8. Effect of delay time on *S/N* ratio: (△) B(ghi)per; (●) B(a)py.

completely constant. Thus the *S/N* ratios decrease monotonically with decreasing fluorescence intensities. Under these conditions the slopes of the *S/N* ratios should be identical with the fluorescence lifetimes of the substances; this is verified within the experimental error. Benzo(ghi)perylene fluorescence has a relatively long lifetime so that the *S/N* ratio is large up to 200 ns. It is important to optimize the delay time of the fluorescence detection in order to reduce the contribution of unwanted emission.

Application to an airborne particulate sample

The chromatograms based on time-resolved fluorescence detection of a sample extracted from airborne particulates are shown in Fig. 9. When the delay time is adjusted to 0 ns, strong background emission appears and the chromatogram obtained is poor. Peaks denoted as (a), (b), and (c) are apparent in the chromatogram measured at a delay time of 20 ns. The retention time (6.9—7.1 min) and the fluorescence lifetime (43 ns) of peak (b) are similar to those of the standard sample of B(a)py in methanol (7.4 min, 42 ns), so that this peak can be assigned to B(a)py. The retention time of peak (c) is 10 min, which is close to that of B(ghi)per (10.5 min). However, the fluorescence lifetime of the substance providing this peak is 20—30 ns, which is very different from the lifetime for B(ghi)per (97 ns). Thus, peak (c) must originate from some other species. The fluorescence corresponding to peak (a) was found to have a relatively short lifetime (14 ns). For the assignment of this component, it would be necessary to measure the fluorescence lifetimes of various standard PAHs.

In a conventional h.p.l.c. system, assignment of peaks is usually based on retention times. However, it is well known that retention times change, depending on the packing materials and even the packing procedure, so that internal standards are required. Assignment by means of excitation and fluorescence spectra is possible for a stopped-flow system [41]. However, the features of the spectra may be complicated if several components are present at a particular retention time. The use of lifetime data provides additional information and should reduce such disadvantages, because fluorescence lifetimes should be identical for a particular solvent. Even if two components were superimposed in the peak of the chromatogram, a double exponential decay might be observed if the lifetimes of the components were sufficiently different. Such assignments would, of course, require fluorescence lifetime tables of the PAHs. Unfortunately, in the present system, it is necessary to measure the chromatogram several times (at least twice) for measurements of fluorescence lifetimes, which becomes tedious and time-consuming. Improvements in the data processing equipment should make it possible to measure fluorescence lifetimes at a particular retention time in the chromatogram.

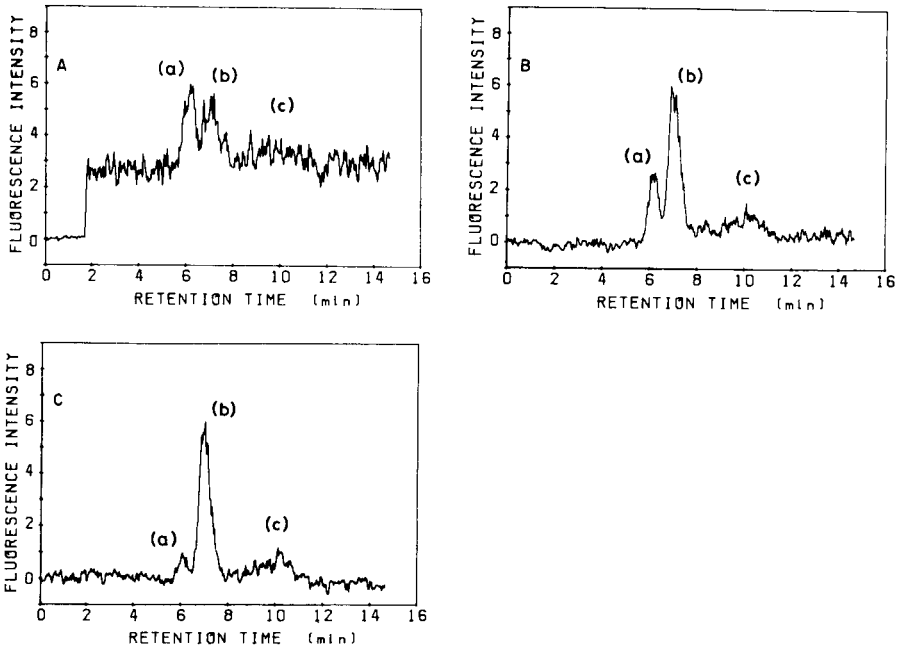

Fig. 9. Chromatograms for the sample extracted from airborne particulates based on time-resolved fluorescence detection. Delay time: (A) 0 ns; (B) 20 ns; (C) 40 ns. See text for explanation of (a)—(c).

The authors thank Kazumi Fukamachi for his gift of the real PAH sample extracted from airborne particulates in Omuta City. The authors also thank Kenji Mori, Toshinori Hayashi, and Yuji Kawabata for their cooperation in experiments and helpful discussions. This research was supported by Grants-in-Aids for Scientific Research (Grant no. 56550536) from the Ministry of Education of Japan and by the Toyata Foundation.

REFERENCES

1 J. M. Daisey and M. A. Leyko, Anal. Chem., 51 (1979) 24.
2 B. A. Tomkins, H. Kubota, W. H. Griest, J. E. Caton, B. R. Clark and M. R. Guerin, Anal. Chem., 52 (1980) 1331.
3 M. L. Yu and R. A. Hites, Anal. Chem., 53 (1981) 951.
4 G. A. Eiceman, R. E. Clement and F. W. Karasek, Anal. Chem., 53 (1981) 955.
5 D. Schuetzle, T. L. Rlley, T. J. Prater, T. M. Harvey and D. F. Hunt, Anal. Chem., 54 (1982) 265.
6 D. R. Choudhury and B. Bush, Anal. Chem., 53 (1981) 1351.
7 J. B. F. Lloyd and I. W. Evett, Anal. Chem., 49 (1977) 1710.
8 J. C. Andre, M. Bouchy and M. Niclause, Anal. Chim. Acta, 92 (1977) 369.
9 T. V. Dinh and P. R. Martinez, Anal. Chim. Acta, 125 (1981) 13.
10 T. V. Dinh, R. B. Gammage and P. R. Martinez, Anal. Chem., 53 (1981) 253.
11 D. W. Armstrong, W. L. Hinze, K. H. Bui and H. N. Singh, Anal. Lett., 14 (1981) 1659.

12 T. F. V. Geel and J. D. Winefordner, Anal. Chem., 48 (1976) 335.
13 J. H. Richardson and M. E. Ando, Anal. Chem., 49 (1977) 955.
14 M. Kunitake, T. Imasaka and N. Ishibashi, Nippon Kagaku Kaishi, (1981) 55.
15 E. L. Wehry and G. Mamantov, Anal. Chem., 51 (1979) 643A.
16 R. B. Dickinson, Jr. and E. L. Wehry, Anal. Chem., 51 (1979) 778.
17 J. R. Maple, E. L. Wehry and G. Mamantov, Anal. Chem., 52 (1980) 920.
18 A. L. Colmsjö and C. E. Östman, Anal. Chem., 52 (1980) 2093.
19 Y. Yang, A. P. D'Silva and V. A. Fassel, Anal. Chem., 53 (1981) 894, 2107.
20 L. A. Bykovskaya, R. I. Personov and Y. V. Romanovskii, Anal. Chim. Acta, 125 (1981) 1.
21 J. R. Maple and H. L. Wehry, Anal. Chem., 53 (1981) 266, 1244.
22 I. Chiang, J. M. Hayes and G. J. Small, Anal. Chem., 54 (1982) 315.
23 J. Müller and E. Rohbock, Talanta, 27 (1980) 673.
24 H. Matsushita, T. Shiozaki, Y. Kato and S. Goto, Bunseki Kagaku, 30 (1981) 362.
25 B. A. Tomkins, R. R. Reagan, J. E. Caton and W. H. Griest, Anal. Chem., 53 (1981) 1213.
26 L. W. Hershberger, J. B. Callis and G. D. Christian, Anal. Chem., 53 (1981) 971.
27 K. Ogan, E. Katz and W. Slavin, Anal. Chem., 51 (1979) 1315.
28 B. S. Das and G. H. Thomas, Anal. Chem., 50 (1978) 967.
29 E. S. Yeung and M. J. Sepaniak, Anal. Chem., 52 (1980) 1465A.
30 G. J. Diebold and R. N. Zare, Science, 196 (1977) 1439.
31 G. J. Diebold, N. Karny and R. N. Zare, Anal. Chem., 51 (1979) 67.
32 S. D. Lidofsky, T. Imasaka and R. N. Zare, Anal. Chem., 51 (1979) 1602.
33 W. D. Hinsberg, III, K. H. Milby and R. N. Zare, Anal. Chem., 53 (1981) 1509.
34 J. H. Richardson, K. M. Larson, G. R. Haugen, D. C. Johnson and J. E. Clarkson, Anal. Chim. Acta, 116 (1980) 407.
35 T. Imasaka and N. Ishibashi, Anal. Chem., 52 (1980) 2083; Opt. Commun., 41 (1982) 219.
36 T. Imasaka, Y. Kawabata and N. Ishibashi, Rev. Sci. Instrum., 52 (1981) 1473.
37 K. Morita and K. Fukamachi, Eisei Kagaku, 27 (1981) 169.
38 A. Andreoni, R. Cubeddu, S. D. Silvestri and P. Laporta, Opt. Commun., 33 (1980) 277.
39 S. D. Silvestri, F. Docchio, P. Laporta, A. Longoni and F. Zaraga, Opt. Commun., 37 (1981) 20.
40 I. B. Berlman (Ed.), Handbook of Fluorescence Spectra of Aromatic Molecules, Academic Press, New York and London, 1971.
41 Z. Tamura, N. Ishibashi, Y. Ohkura, T. Tanimura and A. Tsuji (Eds.), LC Fluorimetry, Koudansha Scientific, Japan, 1978, p. 114.

Analytica Chimica Acta, 142 (1982) 13—29
Elsevier Scientific Publishing Company, Amsterdam — Printed in The Netherlands

THE HIGH-PERFORMANCE LIQUID CHROMATOGRAPHY AND DETECTION OF PHOSPHOLIPIDS AND TRIGLYCERIDES
Part 2. Comparison of an Ultraviolet Absorption and Post-Column Reactor Detector

BRUCE JON COMPTON[a] and WILLIAM C. PURDY*

Department of Chemistry, McGill University, 801 Sherbrooke St. W., Montreal, Quebec H3A 2K6 (Canada)

(Received 15th February 1982)

SUMMARY

A liquid chromatographic ultraviolet absorption detector (at 195 nm) and a novel post-column reactor detector are compared for use in the detection of triglyceride and phospholipid molecular species. The detection limit for the u.v. detector depends on the degree of unsaturation of the lipid sample (3×10^{-6}—2×10^{-8} M in the detector cell for 0—3 double bonds per acyl group). The post-column reactor detector is responsive to equivalents of lipid and has detection limits of 5×10^{-7} M for triglycerides and 2×10^{-6} M for phospholipids. The log u.v./post-column reactor detector response ratios are linearly related to the log of the degree of unsaturation of the lipid, indicating the usefulness of both detectors for quantifying triglycerides and phospholipids.

The diverse nature of acylglyceride and phosphatide molecular species makes their quantification a particularly arduous task. In Part 1 of this series [1], the retention behavior of these two lipid classes was described in a nonpolar stationary (reverse) phase liquid chromatographic system. It was shown that ultraviolet transparent mobile phases could be used with a hexyl (C_6)-bonded stationary phase and a column heated to 60°C. The information content of the retention data was questioned because it was noted, as in earlier studies [2, 3], that unequivocal structural assignment was complicated by retention redundancy arising from the effects of acyl unsaturation. To resolve this problem, additional information on acyl structure (i.e., the degree of unsaturation) must be obtained. One logical approach to acquiring this necessary information is by detector design.

Conventional on-line detection methods employed with liquid chromatographic fractionation of triglycerides and phospholipids are based on differential refractometry, ultraviolet absorbance (u.v.), infrared absorbance (i.r.), and moving-wire flame-ionization detectors [1—6]. None of these detectors has been shown to be satisfactory for these classes of lipids, lacking sensitivity

[a]Present address: Merck Sharp and Dohme Research Laboratories, P.O. Box 2000, Rahway, NJ 07065, U.S.A.

0003-2670/82/0000-0000/$02.75

(i.r. and refractive index), selectivity (refractive index and u.v.), predictable response (flame ionization), or general response for all triglyceride and phospholipid species (u.v.). While numerous detectors might be envisioned as usable for these lipids, to date none has the desired sensitivity, class selectivity, or general within-class response characteristics required for quantifying diverse lipid molecular species. With this in mind, an investigation of a post-column reactor detector was undertaken.

By judicial choice of the chemistry involved, a post-column reactor can possess the desired features of (i) class or compound selectivity, (ii) adequate sensitivity, and (iii) molar response as described herein. This last capability is particularly useful when dealing with complex samples like triglyceride and phospholipid molecular species where detector calibration becomes impractical. Molar response detectors can also be combined with other detector systems, such as refractive index, u.v., and i.r., to yield, through response ratios, information on the molar refractivity, u.v. absorptivity, or i.r. absorptivity of the compound being detected. This additional information can be used to augment retention data, specifically regarding the unsaturation of a lipid, and help resolve the retention redundancy problem cited in Part 1 of this study [1]. It is to this end that the post-column reactor described below was developed. Also presented is a comparison of the response characteristics of the post-column reactor and the u.v. detector.

DETECTOR CHARACTERISTICS

The features of interest of the u.v. and post-column reactor detectors are their selectivity, measured as response (R_D), sensitivity, linear dynamic range, and sources and magnitude of noise. This last characteristic is important so that recommendations for future detector improvement can be made.

The ultraviolet absorption detector

The general operating characteristics of the u.v. detector have been investigated [7, 8] and reviewed [9]. The unit used in this study, the Schoeffel Model SF770 with GM770 monochromator (Schoeffel Instrument Corp., Westwood, NJ 07675) has been described in detail [10]. The SF770 compares favorably with other variable-wavelength absorption detectors and is not expected to be unique to this application. It has a reported 5-nm bandpass and a cell volume of 8 μl.

The u.v. response, R_{uv}, can be described by

$$R_{uv} = a_\lambda C_s D V \tag{1}$$

where a_λ is the absorptivity of the analyte at the wavelength setting of the detector, C_s is the analyte concentration, D is the chromatographic dilution factor, and V is the volume of the injected sample. The optical cell length is assumed to be unity. The absorptivity can be expressed by $a_\lambda = \Sigma a_x, a_y, a_z, a_g$, where a_x and a_y refer to group absorptivity of isolated and conjugated

double bonds, respectively, a_z refers to other chromophores substituted on the acyl moieties (i.e., epoxides, hydroxyl, etc.), and a_g refers to the absorptivity of the glycerol or phosphoglycerol moiety. This equation assumes that the respective chromophores are not auxochromes of one another.

The absorptivity a_x and a_y can be predicted from the quantum mechanical "particle-in-a-box" model by the relationship [11]

$$a_{x,y} = 32Ne^2L^2\nu/3000\,\pi hc \tag{2}$$

where L is the box length, N is Avogadro's number, e is the charge on the electron, h is Planck's constant, c is the velocity of light, and ν is the frequency of the incident radiation. For the purpose of simplifying notation, a_x and a_y have been combined as $a_{x,y}$. If L can be approximated by $L = kD_b$, where k is the unit length of the carbon—carbon double bond and D_b is the number of double bonds in the entire molecule, then Eqn. (2) can be modified to give

$$a_{x,y} = c^*D_b^2 \tag{3}$$

where c^* is a constant equal to $(32\ Ne^2k^2\nu)/(3000\,\pi hc)$.

The limitations of Eqn. (3) are obvious from its derivation because of the simplifications implicit in $L = kD_b$. The usefulness of Eqn. (3) resides, however, in its ability to predict the value of $a_{x,y}$ for the acyl portion of phospholipid and triglyceride molecular species at a constant wavelength (c/ν). It is well known that both the λ_{max} and absorptivity increase with increasing D_b but this information is difficult to correlate with fixed-wavelength measurements. Because Eqn. (3) is derived for simple, conjugated, unsaturated triglycerides and phospholipids, these being the most frequently encountered in nature, it is expected to be useful in obtaining qualitative information on the degree of unsaturation of a triglyceride or phospholipid sample.

The u.v. signal-to-noise ratio (SNR) can be described in terms of the detector response, R_{uv}, and associated noise in the frequency domain of the signal. The SNR expression at the noise-limited detection limit is

$$\text{SNR} = c^*D_b^2C_sDV/2\sigma \tag{4}$$

where 2σ is the amplitude of the baseline noise (i.e., encompassing 95% of the noise). If the lower detectable signal is defined as positive signals twice the 2σ-noise level (95% confidence on a one-tail test), then the detection limit, C_{SDL}^{uv}, should be inversely proportional to the square of the number of double bonds in the triglyceride or phospholipid molecular species.

The linear dynamic range of the detector is a function of C_{SDL}^{uv}, R_{uv}, and the detector upper range. Upper range deviations from linearity (caused by optical and electronic non-linearity as well as chemical deviations from ideal behavior) are not of great interest in this discussion because on-line chromatographic detectors are also subject to column loading and overloading effects.

The post-column reactor detector

The detector described here has response originating from fluorescent intensity measurements. These measurements are addressed in this discussion.

The Schoeffel spectrofluorimeter Model FS970 with GM770 monochromator was used. Because the detector has a unique frontal fluorescent cell design it is not easy to predict whether other types of detectors will behave in a similar manner. This is especially true because the detector was used with the segmentation gas in the post-column reactor passing through the cell.

The relationship between fluorescent signal and analyte concentration is

$$F = k_{f,n}\phi_{f,n}(abC_s) \tag{5}$$

where $\phi_{f,n}$ is the fluorescent quantum efficiency of the species n and the term abC_s is derived from the Beer—Lambert Law to account for absorbed photons [12]. The constant $k_{f,n}$ is an instrumental factor accounting for the total optical—electronic efficiency of the FS970.

The response expression for the FS970 is

$$R_{Flr,n} = k'_n C_s DV \tag{6}$$

where k'_n is equal to $abk_{f,n}\phi_{f,n}$ and D and V have the same meanings as in Eqn. (1). Equation (6) is only valid for dilute ($< 10^{-4}$ M), moderately-fluorescing samples because at higher concentrations, k'_n is expected to change. For the present study, Eqn. (6) requires additional terms to account for the chemistry involved in the post-column reactor. This can be expressed as follows

$$C_{PCR,n} = k_{PCR,n}C_{s,n} \tag{7}$$

where $C_{PCR,n}$ is the concentration of the detectable substance resulting from the chemical reactions of the reactor on n, and $k_{PCR,n}$ is the chemical and hydrodynamic efficiency of the reactor (a function of n). Equations (6) and (7) can be combined to give

$$R_{Flr,n} = k_n C_{s,n} DV \tag{8}$$

where $k_n = k'_n k_{PCR,n}$.

The selectivity of the post-column reactor is determined both by the chemistry and fluorescent detector stages of the system. Thus the detector will detect any compound converted by the reactor or having endogenous fluorescence similar to the detected fluorophore.

In terms of selectivity for triglycerides or phospholipids, if k_n is the same for all molecular species, the reactor is a molar response detector for these two classes of compounds. The noise associated with the reactor will be described later. However, it can be expressed as

$$N_{2\sigma} = k'_b k_{PCR,b} C_b P_b \phi_{Cb} \tag{9}$$

where b refers to the background and $P_b \phi_{Cb}$ is a function associated with peristaltic pump noise and reactor mixing, respectively. This is a general expression for the efficiency of the reactor. The SNR expression is SNR = $K_{SNR}\ C_{s,n}\ C_b^{-1}$, where $K_{SNR} = k_n(k_b P_b \phi_{Cb})^{-1}$. The SNR is seen to be related to background by $C_{s,n}\ C_b^{-1}$. The lower limit of detection, $C^{Flr}_{SDL,n}$, is

$$C^{Flr}_{SDL,n} = 2C_b K^{-1}_{SNR} \tag{10}$$

The linear dynamic range arguments for this detector follow those of the u.v. detector with one additional factor. Because the post-column reactor used in this study is optimized for first-order reaction kinetics, if solute concentration is increased to overcome this condition, detector response may be affected. Examination of the reagent concentrations, as described below in Table 2, indicates that column overloading is expected to occur before this condition is encountered.

Comparison of the u.v. and post-column reactor detectors

The expected detection limits for the u.v. and fluorimetric detectors have been studied [13]. Comparison of the two detectors indicates that selectivity plays a major role in detector response and the detection-limit expression. Both R_{uv} and C^{uv}_{SDL} are functions of D_b while $R_{Flr,n}$ and $C^{Flr}_{SDL,n}$ are independent of the molecular weight of phospholipid or triglyceride. Both detectors are expected to give responses in direct proportion to the concentration of the solute present.

The molar response characteristic of the post-column reactor can be connected with that of the u.v. detector in a meaningful way. The ratio of R_{uv} to $R_{Flr,n}$ gives a result analogous to the absorptivity of the lipid investigated. This yields the expression

$$R^{uv}_{Flr(PCR)} = c^* D_b^2 / a \tag{11}$$

where a is 2.3 $a_n b k_{PCR,n} k_{f,n} \phi_{f,n} k'_n$ and c^* is defined as above.

THE POST-COLUMN REACTOR DETECTOR

During the development of the detector, it was noted that typical "automated" methods for quantifying triglycerides involve either classical chemical or enzymatic techniques. The more selective enzymatic methods [14, 15] compromise the choice of chromatographic mobile phase; thus the more classical chemical methods [16, 17] were studied for the present application. These chemical methods were developed by Lofland [16] and Kessler and Lederer [17], and involve the general reaction sequence of converting the acylglycerides (and phospholipids) to a detectable product. The reaction steps were studied from the standpoint of enhancing detector sensitivity. Hardware associated with the detector was investigated to optimize hydrodynamic efficiency. This was necessary because the automated method for the determination of serum triglyceride levels that was studied did not require a highly efficient or sensitive detection system.

(I) Acylglycerides + Base ⟶ Glycerol + fatty acids

(II) Glycerol + $NaIO_4$ ⟶ HCHO + HCOOH

(III) HCHO + Fluoral-P ⟶

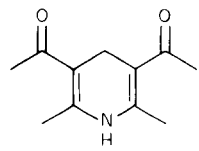

3,5-Diacetyl-2,6-dihydrolutidine

Design of the reactor

The reactor is shown schematically in Fig. 1. Continuous segmented flow processing [18] using helium-plugged flow was required to limit dispersion in the three stages of the reactor. Studies on reactor designs of this type have been presented [19—22] but the optimum theoretical conditions for the segmented flow reactor were often difficult to execute experimentally, necessitating some design compromise.

Consideration of the length of the reaction delay coil (D_c) vs. delay time indicated that 1-mm i.d. tubing offered wide volumetric flow range with easily handled tube lengths. Thus the reactor tubing was chosen to be stainless-steel 316 standard (1/16-in. (0.159 cm) o.d. and 0.03-in. (ca. 1 mm) i.d.) coiled into a 1-cm diameter coil.

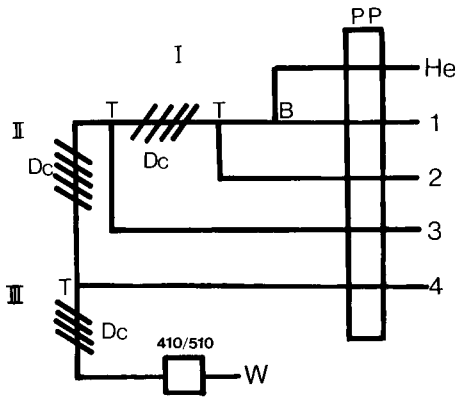

Fig. 1. Schematic representation of the post-column reactor manifold and associated equipment. See text for description of components. Reagent lines are as follows: (1) effluent from chromatograph; (2) KOH line; (3) periodate line; (4) Fluoral-P line. W is waste.

The bubbler (B) was made from a standard Swagelok 1/16-in. T-connector using standard compression nuts and ferrels for inlet (unsegmented) and outlet (segmented) flow. The gas line and all other reagent and connector lines were made of 0.01-in. i.d., 1/16-in. o.d. teflon tubing. Because bubble surging is often encountered in segmented flow systems, special attention was paid to this problem. It was found that decreasing the gas inlet volume from the gas delivery pump to the bubbler to as small a volume as possible, effectively prevented surging. When surging did occur, it indicated high resistance in the reactor lines caused by sample or reagent precipitation.

Evaluation of various conventional T-type debubbler designs indicated that this component contributed greatly to potential band broadening. Thus the debubbler was eliminated and bubbles were allowed to pass directly through the detector cell. As will be seen below, the effects of bubbled flow on noise in the fluorescent detector can be tolerated if appropriate signal processing (in this case a simple RC filter) is applied.

The reagent-addition T-joints (T) were standard Swagelok design (1/16-in.) and the segmentation gas was helium. The reagent delivery system (PP) was a Technicon Pump III (Technicon Instrument Corp., Tarrytown, NY); the air bar of this model was not used. The detector was a Schoeffel FS970 spectrofluorimeter with the monochromator set at 410 nm for excitation and 480- and 550-nm emission filters ganged together (standard supplies from Schoeffel). Excitation and emission spectral overlap was estimated to be less than 0.001%.

Chemistry of the reactor

The chemistry used for detection was developed from the triglyceride methods previously mentioned. The detector stages and relevant reagents and products are outlined above. The three stages are deacylation with saponification of triglyceride or phospholipid to glycerol or phosphoglycerol, respectively; periodate oxidation of glycerol or phosphoglycerol to formaldehyde (two equivalents for glycerol, one for phosphoglycerol); and detection of formaldehyde using Fluoral-P (4-amino-3-penten-2-one), a new fluorogenic agent specifically developed for this application [23, 24], to the final product 1,4-diacetyl-2,5-dihydrolutidine.

The literature contains a large number of references to deacylation of fatty-acid esters [25—28]. Transesterification was found to be the most expedient for accomplishing this [27, 28]. Unfortunately, alcohol solutions contain high aldehyde contamination and were thus eliminated from the post-column reactor. Saponification was used for deacylation.

Periodate oxidation is normally considered a selective process involving 1,2-diols [29, 30]. Because the selectivity of this reaction decreases above 50°C [31], excess of periodate should be removed by using high concentrations of either sodium arsenite or rhamnose [32—35]. Periodate was found to decompose the dihydrolutidine product of the post-column reactor but excess of periodate was not removed in this application because interferences from the high concentrations of scavenging agents were found to be significant.

In the original method, formaldehyde was detected by using the Nash reagent (0.1 M 2,4-pentanedione in 2 M ammonium acetate [36]). This reagent was found to have high background and viscosity along with a low reaction rate for formaldehyde. Fluoral-P [23, 24] had the desirable properties of a very high reaction rate for formaldehyde, selectivity for aldehydes (mainly formaldehyde with fluorimetric detection), low viscosity, and low background.

Materials

Chromatographic equipment and lipid standards were described in Part 1 of this series [1]. Specific triglyceride and phospholipid standards and the chromatographic conditions used in this study are presented in Table 1. The mixtures were stored desiccated at −20°C when not in use. Phosphatidylcholine (PC) dilinoleoyl and PC dilinolenoyl were obtained from Sigma Chemical Co.

Preparation of Fluoral-P has been described [23, 24]. Acetonitrile (Gold label) was purchased from Aldrich Chemicals. All other chemicals were of reagent grade.

TABLE 1

Triglyceride and phospholipid standard mixtures used for detector evaluation (Chromatographic conditions: column, 5 μm C_6 reverse-phase, in-lab design; temperature, 60 ± 1°C; flow rates, 1 ml min^{-1} for u.v. detector, and 0.5 ml min^{-1} for post-column reactor. Eluent varied as follows: TG-I, 100% CH_3CN; TG-II and TG-III, 90 CH_3CN/10% H_2O; PL-I, 95 CH_3CN/5% H_2O/0.1% conc. H_3PO_4)

Sample	Composition	Concentration (10^{-3} M)
Individual	Trilaurin	6.26
Individual	Tripalmitolein	4.99
Individual	Triolein	4.50
Individual	Tripetroselinin	4.52
TG-I	Triolein	2.25
	Trilinolein	2.30
TG-II	Trimyristin	5.53
	Trilaurin	6.26
	Tripalmitolein	4.99
	Trilinolein	4.60
TG-III	Tricaprin	7.20
	Trilaurin	6.26
	Trimyristin	5.53
	Tripalmitolein	4.99
PL-I	Dihexanoyl PC	0.524
	Didecanoyl PC	2.10
	Dioleoyl PC	1.51
	Dilinoleoyl PC	1.50
	Dilinolenoyl PC	1.50

Optimization of the reactor

One problem often encountered in developing a mechanized analytical system is determining what combination of reagents, solvents and buffers, delay times, etc., constitute an optimum state. Also of concern is whether an "optimum" system is required for a particular application. The approach taken in this work for the optimization of the reactor has been to choose the hardware and chemical parameters on the basis of hydrodynamic considerations (i.e., using low viscosity reagents) and extensive knowledge of the bench chemistry of the particular procedure. The optimization is then reduced to the selection of the appropriate delay times for each reactor stage. This was done in the present instance by using the previously described "stop-flow optimization" technique specifically developed for this application [37].

The optimized conditions used with the post-column reactor are given in Table 2.

Experimental procedures

The u.v. and reactor detectors were run in series in that order. Two general experimental procedures were followed. First, detector response vs. amount of sample injected was studied by injecting standard mixtures TG-I and PL-I in 2—25-μl quantities. Responses were reported as peak height, measured from a line defining the top boundary of the baseline noise to the

TABLE 2

Summary of the optimized conditions for the post-column reactor

Stage	Measured D_c vol. (ml)[a]	Nominal flow rate through stage (ml s^{-1})	Calculated delay time (s)[b]
I KOH	2.48	0.020	125
II $NaIO_4$	3.17	0.027	120
III Fluoral-P	0.99	0.033	30

Stage[c]	Nominal pump flow rate (ml s^{-1})[b]	Pump tube
I 0.5 M KOH in H_2O	0.0038	PVC-O/W
II 0.02 M $NaIO_4$ in 0.3 M $HClO_4$	0.0070	PVC-O/O
III 0.18 g Fluoral-P in CH_3CN	0.0070	Silicon-O/O
H.p.l.c.	0.0083	Waters 6000A
He	0.0070	Silicon-O/O

[a]Measured by repetitive (10) injections of lutidine into a unit using the Waters 6000A pump, delay coil of interest, and FS970 detector. Relative standard deviation of volumes was less than 1%. [b]Because of pump tube aging and variations, these values are reproducible to ±5%. The calculated total flow rate of 1.99 ml min^{-1} was evaluated by pumping water through all lines. The measured total flow rate was 1.97 ml min^{-1}. [c]Concentration of each reagent as it occurs in the reaction (assuming no reaction): (I) 0.16 M KOH; (II) 0.0073 M $NaIO_4$; (III) 0.048 M Fluoral-P.

uppermost deflection of the detector response. These results were given in absorbance (at 195 nm) and relative fluorescent intensity units and were self-consistent within each experiment. Noise was measured directly from the chromatograms as peak-to-peak noise by drawing parallel lines that encompassed approximately 95% of the noise over three peak base-widths of the broadest chromatographic band. Secondly, the detector response ratio, R_{PCR}^{uv}, was investigated by using 2—10-μl injections of mixtures TG-II and PL-I, repeated 6—15 times.

RESULTS AND DISCUSSION

The normal physiological range for triglycerides in serum is from zero to ca. 2×10^{-3} M [38]. In terms of triolein, the lower limit of detection for clinical triglyceride determinations has been calculated to be 5×10^{-5} mol per sample introduction [39]. This illustrates that conventional manifolds are designed with upper rather than lower triglyceride ranges in mind.

Noise

The post-column reactor system should be superior to conventional systems because of the care taken to lower band dispersion and detector noise. With distilled water in all reactor channels, lutidine was detectable at 1.6×10^{-10} mol per injection. A flow-injection system using Fluoral-P reagent [24] determined formaldehyde at 3×10^{-9} mol per injection. That system contained Fluoral-P reagent and dilute phosphoric acid. It had a higher background than the distilled water system, resulting in greater detector noise and higher detection limits at comparable signal intensities. The value of 1.6×10^{-10} mol per injection can be taken as the absolute fluorimeter-limited lower detection limit for the post-column reactor with 3×10^{-9} mol per injection being a more realistic value.

In developing the post-column reactor, the noise of concern was of two types, $1/f$ and synchronous (less than 1 Hz) noise, because the chromatographic signal was typically in the range of 0.01—0.1 Hz. Observations made during the development of the reactor indicated the noise sources to be (i) proportioning pump pulsations, (ii) heating bath cycling and other synchronous low-frequency sources, (iii) particles in the detector cell, and (iv) bubbles passing through and forming in the detector cell.

The Technicon Pump III possessed, per channel, periodic noise in the range up to 0.1 Hz. The multiple channel nature of the reactor, four channels shown in Fig. 1, meant that individual noise patterns arising from each channel combined in a complex phase-dependent fashion. It was noted that, in some manifold configurations, individual noise channels would add in constructive or destructive fashion depending on their respective phases, a function of the length of reagent lines used and delay-coil volumes. Because noise was observed to increase up to a certain level with background, the main approach employed to limit noise in the reactor was to decrease background, thus increasing signal-to-noise directly.

Detector noise was reduced by several orders of magnitude over previous mechanized designs by the development of the Fluoral-P reagents [23, 24] and the replacement of potential sources of aldehyde contamination (acetic acid, alcohols) in the original design with aldehyde-free chemicals [24].

Major synchronous noise sources were minimized through changes in their duty cycles (such as better thermal insulation in the case of heaters) and isolation. Total random noise from bubble formation and particles in the detector cell was eliminated by allowing the gas segments to pass through the detector cell. This permitted normally low-frequency random noise to be synchronized to a higher frequency than was usually encountered in liquid chromatographic signals. These higher-frequency noise sources were then minimized by RC filtering.

Response characteristics

The response characteristics of the post-column reactor were studied with the Schoeffel SF770 spectrometer (at 195 nm) in line preceding the reactor. The results shown in Table 3 compare the SF770 response with that of the reactor in a bubbled (segmentation bubbles allowed to pass through the FS970 detector) and debubbled (using a stainless-steel T-debubbler, 70% pull-through) stream mode. Debubbling was found to be an extremely inefficient means of dealing with the segmenting gas. The high relative standard deviation (16.1%) in this mode was attributed, in part, to bubble formation in the fluorimetric cell. This cell has a very large pressure drop and debubbler pull-through promotes bubble formation (seen as a decrease in background and signal caused by lower solution volume). The detector was subsequently used in the bubble mode with the bubble frequency set at approximately 5 Hz (i.e., 5 bubbles per second).

A plot of the logarithm of the peak-to-peak 2σ noise vs. the RC filter time constant (τ) of the FS970 showed that a 4-s time constant was effective in reducing noise by an order of magnitude, increasing the band width by 20% at half peak height and decreasing the peak height by 10%. Electronic debubbling [40, 41] would be a more efficient but costly approach to improving the detector response characteristics.

TABLE 3

Comparison of the effect of various detector modifications on band dispersion (measured as half band width, $W_{1/2}$, at the peak) and concentration (measured as peak height)

Mode	$W_{1/2}$(s)	n	Peak height[a]	R.s.d. (%)
Bubbles through detector[b]	17.5 ± 0.0	8	123.6 ± 7.6	6.1
Bubbles eliminated	26.0 ± 0.8	8	33.5 ± 5.4	16.1
SF770 response (λ_{195} nm)	14.7 ± 0.8	19	0.097 ± 0.004	3.7

[a]Average fluorescent intensities for the first two lines are not comparable to absorbance in the third line. [b]τ = 4 s.

Of immediate interest to this study was the possibility that the post-column reactor would have molar response characteristics for triglycerides and phospholipids. Table 4 shows results of reactor response measured as solute band area (determined as area weights). The detector was found to have the desired constant response to equivalents of triglycerides and phospholipids.

The class selectivity of the detector is demonstrated by the chromatogram shown in Fig. 2 where the off-set u.v. vs. reactor response is seen. The saturated triglyceride standards tricaproin and trilaurin were not detected in the u.v. detector but were well detected in the reactor. In addition, the chloroform void-volume peak was not seen to any appreciable extent by the post-column reactor. Thus the reactor was found to have the desired class selectivity for triglycerides and phospholipids.

Both the u.v. and reactor detectors are expected to give a response directly proportional to the amount (volume) of sample injected. This was found to be the case and the results are summarized in Table 5. The chromatographic dilution factor, D, is expected to affect detector response and accounts for the different detector responses (B in Table 5) seen for different lipids.

The concentration ranges used to evaluate R_D were narrow because of the limited solubility of some of the lipid standards in the chromatographic mobile phase. Also, injections of chloroform greater than 25 μl resulted in a high probability of precipitation and blockage in the reactor. This effect may be minimized in the future by substituting sodium for potassium hydroxide in reactor stage I. The precipitate is most likely potassium periodate. The concentration range investigated in this study shows the great sensitivity of the post-column reactor. Standards were used in the lower nanomole per injection range.

Detection limits are presented in Table 6. These were calculated from the data in Table 5 and measurements of the baseline noise. The values were

TABLE 4

Response of the post-column reactor measured as band area[a]

Triglycerides — individual standards			Phospholipids — mixture PL-I		
Standard	ACN:D_b	Response[b]	Standard	ACN:D_b	Response[b]
Trilaurin	C_{12}	140 (±6)	Dicaprinoyl	C_{10}	79 (±6)
Tripalmitolein	$C_{16:1}$	149 (±18)	Dioleoyl	$C_{18:1}$	67 (±5)
Triolein	$C_{18:1}$ Δ9	170 (±6)	Dilinoleoyl	$C_{18:2}$	67 (±5)
Tripetroselinin	$C_{18:1}$ Δ6	152 (±25)	Dilinolenoyl	$C_{18:3}$	88 (±6)
Mean		152 (±13)	Mean		75 (±6)

[a] ACN:D_b is the ratio of acyl carbon number to the number of double bonds. The Δ9 and Δ6 indicate double-bond placement. [b] The fluorescence responses given are the mean (± s.d.) of 6 readings for triglycerides and 3 readings for phospholipids. Response ratio for triglycerides to phospholipids is 2.02.

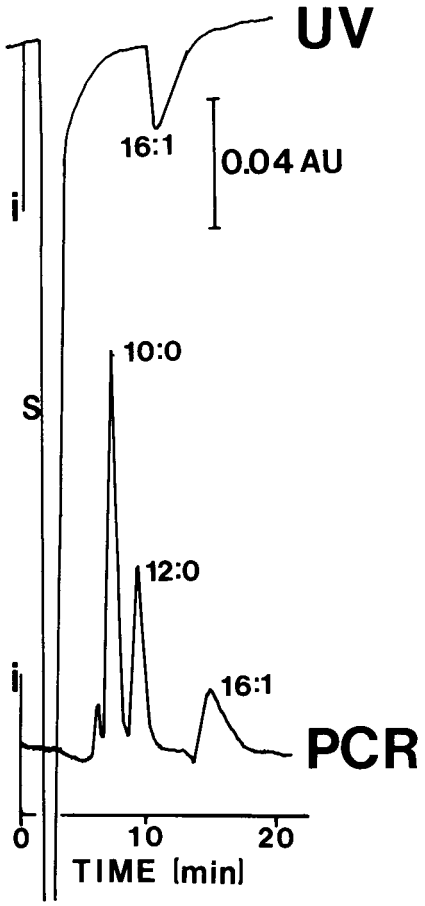

Fig. 2. Fractionation and detection of tricaprin ($C_{10:0}$, 12.5 nmol), trilaurin ($C_{12:0}$, 11.1 nmol) and tripalmitolein ($C_{16:1}$, 9.98 nmol) using the SF770 at 195 nm and the reactor detectors. The difference in the location of the responses is due to the dwell time in the reactor. S is the chloroform solvent response in the u.v. detector and I is the point when the sample was injected.

determined for bands eluting with a capacity factor, k', in the range 5—15. Thus they should be considered as realistic, if not conservative, and subject to improvement with decreases in the chromatographic dilution factor (i.e., improved column technology).

One detector characteristic of interest, related to future improvements (decreases) in C^{D}_{SDL}, is the detector baseline stability. The u.v. detector showed characteristic $1/f$ noise from fundamental long-term thermal and pressure fluctuation. Its performance is not expected to show improvement. In contrast, the post-column reactor showed no baseline drift and was noise-limited by high-frequency bubble noise. Thus it is expected that the detection limit for the reactor system might be improved by decreasing further the detector background and with more high frequency filtering.

TABLE 5

Linear regression analysis data for calibration curves relating u.v. or reactor detector response to volume of sample injected
(Analysis based on $R_D = BV + A$)

Detector	Standard	Slope (B)	Intercept (A)
U.v.	Trioleinglycerol	$3.4\ (\pm 0.63) \times 10^{5}$	$1.8\ (\pm 1.44) \times 10^{-3}$
Reactor	Trioleinglycerol	$9.9\ (\pm 0.74) \times 10^{8}$	$3.1\ (\pm 5.53) \times 10^{-1}$
Reactor	Trilinoleinglycerol	$2.5\ (\pm 0.10) \times 10^{9}$	$4.9\ (\pm 7.73) \times 10^{-1}$
U.v.	Dilinoleoyl lechithin	$1.5\ (\pm 0.18) \times 10^{6}$	$4.1\ (\pm 4.2) \times 10^{-3}$
U.v.	Dilinolenoyl lechithin	$5.3\ (\pm 0.30) \times 10^{6}$	$1.2\ (\pm 0.69) \times 10^{-1}$
Reactor	Dilinoleoyl lechithin	$3.8\ (\pm 0.17) \times 10^{8}$	$5.9\ (\pm 0.22)$
Reactor	Dilinolenoyl lechithin	$6.7\ (\pm 0.56) \times 10^{8}$	$7.5\ (\pm 0.73)$

The C^{D}_{SDL} data are expressed in units of mol l^{-1} and correspond to the concentration of the solute in the detector cell. The results indicate that the u.v. detector is as sensitive as the reactor detector (PCR) for saturated standards. This is crucial as both detectors are to be used simultaneously in investigating R^{uv}_{PCR}. The C^{D}_{SDL} data of Table 6 can be converted to the approximate amount of standard injected by multiplying these values by 10^{-2}, the dilution factor for the chromatographic system. While these values are only approximate, they show the post-column is conservatively responsive to nanomolar quantities of triglycerides and phospholipids; this is about

TABLE 6

Detection limits (C^{D}_{SDL})[a]

Type	Standard	ACN:D_b[b]	Detection limit (M)	
			U.v.	Reactor
Triglycerides	Trilaurin	C_{12}	3×10^{-6}	$4\text{—}5 \times 10^{-7}$
	Trimyristin	C_{14}	3×10^{-6}	
	Triolein	$C_{18:1}$	2×10^{-7}	
	Trilinolein	$C_{18:2}$	2×10^{-8}	
Phospholipids	Dihexanoyl PC	C_{6}	2×10^{-6}	$1\text{—}2 \times 10^{-6}$
	Didecanoyl PC	C_{10}	2×10^{-6}	
	Dioleoyl PC	$C_{18:1}$	2×10^{-7}	
	Dilinoleoyl PC	$C_{18:2}$	8×10^{-8}	
	Dilinolenoyl PC	$C_{18:3}$	2×10^{-8}	

[a]Calculated as molar concentration of the sample in the detector by: $C^{D}_{SDL} = (VC_s)(2\sigma \text{ noise})/(F_L W_{base})(H)$ where V and C_s are as previously defined, 2σ noise is the noise amplitude in response units, F_L is the detector response constant, W_{base} is the signal base width in time units and H is the detector response. [b]ACN:D_b is the ratio of the acyl carbon number to the number of double bonds.

four orders of magnitude more sensitive than its counterpart in the clinical chemistry laboratory [39].

Equation (11) can be expressed as

$$\log R^{uv}_{PCR} = 2 \log D_b + \log c^* a^{-1} \quad (12)$$

This equation predicts that a log–log plot of R^{uv}_{PCR} vs. D_b should have a slope of 2. Values for R^{uv}_{PCR} are summarized in Table 7. For triglycerides, d log R^{uv}_{PCR}/d log D_b was found to be 2.2 (standards contained 3 and 6 double bonds).

TABLE 7

Detector response ratios, R^{uv}_{PCR}, for triglyceride and phospholipid standards[a]

Type	Standard	R^{uv}_{PCR}	n	D_b
Triglycerides	Trilaurin	0.06 ± 0.007	15	0
	Trimyristin	0.06 ± 0.007	15	0
	Tripalmitolein	2.98 ± 0.14	15	3
	Trilinolein	13.58 ± 1.03	6	6
Phospholipids	Dicaprinoyl PC	0.88 ± 0.13	4	0
	Dioleoyl PC	1.42 ± 0.34	4	2
	Dilinoleoyl PC	6.77 ± 1.67	4	4
	Dilinolenoyl PC	14.70 ± 1.86	6	6

[a]Log R^{uv}_{PCR} = (2.36 ± 0.177) log D_b − 0.64 ± 0.105 (correlation coefficient 0.9972). Values are given ± s.d. for n = 3.

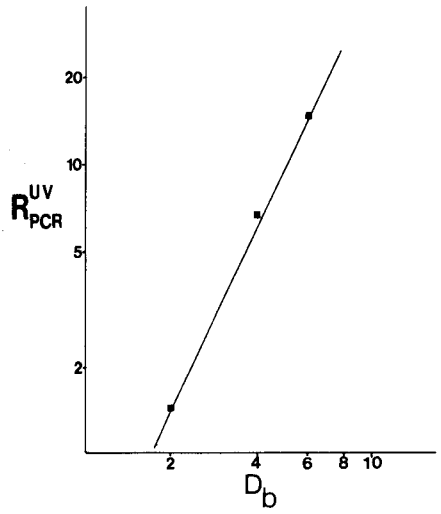

Fig. 3. Plot of log R^{uv}_{PCR} vs. log D_b for phospholipid standards to evaluate Eqn. (12). See Table 5 for uncertainty of results and linear-regression analysis.

Results for phospholipids were evaluated graphically and are shown in Fig. 3. Linear-regression analysis data are given in Table 7. The slope of the line in Fig. 3 is 2.36. This correlation between $\log R^{uv}_{PCR}$ and $\log D_b$, 2.2 and 2.36 for triglycerides and phospholipids, respectively, vs. the predicted value of 2, supplements previously reported results [42] in which a linear relationship was found but no basis was given for that relationship. The present results show that the post-column reactor is giving a molar-sensitive response independent of the identity of the triglyceride or phospholipid molecular species.

The standards used in this study were well suited for the determination of R^{uv}_{PCR} because they were conjugated alkenes. The predictive values of R^{uv}_{PCR} will have to be studied in greater detail and for other standards before they can be applied practically.

The work presented in these two parts of the study lays a firm foundation for implementing future investigations on a system for positive identification of individual triglyceride and phospholipid species in a complex matrix. It also demonstrates that post-column reactor detectors can be developed for detecting compound classes that are otherwise difficult to detect. The molar response of the reactor is seen as its greatest asset, aiding in the quantification of diverse chemical species which otherwise cannot be determined with reliability.

The authors acknowledge the assistance of J. R. Weber and the financial support of the Natural Sciences and Engineering Research Council of Canada.

REFERENCES

1 B. J. Compton and W. C. Purdy, Anal. Chim. Acta, 141 (1982) 405.
2 R. D. Plattner, G. F. Spencer and R. Kleiman, J. Am. Oil Chemists' Soc., 54 (1977) 511.
3 N. A. Porter, R. A. Wolf and J. R. Nixon, Lipids, 14 (1979) 20.
4 B. J. Compton and W. C. Purdy, J. Liq. Chromatogr., 3 (1980) 1183.
5 B. Vonach and G. Schomburg, J. Chromatogr., 149 (1978) 417.
6 W. L. Erdahl and O. S. Privett, Lipids, 12 (1977) 797.
7 M. N. Munk, J. Chromatogr. Sci., 8 (1970) 491.
8 M. Krejci and N. Pospisilova, J. Chromatogr., 73 (1972) 105.
9 R. J. Magg, in C. F. Simpson (Ed.), Practical High-Performance Liquid Chromatography, Heyden, London, 1979, p. 276.
10 J. F. Lawrence and R. W. Frei, Journal of Chromatography Library, Vol. 7, Elsevier, Amsterdam, 1976, p. 90.
11 G. M. Barrow, Introduction to Molecular Spectroscopy, McGraw-Hill, New York, 1962, p. 276.
12 G. H. Schenk, Absorption of Light and Ultraviolet Radiation, Allyn and Bacon, Boston, 1973, pp. 15—19.
13 W. Baumann, Fresenius Z. Anal. Chem., 284 (1977) 31.
14 G. Bucolo and H. David, Clin. Chem., 19 (1973) 476.
15 G. Bucolo and R. McCroskey, Clin. Chem., 21 (1975) 424.
16 H. B. Lofland, Jr., Anal. Biochem., 9 (1964) 393.
17 G. Kessler and H. Lederer, in L. T. Skeggs, Jr. (Ed.), Automation in Analytical Chemistry, Technicon Symposia 1965, Medical Inc., New York, 1966, p. 341.

18 L. T. Skeggs, Jr., Am. J. Clin. Pathol., 28 (1957) 311.
19 R. D. Begg, Anal. Chem., 43 (1971) 854.
20 L. R. Snyder and H. L. Adler, Anal. Chem., 48 (1976) 1017.
21 L. R. Snyder and H. L. Adler, Anal. Chem., 48 (1976) 1022.
22 L. R. Snyder, J. Chromatogr., 125 (1976) 287.
23 B. J. Compton and W. C. Purdy, Can. J. Chem., 58 (1980) 2207.
24 B. J. Compton and W. C. Purdy, Anal. Chim. Acta, 119 (1980) 349.
25 W. W. Christie, in F. D. Gunstone (Ed.), Topics in Lipid Chemistry, Vol. 3, Wiley, New York, 1972, p. 171.
26 A. J. Sheppard and J. J. Iverson, J. Chromatogr. Sci., 13 (1975) 448.
27 R. L. Glass, Lipids, 6 (1971) 919.
28 S. W. Christopherson and R. L. Glass, J. Dairy Sci., 52 (1969) 1289.
29 J. March, Advanced Organic Chemistry: Reactions, Mechanisms and Structure, McGraw-Hill, New York, 1968.
30 F. L. Jackson, Reactions, 2 (1944) 341.
31 P. Fleury and S. Boisson, C.R. Acad. Sci., 204 (1937) 1264; J. Pharm. Chem., 30 (1939) 145, 307; C.R. Acad. Sci., 208 (1939) 1509.
32 F. G. Soloni, Clin. Chem., 17 (1971) 529.
33 P. J. Martin, Clin. Chim. Acta, 62 (1975) 79.
34 V. E. Vas'kovskii and S. V. Isai, Anal. Biochem., 30 (1969) 25.
35 W. Goedicke and U. Gerike, Mikrochim. Acta, (1972) 603.
36 T. Nash, Biochem. J., 55 (1953) 416.
37 B. J. Compton, J. R. Weber and W. C. Purdy, Anal. Lett., 13 (1980) 861.
38 N. Tietz, Fundamentals of Clinical Chemistry, 2nd edn., W. B. Saunders, Philadelphia, 1976, p. 1225.
39 W. R. Holub, Clin. Chem., 19 (1973) 1391.
40 W. E. Neely, S. C. Wardlaw, T. Yates, W. G. Hollingsworth and M. E. T. Swinnen, Clin. Chem., 22 (1976) 227.
41 W. C. Furman, Continuous Flow Analysis: Theory and Practice, Dekker, New York, 1976, p. 223.
42 F. B. Jungalwala, J. E. Evans and R. H. McCleur, Biochem. J., 155 (1976) 55.

Analytica Chimica Acta, 142 (1982) 31—45
Elsevier Scientific Publishing Company, Amsterdam — Printed in The Netherlands

AMPEROMETRIC DETECTION OF AMINO ACIDS WITH A PASSIVATED COPPER ELECTRODE

W. TH. KOK, H. B. HANEKAMP, P. BOS and R. W. FREI*

Department of Analytical Chemistry, Free University, de Boelelaan 1083, 1081 HV Amsterdam (The Netherlands)

(Received 12th May 1982)

SUMMARY

The amperometric behaviour of a copper electrode towards amino acids is studied by means of a rotating disc electrode. A theoretical model describing the anodic background current in a buffer solution and the increase of the current caused by amino acids is checked experimentally. The influences of the amino acid concentration, the rotation speed of the electrode and the composition of the buffer solution are studied. It is proved that chemical dissolution of a passivating film on the electrode surface, which is enhanced by the complexation reaction between the amino acid and copper(II) ions, is the principle of the phenomena observed. The applicability to flow systems is demonstrated.

The formation of complexes with copper(II) ions has been used by various workers as the principle for the detection of amino acids and other complexing agents [1—4]. The use of a copper-selective membrane electrode as the indicator electrode for the titration of amino acids with copper(II) solutions is well known. A copper-selective electrode has been used as a potentiometric detector for amino acids in high-performance liquid chromatography (h.p.l.c.) [1]. A copper(II) solution was added after the column and the loss of copper(II) activity caused by the complexation reaction was taken as a measure for the amino acid concentration in the column effluent. It has been shown that a copper-selective electrode responds to complexing agents even in the absence of copper(II) ions in the solution [2]. Instead of a membrane electrode, an electrode made of copper can be used. Potentiometric detection of amino acids in h.p.l.c. is possible with copper wire and tubular electrodes [3, 4]. These electrodes were also shown to respond directly to the amino acids and addition of copper(II) ions to the column effluent was thus unnecessary.

The main disadvantage of these potentiometric measurements is the fact that, according to theory, the calibration curves are inherently non-linear. Only when a large excess of copper(II) ions is added to the solution, can the electrode response be expected to be proportional to the concentration of amino acid. However, in this case the changes in electrode potential will be small. For direct quantitative measurements, an amperometric method would be preferable.

0003-2670/82/0000-0000/$02.75

When a solid copper electrode is anodized in a weakly acidic or alkaline buffer solution, the copper surface is quickly covered with a layer of oxide or hydroxide [5, 6] and the copper will not make direct contact with amino acids in the solution. Dissolution of the copper at a more negative potential by complexation with amino acids, such as has been observed with a dropping copper amalgam electrode [7], is therefore not expected. However, it has been shown with a lead/lead dioxide electrode that a metal electrode "passivated" with an oxide layer can respond to complexing agents [8]. Because the current flowing through the lead dioxide electrode at a fixed potential increased proportionally with the concentration of complexing agent, amperometric determination of this concentration was possible.

In the work described below, the amperometric behaviour of an anodized copper electrode towards amino acids in buffer solutions was investigated. A rotating disc electrode was used, because parameters are easily varied with this electrode and results can be used to predict those obtained in flow-through systems [9]. The latter was verified by means of flow injection experiments.

THEORY

Anodization of the copper electrode

Electrochemical and x-ray photo-electron spectroscopic studies have shown that when a copper electrode is anodized in a buffer solution, different layers of copper oxide (or hydroxide) are formed [5, 6]. First, a layer of copper(I) oxide is deposited on the copper surface; its thickness does not depend on the potential. The layer is extremely insoluble and is reduced only at fairly negative potentials. Because such potentials were not normally applied here, the copper electrode in use can be regarded as covered with an "inert" layer of copper(I) oxide. In the more positive potential region studied, only copper(II) ions are formed and these can diffuse through the copper(I) oxide layer.

If it is assumed that the copper(I) oxide film is not influenced by changes in potential and that the electrode kinetics are fast, the concentration of copper(II) ions at the electrode—solution interface, $[Cu^{2+}]_0$, at low potentials is given by the Nernst-Kirchhoff equation

$$E = E'_0 + RT(2F)^{-1} \ln [Cu^{2+}]_0 + iR_I \qquad (1)$$

where iR_I is the potential barrier across the copper(I) oxide film. The value of E'_0 in Eqn. (1) will not be equal to the standard potential of the Cu/Cu^{2+} couple because of the presence of the copper(I) oxide layer. Besides, in many buffer solutions, complex species of copper(II) are in reversible equilibrium with the free, aquated copper(II) ions. If these species are included in the $[Cu^{2+}]_0$ of Eqn. (1), E'_0 will depend on the buffer composition.

The solubility of copper(II) ions in weakly acidic or alkaline buffers is limited. Therefore, if the electrode potential is increased, the copper(II)

concentration at the electrode surface will increase only upto a certain value $[Cu^{2+}]_{max}$ at a potential E_{max}. Above this potential a layer of copper(II) oxide or hydroxide will be deposited on top of the copper(I) oxide layer. A further increase of potential will only lead to a thicker oxide layer [5] and an increase in the ohmic drop across this layer. Under the condition that $E \geqslant E_{max}$, Eqn. (1) can be modified

$$E = E_0' + RT(2F)^{-1} \ln [Cu^{2+}]_{max} + iR_I + iR_{II}(E) \quad (2)$$

where $R_{II}(E)$ is the potential-dependent resistance of the copper(II) film.

The background current

The transport processes occurring near a rotating disk electrode are conveniently described by the diffusion layer model. This model assumes the existence of a layer of solution of uniform thickness δ near the electrode surface, where convection normal to the electrode can be neglected. For distances normal to the electrode $z > \delta$, all concentrations are assumed to be equal to the bulk concentrations. The thickness of the diffusion layer is given by the Levich equation [10]

$$\delta = 1.62\, \omega^{-1/2}\, \nu^{1/6}\, D_i^{1/3} \quad (3)$$

where ω is the rotation speed of the electrode (in rad s^{-1}), ν the kinematic viscosity of the solution, and D_i the diffusion coefficient of the species studied.

For the copper electrode in a buffer solution at potentials where copper(II) ions are formed, the transport equation for the steady state ($\delta c/\delta t = 0$) is simply

$$D_{Cu}\, d^2[Cu^{2+}]/dz^2 = 0 \quad (4)$$

with boundary conditions $z = 0$, $[Cu^{2+}] = [Cu^{2+}]_0$ and $z = \delta$, $[Cu^{2+}] = 0$. This equation is easily solved; the current i is given by

$$i = A\, 2FD_{Cu}\, (d[Cu^{2+}]/dz)_0 \quad (5)$$

where A is the surface area of the electrode, and for potentials above E_{max}, where $[Cu^{2+}]_0 = [Cu^{2+}]_{max}$, the limiting background current i_0 observed can be written as

$$i_0 = A\, 2FD_{Cu}\, [Cu^{2+}]_{max}/\delta \quad (6)$$

According to Eqn. (3), δ is proportional to $\omega^{-1/2}$, so that the limiting current will be proportional to $\omega^{1/2}$.

Instantaneous complexation reactions

Amino acids form very stable complexes with copper(II) ions, the stability constants being of the order of 10^8 for the 1:1 complexes and 10^{15} for the 1:2 complexes [11]. Under suitable conditions, the forward reaction rates can be very high, whereas the reverse reaction will obviously be slow

[12], so that complexation may be regarded as an instantaneous, irreversible reaction

$$Cu^{2+} + pA^- \rightarrow Cu\,A_p^{2-p} \tag{7}$$

A^- being the amino acid anion; for simple amino acids, $p = 2$. When the reaction is instantaneous, the diffusion layer must contain a reaction boundary at some distance z_r from the electrode surface; only copper(II) ions will be present on one side of the boundary, and only amino acid on the other. For the copper(II) zone ($0 < z < z_r$), Eqn. (4) is valid but the boundary conditions become $z = 0$, $[Cu^{2+}] = [Cu^{2+}]_0$ and $z = z_r$, $[Cu^{2+}] = 0$.

For the amino acid zone ($z_r < z < \delta$), the transport equation is similar

$$D_A\, d^2[A]/dz^2 = 0 \tag{8}$$

with the boundary conditions $z = z_r$, $[A] = 0$ and $z = \delta$, $[A] = [A]^*$. Here $[A]^*$ is the bulk concentration of the amino acid.

Because of reaction scheme (7), another boundary condition must be met $z = z_r$, $D_A\, d[A]/dz = p\, D_{Cu}\, d[Cu^{2+}]/dz$. Solution of Eqns. (4) and (8) with the stated boundary conditions yields for z_r the equation

$$z_r = \delta\, D_{Cu}[Cu^{2+}]_0/(D_{Cu}[Cu^{2+}]_0 + p^{-1}\, D_A[A]^*) \tag{9}$$

which, combined with Eqn. (5), gives the current as

$$i = A\ 2F\,(D_{Cu}[Cu^{2+}]_0 + p^{-1}\, D_A[A]^*)/\delta \tag{10}$$

The increase in the current caused by the presence of the amino acid in the buffer solution at potentials above E_{max} is found by substituting Eqn. (6) in Eqn. (10)

$$\Delta i = A\ 2FD_A[A]^*/p\delta \tag{11}$$

This equation states that the current increase for instantaneous reactions will be proportional to $[A]^*$ and, like the background current, to δ^{-1}, and thus to $\omega^{1/2}$.

Second-order complexation reactions

When the complexation reaction is not instantaneous, the zones of copper(II) and amino acid in the diffusion layer will overlap. To evaluate the influence of the amino acid on the current, the kinetics of the complexation reaction must be considered. The reaction scheme for the formation of the 1:2 complex is

$$Cu^{2+} + A^- \underset{k_{-A}}{\overset{k_{2A}}{\rightleftharpoons}} CuA^+ \text{ and } CuA^+ + A^- \underset{k_{-B}}{\overset{k_{2B}}{\rightleftharpoons}} CuA_2 \tag{12}$$

In most cases, the reverse reactions can be neglected. Then the following three transport equations have to be considered for the three species involved (for simplicity the various diffusion coefficients are assumed to be equal)

$$D\,d^2[Cu^{2+}]/dz^2 - k_{2A}\,[Cu^{2+}]\,[A] = 0 \quad (13)$$

$$D\,d^2[CuA^+]/dz^2 + k_{2A}\,[Cu^{2+}]\,[A] - k_{2B}\,[CuA^+]\,[A] = 0 \quad (14)$$

$$D\,d^2[A]/dz^2 - k_{2A}\,[Cu^{2+}]\,[A] - k_{2B}\,[CuA^+]\,[A] = 0 \quad (15)$$

Here [A] is the concentration of the amino acid irrespective of its ionic form. The boundary conditions are $z = 0$, $[Cu^{2+}] = [Cu^{2+}]_0$, $d[CuA^+]/dz = 0$, $d[A]/dz = 0$ and $z = \delta$, $[Cu^{2+}] = 0$, $[CuA^+] = 0$, $[A] = [A]^*$.

The set of non-linear differential Eqns. (13—15) cannot be solved analytically. However, the concentration of each species can be regarded as a power series of z

$$[Cu^{2+}] = c_0 + c_1 z + c_2 z^2 + c_3 z^3 + \ldots \quad (16)$$

$$[CuA^+] = b_0 + b_1 z + b_2 z^2 + b_3 z^3 + \ldots \quad (17)$$

$$[A] = a_0 + a_1 z + a_2 z^2 + a_3 z^3 + \ldots \quad (18)$$

Approximate solutions of Eqns. (13—15) can be found by taking only the first N terms of Eqns. (16—18), substituting these in Eqns. (13—15), and neglecting all terms which contain z to the power $(N - 2)$ or larger; the diffusional terms are only in z to the power $(N - 3)$. Because the formulae obtained in this way must be valid for all values of z $(0 < z < \delta)$, $3 \times (N - 2)$ equations of the coefficients a_n, b_n and c_n are obtained; from these, together with the six boundary conditions, the $3N$ coefficients of Eqns. (16—18) can be calculated numerically for every value of k_{2A}, k_{2B}, δ, $[A]^*$ and $[Cu^{2+}]_0$. When these coefficients are known, the current can be calculated from Eqn. (5)

$$i = -A\,2FD\,c_1 \quad (19)$$

Calculations were done by taking the first four and the first five terms of Eqns. (16—18). As long as $\Delta i/i_0$ was below 0.8, addition of the fifth term never changed the calculated $\Delta i/i_0$ value by more than 10%. Therefore, it may be assumed that in this range the calculation with five terms is a close enough approximation. The calculated dependence of the current on the reaction rate constants is shown in Fig. 1. At low reaction rates, the current increase is proportional to the rate constant, while it approaches a constant value at high reaction rates. Figure 2 shows the dependence on the concentration of amino acid. It can be seen that the current increase will be proportional to the amino acid concentration over a wide range, especially for low reaction rates. The inflexion of the curves calculated for high concentrations of amino acid may be partly due to the increasing significance of 1:2 complex formation. However, another cause is that the approximations used to calculate the current become less valid. The coefficients of the higher-order terms of the power series (16—18) increase for increasing values of i.

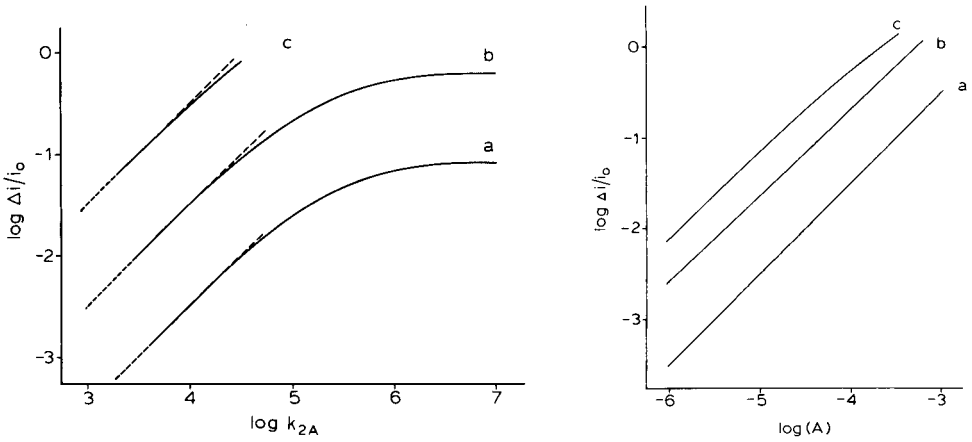

Fig. 1. Dependence of the currents on the reaction rate constants: (——) second order; (---) pseudo-first order. Values used: $k_{2A} = k_{2B}$ (second order); $k_{2B} = 0$ (pseudo-first order); $\delta = 10^{-3}$ cm; $D = 10^{-5}$ cm^2 s^{-1}; $[Cu^{2+}]_0 = 10^{-4}$ M. Value of [A]*: (a) 10^{-5} M, (b) 10^{-4} M; (c) 10^{-3} M.

Fig. 2. Dependence of the currents on the amino acid concentration, considering a second-order reaction. Values used: $k_{2A} = k_{2B}$; $\delta = 10^{-3}$ cm; $D = 10^{-5}$ cm^2 s^{-1}; $[Cu^{2+}]_0 = 10^{-4}$ M. Value of k_{2A}: (a) 10^4; (b) 10^5; (c) 10^6 mol^{-1} l s^{-1}.

Pseudo-first order complexation reactions

When the reaction rate is very small, the amount of CuA^+ formed within the diffusion layer will be small. Usually $k_{2B} < k_{2A}$ [12], and the second step can then be neglected. The amount of amino acid consumed in the diffusion layer will also be small, and the concentration of amino acid in the diffusion layer will be nearly equal to the bulk concentration. The reaction is then pseudo-first order in $[Cu^{2+}]$. The transport equation for this pseudo-first order reaction is

$$D_c \, d^2 [Cu^{2+}]/dz^2 - k_1 [Cu^{2+}] = 0 \tag{20}$$

where $k_1 = k_{2A} [A]^*$. The boundary conditions for $[Cu^{2+}]$ are the same as in the second-order situation. Equation (20) can be solved analytically, and substitution of Eqns. (5) and (6) gives

$$i = i_0 K^{1/2} \coth K^{1/2} \tag{21}$$

where $K = k_1 \delta^2 / D_{Cu}$. For small values of K, $K^{1/2} \coth K^{1/2} \approx 1 + K/3$. It follows that $\Delta i \approx i_0 K/3$. Because i_0 is proportional to $\omega^{1/2}$ and K to ω^{-1}, the current increase will be proportional to $\omega^{-1/2}$. Values of $\Delta i/i_0$ calculated from the given approximation are shown in Fig. 1 as dashed lines. It can be seen that for low values of k_{2A} this method of calculation is in good agreement with the numerical approximation.

EXPERIMENTAL

Apparatus and reagents

The copper disk electrode (diameter 6 mm) was embedded in a Kel-F shaft and driven by a servomotor with tachogenerator. The rotation speed was variable from zero to 80 r.p.s. The cell consisted of a main compartment of about 100 ml, a compartment for the platinum wire auxiliary electrode and a compartment for the reference electrode, which were connected to the main compartment via a glass frit and a Luggin capillary, respectively. Potentials were measured against a Ag/AgCl/1 M LiCl in methanol—water (1 + 1) reference electrode. Currents were measured with a home-made potentiostat/amplifier connected to a home-made potential sweep generator with digital potential control. Voltammograms were recorded on a Kipp and Zonen BD30 x—y—t recorder.

In the flow injection experiments, a Metrohm (Herisau, Switzerland) EA 1096/2 flow-through cell was used, with a copper electrode of 3-mm diameter, a platinum auxiliary electrode and a Ag/AgCl/1 M LiCl in methanol—water (1 + 1) reference electrode. The potential of the working electrode was kept at + 100 mV. The solution was pumped by means of a Waters 6000A pump, and samples were injected with a Rheodyne valve with a 1-ml loop.

L-Amino acids (Sigma grade) were obtained from Sigma Chemical Company. Distilled demineralized water was used. All other reagents (analytical grade) were used as received. No precautions were taken to remove oxygen or carbon dioxide from the solutions used.

Procedure

The copper electrode was lightly polished with Gamal (Fisher Scientific Company) and rinsed with 5 M nitric acid before each series of experiments. Before measurements the electrode was held at a potential of −250 mV for at least 15 min.

RESULTS AND DISCUSSION

The solubility of copper(II)

Some voltammograms obtained with a rotating copper electrode in a phosphate buffer solution are presented in Fig. 3. It can be seen that when the potential is changed from −250 mV in the positive direction, the recorded curve resembles a d.c. voltammogram. The limiting current was not changed significantly upto applied potentials of + 800 mV, but above + 800 mV the current became very irregular. Apparently the oxide films on the electrode surface were disrupted at very positive potentials. Addition of amino acid to the solution raised the limiting current reproducibly. The increase of the limiting current was proportional to the amino acid concentration.

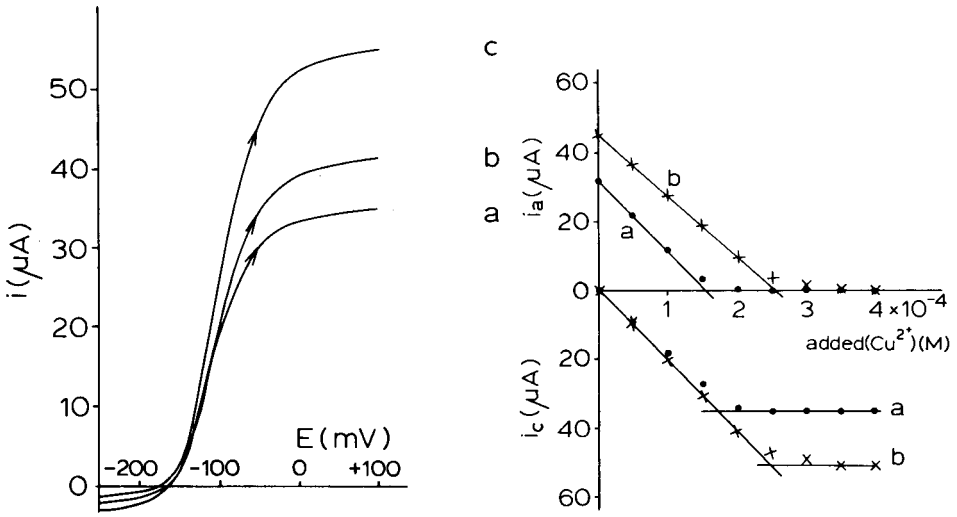

Fig. 3. Voltammograms in 0.1 M phosphate buffer, pH = 6.7. Scan rate 1 mV s^{-1}; 20 r.p.s. L-Alanine concentration: (a) 0; (b) 10^{-4} M; (c) 3×10^{-4} M.

Fig. 4. Anodic and cathodic limiting currents. Phosphate buffer, 0.1 M, pH = 6.7; 20 r.p.s. L-Alanine concentration: (a) 0; (b) 2×10^{-4} M.

The determining role of the solubility of copper(II) ions is clearly demonstrated in Fig. 4. When copper(II) ions were added to the phosphate buffer, two closely spaced cathodic waves could be observed with halfwave potentials of about −100 and −150 mV, reflecting the two-step reduction of Cu(II) to Cu(0). The cathodic limiting current, measured at −250 mV, increased with the concentration of Cu(II) added. However, above a copper(II) concentration of 1.6×10^{-4} M, a precipitate was observed and the current did not increase further. The anodic current, measured at +100 mV, decreased when copper(II) ions were added to the solution. At the copper concentration where precipitation began, the anodic current was zero. Apparently chemical dissolution of the copper(II) film, the cause of the anodic current, was no longer possible. Addition of 2×10^{-4} M L-alanine to the buffer solution increased the amount of copper(II) that could be added before precipitation started, by about 1×10^{-4} M. That means that formation of the 1:2 copper(II)—amino acid complex predominates in the bulk solution. The cathodic and anodic currents had to be measured in different series of experiments. The cathodic deposition of copper changed the surface properties of the electrode so that polishing was necessary afterwards.

Similar experiments were done with carbonate and borate buffers. Voltammograms with a 0.1 M carbonate buffer (pH 10.0) are shown in Fig. 5A. Again the anodic current first increases exponentially with the potential until a limiting current is reached. This limiting background current is considerably higher than in phosphate buffers. Experiments in which

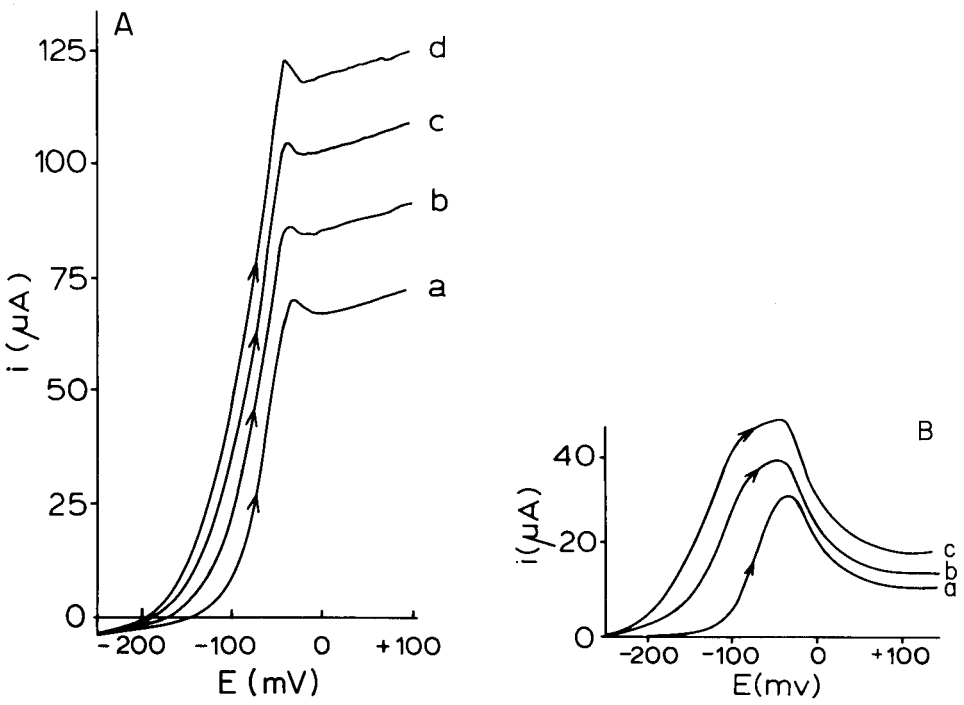

Fig. 5. Voltammograms in (A) 0.1 M carbonate buffer pH 10.0, and (B) 0.1 M borate buffer pH 8.9. Scan rate 1 mV s^{-1}; 20 r.p.s. L-Alanine concentration: (a) 0; (b) 10^{-4}; (c) 2×10^{-4}; (d) 3×10^{-4} M.

copper(II) ions were added indicated a maximum copper(II) solubility of 4.5×10^{-4} M. Because the pH of the carbonate buffer was higher than that of the phosphate buffer, copper(II) ions clearly form much stronger complexes with carbonate than with phosphate ions.

Voltammograms measured in a 0.1 M borate buffer (pH 8.9) showed a maximum at about −40 mV (Fig. 5B). The height of this maximum was strongly dependent on the history of the electrode. When the electrode was freshly polished, the maximum was lower than after the measurement of a few voltammograms. At more positive potentials (about +100 mV), a lower but much more reproducible limiting current was observed. The occurrence of these two distinct regions is probably connected with a change in structure of the oxide film on the electrode surface. Cathodic waves observed with copper(II)-containing borate buffers were drawn out; precise measurement of the maximum solubility of copper(II) was therefore impossible.

Influence of the rotation speed

The dependence of the anodic background current in a phosphate buffer on the rotation speed of the electrode is shown in Fig. 6A. Linear regression of the log i_0 vs. log ω relation gives a straight line with a slope of 0.48, in

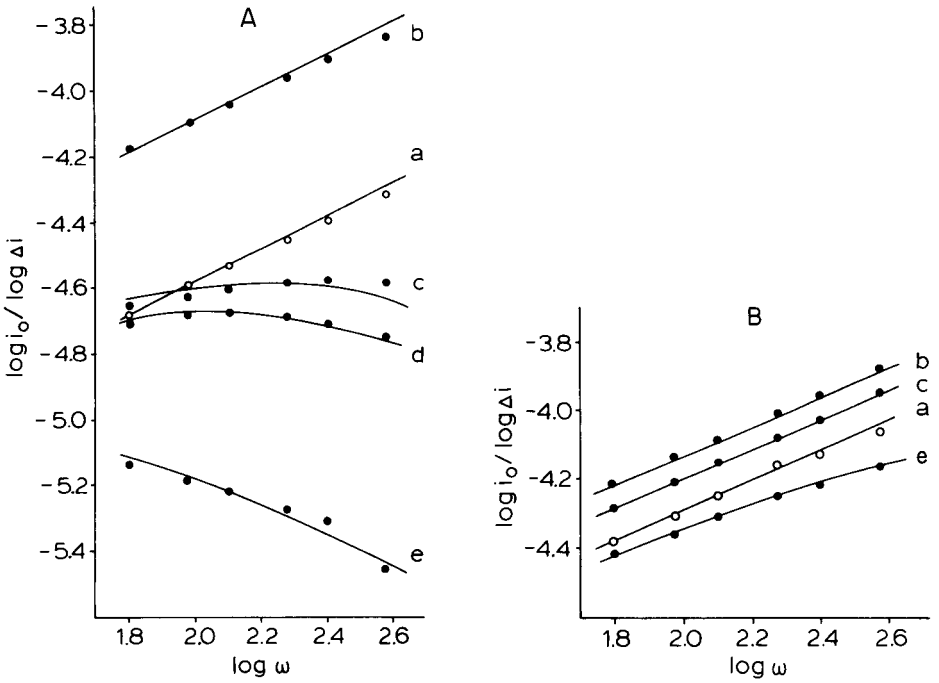

Fig. 6. Dependence of the currents on the rotation speed in (A) 0.1 M phosphate buffer pH 6.7, and (B) 0.1 M carbonate buffer pH 10.0. Points are experimental values; lines in (A) were calculated with the second-order approximation method. Curves: (a) background current; (b) current increase, L-histidine added; (c) L-alanine added; (d) L-leucine added; (e) L-proline added. All 5×10^{-4} M amino acid.

close agreement with the theoretical value of 0.5. The diffusion coefficient of the copper(II) ion can be calculated from the experimental data by means of Eqn. (6). The mean value found is 0.34×10^{-5} cm^2 s^{-1}, assuming that the kinematic viscosity of the solution is 0.01 cm^2 s^{-1}. Line (a) in Fig. 6A represents the current calculated from Eqn. (6), with the above values for D and ν, and $[Cu^{2+}]_{max} = 1.6 \times 10^{-4}$ M.

Figure 6A also shows the values of Δi measured when 5×10^{-4} M L-histidine was added to the solutions. Linear regression of log Δi for L-histidine against log ω gives a straight line with a slope of 0.43. This value is fairly close to the theoretical value of 0.5 for an instantaneous reaction, and it can be concluded that the complexation reaction is fast. Equation (11) predicts the current increase for an instantaneous reaction. If it is assumed that the 1:2 complex is formed, the values calculated for Δi (line (b) in Fig. 6A) fit the experimental data best when a value of 0.98×10^{-5} cm^2 s^{-1} is used for D_A.

The reaction rates of other amino acids, L-alanine, L-leucine and L-proline with copper(II) ions are much lower than that of L-histidine in phosphate

buffers. This results in a smaller current increase and another dependence on the rotation speed. The second-order numerical approximation method described above can be used to estimate the rate constants of the complexation reaction. A mean diffusion coefficent of 0.6×10^{-5} cm^2 s^{-1} was used for the species involved and the rate constants k_{2A} and k_{2B} of the two steps in the complexation reaction were assumed to be equal. Calculation of the values of Δi agreed with the experimental data best when the following rate constants (mol^{-1} l s^{-1}) were used: 4.8×10^4 for L-alanine, 3.2×10^4 for L-leucine, and 5.7×10^3 for L-proline. The lines (c—e) in Fig. 6A represent the results of the calculations.

When a carbonate buffer (0.1 M, pH 10.0) is used, the plot of log i_0 vs. log ω (Fig. 6B, line a) has a slope of 0.42. This value is smaller than that measured in a phosphate buffer, suggesting that electrode kinetics play a more important role. Plots of log Δi vs. log ω for 5×10^{-4} M L-histidine and L-alanine both have slopes of 0.44, indicating that complex formation with these amino acids is fast. For L-proline (Fig. 6B, line e), the slope of the plot is smaller, especially at high rotation speeds. Obviously reaction kinetics are a limiting factor for the current increase, but the reaction rate is still too high for estimation of the rate constant.

With a borate buffer (0.1 M, pH 8.9), both i_0 and Δi for 5×10^{-4} M L-alanine are small and hardly depend on the rotation speed of the electrode. It can be concluded that the currents are mainly determined by slow electrode kinetics. The cause of this different electrode behaviour must be sought in the structure of the oxide layers on the electrode surface; copper(II) ions formed by the electrode reaction must diffuse through the oxide (or hydroxide) layers and the permeability of these layers will therefore determine the rate of the electrode kinetics. X-ray photoelectron studies [5] have shown that the oxide layer formed in a borate buffer contained no boron. When the electrode was anodized in a phosphate buffer, small traces of phosphorus were found in the surface film. Formation of insoluble phosphate films on a copper anode has been observed before and has even been used for determination of phosphate by cathodic stripping [13]. In the present work, some proof for the participation of phosphate in film formation was also found. Normally when a 0.1 M acetate buffer was used, the current kept on increasing exponentially when the electrode potential was raised, but when phosphate (10^{-2} M) was added to the acetate buffer, a (high) limiting current was observed. The higher permeability of the oxide (or hydroxide) layer formed in phosphate buffers, compared to that in borate buffers, may therefore be explained by the incorporation of phosphate ions in the layer. For the films found in carbonate buffers, which are also permeable, a comparable explanation might be valid.

Influence of the buffer composition

The influence of the concentration of the buffer solution on the i_0 and Δi value for 5×10^{-4} M L-alanine is shown in Fig. 7. It can be seen that the

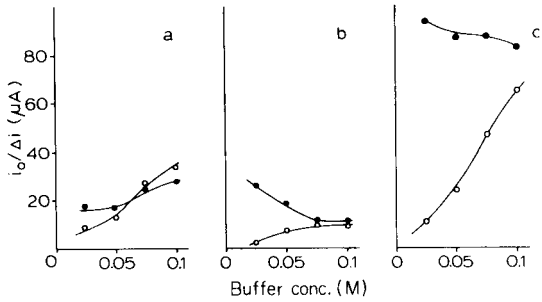

Fig. 7. Influence of the buffer concentration on the currents at a rotation rate of 20 r.p.s. (○) Background current; (●) current increase for 5×10^{-4} M L-alanine. Buffer: (a) phosphate, pH 6.7; (b) borate, pH 8.9; (c) carbonate, pH 10.0.

background current in phosphate and carbonate buffers is about proportional to the buffer concentration. This is logical because the solubility product of $Cu(OH)_2$ [14] indicates that most of the copper(II) ions in the diffusion layer must be present as complexes with buffer species in the pH range studied. The current increase is much less influenced by the buffer concentration, except for the borate buffer. In Fig. 8 the influence of the buffer pH is shown. The background current decreases strongly with pH, reflecting the decreased solubility of copper(II). For phosphate buffers, the current increase for 5×10^{-4} M L-alanine is not much influenced by the pH. Because Δi is a function of $[Cu^{2+}]_0$ when complexation is not instantaneous, the reaction rate constant must increase with pH in phosphate buffers. This agrees with observations [12] that the amino acid anion is the dominant reacting species. With borate buffers the situation is less clear because of the irreversibility of the electrode reaction. Although Δi decreases with pH in carbonate buffers, the value of $\Delta i/i_0$ increases.

Application to flow systems

The passivated copper electrode is not suitable for determination of amino acids in batch experiments, because the current measured depends

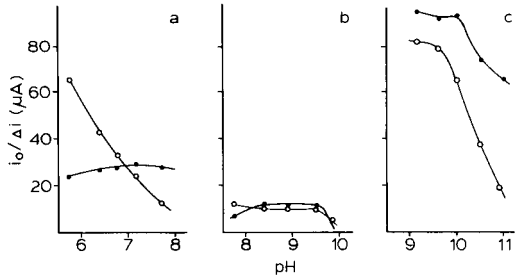

Fig. 8. Influence of the pH on the currents at a rotation rate of 20 rps. (○) Background current; (●) current increase for 5×10^{-4} M L-alanine. Buffer: (a) 0.1 M phosphate; (b) borate; (c) carbonate.

not only on the amino acid concentration, but also on the pH and composition of the matrix solution. However, in h.p.l.c., matrix effects of the sample will only influence the unretained peak, and (retained) amino acids may well be quantifiable.

To examine the applicability of the detection principle to flow systems, a flow injection method was tested. The detector was a Metrohm 1096/2 cell with a copper working electrode (diameter 3 mm) kept at a potential of + 100 mV. A phosphate buffer solution (pH 7.2) containing 10% (v/v) methanol was used, because this is a common mobile phase in reverse-phase h.p.l.c. Sample solutions were prepared by diluting amino acid stock solutions in mobile phase solution. Large (1 ml) sample plugs were injected to eliminate dilution effects by band broadening.

Baseline current and current increase for several amino acids were measured as a function of the flow rate F (Fig. 9). The plot of $\log i_0$ vs. $\log F$ is a straight line with a slope of 0.30. This value is considerably different from the values predicted theoretically for a wall-jet (0.75) or thin-layer cell (0.50). It is also smaller than the value of 0.44 measured before for the same Metrohm cell [15] when a glassy carbon electrode of larger diameter (6 mm) was used.

The current increase for the rapidly complexing amino acid L-histidine shows virtually the same dependence on flow rate as does the baseline current. The current increase for the slower-reacting L-alanine and L-proline depends on the flow rate analogously to the dependence on the rotation

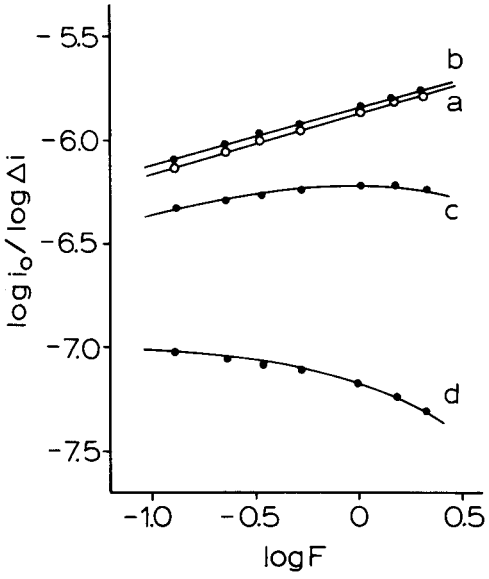

Fig. 9. Influence of the flow rate in a flow system. Carrier, 0.025 M phosphate buffer—10% methanol, pH 7.2. Curves: (a) baseline current; (b) peak heights for 10^{-4} M L-histidine; (c) L-alanine and (d) L-proline.

speed with the RDE. The detector response is fast. With a flow rate of 1 ml min^{-1}, the detector time constant was less than 1 s.

Conclusions

Amperometric detection of amino acids in various buffer systems is possible by means of the enhanced chemical dissolution of the passivating film on a copper anode. The method can be applied in the pH range 6—11. The increase of the anodic current measured when amino acid is added to the solution is proportional to the amino acid concentration and is a function of the rate of complexation reaction between the amino acid and copper(II) ions. The theoretical model which describes this function is confirmed fairly well by the experimental results. The second-order rate constants of the complexation reaction can be estimated by means of this model up to a value of about 10^6 mol^{-1} l s^{-1}. However, precise measurements are impossible because too many unknown factors (diffusion coefficients, relative rates of the two complexation steps) have to be included in the calculations.

In phosphate and carbonate buffers, the electrode kinetics is fast, while in borate buffers the electrode kinetics is the main limiting factor for the current. Therefore, when a fast electrode reaction is required, the borate system is not recommended.

In a flow system, analogous results are obtained, and the detection principle seems promising for h.p.l.c.

For analytical application, the quality of the method can be judged from the value of $\Delta i/i_0$, because Δi gives the signal measured and i_0 determines the reproducibility and noise. From the experimental results, some general indications for obtaining high $\Delta i/i_0$ values can be given for the phosphate and carbonate systems: (1) the buffer concentration should be as low as possible; (2) the pH should be as high as possible, within the pH ranges studied; and (3) when the amino acid does not react instantaneously with copper(II) ions, convection towards the electrode should be as slow as possible.

This study shows that simple batch experiments with a rotating disc electrode can be used to predict the results that will be obtained under dynamic conditions.

REFERENCES

1 C. R. Loscombe, G. B. Cox and J. A. W. Dalziel, J. Chromatogr., 166 (1978) 403.
2 M. F. El-Taras, E. Pungor and G. Nagy, Anal. Chim. Acta, 82 (1976) 285.
3 P. W. Alexander, P. R. Haddad, G. K. C. Low and C. Maitra, J. Chromatogr., 209 (1981) 29.
4 P. W. Alexander and C. Maitra, Anal. Chem., 53 (1981) 1590.
5 H.-H. Strehblow and B. Titze, Electrochim. Acta, 25 (1980) 839.
6 Y. A. El-Tantawy, F. M. Al-Kharafi and A. Katrib, J. Electroanal. Chem., 125 (1981) 321.

7 J. Hernandez Mendez, A. Sanchez Perez and F. Lucenda Conde, J. Electroanal. Chem., 66 (1975) 53.
8 T. Yoshimura, Fresenius Z. Anal. Chem., 307 (1981) 197.
9 H. B. Hanekamp, Doctoral Thesis, Free University, Amsterdam, 1981.
10 V. G. Levich, Acta Physicochim. URSS, 17 (1942) 257.
11 A. E. Martell and R. M. Smith, Critical Stability Constants, Vol. 1, Plenum Press, New York, 1974.
12 R. F. Pasternack, E. Gibbs and J. C. Cassatt, J. Phys. Chem., 73 (1969) 3814.
13 G. L Lundquist and J. A. Cox, Anal. Chem., 46 (1974) 360.
14 A. E. Martell and R. M. Smith, Critical Stability Constants, Vol. 4, Plenum Press, New York, 1976.
15 H. B. Hanekamp and H. J. van Nieuwkerk, Anal. Chim. Acta, 121 (1980) 13.

Analytica Chimica Acta, 142 (1982) 47—54
Elsevier Scientific Publishing Company, Amsterdam — Printed in The Netherlands

COMPARISON OF ANALYTICAL FIGURES OF MERIT OF AN ACTIVE NITROGEN AFTERGLOW AND A FLAME IONIZATION DETECTOR FOR GAS CHROMATOGRAPHY

G. W. RICE, J. J. RICHARD, A. P. D'SILVA and V. A. FASSEL*

Ames Laboratory and Department of Chemistry, Iowa State University, Ames, IA 50011 (U.S.A.)

(Received 7th June 1982)

SUMMARY

A comparison of the analytical figures of merit of an atmospheric pressure, active nitrogen afterglow and a conventional flame ionization detector revealed that the latter had slightly superior powers of detection and a considerably higher range of linear response. The selectivity of the afterglow detector was far superior because of its specific response to carbon-containing compounds and its potential, as previously demonstrated, of being a metal-specific, multielement detector as well.

The requirements for detecting trace levels of organic contaminants in a large variety of sample matrices has made it necessary to devise new and highly sensitive detectors for gas chromatography (g.c.). Among these, the widely used flame ionization detector (FID) has an excellent linear response (up to 10^7) and limits of detection (10—100 pg). Substantial interest has also been shown in utilizing a variety of emission type detectors for g.c. including microwave-induced plasmas, direct current argon plasmas, and inductively-coupled plasmas. The applications of these plasma detectors have been summarized in recent detailed reviews [1, 2].

A chemiluminescence detector, based on the reaction of organic compounds with active nitrogen sustained at low pressures (10—20 torr) to form excited CN ($B^2\Sigma^+$) molecules has also been reported [3, 4]. The reactions of a variety of organic compounds in low-pressure active nitrogen afterglows have been extensively studied over several decades [5]. In such reactions, the fragmentation of organic compounds, which leads to formation of the excited CN ($B^2\Sigma^+$) state, has been predicted to be the result of energy transfer from metastable atomic and molecular nitrogen species present in the discharge source.

In recent communications, it was demonstrated that an atmospheric pressure, active nitrogen (APAN) afterglow could also be utilized as a selective g.c. detector for organometallic compounds by observing atomic emissions from the metal constituents of the compounds [6, 7]. In those investigations it was also observed that the APAN afterglow could function as a selective

0003-2670/82/0000-0000/$02.75

detector for organic compounds at nanogram levels through the detection of CN ($B^2\Sigma^+ \rightarrow X^2\Sigma^+$) emission at 388.3 nm [6]. The results were obtained after chromatographic separations on packed columns. This paper reports on: (a) further improvements in the APAN detector for organic compounds and its performance with fused-silica capillary, gas chromatographic columns; and (b) a comparison of several g.c.-APAN figures of merit with those obtained with commercial flame ionization detectors.

EXPERIMENTAL

Apparatus

A schematic diagram of the electrodeless ozonizer-type discharge tube utilized in these investigations is shown in Fig. 1. This tube was considerably modified from the design previously described [6, 7]. The discharge region was reduced from a length of 40 cm to 15 cm and the outer tube diameter from 18 mm to 10 mm. The copper electrodes previously utilized were replaced with platinum to prevent the formation of oxide layers on the electrode surface by the electrical discharge, thus providing for a more stable and uniform discharge. The internal diameter of the afterglow tube was also reduced from 6 mm to 3 mm, which effectively concentrated the emitting afterglow into a smaller radiating volume.

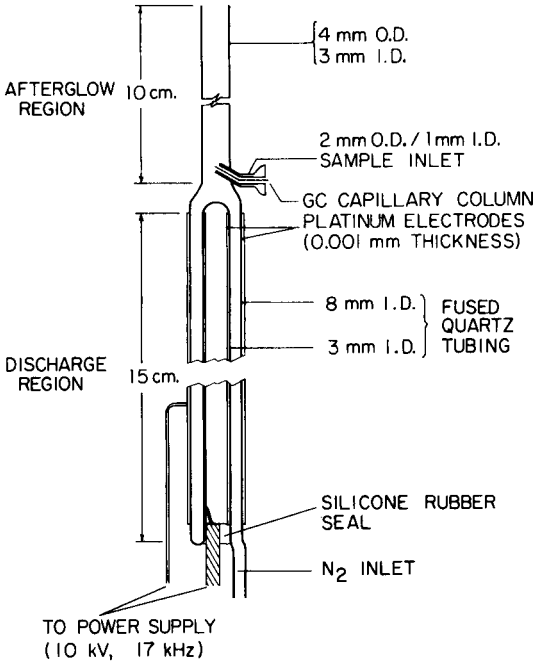

Fig. 1. Schematic diagram of the APAN discharge tube.

A schematic diagram of the analytical facilities employed in this investigation is shown in Fig. 2. The boil-off from liquid nitrogen, adjusted to a flow rate of 12 l min^{-1} by a flow meter, sustained the primary discharge that produced the active nitrogen species. Prior to entering the discharge tube, the nitrogen was passed through a copper coil immersed in liquid nitrogen in order to cool the discharge tube and remove any hydrocarbon impurities in the gas stream. The oxygen content of the nitrogen entering the discharge tube was <10 ppm.

A new power supply assembly, consisting of a 1000-W a.c. power amplifier coupled to a 10-kV impedance matching transformer (ENI Power Systems, Rochester, NY) was found to be superior in performance and stability to the power supply utilized in our prior investigations. The best analytical performance with the present discharge tube design was obtained at a frequency of 17 kHz with an incident power of 175 W. Further increases in the incident power resulted in a red glow from the inner electrode of the discharge tube due to overheating.

Emission from organic effluents in the afterglow was monitored at the $\Delta v = 0$, CN ($B^2\Sigma^+ \rightarrow X^2\Sigma^+$) transition at 388.3 nm, thus providing a selective detector for organic compounds. The central 1.5 cm along the axis of the afterglow tube was placed directly against the slit of a 0.2-m monochromator (Model H20, Instruments SA, Metuchen, NJ) for spectral observations. A bandpass of 4 nm (f.w.h.m.) was used throughout this study. An EMI 6256 photomultiplier tube was used as the detector and maintained with a high voltage input of 1320 V. The photocurrents produced were amplified by an electrometer amplifier (Model 417, Keithley Instruments, Cleveland, OH) and the chromatographic information recorded on a strip chart recorder (Supercribe Series 4910, Houston Instruments, Austin, TX).

A Hewlett-Packard Model 5710A capillary gas chromatograph (Hewlett-Packard, Avondale, PA) was interfaced to the APAN afterglow tube in the manner shown in Fig. 3. Either 30-m narrow-bore SE-52 or SE-54 fused silica capillary columns (J&W Scientific, Rancho Cordova, CA) were inserted directly into the sample inlet of the discharge tube at the base of the afterglow region, with no intermediate transfer lines or gas mixing being required.

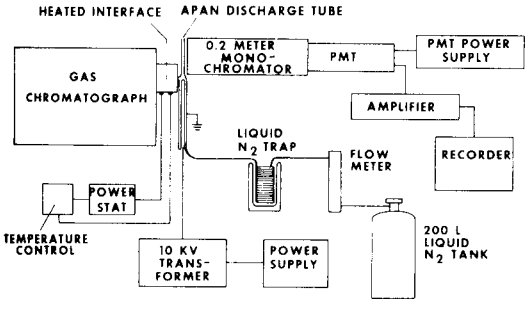

Fig. 2. Schematic diagram of instrumentation required for the APAN system.

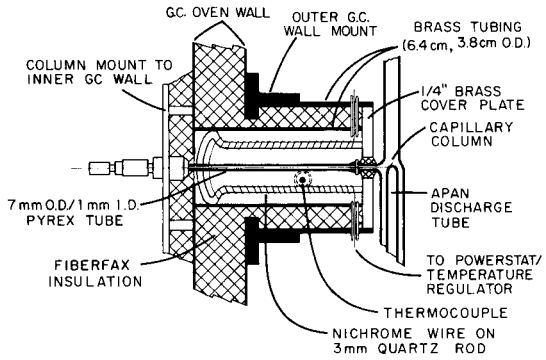

Fig. 3. Schematic diagram of the heated interface between the g.c. and the APAN afterglow sample inlet.

A 7-mm o.d., 1-mm i.d. glass insert between the g.c. oven wall and the sample inlet of the discharge tube was used to guide the column into the discharge tube. A small oven interface, shown in Fig. 3, bridged the gap between the g.c. oven wall and the discharge tube. To reduce the possibility of band broadening, the oven was designed so that a constant temperature was maintained along the length of the capillary column interface. The normal operating temperature of 325° C in the oven was maintained by a variable temperature controller (Omega Engineering, Inc., Stamford, CT).

Because the Hewlett-Packard g.c. was obtained without detector accessories, a Carlo-Erba g.c. equipped with a standard FID unit was utilized to compare the performance of the APAN detector to the FID. Differences in operating characteristics and temperature programming parameters allowed for only approximate matching of the chromatographic conditions used for comparing the two detectors. All injections were performed in the splitless mode using an injection port temperature of 300° C. Nitrogen or hydrogen were normally used as the carrier gases.

Organic reference samples

A stock solution of even numbered alkanes ranging from C_6 through C_{24} was prepared in pentane at a concentration of 60 μg ml^{-1}, with the exception of the C_{12} and C_{18} alkanes, which were at 120 μg ml^{-1}. Serial dilutions were also prepared down to concentrations of 0.01 μg ml^{-1}. A stock solution and subsequent dilutions of a mixture of ten polycyclic aromatic hydrocarbons (PAH), ranging in molecular weights from naphthalene to coronene, were also prepared in the same manner, utilizing hexane as the solvent.

RESULTS AND DISCUSSION

Chromatographic comparisons

Chromatograms obtained from the separation of an alkane hydrocarbon mixture by capillary g.c., for both the flame ionization and APAN detectors,

are shown in Fig. 4. Each compound was present at a 0.6 ng level except for the C_{12} and C_{18} alkanes, which were at 1.2 ng each. Comparative chromatograms for a mixture of PAH compounds are shown in Fig. 5. For the FID, each compound was present at a 1.8 ng level, while for the APAN detector each compound was at a 1.0 ng level. The unidentified peaks in the chromatogram obtained from the Hewlett-Packard g.c. with the APAN detector appeared to be due to contaminations in the injection system of the g.c.

The background scatter from the FID was observed to be considerably less than that obtained from the APAN detector at instrument settings which provided approximately the same peak magnitudes. Much of the baseline signal, as well as background scatter, in the APAN afterglow appears to arise from internal reflections in the quartz tubing from emissions originating in the discharge region.

At the higher g.c. oven temperatures where column bleed begins to occur, the APAN detector maintained a more constant baseline signal than the FID, which can be attributed to the selective detection of only CN emission. In contrast, the FID, being a non-selective detector, reflects the increasing baseline signals from detection of column bleed of carbon and non-carbon species. This factor is especially evident in the PAH chromatograms (Fig. 5), where high column temperatures were required for elution of the larger PAH compounds. A significant increase in the baseline signal was observed with the FID, even when the signal was attenuated by a factor of four. No further change in baseline signal, other than that shown, was observed from the APAN detector even at column temperatures sustained at 320°C.

No significant differences in peak shapes or resolution were observed between the two detectors. The direct insertion of the capillary column into the APAN afterglow and the high nitrogen flow rates used in the afterglow insured rapid mixing and reaction with the organic effluents. It is interesting to note that the violet CN emission from organic effluents in the afterglow could be visually observed at levels as low as 100 ng.

Quantitative potential

Limits of detection for the FID and APAN detectors are given in Table 1 for the two classes of compounds studied. The limits of detection were based on a signal/background scatter of three. Although the limits of detection for the FID were found to be three to ten times better than those obtained with the APAN detector, this range is considerably less if the short chain alkanes are excluded. The APAN detector was observed to be less sensitive for alkane compounds containing eight carbons or less, which appeared to be just the opposite of that observed with the FID. The FID limits of detection for the less volatile effluents (i.e., coronene, $C_{24}H_{50}$) would in practice be considerably poorer, because at low or no attenuation, the rising baseline signal would eventually saturate the electrometer signal.

It was expected that all carbon species in the afterglow would ultimately lead to the CN ($B^2\Sigma^+$) state. The emission intensity could then be directly

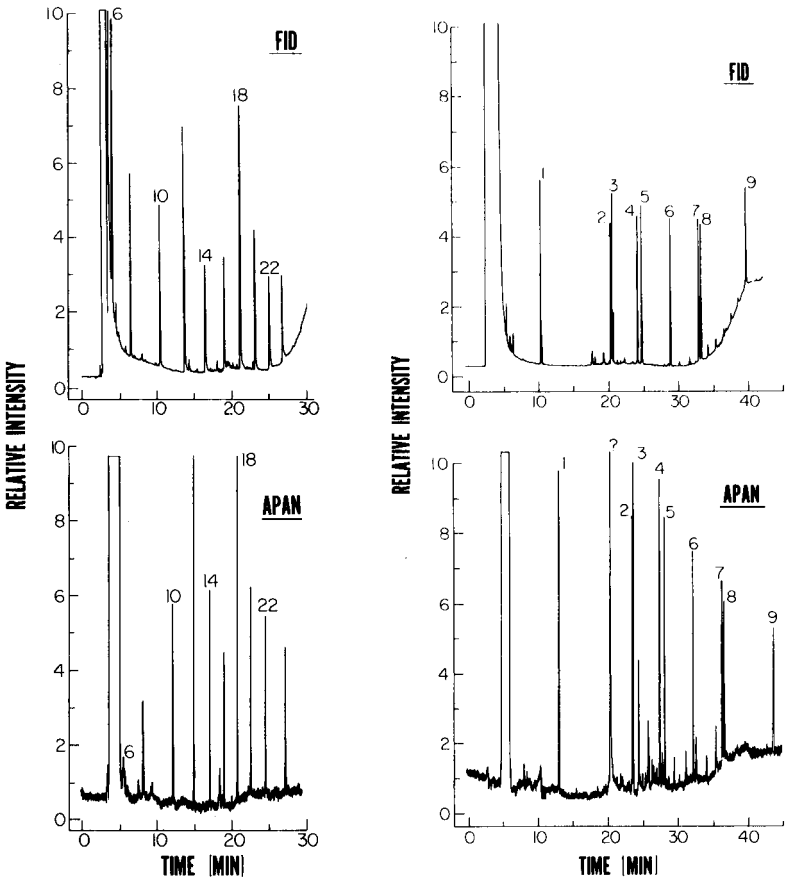

Fig. 4. (left) Chromatograms obtained from the separation of a standard hydrocarbon mixture containing even numbered carbons from C_6 to C_{24}. Each component present at 0.6 ng except for C_{12} and C_{18} at 1.2 ng. Numbers above peaks refer to carbon number. (A) Top chromatogram: FID (Carlo-Erba); 30 m SE-52 column; temperature program 30° C (4 min)—10° C min^{-1}—300° C; attenuation 2×. (B) Bottom chromatogram: APAN detector; 30 m SE-54 column; temperature program 40° C (4 min)—16° C min^{-1}—290° C; gain 3 × 10^{-8} A.

Fig. 5. (right) Chromatograms obtained from the separation of a standard polycyclic aromatic hydrocarbon mixture. (A) Top chromatogram: FID (Carlo-Erba); compound amount, 1.8 ng each; 30 m SE-52 column; temperature program 55° C (2 min)—8° C min^{-1}—315° C (5 min); attenuation 2×. (B) Bottom chromatogram; APAN; compound amount, 1.0 ng each; 30 m SE-54 column; temperature program 70° C (2 min)—8° C min^{-1}—300° C (8 min); gain 3 × 10^{-8} A. Compound identification: (1) naphthalene, (2) phenanthracene, (3) anthracene, (4) fluoranthrene, (5) pyrene, (6) chrysene, (7) benzo[e]pyrene, (8) perylene, and (9) coronene.

TABLE 1

Comparison of the limits of detection for the APAN detector and the FID

Compound class	Limits of detection[a] (ng)	
	FID[b]	APAN[c]
Aliphatic	0.02—0.05	0.06—0.3
Aromatic	0.02—0.04	0.06—0.1

[a]Signal/background scatter = 3. [b]No attenuation 1×. [c]Maximum gain = 3×10^{-8} A.

correlated to the number of carbon atoms in each respective compound. This dependence was not observed. Evidently reactions other than those responsible for the formation of the CN ($B^2\Sigma^+$) state occur in the afterglow.

The APAN detector responded linearly from near the detection limit concentration (≈0.06—0.3 ng of column loading) up to ≈300 ng of loading. The departure from linearity above 300 ng presumably arose from depletion of the active species responsible for the formation of the CN ($B^2\Sigma^+$) state. The three to four orders of magnitude of linearity is markedly less than the six to seven orders of magnitude range for FID detectors. This difference is not of primary importance because the loading capacity of capillary g.c. columns is typically limited to 100 ng or less of each compound.

The substitution of hydrogen or helium for the nitrogen carrier gas caused reductions in signal ranging from 10 to 35% for hydrogen and 70 to 95% for helium. The preference for hydrogen as a carrier gas in capillary g.c. applications therefore involves a small reduction in powers of detection when the APAN detector is used.

The operating stability of the APAN detector was found to be very similar to the FID over extended periods of operation. The simple operating parameters associated with the APAN system allowed for excellent long term reproducibility in chromatographic measurements. Peak heights were found to deviate only ±5% or less on a day-to-day basis. There were no visual signs of contamination in the afterglow tube after approximately 100 h of operation, which can be attributed to the high flow rates of nitrogen through the reaction zone.

A mixture of nitrogen-, oxygen-, fluorine- and sulfur-containing compounds was also examined to insure that the formation of CN was not strictly limited to only C- and H-containing compounds. A chromatogram obtained from this mixture is shown in Fig. 6, with each component being present at an 8 ng level. Excellent baseline stability and peak resolution were observed throughout the chromatogram. Thus, the APAN detector appears to be responsive to a large variety of carbon containing compounds.

The Ames Laboratory is operated for the U.S. Department of Energy by Iowa State University under Contract No. W-7405-Eng-82. This research was supported by the Division of Chemical Sciences, Budget Code KC-03-02-03, Office of Energy Research.

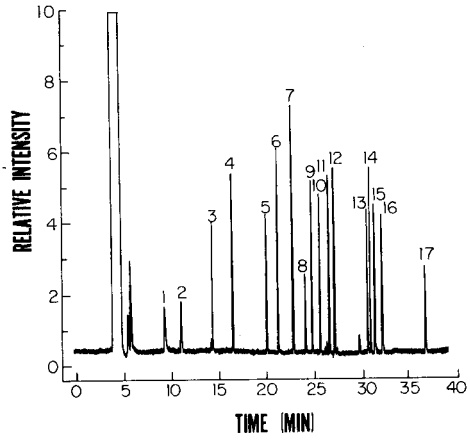

Fig. 6. Chromatogram obtained in conjunction with the APAN detector of a standard mixture used for fly-ash leaching studies at the Ames Laboratory. Concentration of compounds, 8 ng each; 30 m SE-52 column; temperature program 35° C (4 min)—8° C min^{-1}—250° C; gain 1 × 10^{-8} A. Compound identification: (1) picoline, (2) fluorophenol, (3) phenol, (4) cresol, (5) naphthalene, (6) quinoline, (7) azulene, (8) naphthoquinone, (9) tetradecane, (10) acenaphthalene, (11) naphthol, (12) naphthylamine, (13) dibenzothiophene, (14) phenanthrene, (15) carbazole, (16) fluoranthrene, and (17) benz[a]anthracene.

REFERENCES

1 I. S. Krull and S. Jordan, Am. Lab., 12 (1980) 21.
2 J. W. Carnahan, K. J. Mulligan and J. A. Caruso, Anal. Chim. Acta, 130 (1981) 227.
3 D. G. Sutton, K. R. Westburg and J. E. Melzer, Anal. Chem., 51 (1979) 1399.
4 J. E. Melzer and D. G. Sutton, Appl. Spectrosc., 34 (1980) 434.
5 A. N. Wright and C. A. Winkler, Active Nitrogen, Academic Press, New York, 1968, Ch. 5.
6 G. W. Rice, J. J. Richard, A. P. D'Silva and V. A. Fassel, Anal. Chem., 53 (1981) 1519.
7 G. W. Rice, J. J. Richard, A. P. D'Silva and V. A. Fassel, J. Assoc. Off. Anal. Chem., 65 (1982) 14.
8 A. P. D'Silva, G. W. Rice and V. A. Fassel, Appl. Spectrosc., 34 (1980) 578.

Analytica Chimica Acta, 142 (1982) 55—62
Elsevier Scientific Publishing Company, Amsterdam — Printed in The Netherlands

DETERMINATION OF METALS AT TRACE LEVELS VIA PRE-COLUMN DERIVATIZATION AND NONPOLAR STATIONARY-PHASE HIGH-PERFORMANCE LIQUID CHROMATOGRAPHY WITH *n*-BUTYL-2-NAPHTHYLMETHYLDITHIOCARBAMATE COMPLEXES

YOUNG-TZUNG SHIH and PETER W. CARR*
Department of Chemistry, University of Minnesota, Minneapolis, MN 55455 (U.S.A.)
(Received 2nd April 1982)

SUMMARY

A new, very stable dithiocarbamate, bis(*n*-butyl-2-naphthylmethyldithiocarbamate) zinc(II), has been synthesized and its use in trace metal determination by high-performance liquid chromatography (h.p.l.c.) has been investigated. Metal complexes of this ligand are thermodynamically stable and kinetically inert at the 1×10^{-8} M level. Various metal complexes including nickel(II), iron(III), copper(II), mercury(II), and cobalt(II) have been "baseline" separated by nonpolar stationary-phase h.p.l.c. The detection limits are about 1—2 ng with a variable-wavelength absorbance detector.

Dithiocarbamates are useful reagents for the separation and spectrophotometric detection of heavy metals [1, 2]. Their extraction chemistry is well understood [3] and they form thermodynamically stable complexes. Separation of diethyldithiocarbamate complexes by polar stationary phase h.p.l.c. on silica gel has been studied extensively [4—6]. Separations of various dialkyldithiocarbamate complexes on hydrocarbon stationary phases have also been reported [7, 8]. In either mode, the methodology is limited by both the dissociation and decomposition of the complexes on the column, and by variations in the spectroscopic properties of different metal complexes. Because of the very significant differences in the wavelength of maximum absorbance of the most intense bands, it is not possible to work at optimum sensitivity for more than a few judiciously selected metals. Thus it is not possible to optimize the overall performance of the methodology without a multi-channel spectrometric detector. Furthermore, the dissociation of metal dithiocarbamate complexes [4] at very low concentration, limits their utility for trace determinations by h.p.l.c. unless excess of ligand can be added to the mobile phase.

An ideal ligand for use as a pre-column derivatization agent will rapidly form very stable, kinetically inert, easily detectable complexes with a wide variety of metals. To this end, a novel dithiocarbamate ligand, *n*-butyl-2-naphthylmethyldithiocarbamate (BNMDTC) has been synthesized.

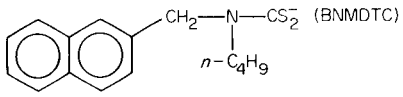

(BNMDTC)

It has been found that the naphthyl group imparts very high absorptivities to the complex, and the combination of the bulky naphthyl and butyl groups tends to stabilize metal complexes formed with this reagent.

EXPERIMENTAL

Synthesis of the reagent

The hydrobromide salt of the *n*-butyl-2-naphthylmethylamine was first made as described by Hutton et al. [9]. The zinc salt of BNMDTC was formed from the hydrobromide salt of the *n*-butyl-2-naphthylmethylamine as follows.

Add 8.6 g of the hydrobromide salt of *n*-butyl-2-naphthylmethylamine to 60 ml of aqueous 1 M sodium hydroxide and add the minimum quantity of isopropanol (~5 ml) to dissolve the amine. Add 1.75 ml of carbon disulfide slowly (10 min) via a dropping funnel. Allow the mixture to react for 2 h at room temperature with constant stirring. Acidify the solution by addition of 100 ml of 0.1 M sodium acetate (pH 5.5) buffer. Add 40 ml of a 0.4 M solution of zinc nitrate with occasional stirring. Digest the mixture overnight and remove the precipitate by filtration. Recrystallize the zinc BNMDTC salt by dissolving it in chloroform. Remove insoluble material by filtration and reduce the volume of chloroform to about 5 ml by gentle heating. Add methanol to precipitate the zinc salt. The filtered product is dried in air (m.p. 115—118°C). Elemental composition found: C, 59.8; H, 5.7; N, 4.4; S, 19.8; Zn, 10.1%. $C_{32}H_{36}N_2S_4Zn$ calcd: C, 59.85; H, 5.6; N, 4.4; S, 20.0; Zn, 10.2%. Molecular weight found 641 (calcd. 641.9). N.m.r., m.s., and i.r. analysis are consistent with the desired product. It was not possible to isolate the sodium, potassium, or calcium salt of this ligand.

Apparatus

An h.p.l.c. system similar to that described elsewhere [10] was employed in this work. It should be noted that two pre-columns were employed. First a silica column (25 cm × 4.6 mm) is used to "saturate" the mobile phase with dissolved silica and thereby minimize loss of column packing in the analytical column; a second pre-column (10 cm × 4.6 mm) filled with silica gel derivatized with a diaminosilane [11] is used to remove trace metals from the mobile phase (buffer, etc.). These pre-columns can be used for a minimum of one month. The analytical column is a Waters RCM-100 C_{18} column (10-μm particles, 10 cm × 5 mm) which is employed to minimize generation of interferences from the metal frits of conventional columns. A Hitachi (Model 100-10) variable-wavelength adsorbance detector set at 221 nm was used throughout this work. The mobile phase is 96/5 methanol/

water containing 1.0 mM Tris adjusted to pH 8.25 by addition of phosphoric acid prior to the addition of methanol.

All the metal complexes injected were prepared by adding metal salts (nitrate or chloride) into zinc BNMDTC which was predissolved in the mobile phase and which should be present in at least two-fold excess.

Application of the method to trace metal analysis via preconcentration of the metal complexes on to XAD resin (Applied Science, 20—60 mesh) was attempted as follows. Add 10 μl of a 1×10^{-2} M solution of each metal (iron(III), nickel(II), mercury(II), and cobalt(II)) to 1 l of 1 mM Tris (pH 7.0) buffer in a polyethylene bottle which has been precleaned as described by Laxen and Harrison [12]. The final concentration of each metal is 1×10^{-7} M. Add 1.5 ml of 1 mM zinc BNMDTC, dissolved in methanol, to this mixture. Stir the solution for 1 h at room temperature. Add ca. 1 g of XAD to the solution. After another 3 h with constant stirring, quantitatively transfer the resin to a small buret filled with a coarse fritted disk at a flow rate of 30 ml min^{-1}. The flow rate is maintained by means of suction with an aspirator. Elute the metal complexes off the XAD resin by use of pure methanol without applying a vacuum. Collect the first 10 ml of solution as the 100-fold preconcentrated metal complex mixture. Then inject this sample into the liquid chromatograph and compare with a freshly prepared 1×10^{-5} M mixture of metal complexes in order to study the recovery of this preconcentration method.

RESULTS AND DISCUSSION

A typical chromatogram for the separation of the BNMDTC complexes of iron(III), nickel(II), copper(II), mercury(II) and cobalt(II) is shown in Fig. 1. It is clear that these metals at least are very easily separated.

The spectroscopic properties of these materials are summarized in Table 1. It is evident that the absorptivity of the naphthyl moiety at 221 nm is reasonably consistent from metal to metal and it is always very much greater than at longer wavelengths. Thus it is possible to achieve multi-component determinations at one wavelength. It should be noted that no fluorescence was observed from either BNMDTC or any of its metal salts despite the presence of the naphthyl group.

In general, metal dithiocarbamate complexes are thermodynamically more stable than the corresponding EDTA complexes [1]. In the case of BNMDTC, it was shown that addition of BNMDTC to EDTA complexes of a variety of metals results in the color typical of that metal dithiocarbamate complex. It was also observed that under identical solution conditions (95/5 methanol/water at pH $\approx$ 2.0), the color of 1×10^{-5} M solution of the above BNMDTC complexes, stored in the dark, persisted almost indefinitely whereas the color of the diethyldithiocarbamate complexes of many metals (copper(II), nickel(II), iron(III) and cobalt(II)) can fade quite rapidly (one hour).

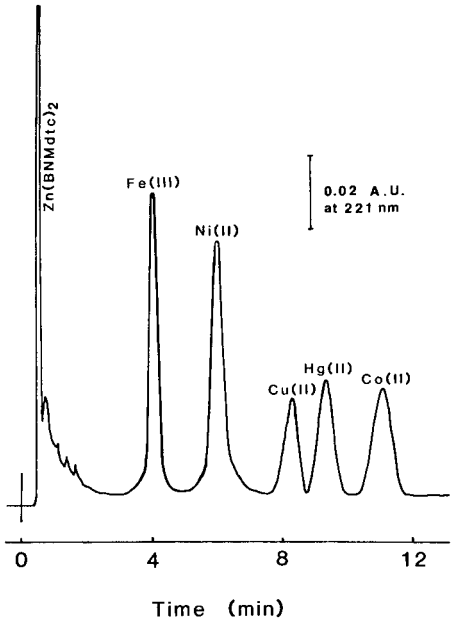

Fig. 1. Chromatogram of the metal $(BNMDTC)_n$ complexes. Sample was 20 μl of a synthetic mixture which was 1×10^{-4} M in each complex. Flow rate 2 ml min^{-1}; pressure drop less than 1500 psi.

TABLE 1

U.v. spectroscopic data for the metal $(BNMDTC)_n$ complexes[a]

Metal	Wavelength (nm)	Molar absorptivity ($l\ mol^{-1}\ cm^{-1}$)	Metal	Wavelength (nm)	Molar absorptivity ($l\ mol^{-1}\ cm^{-1}$)
Zn^{2+}	221	150 000	Ni^{2+}	221	176 000
	265	77 600		245	52 500
Cu^{2+}	221	>200 000		325	46 900
	265	52 000	Co^{2+}	221	149 000
	390	9 400		276	38 600
Fe^{3+}	221	268 000		320	18 200
	265	57 500			

[a]The samples were dissolved in 95/5 methanol/water.

The stability of BNMDTC complexes at very low concentration at which the color is too low to observe (10^{-8} M), was tested in the following fashion. In acidic solution the dithiocarbamate ligand decomposes to carbon disulfide and the free amine:

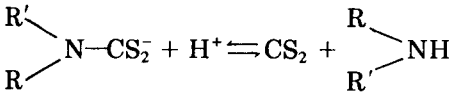

(1)

In the case of BNMDTC the free amine is extremely fluorescent. Thus if the pH is adjusted to a low value, any dissociation of the metal—BNMDTC complex will liberate the free ligand which will rapidly decompose to the free amine which can be measured by h.p.l.c. with fluorescence detection. The results of a series of such experiments are summarized in Table 2. It is clear that BNMDTC complexes are very stable and on a chromatographic time scale (15 min) dissociation and decomposition will be altogether negligible. As expected, the zinc—BNMDTC complex is the least stable of the metals tested here.

The separation of these metal complexes was assessed in a variety of mobile phases (acetonitrile—water, tetrahydrofuran—water, isopropanol—water and methanol—water). Preliminary experiments indicated that methanol—water mixtures gave the best chromatographic selectivities and therefore the most easily optimized resolution. The chromatographic results differ very considerably between different nonpolar phase columns (Table 3). Total retention (k') varied dramatically with a given mobile phase as the column was varied. It is tentatively inferred that the complexes are interacting in part with free silanol groups because very heavily loaded (22% weight carbon) C_{18} columns gave very poor selectivity and diminished retention.

In order to forestall decomposition of complexes in acidic or neutral solution, Tris buffer at pH 8.25 was included in the mobile phase. This buffer is relatively non-corrosive towards nonpolar packing materials [13] in comparison to other alkaline buffering agents and has low formation constants for metal complexes [14]. Under the isocratic elution conditions given in Fig. 1, five important metals, iron(III), nickel(II), copper(II),

TABLE 2

Inertness of the metal $(BNMDTC)_n$ complexes

Metal	Conc. (M)	Conditions[a]		Decomposition (%)
		pH	Time (h)	
Zn^{2+}	10^{-7}	8.2[b]	24	10
	10^{-7}	2[c]	2	50
Fe^{3+}	10^{-7}	8.2	2	0
	10^{-7}	2	2	10
Cu^{2+}	10^{-7}	2	24	0
	10^{-8}	2	24	0
Hg^{2+}	10^{-7}	2	24	0
	10^{-8}	2	24	0

[a]Solutions are stored in the dark. [b]pH 8.25, 0.1 M Tris buffer. [c]0.01 M HCl.

TABLE 3

Retention (k') of the metal $(BNMDTC)_n$ complexes

Metal	Waters Radial-PAK A[a]	Supelco Supelcosil[b]	Waters μ-Bondapak[c]
Fe(III)	3.9	4.6	2.3
Ni(II)	6.2	6.4	3.6
Cu(II)	8.5	9.2	5.2
Hg(II)	10.1	10.9	5.5
Co(II)	12.1	—	8.1

[a]Column: Waters RCM-100 C_{18}, 10-μm particles, 100 × 8 mm. Mobile phase: 95/5 methanol/water, 1 mM Tris at pH 8.25, 2.0 ml min^{-1}. [b]Column: Supelcosil LC-8, 5-μm particles, 150 × 4.6 mm. Mobile phase: 85/15 methanol/water, 1 mM Tris at pH 8.25, 2.5 ml min^{-1}. [c]Column: Waters μ-Bondapak C_{18}, 10-μm particles, 90 × 4.6 mm. Mobile phase: 93/7 methanol/water, 1 mM Tris at pH 8.25, 1.0 ml min^{-1}.

mercury(II), and cobalt(II), can be nearly baseline-separated within 12 min, at a flow rate of 2 ml min^{-1}, with peak asymmetry less than 1.2 in all cases.

Calibration curves (Fig. 2) are clearly linear. Statistical analysis indicates that the intercepts are zero, from which one can conclude that over the range of concentrations employed in this work, dissociation and decomposition are negligible. This is in marked contrast to the results of Moriyasu and Hashimoto [4] who found that at low concentration ($< 1 \times 10^{-5}$ M) most metal dithiocarbamate complexes dissociate, and therefore calibration curve intercepts are non-zero and the curves are not linear at low concentration.

Table 4 summarizes the reproducibility of peak area measurements. At concentrations above 10^{-6} M, precision better than 2.0% can generally be achieved. Below this level, baseline instability (drift) limits the measurement system. According to the detection limit criteria developed by Hubaux and Vos [15], detection limits for mercury(II), copper(II) and iron(III) are 3, 1, and 10 ng, respectively.

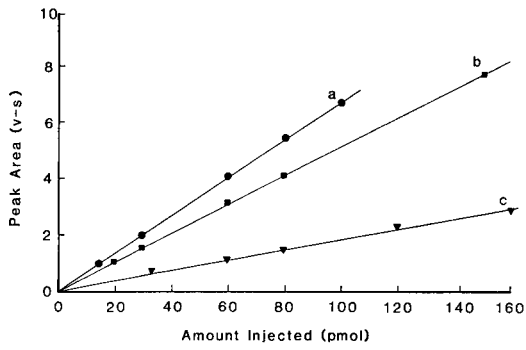

Fig. 2. Calibration curves for various metal ions: (a) $Hg(BNMDTC)_2$; (b) $Cu(BNMDTC)_2$; (c) $Fe(BNMDTC)_3$. These complexes are very strong, stable, and less stable, respectively.

TABLE 4

Precision of peak area measurement at different concentrations of the metal $(BNMDTC)_n$ complexes

Concentration (μM)	Coefficient of variation[a]		
	Hg(II)	Cu(II)	Fe(III)
0.75	3.3	—	—
1.0	—	3.1	—
1.5	1.5	1.6	3.5
3.0	0.2	0.5	1.6
4.0	0.5	0.5	0.9
5.0	0.2	—	—
6.0	—	—	0.5
7.5	—	0.2	—
8.0	—	—	0.5

[a]Defined as (100 SD/mean) and based on a minimum of 5 replicates.

The use of BNMDTC as a preconcentration reagent is summarized in Table 5. Although Waters C_{18} Sep-Pak cartridge has been used to preconcentrate trace metals from natural water samples [16, 17], XAD resin was found to give better recovery of metal BNMDTC complexes. The longer the contact time between the samples and the resin, the greater the recovery. However, in the case of $Fe(BNMDTC)_3$, prolonged extraction time decreases the recovery because of decomposition of the complex in the pH 7.0 solution. This preliminary recovery study demonstrates the possibility of preconcentrating trace metals from real samples provided that other organic matter in the sample does not interfere with formation of the metal complexes.

This work was supported by a grant from the National Institute of Occupational Safety and Health (1 R01 0H00876-01).

TABLE 5

Recovery of metal BNMDTC complexes

Metal	Recovery from resins (%)			
	C_{18} Sep-Pak[a]	XAD with contact time of		
		1 h	3 h	16 h
Fe(III)	~ 40	84	92	80
Ni(II)	~ 60	101	101	102
Hg(II)	~ 60	97	99	99
Co(II)	~ 50	93	94	95

[a]The flow rate of sample through the cartridge is about 10 ml min^{-1}.

REFERENCES

1 G. D. Thorn and R. A. Ludwig, The Dithiocarbamates and Related Compounds, Elsevier, New York, 1962.
2 E. S. Sandell and H. Onishi, Photometric Determination of Traces of Metals, 4th edn., Wiley—Interscience, New York, 1978, pp. 512—532.
3 J. Stary and K. Kratzer, Anal. Chim. Acta, 40 (1968) 93.
4 M. Moriyasu and Y. Hashimoto, Anal. Lett., A11 (1978) 593.
5 P. Heizmann and K. Ballschmiter, J. Chromatogr., 137 (1977) 153.
6 D. Liska, J. Lehotay, E. Brandsteterova, G. Guiochon and H. Colin, J. Chromatogr., 172 (1979) 384.
7 G. Schwedt, Chromatographia, 12 (1979) 289.
8 R. F. Borch, J. H. Markovitz and M. E. Pleasants, Anal. Lett., 12 (1979) 917.
9 R. C. Hutton, S. A. Salam and W. I. Stephen, J. Chem. Soc. A, (1966) 1573.
10 Y. T. Shih and P. W. Carr, Talanta, 28 (1981) 411.
11 D. E. Leyden, in T. G. Dzubay (Ed.), X-ray Fluorescence Analysis of Environmental Samples, Ann Arbor Science Publications, Ann Arbor, 1977, p. 145.
12 D. P. H. Laxen and R. M. Harrison, Anal. Chem., 53 (1981) 345.
13 A. Wehrli, J. C. Hildebrand, H. P. Keller and R. Stampfli, J. Chromatogr., 149 (1978) 199.
14 N. E. Good, G. D. Winget, W. Winter, T. N. Connolly, S. Izawa and R. M. M. Singh, Biochem. J., 5 (1966) 467.
15 A. Hubaux and G. Vos, Anal. Chem., 42 (1970) 849.
16 G. L. Mills and J. G. Quinn, Mar. Chem., 10 (1981) 93.
17 R. E. Sturgeon, S. S. Berman and S. N. Willie, Talanta, 29 (1982) 167.

Analytica Chimica Acta, 142 (1982) 63—72
Elsevier Scientific Publishing Company, Amsterdam — Printed in The Netherlands

THE EFFECT OF END-CAPPING REAGENT ON LIQUID CHROMATOGRAPHIC PERFORMANCE

C. H. LOCHMÜLLER* and DAVID B. MARSHALL[a]
P. M. Gross Chemical Laboratory, Duke University, Durham, NC 27706 (U.S.A.)
(Received 21st April 1982)

SUMMARY

Luminescence and photoacoustic spectroscopies are used to evaluate the nature of octadecylated silica surfaces as a function of trimethylsilyl "end-capping" reagent. These differences are compared to the chromatographic behavior of similar phases. It is concluded that end-capping with hexamethyldisilazane (HMDS) yields a phase with greater chemical heterogeneity, though lower average polarity, than phases end-capped with trimethylchlorosilane (TMCS). Some of these differences are attributed to the production of basic sites on the surface when HMDS is used. This property may make HMDS more suitable than TMCS as an end-capping reagent for phases used in the separation of basic solutes.

The development of theoretical models of retention in high-performance liquid chromatography (h.p.l.c.) [1—6] and the use of this chromatography for the evaluation of physical parameters [7—9] are areas of increasing interest. Both the construction of realistic retention theories and the reliable extraction of physical parameters depend on knowledge of the molecular nature of the stationary phase (and its interactions with mobile phase and solute) and how this nature is expressed in the macroscopic chromatographic behavior. Among the information necessary (particularly for reversed-phase and other bonded-phase chromatographies), are the following points: the actual composition of the stationary phase; how it is wetted by the mobile phase; its conformation and any changes in this conformation with such factors as chain length, temperature, and mobile phase composition; the homogeneity of the surface with respect to variations in local carbon chain and residual silanol density; the variation of these properties with the structure of the silica support (particle size, pore diameter, distribution, etc.).

Chromatographic studies alone cannot provide the kinds of molecular-level information needed to understand the nature of bare and chemically-modified silica surfaces. Spectroscopic methods are being employed with increasing frequency in order to provide this information (for earlier references, see

[a]Current address: Department of Chemistry, University of Idaho, Moscow, ID 83843, U.S.A.

[10]). Electron spin resonance (e.s.r.) has been used recently to study the restriction of water mobility in narrow silica pores [11] and the preferential adsorption of ammonia from aqueous solution as a function of pore size [12, 13]. Such studies are useful in understanding long-range ordering of liquids by solid surfaces. Nuclear magnetic resonance (n.m.r.), particularly with cross-polarization, magic-angle spinning techniques, has been used to detect residual silanols on the surface of chemically modified silica [14], to identify surface-bound species [15], and to detect the various types of bonding present (e.g., the proportion of monomeric to dimeric linkages formed when a difunctional silylating agent is used) on the modified surface [16]. Silica labelled with a luminescent probe molecule has been used to study the surface via fluorescence spectroscopy [10]. This method was shown to be useful for investigating changes in effective surface polarity with variations in the conditions of, and reagents used in, chemical modification, as well as variations in surface coverage, composition of the liquid used to wet the surface, density and length of alkyl chains that were also attached to the surface, etc. The variation in emission maximum with excitation wavelength was shown to be a potentially useful indicator of the micro-heterogeneity of the chemically modified surface [17].

Silanol groups on the surface of silica act as strong adsorptive sites in normal-phase liquid chromatography as well as sites of surface attachment in the synthesis of bonded phases. Synthesis of nonpolar silica for use in reversed-phase liquid chromatography involves reaction of silica gel with a reactive (usually chloro- or alkoxy-) alkylsilane. The nature of the chemically modified surface will depend on surface coverage and distribution of the bonded alkyl chains and on the number and type of residual silanols. These factors are governed by the physical accessibility and chemical reactivity of the silanol groups on the original silica substrate. Silanol groups are usually classified as "reactive" or "unreactive" with respect to some derivatizing reagent. They are also classified as "free" or "associated" (two adjacent silanols, hydrogen-bound to each other (vicinal) or a silanol bound to a siloxane oxygen). The presence of geminal silanols is sometimes also inferred. A review of the literature to 1968 is given by Snyder [1] who concludes that associated silanols are "reactive" with respect to trimethylchlorosilane (TMCS) whereas "free" silanols are unreactive. These less tractable silanols are determined via reaction with hexamethyldisilazane (HMDS), an apparently more reactive trimethylsilylating reagent. This particular assignment of silanol association with reactivity has, however, been a matter of some dispute [18], with the opposite being suggested by the work of others [19, 20]. It is interesting in this regard to note that an *ab initio* study of model silanols concludes that an unassociated silanol has an absolute acidity between that of phenol and hydrogen cyanide, whereas a silanol in which the oxygen atom is associated with a Lewis acid is more acidic than hydroiodic acid [21].

The synthesis of nonpolar stationary phases often involves "end-capping", or trimethylsilylation of residual silanols after initial reaction with the

alkylsilylating reagent of choice (usually an octadecylsilane). Reaction conditions for such stationary phases have recently been optimized, and it is suggested that end-capping be done with TMCS [22]. The greatest degree of surface deactivation has, however, been achieved via end-capping with a mixture of TMCS and HMDS in pyridine [23]. It seems important to determine how end-capping with TMCS versus HMDS changes the properties of the chemically modified surface on the molecular level, and how those changes affect the macroscopic chromatographic properties of such surfaces. This paper reports the investigation via fluorescence spectroscopy (using luminescent probe methods) and photoacoustic spectroscopy of octadecylated silica surfaces that have been end-capped with TMCS or HMDS. Correlations with the chromatographic performance of similar materials are made in an attempt to understand the relationship between the microscopic and macroscopic properties of these materials.

EXPERIMENTAL

Chemicals and reagents

The silanes examined (aminopropyldimethylethoxysilane, octadecyldimethylchlorosilane, octadecylmethyldichlorosilane, trimethylchlorosilane, hexamethyldisilazane; Petrarch Systems, Bristol, PA) were used as received without further purification. The silica used for the spectroscopic studies was LiChrosorb SI-100 (EM Laboratories, Elmsford, NY) with a mean particle size of 10 μm and a nominal surface area of 240 $m^2\ g^{-1}$. The silica for the chromatographic studies was Whatman Partisil-10 with a mean particle size of 7.5 μm and a surface area of 323 $m^2\ g^{-1}$. All solvents used for synthesis were distilled at least once from the appropriate drying agent and stored under dry nitrogen. All syntheses were done in oven-dried (140° C) glassware and silica, under dry nitrogen. Liquid chromatographic-grade (Omnisolv) solvents were used for the chromatographic studies. Dansyl chloride (5-dimethylaminonaphthalenesulfonyl chloride; Aldrich Chemical Co.) was recrystallized prior to use.

Preparation of chemically modified silicas

A batch of silica was sparingly dansylated by amination followed by reaction of the sparingly aminated silica with dansyl chloride, as detailed earlier [10]. This luminescent probe-labelled silica was exhaustively alkylated with octadecyldimethylchlorosilane by the procedure of Evans et al. [22]. Aliquots of this material were then treated with TMCS or HMDS or both. Chromatographic phases were synthesized by the same general procedure with octadecylmethyldichlorosilane under dry conditions to minimize polymerization, and end-capped with either TMCS or HMDS. Elemental determinations indicated 18.6% carbon for the octadecyl, HMDS end-capped material (O/H), and 19.0% for the octadecyl, TMCS end-capped material (O/T).

Spectroscopic and chromatographic measurements

Fluorescence measurements were made with a Perkin-Elmer MPF-3 spectrofluorimeter, as previously described [10, 17]. Photoacoustic measurements were made with a PAR 6001 photoacoustic spectrometer, as previously described, in the visible [24] and near-i.r. [25, 26] regions.

Liquid chromatography was conducted at ambient temperature. Bonded phases were packed by the upward-slurry method into the same stainless-steel column (20-cm, 0.4-cm i.d.) for each experiment. The mobile phase was 80/20 (by volume) methanol/water.

RESULTS

Spectroscopic studies

The emission of the dansylamide group is a sensitive indicator of changes in polarity or polarizability of the environment. The emission of the model compound *n*-propyldansylamide in free solution undergoes a red-shift of about 100 nm in going from *n*-hexane to water as solvent. This wavelength shift is compressed when the probe is bound to the silica surface, with the emission maximum varying as a function of surface coverage, solvent(s) used to wet the surface, the functionality of the aminating reagent (used to anchor the dansyl group via reaction of dansyl chloride with the surface-bound primary amine), and the identity and surface coverage of other (e.g., alkyl) surface-bound moieties [10]. In this study, a sparingly dansylated silica (DS) was exhaustively octadecylated (DS/OD) and aliquots of this material were end-capped with TMCS (DS/OD/T) or HMDS (DS/OD/H). The emission maximum is expected to blue-shift as the polarity of the surface is lowered by reaction of the surface silanols with alkylsilylating agents. This trend is shown by the data in Table 1, with the surprising exception of OD in dry form, emission from which is red-shifted with respect to the sparingly dansylated precursor, DS.

The carbon content of chemically modified silicas may be determined by photoacoustic spectroscopy [26]. The relative carbon content of the dansyl silicas, using an octadecylated silica standard with 16.57% carbon, is 0.000 for DS, 0.822 for DS/OD, 0.946 for DS/OD/T, and 1.07 for DS/OD/H.

The variation of emission maximum with excitation wavelength of dansylated silicas has been suggested as a qualitative indicator of the microheterogeneity of the surface [17]. This variation for the materials in this study is also shown in Table 1. It was expected that the DS/OH/H material would be the most homogeneous of the alkylated dansyl silicas, but instead appears to be the least. Treatment of the DS/OD/H material with TMCS produced no significant change in its luminescence characteristics.

The absorption maximum of the dansyl amide model compound in free solution undergoes a red-shift in aprotic solvents of increasing polarity (the magnitude of the shift being about one-third that of the emission shift in the same solvents), but blue-shifts in solvents of increasing acidity such that the

TABLE 1

Emission and photoacoustic maxima of dansyl silicas as a function of excitation wavelength (nm)

Excitation wavelength	Emission maximum			
	DS	DS/OD	DS/OD/T	DS/OD/H
Dry powder				
290	—[a]	492	478	460
350	484	492	480	462
400	—[a]	492	480	464
	Photoacoustic maximum			
	314	302	293	313
ACN slurry[b]				
290	495	502	496	488
350	510	502	496	492
400	500	502	496	490

[a]Intensity too low to obtain reliable values. [b]Slurries allowed to stand for 24 h before measurement.

absorption in water is 5 nm to the blue of the value in *n*-heptane [17]. The emission by contrast undergoes a red-shift in solvents of increasing polarity regardless of their acidity. The emission is somewhat sensitive to protonation, however, as evidenced by a blue-shift of 5 nm in pH 2 solution versus its value in neutral pH water [10]. Comparison of emission maxima with the photoacoustic maxima reported in Table 1 thus allows an assessment of the extent of hydrogen bond formation in these dansyl silicas. The blue shift in photoacoustic maximum of DS/OD versus the DS precursor despite the slight red-shift in emission suggests an enhanced degree of hydrogen bonding to the dansyl moiety. The further blue shift of DS/OD/T may be due simply to the decrease in polarity as indicated by the blue emission shift. The shift back to longer wavelengths for DS/OD/H is expected for a decrease in hydrogen bonding, but the magnitude of the shift is rather large, a photoacoustic maximum of 300 nm being more reasonable.

Chromatographic studies

The chromatographic properties of octadecyl, reversed-phase materials were investigated by evaluating the retention and bandwidth behavior of the test solutes aniline, phenol, benzene, anthracene, pyrene, 2-picoline, 2-*p*-tolylpyridine and 2,6-di-*t*-butylpyridine at flow rates of 0.5, 1, 1.5 and 2 ml min^{-1}. The mobile phase used was the same batch of 80/20 (by volume) methanol/water. The peaks were not assumed to be gaussian; rather k' and plate height values were determined using the first and second moments assuming exponentially modified gaussian peak shapes. The statistical

moments were determined by using the graphical method of Barber and Carr [27] from the peak asymmetry, width, and retention time values. Sodium nitrate was used to determine t_0, so the values of k' reported in Table 2 cannot be considered absolute, but are easily correctable should the chemically and philosophically perfect "unsorbed tracer" ever be found. The values are

TABLE 2

Capacity factors (k'), peak asymmetry and effective reduced plate height values for test solutes on the end-capped octadecyl bonded phases

	Solute[a]							
	1	2	3	4	5	6	7	8
Flow rate 0.5 ml min^{-1}								
k', O/T	0.35	0.36	1.11	4.55	6.93	0.69	1.41	
k', O/H	0.36	0.38	0.97	4.19	6.50	0.61	1.32	
A_s, O/T	2.6	2.5	2.4	2.3	2.4	2.8	2.5	
A_s, O/H	4.1	3.6	3.0	2.3	2.1	3.4	2.6	
h_{eff}, O/T	2600	2500	360	87	72	1200	380	
h_{eff}, O/H	4100	3400	510	85	61	1500	400	
Flow rate 1.0 ml min^{-1}								
k', O/T	0.25	—	0.98	4.04	6.92	0.69	1.41	
k', O/H	0.34	0.36	0.96	4.29	6.58	0.59	1.34	
A_s, O/T	2.6	2.8	2.3	2.3	2.3	1.9	2.4	
A_s, O/H	3.7	3.3	3.1	2.6	2.4	2.7	2.2	
h_{eff}, O/T	6000	—	360	120	58	1200	330	1
h_{eff}, O/H	3200	2800	650	150	96	1300	320	
Flow rate 1.5 ml min^{-1}								
k', O/T	0.32	0.36	0.96	4.74	6.00	0.68	—	
k', O/H	0.32	0.34	0.89	4.06	6.26	0.53	1.26	
A_s, O/T	2.8	3.2	2.8	2.5	1.8	2.9	—	
A_s, O/H	3.8	3.6	2.0	2.0	1.8	2.7	2.3	
h_{eff}, O/T	2900	3200	560	140	110	1500	—	1
h_{eff}, O/H	4300	3300	450	92	88	1300	460	1
Flow rate 2.0 ml min^{-1}								
k', O/T	0.31	—	—	4.74	7.28	—	—	
k', O/H	0.30	0.26	0.93	4.20	6.37	—	—	
A_s, O/T	2.5	4.4	4.3	3.3	3.0	—	—	
A_s, O/H	3.1	3.2	2.8	2.6	2.0	—	—	
h_{eff}, O/T	3800	—	—	260	250	—	—	1
h_{eff}, O/H	3200	4400	580	170	130	—	—	1

$k' = (t_R - t_0)/t_0$, $h_{eff} = (m^2 L/(d_p t_0^2 k'^2)$, A_s = B/A at 10% per min.

[a]Solutes: (1) phenol, (2) aniline, (3) benzene, (4) anthracene, (5) pyrene, (6) 2-picoline, (7) 2-*p*-tolylpyridine, (8) 2,6-di-*t*-butylpyridine.

quite appropriate, however, for comparing the TMCS-capped column (O/T) to the HMDS-capped column (O/H).

Several interesting trends can be seen in these data. Retention is generally less in the HMDS end-capped column that in the TMCS end-capped column. Efficiency as measured by the effective reduced plate height is greater for the solutes with greater retention for the O/H column than the O/T column. Peak asymmetry values are generally greater for the O/H column, with the tailing for phenol (a hydrogen bond donor) being greater, except for the values at the 2.0 ml min^{-1} flow rate, than the tailing for aniline (a hydrogen bond acceptor). This order is reversed for the O/T column, with aniline exhibiting greater tailing than phenol. It is also interesting to note the differences in retention between sodium nitrate, used here as an estimate of t_0, and deuterium oxide (Table 3). While the retention volumes are essentially the same for sodium nitrate for both phases and all flow rates (except at 2.0 ml min^{-1} for the O/H column), retention of D_2O is greater than that of sodium nitrate on both phases and greater on O/H than on O/T.

Although the two stationary phases were packed in the same column, and identical operating conditions, equipment, and mobile phase was used for both, it is possible that the differences observed are due to extra-column and/or other effects such as packing efficiency rather than some real chemical difference between the two phases. Therefore, the plate height analysis method of Horvath and Lin [28] was used to evaluate the kinetic contribution (i.e., the contribution of the actual sorption-desorption kinetics, not other kinetic processes such as mass transfer) to the total band broadening. The applicability of the method was tested by plots of the second moment of the solute peaks vs. the k' values. Linear plots with acceptable correlation coefficients (greater than 0.99) were obtained for all except the values obtained at the 1.0 ml min^{-1} flow rate. The results from this flow rate were therefore not used. Given the many restrictions on the method [28], and the fact that irregularly shaped silica particles were used, the calculation of absolute values for the various contributions was not attempted. It is sufficient for this study to compare the kinetic contribution of one phase to the other. This was done by fitting effective plate height to k' values via non-linear

TABLE 3

Retention volumes (ml) of sodium nitrate and D_2O

	Flow rate (ml min^{-1})			
	0.5	1.0	1.5	2.0
$NaNO_3$, O/T	1.05	1.05	1.07	1.06
D_2O, O/T	1.08	1.15	1.17	1.16
$NaNO_3$, O/H	1.05	1.07	1.08	1.13
D_2O, O/H	1.25	1.20	1.20	1.26

regression to the second degree polynomial to determine values of the three coefficients of Eqn. (1)

$$h_{eff} = a + 2b/k' + c/k'^2 \quad (1)$$

The difference $a - b$ was determined for both phases. The kinetic contribution to the total broadening is given [28] by

$$h_{kin} = R'[a - b - (1 + k_0)h_0/k_0] \quad (2)$$

Assuming that the non-sorbed tracer term is the same for both and negligible, the difference

$$h_{kinH} - h_{kinT} = R_H(a_H - b_H) - R_T(a_T - b_T) \quad (3)$$

is consistently large and positive for O/H — O/T for all solutes, indicating that the efficiency of the O/H phase itself is less than that of the O/T phase. Representative values are given in Table 4. In Eqns. (2) and (3), $R_i = [k'_i/(1 + k'_i)]^2$.

DISCUSSION

The luminescence and photoacoustic results together suggest that end-capping with HMDS produces a surface that is more heterogeneous than end-capping with TMCS, despite the decrease in polarity (presumably via reduction of the number of surface silanols) in going from DS/OD to DS/OD/T to DS/OD/H. The marked red-shift in emission and blue-shift in photoacoustic maximum in going from DS to DS/OD may indicate an enhancement of dansyl chain associations with each other. Attachment of octadecyl chains to the surface, though lowering the average polarity of the surface, may be sterically hindered within the boundaries of a cluster of dansyl chains, thus the local polarity of the dansyl clusters may actually increase, perhaps with the formation of excimers [10]. End-capping with TMCS lowers the polarity, perhaps because the less bulky reagent can penetrate these clusters. The HMDS lowers the polarity even further, probably because of its higher reactivity. The magnitude of the red-shift in the photoacoustic maximum in going from DS/OD/T to DS/OD/H, and the increase in heterogeneity noted above, suggest the formation of basic species on the surface (perhaps via chemisorption of ammonia generated from the reaction of HMDS with surface silanols) that are not removed despite thorough washing.

TABLE 4

h_{kin} (O/H) — h_{kin} (O/T) for several test solutes

Solute	Flow rate (ml min^{-1})		
	0.5	1.5	2.0
Benzene	95	210	—
Anthracene	240	—	360
2,6-Di-*t*-butylpyridine	280	690	420

The chromatographic results support the notion that a basic species is bound to the surface when HMDS is used as an end-capping reagent. Elemental determination of chlorine and nitrogen in the two materials showed low but detectable (about 0.1% by weight) levels of nitrogen on the O/H material but no detectable chlorine on the O/T material. Addition of a methanol solution of the dansyl model compound to a suspension of the chromatographically-studied silicas yielded emission maxima of 494 nm for O/H and 498 nm for O/T, indicating that the polarity difference between the chromatographic phases is comparable to the polarity differences observed for the dansyl silicas (see Table 1). In conclusion, the slight improvement in peak tailing for the more retained solutes, particularly the substituted pyridines, suggests that end-capping with HMDS may actually be the method of choice for the separation of basic solutes, whereas TMCS should be used for acidic or neutral solutes.

This work was supported, in part, by a grant (to CHL) from the National Science Foundation CHE-8119600. The Partisil-10 used was made available from the reference substrate collection at Duke University founded by a gift from Whatman-Reeve Angel. Aliquots from this collection are available to serious researchers upon application.

REFERENCES

1 L. R. Snyder, Principles of Adsorption Chromatography, M. Dekker, New York, 1968.
2 E. Soczewinski and W. Golkiewicz, Chromatographia, 6 (1973) 269.
3 L. R. Snyder and H. Poppe, J. Chromatogr., 184 (1980) 363.
4 R. P. W. Scott and P. Kucera, J. Chromatogr., 112 (1975) 425.
5 Cs. Horvath, W. Melander and I. Molnar, J. Chromatogr., 125 (1976) 129.
6 Cs. Horvath and W. Melander, J. Chromatogr. Sci., 15 (1977) 393.
7 E. H. Slaats, J. C. Kraak, W. J. T. Brugman and H. Poppe, J. Chromatogr., 149 (1978) 255.
8 Cs. Horvath, W. Melander and A. Nahum, J. Chromatogr., 186 (1979) 371.
9 A. Nahum and Cs. Horvath, J. Chromatogr., 192 (1980) 315.
10 C. H. Lochmüller, D. B. Marshall and D. R. Wilder, Anal. Chim. Acta, 130 (1981) 31.
11 G. Martini, J. Colloid Interface Sci., 80 (1981) 39.
12 G. Martini and L. Burlamacchi, J. Phys. Chem., 83 (1979) 2505.
13 G. Martini and V. Bassetti, J. Phys. Chem., 83 (1979) 2511.
14 M. Holik and B. Matejkova, J. Chromatogr., 213 (1981) 33.
15 D. E. Leyden, D. S. Kendall and T. G. Waddell, Anal. Chim. Acta, 126 (1981) 207.
16 D. W. Sindorf and G. E. Maciel, J. Am. Chem. Soc., 103 (1981) 4263.
17 C. H. Lochmuller, D. B. Marshall and J. M. Harris, Anal. Chim. Acta, 131 (1981) 263.
18 L. Boksanyi, O. Liardon and E. Sz. Kovats, Adv. Colloid Interface Sci., 6 (1976) 95.
19 V. Ya. Davydov, L. T. Zhuravlev and A. Kiselev, Russ. J. Phys. Chem., 38 (1964) 1108.
20 A. V. Kiselev and V. I. Lygin, Infrared Spectra of Surface Compounds, Wiley—Interscience, New York, 1975.
21 D. Heidrich, D. Volkmann and B. Zurawski, Chem. Phys. Lett., 80 (1981) 60.
22 M. B. Evans, A. D. Dale and C. J. Little, Chromatographia, 13 (1980) 5.
23 J. M. McCall, J. Med. Chem., 18 (1975) 549.
24 C. H. Lochmüller, S. F. Marshall and D. R. Wilder, Anal. Chem., 52 (1980) 19.

25 C. H. Lochmüller and D. R. Wilder, Anal. Chim. Acta, 116 (1980) 19.
26 C. H. Lochmüller and D. R. Wilder, Anal. Chim. Acta, 118 (1980) 101.
27 W. E. Barber and P. W. Carr, Anal. Chem., 53 (1981) 1939.
28 Cs. Horvath and H.-J. Lin, J. Chromatogr., 149 (1978) 43.

Analytica Chimica Acta, 142 (1982) 73—87
Elsevier Scientific Publishing Company, Amsterdam — Printed in The Netherlands

PRECONCENTRATION METHODS FOR THE DETERMINATION OF TRACE ELEMENTS IN WATER BY X-RAY FLUORESCENCE SPECTROMETRY
Part 1. Response Characteristics

ANDREW T. ELLIS and DONALD E. LEYDEN*
Colorado State University, Fort Collins, CO 80523 (U.S.A.)
WOLFHARD WEGSCHEIDER
Technical University, Graz (Austria)
BRUCE B. JABLONSKI
Shell Development, Houston, TX 77001 (U.S.A.)
WILLIAM B. BODNAR
Storage Technology Corporation, Boulder, CO 80309 (U.S.A.)
(Received 22nd March 1982)

SUMMARY

Seven methods for the preconcentration of the elements Cr, Mn, Fe, Co, Ni, Cu, Zn, As, Se, Ag, Cd, Sb, Hg, Tl, and Pb in trace quantities from water have been evaluated. All the methods involved incorporation of the dissolved species into a solid resulting in large concentration factors and yielded samples well-suited to quantitation by either energy- or wavelength-dispersive x-ray fluorescence. On the basis of measurable criteria such as method sensitivity, linear range, and overall reproducibility, a scheme for ranking the seven methods is proposed. Application of such a rating scheme has enabled an objective, critical comparison of the available methods to be made on the basis of performance characteristics.

As the amount and diversity of the anthropogenic input to the environment changes, so too does the demand upon analytical techniques to monitor environmental changes. This is particularly so in the case of trace (heavy) metals in the natural and processed water systems where the balance between biological toxicity and dietary necessity is narrow and frequently ill-defined. It is, therefore, becoming necessary to determine a wide range of elements at ever lower concentrations in an increasingly wide variety of samples. In addition, improved accuracy and precision are constantly being sought. In recent years, the use of atomic absorption spectrometry [1] (a.a.s.) with either conventional flame or electrothermal atomization has enabled the widespread, routine determination of many elements, especially metals, in the low mg l^{-1} and $\mu g\ l^{-1}$ ranges, respectively. However, with

0003-2670/82/0000-0000/$02.75

the large number of elements now being requested for determination in any one particular sample the difficulty of implementing multielement analyses by a.a.s. is becoming an increasing limitation of that method. The more recent and highly successful introduction of atomic emission spectrometry (a.e.s.) using inductively-coupled plasma (i.c.p.) sources shows most of the benefits of a.a.s. with the additional advantage of simultaneous multielement determination capability [2]. This latter advantage may be brought about either in a truly simultaneous mode through the use of detector arrays (as in more classical arc/plasma spectrometry) or by the use of rapid-scan sequential element determination. By using these approaches it is possible to determine up to 40 elements over very wide linear working ranges down to the $\mu g\, l^{-1}$ level. Despite these advances, multielement determination in natural water samples in the low $\mu g\ l^{-1}$ (ppb) range is not without problems. Many of the difficulties arise from the complex matrices frequently encountered in environmental samples. Other techniques such as neutron activation—γ-spectrometry and spark-source mass spectrometry (s.s.m.s.) are multielement techniques which must be considered. However, these techniques are plagued by slow turn-around times and low sample through-put as well as lack of general instrument availability.

The multielement capability of a.e.s. is a significant advantage which is shared by comparatively few other analytical techniques. Energy-dispersive x-ray fluorescence spectrometry (e.d.x.r.f.) is one such technique applicable to all elements with atomic number greater than eleven. Unfortunately, e.d.x.r.f. has insufficient sensitivity for the determination of trace amounts of the elements. If this technique is to be used for the determination of trace elements in water, then a preconcentration step is mandatory. This may not be such a disadvantage as by its very nature, preconcentration may yield a sample less subject to potential matrix interferences. It is methods of preconcentration for x-ray spectrometry and particularly e.d.x.r.f. which are addressed in this paper. The justification for the emphasis of e.d.x.r.f., rather than the wavelength-dispersive technique lies in the fact that to be competitive, a variety of operating conditions such as x-ray tube changes are required for wavelength-dispersive x-ray fluorescence (w.d.x.r.f.). Although modern w.d.x.r.f. instrumentation is operated under computer control, the instruments by their very nature are not well suited for simultaneous measurements.

There are many published methods available for the preconcentration of environmentally important elements [3, 4]. Of these seven have been selected for extensive comparison. These seven were selected as they had been previously reported to perform well in natural water samples, and were capable of forming homogeneous thin-film samples well-suited to x-ray analysis. This latter benefit meant that such samples would not suffer from matrix or interelement absorption/enhancement effects yielding much simpler spectral analysis and quantification.

Other factors were also considered in the selection such as simplicity of procedure, ruggedness of the method toward variation resulting from different analysts, and availability of reagents and materials. In some cases, a method was selected because it was specifically developed and reported for the determination of trace elements in environmental waters by x-ray spectrometry. In some cases, a method was rejected because evaluation of literature data showed a high degree of interelement interference or because the chemical capacity was too low to permit reasonable application to diverse environmental samples. It is beyond the scope of this report to review all such methods and the arguments for the individual selection [2]. The methods chosen for evaluation used several different chemical approaches that include:

(1) precipitation by a dithiocarbamate salt [5, 6, 7]; (2) complexation by 8-quinolinol (oxine) and adsorption of the complexes on activated carbon [8, 9]; (3) complexation by a dithiocarbamate immobilized on controlled pore glass [10, 11]; (4) precipitation with the combined reagents thionalide/poly(vinylpyrrolidone) [12]; and (5) filtration through a cation-exchange resin-impregnated filter paper [13, 14].

These methods were evaluated in their published forms on the basis of the following criteria: (a) ability to form a homogeneous thin-film sample; (b) number of elements on the EPA Priority Pollutants [15] list recoverable; (c) extent of calibration range; (d) linearity of calibration; (e) overall method precision; (f) applicability to natural water samples; (g) general analytical utility, ruggedness and availability of reagents and materials.

From the results of the critical comparison of the methods with regard to the above criteria, it is possible to propose a procedure for ranking the methods considered. Rankings resulting from these procedures have been found to agree closely with the order of merit found intuitively during the evaluation study. The work reported here presents the results of response evaluation of all the methods outlined and indicates the optimum method as determined by the response criteria proposed above. The evaluation of each method for its ability to withstand potential interferences is detailed in Part 2 of this series [16].

EXPERIMENTAL

Reagents and materials

Standard aqueous solutions (1000 mg l^{-1} as the metal) were prepared, whenever possible, by dissolution of the pure metal or oxide in nitric acid with the exceptions of $NiCl_2 \cdot 6H_2O$, $AgNO_3$, $Pb(NO_3)_2$, $TlNO_3$, and $Mn(NO_3)_2 \cdot 6H_2O$ ("Gold Label", Aldrich Chemical Co.). Final acid concentrations were 1% (v/v) and acids of the highest purity were used throughout (Ultrex, J. T. Baker). Carbon-filtered and double-deionized water was used for dilution. Solutions and samples were stored in acid-washed (50% nitric acid, 1 week) linear polyethylene containers.

Poly(vinylpyrrolidone) was obtained as a dry powder (type NP-K90, GAF Corp., 140 W. 51st Street, New York, NY 10020) of average molecular weight 360 000. Activated carbon (Merck) was purified according to a previously published method [17]. Controlled pore glass 200—400 mesh (CPG-10, ElectroNucleonics, Fairfield, NJ) having a nominal particle diameter of 7.5 μm, pore volume of 4.0 ml g^{-1} and a surface area of 110 m^2 g^{-1} was used as substrate for the immobilization of *N*-β- aminoethyl-γ-aminopropyltrimethoxysilane (Z6020, Dow-Corning) as described previously [10, 18]. The resulting surface-bound amine yielded an exchange medium with a capacity of 0.5 mmol g^{-1} Cu^{2+}. Subsequent reaction of the bonded amine with carbon disulfide yielded the bis-dithiocarbamate functionality. Membrane filters (25-mm diameter, 0.45-μm pore size; GA-6, Gelman Sciences, Ann Arbor, MI 48106) were used to collect precipitates. Strong acid cation-exchange resin-impregnated filter papers (SA-2, Reeve-Angel, Clifton, NJ) were prewashed with three 40-ml aliquots of saturated brine followed by 5 ml of deionized water. This procedure ensured presence of the resin in the Na^+ form and removed most of the copper and iron contamination generally found in the filters.

Apparatus

Wavelength-dispersive x-ray spectra were collected using a Philips Model PW-1410 spectrometer. The choice of Mo, Cr, or W anode x-ray tubes, tube voltage and filament current was optimized for each element. A LiF 200 analyzing crystal in conjunction with a proportional gas flow (operated at 1.6 kV) and/or scintillation detector was used. Counting times were usually 100 s but never exceeded 200 s, and instrument control was under an APPLE II (Apple Computer, Inc.) computer [19].

Energy-dispersive x-ray analyses were done with a Spectrace 440 spectrometer (Tracor X-Ray Corporation, Mountain View, CA) in conjunction with a Si(Li) detector and interfaced to a NS880 analyzer (Tracor Northern, Middleton, WI 53562) under the control of a PDP 11/05 computer (Digital Equipment Corporation, Maynard, MA). A silver anode 50-W side window x-ray tube was operated in a pulsed mode at an anode voltage of 30 kV for all elements except mercury (40 kV) and at an anode current (usually 300 μA) ensuring a dead time of $\leqslant$50% through the whole system. For the activated carbon and CPG methods, 200 μA was used. A 0.025-mm thick silver foil filter was used to reduce spectral background. All samples, with the exception of those produced by the controlled pore glass method and blanks (1000 s) were irradiated for 200 s real time.

Thin-film samples were mounted between Mylar films (0.000025 in. thick; Chemplex Ind., Eastchester, NY 10707) in a polypropylene sample holder (Type 1430, Chemplex Ind.).

Preconcentration procedures

Sodium diethyldithiocarbamate (NaDDC). Samples (100 ml) were adjusted to pH 4 ± 0.05 and buffered with 2 ml of 0.1 M potassium hydrogenphthalate solution (pH 4); then 5 ml of aqueous 0.1% (w/v) solution of NaDDC (Baker) was added with stirring. After the precipitate had aged for 15 min, the solution was filtered under vacuum through a 25-mm 0.45-μm pore membrane filter and the filter was air-dried and mounted between Mylar films.

1-Pyrrolidinecarbodithioic acid, ammonium salt (APDC). This procedure was as for NaDDC with the exceptions that 1 ml of aqueous 1% (w/v) APDC solution was added and the precipitates were aged for 20 min before filtration.

Sodium dibenzyldithiocarbamate (DBDTC). This procedure was as for NaDDC with the exceptions that 1 ml of methanolic 1% (w/v) solution was used and precipitates were aged for a total of 30 min.

Complexation with 8-quinolinol (oxine) and adsorption of complexes on activated carbon (AC). Samples (100 ml) were adjusted to pH 8 ± 0.1 and buffered with NH_4Cl/NH_4OH solution (10 ml, pH 8). An amount of oxine solution (8 mg ml^{-1} in acetone) as determined from the recommendations of Vanderborght et al. [8, 9] was added followed by 100 mg of activated carbon. The resulting suspension was then rotated in a glass vessel on a pot mill for 1 h, after which time the activated carbon was collected by filtration of the solution through a membrane filter. The filter with the collected activated carbon was mounted between Mylar films while still moist. The lower Mylar support was perforated and the sample dried under vacuum.

Dithiocarbamate immobilized on controlled pore glass (CPG). Derivatized glass beads (200 mg) were loaded into a PTFE column (50 mm long, 4-mm i.d.) and supported at each end by polypropylene frits. Samples (100 ml) adjusted to pH 8 and buffered with NH_4Cl/NH_4OH (pH 8) solution were forced down the column under nitrogen pressure (filtration rate 30—40 ml min^{-1}, N_2 pressure 25 psi). The glass beads were then removed from the column, dried in a vacuum desiccator, homogenized and mounted between Mylar films.

Ion-exchange resin-impregnated filter papers. Samples (100 ml) were adjusted to pH 3 ± 0.05 and filtered seven times through the same 25-mm ion-exchange filter paper at a flow rate of 40 ± 10 ml min^{-1}. The air-dried filters were then mounted between Mylar films.

Precipitation with thionalide and poly(vinylpyrrolidone) (PVP). To a 100-ml sample were added 5 ml of an aqueous 0.1% (w/v) solution of PVP and 5 ml of a 0.1% (w/v) solution of thionalide (mercaptoacetic acid naphthylamide) in glacial acetic acid. The pH was adjusted to 4 ± 0.05 and the solution was filtered through a membrane filter (47-mm diameter, 0.45-μm pore size) after 15 min stirring and 5 min aging. Then 25-mm diameter sections of these filters were punched out, air-dried, and mounted between Mylar films for x-ray analysis.

Calibration curves

Single element calibrations were established over the range 0—100 μg. Twenty-one standards were used for each calibration curve, five of which were reagent blanks, five of 1 μg, five of 30 μg and duplicates at each of 20, 50, and 100 μg of the element. From these data, a detection limit as defined by Currie [20], the precision at 30 μg (300 ppb), the calibration slope, linearity, and linear range were established.

RESULTS AND DISCUSSION

At the outset of a large comparison study such as the one reported here, several requirements must be identified in order to develop meaningful evaluation experiments. In this study, interest was confined to elements of environmental importance and concern as defined in the EPA Priority Pollutants List [15]. Beryllium is the exception and is not included here as routine x-ray spectrometry is unable to detect elements of such low atomic number. As the levels of elements commonly found in natural waters are concerned, the methods for preconcentration should have a linear dynamic range extending from the low (~10) μg l^{-1} (ppb) region into the low mg l^{-1} (ppm) region. The inherent specificity of the x-ray spectrometric technique means that selective preconcentration methods are largely unnecessary and even undesirable unless used to determine selected species. Thus, methods should be capable of quantitative recovery of the Priority Pollutant elements in the presence of the "macro" (Group I and IIa) elements at environmental levels. In addition to the chemical requirements, the method of choice would be one which is simple, inexpensive and insensitive to operator and laboratory variations.

The evaluation of methods has been divided into two parts: the single element response characteristics inherent to the method and the ability to withstand interference. In order to evaluate the response, three analytical criteria were chosen for study; these were (1) linear range, (2) sensitivity and (3) reproducibility.

The linear range of all the preconcentration methods is governed, at the lower limit, by the ability of the x-ray analytical instrumentation to detect the element of interest. In turn, the lower limit of detection (LLD) is influenced by the background in the spectral region of interest. This spectral background in both the energy- and wavelength-dispersive instruments arises from many sources but is principally due to scatter of the exciting radiation by the sample. This scatter becomes particularly severe as the average atomic number of the matrix decreases and may be expected to be particularly evident in the predominantly organic matrices used in this study. A limit of detection based on the standard deviation of the blank determination has been used throughout. In addition to the lower limit determined by the x-ray measurement process, the recovery of the elements of interest must be consistent at low ppb levels to permit presentation of the analyte to the

instrument. The upper limit of the range is also governed by both instrumental and chemical influences. Chemically, methods may experience limited reagent capacity, inconsistency of recovery at higher analyte concentrations and depressed recovery in the presence of other species. Instrumentally, there are few limitations at the upper limit when considering the range of analyte masses (0—100 μg) of concern in this study.

The sensitivity is very much governed by chemical and spectroscopic factors. Sensitivity in the context used here is defined in units of x-ray counts per second per μg of analyte element (cps μg^{-1}). The recovery of an element has a direct effect on the amount of material irradiated and the effect of this is serious but obvious. The matrix in which the element is bound will influence sensitivity as will the instrumental parameters for the two spectrometer types used.

Energy-dispersive x-ray spectrometer (e.d.x.r.f.). The main parameters controlling sensitivity are anode material, tube voltage and current, and primary filter characteristics. Provided that these parameters are standardized, then the mass absorption coefficient of the analyte element at the effective excitation energy of the source governs overall sensitivity. Thus, the lower the element analytical line absorption edge lies below the excitation energy the lower is the sensitivity (for the same spectral series).

Wavelength-dispersive x-ray spectrometer (w.d.x.r.f.). The parameters are similar in this case but the ability to influence sensitivity of any one element is increased by greater instrument flexibility. In particular, the choice of analyzing crystal and detector type along with the higher x-ray tube powers obtainable and the higher input count rate tolerance usually results in higher sensitivity and extended linear range for this instrument when compared to e.d.x.r.f. Inevitably, the sensitivity influences the LLD, thus, the higher the sensitivity, then, usually the lower the LLD.

The reproducibility of a method is reflected in the percent relative standard deviation (% RSD = $S/\bar{x} \times 100$) of replicate determinations. The level of this determination must be consistent for all methods and has been standardized to 300 ppb in this instance. All other factors being equal, the lower the % RSD the better the method. In particular, the % RSD of blank determinations governs the LLD of a method. The reproducibility generally deteriorates with each stage of sample handling and each of these increases in % RSD is difficult to predict. Spectroscopically, the actual precision is governed by well-defined statistics of counting and can be predicted. Overall method reproducibility is better obtained experimentally by replicate determinations and will incorporate all effects into the figure of merit obtained. Precision obtained in this way yields a figure more amenable to an inter-method comparison study. The three analytical criteria/figures of merit have been determined for each method and element using both wavelength and energy dispersive x-ray spectrometric techniques. The results of these single element/method evaluations are collected in Table 1. In this table, the general trend of higher w.d.s. sensitivity is seen, but it may be better to treat the figures of merit method by method.

TABLE 1

Figure of merit data for preconcentration methods

Method			Cr	Mn	Fe	Co	Ni	Cu	Zn	As	Se	Ag	Cd	Sb	Hg	Tl	Pb
AC	E.d.x.r.f.	Sens.[a]	0.4	0.6	0.9	0.9	2.3	1.6	3.4	NR[d]	NR	**[e]	**	0.1	1.2	0.4	1.5
		LLD[b]	1.7	1.4	8.6	0.4	8.1	2.0	3.9	NR	NR	**	**	25.0	1.5	1.8[f]	0.8
		%RSD[c]	13.4	10.1	12.4	10.7	6.4	12.0	13.7	NR	NR	**	**	5.9	3.4	20.5	5.5
	W.d.x.r.f.	Sens.	35.8	48.4	7.9	5.1	12.0	2.0	3.4	NR	NR	1.9	2.0	1.5	10.0	4.6	11.0
		LLD	1.3	0.3	8.9	0.5	2.3	6.0	4.9	NR	NR	1.8	2.6	6.8	0.6	1.3[f]	0.7
		%RSD	5.0	2.8	11.7	6.8	7.5	6.6	4.7	NR	NR	2.9	14.8	12.6	9.5	10.7	3.4
APDC	E.d.x.r.f.	Sens.	NR	NR	2.9	2.1	4.7	5.6	2.5	9.4	8.2	**	**	0.2	3.8	NR	3.0
		LLD	NR	NR	0.3	0.4	1.7	0.4	0.3	0.3	0.6	**	**	14.0	0.3	NR	0.5
		%RSD	NR	NR	4.8	4.5	5.5	5.5	10.9	6.4	6.8	**	**	27.0	6.1	NR	4.7
	W.d.x.r.f.	Sens.	NR	NR	15.8	20.0	19.0	12.0	19.0	15.0	24.0	2.2	2.4	2.2	12.0	NR	14.0
		LLD	NR	NR	0.3	0.3	1.5	0.8	0.3	0.5	2.6	3.9	2.8	3.0	0.3	NR	0.4
		%RSD	NR	NR	3.4	3.4	4.2	6.3	8.0	4.1	7.3	4.5	10.9	6.8	4.1	NR	3.1
CPG	E.d.x.r.f.	Sens.	0.3	0.2	0.4	1.1	1.5	0.8	2.1	NR	NR	**	**	1.2	0.5	1.5	0.6
		LLD	1.8	2.7[f]	4.3	0.8	0.5	1.0	2.1	NR	NR	**	**	2.6[f]	1.3	2.0	3.3
		%RSD	10.7	12.5	19.7	9.9	8.5	11.5	11.0	NR	NR	**	**	15.0	8.5	8.9	7.0
	W.d.x.r.f.	Sens.	2.4	6.2	2.9	5.1	4.3	4.3	4.1	NR	NR	1.3	1.4	1.4	5.7	8.7	4.3
		LLD	1.6	0.5[f]	2.6	0.3	0.9	1.0	0.9	NR	NR	6.0	4.3	5.0[f]	0.8	0.7	2.3
		%RSD	11.1	5.9	24.2	4.1	11.6	7.9	10.2	NR	NR	4.3	11.4	7.8	8.7	11.8	8.0
DBDTC	E.d.x.r.f.	Sens.	NR	1.3	2.2	2.9	3.3	3.6	3.7	6.2	6.2	**	**	1.0	2.7	0.9	2.3
		LLD	NR	0.4	0.4	0.2	0.2	0.4	0.4	0.2	0.3	**	**	1.0	0.4	1.1	0.6
		%RSD	NR	2.9	3.0	4.0	3.0	2.2	4.6	3.8	4.8	**	**	5.0	4.2	2.3	7.0
	W.d.x.r.f.	Sens.	NR	16.0	4.4	8.2	11.1	12.2	24.0	9.1	8.9	4.5	4.0	4.9	2.7	7.4	3.4
		LLD	NR	0.3	3.4	0.3	0.3	0.9	0.4	0.8	0.4	2.0	2.1	0.9	0.6	0.7	0.8
		%RSD	NR	5.7	9.9	6.9	1.6	4.6	5.0	7.6	4.8	8.0	28.9	2.3	4.2	5.2	3.1
NaDDC	E.d.x.r.f.	Sens.	NR	NR	2.1	5.7	5.4	7.6	3.8	NR	NR	**	**	1.0	2.6	NR	3.9
		LLD	NR	NR	0.9[f]	0.4	0.3	0.5	2.2	NR	NR	**	**	20.0	0.4	NR	0.2
		%RSD	NR	NR	4.9	4.5	1.6	9.1	11.9	NR	NR	**	**	7.0	13.0	NR	5.6

	W.d.x.r.f.	Sens.	NR	NR	19.3	5.5	5.3	2.6	10.0	NR	NR	2.3	2.5	2.1	7.7	NR	16.0
		LLD	NR	NR	0.9[f]	0.5	0.3	0.4	1.4	NR	NR	2.3	3.5	4.6	0.7	NR	0 2
		%RSD	NR	NR	5.5	8.8	6.5	4.4	9.7	NR	NR	5.1	10.4	17.4	17.6	NR	5.7
PVP-T	E.d.x.r.f.	Sens.	NR	NR	NR	NR	NR	1.1	NR	0.3	3.0	**	**	NR	1.2	NR	0.8
		LLD	NR	NR	NR	NR	NR	1.7[f]	NR	8.3	0.4	**	**	NR	1.6	NR	3.9
		%RSD	NR	NR	NR	NR	NR	8.0	NR	13.0	3.0	**	**	NR	3.0	NR	22.0
	W.d.x.r.f.	Sens.	NR	NR	NR	NR	NR	1.7	NR	0.8	1.4	0.7	NR	NR	1.2	NR	1.3
		LLD	NR	NR	NR	NR	NR	2.5[f]	NR	13.0	1.5	17.5	NR	NR	1.5	NR	5.3
		%RSD	NR	NR	NR	NR	NR	5.7	NR	18.0	3.1	19.0	NR	NR	6.0	NR	20.2
SA-2	E.d.x.r.f.	Sens.	0.6	0.9	1.4	3.5	3.0	4.9	3.3	NR	NR	**	**	NR	0.2	1.6	2.9
		LLD	0.3	0.4	0.1	0.4	0.5	3.0	2.8	NR	NR	**	**	NR	13.0	0.6	0.5
		%RSD	5.8	4.6	12.7	6.0	7.0	13.0	6.0	NR	NR	**	**	NR	21.0	12.0	14.4
	W.d.x.r.f.	Sens.	55.9	32.5	14.2	7.0	10.0	12.0	3.0	NR	NR	1.4	2.2	NR	0.7	12.0	14.0
		LLD	0.2	0.5	1.9	0.6	1.2	1.0	9.6	NR	NR	6.0	4.0	NR	4.0	0.6	0.6
		%RSD	6.3	4.3	12.5	4.8	3.2	13.0	4.9	NR	NR	15.0	6.4	NR	14.4	10.2	14.9

[a]Sensitivity, i.e., the slope (cps μg^{-1}) of the single element calibration line. [b]Lower limit of detection as defined by Currie [20]. [c]% Relative standard deviation as determined from 5 replicate samples at 300 $\mu g\ l^{-1}$. [d]NR, Not recovered. [e]Not determined because of e.d.s. anode material (Ag). [f]Linear ranges extend only to 50 μg; but 100 μg in all other cases.

Chelation with 8-quinolinol and adsorption on activated carbon (AC)

The ability of oxine to recover several elements from aqueous solution is well-known as is its inability to recover As(III) and Se(IV). This behavior is again seen in the results of this study. Sensitivities (cps μg^{-1}) by e.d.x.r.f. are generally low partly because of the low tube current employed (200 μA) and partly because of the background correction made necessary by the large scatter from the sample. The low sensitivity for antimony and consequent high LLD are due to the enforced use of the $L_{\alpha 1}$ emission line which is very inefficiently excited by the silver K_α irradiation. The more generally low sensitivities and high limits of detection for the other elements may be attributed to two factors. Firstly, the complexed metal is diluted by the activated carbon reducing sensitivity, and secondly, the relatively low atomic number carbon matrix causes increased scatter, yielding decreased detectability as a result of the high background. This generally poor sensitivity is also reflected to some extent in the relatively high % RSD figures and the latter are compounded by problems of sample handling. The much higher x-ray sensitivities to be gained by the use of w.d.x.r.f. yield better overall performance. Despite this advantage, the % RSD remains high using w.d.x.r.f., thereby reflecting the handling difficulties experienced with the rather intractable activated carbon adsorbent.

Precipitation with 1-pyrrolidinecarbodithioic acid (APDC)

All the elements considered with the exceptions of Cr(III), Mn(II), and Tl(I) were recovered. Chromium(III) is largely inert because of the stability of the $Cr(H_2O)_6^{3+}$ species whilst Mn(II) complexes are particularly unstable and Tl(I) complexes are soluble [21]. Sensitivities by e.d.x.r.f. are good for all elements except Sb(III) (poor excitation of the L_α emission line) yielding LLD values of ca. 0.3 μg (3 ppb) and % RSD values $\leqslant 5\%$. The w.d.x.r.f. data are similar with slight benefits through the range resulting from increased x-ray sensitivity. This latter advantage is reflected in the generally good % RSD figures. In addition to the analytical advantages outlined above, the method is attractive in its simplicity, lack of practical problems, and availability of reagents.

Chelation with immobilized dithiocarbamate (CPG)

When e.d.x.r.f. was used, this method yielded even lower sensitivities than the activated carbon method. Firstly, only a 200-μA x-ray tube current was used as the low atomic number matrix caused a large amount of scatter thereby generating high dead times at the 300-μA tube current normally used. Secondly, the glass matrix dilutes the sample and generates high background which leads to reduced sensitivity and to decreased detectability, respectively. Additionally the sample is becoming relatively thick and the presence of surface coating alone causes effective volume and mass dilution of the analyte. The different elements recovered by the CPG method when compared to methods based on dithiocarbamate precipitation might be explained in the following ways.

Chromium(III) is generally not recovered at all by dithiocarbamates. Its recovery by an immobilized dithiocarbamate may be a result of factors not directly influenced by the immobilized group itself. Thus, at the high pH on the column (pH 8) significant hydrolysis of the trivalent chromium ion is to be expected. Such a hydrolyzed species may easily be adsorbed onto the unreacted/exposed surface of the siliceous substrate [22]. In addition to this, the pH is sufficiently high to form $Si—O^-$ groups on the glass surface which may themselves complex chromium species.

Manganese(II) is also not usually recovered by dithiocarbamates, but as in the case of chromium(III), extensive hydroxide formation is to be expected at pH 8 and subsequent adsorption of such species onto the support will yield a measurable recovery of manganese.

The high pH of complexation may also explain the surprising lack of recovery of both As(III) and Se(IV), as it has been found [23] that As(III) and Se(IV) are not recovered at pH $\geqslant$ 5.5 by dithiocarbamates. The relatively low recovery of copper(II) may also arise from high pH as it has been reported [23] to be difficult to form Cu(II) dithiocarbamates at pH $\geqslant$ 8. The recovery of thallium(I) by the immobilized dithiocarbamate is not surprising. Usually Tl(I) complexes are soluble [21], but the immobilization of the reagent clearly removes the possibility of complex elution.

When e.d.x.r.f. is used, sensitivities, and therefore limits of detection, are poor with LLD figures in the region of 20—30 ppb (100-ml sample). The low sensitivity accompanied by the difficulties of handling tend to result in poor (high) % RSD values in the range 10—20%. When w.d.x.r.f. is used, all the figures of merit are proportionately improved because of enhanced sensitivity but these improvements are not as large as might be expected.

Precipitation with sodium dibenzyldithiocarbamate (DBDTC)

All the elements considered, with the exception of chromium(III) are recovered by this precipitant. An advantage of DBDTC over other dithiocarbamates is the recovery of both manganese(II) and thallium(I). One is led to assume that the Mn—DBDTC precipitate is more stable than for other dithiocarbamates and that the Tl—DBDTC complex is not soluble in this instance. When e.d.x.r.f. is used, sensitivity is generally good, resulting in LLD values <0.5 μg (5 ppb) for almost all the elements considered. Additionally, method precision is good as indicated by the low % RSD figures ($\leqslant$ 5%). Data obtained by w.d.x.r.f. are similarly good with a slight improvement in sensitivity leading to lower LLD values and precision better than 5% relative. The method has all the other advantages of APDC with the exception of wide commercial availability of the reagent.

Precipitation with sodium diethyldithiocarbamate (NaDDC)

Of all the dithiocarbamate reagents used, this one recovered the least number of elements. Chromium(III), Mn(II) and Tl(I) were not recovered, for the same reasons as discussed for APDC. The inability of the reagent to

recover either As(III) or Se(IV) is less explicable and was entirely unexpected. When e.d.x.r.f. was used, all elements showed good sensitivity because of the very thin precipitate films formed. Antimony(III) showed low sensitivity and high LLD for reasons discussed earlier, whilst zinc(II) showed poor and variable recovery reflected in low sensitivity, high LLD and poor reproducibility. Precision was, in general, approximately 5% relative for the K_α lines but was higher for the L_α analyte lines (Sb, Hg, Tl and Pb). When w.d.x.r.f. was used, a similar performance was observed with little or no advantage to be gained, indicating the method constraints to be of a chemical rather than spectroscopic nature.

Precipitation with poly(vinylpyrrolidone) and thionalide (PVP-T)

Of all the methods considered, PVP-T recovered the least number of elements, only six out of the fifteen studied. Previous reports indicated more elements to be recovered; but this was found not to be the case in this study even after attempts by several people and after consultation with one of the original authors [12]. Thionalide has suitable vacant orbitals on the sulfur atom such that back-bonding from the coordinated metal is possible and, indeed, preferred. Thus, metals with filled *d*-orbitals (i.e., not transition metals) are favored for bonding with the ligand. Of the first transition series only copper(I) is expected to form complexes on the basis of the above criterion. Of the elements which might be expected to form stable complexes (Ag, Cd, Hg(II), Tl, Pb, As, Se, and Sb), only Cd, Sb and Tl were found not to do so. The presence of PVP appears to change little of these thionalide properties. In general, the sensitivity for the elements which were recovered was low for both x-ray spectrometric methods and is the result of two effects. Primarily, the need to filter the precipitates through a 47-mm diameter filter in order to obtain reasonable ($<$1 h) filtration times and then cut this down to fit a 32-mm sample holder resulted in discarding 54% of the analyte material. Secondly, the recovery of some elements was frequently less than quantitative, though reproducibly so. Largely because of these low sensitivities the LLD figures are high ($\geqslant$20 ppb). Observed % RSD figures are, for both instrumental finishes, similar and range from 3 to 20% relative, the majority of the imprecision arising from sample handling.

Collection on cation-exchange resin-impregnated filter papers (SA-2)

The strong acid cation exchanger used in this filter paper was able to preconcentrate all the elements considered which exist as cations in solution. Thus, elements existing as anions in aqueous solution [As(III), Se(IV), and Sb(III)] were not recovered. When e.d.x.r.f. was used, sensitivities were good with the exception of mercury (0.22 cps μg^{-1}) leading to LLD figures usually less than 0.5 μg ($<$5 ppb). Precision (% RSD) was generally in the 5—15% region except for mercury, for which the low sensitivity tended to result in poor performance generally. When w.d.s. was used, sensitivities were, as expected, improved. However, little improvement in precision was seen and

this tended to raise LLD figures to higher values than would be hoped for on the basis of sensitivity alone.

From the foregoing response data it is evident that each method has its merits and disadvantages. Not only are there merits and disadvantages of a purely objective nature based on meeting analytical criteria, but there are those based on more subjective criteria such as convenience, cost and simplicity. The latter are more difficult to assess but the former might be evaluated by using a figure of merit derived from assessment of analytical performance. An additional advantage of the figure of merit approach is the reduction of all the response data to manageable proportions. Such a figure of merit has been derived on the basis of the semi-empirical equation for rating, R

$$R = \sum_{i=1}^{n} \ln [(\text{linear range})/(2\pi e)^{1/2} s] \quad (1)$$

where n is the number of elements recovered, linear range is the upper calibration limit (50 or 100 μg minus LLD), and s is the standard deviation as determined at 30 μg (300 ppb).

When the response data are evaluated by using this equation one obtains the figures of merit shown in Table 2. As would be expected, the method ranking is independent of the instrument used. On the basis of the ratings in Table 2, the PVP-T method is clearly the worst, the major reason for this lying in the few elements recoverable. Two of the precipitation methods (APDC and DBDTC) are indicated as the optimum methods. This is not surprising as these methods reliably concentrate most of the elements of concern and they are particularly rugged, i.e., they present no handling problems and yield good reproducibility irrespective of the analyst. The formation of a very thin precipitate film which is then entirely irradiated leads to high sensitivities for these methods. The activated carbon, CPG, and

TABLE 2

The rating (Eqn. 1) of preconcentration methods for x.r.f. spectrometry on the basis of response characteristics

Method	Rating R			Rank
	e.d.x.r.f.	w.d.x.r.f.	Total	
AC	23	33	56	3
APDC	25	33	58	2
CPG	21	27	48	5
DBDTC	40	38	78	1
NaDDC	20	22	42	6
PVP-T	11	12	23	7
SA-2	22	28	50	4

SA-2 methods lie in an intermediate group where the techniques are widely applicable. However, because of either their dilution of the analyte (AC/CPG) or poor capacity (CPG/SA-2), they are generally inferior to the dithiocarbamate methods. In addition, the activated carbon and CPG methods are rather time-consuming and the former method has particular handling problems which are reflected in overall poor performance but especially in the lack of precision. Of the dithiocarbamates, NaDDC is anomalously poor mainly because of its inability to recover several elements. In particular its inability to recover arsenic(III) and selenium(IV) is a disadvantage and is somewhat surprising.

Conclusions

Seven published methods for the preconcentration of trace elements from aqueous solution have been evaluated for their applicability to x-ray fluorescence spectrometry. A figure of merit approach was used to evaluate the methods for their utility in the determination of fifteen environmentally important elements. The figure of merit proposed takes into account contributions from the lower limit of detection (which is, in turn, related to sensitivity) and the reproducibility of the overall method. On the basis of this figure of merit, methods based on precipitation by a dithiocarbamate have been found to be optimal. The effect of interfering species on the above methods and their ranking based on both response and interference criteria are presented in Part 2 [16].

This work was supported in part by Cooperative Agreement No. R80652-0010 from the Environmental Protection Agency and by the AMAX Foundation.

REFERENCES

1 U.S. Environ. Prot. Agency, Methods for Chemical Analysis of Water and Wastes, EPA-600/4/79-020, Washington, DC, March 1979.
2 V. A. Fassel, Anal. Chem., 51 (1979) 1291A.
3 D. E. Leyden and W. Wegscheider, Anal. Chem., 53 (1981) 1059A.
4 P. Burba and K. H. Lieser, Fresenius Z. Anal. Chem., 297 (1979) 374.
5 H. Watanabe, S. Berman and D. E. Russell, Talanta, 19 (1972) 1363.
6 J. F. Elder, S. K. Perry and F. P. Brady, Environ. Sci. Technol., 9 (1975) 1039.
7 H. Linder, H. Seltner and B. Schreiber, Anal. Chem., 50 (1978) 896.
8 B. M. Vanderborght, J. Verbeeck and R. E. van Grieken, Bull. Soc. Chim. Belg., 86 (1977) 23.
9 B. M. Vanderborght and R. E. van Grieken, Anal. Chem., 49 (1977) 311.
10 D. E. Leyden and G. H. Luttrell, Anal. Chem., 47 (1975) 612.
11 D. E. Leyden, G. H. Luttrell, A. E. Sloan and N. J. de Angelis, Anal. Chim. Acta, 84 (1976) 97.
12 R. Panayappan, D. L. Venezky, J. V. Gilfrich and L. S. Birks, Anal. Chem., 50 (1978) 1125.
13 W. J. Campbell, E. F. Spano and T. E. Green, Anal. Chem., 38 (1966) 987.

14 D. T. Carlton and J. C. Russ, X-Ray Spectrom., 5 (1976) 172.
15 U.S. Environ. Prot. Agency, Fed. Reg., 45 (2310) (1980) 79318.
16 A. T. Ellis, D. E. Leyden, W. Wegscheider, B. B. Jablonski and W. B. Bodnar, Anal. Chim. Acta, 142 (1982) 89.
17 B. Vanderborght and R. E. van Grieken, Anal. Chim. Acta, 89 (1977) 399.
18 D. E. Leyden, in T. G. Dzubay (Ed.), X-ray Fluorescence Analysis of Environmental Sciences, Ann Arbor Scientific Publ., Ann Arbor, 1977, p. 165.
19 B. B. Jablonski and D. E. Leyden, X-ray Spectrom., 10 (1981) 177.
20 L. A. Currie, Anal. Chem., 40 (1968) 586.
21 F. A. Cotton and G. Wilkinson, Advanced Inorganic Chemistry, Interscience, New York, 1972, p. 281.
22 R. K. Iler, The Chemistry of Silica, Wiley, New York, 1979, p. 659.
23 T. Török, J. Mika and E. Gegus, Emission Spectrochemical Analysis, Adam Hilger, Bristol, 1978, p. 63.

Analytica Chimica Acta, 142 (1982) 89—100
Elsevier Scientific Publishing Company, Amsterdam — Printed in The Netherlands

PRECONCENTRATION METHODS FOR THE DETERMINATION OF TRACE ELEMENTS IN WATER BY X-RAY FLUORESCENCE SPECTROMETRY
Part 2. Interference Studies

ANDREW T. ELLIS and DONALD E. LEYDEN*
Colorado State University, Fort Collins, CO 80523 (U.S.A.)
WOLFHARD WEGSCHEIDER
Technical University, Graz (Austria)
BRUCE B. JABLONSKI
Shell Development, Houston, TX 77001 (U.S.A.)
WILLIAM B. BODNAR
Storage Technology Corporation, Boulder, CO 80309 (U.S.A.)
(Received 22nd March 1982)

SUMMARY

Seven methods for the preconcentration of fifteen elements for their subsequent measurement by x-ray fluorescence spectrometry have been evaluated for their susceptibility to interferences. A two-level factorial experimental design has been used, enabling an economical and meaningful comparison of the seven methods to be made. A scheme for rating the methods on the basis of the effect of several interfering species is proposed. Use of such a scheme has enabled an objective comparison of the methods considered to yield their relative ranks. It is also shown that spectral and chemical interferences can be discerned to some extent. Combination of the response rating proposed earlier and the interference rating schemes reported here gives rise to an overall comparison and rank for the methods, allowing an objective choice of the optimal method(s) to be made.

The preceding publication [1] has detailed the evaluation and critical comparison of seven methods of preconcentration applicable in the determination of several trace elements in natural water by x-ray fluorescence spectrometry. The seven methods have been ranked on the basis of their response characteristics without regard to the effect of interferences. There are two types of interference which may be encountered, the first of which is spectral and the second chemical.

Spectral interferences in terms of partial or total peak overlap are more common in energy-dispersive than wavelength-dispersive x-ray fluorescence spectrometry. This is a direct consequence of the resolution of the former system. The possibilities for these spectral interferences are many, but are

0003-2670/82/0000-0000/$02.75

easily predictable with knowledge of the analyte matrix and the analytical conditions, and are frequently simple to correct.

Chemical interferences on the preconcentration methods are more difficult to predict and are usually more difficult to correct. Thus, results may exhibit depressed or enhanced values caused by reagent saturation or coprecipitation, respectively. In order to correct for such interferences, e.g., by the use of masking reagents, it is first necessary to assess the interference effects for each method/element/interference situation. This assessment may be achieved by using a "one-factor-at-a-time" approach. However, because of the large number of experiments required to assess interference on seven methods for fifteen elements by ten possibly interfering species, a factorial experiment design was chosen. On the basis of the data obtained from this design, it is possible to propose a method for ranking the preconcentration methods. Such a ranking method can be combined qualitatively with the rating method from the response study [1] to enable an objective choice of the optimum method to be made.

EXPERIMENTAL

Reagents, materials and apparatus

These were as reported in Part 1 [1] with the addition of reagent-grade calcium nitrate and sodium chloride.

Energy-dispersive x-ray spectra were collected by means of a Spectrace 440 spectrometer (Tracor X-Ray Corporation, Mountain View, CA) as described in Part 1.

Procedure

The preconcentration methods for each of the fifteen elements were assessed at an analyte concentration of 200 $\mu g\ l^{-1}$ (ppb). A five-fold excess (1 ppm) of the interfering species Cr, Mn, Fe, Co, Cu, Zn, Pb, and Cd was used whereas sodium chloride (salinity) was 0.5% (w/v) and calcium was at a level of 100 ppm (as Ca^{2+}). The study was done by means of a two-level factorial design with complete confounding of second and higher order effects [2, 3]. The error estimate of this procedure was derived indirectly by running an experimental unit with sixteen separate measurements for only ten potential interferents. The five additional degrees of freedom were carried along, without assigning them a specific effect, as "dummy" parameters. The results from these "dummy" parameter determinations were taken as an error estimate [4].

RESULTS AND DISCUSSION

The effects of interfering species on methods were assessed by means of a two-level factorial experimental design [2, 3]. This procedure was used in preference to a "one-factor-at-a-time" design as the former afforded

greater economy with somewhat better representation of real samples containing several potentially interfering concomitants [4]. A lower level of interferent concentration equal to zero (i.e., absence of interference) was chosen, whereas the higher level was selected to reflect a reasonable environmental level of interference. Thus, the evaluation was conducted at a level of analyte of 20 μg/100 ml (200 ppb) with the potential interferences Cr(III), Mn(II), Fe(III), Co(II), Cu(II), Zn(II), Pb(II), and Cd(II) in a five-fold excess (1 ppm). Sodium chloride was present at 0.5% (w/v) and calcium at 100 ppm. These elements and levels were chosen for their approximation to levels anticipated in water samples. Interferences were compared by using spectra collected from energy-dispersive x-ray spectrometry (e.d.x.r.f.) except in the cases of silver and cadmium where wavelength-dispersive x-ray spectrometry (w.d.x.r.f.) was used through necessity. Figures of merit were produced for each method and element/interferent interaction, and expressed as percent enhancement or suppression of the observed 200 ppb element signal.

There are general trends observable in this part of the study, but the complexity of the possible interaction makes some interpretations particularly difficult. However, one prevalent effect which is explicable and large is that of neighboring element spectral interference. This may occur basically in two possible ways, both of which are severe, but which give rise to effects of opposite sign (enhancement and suppression). The possibilities in the case of manganese are seen in Fig. 1.

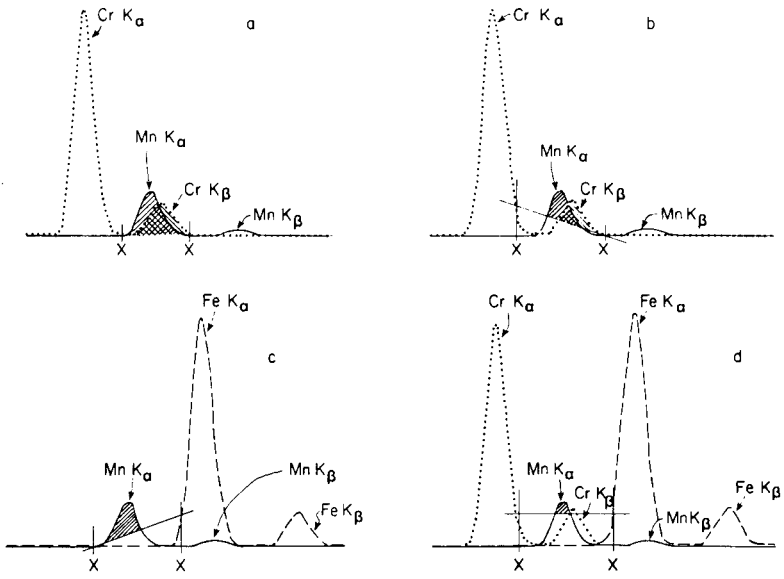

Fig. 1. (a) Effect of Cr K_β on Mn K_α (enhancement). (b, c, d) Effects of neighboring peaks on the integral Mn K_α peak above background with varying energy windows (X—X).

Figure 1(a) shows the effect of the Cr K_β on the analyte Mn K_α peak. The five-fold excess of chromium over manganese causes a large enhancement of the analyte signal. Typically, the K_β intensity is approximately 13% of the K_α intensity for elements such as Cr, Mn, and Fe. Therefore a sample consisting of 20 μg of manganese and 100 μg of chromium will give an effective Mn K_α peak enhancement equivalent to 13 μg of manganese (or 165% of expected). Other effects of neighboring spectral lines may result from the choice of energy windows for the peak-above-background integration of the analyte K_α (or L_α) peak. If these windows are chosen in the absence of interferences, then the effects shown in Fig. 1 (b, c, d) may cause suppression of the analyte peak (hatched area). These effects presuppose that the background is computed on the basis of a straight line drawn from the low to the high energy limit of the window. Thus, as the energy window is made wider, the neighboring interferent peak (5 times more intense than the analyte peak) begins significantly to affect the location of the "baseline" which is no longer computed from the true background on either side of the analyte peak, but from some way up one or more of the neighboring peaks. The effect on the net analyte peak intensity is a depression as the background is overly compensated.

There is a further special case of enhancement resulting from peak overlap, illustrated by lead and arsenic. X-ray fluorescence spectra containing the As K_α and Pb L_α peaks show direct peak superposition and enhancement effects are expected to be severe. Thus, the As K_α/Pb L_α enhancement is expected along with several neighboring K_α/K_β enhancement or adjacent K_α/K_α suppressions for the first row transition elements. There are, of course, other spectral possibilities and these will be discussed as they arise. Spectral interferences will be compounded with chemical effects (and vice versa) in some instances, but in all cases it is worthwhile to take the observed effects method by method.

Preconcentration with 8-quinolinol and adsorption on activated carbon (AC)

When this method is used, four elements (Co, Ag, Cu, and Hg) were unaffected by any of the interferents, whereas As(III) and Se(IV) were not recovered as shown in Table 1. Of the interferences, NaCl and calcium both suppressed the observed iron signal. Several interferences (Mn/Cr, Fe/Mn, Ni/Co, Ni/Cu, Zn/Cu, and Sb/Cd) were observed, all of which can be explained in terms of spectral factors outlined earlier for $Z \pm 1$ interactions. Cobalt(II) caused a depression on many analyte elements which may have been a result of the particularly effective complexation of cobalt(II) by 8-quinolinol, leading to some reagent deficiency for the analyte. Those elements for which the highest % RSD figures were observed tended to show the largest number of interferences (e.g., for w.d.x.r.f., the % RSD values were Fe = 11.7; Cd = 14.8; Sb = 12.6; Hg = 9.5; and Tl = 10.7). This perhaps indicates that those elements whose recovery is sensitive to experimental parameters suffer even wider variation when interfering species are present in excess.

Preconcentration by precipitation by ammonium pyrrolidinedithiocarbamate (APDC)

Chromium(III), Mn(II), and Tl(I) were not recovered with this precipitant and lead(II) was unaffected by all potential interferences as shown in Table 2. Of the observed interferences, the largest numerical values were in cases in which spectroscopic interference was expected (Fe/Co, Co/Fe, Ni/Co, Cu/Zn, Zn/Cu, As/Pb, and Sb/Cd). In the case of antimony, there is the possibility of overlap/interference with the Sb L_α by the Cd L_β line. Of the other interactions, copper was most affected but the variation for all the mainly "chemical" interferences was small, suggesting that the method is generally effective under the conditions studied.

Extraction onto controlled-pore glass containing immobilized dithiocarbamate (CPG)

When this method was used, neither As(III) or Se(IV) are recovered and the elements Cr, Cu, and Ag are not influenced by any of the potential interferences (Table 3). Nine possible spectroscopic effects were observed (Mn/Cr, Fe/Mn, Fe/Co, Co/Fe, Ni/Co, Ni/Cu, Zn/Cu, Sb/Cd, and Tl/Pb) and, as expected, these interactions were of large magnitude. Many interferences are noticeable in this method; several of them are largely inexplicable. For example, iron suffers from seven of nine potential interferences investigated. In general, the imprecision of the CPG method does not justify more detailed or exhaustive investigation.

Preconcentration with precipitation by dibenzyldithiocarbamate (DBDTC)

The DBDTC method did not recover chromium(III). The elements Zn, Se, Ag, Cd, Sb, Hg, and Pb were unaffected by the possible interferences studied. Of the interferences, salinity (NaCl), Ca, Cr, Mn, and Cd showed no effect. Of the few remaining observed interferences shown in Table 4, several may be due in part to spectral interference (Mn/Fe, Fe/Co, Co/Fe, Ni/Co, As/Pb, and Tl/Pb). The remaining five effects may be explicable from a chemical standpoint. In the case of cobalt, consumption of reagent by the excess of cobalt interference appears to result in a depressed recovery for a few elements. The problem of reagent competition is best illustrated with manganese as analyte where Co, Cu, and Zn are found to cause a decreased signal. This particular chemical suppression can be eliminated by increasing the amount of precipitating agent as required. When this is done, the only interference is from iron which depresses the manganese signal by 27% and may be a result of spectral proximity as discussed earlier. The reason that manganese is subject to the most severe chemical interferences (depression) is assumed to result from the instability of the Mn—dibenzyldithiocarbamate complex.

TABLE 1

Effect of interferences on the determination of several elements with preconcentration by 8-quinolinol and activated carbon

Interferent	Cr	Mn	Fe	Co	Ni	Cu	Zn	As	Se	Ag	Cd	Sb	Hg	Tl	Pb
NaCl	0	0	−12	0	0	0	0	*	*	0	13	0	0	4.6	0
Ca	−14	0	−13	0	0	0	0	*	*	0	−9.9	0	0	0	0
Cr	**	−61	0	0	−10	0	5	*	*	0	0	0	0	0	0
Mn	0	**	−11	0	−9.5	0	0	*	*	0	−13	12	0	4.6	0
Fe	40	0	**	0	0	0	0	*	*	0	0	0	0	0	0
Co	0	0	0	**	−33	0	0	*	*	0	−10	−13	0	−4.4	−6.6
Cu	0	0	0	0	9.9	**	−21	*	*	0	0	0	0	0	−7
Zn	0	0	0	0	0	0	**	*	*	0	0	0	0	−7.8	0
Cd	0	0	0	0	0	0	0	*	*	0	**	−34	0	0	0
Pb	0	0	0	0	0	0	0	*	*	0	17	0	0	0	**

*Not recovered. **Not possible.

TABLE 2

Effect of interferences on the determination of several elements by ammonium pyrrolidinedithiocarbamate

Interferent	Cr	Mn	Fe	Co	Ni	Cu	Zn	As	Se	Ag	Cd	Sb	Hg	Tl	Pb
NaCl	*	*	−7.5	0	0	−2	0	0	−20	0	0	0	0	*	0
Ca	*	*	0	0	0	−3.4	0	0	0	0	−12	0	0	*	0
Cr	**	*	17	0	0	−3.5	0	0	18	2.6	−12	0	0	*	0
Mn	*	**	0	−3	−8.5	0	0	0	0	0	−13	0	0	*	0
Fe	*	*	**	−3.5	0	−4	10	−7	0	−2.4	0	0	0	*	0
Co	*	*	−23	**	−67	−5.5	0	0	0	−3.6	11	0	0	*	0
Cu	*	*	0	0	0	**	−24	−5	−9.2	0	0	0	0	*	0
Zn	*	*	0	0	0	−3.7	**	0	0	0	0	−7.6	−2.8	*	0
Cd	*	*	−14	−3	−8.7	−6.9	0	0	0	0	**	−55	0	*	0
Pb	*	*	0	3.7	0	−1.3	0	106	0	0	0	12	0	*	**

*Not recovered. **Not possible.

TABLE 3

Effect of interferences on the determination of several elements by preconcentration with dithiocarbamate immobilized on controlled pore glass

Interferent	Cr	Mn	Fe	Co	Ni	Cu	Zn	As	Se	Ag	Cd	Sb	Hg	Tl	Pb
NaCl	0	0	−11	34	0	0	0	*	*	0	0	−9.7	0	−9.8	31
Ca	0	0	32	28	9.6	0	0	*	*	0	19	0	0	−8.9	26
Cr	**	35	−13	−29	0	0	0	*	*	0	−13	0	20	0	0
Mn	0	**	−10	0	13	0	−15	*	*	0	0	0	0	0	0
Fe	0	0	**	40	9	0	15	*	*	0	9.5	0	−12	0	0
Co	0	0	−10	**	−31	0	−25	*	*	0	0	−8	0	12	0
Cu	0	−29	7.6	0	−6.9	**	−28	*	*	0	0	0	0	0	0
Zn	0	0	0	0	0	0	**	*	*	0	0	0	0	−10	0
Cd	0	0	0	−16	0	0	0	*	*	0	**	−57	−12	0	0
Pb	0	−31	−7.5	−14	−7.4	0	0	*	*	0	8.7	0	0	−28	**

*Not recovered. **Not possible.

TABLE 4

Effect of interferences on the determination of several elements with preconcentration by sodium dibenzyldithiocarbamate

Interferent	Cr	Mn	Fe	Co	Ni	Cu	Zn	As	Se	Ag	Cd	Sb	Hg	Tl	Pb
NaCl	*	0	0	0	0	0	0	0	0	0	0	0	0	0	0
Ca	*	0	0	0	0	0	0	0	0	0	0	0	0	0	0
Cr	**	0	0	0	0	0	0	0	0	0	0	0	0	0	0
Mn	*	**	0	0	0	0	0	0	0	0	0	0	0	0	0
Fe	*	−32	**	30	0	0	0	0	0	0	0	0	0	0	0
Co	*	−21	−29	**	−49	−39	0	0	0	0	0	0	0	0	0
Cu	*	−33	−14	0	0	**	0	0	0	0	0	0	0	0	0
Zn	*	−17	0	0	0	0	**	0	0	0	0	0	0	0	0
Cd	*	0	0	0	0	0	0	0	0	0	**	0	0	0	0
Pb	*	0	0	0	0	0	0	0	0	0	0	0	0	164	**

*Not recovered. **Not possible.

Preconcentration by precipitation with sodium diethyldthiocarbamate (NaDDC)

As shown in Table 5, five elements (Cr, Mn, As, Se, and Tl) were not recoverable with NaDDC, and of the rest, the interferences were few and generally small. Three possible spectral interactions were observed (Fe/Co, Ni/Co, and Sb/Cd). The remaining interferences are due to chemical interactions which are difficult to evaluate. There is little or no interference from NaCl and calcium indicating the general utility of this method in natural water analysis may be favorable.

Preconcentration by precipitation with thionalide using poly(vinylpyrrolidone) as a carrier (PVP-T)

This method recovered the least number of elements of all the methods considered, as shown in Table 6. No response was observed for eight elements (Cr, Mn, Fe, Co, Ni, Zn, Cd, and Tl). Despite this poor overall performance, the number of observed interferences was low, with Ca, Cr, Mn, Fe, and Cd having no effect on any of the recovered elements. Of the observed interferences, two (Cu depression by Zn, and As enhancement by Pb) are explicable spectroscopically. The interference on selenium is not easily understood.

Preconcentration by precipitation on ion-exchange resin-impregnated filter paper (SA-2)

Three elements (As, Se, and Sb) were not recovered on the cationic resin. No interference from manganese was observed for any of the elements studied. However, as shown in Table 7, the remaining interferences were numerous. Of these, four may be attributed to spectral effects (Mn/Cr, Ni/Co, Zn/Cu, and Tl/Pb). The most widespread interference was caused by calcium. Almost all the elements exhibited markedly depressed analyte signals caused by depletion of ion-exchange capacity resulting from calcium uptake. Thus, in the presence of 100 mg l^{-1} calcium ion, the cationic resin exchange sites are rapidly taken up by the large excess of calcium (which is strongly exchanged from solution) leaving the analyte ions in the filtrate liquor.

Ranking of methods

In general, the observed interferences in the various methods are explicable by either chemical or spectroscopic effects. However, several effects are not understood on the basis of first-order effects alone. The two-level factorial experimental design has been capable of identifying many potential interferences. It is important to realize that by proper use of a spectral deconvolution routine, the effects of spectroscopic interaction, e.g., As/Pb overlap, can be minimized.

On the basis of the foregoing interference data, an attempt has been made to quantify and rank the methods in a relative manner through the use of the equation

TABLE 5

Effect of interferences on the determination of several elements with preconcentration by sodium diethyldithiocarbamate

Interferent	Cr	Mn	Fe	Co	Ni	Cu	Zn	As	Se	Ag	Cd	Sb	Hg	Tl	Pb
NaCl	*	*	0	0	0	0	18	*	*	0	0	0	0	*	0
Ca	*	*	0	0	0	0	0	*	*	0	0	4.2	0	*	0
Cr	**	*	0	0	−4.8	0	0	*	*	0	0	0	0	*	0
Mn	*	**	0	−3.6	0	0	0	*	*	0	0	0	0	*	0
Fe	*	*	**	0	−4.8	0	0	*	*	0	−18	0	−8	*	0
Co	*	*	−12	**	−104	0	0	*	*	0	0	10	0	*	0
Cu	*	*	0	0	0	**	0	*	*	0	16	0	0	*	−9
Zn	*	*	0	3.5	12	0	**	*	*	0	0	0	0	*	0
Cd	*	*	0	0	0	−5	0	*	*	0	**	−40	0	*	0
Pb	*	*	0	0	0	0	−22	*	*	0	0	0	0	*	**

*Not recovered. **Not possible.

TABLE 6

Effect of interferences on the determination of several elements with preconcentration on poly(vinylpyrrolidone)—thionalide

Interferent	Cr	Mn	Fe	Co	Ni	Cu	Zn	As	Se	Ag	Cd	Sb	Hg	Tl	Pb
NaCl	*	*	*	*	*	0	*	0	0	0	*	*	0	*	84
Ca	*	*	*	*	*	0	*	0	0	0	*	*	0	*	0
Cr	**	*	*	*	*	0	*	0	0	0	*	*	0	*	0
Mn	*	**	*	*	*	0	*	0	0	0	*	*	0	*	0
Fe	*	*	**	*	*	0	*	0	0	0	*	*	0	*	0
Co	*	*	*	**	*	0	*	0	18	0	*	*	0	*	0
Cu	*	*	*	*	*	**	*	0	0	0	*	*	0	*	117
Zn	*	*	*	*	*	−18	**	0	−15	0	*	*	0	*	0
Cd	*	*	*	*	*	0	*	0	0	0	**	*	0	*	0
Pb	*	*	*	*	*	0	*	100	0	0	*	*	0	*	**

*Not recovered. **Not possible.

TABLE 7

Effect of interferences on the determination of several elements with preconcentration by resin-impregnated filter papers

Interferent	Cr	Mn	Fe	Co	Ni	Cu	Zn	As	Se	Ag	Cd	Sb	Hg	Tl	Pb
NaCl	0	0	0	2	0	−8	0	*	*	0	−3.7	*	98	−2.7	−40
Ca	−27	−62	−65	−30	−7.8	−70	−24	*	*	−9	−169	*	0	9.3	−64
Cr	**	5	0	−2	0	0	0	*	*	0	−8.7	*	0	−3.8	0
Mn	0	**	0	0	0	0	0	*	*	0	0	*	0	0	0
Fe	0	0	**	0	0	0	0	*	*	−14	0	*	0	−2.6	−12
Co	0	0	0	**	−18	0	0	*	*	0	0	*	0	−2.9	0
Cu	0	0	−6.1	0	0	**	−33	*	*	0	0	*	0	2.9	0
Zn	0	3	8.5	3	0	0	**	*	*	−12	0	*	52	0	−12
Cd	0	0	0	0	4.2	0	0	*	*	0	**	*	50	−24	0
Pb	0	−4	−9.6	0	0	0	0	*	*	0	0	*	0	−92	**

*Not recovered. **Not possible.

$$R_I = \sum_{i=1}^{n} |I|/N \quad (1)$$

where I is the percent interference, i is the index of the observed interference I, and N is the number of elements recoverable.

Based on the total data, the figures shown in Table 8 are obtained for rating and ranking of the methods. From this rating, it is evident that the precipitation and activated carbon methods are subject to the least interference (lowest R_I values) whereas the CPG and SA-2 methods are most sensitive to interference.

If the interferences confidently assigned as spectral effects only are disregarded in the calculation of the R_I values, the rating and ranking also shown in Table 8 are obtained. The only change in the ranking is that the activated carbon method is moved below DBDTC. Detailed inspection of the data shows that the methods appear to fall into two main groups: the dithiocarbamate methods (where <50% of interference is chemical), and CPG, PVP-T and SA-2 methods (where >65% of the interference is due to chemical interference).

The activated carbon method appears to be intermediate between these two groups. These observations show that for dithiocarbamates, more than half the observed interference is spectral and can be compensated through the careful use of a peak deconvolution routine. This is particularly true for the DBDTC method. Removal of the remaining chemical effects may require modification of the method or the use of masking agents where large amounts of potential interferences are known to be present. The remaining methods show increasing chemical interferences, thereby becoming less suitable for routine analysis of, for instance, widely varying environmental samples. The data are useful to direct the way to corrective measures.

TABLE 8

Rating and ranking of the methods with regard to both chemical and spectral interferences, and after disregarding interferences assigned to spectral effects

Method	Chemical and spectral effects		Chemical effects only	
	R_I	Rank_A	R_I	Rank_B
AC	31	2	18	3
APDC	44	4	20	4
CPG	62	6	43	6
DBDTC	39	3	11	1
NaDDC	30	1	13	2
PVP-T	50	5	30	5
SA-2	90	7	77	7

Conclusions

Seven methods of preconcentration for their use in the x-ray spectrometry of trace elements in aqueous media have been evaluated. Figures of merit and relative ranks have been determined through the use of empirical equations applied to interference data. These equations may be extended to indicate whether a method suffers most from chemical or from spectral interferences. The ability to discern interference types is invaluable, as spectroscopic interferences are frequently simple to correct whereas chemical interferences are not. On the basis of such equations, the preconcentration methods may be grouped and ranked according to interference effects. The methods which appear best are those utilizing dithiocarbamate precipitation, as they are relatively free from chemical interference and show good response characteristics. Of these methods, the use of sodium dibenzyldithiocarbamate precipitation is indicated to be the optimum method. However, it should be understood that the rating techniques summarize in an objective way response parameters selected subjectively, and it may not be possible to evaluate any one particular application from the pooled data.

REFERENCES

1 A. T. Ellis, D. E. Leyden, W. Wegscheider, B. B. Jablonski and W. B. Bodnar, Anal. Chim. Acta, 42 (1982) 73.
2 G. Wernimont, in J. R. de Voe (Ed.), Validation of the Measurement Process, ACS Symp. Ser., No. 63, ACS, Washington, DC, 1977, p. 1.
3 R. L. Plackett and J. P. Burman, Biometrika, 33 (1946) 305.
4 W. Wegscheider, G. Knapp and H. Spitzy, Fresenius Z. Anal. Chem., 283 (1977) 9.

Analytica Chimica Acta, 142 (1982) 101—107
Elsevier Scientific Publishing Company, Amsterdam — Printed in The Netherlands

DETERMINATION OF MOLYBDENUM IN NATURAL WATERS AFTER SELECTIVE ADSORPTION ON SEPHADEX GEL

KAZUHISA YOSHIMURA*, SOICHI HIRAOKA and TOSHIKAZU TARUTANI

Department of Chemistry, Faculty of Science, Kyushu University 33, Hakozaki, Higashiku, Fukuoka 812 (Japan)

(Received 22nd February 1982)

SUMMARY

Molybdenum(VI) ions are adsorbed on Sephadex G-25 gel at pH 3.5, and are desorbed reversibly with a complexing agent, EDTA. The adsorbability is much greater than that for boron(III) and vanadium(V). Large amounts of sodium chloride have little effect on the adsorption. Molybdenum concentrations in natural waters, especially in seawater, can be determined with good precision and accuracy after selective preconcentration of molybdenum by a Sephadex G-25 gel column. The detection limit for 250-ml water samples is about 1 $\mu g\ l^{-1}$ by atomic absorption spectrometry or by spectrophotometry with bromopyrogallol red as reagent.

Selective concentration methods for boron(III) and vanadium(V) by use of a Sephadex G-25 gel column have already been described [1, 2]. Borate and vanadate ions are adsorbed on Sephadex G-25 gel from solutions at pH 9.5—11 and 3—7, respectively, and desorbed into 0.01—0.1 M hydrochloric acid solution. Complex formation of these oxo-anions with the hydroxyl groups of the dextran matrix may be responsible for the reversible adsorption.

Molybdenum is one of the important elements for many organisms and its abundance in natural waters is of interest. It is difficult, however, to determine molybdenum directly in natural waters because of its low $\mu g\ l^{-1}$ levels. A simple, rapid, and quantitative method for the determination of molybdenum is needed. It is well known that molybdate(VI) forms complexes with polyhydroxy compounds [3]. Adsorption of molybdate on Sephadex gels has been already reported [4, 5] and has been utilized for the separation of molybdenum as matrix element from traces of alkali and alkaline earth metals [6]. In this study, a separation and concentration method for traces of molybdenum in natural waters has been developed by taking advantage of the reversible adsorption on Sephadex G-25 gel. The molybdenum can be determined by atomic absorption spectrometry or by solution spectrophotometry with bromopyrogallol red [7].

EXPERIMENTAL

Chemicals

All the chemicals used were of analytical grade and the water was deionized.

La(III) solution (5000 ppm). Dissolve 5.9 g of La_2O_3 in 50 ml of concentrated hydrochloric acid, evaporate to dryness and add 1 l of 0.01 M hydrochloric acid solution.

Procedures

Separation and concentration of molybdenum(VI) on a Sephadex G-25 gel column. Filter the water sample at the sampling point through a glass-fiber filter paper (Whatman GF/D) if necessary. Add 7.5 ml of anhydrous acetic acid to a 250-ml sample and adjust to pH 3.5 with ammonia solution.

Use an acrylic resin column (16-mm i.d., 100 mm long) containing 15 ml of Sephadex G-25 gel (Medium, Pharmacia). Condition the column with 0.5 M acetate buffer (pH 3.5) and then pass the sample solution through at a rate of 8 ml min^{-1}. Wash the column with 25 ml of 0.1 M ammonium acetate buffer (pH 3.5) and then desorb the molybdenum with 20 ml of 0.01 M EDTA (disodium salt) solution. Reject the first 5 ml of effluent and collect the next 15 ml in a 50-ml beaker or in a 25-ml volumetric flask.

Determination of molybdenum. To the evaporated sample containing 0.5—50 μg of molybdenum in the beaker, add 2 ml of the La(III) solution. After dissolving, determine the molybdenum by atomic absorption spectrometry with a Nippon Jarrell-Ash spectrometer, Model AA-781. Instrumental conditions are as follows: analytical wavelength 313.26 nm, nitrous oxide—acetylene flame, 5-cm long burner. Use peak heights relative to 5-ppm molybdenum solution for the calculation.

Alternatively, add 5 ml of 1 M hydrochloric acid, 1.5 ml of 0.01 M zephiramine and 1 ml of 0.03% (w/v) bromopyrogallol red (50% ethanolic solution) to the sample containing 0.2—5 μg of molybdenum in the 25-ml volumetric flask. Stand for 20 min after mixing the solutions. Measure the absorbance at 629 nm using a cell of 5-cm light path against a reagent blank. A Hirama Model 6B spectrophotometer was used.

In each case, use a calibration graph obtained by taking standards throughout the gel adsorption procedure.

Distribution measurements. To investigate the adsorption of molybdenum(VI) on Sephadex G-25, the distribution coefficient K_d was measured by the batch technique, using 0.5 g of Sephadex G-25 and 50 ml of solution. The mixture was stirred overnight and the molybdenum in the equilibrated solution was determined. The detailed experimental procedure was described previously [1].

RESULTS AND DISCUSSION

The adsorption of molybdenum(VI)

The pH dependence of the distribution coefficient (K_d), the measure of uptake of molybdenum by the gel, is shown in Fig. 1. The uptake was maximal at pH 3.5. The value of K_d was much larger than those for borate and vanadate(V) [1, 2]. The loss of traces of molybdenum in glass vessels can almost be neglected in solutions at any pH values [8]. Therefore, glassware was used for all the batch experiments.

The mole fraction diagram of each species of molybdate, also shown in Fig. 1, was calculated using the acidic dissociation constants of MoO_2^{2+}: $pK_1 = 1.0$, $pK_2 = 2.0$, $pK_3 = 2.4$, and $pK_4 = 3.8$ (1 M $NaClO_4$) [9]. The diagram corresponds to conditions under which there is no polymerization of molybdate [10]. More precise pK_a values under the same conditions as those of the present study could not be found in the literature. However, the pH dependence curve of K_d values agrees fairly well with that of mole fraction of $HMoO_4^-$ species, suggesting that the active species for adsorption is $HMoO_4^-$. Bourne et al. [3] examined the paper ionophoresis of a number of cyclic carbohydrates in molybdate solution and showed that molybdate forms complexes more strongly in acidic than in alkaline solution and that the complex formation depends on the configuration of the hydroxyl groups in carbohydrates. Complex formation of molybdate with hydroxyl groups of the dextran matrix of the gel may be responsible for the adsorption. Karajannis et al. [6] suggested the formation of a Mo—NH_3—glucose complex in the G-10 gel at pH 2.5. However, such complex formation is unlikely under their conditions.

The K_d value decreased with increasing concentrations of molybdenum, also in the case of borate and vanadate. Polymerized oxo-anions may be excluded from the gel, or may show lower affinity with the gel.

Figure 2 shows the effects of coexisting electrolytes on the adsorption of

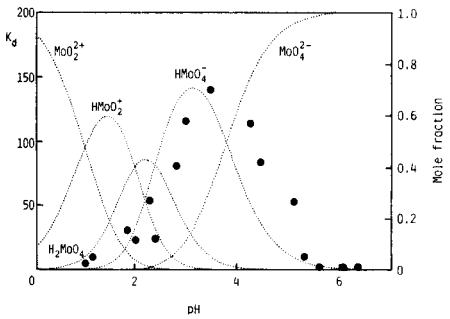

Fig. 1. pH-dependence of the adsorption of molybdenum(VI) on 0.5 g of Sephadex G-25 for a 50-ml sample of 2×10^{-4} M Na_2MoO_4 in 0.1 M NaCl (HCl—NaOH). Dotted lines indicate the mole fraction curves.

molybdenum on the gel. The presence of acetate (used for maintaining the pH of the sample solution), perchlorate, and calcium ions results in decreased adsorption. Acetate and calcium ions may form complexes with molybdenum(VI). Perchlorate is known to be adsorbed on the gel and thus may exclude molybdenum.

Selective concentration of molybdenum(VI) on a Sephadex gel column

When the characteristic adsorption of molybdenum on Sephadex gel is applied to selective concentration by the column method, an effective agent is necessary for desorption of molybdenum from the column. Hydrochloric acid higher than 0.1 M may hydrolyze the gel matrix. The use of sodium hydroxide as eluent caused tailing on the elution peak of molybdenum. Molybdenum(VI) forms fairly stable complexes with aminopolycarboxylates [11]. It is shown in Fig. 3 that the use of 0.01 M EDTA (disodium salt) makes it possible to desorb molybdenum completely from the column and to concentrate the molybdenum content of a sample into about 10 ml. Therefore, the first 5 ml of effluent was rejected and the next 15 ml was collected in a 50-ml beaker or in a 25-ml volumetric flask. The pH of the EDTA solution did not affect the recovery of molybdenum within the range 2—11. The molybdenum in the beaker was determined by atomic absorption spectrometry after the solution had been evaporated to dryness and the residue dissolved in 2 ml of the La(III) solution, which suppresses the inter-

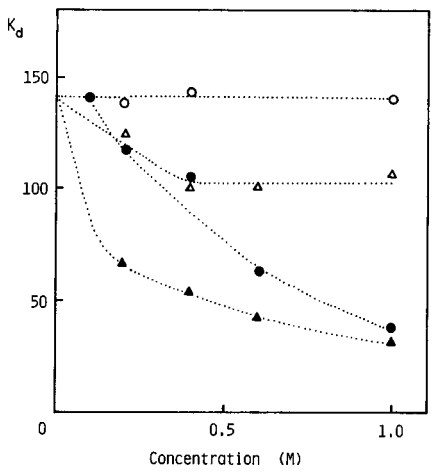

Fig. 2. Effect of electrolytes on the adsorption of molybdenum(VI) on 0.5 g of Sephadex G-25 from 50-ml samples of 2×10^{-4} M Na_2MoO_4: (•) acetate (pH 3.5); in 0.1 M acetate buffer (pH 3.5), (○) NaCl, (△) $NaClO_4$, (▲) $CaCl_2$.

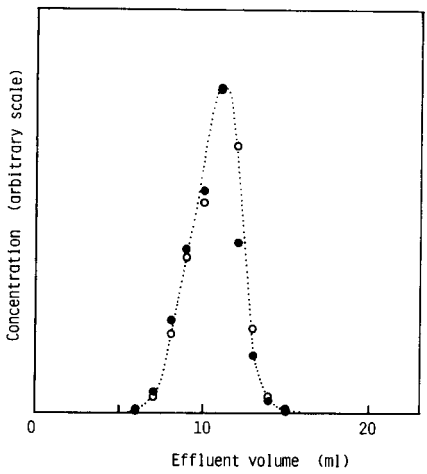

Fig. 3. Desorption of molybdenum(VI) from the column with 0.01 M EDTA solution as eluent (duplicate experiments). Column 16-mm i.d., 100 mm long; 15 ml of Sephadex G-25.

ference by coexisting EDTA. Relative peak height to 5-ppm molybdenum solution was used for calculations, to obtain higher precision and accuracy. Alternatively, the molybdenum in the volumetric flask was determined spectrophotometrically by the bromopyrogallol red method.

Figure 4 shows the absorbance plotted against the volume of solution taken. Molybdenum in up to 600 ml of freshwaters, the pH of the solution being buffered by 0.1 M acetate, could be almost completely recovered into 15 ml of eluate. With seawater, molybdenum could be concentrated into a 15-ml solution from up to 300-ml samples containing 0.5 M acetate.

The recommended procedure was applied to 100-ml solutions containing 1.25 μmol of molybdenum and 1—10000-fold amounts of various ions. The molybdenum was determined by atomic absorption spectrometry. The results are summarized in Table 1. Interference from vanadium(V) and tungsten(VI) is probably due to complex formation with molybdenum. Iron(III) at a 100-fold level lowered the recovery, probably because its hydroxides or hydroxo complexes adsorb molybdenum, but the interference could be overcome in the presence of 0.5 M acetate.

Similar results were also obtained by the bromopyrogallol red method, except in the case of tungsten(VI). When present in a molar ratio of 1:1, tungsten was recovered in part as well as molybdenum, which resulted in positive errors. Its presence in a 1:10 molar ratio to molybdenum hardly interfered with the determination.

Determination of molybdenum in natural waters

The present method makes it possible to determine molybdenum at $\mu g\ l^{-1}$ levels. Sugawara et al. [12] reported that the molybdenum content of river waters in Japan ranges from 0.2 to 0.6 $\mu g\ l^{-1}$. As an aid to geochemical prospecting, the method should be convenient for routine determinations of

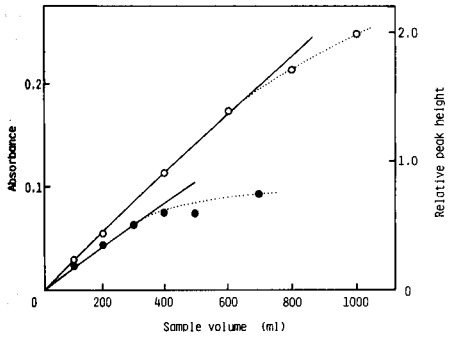

Fig. 4. Effect of sample volume on the recovery of molybdenum(VI): (○) 0.1 M acetate buffer (pH 3.5) containing 2×10^{-7} M Na_2MoO_4, absorbance being measured spectrophotometrically [7]; (●) seawater from Wajiro, Fukuoka, containing 0.5 M acetate buffer (pH 3.5), peak height being measured relative to a 5-ppm reference molybdenum solution.

TABLE 1

Effects of foreign ions on the recovery of molybdenum[a]

Species	Molar ratio to Mo	Mo found ($\times 10^{-6}$ M)	Species	Molar ratio to Mo	Mo found ($\times 10^{-6}$ M)
Al	1000	1.27	Fe(III)	100	1.15
	10000	1.21		100[b]	1.24
V(V)	10	1.20	W(VI)	1	1.24
	100	1.03		10	0.65
Cr(VI)	100	1.26	SiO_2	1000	1.27
Mn(II)	100	1.21		10000	1.13
	1000	1.18	PO_4^{3-}	100	1.25
Mn(VII)	10	1.25			
	100	1.20			

[a]Molybdenum(VI) in a 100-ml sample solution was separated and concentrated to 15 ml on the Sephadex column and finally to 2 ml. The sample solution was 100 ml of 1.25×10^{-6} M Na_2MoO_4, 0.1 M in acetate (pH 3.5). Peak heights were measured relative to a 5-ppm reference molybdenum solution, which exhibited about 2.5-cm peak height. [b]Sample solution contains 0.5 M acetate (pH 3.5).

molybdenum in freshwater samples in which somewhat elevated concentrations are present. The method itself is simple in operation and easily adapted for an automated system.

The proposed method is particularly effective for seawater. There are no elements present which affect the recovery of molybdenum or the selective concentration by the column method [13]. Table 2 shows the recoveries of added molybdenum from 250 ml of a seawater sample. The molybdenum was determined by atomic absorption spectrometry. It is desirable to use a calibration graph prepared by the column method. Recovery was almost complete. The analytical results obtained are presented in Table 3. Standard deviations were within ±3% for each sample. Molybdenum concentration ranges were reported as 8.6—11.6 $\mu g\ l^{-1}$ in the western North Pacific Ocean and 8.6—11.8 $\mu g\ l^{-1}$ in the eastern China Sea [14]. The present results are in good agreement with these values. The concentrations in the Hakata Bay, however, were found to decrease in summer. In the eutrophic Bay in the summer season, molybdenum may be coprecipitated with flocculated

TABLE 2

Recovery of molybdenum(VI)[a]

Mo added (μg)	0	2.39	4.78	7.17
Relative peak height[b]	0.64	1.18	1.76	2.30
Mo found (μg)	2.55	5.02	7.46	9.73

[a]Coastal seawater from Wajiro, Fukuoka (250 ml). [b]Reference solution, 5-ppm molybdenum.

TABLE 3

Molybdenum contents in seawaters (1981)

Sampling point	Mo content ($\mu g\ l^{-1}$)		Sampling point	Mo content ($\mu g\ l^{-1}$)	
	February	August		February	August
Tsuyazaki[a]	10.1	10.3	Wajiro[b]	10.4	7.8
Shingu[a]	—	10.4	Kashii[b]	10.2	7.9
Shikanoshima[a]	10.2	10.2	Hakozaki[b]	—	9.4
			Okinoerabu-jima[c]	—	11.3

[a]Coastal seawater from positions facing the open sea near Fukuoka. [b]Coastal seawater from the Hakata Bay of Fukuoka. [c]Seawater near the island in the western North Pacific Ocean.

hydrated iron or manganese oxide or sulfide, which are supplied from bottom materials under anaerobic conditions, or multiplying organisms such as plankton may incorporate molybdenum.

REFERENCES

1 K. Yoshimura, R. Kariya and T. Tarutani, Anal. Chim. Acta, 109 (1979) 115.
2 K. Yoshimura, H. Kaji, E. Yamaguchi and T. Tarutani, Anal. Chim. Acta, 130 (1981) 345.
3 E. J. Bourne, D. H. Hutson and H. Weigel, J. Chem. Soc., (1960) 4252.
4 C. A. Streuli and L. B. Rogers, Anal. Chem., 40 (1968) 653.
5 N. Yoza, H. Matsumoto and S. Ohashi, Anal. Chim. Acta, 54 (1971) 538.
6 S. Karajannis, H. M. Ortner and H. Spitzy, Talanta, 19 (1972) 903.
7 M. Deguchi, M. Iizuka and M. Yashiki, Bunseki Kagaku, 23 (1974) 760.
8 J. Burclova, J. Prasilova and P. Benes, J. Inorg. Nucl. Chem., 35 (1973) 909.
9 B. I. Nabivanets, Russ. J. Inorg. Chem., 14 (1969) 341.
10 C. F. Baes, Jr. and R. E. Mesmer, The Hydrolysis of Cations, Wiley, New York, 1976.
11 K. Zare, P. Lagrange and J. Lagrange, J. Chem. Soc. Dalton Trans., (1979) 1372.
12 K. Sugawara, S. Okabe and M. Tanaka, J. Earth Sci., Nagoya Univ., 9 (1961) 114.
13 K. K. Turekian, in K. H. Wedepohl (Ed.), Handbook of Geochemistry, Springer-Verlag, Berlin, 1969.
14 K. Sugawara and S. Okabe, J. Earth Sci., Nagoya Univ., 7 (1959) 422.

Analytica Chimica Acta, 142 (1982) 109—118
Elsevier Scientific Publishing Company, Amsterdam — Printed in The Netherlands

DIFFERENZIERUNG DER BINDUNGSFORMEN VON KUPFERSPUREN IN PFLANZLICHEN LEBENSMITTELN MITTELS IONENAUSTAUSCH AN CELLULOSE-MATERIALIEN UND GEL-FILTRATION

R. BISCHOFF und G. SCHWEDT*

Anorganisch-Chemisches Institut der Universität Göttingen, Tammannstr. 4, 3400 Göttingen (B.R.D.)

(Eingegangen den 2. Marz 1982)

SUMMARY

(Differentiation of the chemical forms of trace amounts of copper in peas and soy meal by means of ion-exchange on cellulose materials and molecular exclusion chromatography.)

Studies on the binding forms of the water-soluble copper contents of peas and soy meal in the ppm region are reported. These foodstuffs contain quite different organic substances. For peas, the amount of copper exchangeable on DEAE-Cellulose increases strongly between pH 7 and 7.5 (amphoteric substances); with soy meal, no such pH dependence is observed. Molecular exclusion chromatography indicates that the amphoteric copper compounds consist entirely of high-molecular-weight substances. The copper compounds that are not exchangeable on DEAE-Cellulose at pH 8.6, contain about 50% high-molecular-weight substances and about 25% low-molecular-weight substances. The trace amounts of copper at the microgram-level were determined spectrophotometrically by means of the selective reagent, lead diethyldithiocarbamate, after extraction.

ZUSAMMENFASSUNG

Am Beispiel der Lebensmittel Erbsen und Sojamehl mit unterschiedlicher Zusammensetzung an organischen Stoffen werden die überwiegend wasserlöslichen Gehalte an Kupfer im ppm-Bereich näher charakterisiert. Beim Ionenaustausch an DEAE-Cellulose nimmt die austauschbare Kupfermenge bei Erbsen zwischen pH 7 and 7,5 stark zu (amphotere Verbindungen), bei Sojamehl kann keine pH-Abhängigkeit festgestellt werden. Durch Gel-Filtration kann gezeigt werden, daß es sich bei den amphoteren Kupferverbindungen aus Erbsen ausschließlich um höhermolekulare Substanzen handelt. Die bei pH 8,6 nicht an DEAE-Cellulose austauschbaren Kupferverbindungen bestehen etwa zur Hälfte aus höhermolekularen und zu einem Viertel aus niedermolekularen Substanzen. Die Kupferspuren in den Fraktionen im Mikrogrammbereich wurden mit Hilfe des selektiven Reagenzes Bleidiethyldithiocarbamat extraktiv-photometrisch bestimmt.

In den vorgestellten Untersuchungen werden erste Ergebnisse über die Bindungsformen des Kupfers in pflanzlichen Lebensmitteln an Beispielen dargestellt. Ähnliche Untersuchungen existieren bisher nur in der Wasseranalytik [1, 2] und der Biochemie [z.B. 3, 4]. Die Untersuchungsmethodik beinhaltet den Ionenaustausch an Cellulose-Ionenaustauschern sowie die Gel-Filtration an einem hydrophilen Gel [5—7]. Das Ziel der Arbeiten war es,

0003-2670/82/0000-0000/$02.75

Wege für eine möglichst einfache, in den verschiedensten Laboratorien anwendbare Analysenmethodik zu finden, die Aussagen über die bisher üblichen Gesamtgehalte an Schwermetallen am Beispiel des Kupfers hinaus ermöglicht. Fragen der Löslichkeit der Kupferspezies, nach der Art der Komplexbildung und der Bedeutung höhermolekularer Stoffe als mögliche Komplexbildner standen dabei am Beispiel von zwei ausgewählten Lebensmitteln, Erbsen und Sojamehl, mit relativ hohen Kupfergehalten sowie unterschiedlicher Zusammensetzung an organischen Stoffen im Vordergrund [8].

EXPERIMENTELLER TEIL

Geräte und Lösungen

Geräte. Zeiss Spektralphotometer PM Q II mit 2-cm Glasküvetten; pH-Meter der Fa. Knick Typ 507; Shimadzu-Spectrophotometer Double-Beam UV 200 mit 1-cm Quarzküvetten; Glassäule mit ca. 150 cm^3 Vorratsgefäß, 50 cm Höhe, 12 mm Innendurchmesser.

Reagenzien. Alle verwendeten Reagenzien besitzen den Reinheitsgrad p.a. Es wird bidestilliertes Wasser verwendet. CM-Cellulose (Serva Typ CM, Kapazität 0,76 meq g^{-1}), DEAE-Cellulose (Servacel Typ DEAE 23SS, Kapazität 0,61 meq g^{-1}) und Fractogel TSK HW-55(F), (230—450 mesh, ASTM 14981, Merck).

Bleidiethyldithiocarbamat-Lösung. Bleiacetattrihydrat (0,1 g) in 10 cm^3 Wasser lösen und mit 0,5 g Kaliumnatriumtartrat versetzen; 5%ige Kaliumhydroxidlösung tropfenweise bis zur Lösung des Niederschlages zugeben und anschließend Bleidiethyldithiocarbamat, $Pb(DDTC)_2$, nach Zusatz von 5 cm^3 10% iger KCN-Lösung mit 0,125 g NaDDTC ausfällen. Mit 250 cm^3 Chloroform im Schütteltrichter extrahieren und die wäßrige Phase mit 200 cm^3 Chloroform nachwaschen. Die vereinigten organischen Extrakte je zweimal mit 250 cm^3 Wasser schütteln, um Cyanidspuren zu beseitigen. Durch einsh Faltenfilter in einen 500-cm^3 Meßkolben ablassen und mit Chloroform bis zur Marke auffüllen. Die Lösung ist in einer dunklen Flasche im Kühlschrank mindestens 4 Wochen haltbar.

Ammoniumcitrat-Puffer. 210 cm^3 Ammoniak (0,91 g) mit 150 cm^3 Wasser mischen und mit 218,4 g Citronensäure-Monohydrat unter Rühren und Kühlen versetzen. Mit Ammoniak auf pH 7—8 bringen und mit einer Spatelspitze NaDDTC versetzen. Kupferspuren durch Extraktion mit 150 cm^3 Chloroform entfernen. Durch Erhitzen das gelöste Chloroform vertreiben und den Puffer mit Wasser auf 500 cm^3 auffüllen.

Pufferlösungen pH 6, 7, 8, 9 (Riedel de Haen, Fixanal). pH 6: 12,53 g Citronensäure-Monohydrat und 159,6 cm^3 1 M NaOH werden in 500 cm^3 Wasser gelöst. pH 7: 3,52 g Kaliumdihydrogenphosphat und 7,26 g di-Natriumhydrogenphosphat in 500 cm^3 Wasser lösen. pH 8: 4,77 g Natriumtetraborat-Decahydrat mit 20,5 cm^3 1 M HCl in 500 cm^3 Wasser lösen. pH 9: 4,77 g Natriumtetraborat-Decahydrat mit 4,6 cm^3 1 M HCl in 500 cm^3 Wasser lösen.

Elutionslösungen. Für die CM-Cellulose, 58,45 g NaCl und 0,4 g NaOH werden in 1 dm^3 Wasser gelöst. Für die DEAE-Cellulose, 68,8 g $Na_3PO_4 \cdot 10$ H_2O werden in 1 dm^3 Wasser gelöst.

Durchführung des Ionenaustausches

Herstellung des wäßrigen Extrakts. Die Probe (1—2 ± 0,01 g) in einen 100-cm^3 Erlenmeyerkolben einwiegen und 1 h mit 50 cm^3 Wasser unter Rühren auf 60° C erwärmen. Den ungelösten Rückstand 10 min mit 6000 U min^{-1} abzentrifugieren. Durch Zugabe von ca. 10 cm^3 Puffer wird der gewünschte pH-Wert eingestellt.

Ionenaustausch. Ionenaustauscher (3 g) mit ca. 100 cm^3 Wasser aufrühren und die überstehende Flüssigkeit mit den feinen Teilchen, die sich nach ca. 1 min noch nicht abgesetzt haben, abgießen. Den mit neuem Wasser aufgeschlämmten Ionenaustauscher in eine mit Glaswolle verschlossene Säule (16 mm Innendurchmesser) geben. Den pH-Wert des Ionenaustauschers mit 25 cm^3 Puffer einstellen. Den gepufferten wäßrigen Extrakt mit einer Durchlaufgeschwindigkeit von ca. 2,5 cm^3 min^{-1} durchlaufen lassen und mit 25 cm^3 Wasser nachwaschen. Zur Kontrolle sollte der pH-Wert dieser Lösung bestimmt werden. Die ausgetauschten Verbindungen mit 25 cm^3 Elutionslösung eluieren und den Ionenaustauscher mit 25 cm^3 Wasser nachwaschen. Von den beiden Lösungen (Durchlauf + Waschwasser und Eluat + Waschwasser) werden je 100 μl in eine 1-cm Quarzküvette pipettiert und mit 3 cm^3 Wasser verdünnt. Es wird die UV-Extinktion bei 260 nm bestimmt. Anschließend dampft man die Lösungen ein und bestimmt den Kupfergehalt nach Aufschluß.

Zusatz von Cu(II)-Ionen. Vor der Extraktion von 2 g Erbsen werden 25 μg Cu(II)-Ionen zugesetzt. Ansonsten verfährt man wie oben beschrieben.

Durchführung der Gel-Filtration

Einen wäßrigen Extrakt von 2 g Erbsen herstellen und auf pH 6,2 bzw. 8,65 bringen. Ionenaustausch an DEAE-Cellulose wie oben beschrieben durchführen. Den Durchlauf in einem 50° C warmen Wasserbad im Wasserstrahlpumpenvakuum vorsichtig eindampfen (Schäumen!). Das zurückbleibende gelbliche Pulver mit 3 cm^3 verdünntem Puffer (1 + 4) rühren und leicht erwärmen. Den ungelösten Anteil über eine Fritte absaugen und zur Kupferbestimmung mit konzentrierter Salpetersäure aufschließen. Die Probe auf die folgendermaßen vorbereitete Gelsäule geben.

Die benötigte Gelmenge über eine Fritte absaugen und mit dem 7-fachen Volumen Wasser aufschlämmen. Nach 2 h gießt man die überstehende Flüssigkeit ab und wiederholt den Vorgang noch zweimal. Nach dem letztenmal saugt man des Gel über eine Fritte ab und rührt es mit ca. 100 cm^3 verdünntem Puffer (1 + 4) auf. Diese Gel-Slurry gibt man in eine Säule, in der schon 25 cm^3 Puffer (1 + 4) sind und die mit Glaswolle verschlossen ist. Nachdem sich das Gel abgesetzt hat, gibt man die Probelösung auf die Säule und benutzt die verdünnte Pufferlösung als Laufmittel. Die ersten 25 cm^3 fängt

man in 5-cm^3 Fraktionen auf und die weiteren in 2-cm^3 Fraktionen. Von diesen Fraktionen pipettiert man 100 bzw. 200 μl in eine 1-cm Quarzküvette und verdünnt mit 2 cm^3 Wasser. Anschließend mißt man die UV-Extinktionen bei 260 nm.

Zur Bestimmung der Kupfermengen müssen aufgrund der zu geringen Nachweisgrenze mehrere Fraktionen zusammengefaßt werden (siehe Abb. 4 und 5). Die zusammengefassten Fraktionen werden eingedampft, aufgeschlossen und analysiert.

Aufschluß der organischen Substanz und Kupferbestimmung [9]

Die Probensubstanz wird in einem 100-cm^3 Erlenmeyerkolben mit 10 cm^3 konzentrierter Salpetersäure auf einem Sandbad erhitzt. Der Kolben wird mit einem Uhrglas verschlossen, an dem die Salpetersäure fortwährend kondensieren sollte. Man läßt das Gemisch auf diese Weise reagieren und dampft die Salpetersäure am nächsten Morgen ein.

Man löst die aufgeschlossene Substanz in 10 cm^3 Wasser und 5 cm^3 Ammoniumcitrat-Puffer, extrahiert mit 10 cm^3 $Pb(DDTC)_2$-Lösung und läßt die organische Phase durch einen Faltenfilter in einen 30-cm^3 Spitzkolben ab. Nachdem das Chloroform am Rotationsverdampfer abdestilliert worden ist, nimmt man den Rückstand in 8 cm^3 Chloroform auf. Man photometriert in 2-cm Küvetten gegen reines Chloroform.

ERGEBNISSE UND DISKUSSION

Das wesentliche Ergebnis dieser Untersuchungen ist ein einfaches Analysenschema, mit Hilfe dessen erste Aussagen über die Bindungsformen von Kupfer in den untersuchten Lebensmitteln gemacht werden können (Abb. 1). In den untersuchten Erbsen befinden sich 8,51 ppm und im Sojamehl 13,92 ppm Kupfer (Tabelle 1). Diese Werte stimmen mit Literaturangaben gut überein [10].

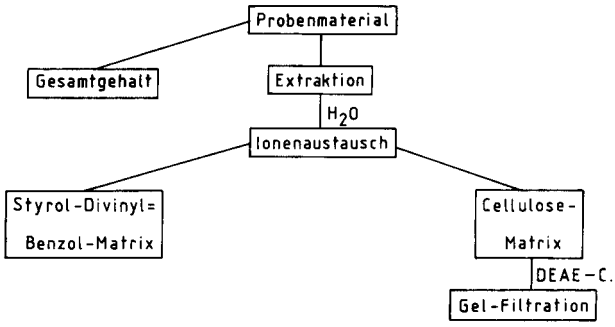

Abb. 1. Analysenschema zur differenzierenden Analytik von Kupferbindungsformen in pflanzlichen Lebensmitteln.

TABELLE 1

Literaturwerte [9] der Kupfergesamtgehalte in den untersuchten Lebensmitteln im Vergleich mit eigenen Meßwerten

Lebensmittel	Kupfergehalt (ppm)	Meßwerte (ppm)
Erbsen (grün, getrocknet)	4,9—14	8,51
Sojamehl	10,0	13,92

Der erste Schritt im Analysenschema besteht darin, ein Extraktionsmittel zu finden, mit dem ein möglichst großer Teil des Kupfergehaltes in Lösung gebracht werden kann. Bei den untersuchten Lebensmitteln nimmt die extrahierbare Kupfermenge mit steigender Polarität des Extraktionsmittels zu (Abb. 2). Mit Wasser wird bei beiden Lebensmittel ein Anteil von über 80% des Gesamtkupfergehaltes in Lösung gebracht. Der wäßrige Extrakt gibt also ein repräsentatives Bild der Kupferverbindungen dieser Lebensmittel wieder, die somit offensichtlich hydrophiler Natur sind.

Im nächsten Schritt wurden unterschiedliche Ionenaustauscher zur weiteren Differenzierung der wasserlöslichen Kupferverbindungen eingesetzt. Dabei stellte sich heraus, daß Ionenaustauscher mit einer Styrol—Divinylbenzol-Matrix sehr stark denaturierend auf die in Lösung befindlichen Proteine wirken. Bei ihrer Anwendung kommt es neben einer Denaturierung, die mit der Bildung eines weißen Niederschlages verbunden ist, auch zu einer

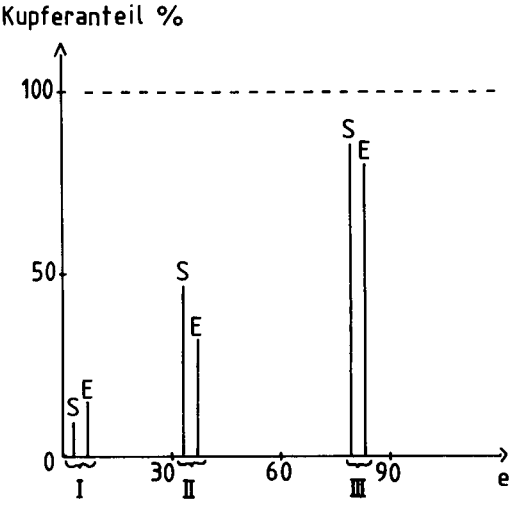

Abb. 2. Löslichkeitsverhalten der Kupferverbindungen in Abhängigkeit von der Polarität des Extraktionsmittels. *e*, Dielektrizitätskonstante des Extraktionsmittels. Kupferanteil%, Prozentualer Anteil der extrahierten Kupfermenge am Gesamtkupfergehalt. S, Sojamehl. E, Erbsen. I, Essigsäureethylester (*e* = 6,11); II, Methanol (*e* = 33,6); III, Wasser (*e* = 80,4).

Abnahme des pH-Wertes um 1—2 Einheiten während des Ionenaustauschvorganges. Da diese Ionenaustauscher sehr wahrscheinlich den Bindungszustand des Kupfers erheblich verändern, wurden sie zu weiteren Untersuchungen nicht eingesetzt. Demgegenüber stellt der Ionenaustausch an Cellulose-Materialien eine gute Möglichkeit der Differenzierung dar. Cellulose-Ionenaustauscher haben dafür drei wichtige Vorteile: aufgrund ihrer hydrophilen Natur kommt es zu keiner Denaturierung; die ausgetauschten Verbindungen können unter milden Bedingungen ohne Zersetzung wieder eluiert werden; der pH-Wert kann während des Ionenaustausches auf einem bestimmten Wert gehalten werden.

Zunächst wurde die CM-Cellulose als schwach saurer Kationenaustauscher bei pH 7 eingesetzt. Es zeigte sich aber, daß bei beiden Lebensmitteln weniger als 5% der wasserlöslichen Kupferverbindungen ausgetauscht wurden. Offensichtlich liegt kein Kupfer in Form schwach basischer kationischer Komplexe vor.

An DEAE-Cellulose lassen sich dagegen bei beiden Materialien höhere Anteile (20—30%) der wasserlöslichen Kupferverbindungen bei pH 7 austauschen. Deshalb wurden hiermit Meßreihen über einen pH-Bereich zwischen 6,2 und 8,6 durchgeführt (unterhalb pH 6,2 treten weiße Fällungen auf: Denaturierung). Die Menge an ausgetauschter organischer Substanz wird anhand ihrer Absorption bei 260 nm detektiert, während die Kupfermenge in den Fraktionen nach Aufschluß photometrisch bestimmt wird. Die Ergebnisse dieser Versuche sind in den Abb. 3 dargestellt. Weitere quantitative Angaben sind in Tabelle 2 zusammengestellt.

Während sich die organische Substanz bei beiden Lebensmitteln ähnlich verhält, ist bei den Kupferverbindungen ein sehr unterschiedliches Verhalten feststellbar. Bei den wasserlöslichen Kupferverbindungen aus Erbsen lassen sich drei Substanzgruppen unterscheiden, von denen jede etwa ein Drittel des Kupfers enthält (s. Tabelle 3).

(a) Saure Verbindungen. Sie sind bei pH 6,2 an DEAE-Cellulose austauschbar. Unter ihnen können sich organische Säuren, Phytin oder auch saure Proteine als Liganden befinden.

(b) Amphotere Verbindungen. Sie sind bei pH 7,5, nicht aber bei pH 7 an DEAE-Cellulose austauschbar. Für diese Gruppe kann man annehmen, daß überwiegend Proteine als Liganden fungieren.

(c) Nicht austauschbare Verbindungen. Sie sind bei pH 8,6 nicht an DEAE-Cellulose austauschbar. Über sie können aus den bisherigen Untersuchungen keine näheren Aussagen gemacht werden. Die Kupferverbindungen aus Sojamehl lassen sich nur in die Gruppen (a) und (c) einteilen. Die amphotere Gruppe fehlt. In weiteren Untersuchungen wurden vor der Extraktion mit Wasser den Erbsen 25 μg an Kupferionen zugesetzt, um deren Verteilung auf die drei Substanzgruppen zu untersuchen. Von den 25 μg befanden sich nach der Extraktion noch 17 μg im wäßrigen Extrakt, deren Verteilungsmuster in Abb. 4 wiedergegeben ist. Aus dieser Verteilung ist zu entnehmen, daß sich der Hauptteil der Kupferionen in der sauren Substanzgruppe (a)

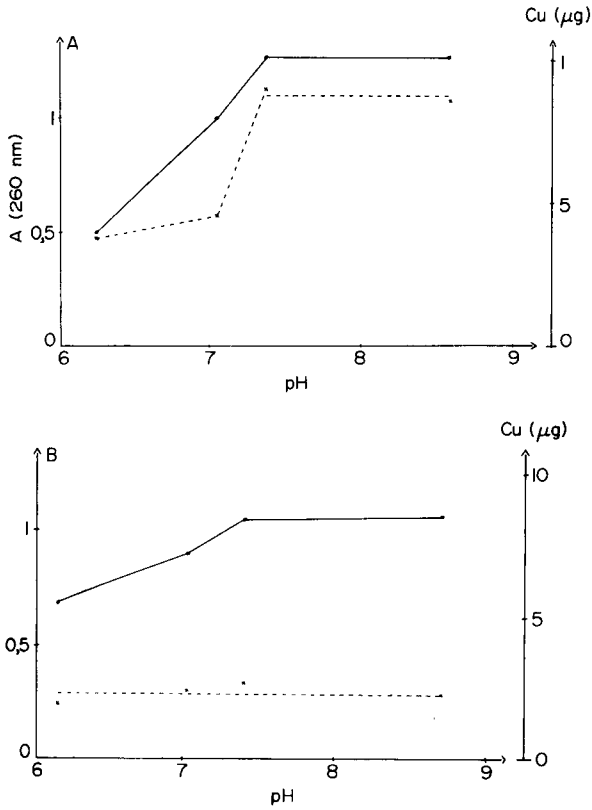

Abb. 3. Verhalten der organischen Substanzen, sowie der Kupferverbingungen gegenüber DEAE-Cellulose in Abhängigkeit vom pH-Wert: A, Erbsen; B, Sojamehl. (—) Extinktion der bei diesem pH-Wert nicht ausgetauschten Substanzen. (---) Kupfergehalt der bei diesem pH-Wert nicht ausgetauschten Substanzen.

TABELLE 2

Ergänzende Tabelle zu den Abb. 3

Probe	pH-Wert		Anteil (%)[a]		Wiederfindung (%)
	vorher	nachher	Durchlauf	Eluat	
2 g Erbsen	6,30	6,15	67,5	29,1	96,8
	7,05	7,05	59,0	35,8	94,8
	7,50	7,50	28,4	67,2	95,6
	8,50	8,60	31,7	63,4	95,1
1 g Sojamehl	6,20	6,10	84,5	16,7	101,2
	7,05	7,00	78,5	20,6	99,1
	7,55	7,35	75,5	22,7	98,2
	8,75	8,60	79,4	20,2	99,6

[a]Organischen Substanzen.

TABELLE 3

Einteilung der kupferhaltigen Verbindungen in Substanzklassen gemäß ihrem Verhalten gegenüber DEAE-Cellulose bei verschiedenen pH-Werten

Probe	Kupfermenge (μg) (% Anteil)		
	Bei pH 7 austauschbar	Zwischen pH 7 und 7,5 austauschbar	Bei pH 7,5 nicht austauschbar
2 g Erbsen	4,80 (35,8%)	3,95 (29,5%)	4,025 (30,0%)
1 g Sojamehl	2,35 (20,2%)	—	9,26 (79.5%)

befindet; die amphotere Gruppe (b) kann kaum noch Kupfer aufnehmen. Aus diesen Ergebnissen ist zu schließen, daß in einem wäßrigen Extrakt aus Erbsen keine freien Kupferionen vorliegen, da noch genügend freie Komplexkapazitäten vorhanden sind.

Der letzte Schritt innerhalb des Analysenschemas (Abb. 1) besteht in einer Gel-Filtration. Mit ihrer Hilfe können Aussagen über die Molekülgrößenverteilung der Kupferverbindungen gemacht werden. Das Hauptproblem stellt das Einengen der wäßrigen Lösungen im Anschluß an den Ionenaustausch dar. Es müssen Temperaturen über 60° C vermieden werden, die zu Veränderungen der organischen Matrix führen würden. Deshalb wurde im Vakuum eingedampft, wobei auf ein störendes Schäumen geachtet werden muß. Zum zweiten läßt sich aus dem Rückstand nur bei den an DEAE-Cellulose nicht ausgetauschten Verbindungen ein genügend hoher Kupferanteil wieder in Lösung bringen (Tabelle 4). Dennoch lassen sich Aussagen über die Molekül-

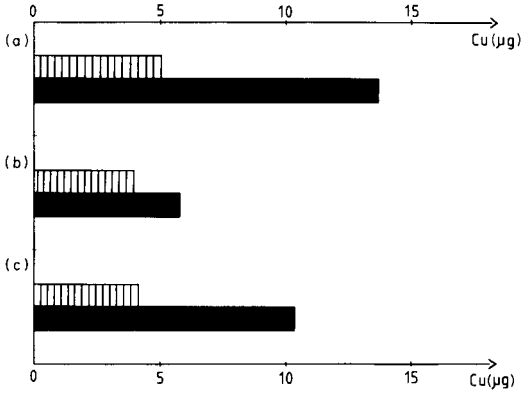

Abb. 4. Verteilung des Kupfers auf die mit Hilfe von DEAE-Cellulose unterscheidbaren Substanzgruppen mit und ohne Zusatz von 25 μg Cu(II)-Ionen (Erbsen). (a) Verbindungen, die unterhalb von pH 7,05 als Anionen vorliegen; (b) Verbindungen, die ihre Ladung im Bereich von pH 7—7,5 wechseln; (c) Verbindungen, die sich nicht an DEAE-Cellulose austauschen lassen. Gestreifte Balken: Kupfermenge ohne Kupferzusatz. Schwarze Balken: Kupfermenge nach Kupferzusatz.

größenverteilung gewinnen, wie die Abb. 5 zeigt. Es ist zu entnehmen, daß die bei pH 6,2 nicht an DEAE-Cellulose ausgetauschten Kupferverbindungen (Gruppe b und c) weitgehend höhermolekularer Natur sind. Führt man den Ionenaustausch dagegen bei pH 8,65 durch, so kommen nur noch die nicht austauschbaren Kupferverbindungen zur Gel-Filtration (Gruppe c). Sie enthalten in der niedermolekularen Fraktion etwa genau so viel Kupfer wie bei pH 6,2. In der höhermolekularen Fraktion ist die Kupfermenge um etwa 5 µg geringer geworden. Dieses Ergebnis läßt sich durch die Annahme erklären, daß die amphoteren Verbindungen aus höhermolekularen Substanzen bestehen. Auch in der Gruppe der nicht austauschbaren Kupferverbindungen sind etwa 50% höhermolekularer Natur.

Die durchgeführten Untersuchungen haben besonders zwei Probleme in der Analytik chemischer Bindungsformen von Elementspuren deutlich werden lassen: Die relativ hohen Blindwerte sowohl in Celluloseaustauschmaterialien als auch in dem eingesetzten hydrophilen Gel (störend bereits für Analysen im Mikrogrammbereich) und die Veränderungen von Bindungsverhältnissen in der Matrix durch die Anwendung der verschiedensten Analysenschritte. Die Untersuchungen haben außer diesen grundsätzlichen Problemen aber auch erste Ansätze für eine differenzierende Analytik von Elementspuren in Lebensmitteln gezeigt, deren Aufgabe es sein soll, über die bisher üblichen

TABELLE 4

Kupfermenge in der chromatographierten Probe bzw. im Rückstand

Probe	pH-Wert	Gelöste Kupfermenge (µg)	Kupfermenge im Rückstand (µg)
2 g Erbsen	6,2	7,70	1,35
2 g Erbsen	8,65	3,325	0,70

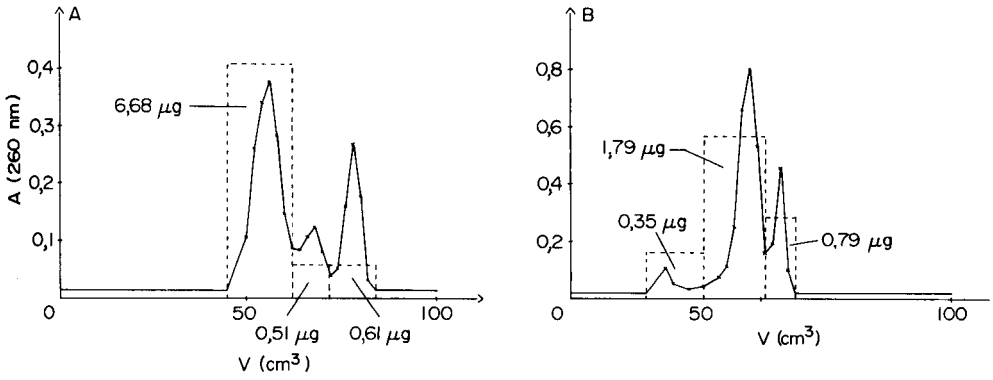

Abb. 5. Gel-Chromatogrammen der nicht an DEAE-Cellulose austauschbaren Verbindungen: A, bei pH 6,2; B, bei 8,65. (———) Extinktion bei 260 nm. (– – –) Kupfergehalt in den Fraktionen.

Gesamtgehalte Anhaltspunkte für Elementbindungsformen im Hinblick auf Fragen der Schwermetallkontamination, der biochemischen und der toxikologischen Wirkungen zu vermitteln.

LITERATUR

1 G. Schwedt, in R. Bock, W. Fresenius, H. Günzler, W. Huber und G. Tölg (Hrsgb.), Analytiker-Taschenbuch, Band 2, Springer-Verlag, Berlin, 1981, p. 255.
2 M. J. Stiff, Water Res., 5 (1971) 585.
3 J. B. Dawson, M. H. Bahreyni-Toosi, D. J. Ellis und A. Hodgkinson, Analyst, 106 (1981) 153.
4 F. J. Langmyhr, B. Eyde und J. Jonson, Anal. Chim. Acta, 107 (1979) 211.
5 T. Hashimoto, H. Sasaki, M. Aiura und Y. Kato, J. Chromatogr., 160 (1978) 301.
6 Y. Kato, H. Sasaki, M. Aiura und T. Hashimoto, J. Chromatogr., 153 (1978) 546.
7 Y. Kato, H. Sasaki, K. Komiya und T. Hashimoto, J. Chromatogr., 190 (1980) 297.
8 R. Bischoff, Diplomarbeit, Universität Göttingen, 1981.
9 A. Claasen und L. Bastings, Fresenius Z. Anal. Chem., 153 (1956) 30.
10 D. Schlettwein-Gsell und S. Mommsen-Straub, Spurenelemente in Lebensmitteln, Verlag H. Huber, Bern, 1973.

Analytica Chimica Acta, 142 (1982) 119—127
Elsevier Scientific Publishing Company, Amsterdam — Printed in The Netherlands

AUTOMATED DETERMINATION OF NITRATE IN WATERS WITH A REDUCTION COLUMN IN A MICROCOMPUTER-BASED STOPPED-FLOW SAMPLE PROCESSING SYSTEM

M. A. KOUPPARIS[a], K. M. WALCZAK and H. V. MALMSTADT*
School of Chemical Sciences, University of Illinois, Urbana, IL 61801 (U.S.A.)
(Received 20th November 1981)

SUMMARY

An automated method for the determination of nitrate in waters with a microcomputer-based stopped-flow mixing system is described. Nitrate is reduced to nitrite with a copperized cadmium—silver alloy or cadmium tube column fitted to the stopped-flow system. Nitrite is determined using fast kinetic, multi-point or single-point procedures with *N*-(1-naphthyl)ethylenediamine dihydrochloride as the color reagent. Reduction time parameters are evaluated and optimized. Water samples in the range of 0.025—3 ppm NO_3^-—N can be processed with a throughput of up to 100 samples per hour and a detection limit of 0.013 ppm. Interference studies show that cyanide, dichromate, iodide, sulfide, copper and tin ions cause negative results.

Determination of nitrate in waters is frequently required in environmental investigations. Numerous analytical methods, including ion-selective electrode [1] and direct and indirect spectrophotometric methods, have been presented. The spectrophotometric methods are based on the reduction of nitrate to nitrite with subsequent quantitation of the nitrite formed. Hydrazine [2, 3] and reductors prepared with zinc [4—6], cadmium [7—10], cadmium amalgam [11, 12], and copperized cadmium [13—15] are used as reducing agents. Methods based on these reducing agents have been developed for use with the air-segmented continuous flow (Technicon Autoanalyzer) [3, 8, 16—22] and flow injection systems [23—25]. Nydahl [26] compared Hg—Cd and Cu—Cd columns and concluded that the Cu—Cd column is superior for its faster rates of reduction.

Reductor columns prepared from copperized cadmium give a nearly quantitative yield of nitrite and their use is approved by the United States Environmental Protection Agency as the "official" colorimetric method for nitrate [27]. The reduction column used in most automated systems consists of a glass column or coil packed with cadmium filings or granules that have been pretreated with a dilute copper sulfate solution to provide a thin film of elemental copper. Several problems arise with this type of column such as

[a]Present address: Laboratory of Analytical Chemistry, University of Athens, Greece.

0003-2670/82/0000-0000/$02.75

large dead-volume because of the large bore of the column (3—5 mm), large sample and wash solution volumes which decrease the throughput rate, and the rather difficult and time-consuming regeneration. Otsuki [28] suggested the reactivation of the copperized cadmium column after extensive use by pumping a solution of 0.05 M copper(II) in 0.1 M EDTA adjusted to pH 7. Stainton [29] reported on the use of a coil of teflon tubing containing a cadmium wire treated with copper sulfate. This arrangement overcame several disadvantages of the column reductor but pure cadmium wire of the dimensions needed (1 mm diameter) is very soft and difficult to handle, rather expensive, and difficult to obtain. Willis [30] described the use of an alloy of 95% cadmium and 5% silver instead of pure cadmium wire. This is stronger and more readily available, it does not need to be regenerated once copperized, and it was found to have a reduction efficiency of 100%.

This paper describes the adaptation of the copperized cadmium reduction to an automated procedure for the determination of nitrate at the parts per million (ppm) level using a microcomputer-based stopped-flow system. The automated stopped-flow technique [31] for the rapid mixing of chemical reagents has been shown to be a useful routine analytical method with rapid and precise results. The copperized cadmium alloy reductor introduced by Willis [30] and a new copperized drilled cadmium rod column are used for the reduction of nitrate to nitrite. The spectrophotometric quantitation of the nitrite is based on a kinetic stopped-flow procedure [32] using sulfanilamide and *N*-(1-naphthyl)ethylenediamine dihydrochloride as color reagent.

EXPERIMENTAL

Apparatus

The automated microcomputer-based stopped-flow system (s.f.s.) has been described by Malmstadt et al. [33]. This inexpensive and compact system, interfaced with an AIM 65 (Rockwell International) microcomputer, provides for automatic aliquoting and mixing of sample and reagent and delivery of the mixed solution into the measurement cuvet (1 cm pathlength). Each syringe delivers 150 μl of sample or reagent. The reduction column is fitted to the inlet port of the sample 3-way valve using a 0.25 in. —28 thread tube end fitting. An interference filter with a bandpass of about 10 nm at 540 nm is used in the photometer unit.

Reduction columns. The cadmium alloy reductor was made from teflon tubing (15 cm long, 2.0-mm i.d., 12 GA; Alpha Wire Corp.). A 1.6-mm o.d. wire of the same length, made of 95% cadmium —5% silver (Kapp Alloy and Wire Inc., Franklin, PA), was inserted into the tubing. The cadmium tube column was made from a cadmium metal rod (13 cm long, 1-cm o.d.) drilled to provide a 0.8-mm i.d. cylinder. Tube end fittings of 0.25 in. —28 thread were fitted to both ends for easy connection with the 3-way sample valve and a short teflon tube for aliquoting. The reductors were copperized by using a syringe to force through the column 10 ml each of the following

solutions: (1) 1 M HCl, (2) deionized water, (3) 2% (w/v) copper sulfate solution, and (4) deionized water in that sequence at about 20 ml min^{-1}. Slower and prolonged flushing with copper solution causes the formation of red copper particles that may block the flow system of the analyzer.

Reagents and samples

All reagents were of analytical grade and deionized water was used in all experiments. Standard stock solutions prepared to contain 1000 ppm NO_3^-—N (6.07 g $NaNO_3$ l^{-1}) and 1000 ppm NO_2^-—N (4.93 g $NaNO_2$ l^{-1}) were treated with a few drops of chloroform and kept in a refrigerator. A pellet of sodium hydroxide was added to the nitrite stock solution to prevent liberation of nitrous acid. Working standard solutions in the range 0.025—3 ppm NO_3^-—N and 0.025—2 ppm NO_2^-—N were prepared daily by appropriate dilution.

The color reagent was prepared by dissolving 10.0 g of sulfanilamide, 0.50 g of *N*-(1-naphthyl)ethylenediamine dihydrochloride and 30 ml of 85% phosphoric acid in water and diluting to 1 l. This solution was stored in an amber bottle in a refrigerator. The reduction buffer was prepared to contain 15 g of sodium tetraborate decahydrate, 80.2 g of ammonium chloride and 0.8 g of Na_2EDTA per liter of deionized water. This buffer has a pH of ca. 8. Acetate, phosphate and Tris buffers (0.025 M), containing 1.50 M NH_4Cl and 0.0024 M EDTA, in the pH range 4—9 were prepared. Various solutions of interfering ions were prepared to contain 1000 ppm of each ion to be tested.

Nitrate was determined in water samples from lakes and rivers near fields treated with nitrate fertilizers in Central-East Illinois.

Procedure

Determination of nitrate. Premix 2 ml of nitrate standards or water samples with 0.5 ml of the reduction buffer solution in 5-ml disposable polystyrene micro beakers by means of a dispenser-dilutor (Labindustries). Use one channel of the stopped-flow system to aliquot the reagent solution and the other channel (the reductor) for the standards and samples on the turntable. Load the appropriate basic and machine language programs from the cassette recorder into computer memory. For the multipoint reaction-rate procedure (concentration range 0.2—3 ppm NO_3^-—N) use a 0.8-s delay time, 1.5-s measurement time, and total reduction time of 15, 20 or 25 s dependent on the relevant nitrate concentration range. For the single-point kinetic procedure (concentration range 0.025—3.0 ppm NO_3^-—N) use a delay time of 10, 15 or 20 s and a measurement time of 0.7 s (one integration). In the execution of the program, a 150-μl aliquot of each standard is held in the reductor column during the reduction time selected and then is mixed with an equal volume of color reagent and transferred in the observation cell. The reaction rates or the absorbance values are printed, and by utilizing the concentrations of standards provided by the operator, the calibration curve is constructed. Each sample is then measured and its concentration is printed out. This value should be automatically corrected for any predilution of the sample.

Determination of nitrite and nitrate in mixture. The nitrite determination in the range 0.025—2 ppm is done first without the use of the reduction column as described earlier [32]. Then the reductor is fitted to the system and the samples, including three nitrite standards, are processed as described above. In the execution of the program, two calibration curves are constructed and the operator provides the nitrite concentration found for each sample. The computer calculates the nitrate concentration using the equation

$$\text{Rate or Absorbance} = a + S_{NO_2} \times \text{ppm}_{NO_2} + S_{NO_3} \times \text{ppm}_{NO_3}$$

(rate for multipoint kinetic and absorbance for single-point procedure) where a is the average of the intercepts of the two calibration curves and S the slope of the respective calibration curve.

RESULTS AND DISCUSSION

In choosing the most suitable reduction column for the stopped-flow system, the rapid aliquoting stroke of the sampling syringe (in about 100 ms) must be considered. The resistance of the column must be low to avoid incomplete aliquoting and the generation of air bubbles in the syringe. Therefore, columns that consisted of zinc granules or cadmium filings were found to be unsuitable, with poor precision in aliquoting and serious carry-over contamination. The copperized cadmium wire column introduced by Stainton [29] was shown to overcome the above problems but there was a gradual removal of copper from the soft thin cadmium wire.

The copperized cadmium—silver alloy reductor was found to be the most suitable column for the system. The resistance of the column is not very high and a stable copper surface can be obtained easily and in a short time. During the one month of continuous use with the usual water samples, its reduction efficiency remained constant.

Although this column is superior to those previously tried, the carry-over contamination is a concern because the sample solution is in contact with two surfaces, the inner surface of the teflon tubing and the copperized surface of the alloy wire. Therefore, an increased number of flushes (5—7) is needed to change from one sample to another. Four flushes are usually needed without the reductor. For this reason, the use of a new reductor consisting of a 1-cm o.d. cadmium rod with a 0.8-mm i.d. hole was examined. The copperized inner surface of this cadmium tube provided a stable and sufficient reduction efficiency with very low flow resistance and without the previously described carry-over problem. Based on these results, a coil of a cadmium—silver alloy tubing with i.d. less than 1 mm should be the best reductor for automated systems.

The reduction efficiencies of the cadmium alloy wire and cadmium tube columns were found to be 50—90%, dependent on the length of the column and the reduction time. The less than 100% efficiency is because not all the solution comes in contact with the reducing surface. There is no movement

of the sample in the column during the reduction period. This problem does not decrease the precision of the method because the aliquoting is very precise and the timing of the operations provided by the computer is very reproducible. The lower reduction efficiency causes a somewhat lower sensitivity for nitrate but rarely do water samples contain less than 0.05 ppm NO_3^-—N, which is within the sensitivity obtained by this method. A redesign of the standard stopped-flow system to improve the sensitivity is not necessary for typical water samples.

The effect of the pH on the reduction of nitrate was studied with the copperized cadmium alloy column, and the results are shown in Table 1. A borate buffer of pH 8.0 was found to be optimum. The concentration chosen ensures stability of the final pH (1.4) in the reaction cell in conjunction with the phosphoric acid concentration of the color reagent.

Because the chloride concentration in water samples varies greatly, the effect of this ion on nitrite and nitrate determination was studied over a wide concentration range. As shown in Table 2, chloride interferes with both nitrate and nitrite determinations. By obtaining calibration curves for nitrite and nitrate in the absence and the presence of 0.3 M chloride (which roughly represents the chloride concentration in seawater), decreases of 19% and 27%, respectively, on the slopes were found. The chloride in high concentration interferes primarily with the color reaction but also with the nitrate reduction, as also observed by Nydahl [26]. However, by preparing the reduction buffer to be 0.3 M chloride (in the diluted sample) the standards and samples will be similar and the chloride interference will be small. The interference was not observed by previous investigators because they were using color reagent prepared in hydrochloric acid (i.e., high chloride concentration) instead of phosphoric acid.

The effect of the reduction time on the reduction efficiency and the maximum sample throughput is shown in Table 3. The reduction efficiency increases when longer reduction times are used but the sample throughput decreases. There is also a decrease in the nitrite concentration as the reduction time increases because of the over-reduction of nitrite to ammonia. By

TABLE 1

Effect of pH on the reduction of nitrate

pH	Buffer[a]	Rate[b] (mA s^{-1})	%RSD (n = 5)	pH	Buffer[a]	Rate[b] (mA s^{-1})	%RSD (n = 5)
4.0	Acetate	41.4	5.7	8.0	Tris	155.5	1.5
5.0	Acetate	115.6	1.0	8.0	Borate	160.1	0.4
6.0	Phosphate	142.5	0.9	9.0	Tris	157.5	0.4
7.0	Phosphate	125.7	2.3				

[a]Buffer concentration 5×10^{-3} M with 0.30 M NH_4Cl and 4.8×10^{-4} M EDTA, in the diluted sample. [b]Nitrate 1 ppm. Reduction time 25 s.

TABLE 2

Effect of chloride concentration on the nitrite and nitrate determinations

[Cl] (mol l^{-1})	0.00	0.01	0.10	0.30	0.50
Rate (mA s^{-1})					
1 ppm NO_2^-—N[a]	317.5	318.2	278.1	252.2	248.6
1 ppm NO_3^-—N	227.6	—	170.2	166.1	167.6

[a]Without the reduction column. All concentrations refer to those in the diluted samples.

TABLE 3

Effect of reduction time on reduction efficiency and the maximum sample throughput with the cadmium alloy wire column

Reduction time (s)	Rate (mA s^{-1})		Reduction[a] efficiency (%)	Sample[b] throughput (samples/h)
	1 ppm NO_3^-—N	1 ppm NO_2^-—N		
15	130.6	256.2	51	97
20	147.9	255.8	58	76
25	160.1	254.4	63	63
30	172.1	253.1	68	53
35	177.5	252.3	70	46

[a]Expressed as the nitrate/nitrite rate. [b]Assuming five flushes and one measurement per sample.

obtaining calibration curves for nitrite standards without and with the reduction column (reduction time 25 s) a decrease of 1.5% on the slope was found.

The reduction efficiency can also be increased by using longer reduction columns so that sample aliquots are held in the column during two reduction cycles. Two typical cadmium alloy wire columns were examined with lengths of 15 and 30 cm. For a reduction time of 25 s, the reduction efficiency was increased from 63 to 87%, the flushes needed were increased from 5 to 7, and the maximum throughput was decreased from 63 to 43 samples per hour.

Statistical equations for typical nitrate calibration curves, using the two procedures are as follows:

(a) Multipoint kinetic procedure (reduction time 25 s):

$$\text{Rate (mA s}^{-1}) = (243.9 \pm 1.99) \times C + (9.14 \pm 3.02); S_{yx} = 3.90, r = 0.99991$$

The measured rates ranged from 54.7 to 616.3 mA s^{-1} with %RSD (n = 5) 0.2—2.1%.

(b) Single-point kinetic procedure (reduction times 10, 15 and 25 s):

$$A = (0.542 \pm 3.25 \times 10^{-3}) \times C + (1.09 \times 10^{-3} \pm 5.02 \times 10^{-3});$$

$$S_{yx} = 8.34 \times 10^{-3}, r = 0.99993$$

$A = (0.657 \pm 3.38 \times 10^{-3}) \times C + (1.67 \times 10^{-3} \pm 3.17 \times 10^{-3})$;

$S_{yx} = 5.68 \times 10^{-3}$, $r = 0.99995$

$A = (0.788 \pm 1.88 \times 10^{-3}) \times C - (1.61 \times 10^{-3} \pm 8.75 \times 10^{-4})$;

$S_{yx} = 1.59 \times 10^{-3}$, $r = 0.99998$

The measured absorbance values ranged from 0.020 to 1.620 with %RSD ($n = 5$) 0.1—6.7%.

In these equations, A = absorbance, C = nitrate concentration in ppm NO_3^-—N, and S_{yx} = standard error of estimate. Similar results were obtained when the drilled cadmium rod column was used, with less reduction efficiency but with only 4 flushes and thus higher sample throughput. From the results obtained, the multipoint reaction-rate procedure had better precision but less sensitivity than the single-point procedure.

The accuracy of the proposed method was examined by measuring the nitrite and nitrate concentrations of synthetic mixtures using the reaction-rate multipoint procedure. Eight samples, containing 0—1 ppm NO_2^-—N and 0—1.5 ppm NO_3^-—N (maximum sum 2 ppm N), were measured and absolute errors ranged from 0 to 0.074 ppm (av. rel. error 1.3%).

A recovery study was also done for ten lake and river water samples by measuring the nitrate concentration before and after standard addition. Samples were also assayed for nitrite and the equation for the determination of nitrite and nitrate in the mixture was used. The nitrite content was found to be equivalent to <0.2 ppm N. Samples higher than 3 ppm were diluted with distilled water. The results obtained (Table 4) show an average recovery of 100.2%.

TABLE 4

Recovery data for the determination of nitrate in lake and river water samples with the multipoint kinetic procedure and cadmium alloy column

Sample	Nitrate content (ppm NO_3^-—N)			Recovery (%)
	Before std. addition	After std. addition		
		Expected	Determined	
1	1.90	6.90	7.05	102.2
2	10.50	13.00	13.00	100.0
3	11.95	14.45	14.25	98.6
4	0.10	1.10	1.11	100.9
5	0.40	1.40	1.41	100.7
6	10.70	13.20	13.15	99.6
7	10.90	13.40	13.55	101.1
8	12.90	14.15	14.20	100.4
9	5.20	7.70	7.65	99.4
10	0.39	1.39	1.37	98.6
			Average	100.2

TABLE 5

Effect of diverse ions on the determination of nitrate by the multipoint reaction-rate procedure with the cadmium alloy wire column

Interferent[a]	Ion: nitrate[b]	Error[c] (%)	Interferent[a]	Ion: nitrate[b]	Error[c] (%)
Cyanide	100	−99.5	Copper	100	−50.5
	10	−7.0		10	None
	1	None	Iron(III)	10	None
Dichromate[d]	10	−21.5	Magnesium	100	+6.5
	1	−10.4		10	None
Iodate	100	−7.5	Mercury	100	−2.5
Iodide	100	−14.1	Tin(II)	10	−88.5
	10	None		1	−15.2
Sulfide[d]	10	−12.0	Nickel[d]	100	−11.0
	1	−2.6		10	None
Cobalt	100	−3.5	Phenol	100	−6.1

[a]The following ions in 100 concentration ratio showed negligible interference: acetate, bromide, carbonate, fluoride, oxalate, perchlorate, sulfate, sulfite, cadmium, calcium, manganese, zinc, silicate, urea, and hypochlorite. [b]Nitrate concentration 2 ppm. [c]None means <2%. [d]Permanent decrease in the reduction efficiency of the column; regeneration is needed.

The effect of various potential interferences was also investigated. The results of these experiments are shown in Table 5. Most of the common ions present in water samples do not interfere even in high concentrations. Those ions that showed serious interference rarely are found in water samples at the highest concentrations examined.

The authors are grateful to the National Institute of Health for partial support of this research through grant PH5-SR01 GM 21984.

REFERENCES

1 D. R. Keeney, B. H. Byrnes and J. J. Genson, Analyst, 95 (1970) 383.
2 J. B. Mullin and J. P. Riley, Anal. Chim. Acta, 12 (1955) 464.
3 M. T. Downes, Water Res., 12 (1978) 673.
4 R. H. Bray, Soil Sci., 60 (1945) 219.
5 E. Foyn, Rep. Norw. Fish. Mar. Invest., 9 (1951) 7.
6 T. J. Chow and M. S. Johnstone, Anal. Chim. Acta, 27 (1962) 441.
7 L. Potzl and R. Reiter, Z. Aerosol-Forsch. Ther., 8 (1960) 252.
8 M. Bernard and G. Macchi, Automation in Analytical Chemistry, Technicon Symposia, 1965, Mediad, NY, 1966, p. 255.
9 P. G. Brewer and J. P. Riley, Deep-Sea Res., 12 (1965) 765.
10 J. H. Margeson, J. C. Suggs and M. R. Midgett, Anal. Chem., 52 (1980) 1957.
11 A. W. Morris and J. P. Riley, Anal. Chim. Acta, 29 (1963) 272.
12 K. Grasshoff, Kiel. Meeresforsch., 20 (1964) 5.

13 E. D. Wood, F. A. Armstrong and F. A. Richards, J. Mar. Biol. Assoc. U.K., 47 (1967) 23.
14 A. Henriksen and A. R. Selmer-Olsen, Analyst, 95 (1970) 514.
15 R. S. Lambert and R. J. Dubois, Anal. Chem., 43 (1971) 955.
16 R. D. Britt, Jr., Anal. Chem., 34 (1962) 1728.
17 A. Henriksen, Analyst, 90 (1965) 83.
18 M. R. Galley, Automation in Analytical Chemistry, Technicon Symposium, 1966, Vol. 1, p. 643.
19 P. G. Brewer and J. P. Riley, Deep-Sea Res., 12 (1965) 765.
20 F. A. J. Armstrong, C. R. Stearns and J. D. H. Strickland, Deep-Sea Res., 14 (1967) 381.
21 A. Henriksen and A. R. Selmer-Olsen, Analyst, 95 (1970) 514.
22 Technicon Method., No. 158-71 W, 1972. Technicon Corp., Tarrytown, N.Y. 10591.
23 L. Andersen, Anal. Chim. Acta, 110 (1979) 123.
24 M. F. Giné, H. Bergamin F°, E. A. G. Zagatto and B. F. Reiss, Anal. Chim. Acta, 114 (1980) 191.
25 B. C. Madsen, Anal. Chim. Acta, 124 (1981) 437.
26 F. Nydahl, Talanta, 23 (1976) 349.
27 APHA—AWWA—WPCF, Standard Methods for the Examination of Water and Wastewater, 15th edn., Washington, D.C., 1980, pp. 370, 376.
28 A. Otsuki, Anal. Chim. Acta, 99 (1978) 375.
29 M. P. Stainton, Anal. Chem., 46 (1974) 1616.
30 R. B. Willis, Anal. Chem., 52 (1980) 1376.
31 D. L. Krottinger, M. S. McCracken and H. V. Malmstadt, Am. Lab., 9 (1977) 51.
32 M. A. Koupparis, K. M. Walczak and H. V. Malmstadt, Analyst, 108 (1982) in press.
33 M. A. Koupparis, K. M. Walczak and H. V. Malmstadt, J. Autom. Chem., 2 (1980) 66.

Analytica Chimica Acta, 142 (1982) 129—142
Elsevier Scientific Publishing Company, Amsterdam — Printed in The Netherlands

INVESTIGATIONS OF REACTIONS INVOLVED IN ELECTROTHERMAL ATOMIC ABSORPTION PROCEDURES

Part 11. A Theoretical and Experimental Investigation of Factors Influencing the Determination of Tin

ERIK LUNDBERG*, BJÖRN BERGMARK and WOLFGANG FRECH
Department of Analytical Chemistry, University of Umeå, S-901 87 Umeå (Sweden)
(Received 12th May 1982)

SUMMARY

Factors of importance for the determination of tin by graphite-furnace atomic absorption spectrometry have been investigated. Losses of tin during the drying and ashing stages were monitored by use of radioactivity measurements. It was found that tin could be lost at 100°C when ordinary graphite or glassy carbon surfaces were used. However, if the sample was dispensed into a droplet of ammonia, no losses occurred until 800°C, independent of the graphite surface, because tin is stabilized as SnO_2 (s, l) and chloride is removed as ammonium chloride. High-temperature equilibrium calculations indicate that tin forms volatile oxides, halides and sulphides which are stable up to relatively high temperatures. As is shown experimentally with commercial non-isothermal atomizers, these molecules might be removed from the system before their decomposition temperature is reached. A recently developed constant-temperature furnace was used to vaporize the sample into an environment of high and constant temperature, in which interference effects from chlorine and sulphur were minimized, as predicted by theory.

Tin can be regarded as one of the more troublesome elements to determine by graphite-furnace atomic absorption spectrometry. This can be explained by the tendency of tin to form volatile compounds and to interact with graphite. From thermodynamic data [1, 2], its gaseous oxides, halides and sulphides are stable up to relatively high temperatures. This means that tin can be lost in molecules before a temperature sufficiently high for decomposition of the molecules is reached, which probably is the main reason for the numerous interference problems reported in the literature [3—12]. Thermodynamic data for compounds between tin and carbon are not available in standard tables [1, 2]. However, pretreatment of the graphite tube surface with elements that form refractory carbides (W, Ta, Zr, Mo) has produced better sensitivity [8, 10, 13], and it is likely that tin reacts with graphite.

Most papers dealing with tin determinations have described only effects caused by a number of matrix constituents in connection with different atomizer surfaces. In this paper, attempts are made to differentiate between the various parameters influencing the atomic absorption signal. The role of

0003-2670/82/0000-0000/$02.75

the graphite surface was investigated by employing the platform technique [14] which makes it possible to study the single effect of the surface in contact with the sample, independently of the atomizer material. Losses of tin during thermal pretreatment of the tube were monitored by using radioactivity measurements. A recently developed constant-temperature furnace [15] was used to accomplish efficient atomization, thus minimizing interference effects. In addition, an on-line data acquisition system was used to obtain information from the shape of the tin signals [16]. Alongside the experimental work, a theoretical study was made using high-temperature equilibrium calculations in order to establish the reactions leading to the formation of tin atoms.

EXPERIMENTAL

Instrumentation

A Varian-Techtron AA-6 atomic absorption spectrometer provided with background correction was fitted with a carbon rod atomizer (CRA 63). The original transformer of the CRA 63 power supply was replaced by a more powerful transformer capable of delivering 7.5 kW. To this transformer was connected a Varian CRA 90 workhead (only for measurements under isothermal conditions) or a Perkin-Elmer HGA 74. The power supply was modified to provide a burning-out step immediately after the atomization step. Facilities for close temperature control of the graphite tube of each furnace were installed. A fibre optic cable, directed towards the outer surface of the tube, was mounted on each furnace and the light emitted from the tube was monitored with a photodiode sensitive to infrared radiation. The principle of this optical feedback control has been described earlier [17]. Temperature settings referring to the inner surface of the graphite tube (or bottom of the CRA 90 cup) were calibrated with a NiCr—Ni thermocouple (below 1000°C) and with an optical pyrometer (Keller Spezialtechnik Pyro Werk GmbH, Model PB0 6AF3) for higher temperatures.

The signal damping of the AA-6 readout module was modified to obtain a faster response time of the electronics. The value of the DAMP A time constant was thus altered from the original 260 ms to 10 ms, as described earlier [18]. To the recorder output of the spectrometer a peak reader module was connected [19], providing simultaneous recording of the peak height and the peak area. To be able to study in detail the time dependence of the analytical signals as well as the temperature, a fast on-line data acquisition system was connected to the spectrometer [16]. After data processing, the atomic absorption as well as the temperature signals were plotted on a X—Y recorder. The instrumental parameters are summarized in Table 1. Background correction was used throughout.

The equipment for radioactivity measurements (γ-radiation) consisted of a 45 × 50-mm NaI(Tl) well-type scintillation detector (Berthold, SZ44/50-W-N) connected to a high-voltage power supply (Berthold, LB2210), a linear

TABLE 1

Instrumental parameters

	Time (s)	Temp. (°C)	Heating rate (°C s^{-1})
Drying	35	100	5
Ashing	35	800	50
Atomization[a]	3	2100	1900
Cleaning	2	Max	—
Wavelength (nm)			286.3
Spectral bandwidth (nm)			0.7
Lamp current (mA)			8
Hydrogen lamp current (scale division)			3
Argon flow (l min^{-1})			
internal			0.050
external			1.4

[a]Temperatures given for standard tubes; for tungsten-treated and glassy carbon tubes, the same instrumental settings were used.

amplifier with integral discriminator (Berthold, LB2220), and a scaler-timer unit (Berthold, BF2270-1).

Reagents and materials

A 1000-μg ml^{-1} stock solution of tin was prepared by dissolving 0.1000 g of tin (99.9%, Analar) in 10 ml of concentrated hydrochloric acid and 1 ml of 90% formic acid (gentle heating), followed by dilution to 100 ml with distilled water. Standard solutions were prepared by dilution with 10% hydrochloric acid, and were stored in acid-washed polyethylene bottles. To some standard solutions, glucose was added to a final concentration of 1%. The radioactive stock solution of ^{113}Sn ($t_{1/2}$ = 115 d) used contained 46 μg Sn ml^{-1} in 6 M hydrochloric acid in the form of $SnCl_6^{2-}$ (Radiochemical Centre, Amersham). A 0.46 μg Sn ml^{-1} radioactive standard solution was prepared by dilution with the 10% acid and was used in all experiments. All gases used were of SR-grade purity, and the chemicals were of analytical grade.

Three types of graphite tubes were used: glassy carbon tubes (Tokai Lux Ore and Chemical, Tokyo) manufactured in this Department, standard graphite tubes (Perkin-Elmer), and tungsten-impregnated tubes. The impregnation was done as described by Fritzsche et al. [10].

Platforms of rectangular shape were manufactured from standard or glassy carbon tubes. The platforms were 8 mm long, 5 mm wide and 1 mm thick; in order to minimize heating by conduction from the furnace walls, cuts were made along the lateral edges of the platform so that only 1 mm in each corner was in contact with the wall. The platforms were cleaned before use by heating at 2800°C for 10 s.

Procedures

Procedure for radioactive measurements. Standard ^{113}Sn solution (3 μl) was injected onto a platform installed in the middle of the tube and was thermally treated ("ashed") at different temperatures, 90 s at each temperature. After each 90-s ashing step, the platform was removed and the amount of ^{113}Sn left was measured. Care was taken in positioning the platform in a reproducible way in the detector in order to ensure a similar geometry for all counts. Relative losses of ^{113}Sn at different temperatures were compared with the undried droplet.

Measurements under isothermal conditions. Graphite of quality RWO (Ringsdorff Werk GmbH) was cut into pieces of 3 ± 0.3 mg and cleaned by heating in a graphite tube at its maximum temperature for 10 s. A 1-μl aliquot of a 100-μg g^{-1} tin standard solution was pipetted onto these pieces with an Oxford micropipette, followed by careful drying under an electric bulb. The graphite pieces were dropped into a Varian CRA 90 graphite cup after the preset final temperature had been reached. Measurements were made at the resonance wavelength, 300.9 nm.

Measurements with addition of $NiCl_2$, HCl and H_2SO_4. A portion (2 μl) of 5% nickel chloride or 10 μl of 1.2 M hydrochloric acid or 10 μl of 0.008 M sulphuric acid was added to each end of the graphite tube after the sample (3 μl of 2 μg Sn g^{-1} and 10 μl of 10% ammonia) had been ashed at 800°C. The droplets were dried at 100°C, whereafter the temperature was raised to 2100°C.

Confirmatory experiments

A recently developed furnace for constant-temperature measurements, consisting of two Varian CRA 90 workheads, was used [15]. Samples were dosed into a graphite cup (5-mm o.d., 3-mm i.d., 9 mm high) which was fastened tightly to an aperture of a graphite tube (6-mm o.d., 4-mm i.d., 13 mm long). To accomplish atomization, the tube was heated to a preselected temperature (2100°C) followed by heating of the cup by means of a separate power supply. The heating rate of the tube was 2500°C s^{-1} and of the cup 1000°C s^{-1}.

During the measurements under non-isothermal conditions, the cup was taken away and the tube described above was replaced by a tube with the same dimensions but without the aperture. All graphite parts used in these experiments were made from high-density graphite.

High-temperature equilibrium calculations

The calculations were done as described in Part 1 [20]. The elements and compounds considered are given in Table 2.

TABLE 2

Species considered in the equilibrium calculations

Gaseous:	Ar, H_2, H, O_2, O, N_2, N, NO, NO_2, N_2O, C, CO, CO_2, CN, H_2O, CH_2, CH_4, HCO, HCl, CCl_2, COCl, S_2, S, H_2S, CS, CS_2, COS, SO, SO_2, Si, SiO, SiS, $SiCl_2$, Cl_2, Cl, ClO, W, WCl, WCl_2, WCl_4, WO, WO_2, WO_3, Sn, SnH_4, SnO, $SnCl_2$, $SnCl_4$, SnS.
Condensed:	C, SiO_2, W, WCl_2, WCl_4, WO_2, WO_3, W_2C, WC, Sn, SnO, SnO_2, $SnCl_2$, $SnCl_4$, SnS, SnS_2, Sn_2S_3.

RESULTS AND DISCUSSION

General survey

Figure 1 shows the calculated distribution of tin species as a function of temperature and partial pressure of diatomic oxygen. Because the reaction between carbon and oxygen proceeds to a greater extent at higher temperatures, the decrease in the partial pressure of oxygen was taken into account. The partial pressure of oxygen inside the graphite tube at the beginning of the atomization step (1100 K) was estimated to be 10^{-6} atm, in accordance with earlier work [21].

Figure 2A shows an ashing curve for tin when vaporized from a glassy carbon tube, whereas Fig. 2B shows an absorbance signal for tin from the same tube. As can be seen, an atomic vapour of tin sufficiently dense to give a measurable signal is not obtained until 1700 K. In contrast, losses of tin are observed at temperatures above 1100 K. These observations can be explained

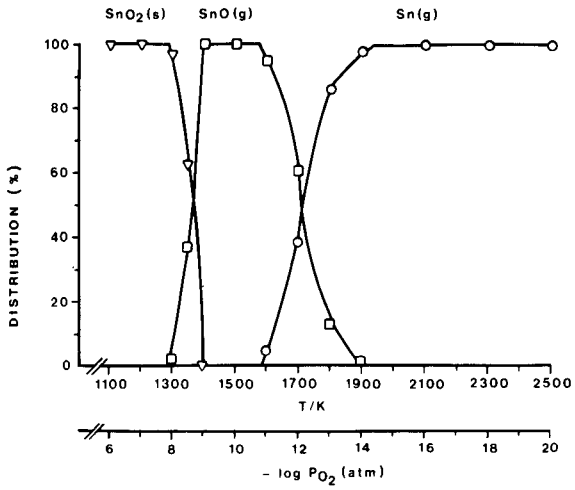

Fig. 1. Calculated distribution of tin species as a function of temperature and partial pressure of diatomic oxygen. The input amounts (μmol) used in the calculations were: Ar = 4, C = 1, H_2 = 0.014, Cl_2 = 5 × 10^{-5} and Sn = 1 × 10^{-4}.

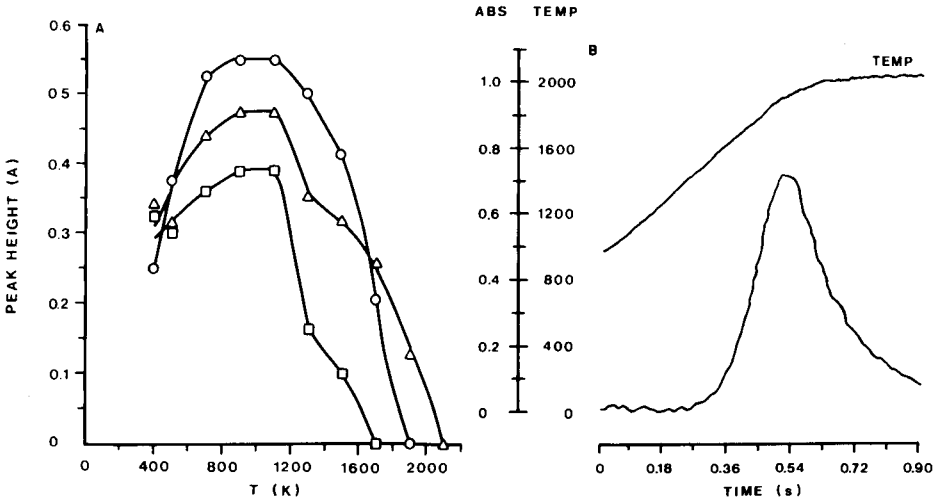

Fig. 2. A, Absorbance for 3 μl of 2 μg Sn g^{-1} + 10 μl of 10% NH_3 as a function of the final ashing temperature, when vaporized from (○) ordinary, (△) tungsten-treated, (□) glassy carbon tubes. B, Transient signal obtained from a typical experiment in A, with a glassy carbon tube, and the variation of temperature (°C) with time.

by the theoretical calculations shown in Fig. 1, according to which SnO(g) is formed between 1300 and 1900 K and is lost without causing absorbance up to ca. 1600 K. These results thus show that the main pathway for the formation of tin atoms can be described by the reaction $SnO_2(s) \rightarrow SnO(g) \rightarrow Sn(g)$. However, this result is in disagreement with the mechanism proposed by Sturgeon and Chakrabarti [22], which involves $SnO_2(l) \xrightarrow{\text{reduction}} Sn(l) \rightleftharpoons Sn_2(g) \rightarrow Sn(g)$.

To investigate possible effects of oxygen on the mechanism of formation of tin atoms, the distribution of tin species at 1400 K was calculated for different partial pressures of oxygen (Fig. 3). For $P(O_2) > 10^{-13}$, the first mechanism is applicable, whereas for $P(O_2) < 10^{-17}$, the second applies. In the range between these extremes, a mixture of the two mechanisms is likely to occur. According to Fig. 3, the experimental results show that the first mechanism is predominant.

Large deviations with regard to appearance temperatures for tin have been reported [14]. Figure 4 shows the highest calculated partial pressure of oxygen which gives rise to 2% of the input amount of tin as Sn(g) at different temperatures. As can be seen, the magnitude of $P(O_2)$ is likely to be one reason for the large deviation in reported values.

Condensed-phase interference effects

Standard solutions of tin have to be prepared in strong hydrochloric acid in order to avoid formation of gels and precipitates. This means that chlorides will be present during the drying and ashing steps. Losses of tin during these

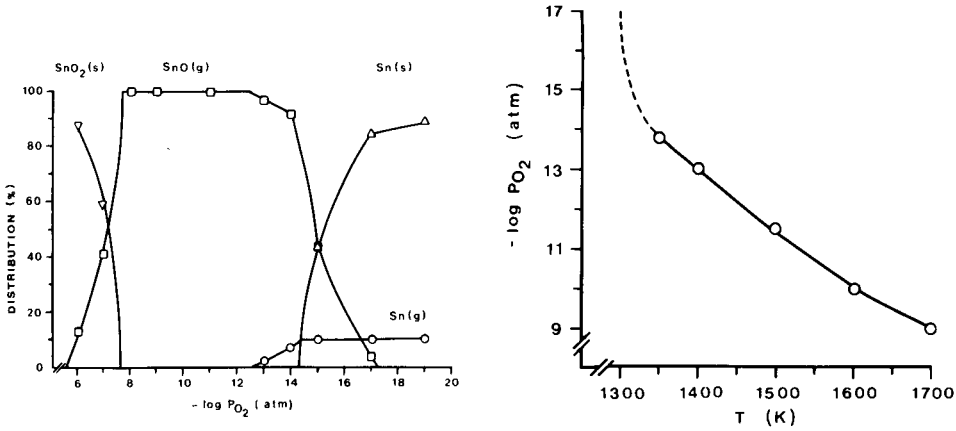

Fig. 3. Calculated distribution of tin species as a function of partial pressure of diatomic oxygen at 1400 K. The input amounts (μmol) used in the calculations were as in Fig. 1.

Fig. 4. Highest calculated partial pressure of diatomic oxygen which gives rise to 2% of the input amount of tin (2×10^{-6} μmol) as Sn(g) at different temperatures. At < 1350 K, the amount of Sn(g) formed will be < 2% regardless of $P(O_2)$. The input amounts (μmol) used in the calculations were as in Fig. 1.

steps, when different surfaces were used, were established by means of radioactivity measurements (Fig. 5). Curves b and c of Fig. 5A show that tin in 10% hydrochloric acid was already lost at 400 K when ordinary or glassy carbon surfaces were used. In contrast, when a tungsten-treated graphite surface was used (curve a), no losses occurred until 1000 K. One reason might be the formation of tin—tungsten compounds like $Sn_2W_3O_8$ [23].

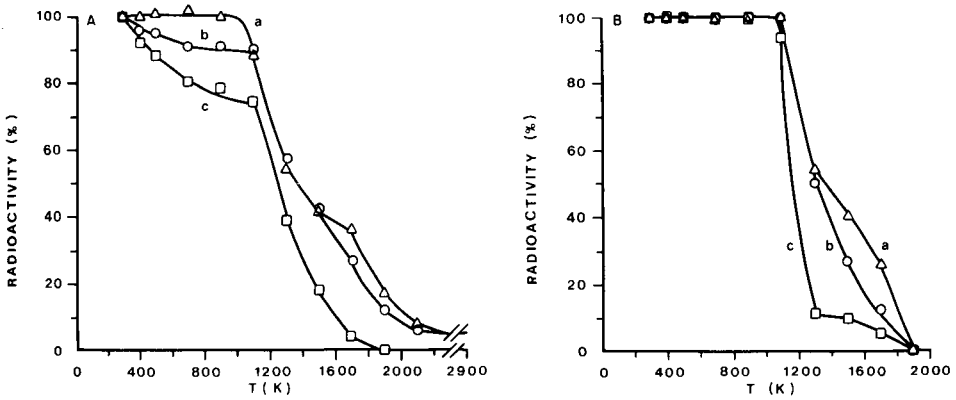

Fig. 5. Relative amounts of 3 μl of 0.46 μg ^{113}Sn g^{-1} left after ashing at different temperatures when (a) tungsten-treated, (b) ordinary, and (c) glassy carbon platforms were used. A, Normal injection; B, injection into 10 μl of 10% ammonia.

Another reason is that tungsten competes with tin for chlorine (see below). Figure 5B shows corresponding measurements when the sample was dispensed into a droplet of 10% ammonia. As can be seen, curves a–c coincide up to about 1100 K, which is in rough agreement with Fig. 1. The addition of ammonia thus probably eliminates interferences from chlorine during the ashing step. A comparison between Fig. 5A and B with respect to curves a and b shows that ammonia prevents the formation of stable tin–graphite compounds, probably because of the initial formation of $SnO_2(s)$.

The results shown in Fig. 5 were obtained for aqueous standard solutions. However, dissolved samples usually contain a matrix material, and interferences from chlorine might then be much more pronounced than those shown in Fig. 5. In order to give an idea of the tendency of tin to form chlorides, the distribution of tin species at 900 K was calculated for different input amounts of chlorine (Fig. 6). As can be seen, even partial pressures of chlorine as low as 10^{-6} atm give rise to the formation of $SnCl_4(g)$. It should also be mentioned that the consideration of tungsten in the calculations resulted in a displacement of the equilibria, so that less $SnCl_4(g)$ was formed.

In order to establish the relevance of the calculations in Fig. 6, the experiment given in Fig. 5B (curve c) was repeated with the addition of palladium chloride. This salt decomposes at 770 K [24], thus giving rise to the formation of chlorine at a temperature where $SnO_2(s)$ is stable (Fig. 5B). As can be seen from Table 3, great losses can occur during the ashing step if large amounts of chlorine are present.

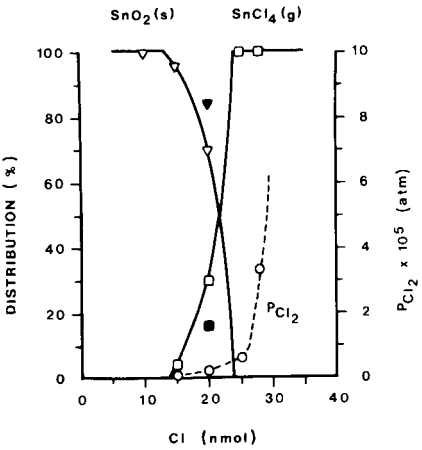

Fig. 6. Calculated distribution of tin species and partial pressure of chlorine as a function of input amounts of chlorine at 900 K. The input amounts (μmol) used in the calculations were: Ar = 4, C = 1, H = 0.014, Sn = 1×10^{-4}, W = 0 (unfilled symbols) or 0.1 (filled symbols); $P(O_2) = 10^{-8}$ atm.

TABLE 3

Relative amounts of ^{113}Sn left on a glassy carbon platform after ashing at different temperatures when $PdCl_2$ was added to the tin solution[a]

Temperature (K)	370	470	570	670	770	870
Radioactivity (%)	96	97	90	74	64	25

[a] 3 μl of 0.46 μg ^{113}Sn g^{-1}, 10 μl of 10% NH_3 and 3 μl of 1000 μg $PdCl_2$ g^{-1}.

Gas-phase interference effects

Theoretically, tin can form stable molecules even at relatively high temperatures. This is exemplified in Fig. 7, which shows the distribution of tin species at 1800 K as a function of the input amount of chlorine. For an input of 10 nmol of Cl, 65% of the tin will be present as $SnCl_2(g)$. The equilibrium partial pressure of Cl_2 at this point is as low as 0.16×10^{-8} atm. The input amount of H_2 was estimated to 14 nmol, which corresponds to 0.01% of the water originally dispensed into the tube. If the H_2 is increased to 140 nmol, the fraction of tin present as $SnCl_2(g)$ is decreased to 10%. It should be mentioned that, in contrast to the calculations performed at 900 K (Fig. 6), the addition of tungsten has no effect on the distribution of tin species at 1800 K.

The calculations used to obtain Fig. 7 can be used to explain the shapes of the ashing curves in Fig. 2A. As can be seen, the sensitivity increases with temperature up to 1100 K. This can be explained by the more efficient removal of chlorides and water at higher temperatures. This means that less

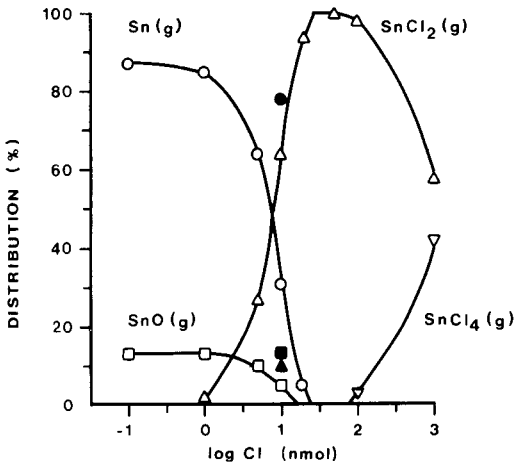

Fig. 7. As Fig. 6, at 1800 K, except for H_2 = 0.014 (unfilled symbols) or H_2 = 0.14 mol (filled symbols) and W = 0 or 0.1 μmol; $P(O_2) = 10^{-13}$ atm. The partial pressure of chlorine was 0.11×10^{-10} atm for log Cl = 0, 0.30×10^{-9} atm for log Cl = 0.7 and 0.16×10^{-8} atm for log Cl = 1.

chlorine is available during atomization. As was shown earlier (Fig. 5B), no losses of tin occur below 1100 K under the conditions used.

A strong suppressive effect of sulphuric acid on the tin signal has been reported [10]. Figure 8 shows thermodynamic calculations at 1800 K which include the presence of sulphur, silicon and tungsten. As can be seen, even stoichiometric input amounts of Sn and S give rise to the formation of considerable amounts of SnS(g) for a wide range of $P(O_2)$. An increase in the input amount of H_2 to 0.14 μmol yields the following distribution of tin species at the point $P(O_2) = 10^{-13}$ atm: Sn(g) = 12, SnO(g) = 2, $SnCl_2$(g) = 2 and SnS(g) = 84 pmol. This means that interferences from sulphur (in contrast to chlorine) cannot be removed by the addition of H_2 during atomization. The possibilities for decreasing interferences from sulphur include the addition of a stabilizing agent for sulphur (e.g., lanthanum) or increasing the temperature into which the sample is vaporized (e.g., the platform technique). If the temperature used for Fig. 8 is increased to 2400 K at the point $P(O_2) = 10^{-13}$ atm (S = 0.1 nmol), then 97% of the tin will be present as Sn(g). Similarly, if 2400 K is used in Fig. 7 at the point log Cl = 1 (H_2 = 0.014 μmol and $P(O_2) = 10^{-13}$ atm), the fraction of tin present as Sn(g) will be 99%.

The effect of oxygen on the tin signal was investigated with an open atomizer (CRA 90), where higher partial pressures of oxygen can be expected. Figure 9 shows signals for tin obtained at constant temperature, as a function of the argon flow rate. The higher sensitivity seen for higher argon flow rates

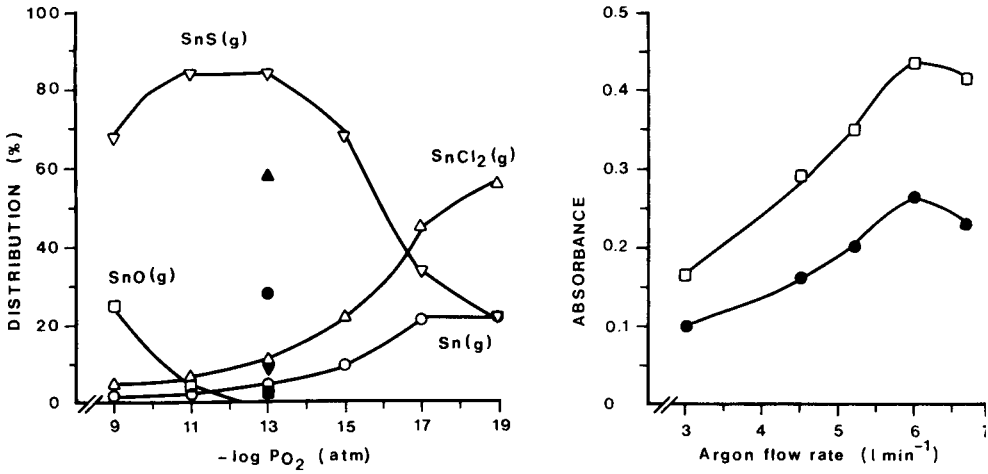

Fig. 8. Calculated distribution of tin species as a function of partial pressure of diatomic oxygen at 1800 K. The input amounts (μmol) used in the calculations were: Ar = 4, C = 1, H_2 = 0.014, Cl_2 = 5 × 10^{-3}, Sn = 1 × 10^{-4}, S = 1 × 10^{-4} (unfilled symbols) or S = 1 × 10^{-5} (filled symbols), W = 0.1 and Si = 1 × 10^{-4}.

Fig. 9. Absorbances for tin obtained at constant temperature (2500 K), as a function of argon flow rate: (□) peak height; (•) peak area.

(i.e., lower partial pressures of oxygen) can be explained by the results of the calculations which are shown in Fig. 10. If hydrogen is added to the argon, the amount of Sn(g) formed is considerably increased, as shown in Figs. 10 and 11. It is also evident from Fig. 11 that the sensitivity will in this case be less susceptible to changes in the argon flow rate. These findings are in agreement with results recently reported by Rayson and Holcombe [25].

Condensed and gas phase interference effects

In practical work it is difficult to relate the interference effects obtained to a specific stage of the heating sequence. Figure 12 shows absorbance signals for tin with and without added nickel chloride; also included is the specific signal for nickel. As can be seen, the tin signal is almost completely suppressed in the presence of nickel chloride. The relative position of the specific signals indicates that chlorine will be present during the formation of tin atoms. However, possible interaction between Sn and Cl_2 when the ashing temperature region 400—1100 K is passed cannot be excluded.

Graphite is known to retain H_2O, HCl and H_2SO_4 [26—28]. If these compounds are present during the atomization step, interferences can be expected. In order to get an idea about the magnitude of such interferences, hydrochloric or sulphuric acid was added to each end of the tube after the sample had been ashed. The results of these experiments are shown in Table 4.

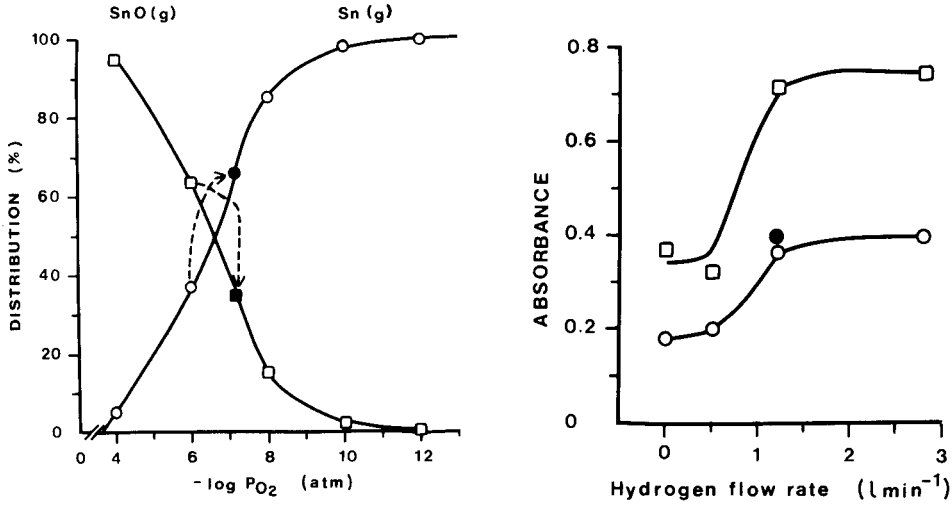

Fig. 10. Calculated distribution of tin species as a function of $P(O_2)$ at 2500 K. The input amounts (μmol) used in the calculations were: Ar = 4, C = 1, H_2 = 0.014 (unfilled symbols) or H_2 = 0.4 corresponding to 10% H_2 (filled symbols), Cl_2 = 5 × 10^{-5} and Sn = 1 × 10^{-4}.

Fig. 11. Absorbances for tin obtained at constant temperature (2500 K), as a function of added hydrogen flow rate. The argon flow rate was 6.0 (unfilled symbols) or 4.5 l min^{-1} (filled symbol). (□) Peak height; (○) peak area.

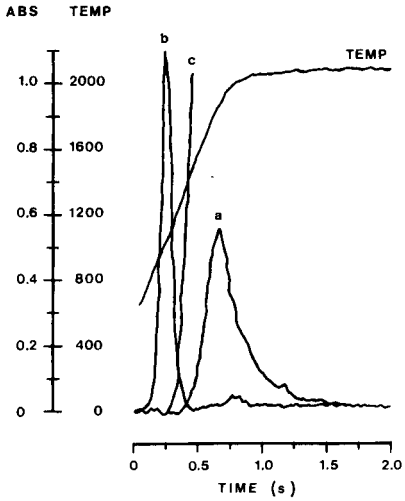

Fig. 12. Transient signals: (a) 3 μl of 2 μg Sn g^{-1} + 10 μl of 10% NH_3 (tin lamp, no background correction); (b) 3 μl of 2 μg Sn g^{-1} + 10 μl of 10% NH_3 + 2 × 2 μl of 5% $NiCl_2$ (tin lamp, no background correction); (c) 2 × 2 μl of 5% $NiCl_2$ (nickel lamp, background correction), when vaporized from a tungsten-treated tube. The variation of temperature (°C) with time is also shown.

TABLE 4

Effect of HCl and H_2SO_4 addition on the tin signal[a]

	Peak height[b]	Peak area[b]
6 ng Sn	0.540 ± 0.026	0.180 ± 0.005
+ 2 × 10 μl 1.2 M HCl	0.361 ± 0.040	0.084 ± 0.010
+ 2 × 10 μl 0.008 M H_2SO_4	0.256 ± 0.014	0.067 ± 0.005

[a]Added after the sample had been ashed; see Experimental. [b]Mean ± standard deviation of 4—8 determinations.

Confirmatory experiments

As has been shown, tin forms volatile molecules with oxygen, chlorine and sulphur. With commercial non-isothermal atomizers, these molecules might be removed from the system before a temperature sufficiently high for their decomposition is reached. As a consequence, the analytical tin signal will be very susceptible to variations in matrix composition, the quality of the purge gas and the properties of the graphite surface with respect to retaining interferents as well as the analyte.

In order to achieve efficient atomization, the sample should be vaporized into an environment of high and constant temperature. A recently developed constant-temperature furnace [15] was used to confirm this conclusion. Table 5 shows a comparison between vaporization/atomization from the tube

TABLE 5

Comparison between interference effects obtained when vaporization/atomization is made from the tube wall or from a graphite cup beneath the tube

	Non-isothermal conditions[a,c]	Isothermal conditions[b,c]
4 ng Sn	0.396 ± 0.005	0.361 ± 0.007
+ 10 μg $NiCl_2$[d]	0.105 ± 0.006	0.366 ± 0.007
+ 0.1 μg $CaSO_4$[d]	0.262 ± 0.008	0.354 ± 0.008

[a]CRA 90 configuration. [b]Double CRA 90 configuration, tube and cup. [c]Peak area values, mean ± standard deviation of 4—12 determinations. [d]Added after drying and ashing of sample (2 μl of 2 μg Sn g^{-1} + 10 μl of 10% NH_3).

wall and a graphite cup beneath the tube, with nickel chloride and calcium sulphate used as interferents. From a theoretical point of view, the sensitivity should be higher for the cup—tube combination. However, it is difficult to establish the relative sensitivity between the two furnace configurations because the rate of vaporization/atomization differs (affecting the peak height) and the temperature at which the measurement takes place is different (affecting the diffusion rate and thus the peak area). Nevertheless, the interference effects obtained during non-isothermal conditions could be completely removed by use of the constant-temperature furnace.

The authors thank Prof. Anders Cedergren for valuable discussions and Drs. Per Beronius and Ingvar Brentel for help with the radioactivity measurements. This work was supported by grants from the Swedish Natural Science Research Council.

REFERENCES

1 JANAF, Thermochemical Tables, Natl. Stand. Ref. Data Ser., Nat. Bur. Stand., (1971) 37.
2 I. Barin and O. Knacke, Thermochemical Properties of Inorganic Substances, Springer-Verlag, New York, 1973.
3 E. G. Harsányi, L. Pólos and E. Pungor, Acta Chim. Acad. Sci. Hung., 101 (1979) 139.
4 W. B. Barnett and E. A. McLaughlin, Jr., Anal. Chim. Acta, 80 (1975) 285.
5 D. B. Ratcliffe, C. S. Byford and P. B. Osman, Anal. Chim. Acta, 75 (1975) 457.
6 G. Del Monte Tamba and N. Luperi, Analyst, 102 (1977) 489.
7 M. Tominaga and Y. Umezaki, Anal. Chim. Acta, 110 (1979) 55.
8 P. Hocquellet and N. Labeyrie, At. Absorpt. Newsl., 16 (1977) 124.
9 K. Ohta and M. Suzuki, Anal. Chim. Acta, 107 (1979) 245.
10 H. Fritzsche, W. Wegscheider, G. Knapp and H. Ortner, Talanta, 26 (1979) 219.
11 W. Slavin and D. C. Manning, Spectrochim. Acta, 35B (1980) 701.
12 M. L. Kaiser, S. R. Koirtyohann, E. J. Hinderberger and H. E. Taylor, Spectrochim. Acta, 36B (1981) 773.
13 T. M. Vickrey and G. V. Harrison, Anal. Chem., 53 (1981) 1573.
14 B. V. L'vov, Spectrochim. Acta, 33B (1978) 153.

15 W. Frech and S. Jonsson, Spectrochim. Acta, accepted.
16 E. Lundberg and W. Frech, Anal. Chem., 53 (1981) 1437.
17 G. Lundgren, L. Lundmark and G. Johansson, Anal. Chem., 46 (1974) 1028.
18 E. Lundberg, Chem. Instrum., 8 (1978) 197.
19 E. Lundberg, Appl. Spectrosc., 32 (1978) 276.
20 W. Frech and A. Cedergren, Anal. Chim. Acta, 82 (1976) 83.
21 W. Frech, J.-Å. Persson and A. Cedergren, Prog. Anal. At., Spectrosc., 3 (1980) 279.
22 R. E. Sturgeon and C. L. Chakrabarti, Prog. Anal. At. Spectrosc., 1 (1978) 5.
23 I. J. McColm, R. Steadman and C. Dimbylow, J. Solid State Chem., 14 (1975) 185.
24 Handbook of Chemistry and Physics, 1972—1973, The Chemical Rubber Company.
25 G. D. Rayson and J. A. Holcombe, Anal. Chim. Acta, 136 (1982) 249.
26 G. R. Henning, J. Chem. Phys., 58 (1961) 12.
27 W. Frech and A. Cedergren, Anal. Chim. Acta, 82 (1976) 93.
28 I. Martinsen and F. J. Langmyhr, Anal. Chim. Acta, 135 (1982) 137.

Analytica Chimica Acta, 142 (1982) 143—150
Elsevier Scientific Publishing Company, Amsterdam — Printed in The Netherlands

MOLECULAR EMISSION CAVITY ANALYSIS
Part 22. Determination of Selenium and Tellurium by Direct Injection into the Cavity

A. SAFAVI

Chemistry Department, Birmingham University, P. O. Box 363, Birmingham B15 2TT (Gt. Britain)

ALAN TOWNSHEND*

Chemistry Department, University of Hull, Hull HU6 7RX (Gt. Britain)

(Received 2nd April 1982)

SUMMARY

Selenium (>50 ng) as selenite or selenate, and tellurium (1—15 μg) as tellurate may be determined by measuring the intensities of the Se_2 and Te_2 emissions, in a carbon cavity situated in a hydrogen—air flame. Certain organic compounds (e.g., citric acid, ascorbic acid and glucose) enhance the intensities, especially of tellurium.

The determination of inorganic sulphur anions by molecular emission cavity analysis (m.e.c.a.) based on S_2 emission is well documented [1—4]. Detection limits are below 1 ppm, mixtures of different anions can be resolved on the basis of their t_m values (time to maximum intensity), and cationic interferences may be relieved by adding phosphoric acid. The behaviour of the corresponding selenium and tellurium anions in the m.e.c.a. cavity, however, has received only cursory attention. Elemental selenium gives a blue emission, which has a band spectrum covering the range 350—550 nm, with the most intense peak at 411 nm [5]. It has been suggested that this emission arises from SeO [6] or Se_2 [7] below 410 nm, and Se_2 (or possibly SeO) above 410 nm [8]. Tellurium gives rise to a green emission in the cavity, and a blue colour in the flame above the cavity [5]. Selenium (≥0.3 μg) in organoselenium compounds has been determined by oxygen-flask combustion and subsequent reduction to elemental selenium. The precipitate was filtered onto a very small glass-fibre filter, which could be inserted into a cavity for m.e.c.a. Inorganic selenium compounds have likewise been determined after reduction [5]. The method has been applied in the analysis of shampoo and sulphuric acid.

As in atomic spectrometric methods, selenium can be determined more sensitively after volatilization as hydrogen selenide. The gas is transported into the cavity through a small tube [9]. The blue emission provides a detection limit of 7 ng of selenium. A much poorer detection limit (0.3 μg) was

achieved when the hydride was transported to a flame contained entirely within a cavity [10].

Because of the greater sensitivity of these volatilization techniques, the determination of selenium and tellurium by direct injection of solution into the cavity has not previously been investigated in detail. This paper describes such a study, and compares the findings with those for the corresponding sulphur anions.

EXPERIMENTAL

Reagents and apparatus

Doubly-distilled water was used throughout. Stock (500 ppm Se) solutions of selenium dioxide, sodium selenite and sodium selenate were prepared by dissolving 0.703 g, 1.095 g and 2.337 g, respectively, of the reagent-grade compounds in double-distilled water and diluting to exactly 1 l with water. A 10000 ppm tellurium solution as telluric acid was prepared by dissolving 17.997 g of telluric acid in water and diluting with water to exactly 1 l. All other chemicals were of analytical-reagent grade.

The instrument used was a prototype MECA spectrophotometer (Anacon, Inc., Houston, TX) as described previously [1]. Stainless steel (3 mm deep × 4.7 mm diameter) and carbon (4 mm deep × 4 mm diameter) cavities were used. The emission from the cavity containing the sample was passed via a 2.5-mm slit (≡42.5 nm) and a grating monochromator to a photomultiplier, the output of which was fed to an Oxford 3000 potentiometric recorder (Oxford Electronic Instruments, Oxford, Gt. Britain), which had a response time of 0.2 s for 90% full scale deflection. Each cavity was pitched at an angle of 7° downward from the horizontal and was ca. 3 mm into the flame. The bottom edge of the cavity was 10 mm above the top of the burner.

General procedure

The gas flows were adjusted to their optimal value, and the flame ignited. Sample solution (5 μl) was injected into the cold cavity, the latter was inserted into the flame, and the emission intensity was measured as a function of time at 411 nm (Se) or 500 nm (Te). For selenium, the cavity was heated for 15—20 s after each measurement in order to burn off any residue deposited in the cavity, which might interfere with the next determination. The cavity was removed from the flame and cooled to room temperature using a cold-air blower before the next sample was injected. The peak height of the response was measured.

Optimization of conditions

The flame composition has a critical role in obtaining an emission from selenium and tellurium compounds. Addition of air to the hydrogen—nitrogen diffusion flame had a similar effect on a solution of selenium dioxide (90 ppm Se) as on sulphur compounds [4, 11] (Fig. 1). Small air-flows extin-

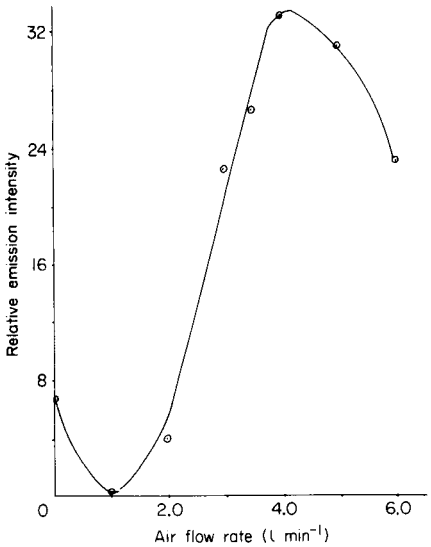

Fig. 1. Effect of air added to a flame of 5.5 l H_2 min^{-1} diluted with 5.0 l N_2 min^{-1} on emission from SeO_2 (100 ppm Se) at 411 nm.

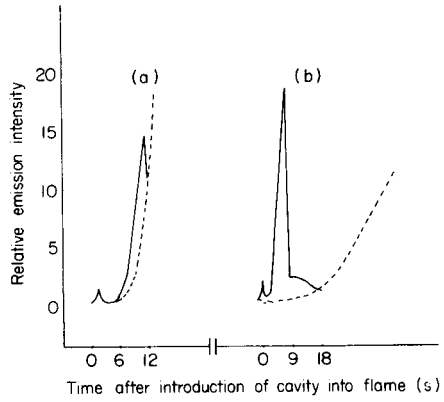

Fig. 2. Responses from 6 μg of Te as H_4TeO_6 in a flame of 5.0 l H_2 min^{-1}, 4.0 l N_2 min^{-1} and 5.5 l air min^{-1} in: (a) a stainless-steel cavity; (b) a carbon cavity.

guished the emission, but larger amounts gave greatly increased intensity. With increasing air flow, the t_m values decreased (e.g., for SeO_2 from 3.1 s to 1.9 s) as would be expected for an increasing flame temperature. The flame conditions which gave maximum selenium intensity were H_2 = 5.8, N_2 = 5.0 and air = 4.0 l min^{-1}. No emission was obtained from telluric acid (10 μg of Te) in the cavity in the absence of air in the flame. The optimal flame composition used for the determination of tellurium was H_2 = 6.5, N_2 = 3.5 and air = 7.5 l min^{-1}.

A stainless-steel cavity was suitable for the determination of selenite or selenate. However, if it was used for tellurium, two peaks occurred [5], the first smaller than the second, with the second superimposed on the incandescent emission of the cavity. However, when a carbon cavity, which takes longer to incandesce, was used for the tellurium determination, the second peak (t_m = 6.3 s) occurred before the incandescence as did a third peak which was observed at higher concentrations of tellurium (t_m = 9.3 s, Fig. 2). A multi-peaked response at higher analyte concentrations was also found for selenium dioxide (Fig. 3) and is a typical feature of the response from large amounts of many compounds [4]. Selenium powder also exhibits two peaks (t_m = 0.5 and 5.5 s) in a hot flame (5.0 l H_2 min^{-1}, 5.0 l N_2 min^{-1}, 5.5 l air min^{-1}). Tellurium dioxide powder gives three peaks (t_m = 1.0, 6.6 and 21.9 s) in a carbon cavity in a flame of 5.8 l H_2 min^{-1}, 5.5 l air min^{-1} and 4.0 l N_2 min^{-1}).

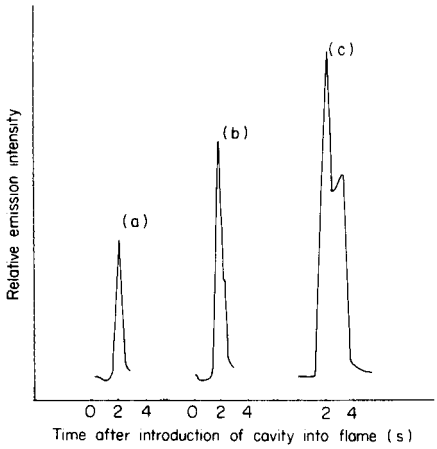

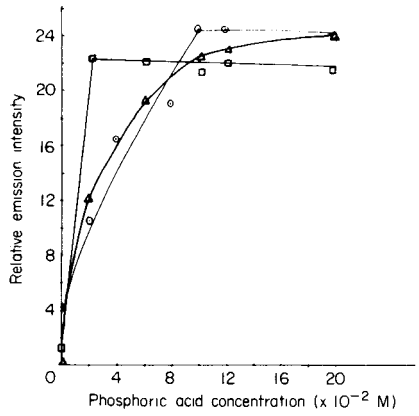

Fig. 3. Responses from: (a) 70; (b) 150; (c) 300 ppm Se as SeO_2. (Stainless-steel cavity; flame 4.3 l H_2 min^{-1}, 5.0 l N_2 min^{-1}, 5.5 l air min^{-1}.)

Fig. 4. Effect of phosphoric acid on emission from 90 ppm Se. Compound used: (⊙) SeO_2; (□) Na_2SeO_4; (△) Na_2SeO_3. (5.8 l H_2 min^{-1}, 5.0 l N_2 min^{-1}, 4.0 l air min^{-1}, stainless-steel cavity.)

Neither sodium selenite or sodium selenate (0.5 μg) gave an emission under the recommended flame conditions, because these compounds are only slowly decomposed under these conditions. Similarly depressed emissions are obtained with the alkali metal sulphates [4], for which phosphoric acid is a very effective releasing agent [1, 12]. Phosphoric acid was also found to be very effective for removing the depressive cationic effects on the selenium anions, as shown in Fig. 4. Phosphoric acid also markedly enhanced the emission from selenium dioxide (Fig. 4), although the t_m value is unaffected. A similar, but less marked effect has been found for sulphuric acid in the presence of phosphoric acid [13].

There was no further increase in intensity above certain concentrations of acid (ca. 0.1 M for the sodium salts, <0.02 M for SeO_2). The intensities above these concentrations were very similar for 90 ppm selenium as each of the three species. In subsequent work, all selenium solutions were made 0.1 M in phosphoric acid. Tellurium solutions could not be treated with phosphoric acid because the green HPO emission band (λ_{max} = 526 nm) interferes with the tellurium emission (λ_{max} = 500 nm).

RESULTS

The calibration graphs obtained for different selenium compounds (Fig. 5) and for telluric acid (Fig. 6) all had a sigmoidal shape similar to those obtained for sulphur compounds [4]. The calibration ranges, precisions and detection limits for each compound, obtained under the recommended conditions,

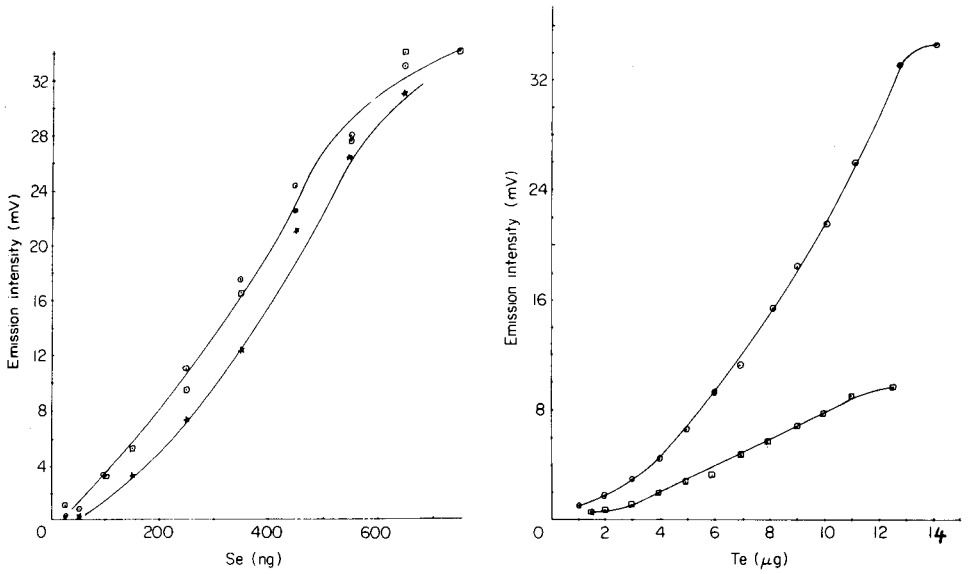

Fig. 5. Calibration graphs for selenium in 0.1 M H_3PO_4: (⊙) SeO_2; (□) Na_2SeO_3; (☆) Na_2SeO_4. (Conditions as for Fig. 4.)

Fig. 6. Calibration graphs for tellurium (second peak) as H_4TeO_6: (□) alone; (⊜) in 0.4 M citric acid. (Carbon cavity; flame 5.8 l H_2 min^{-1}, 4.0 l N_2 min^{-1}, 6.5 l air min^{-1}.)

are given in Table 1. They show that the sensitivities are considerably less than for the corresponding sulphur compounds, and that such tellurium responses are unlikely to have many analytical applications. The log—log slopes for the selenium and tellurium compounds were 1.8 ± 0.1, indicating that the emitting species are predominantly Se_2 and Te_2 rather than oxides as suggested previously [6, 8]. Further evidence that oxide emitters are not involved came from the use of a cavity into which a small flow of oxygen

TABLE 1

Analytical results for determination of selenium and tellurium compounds by m.e.c.a.

Compound[a]	Detection limit[b]		R.s.d.[c] (%)	Calibration range (μg ml^{-1})
	ng	μg ml^{-1}		
SeO_2	10	2	4.0	10—100
Na_2SeO_3	10	2	4.5	10—100
Na_2SeO_4	25	5	3.5	20—110
H_4TeO_6	1000	200	3.3	600—2200
H_4TeO_6[d]	450	90	2.3	700—2400

[a]All Se samples in 0.1 M H_3PO_4. [b]Amount giving 2× s.d. of background. [c]For 7 results for 90 μg Se ml^{-1} or 2000 μg Te ml^{-1}. [d]In the presence of 0.4 M citric acid.

is introduced; no selenium or tellurium emissions were obtained under these conditions.

Organic compounds such as citric acid, ascorbic acid and glucose were found to increase the emission intensity from tellurium. These compounds alone gave no emissions under these conditions. Figure 7 shows the effect of different amounts of citric acid on the tellurium response. Maximum enhancement, by a factor of 2, was obtained in the presence of 0.4 M citric acid. Under these conditions, the small first and third peaks did not appear. The t_m value for the main peak was unaffected by the presence of citric acid. The calibration graph for tellurium under these conditions, included in Fig. 6, confirms the increased sensitivity. The relevant analytical parameters are given in Table 1. The log–log calibration has a slope of 1.8, confirming that Te_2 is still the main emitter. Glucose (Fig. 8), ascorbic acid and tartaric acid had similar effects, but the concentration which gave greatest enhancement (0.05 M) was much less than for citric acid. At high ascorbic acid concentrations, tellurium(VI) was reduced to give a black precipitate of elemental tellurium.

In order to investigate if the increased intensity was due to the effect of a residue in the cavity resulting from decomposition of the organic compound by the flame, 10 μl of 1 M citric acid was injected into a stainless-steel cavity and the cavity was introduced into the flame. This process was repeated several times and then a solution of telluric acid without any organic compound was injected. No increase in tellurium emission was observed. Also, no increase in emission was obtained when a small amount of graphite was put into a stainless-steel cavity. It seems more likely, therefore, that the enhancement may be connected with the simultaneous production of gaseous products by the tellurium and organic compound, but the exact mechanism is not known.

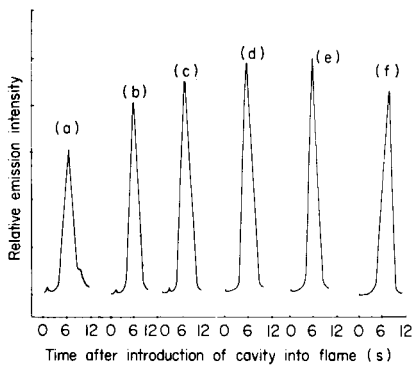

Fig. 7. Effect of citric acid on emission from 2000 ppm Te. Citric acid concentration: (a) 0; (b) 0.05 M; (c) 0.2 M; (d) 0.3 M; (e) 0.4 M; (f) 0.6 M. (Conditions as for Fig. 6.)

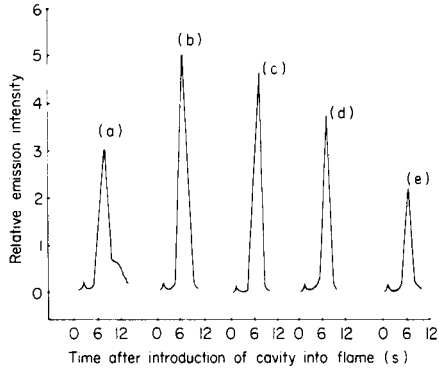

Fig. 8. Effect of glucose on emission from 2000 ppm Te. Glucose concentration: (a) 0; (b) 0.05 M; (c) 0.1 M; (d) 0.3 M; (e) 0.5 M. (Conditions as for Fig. 6.)

It was also of interest to investigate the effect of such organic compounds on selenium emissions. A comparison of the calibration curves for selenium dioxide with and without citric acid (Fig. 9) shows a doubled sensitivity when citric acid is present; 0.05 M citric acid gave the greatest enhancement. However, phosphoric acid provided greater enhancement. The t_m value was unaffected by the presence of either acid. A mixture of 0.1 M phosphoric acid and 0.05 M citric acid was less effective than either acid separately. As mentioned above, larger amounts of selenium dioxide gave rise to a double peak response. Addition of citric acid under these conditions completely removed the minor peak, as was found for tellurium. This provides further support that gas evolution from the organic compound is an important feature, in that it dilutes the analyte vapour, and discourages those polymerization processes that give rise to multipeaked responses.

Sulphuric acid greatly enhanced the emission from telluric acid. When measured at 500 nm, 0.15 M sulphuric acid gave a double peak response, which had disappeared after 3 s. Under similar conditions, telluric acid alone gave a peak at t_m = 4 s, whereas in the presence of 0.15 M sulphuric acid, it gave a peak 8 times more intense, but the t_m had shifted to 3 s, so that the peak was not completely resolved from the sulphuric acid response.

The S_2 intensity was greatly enhanced by water-cooling the cavity, an example of the Salet phenomenon [4]. The effect of water cooling of a stainless-steel cavity on the Se_2 emission from selenium dioxide (aqueous

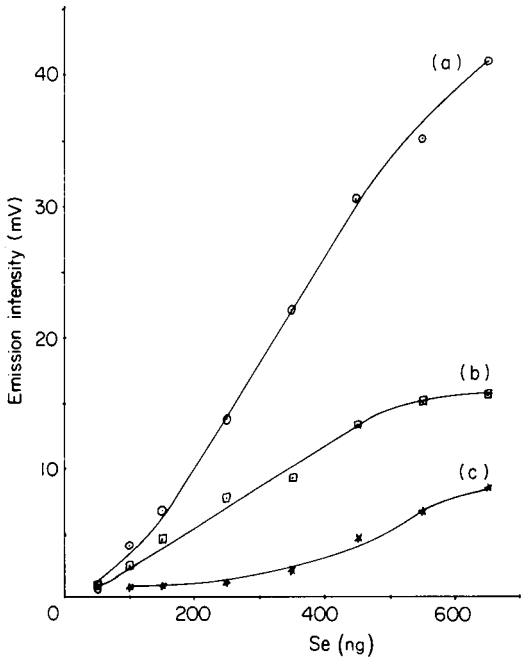

Fig. 9. Calibration graphs for SeO_2 in: (a) 0.1 M H_3PO_4; (b) 0.05 M citric acid; (c) alone.

solution) was therefore investigated to establish whether a similar enhancement occurred. Water cooling gave a peak three times as high as when no cooling was used, and the t_m value increased from 5 to 7 s, because volatilization is delayed by the cool surface. Thus Salet enhancement also occurs for Se_2 emission.

Conclusions

The behaviour of inorganic selenium and tellurium compounds in the m.e.c.a. cavity is similar to that of the corresponding sulphur compounds. Each compound produces a characteristic response, of one or more peaks, with well defined t_m values. The emitting species are Se_2 and Te_2, similar to the S_2 emitter for sulphur compounds, and their emission intensities are enhanced by a cold surface. Unfortunately, the sensitivity decreases in the order S > Se > Te, so that, although various expedients are available that increase sensitivity (addition of organic compounds or sulphuric acid), the tellurium response is not sufficiently sensitive for trace analysis. For applications where sensitivity is required, hydride generation in conjunction with m.e.c.a. will be the preferred approach.

REFERENCES

1 R. Belcher, S. L. Bogdanski, D. R. Knowles and A. Townshend, Anal. Chim. Acta, 77 (1975) 53.
2 R. Belcher, S. L. Bogdanski, I. H. B. Rix and A. Townshend, Mikrochim. Acta, 11 (1977) 91.
3 M. Q. Al-Abachi, R. Belcher, S. L. Bogdanski and A. Townshend, Anal. Chim. Acta, 86 (1976) 139.
4 S. L. Bogdanski, M. Burguera and A. Townshend, Crit. Rev. Anal. Chem., 10 (1980) 185.
5 R. Belcher, T. Kouimtzis and A. Townshend, Anal. Chim. Acta, 68 (1974) 297.
6 R. K. Asundi, M. Jan-Khan and R. Samuel, Nature, 136 (1935) 642.
7 M. Miyanisi, Sci. Pap. Inst. Phys. Chem. Res. (Jpn.), 37 (1940) 79.
8 J. Emeléus and H. L. Riley, Proc. R. Soc. (London), Ser. A., 140 (1933) 378.
9 R. Belcher, S. L. Bogdanski, E. Henden and A. Townshend, Anal. Chim. Acta, 113 (1980) 13.
10 R. Belcher, S. L. Bogdanski, E. Henden and A. Townshend, Anal. Chim. Acta, 116 (1980) 93.
11 R. Belcher, S. L. Bogdanski and A. Townshend, Anal. Chim. Acta, 67 (1973) 1.
12 S. L. Bogdanski, A. Townshend and P. Tuñon Blanco, Anal. Chim. Acta, 131 (1981) 297.
13 T. J. Cardwell, P. J. Marriott and D. J. Knowles, Anal. Chim. Acta, 121 (1980) 175.

Analytica Chimica Acta, 142 (1982) 151—157
Elsevier Scientific Publishing Company, Amsterdam — Printed in The Netherlands

MOLECULAR EMISSION CAVITY ANALYSIS
Part 23. Determination of Nitrite and Nitrate after Conversion to Nitrogen Monoxide

I. Z. AL-ZAMIL[a]

Department of Chemistry, University of Birmingham, P.O. Box 363, Birmingham B15 2TT (Gt. Britain)

ALAN TOWNSHEND*

Department of Chemistry, University of Hull, Hull HU6 7RX (Gt. Britain)

(Received 5th May 1982)

SUMMARY

Molecular emission cavity analysis is applied to the determination of nitrite and nitrate after their reduction to nitrogen monoxide by iodide or zinc. The white emission stimulated from nitrogen monoxide in an oxy-cavity placed in a hydrogen—nitrogen diffusion flame is measured at 526 nm. Calibration graphs are linear up to 300 μg N ml^{-1}; the detection limit is 0.5 μg N ml^{-1} for nitrite and 2 μg N ml^{-1} for nitrate. There are few interferences. Procedures for the determination of nitrite and nitrate in admixture are described.

Most direct conventional spectrometric methods for the determination of nitrogen and its compounds rely on flame emission band spectra of diatomic or triatomic molecules involving nitrogen [1—6]. These methods, in general, are not very sensitive. Nitrite and nitrate have been determined by measuring the CN emission at 388.3 nm with a detection limit of 250 ppm of nitrogen [4]. The NO band at 236 nm has been used to determine nitric acid by aspiration into a hydrogen—air flame; the detection limit was 14 ppm of nitrogen [1]. More recently, Belcher et al. [7] have determined ammoniacal nitrogen in effluents and fertilizers by molecular emission cavity analysis (m.e.c.a.). Ammonium ion was converted to ammonia which was carried to an oxy-cavity wherein a white band emission was produced. From 10—2000 μg N ml^{-1} could be determined, with a detection limit of 1 μg N ml^{-1}. In the present paper, m.e.c.a. methods are described for the determination of nitrite and nitrate after their reduction to nitrogen monoxide, either by iodide or zinc metal, with transfer of the gas to an oxy-cavity.

---

[a]Present address: Department of Chemistry, College of Science, King Saud University, Riyadh, Saudi Arabia.

EXPERIMENTAL

Apparatus and reagents

A modified Evans Electroselenium (EEL) 240 atomic absorption spectrometer operating in the emission mode with the slit opening at its maximal value of 12 (0.91 mm = 3 nm) was used as described previously [8]. The emission intensity was recorded on an Oxford 3000 potentiometric recorder (Oxford Instruments, Oxford) which had a response time of 0.2 s for 90% full-scale deflection. The stainless-steel water-cooled oxy-cavity and the volatilization system used were as described previously [9] unless otherwise stated.

All chemicals used were of analytical-reagent grade. Nitrite and nitrate stock solutions (1 mg N ml^{-1}) were prepared by dissolving 2.4629 and 3.0341 g of the respective sodium salts in 500 ml of distilled water. The nitrite and iodide solutions were freshly prepared.

Procedures

A syringe containing 2 ml of the sample or standard solution was connected to the reaction vessel [9] containing 2 ml of 1 M potassium iodide in 1 M hydrochloric acid or 0.5 g of zinc granules in 2 ml of 7 M hydrochloric acid. Nitrogen carrier gas was passed through the system at 135 ml min^{-1} until the end of the determination. The reaction vessel was placed in a water bath at 96–100°C (iodide method) or 84 ± 3°C (zinc method) and the system was closed and deaerated for $\geqslant$ 15 s to prevent oxidation of nitrogen monoxide. The trap was immersed in liquid nitrogen and cooled for 15 s before the 2 ml of sample or standard solution was injected. The nitrogen monoxide (b.p. −152°C) formed was collected in the trap for 1 min. The cavity was cooled with water flowing at 600 ml min^{-1} and was positioned so as to be 9 mm into the flame, 25 mm above the burner. The oxygen flow to the cavity was set to 85 ml min^{-1} and the flame (3.0 l H_2 min^{-1}, 4.4 l N_2 min^{-1}) was ignited at least 20 s before the measurement. The trap was removed from the liquid nitrogen and quickly immersed in a water bath at 80°C. The released nitrogen monoxide was swept into the cavity and the white emission was recorded at 526 nm as a function of time. Peak heights were measured.

The spectrum of the nitrogen emission was scanned, for the nitrite–iodide reaction. Nitrogen gas (20 ml min^{-1}) was used to carry the nitrogen monoxide produced from a nitrite solution (2 mg N ml^{-1}) directly to the flame via the oxy-cavity. The nitrogen emission reached a maximum intensity 10 s after the nitrite solution had been injected, and remained constant for 5 min during which the spectrum was scanned.

RESULTS AND DISCUSSION

No emission was observed when 10 μl of a solution containing 200 μg N ml^{-1} of sodium nitrite was directly injected into the cavity. However, when nitrite or nitrate was converted to nitrogen monoxide, an intense white emission was obtained showing a broad band spectrum with a maximum intensity at 526 nm, a few shoulders and little fine structure (Fig. 1). Such an emission was also obtained from ammonia. It has also been observed by Dagnall et al. [2] when a 50% ammonia solution in methanol was sprayed into a hydrogen–nitrogen diffusion flame and has been attributed to NH_2 emission.

Generally, when nitrogen monoxide is introduced into a hydrogen flame, the NO—O continuum (from 400 nm to the near i.r.) arising from the reaction $NO + O \rightarrow NO_2 + h\nu$ predominates if the oxygen concentration is fairly high and the temperature is <2500 K [10]. It is likely, therefore, that the nitrogen emission produced from nitrogen monoxide in the oxy-cavity is mainly the NO—O continuum, perhaps with some NH_2 emission. No emission was obtained from the nitrogen carrier gas because the highly stable nitrogen molecules are not broken down in the flame.

When the nitrogen monoxide formed was collected in the cold trap and then volatilized quickly, sharper, higher peaks were obtained compared with direct sweeping of the monoxide into the cavity. The optimal cavity position, gas flow rates and reaction conditions are those given in the procedures. Premixing air with the flame gases caused a decrease in emission intensity.

The iodide method

Iodide reduces nitrous acid as follows:

$$2HNO_2 + 2I^- + 2H^+ \rightarrow I_2 + 2NO + 2H_2O$$

When this reaction was used for the determination of nitrite by m.e.c.a., the calibration graph was linear up to 300 μg N ml^{-1} (Fig. 2). The relative

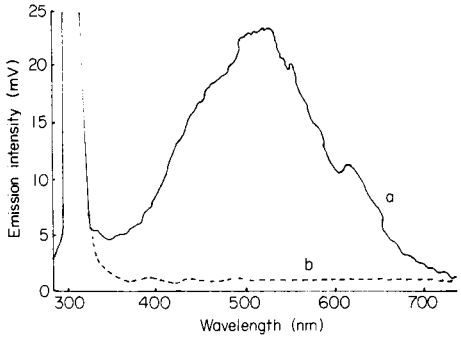

Fig.1. Emission spectrum obtained from (a) nitrogen monoxide; (b) background in the m.e.c.a. oxy-cavity.

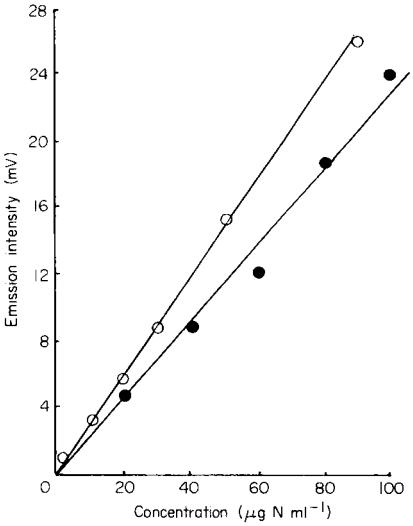

Fig. 2. Calibration graphs for the iodide method: (○) nitrite; (●) nitrate after zinc reduction.

standard deviation for 7 replicate measurements of 2 ml of 100 μg N ml^{-1} was 3%, and the detection limit (signal = twice background noise) was 0.5 μg N ml^{-1} (0.6 mV). The flame background was 3 mV.

The effect of some ions (0.25 mg ml^{-1}) on the generation of nitrogen monoxide from 2 ml of 50 μg N ml^{-1} as nitrite was investigated. An interference was considered significant when it caused a change in signal or more than two standard deviations (i.e., 6%). There were no significant effects from Co(II), Cd(II), Hg(II), Pb(II), Ni(II), Zn(II), SCN^-, SO_4^{2-}, Br^-, PO_4^{3-}, HPO_3^{2-}, NO_3^-, $[Fe(CN)_6]^{3-}$ and $[Fe(CN)_6]^{4-}$. Chromium(III), Fe(III) and Cu(II) depressed the emission slightly (≤10%) while MnO_4^-, CrO_4^{2-} (34%), BrO_3^- (52%) and Ce(IV) (100%) depressed it seriously. These depressive effects were due to oxidation of nitrite to nitrate. Also, compounds that convert nitrite to nitrogen, such as urea, sulphamic acid and ammonium chloride, had to be absent, otherwise very severe depressive effects would have occurred.

Nitrate was determined by the iodide method after its reduction to nitrite by means of the procedure of Chow and Johnstone [11]. As a reducing agent, they used zinc metal in alkaline solution with manganese(IV) as catalyst. The pH of the nitrate solution was adjusted with sodium hydroxide instead of ammonia solution to avoid the spectral interference from the latter. This procedure, when coupled with m.e.c.a., gave a conversion of nitrate to nitrite of 84—90%, which is the same as that reported previously when a spectrophotometric method was used [11]. The calibration graph for the determination of 0—100 μg N ml^{-1} as nitrate is shown in Fig. 2. The relative standard deviation for the determination of 2 ml of 100 μg N ml^{-1} as nitrate was 10% (5 replicates). This is considerably poorer than the

value for nitrite, and also poorer than the deviation for the Devarda's alloy method of determining nitrate [7].

The zinc method

Nitrite and nitrate can both be reduced to nitrogen monoxide by certain metals in deaerated acidic solution. Several granular metals were investigated (Table 1). The maximum intensity was obtained when zinc was used to reduce nitrite and nitrate and also when copper was used to reduce nitrite. The reduction of nitrite and nitrate by zinc metal was complete within 60 and 80 s, respectively. The zinc method is useful for the determination of both nitrite and nitrate in the range 0—200 μg N ml^{-1} (Fig. 3). The relative standard deviation for 7 replicate determinations of 2 ml of 100 μg N ml^{-1} as nitrite or nitrate was 5%. The detection limits were 1 and 2 μg N ml^{-1} for nitrite and nitrate, respectively. It is interesting that the emission obtained from nitrite in the absence of a metal was 50% of that achieved when zinc or copper was present, or when the iodide reduction procedure

TABLE 1

Reduction of 0.4 mg N as nitrite or nitrate by some granular metals in 3.5 M HCl at 84°C

Metal (0.5 g)	Intensity (mV)		Metal (0.5 g)	Intensity (mV)	
	From nitrite	From nitrate		From nitrite	From nitrate
—	19.4	0.0	Zinc	45.0	22.8
Cadmium	36.0	3.2	Iron	40.5	17.0
Copper	45.0	2.8	Tin	28.5	0.0

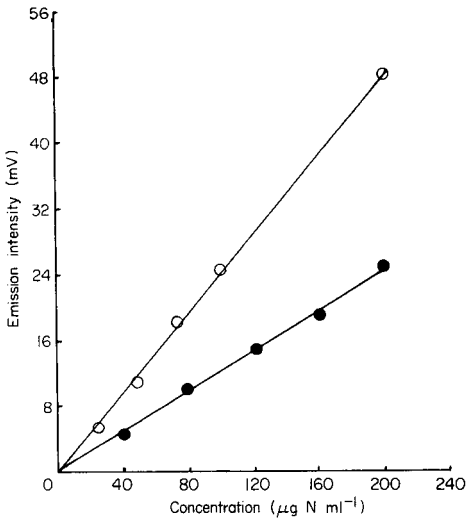

Fig. 3. Calibration graphs for the zinc reduction method: (○) nitrite; (●) nitrate.

TABLE 2

Analysis of nitrite and nitrate mixtures

Experiment no.	Expected (μg N ml^{-1})		Found (μg N ml^{-1})	
	NO_2^-	NO_3^-	NO_2^-	NO_3^-
1	100	100	104	97
2	50	100	48	98
3	100	50	95	53

was used. As the reaction involved is $2HNO_2 \rightarrow NO + NO_2 + H_2O$, this probably indicates that the nitrogen dioxide produced is not detected, possibly because of its much higher boiling point (21°C) and thus slower volatilization from the generator and cold traps, or because nitrogen dioxide is unable to produce the NO—O continuum.

All the interfering ions tested in the iodide method were examined in the zinc method. These ions (0.25 mg ml^{-1} of each) did not show any significant effects on the determination of 100 μg N ml^{-1} as nitrite or nitrate except for bromate, chromate, permanganate and cerium(IV) which decreased the nitrite response as expected.

The zinc procedure was also applied to the simultaneous determination of nitrite and nitrate. The emission intensity from both ions was measured on one aliquot; nitrite was destroyed in another aliquot by addition of excess of iodide (1 M potassium iodide in 1 M hydrochloric acid) and the emission intensity from nitrate was measured as above. The emission intensity from nitrite was obtained by difference. The concentrations of both ions were determined (Table 2) by referring the emission intensities obtained from nitrite and nitrate to calibration graphs prepared from pure solutions (Fig. 3). Good recoveries were obtained.

The iodide method is more sensitive and more precise than the zinc method but the latter is more selective. However, both methods are simple and rapid and provide wide linear calibration ranges. The methods have a similar detection limit to the m.e.c.a. methods for ammoniacal nitrogen and for nitrate after reduction with Devarda's alloy [7], but are somewhat simpler and more rapid.

The authors thank (the late) Emeritus Professor R. Belcher and Dr. S. L. Bogdanski for their interest in this work. I. Z. Al-Zamil thanks the University of King Saud, Saudi Arabia, for the provision of a research scholarship.

REFERENCES

1 P. T. Gilbert, in E. R. Lippincott and M. Margoshes (Eds.), Proceedings Xth Colloquium Spectroscopicum International, Spartan Books, Washington DC, 1963.
2 R. M. Dagnall, D. J. Smith, K. C. Thompson and T. S. West, Analyst, 94 (1969) 871.

3 R. S. Braman, Anal. Chem., 38 (1966) 734.
4 M. Honma and C. L. Smith, Anal. Chem., 26 (1954) 458.
5 B. E. Buell, Anal. Chem., 34 (1962) 635; 38 (1966) 1376.
6 K. J. Krost, J. A. Hodgeson and R. K. Stevens, Anal. Chem., 45 (1973) 1800.
7 R. Belcher, S. L. Bogdanski, A. C. Calokerinos and A. Townshend, Analyst, 102 (1977) 220; 106 (1981) 625.
8 R. Belcher, S. L. Bogdanski and A. Townshend, Anal. Chim. Acta, 67 (1973) 1.
9 R. Belcher, S. L. Bogdanski, E. Henden and A. Townshend, Anal. Chim. Acta, 92 (1977) 33.
10 H. P. Braida, H. I. Schiff and T. M. Sugden, Trans. Faraday Soc., 57 (1961) 259.
11 T. J. Chow and M. S. Johnstone, Anal. Chim. Acta, 27 (1962) 441.

Analytica Chimica Acta, 142 (1982) 159—171
Elsevier Scientific Publishing Company, Amsterdam — Printed in The Netherlands

THE SELECTIVE DETERMINATION OF HALOGENS AND SULPHUR IN SOLUTION BY ATMOSPHERIC-PRESSURE HELIUM MICROWAVE-INDUCED PLASMA EMISSION SPECTROMETRY COUPLED TO AN ELECTROTHERMAL INTRODUCTION SYSTEM

HANS P. J. VAN DALEN*, BERTHA G. KWEE and LEO DE GALAN

Laboratory for Analytical Chemistry, Delft University of Technology, Jaffalaan 9, 2628 BX Delft (The Netherlands)

(Received 14th May 1982)

SUMMARY

Instrumentation is described for the direct determination of Cl, Br, I and S in dissolved samples. A tantalum furnace is coupled directly to a TM_{010} cavity, in which a helium microwave plasma is generated at atmospheric pressure. Samples (20 μl) are dried, ashed and atomized; the free atoms are transported by helium to the cavity, where they are excited. Detection limits are in the sub-mg l^{-1} region. The effect of counter cations is removed by the addition of 50 mg l^{-1} potassium hydroxide, which also helps to suppress interferences by large amounts of matrix constituents, but the standard addition technique remains necessary to permit determinations that are reliable to within 5%.

Since the introduction by McCormack et al. [1] of the microwave-induced plasma (m.i.p.) in argon as an element-selective detector for gas chromatography, the m.i.p. in a noble gas has been used in several forms for the selective determination of metals and non-metals. General as well as analytical aspects have been reviewed recently in an excellent article by Zander and Hieftje [2]. The demonstrated nonthermal excitation mechanism of the m.i.p. provides inherent advantages and disadvantages. The high electronic energy makes the m.i.p. much more suitable for the determination of non-metals than such thermal excitation sources as the d.c. plasma or the inductively coupled plasma (i.c.p.). However, the low kinetic energy of the m.i.p. generally requires volatilization of the sample prior to its introduction into the plasma. Moreover, the low-power m.i.p. is easily overloaded by excess of solvent or matrix, which should therefore be removed before entering the m.i.p. These properties explain the use of the m.i.p. as a gas chromatographic detector, as has been reported in more than 50 publications after the pioneering work of McCormack et al. [1]. A prominent part is covered in a recent review by Carnahan et al. [3]. Obviously, this combination is restricted to the determination of relatively volatile components.

Until 1976, the m.i.p. was either operated at atmospheric pressure in argon or at sub-atmospheric pressure in helium. The former is to be preferred

for the determination of metals. However, for use as a gas-chromatographic detector for metal—organic compounds, the argon m.i.p. is generally inferior to competing excitation sources such as the d.c. plasma and the i.c.p. In contrast, the low-pressure helium m.i.p. offers unique possibilities for the determination of non-metals, as was demonstrated notably by Bache and Lisk [4] for the halogens, sulphur and phosphorus. McLean et al. [5] coupled a low-pressure helium m.i.p. to a gas chromatograph to determine selectively carbon, oxygen, nitrogen, hydrogen, sulphur, phosphorus and halogens and determined atomic ratios and the empirical formulae of organic compounds. However, the high expectations raised in this publication were not confirmed in subsequent studies [6, 7]. In 1976, Beenakker was the first to generate an atmospheric-pressure m.i.p. in helium by using a TM_{010} cavity [8]. With some design improvements suggested by van Dalen et al. [9], this cavity is as easy to use as the previously used Evenson cavities. Again, the atmospheric-pressure helium m.i.p. has been used as an element-specific detector in gas chromatography for the determination of metals and non-metals in volatile compounds. In comparison with other element-selective detectors, the m.i.p. demonstrates its main advantage for the determination of halogens [10].

For the analysis of less volatile compounds, the atmospheric-pressure m.i.p. has been combined with other means of preliminary volatilization. Complete volatilization of solution droplets prior to their excitation in a m.i.p. has been largely restricted to the determination of metals. For this purpose, the m.i.p. has been coupled with a carbon cup [11], a carbon rod [12], a platinum loop [13, 14], a tantalum strip [14] and a micro-arc [15]. As remarked above, such systems offer few if any advantages for the determination of metals over competitive atomic spectrometric methods.

Little has been reported on the determination of non-metals in involatile compounds with a m.i.p. Chemical treatment of aqueous solutions has been used by Alder et al. [16] for the selective volatilization and determination of chloride down to 100 $\mu g\ l^{-1}$. Similarly, Tanabe et al. [17] determined nitrogen in ammonia, nitrate and nitrite by selective volatilization of nitrogen gas down to $1\ \mu g\ l^{-1}$. The combination of an electrothermal introduction system and an atmospheric-pressure helium m.i.p. for the more general determination of non-metals has recently been reported. Rommers and Boumans [18] used 1—10-μl injections onto graphite cord and determined sulphur, chlorine and bromine (as well as Ga, Ca, Mn and Pb). They experienced matrix effects and concluded that the system is best suited for sulphur and the halogens. Their results are described by Beenakker et al. [19]. In the present study, a tantalum furnace is coupled with a m.i.p. for the determination of non-volatile halogens, sulphur, phosphorus, carbon, hydrogen, oxygen and nitrogen in aqueous solution.

EXPERIMENTAL

Equipment

A block diagram of the equipment is shown in Fig. 1.

Microwave equipment. The microwave generator (Electro-Medical Supplies, Microtron 200, Mk III, 2450 MHz, 0—200 W) is equipped with an Addington circulator and a Bendix coaxial load resistor to facilitate the ignition procedure and to protect the generator [9]. The copper TM_{010} cavity [8] with an inner height of 6 mm and an inner diameter of 86.5 mm, is constructed as described by van Dalen et al. [9] and operated at an incident power of 75 W and a reflected power of less than 1 W. Air-cooling through the variable antenna coupling keeps the temperature of the quartz discharge tube relatively low and prevents excessive erosion of the silica discharge tube (2-mm i.d., 7-mm o.d.).

The plasma is initiated as follows. With a helium flow of at least 50 ml min^{-1}, an incident power of 75 W and the antenna rod screwed into the cavity by about 2 mm, the reflected power is tuned to a minimum value (of about 15 W) with the quartz tuning rods. The plasma is then ignited by momentarily inserting a pointed isolated wire into the discharge tube [20, 21]. A small disposable injection needle works quite well. Ignition with a Tesla coil is discouraged, because it may damage electronic components (especially MOS integrated circuits). Next, the reflected power is zeroed by slowly screwing the antenna rod into the cavity while simultaneously pulling out the quartz tuning rods. If necessary, the system may be retuned to zero

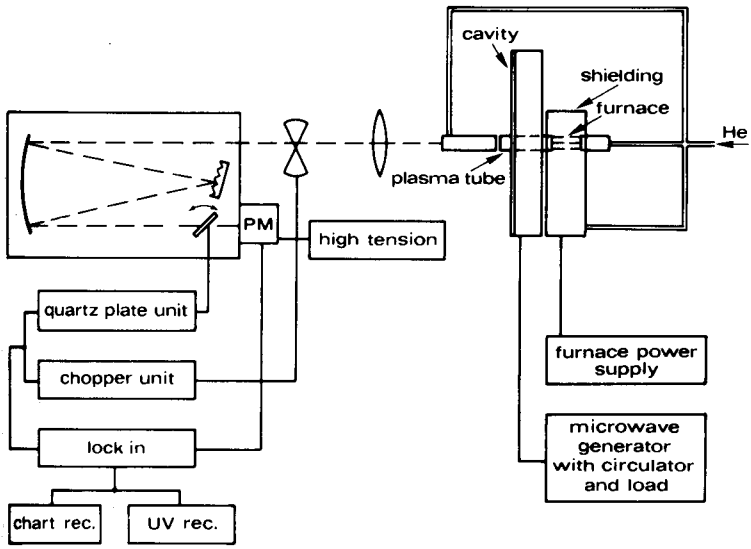

Fig. 1. Block diagram of the equipment and coupling of the atmospheric-pressure m.i.p. to a tantalum furnace.

reflected power after a warm-up time of about 15 min. An (inadvertently) extinguished discharge can easily be re-ignited in the adjusted cavity by re-inserting the injection needle.

For measurements at sub-atmospheric pressure, a cap is fitted onto the discharge tube which permits end-on view of the plasma through a quartz window.

Optics and read-out. A 1:1 image of the axially viewed plasma is focussed with a Suprasil lens (f = 11.8 cm) onto the entrance slit of a 0.5-m Ebert monochromator (Jarrell-Ash 82-001) equipped with a 750-nm blazed grating providing a reciprocal linear dispersion of 1.65 nm mm^{-1}. Slits of 50-μm width stopped to a height of 2 mm are used. For measurement of lines above 450 nm, a Corning filter 3387 is used to reject second-order radiation. Wavelength modulation with a 2-mm thick vibrating quartz plate is employed to discriminate against continuum background radiation. The fundamental frequency of the vibrating quartz plate (117 Hz) is fed to a lock-in amplifier (Princeton Applied Research Model 122) tuned to 234 Hz and used in the $f/2$ mode. A time constant of 0.1 s is used throughout.

The photomultiplier (Hamamatsu R 446) is fed with 750 V from a Philips high voltage supply (PE 1533). The signals were recorded with a Kipp BD 41 chart recorder. Rapid scans of the spectrum at 50 nm s^{-1} were made with a Bausch and Lomb double-grating monochromator (equipped with a fast scan motor). The signal from the photomultiplier was amplified by a Keithley 427 current amplifier and recorded with a u.v. recorder (Honeywell 2206). The peak area of the signal was measured with a Shimadzu C-ElB integrator; the peak height was read from the recorder trace.

Electrothermal introduction system. Although it has been developed independently, our design for the combination of an electrothermal atomizer and a m.i.p. (Fig. 2) is similar to the system described by Volland et al. [12] for the determination of metals in aqueous solution. Both systems have a small, rapidly heated furnace and direct coupling to the discharge tube to minimize cold spots and dead volumes. Volland et al. used a Varian carbon rod assembly; with a somewhat longer home-made graphite furnace [22] severe plasma overloading from excess carbon vapour was experienced here. A metal furnace was therefore preferred; this has the added advantage that carbon can be determined in the samples. Because tungsten, as used by Sychra et al. [23], is difficult to machine and becomes brittle when heated in the presence of traces of oxygen, tantalum was selected. Two profiled strips from 0.2-mm tantalum foil are spot-welded to form a furnace (5-mm i.d., 15 mm long) with two side-arms to connect the electrodes. A dent in the bottom can hold up to 20 μl of solution.

The smoothed ends of the furnace are pressed tightly against the quartz discharge tube at one side and the carrier gas introduction tube at the other. Firm contact is essential to prevent analyte losses and to improve the analytical reproducibility. The connections are not gas-tight and hence the shielding gas around the furnace for protection against oxidation diffuses to a certain extent into the discharge. For this reason the shielding gas is the

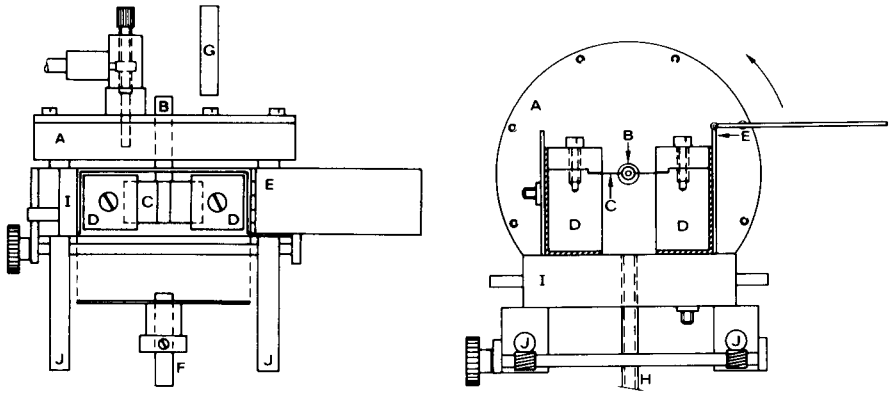

Fig. 2. Top view (left) and end-on view (right) drawing of the coupling of the TM_{010} cavity and the tantalum furnace. (A) TM_{010} cavity with antenna; (B) silica plasma tube; (C) tantalum furnace clamped between (D) water-cooled electrodes; (E) housing around furnace with lid and (F) removable side (for end-on injection) provided with silica tube for plasma helium introduction; (G) silica tube to be rotated in front of plasma tube for flow reversal (during injection and drying); (H) introduction of helium shielding gas; (I) water-cooled mounting block which can be separated from cavity over (J) sliding bars, during injection and drying.

same as the carrier gas to the plasma, i.e., helium. The furnace is enclosed in a metal housing. By monitoring spectral lines of helium, nitrogen and continuously introduced chlorine vapour, the minimum flow rate of the shielding gas was found to be 1.2 l min^{-1}.

In principle, the plasma can be shut off during introduction and drying of the sample, but after re-ignition it takes some time to stabilize. Therefore, it is advisable to keep the plasma running all the time, but to divert the solvent vapour volatilized during drying. This is realized by disconnecting the furnace from the quartz tubes before the sample solution is injected from the side. During this operation and the consecutive drying stage, the helium flow through the discharge tube is reversed. When the sample solution has been desolvated, the furnace is again clamped in position and the original helium flow is restored for the ashing and atomization stages.

The furnace is heated with a Perkin-Elmer HGA 72 graphite furnace power supply. Furnace temperatures were measured with a Leeds and Northrup optical pyrometer and an iron-constantan thermocouple. This relatively slow system can only record the final temperatures of the rapidly heated furnace, which are reported below.

Materials

Standard quality (99.995%) helium gas was passed through a molecular sieve from the central laboratory gas supply system. All chemicals used were of analytical-grade quality or better. Ringsdorf RWA graphite was used for the modified carbon rods. The tantalum foil (99.93%) was supplied by Highways International (Baarn, The Netherlands).

RESULTS AND DISCUSSION

Prominent lines

It is well known that in a helium m.i.p. operated at reduced pressure (10 kPa) the ionic lines of non-metallic elements are much stronger than atomic lines. This can be attributed to the very high electronic temperature of the low-pressure helium m.i.p. [24]. With an increase in pressure to atmospheric, as is possible with the TM_{010} cavity, the electronic temperature may be expected to decrease [2, 25] and consequently, a preference for ionic transitions is not necessarily evident. For a closer investigation, analyte spectra were recorded using continuous sample introduction with diffusion tubes or an exponential diluter as described previously [6].

Spectra recorded at reduced pressure (12 kPa), using either an Evenson cavity or the TM_{010} cavity, and at atmospheric pressure (with the TM_{010} cavity) reveal significant differences. At reduced pressure, the ionic lines are much stronger than the few atomic lines that can be observed. Molecular bands are also very weak. The intensities observed side-on from the Evenson cavity are higher than measured end-on from the TM_{010} cavity and this provides somewhat better detection limits for the former cavity (Table 1). When the pressure is raised to atmospheric level, molecular bands and atomic lines become more prominent. As a result, the most useful spectral line for an element must be selected on the basis of both intensity and freedom from spectral interferences by molecular bands. For the halogens

TABLE 1

Analytical properties of the m.i.p. at low and atmospheric pressure for gaseous samples

Element/ compound	Wavelength (nm)	Low pressure (12 kPa) Evenson[a] and TM_{010} cavity		Atmospheric pressure TM_{010} cavity	
		Detection limit[b] ($\mu g\ ml^{-1}$)	Linear range (decades)	Detection limit ($\mu g\ ml^{-1}$)	Linear range (decades)
Cl/	I 725.7	—	—	0.32	3.4
CCl_4	I 725.7	—	—	0.32	3.4
	II 479.5	0.21 (0.16)	3.4 (3.3)	0.35	3.2
Br/	I 734.9	—	—	0.24	3.4
CH_2Br_2	II 470.5	0.24 (0.11)	3.4 (3.4)	0.56	2.6
I/	I 608.2	—	—	2.7	2.4
CH_2I_2	II 516.1	(0.12)	(3.5)	1.3	2.5
S/	I 675.7	—	—	0.89	2.3
CS_2	II 545.4	(0.19)	(2.8)	1.5	2.0

[a]Values for the Evenson-type cavity are placed in parentheses. They are taken from [6] and were measured on the same equipment. [b]Detection limits are expressed in μg of element per ml of helium at atmospheric pressure.

and sulphur, the optimal atomic and ionic emission lines in the present system were selected. For these lines the detection limit and linear dynamic range were determined by the procedure described previously [6].

In agreement with measured relative intensities, the detection limits presented in Table 1 are similar for ionic and atomic lines when the helium m.i.p. is operated at atmospheric pressure. Whereas for Cl and Br the detection limits are similar at either pressure, those for I and S are significantly poorer at atmospheric pressure. At low pressure the dynamic range is at least three orders of magnitude, but at atmospheric pressure such high values are rarely reached and then only when atomic lines are used. Apparently the atomic transition is more resistant to plasma overloading by excess of analyte atoms introduced into the plasma. Again, this can be attributed to the fact that atomic lines are less sensitive to a decrease in electronic temperature. It can be concluded that at atmospheric pressure the lowest detection limits are obtained for the emission lines (either atomic or ionic) with the highest relative signal, while the highest upper limits of the linear range are reached with atomic lines.

Operating conditions

The two main parameters of the furnace—m.i.p. system are the atomization temperature in the metal furnace and the flow rate of the helium carrier gas. Examples of their influence on the analytical signals are presented in Figs. 3 and 4. From these and similar data collected for other elements, the following conclusions can be drawn.

The heating program of the furnace must include a drying step to remove the solvent. In principle, the solvent vapour could be led through the running m.i.p., but extinguishing the discharge can only be prevented by very slow drying. As described in the experimental section, it is preferable to disconnect the furnace and dry the sample in the usual time of 1 min. It was observed, however, that even at low drying temperatures many organically-bound

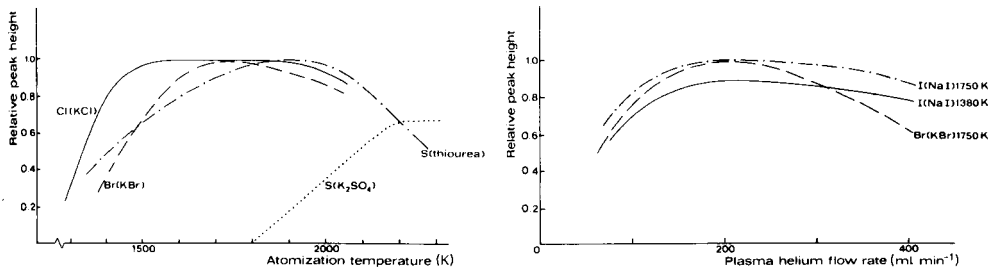

Fig. 3. Influence of atomization temperature on relative signals of 0.5 μg of analyte (maximum values normalized to unity).

Fig. 4. Influence of helium flow rate through the plasma on relative signals of 0.5 μg of analyte (maximum values normalized to unity).

analytes may partially be lost during the drying step. Consequently, if such analytes are to be determined, a preliminary decomposition into an ionic, inorganic form is advisable. Naturally, an ashing step can be incorporated deliberately to remove excess of volatile sample components before the final atomization step. The atomization temperature is selected on the basis of the maximum peak intensity. The example in Fig. 3 shows that for ionic analytes the optimal temperature is not very critical. Moreover, it varies little with the nature of the associated cation. Seven alkali or alkaline earth chlorides showed optimum temperatures between 1800 and 1950 K. At a compromise value of 1850 K, the sensitivity decreased from the maximum value by no more than 20%. Relatively involatile organic analytes that survive the drying step generally atomize at substantially lower temperatures.

As is shown in Fig. 4, the peak height first increases with increasing helium flow rate, passes through a maximum at 200 ml min^{-1} and then decreases. The latter behaviour is expected from the dilution effect of increasing amounts of helium. The initial increase of the signal up to 200 ml min^{-1} of helium has also been observed by Volland et al. [12] and is more difficult to explain. Possibly, at very low helium flow rates, analyte is lost by diffusion or condensation or by reaction with the discharge tube. Whatever the reason, an optimum flow rate of 200 ml min^{-1} was observed for all compounds investigated and this value was maintained throughout this study.

Detection limits and dynamic range

The calibration graph for chlorine present as hexachlorocyclohexane in aqueous solution is linear up to 10 μg ml^{-1}, above which it becomes curved; at 20 μg ml^{-1} the sensitivity is half its value at low concentrations. The detection limit is 0.01 μg ml^{-1}, which corresponds to 0.2 μg Cl for 20-μl samples. The dynamic range is thus about 3 decades, which agrees with the value stated in Table 1 for direct introduction of gaseous carbon tetrachloride with an exponential diluter. In order to compare the detection limits the solution value must be converted to a vapour phase concentration through the expression $c_g = c_l V/\Phi \Delta t$, where c_g and c_l are the detection limits in the vapour and liquid phases, respectively; V is the injected amount of sample solution; Φ is the flow rate of helium; and Δt is the width of the recorded analyte signal. With V = 20 μl, Φ = 200 ml min^{-1}, Δt = 0.15 s and c_l = 0.01 μg ml^{-1}, c_g = 0.4 μg Cl ml^{-1} He. This is again very close to the value of 0.3 μg ml^{-1} stated for chlorine in Table 2. It can be concluded, therefore, that the analytical range observed with electrothermal vaporization is fully determined by the properties of the microwave discharge.

Detection limits and dynamic range for halogens and sulphur introduced as organic or inorganic compounds in solution are presented in Table 2. In addition, data were collected for H, C, O, N, F and P, but for these elements the detection limits are high ($\geqslant$1 μg ml^{-1}) and the dynamic range is rarely more than one decade, so it is clear that the present system provides no useful analytical capabilities for those elements.

TABLE 2

Analytical properties of the furnace—m.i.p. system for various elements

Element and λ(nm)	Compound	Detection limit		Upper limit		Dynamic range (decades)
		(μg)	(μg ml^{-1})[a]	(μg)	(μg ml^{-1})[a]	
Cl	$CH_6H_6Cl_6$	0.2	0.01	400	20	3.3
725.6	NaCl	0.8	0.04	1000	50	3.1
Br	$C_{17}H_{35}Br$	0.4	0.02	300	15	2.9
734.8	NaBr	0.8	0.04	1200	60	3.2
I	$(CH_3)_4NI$	2.6	0.13	300	15	2.7
608.2	KI	4.0	0.20	800	40	2.3
S	$(NH_2)_2CS$	1.6	0.08	240	12	2.2
675.7	K_2SO_4	3.0	0.15	600	30	2.3

[a]Value for the optimal injection volume of 20 μl.

These disappointing results can be attributed to two main causes. For H, C, N and O, high and irreproducible blank values arise from contaminants adsorbed onto the tantalum furnace and released during atomization. The contamination is due to exposure to air during sample introduction and from trace components in helium during the drying and ashing steps. As a result these elements can be determined only when highly purified helium is used and exposure to air is completely avoided. Alternatively, a furnace material might be found that shows considerably less adsorption. In accordance with earlier experience [6], the negative results for fluorine and phosphorus are attributed to reactions with the hot silica discharge tube. Replacement of the silica by alumina or boron nitride might improve the results for these elements. However, the much higher absorption of microwave energy by these materials requires more microwave power and cooling facilities for the discharge tube.

Consequently, the usefulness of the present combination of a tantalum furnace and a m.i.p. excited in a silica tube is restricted to Cl, Br, I and S. Of these elements, inorganic sulphur compounds generally require high atomization temperatures (2300 K), which considerably reduce the lifetime of the tantalum furnace.

Interferences

The susceptibility of the m.i.p. to interferences is well known [2]. This explains its popularity mainly as a gas chromatographic detector, because the chromatographic process removes interfering compounds. In the present application of the m.i.p., where non-metals are determined in aqueous solution without prior separation, matrix effects require special attention. One

possible interference is the appearance of a signal in the absence of the analyte. The selectivity, defined as the sensitivity ratio of analyte to concomitant, both measured at the analyte wavelength, was measured for all elements in Table 3 and found to be at least 1000. In many cases, no signal for the concomitant could be detected up to 1000 μg ml^{-1} at the wavelength of the analyte. At such high concentrations, the plasma is seriously overloaded or even extinguished. The high selectivities observed in the present system are the favourable result of the wavelength modulation used.

A more common and important interference is the variation of analyte signal caused by the presence of other components in the sample solution. As is clear from Table 3, for all four analytes Cl, Br, I (as the corresponding halides) and S (as sulphate or disulphate), the counter cation exerts a significant influence on the peak height. Similar conclusions apply to the peak area. In these tests, 20 μl of 5 μg ml^{-1} analyte solutions were dried at about 200°C, no ashing step was included and atomization proceeded at a single temperature for each analyte. However, the magnitude of the effect far exceeds the influence of a difference in optimum atomization temperature, which accounts for no more than 20% depression. In other words, even if the atomization temperatures had been adapted to the sample composition, which in itself is highly impractical, the analyte sensitivities remain unequal.

The large depressive effects for some counter cations are difficult to explain. If the interference arises within the plasma, the addition of a

TABLE 3

Relative sensitivities for different compounds and influence of added potassium hydroxide

Component	Relative peak height[a]		Component	Relative peak height[a]	
	No KOH	50 ppm KOH present		No KOH	50 ppm KOH present
Chlorine			*Iodine*		
NaCl	1.00	1.08	LiI	1.00	0.50
KCl	0.95	1.07	NaI	0.9	0.54
LiCl	0.88	1.05	KI	0.9	0.54
$MgCl_2$	0.75	1.07	ZnI_2	<0.1	0.54
$BaCl_2$	0.53	1.07			
$CaCl_2$	0.60	1.09	*Sulphur*		
$BrCl_2$	0.83	1.09	K_2SO_4	1.0	
$PbCl_2$	<0.2	1.09	$ZnSO_4$	0.8	
$CuCl_2$	<0.2	1.07	$K_2S_2O_7$	0.8	
$MnCl_2$	<0.2	1.09			
Bromine					
KBr	1.00	1.10			
NaBr	0.98	1.09			
$MgBr_2$	<0.2	1.09			
$CaBr_2$	<0.2	1.10			

[a]For analyte concentrations of 10 μg ml^{-1}.

stabilizing spectroscopic buffer might help. In view of the low analyte concentrations, premature loss of analyte ions through the release of acids (HCl, HBr, HI) cannot be ruled out. This could be counteracted by raising the pH of the sample solution.

Figure 5 shows the favourable influence of increasing amounts of potassium hydroxide added to the sample solution. Whereas the already high signal of sodium bromide is nearly unaltered, the low signal observed for magnesium bromide in the absence of alkali increases to the same level as sodium bromide on addition of 20 μg KOH ml^{-1}. The data in the final column of Table 3 demonstrate the beneficial influence of the addition of 50 μg KOH ml^{-1} to all samples. For all three halides the response becomes independent of the counter cation. For iodine a twofold loss in sensitivity must be accepted, whereas for chlorine and bromine the addition of alkali entails no loss in sensitivity.

Obviously, the variation of counter cations present in the same molar concentration as the analyte represents only a special case of the more general interference situation, in which the analyte may be influenced by other components in the sample. It is typical of the m.i.p. that such components often exert a large, usually depressive influence on the analyte signal. Some examples are shown in Fig. 6. In agreement with the above discussion on the effect of counter cations, many components interfere even at the equimolar level. In some cases, even a moderate excess of interfering component reduces the analyte signal by an order of magnitude.

Fortunately, the situation is again markedly improved by the addition of potassium hydroxide to the sample. As an example, the signal from chlorine in the presence of excess of ammonium sulphate is shown in Fig. 7. Without the addition of alkali, the original chlorine signal is depressed by an order of magnitude. With increasing amounts of alkali, the signal from chloride alone is somewhat enhanced. However, the signal depressed by ammonium sulphate is much more enhanced, and at a potassium hydroxide level of 100 μg ml^{-1} it approaches the value of the chlorine signal in the

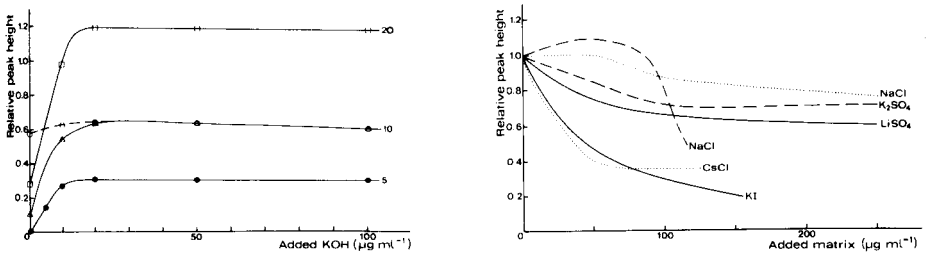

Fig. 5. Influence of KOH on the Br signal from (—) $MgBr_2$ and (---) NaBr. The numbers on the lines indicate the Br concentration in μg ml^{-1}.

Fig. 6. Influence of added salts upon relative peak height of 10 μg ml^{-1} (0.2 μg) of: (—) Cl as NaCl; (---) Br as NaBr; (...) I as KI.

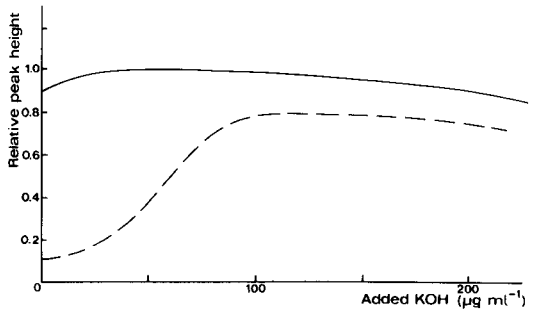

Fig. 7. Influence of KOH on the relative peak height of 5 μg Cl^- ml^{-1} (0.1 μg Cl) as NaCl: (—) without matrix; (---) in the presence of 50 μg $(NH_4)_2SO_4$ ml^{-1} (1 μg).

absence of the interferent. It is clear, however, that the signals do not coincide, and ammonium sulphate at the 50 μg ml^{-1} level still exerts a small depressive influence. However, quantitative analysis is now feasible with the standard addition technique. Indeed, a test solution containing chloride (2.5 μg ml^{-1}) and ammonium sulphate (500 μg ml^{-1}) was analysed in this way after addition of potassium hydroxide (50 μg ml^{-1}) and gave a result of 2.54 ± 0.06 μg Cl^- ml^{-1}.

Conclusions

With the present system of a tantalum furnace atomizer and a silica discharge tube, H, C, N, O, F and P could not be determined reliably. Chlorine, bromine, iodine and possibly sulphur, can be determined at the μg ml^{-1} level, but serious interferences typical of the microwave discharge are encountered. If the excess of foreign components exceeds the 1 mg ml^{-1} level, prior separation of either the analyte or the matrix is mandatory. Techniques such as selective volatilization [16, 17], ion exchange or extraction might be employed. If, however, the interference level can be kept to a few hundred μg ml^{-1}, then the addition of potassium hydroxide permits determinations by means of the standard addition technique. This possibility has been demonstrated for chlorine, bromine and iodine. Extension to other elements probably requires the use of other furnace materials, different discharge tubes and/or other additives.

The authors thank H. Trumpie and P. A. van Gelder for their contributions to the experiments, and G. J. Kleyer for the construction of the furnace system and the coupling to the cavity. This paper was presented in part at the XXI C.S.I.—8 I.C.A.S., Cambridge, England, 1979.

REFERENCES

1 A. J. McCormack, S. C. Tong and W. D. Cooke. Anal. Chem., 37 (1965) 1470.
2 A. T. Zander and G. M. Hieftje, Appl. Spectrosc., 35 (1981) 357.
3 J. W. Carnahan, K. J. Mulligan and J. A. Caruso, Anal. Chim. Acta, 130 (1981) 227.
4 C. A. Bache and D. J. Lisk, Anal. Chem., 39 (1967) 786.
5 W. R. McLean, D. C. Stanton and G. E. Penketh, Analyst, 98 (1973) 432.
6 J. P. J. van Dalen, P. A. de Lezenne Coulander and L. de Galan, Anal. Chim. Acta, 94 (1977) 1.
7 H. A. Dingjan and H. J. de Jong, Spectrochim. Acta, 36B (1981) 325.
8 C. I. M. Beenakker, Spectrochim. Acta, 31B (1976) 483; 32B (1977) 173.
9 J. P. J. van Dalen, P. A. de Lezenne Coulander and L. de Galan, Spectrochim. Acta, 33B (1978) 545.
10 K. Tanabe, H. Haraguchi and K. Fuwa, Spectrochim. Acta, 36B (1981) 633.
11 F. L. Fricke, O. Rose, Jr. and J. A. Caruso, Anal. Chem., 47 (1975) 2018.
12 G. Volland, P. Tschöpel and G. Tölg, Spectrochim. Acta, 36B (1981) 901.
13 J. H. Runnels and J. H. Gibson, Anal. Chem., 39 (1967) 1398.
14 K. M. Aldous, R. M. Dagnall, B. L. Sharp and T. S. West, Anal. Chim. Acta, 54 (1971) 233.
15 A. T. Zander, R. K. Williams and G. M. Hieftje, Anal. Chem., 49 (1977) 2372.
16 J. F. Alder, Q. Jin and R. D. Snook, Anal. Chim. Acta, 120 (1980) 147; 123 (1981) 329.
17 K. Tanabe, K. Matsumoto, H. Haraguchi and K. Fuwa, Anal. Chem., 52 (1980) 2361.
18 P. J. Rommers and P. W. J. M. Boumans, XXI C.S.I.—8 I.C.A.S., Cambridge, England, 1979.
19 C. I. M. Beenakker, P. J. Rommers and P. W. J. M. Boumans, Philips Tech. Rev., 39 (1980) 65.
20 B. D. Quimby, P. C. Uden and R. M. Barnes, Anal. Chem., 50 (1978) 2112.
21 S. A. Estes, P. C. Uden and R. M. Barnes, Anal. Chem., 53 (1981) 1829.
22 M. T. C. de Loos-Vollebregt and L. de Galan, Spectrochim. Acta, 35B (1980) 495.
23 V. Sychra, D. Kolihovà, O. Vyskočilovà, R. Hlaváč and P. Puschel, Anal. Chim. Acta, 105 (1979) 263.
24 P. Brassem and F. J. M. J. Maessen, Spectrochim. Acta, 29B (1974) 203.
25 S. R. Goode and D. C. Otto, Spectrochim. Acta, 35B (1980) 569.

Analytica Chimica Acta, 142 (1982) 173—182
Elsevier Scientific Publishing Company, Amsterdam — Printed in The Netherlands

SOME ANALYTICAL CHARACTERISTICS OF AN ARGON—NITROGEN D.C. PLASMA ARC FOR EMISSION SPECTROMETRY

Y. FUJISHIRO, M. KUBOTA* and R. ISHIDA
National Chemical Laboratory for Industry, 1-chome, Higashi, Yatabe, Ibaraki (Japan)
(Received 15th February 1982)

SUMMARY

A low-power d.c. plasma arc device was used to estimate the analytical characteristics of an Ar—N_2 plasma arc compared to those of an argon plasma arc. When the flow rate of added nitrogen was varied from 0 to 1 l min^{-1}, the Cd I 228.802-nm line showed a maximum signal-to-background ratio at a nitrogen flow rate of approximately 0.3 l min^{-1} which corresponds to 0.23% of the total argon flow rate. Ratios of the signal intensities with the Ar—0.23%N_2 and argon plasma arcs are given for the spectral lines of seventeen elements. Relatively higher ratios were found for the atom lines of the group VIII through IIIA elements in the periodic table. Better precision and lower detection limits were attained for aluminium and cadmium with the Ar—0.23%N_2 plasma arc than with the argon plasma arc.

Direct current (d.c.) plasma arc devices are divided into two classes on the basis of the region of observations; i.e., the current-free type and the current-carrying type [1]. The former comprises most of the plasma jets and d.c. arc plasmas used as excitation sources for emission spectrochemical analysis of solutions. The latter includes a variety of stabilized arcs, which have been used successfully in the analysis of various solutions [2—5]. The capillary arc plasma which was developed primarily for the excitation of a fine aerosol produced with an aerosol generator [6] is also one of the wall-stabilized arc devices. A modified capillary arc plasma source used in conjunction with a nebulizer—desolvation apparatus has proved to be useful for determinations of trace elements in solutions [7—9].

Spectroscopic plasmas commonly require argon as a plasma-forming gas. In inductively-coupled plasma emission spectrometry, however, several papers have appeared describing the use of argon—nitrogen mixtures to decrease consumption of argon gas and/or to improve the power of detection [10—17]. Reports on the argon—nitrogen plasma for d.c. plasma emission spectrometry are relatively few [7, 18], though the Kranz plasma jet operated with only nitrogen has been reported by Schirrmeister [19, 20] and Kranz [21].

This paper describes the effects of added nitrogen on the analytical characteristics of the d.c. argon capillary arc. The aim of using the argon—

nitrogen atmosphere instead of the argon atmosphere is mainly to achieve higher signal-to-background ratios, because the argon flow supplied to the d.c. plasma arc is not so large as to be a serious problem in routine analytical applications.

EXPERIMENTAL

Apparatus and procedure

The apparatus used is listed in Table 1. The nebulizer—desolvation device, capillary arc source unit, and sequential scan spectrometer have been described previously [7, 8]. The heater temperature and the cooling-water temperature of the desolvation device were kept constant at 200°C and 4°C, respectively. The plasma arc is sustained by the main argon flow which carries the sample aerosol. A separate stream of argon (0.1 ml min^{-1}) was supplied around the thoriated tungsten cathode to reduce electrode consumption. Nitrogen was introduced into the arc through an additional gas inlet between the anode and cathode.

A Hamamatsu TV R457 photomultiplier tube replaced the R453 tube used in previous reports [7, 8]. The voltage supplied to the photomultiplier was set to 640 V.

Standard dilutions from 1 or 2 mg ml^{-1} stock solutions were used for all studies. All solutions were prepared with deionized water and stored in polyethylene bottles.

Argon flow rate and arc current

Emission stability of the plasma arc and signal and background intensities depend mainly on the main argon flow rate and the arc current. The concen-

TABLE 1

Apparatus

Sample introduction—excitation system	
Nebulizer	Glass concentric nebulizer
Desolvation device	Heater and water-cooled condenser
Excitation source	D.c. capillary arc source unit
D.c. power supply	Nakano Electronics, model D-8
Spectrometer system	
Spectrometer	JEOL 1.25-m Czerny-Turner mount, model 125B
Dispersion	0.62 nm mm^{-1} in the first order
Slit widths	9-μm entrance; 30-μm exit
Detector system	
Photomultiplier	Hamamatsu TV R457
High voltage power supply	Power Designs, model 2K20
Amplifier	Takeda Riken picoammeter, model TR-8641
Recorder	Hitachi strip-chart recorder, model 056
Integrator	Takeda Riken, model TR-2221

tric nebulizer used operates satisfactorily with argon flow rates of 1—1.5 l min^{-1} [9]. Increasing the argon flow rate increases the solution uptake rate, enhancing emission signals. However, with flow rates above 1.2 l min^{-1}, the signal enhancement became small and the emission stability was slightly reduced. Thus the optimal flow rate for the nebulization—argon arc excitation system is 1.2 l min^{-1}.

The argon plasma arc tends to be unstable at currents of 5 A or less, and fairly rapid erosion of the cathode occurs at currents above 12 A [7]. In the current range 5—12 A, the background increases rapidly and signal-to-background ratios for most elements decrease with increasing arc current. Therefore, measurements with the argon plasma arc were made at a current of 5.2 A.

Relations between the flow rate of added nitrogen and the emission characteristics of the arc were investigated using the same argon flow rate and arc current as those for the argon plasma arc. The optimal conditions for the argon—nitrogen plasma arc will be described later in the present paper.

RESULTS AND DISCUSSION

Effects of added nitrogen on emission characteristics

In order to investigate the influence of varying the flow rate of added nitrogen on the characteristics of the plasma arc, emission measurements were made for the Cd I 228.802-nm, Mg II 279.553-nm, and Ca II 393.367-nm lines. The flow rate of nitrogen was varied from zero to 1 l min^{-1}. The results obtained are shown in Fig. 1. The signal intensity (net signal) of the magnesium line falls to a minimum at about 0.2 l N_2 min^{-1} and then increases with increasing nitrogen flow rate. A similar but greater change occurs for the calcium line intensity. The cadmium line intensity shows the opposite trend; it increases drastically as the nitrogen flow rate is varied from zero to 0.3 l min^{-1} and then decreases with the flow rate. The signal-to-background ratios of these lines follow nearly the same trend as those observed for the signal intensities. It is clear that the addition of nitrogen is effective for improving the signal-to-background ratio of the cadmium line.

Figure 2 shows the effects of added nitrogen on the ratios of atom line intensity to ion line intensity for cadmium and calcium lines. The ratio for the calcium line pair increases as the nitrogen flow rate is increased to 0.3 l min^{-1}. Presumably this behavior can be explained in terms of ionization suppression of calcium atoms. The change in the ratio of the cadmium line pair with the nitrogen flow rate is much smaller than that observed for the calcium line pair; that is, ionization suppression is less pronounced for cadmium. This may appear unconvincing, because the ionization potential of cadmium (8.991 eV) is higher than that of calcium (6.111 eV). The enhancing effect of nitrogen on the cadmium line intensity, illustrated in Fig. 1, was observed not only for different cadmium atom lines (i.e., Cd I 326.105 nm, Cd I 361.051 nm, etc.) but also for ion lines (i.e., Cd II

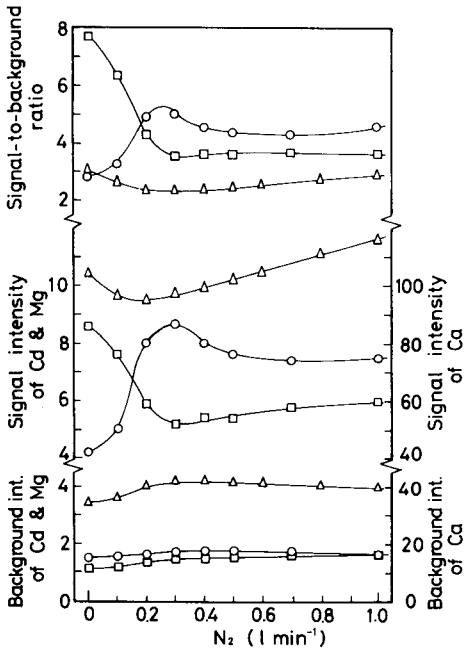

Fig. 1. Signal intensity, background intensity, and signal-to-background ratio of the Cd I 228.802, Mg II 279.553, and Ca II 393.367-nm lines as a function of the flow rate of added nitrogen. (○) Cd, 10 μg ml^{-1}; (△) Mg, 1 μg ml^{-1}; (□) Ca, 1 μg ml^{-1}.

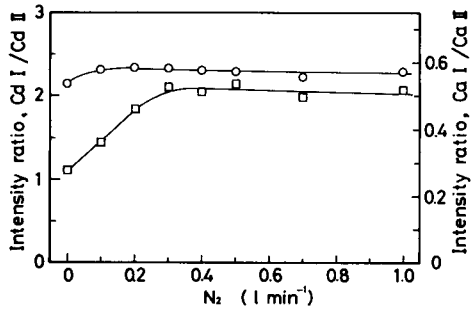

Fig. 2. Ratio of atom line to ion line intensity as a function of the flow rate of added nitrogen. (○) Cd I 228.802 nm/Cd II 226.502 nm; (□) Ca I 422.673 nm/Ca II 393.367 nm.

214.441 nm, Cd II 226.502 nm, etc.). As shown previously [7], the addition of nitrogen results in a slight decrease in the excitation temperature of the arc. Hence, it seems likely that the enhancement found for the cadmium lines is primarily a consequence of the energy transfer from nitrogen species to cadmium compounds, atoms, and/or ions in the plasma arc; and that energy transfer rather than ionization suppression is the dominant process which affects the emission behavior of cadmium in the argon—nitrogen plasma arc.

Variations in the signal intensity and the signal-to-background ratio of the Cd I 228.802-nm line with the nitrogen flow rate were also measured under different conditions of the main argon flow rate. Changing the argon flow rate causes a change in the solution uptake rate as well as a change in the nitrogen-to-argon concentration ratio in the plasma arc. Nevertheless, the results shown in Fig. 3 reveal that the maximum signal-to-background ratio is achieved within a limited range of nitrogen flow rate (0.2—0.3 l min^{-1}), being independent of the argon flow rate. It is also demonstrated in this figure that, for argon flow rates of 0.64—1.20 l min^{-1}, the larger the argon flow rate, the higher the signal-to-background ratio when the nitrogen flow rate is kept constant. However, as the argon flow rate is increased from 1.20 to 1.35 l min^{-1}, the signal-to-background ratio scarcely changes. Further, decreased emission stability was seen when the plasma was operated at the higher flow rate. These phenomena are essentially the same as those observed for the argon plasma arc. Therefore, the optimal argon flow rate for the argon—nitrogen plasma arc is also 1.2 l min^{-1}.

Effects of varying the arc current on the cadmium line emission are shown in Fig. 4. The measurements were made with various nitrogen flow rates up to 0.7 l min^{-1}. Obviously, with the argon—nitrogen plasma arc the signal intensity increases and the signal-to-background ratio decreases with increasing arc current. Hence, to achieve higher signal-to-background ratios, this plasma should be operated with smaller arc currents, though this causes

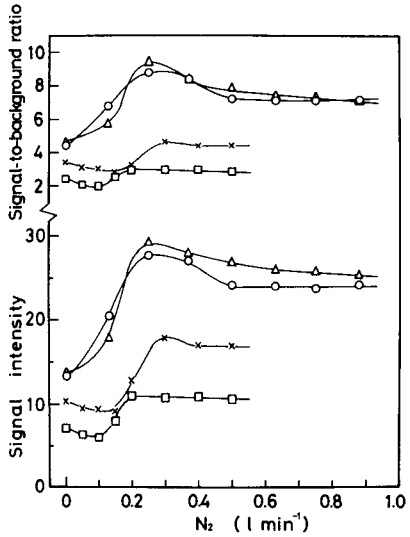

Fig. 3. Signal and signal-to-background ratio of the Cd I 228.802-nm line for different argon flow rates as a function of the flow rate of added nitrogen. Argon flow rate: (□) 0.64 l min^{-1}; (×) 0.90 l min^{-1}; (○) 1.20 l min^{-1}; (△) 1.35 l min^{-1}.

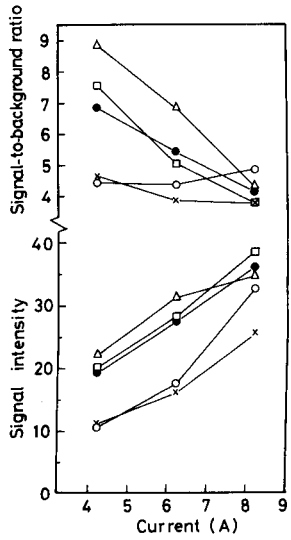

Fig. 4. Signal and signal-to-background ratio of the Cd I 228.802-nm line for different flow rates of added nitrogen as a function of the arc current. Nitrogen flow rate: (○) 0 l min^{-1}; (×) 0.2 l min^{-1}; (△) 0.3 l min^{-1}; (□) 0.5 l min^{-1}; (●) 0.7 l min^{-1}.

a slight decrease in the emission stability especially in the current range below 5 A.

It was indicated previously [8] that an effective means to obtain higher signal-to-background ratios with the argon plasma arc is to employ potassium chloride solutions. To examine the combined effect of nitrogen added to the plasma gas and potassium chloride added to the solutions, measurements were made for the Cd I 228.802-nm line emission from a 0.1 mol l^{-1} potassium chloride solution containing 1 μg ml^{-1} cadmium. The flow rate of added nitrogen was varied over the range 0—1.0 l min^{-1}. It can be seen from Fig. 5 that no improvement in the signal-to-background ratio is attained, although a small increase in the signal intensity occurs as the nitrogen flow rate is increased from zero to 0.2 l min^{-1}. This is probably because the buffer effect of potassium chloride is far stronger than the effect of added nitrogen on the characteristics of the arc.

Comparison of argon and argon—nitrogen plasma arcs

According to the above results, the optimal operation of the argon and the argon—nitrogen plasma arcs is achieved at a main argon flow rate of 1.2 l min^{-1} and an arc current of 5.2 A. Another important parameter for the argon—nitrogen plasma is the flow rate of nitrogen. As illustrated in Fig. 1, the effect of the nitrogen flow rate on signal intensities changes from element to element. However, several elements (including cadmium), which were found to have their signals enhanced by added nitrogen, gave the maximum signal-to-background ratio at a nitrogen flow rate of about 0.3 l min^{-1}.

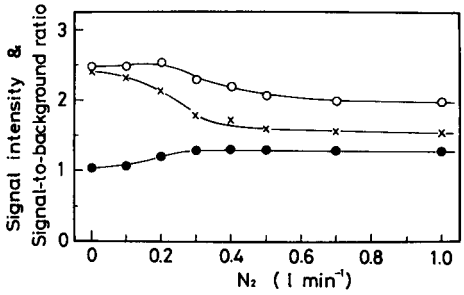

Fig. 5. Effect of added nitrogen on: (○) the Cd I 228.802-nm line intensity; (●) the background intensity; (×) the signal-to-background ratio, obtained with a 0.1 mol l^{-1} KCl solution containing 1 μg ml^{-1} cadmium.

Also, rather rapid erosion of the cathode occurred when the flow rate exceeded 0.4 l min^{-1} and, as indicated previously [7], the emission stability decreased at flow rates in excess of 0.6 l min^{-1}. Based on these observations, a nitrogen flow of 0.3 l min^{-1} was selected. The total flow rate of argon (nebulizer gas plus cathode flush) is 1.3 l min^{-1} and thus the nitrogen flow rate corresponds to approximately 0.23% of the total argon flow rate.

For comparative purposes, emission characteristics, analytical precision, and detection capability were investigated for the argon plasma arc and the Ar—0.23%N_2 plasma arc. Ratios of signal intensity obtained with the Ar—0.23%N_2 plasma arc to that obtained with the argon plasma arc determined for the spectral lines of seventeen elements are shown in Fig. 6. The spectral lines selected are the most sensitive for each element with both arcs. Each solution contained the particular element at a concentration level of 10 μg ml^{-1}. The maximum value of the intensity ratio was 2.06 which was obtained for zinc [Zn I 213.856-nm line], while the minimum value was 0.52 which was observed for calcium [Ca II 393.367-nm line]. No significant correla-

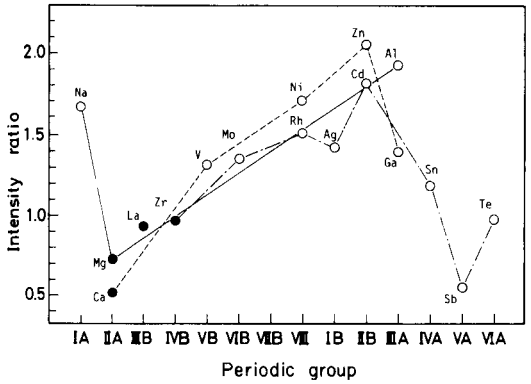

Fig. 6. Ratio of the signal intensity observed for the Ar—0.23%N_2 plasma arc to that observed for the argon plasma arc plotted against group in the periodic table. (○) Atom line; (●) ion line.

tion was found between the intensity ratios for the seventeen elements and spectroscopic parameters such as the ionization potentials of the atoms and the excitation energies of the lines. For instance, zinc and cadmium showed larger intensity ratios (2.06 and 1.82, respectively), whereas antimony and tellurium whose ionization potentials are as high as zinc and cadmium exhibited much smaller intensity ratios (0.53 and 0.97, respectively). The most sensitive lines of magnesium, calcium, lanthanum, and zirconium were ion lines and the intensity ratios of these lines were less than 1, i.e., nitrogen suppressed the emission intensities. The most sensitive lines of the other thirteen elements were atom lines and no suppressing effect from nitrogen occurred for the atom lines except for the antimony and tellurium lines. It is interesting to note that the atom lines of the group VIII through IIIA elements in the periodic table show higher intensity ratios. Unfortunately, we have no conclusive explanation for this phenomena, although it is possible to speculate that the energy transfer from nitrogen species to the species of these elements could be a main factor yielding the signal enhancement in presence of nitrogen, as mentioned in the discussion of Figs. 1 and 2. Very little is known about the actual role played by nitrogen in argon—nitrogen plasmas, e.g., selective energy transfer from active nitrogen and deactivation of metastable argon species by nitrogen molecules [16]. Further study is needed to obtain adequate data to account for the role of nitrogen.

Figure 7 compares the background spectra observed with the argon and the Ar—0.23%N_2 plasma arcs. These spectra were recorded at a scanning speed of 250 nm min^{-1} while pure water was aspirated. It can be seen that nitrogen reduces the emission intensity of the OH bands. With the argon—

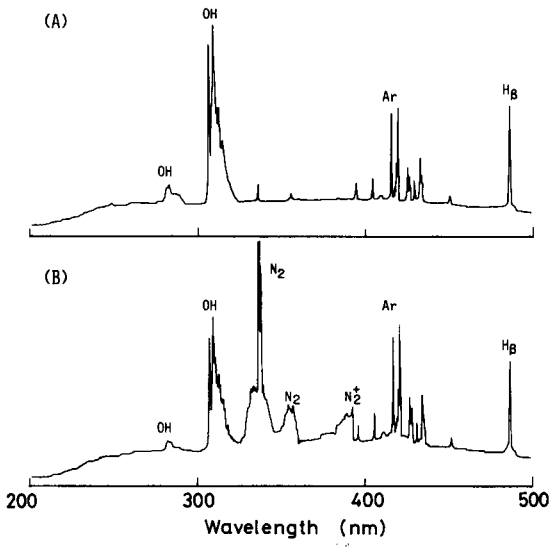

Fig. 7. Spectral scan for (A) argon plasma arc and (B) Ar—0.23%N_2 plasma arc with water aspirated.

nitrogen plasma, the band spectra of the second positive nitrogen system and the first negative nitrogen system appear in the region 330—400 nm, so that spectral interference becomes more serious than with the argon plasma.

Table 2 presents typical precision data for nine elements. For aluminium and cadmium, better precision was obtained with the Ar—0.23%N_2 plasma arc than with the argon plasma arc, but the differences are rarely significant for practical purposes. Background-equivalent concentrations and detection limits determined with the two plasma arcs are compared in Table 3. The detection limit represents the analyte concentration giving a signal-to-noise ratio of 2, where the noise is defined as the standard deviation of ten consecutive measurements of the background intensity. The background-equivalent concentration means the analyte concentration which gives a net signal equal to the background intensity. For aluminium, cadmium, sodium, nickel, and zinc, the background-equivalent concentrations obtained with the Ar—0.23%N_2 plasma arc are lower than those obtained with the argon plasma arc. In most wavelength regions of interest, the noise which expresses the background fluctuation increased when nitrogen was added to the plasma. Because of the increased noise, the detection limits for sodium, nickel, and zinc were not lowered by using the Ar—0.23%N_2 plasma arc.

To reduce the noise, further studies were carried out on the size of the additive gas inlet, the material and configuration of the cathode, and the mixing of nitrogen in the nebulizer gas. Satisfactory results, however, could not be obtained. In conclusion, it is recommended to use the argon—nitrogen plasma arc only for the determination of such elements as aluminium and cadmium, for which the precision and detection capability can be improved by the addition of nitrogen.

TABLE 2

Coefficients of variation (%) for ten repetitive measurements with the argon and Ar—0.23%N_2 plasma arcs

Element and line (nm)	Ar				Ar—0.23%N_2			
	Conc. ($\mu g\ ml^{-1}$)				Conc. ($\mu g\ ml^{-1}$)			
	0.1	1	10	100	0.1	1	10	100
Al I 396.153	—	5.61	2.46	1.26	—	5.31	1.26	1.10
Cd I 228.802	—	4.67	1.96	—	—	4.64	1.79	—
La II 408.672	—	—	2.86	1.61	—	—	15.0	2.01
Mg II 279.553	6.31	3.44	1.64	—	5.71	3.07	2.45	—
Mn II 257.610	19.5	3.25	2.85	—	39.7	5.15	4.10	—
Mo I 386.411	—	7.46	2.75	—	—	17.7	3.08	—
V I 437.924	—	2.80	2.31	—	—	3.49	1.86	—
Zn I 213.856	—	—	6.01	2.73	—	—	4.32	3.80
Zr II 343.823	—	3.00	1.85	—	—	4.62	1.71	—

TABLE 3

Comparison of background-equivalent concentration and detection limit with argon and Ar—0.23%N_2 plasma arcs ($\mu g\ ml^{-1}$)

Element and line (nm)	Background-equivalent concentration[a]		Detection limit[b]	
	Ar	Ar—0.23%N_2	Ar	Ar—0.23%N_2
Ag I 328.068	1.2	2.3	0.03	0.1
Al I 396.153	6.2	4.2	0.03	0.02
Ca II 393.367	0.12	0.22	0.004	0.007
Cd I 228.802	3.1	2.3	0.09	0.05
Ga I 417.205	2.2	2.3	0.03	0.2
La II 408.672	32	52	0.9	2.6
Mg II 279.553	0.24	0.34	0.004	0.006
Mn II 257.610	1.8	2.6	0.04	0.09
Mo I 386.411	4.0	4.4	0.09	0.3
Na I 588.995	0.094	0.083	0.006	0.01
Ni I 352.454	5.2	3.7	0.07	0.2
Rh I 343.489	15	16	0.08	0.3
Sb I 259.805	15	36	0.2	0.7
Sn I 270.651	34	38	0.8	0.7
Te I 214.275	13	16	0.3	0.8
V I 437.924	2.4	2.6	0.02	0.05
Zn I 213.856	0.76	0.44	0.02	0.02
Zr II 343.823	2.2	3.3	0.06	0.08

[a]The analyte concentration giving a net signal equal to the background intensity. [b]The concentration yielding a net signal equal to twice the standard deviation of the background intensity (n = 10).

REFERENCES

1 C. D. Keirs and T. J. Vickers, Appl. Spectrosc., 31 (1977) 273.
2 M. Marinković and B. Dimitrjević, Spectrochim. Acta, 23B (1968) 257.
3 M. Kliska and M. Marinković, Spectrochim. Acta, 25B (1970) 545.
4 D. A. Murdick, Jr. and E. H. Piepmeier, Anal. Chem., 46 (1974) 678.
5 M. Marinković and V. G. Antonijević, Spectrochim. Acta, 35B (1980) 129.
6 J. L. Jones, R. L. Dahlquist and R. E. Hoyt, Appl. Spectrosc., 25 (1971) 628.
7 M. Kubota, Anal. Chim. Acta, 88 (1977) 79.
8 M. Kubota, R. Ishida and Y. Fujishiro, J. Spectrosc. Soc. Jpn., 26 (1977) 63.
9 M. Kubota, J. Spectrosc. Soc. Jpn., 29 (1980) 39.
10 S. Greenfield and P. B. Smith, Anal. Chim. Acta, 59 (1972) 341.
11 S. Greenfield, I. L. Jones, H. McGeachin and P. B. Smith, Anal. Chim. Acta, 74 (1975) 225.
12 S. Greenfield and H. McGeachin, Anal. Chim. Acta, 100 (1978) 101.
13 S. Greenfield and D. T. Burns, Anal. Chim. Acta, 113 (1980) 205.
14 L. Ebdon, D. J. Mowthorpe and M. R. Cave, Anal. Chim. Acta, 115 (1980) 171.
15 A. Montaser and J. Mortazavi, Anal. Chem., 52 (1980) 255.
16 A. Montaser, V. A. Fassel and J. Zalewski, Appl. Spectrosc., 35 (1981) 292.
17 J. A. C. Broekaert, F. Leis and K. Laqua, Talanta, 28 (1981) 745.
18 R. Ishida and M. Kubota, J. Spectrosc. Soc. Jpn., 21 (1972) 255.
19 H. Schirrmeister, Spectrochim. Acta, 23B (1968) 709.
20 H. Schirrmeister, Spectrochim. Acta, 24B (1969) 1.
21 E. Kranz, Spectrochim. Acta, 27B (1972) 327.

Analytica Chimica Acta, 142 (1982) 183—188
Elsevier Scientific Publishing Company, Amsterdam — Printed in The Netherlands

ESSAIS INTERLABORATOIRES: DOSAGE DU CADMIUM, DU CUIVRE ET DU PLOMB DANS L'EAU DE MER PAR SPECTROMETRIE D'ABSORPTION ATOMIQUE ELECTROTHERMIQUE

JANINE LAMATHE*

Service de Chimie, Laboratoire Central des Ponts et Chaussées, 58, Boulevard Lefèbvre, 75732 Paris Cedex 15 (France)

CHARLES MAGURNO et JEAN-CLAUDE EQUEL

Laboratoire Régional des Ponts et Chaussées d'Aix-en-Provence, B.P. 39, 13762 Les Milles Cedex (France)

(Reçu le 30 mars 1982)

SUMMARY

(An interlaboratory study of the determination of cadmium, copper and lead in seawater by electrothermal atomic absorption spectrometry.)

The reproducibility of a selective extraction method on Chelex-100 resin in the Ca^{2+} form, described previously, was tested on seawater with and without addition of Cd, Cu and Pb. The metals extracted were determined by electrothermal atomic absorption spectrometry (a.a.s.). The results obtained by the three laboratories participating in these tests prove the validity of the method for the determination of cadmium and copper. The largest dispersion of results, observed for lead, is related to the poorest precision of electrothermal a.a.s. for this element.

RESUME

La reproductibilité de la méthode d'extraction sélective, sur résine Chelex-100 (forme Ca^{2+}) décrite précédement a été testée sur une eau de mer avec et sans ajouts de Cd, Cu et Pb. Le dosage des métaux extraits a été réalisé par spectrométrie d'absorption atomique (s.a.a.) électrothermique. Les résultats obtenus, par les trois laboratoires qui ont participé à cet exercice, montrent la validité de la méthode expérimentée pour les dosages du cadmium et du cuivre. Pour le plomb, on observe une plus grande dispersion des résultats qui semble liée à une moins bonne précision de la s.a.a. électrothermique pour cet élément.

La détermination des éléments-traces dans le milieu marin, en particulier des métaux lourds, présente une certaine importance non seulement du fait de leur rôle dans les cycles biochimiques et géochimiques des océans mais surtout parce que les niveaux atteints peuvent être des indices de contamination.

Le dosage des métaux lourds dans l'eau de mer présente de grandes difficultés en raison des très faibles teneurs rencontrées, souvent proches des limites de détection des techniques analytiques usuelles, et de la complexité du milieu fortement chargé en sels. De très nombreuses recherches ont été effectuées ces dernières années pour la mise au point de méthodes sensibles et

reproductibles. Actuellement les techniques analytiques les plus couramment utilisées sont la spectrométrie d'absorption atomique électrothermique, après préconcentration par formation de complexes organo-métalliques extractibles par un solvant, et la voltammétrie de redissolution anodique.

En 1979, nous avons étudié la séparation des métaux lourds, présents dans l'eau de mer, par chromatographie sur résine chélatante et mis au point un mode opératoire permettant l'élution sélective des différents cations fixés sur la résine, les dosages étant faits par s.a.a. électrothermique [1]. Cette technique a été utilisée par le Laboratoire Régional d'Aix-en-Provence lors de l'exercice d'intercalibration, pour le dosage du cadmium dans l'eau de mer, organisé en 1979 par le Réseau National d'Observation de la qualité du milieu marin (R.N.O.) dans le cadre du Conseil International pour l'Exploration de la mer (C.I.E.M.). Les résultats de ce laboratoire se situant parmi ceux des laboratoires de haute précision (à ±30%) montrent, en principe, la validité de la technique. Cependant, le Laboratoire d'Aix ayant été le seul à avoir effectué une extraction sur résine chélatante, sur les 33 laboratoires participants, il nous est apparu souhaitable de confirmer ce résultat par un exercice similaire réalisé par trois laboratoires du réseau des Ponts et Chaussées: Aix-en-Provence, Angers et St-Brieuc.

Pour tester la sélectivité des élutions, cet essai interlaboratoires a porté sur des échantillons d'eau de mer avec et sans ajouts de cadmium, de cuivre et de plomb.

ORGANISATION DE L'EXERCICE

Echantillons

Chaque laboratoire devait analyser trois échantillons et effectuer trois déterminations sur chaque échantillon. Les trois échantillons étaient: A, eau de mer sans ajout; B, eau de mer avec ajout faible de cadmium, de cuivre et de plomb (0,75 μg Cd l^{-1}; 5 μg Cu l^{-1}; 3 μg Pb l^{-1}); C, eau de mer avec ajout élevé de cadmium, de cuivre et de plomb (5 μg Cd l^{-1}; 75 μg Cu l^{-1}; 50 μg Pb l^{-1}).

L'eau de mer a été prélevée en Méditerranée sur un site côtier réputé non pollué près de Carry-le-Rouet. Le pompage a été réalisé à 15—20 cm de profondeur et l'eau de mer a été recueillie dans une bonbonne en verre de 30 l. Les échantillons ont été préparés dans la journée qui a suivi le prélèvement, après simple décantation de l'eau de mer, et congelés à —20°C. Les analyses ont été réalisées dans un délai de 1 à 2 mois après réception des échantillons.

Extractions

Sur une micro-colonne de résine Chelex-100, (100—200 mesh, forme Ca^{2+}, diamètre 1 cm, hauteur 4 cm), on fait passer 100 ml d'eau de mer (pH naturel voisin de 8). Après lavage à l'eau déionisée jusqu'à absence d'ions chlorures dans l'effluent, on élue les alcalins et alcalino-terreux par passage

de 250 ml d'acide acétique dilué (1 + 99). Cet éluat est rejeté. On lave la résine avec 25 ml d'eau déionisée afin d'éliminer l'acide acétique restant dans le volume interstitiel du lit de résine. On élue ensuite successivement par 100 ml d'acide nitrique 10^{-2} M le cadmium, puis par 10 ml d'acide nitrique 1 M le cuivre et le plomb (cet éluat est dilué à 100 ml afin d'avoir une concentration en acide nitrique égale à 10^{-1} M au moment du dosage).

Un essai à blanc est réalisé parallèlement par passage de l'ensemble des réactifs sur une micro-colonne de résine.

Pour pallier l'effet "rendement des colonnes", il a été demandé aux participants de procéder par ajouts dosés préalablement aux extractions. Ceci a conduit chaque laboratoire à préparer, pour chaque type d'eau, une série d'échantillons avec des ajouts croissants des trois éléments à doser. Chaque série a été soumise à l'extraction simultanément à celles correspondant aux 3 déterminations imposées. Le Tableau 1 montre un exemple d'une gamme employée par un des laboratoires.

Dosages

Les dosages ont été effectués par spectrométrie d'absorption atomique avec four graphite, le nombre d'injections étant laissé à l'appréciation de l'analyste pour l'obtention d'une moyenne valable. Dans le cas présent, le nombre d'injections se situe entre 3 et 6.

L'équipement des trois laboratoires est différent: (1) Varian-Techtron AA6, CRA 90, automatique; (2) Perkin-Elmer 373, HGA 76B, automatique; (3) Instrumentation Laboratory (IL) 151, IL 555, manuelle.

RESULTATS ET DISCUSSION

Le Tableau 2 donne l'ensemble des résultats obtenus pour les trois échantillons d'eau de mer A, B et C. Pour le cadmium, on observe une bonne répétabilité des mesures sauf pour le laboratoire 3 dont les résultats sont plus dispersés. La valeur de 0,22 $\mu g\ l^{-1}$ pour l'échantillon A est probablement aberrante. Pour le cuivre et le plomb, on obtient une assez bonne répétabilité dans l'ensemble à une exception près. Il est à remarquer que les résultats du laboratoire 3, dont les injections sont faites manuellement, sont les plus dispersés.

TABLEAU 1

Exemple de gamme pour la méthode des ajouts dosés

Extraction	1	2	3	4	5	6	7
Eau de mer (ml)	100	100	100	100	100	100	100
Ajout (μg Cd)	0	0	0	0,05	0,1	0,3	0,6
Ajout (μg Cu)	0	0	0	1,0	2,5	5,0	10,0
Ajout (μg Pb)	0	0	0	1,0	2,5	5,0	7,5

TABLEAU 2

Resultats detaillés

Elément	Echantillon		Teneurs trouvées ($\mu g\ l^{-1}$)[a]								
	Réf.	Ajout ($\mu g\ l^{-1}$)	Laboratoire 1			Laboratoire 2			Laboratoire 3		
			Ex1	Ex2	Ex3	Ex1	Ex2	Ex3	Ex1	Ex2	Ex3
Cadmium	A	0,00	0,00	0,00	0,02	0,03	0,03	0,03	0,00	0,00	0,22
	B	0,75	0,75	0,77	0,92	0,76	0,78	0,79	0,5	0,78	0,81
	C	5,00	5,72	5,84	5,95	5,50	5,50	5,50	3,8	5,8	5,8
Cuivre	A	0,0	0,2	0,5	0,8	0,6	1,0	1,0	0,0	0,6	1,25
	B	5,0	4,8	5,6	6,6	4,5	4,5	4,8	4,65	5,15	5,60
	C	75,0	80,5	81,0	82,0	67,0	67,0	68,0	50,0	67,5	73,0
Plomb	A	0,0	0,0	0,0	0,4	0,0	0,0	0,1	0,0	0,0	0,8
	B	3,0	3,0	3,6	4,0	3,6	3,6	4,0	3,15	5,32	5,9
	C	50,0	60,0	60,0	63,0	55,0	57,0	59,0	47,5	51,5	75,0

[a] Ex = Extraction.

TABLEAU 3

Calcul statistique pour les échantillons B et C

Elément	Cd		Cu		Pb	
Echantillon	B	C	B	C	B	C
Nombre de déterminations	9	9	9	9	9	9
Etendue ($\mu g\ l^{-1}$)	0,5—0,92	3,8—5,95	4,5—6,6	50—82	3—5,9	47,5—75
Teneur moyenne ($\bar{X}$)	0,76	5,49	5,06	70,66	4,02	58,66
Ecart-type (σ)	0,11	0,65	0,69	10,1	0,97	7,7
Coefficient de variation (%)	14,5	11,8	13,6	14,3	24,1	13,1
Précision (%) pour P = 95%[a]	33	27	31	33	55	30

[a] $100\ \sigma\ t/\bar{X}$.

Le Tableau 3 récapitule, pour les échantillons B et C, les principales données statistiques calculées à partir des résultats bruts. Le nombre de déterminations n'est pas assez grand pour faire une exploitation critique, mais ce tableau montre que les résultats obtenus pour le plomb sont les moins satisfaisants.

Les résultats trouvés par chaque laboratoire pour les ajouts des trois métaux dans les échantillons B et C sont indiqués dans le Tableau 4. Pour le cadmium, les résultats sont très satisfaisants, la moyenne générale étant de 0,73 $\mu g\ l^{-1}$ pour un ajout théorique de 0,75 $\mu g\ l^{-1}$ et de 5,45 $\mu g\ l^{-1}$ pour une valeur théorique de 5 $\mu g\ l^{-1}$.

TABLEAU 4

Moyennes, ajouts trouvés et écarts[a]

Elément	Echantillon		Laboratoire 1			Laboratoire 2			Laboratoire 3			Moyenne	
	Réf.	Ajout ($\mu g\ l^{-1}$)	I	II	III	I	II	III	I	II	III	IV	III
Cadmium	A	0,00	0,01			0,03			0,07				
	B	0,75	0,81	0,80	+7	0,78	0,75	0	0,70	0,63	−16	0,73	−3
	C	5,00	5,84	5,83	+17	5,50	5,47	+9	5,13	5,06	+1	5,45	+9
Cuivre	A	0,0	0,5			0,9			0,6				
	B	5,0	5,7	5,2	+4	4,6	3,7	−26	5,1	4,5	−10	4,5	−10
	C	75,0	81,2	80,7	+8	67,3	66,4	−11	63,5	62,9	−16	70,0	−7
Plomb	A	0,0	0,1			0,0			0,3				
	B	3,0	3,5	3,4	+13	3,7	3,7	+23	4,8	4,5	+50	3,9	+30
	C	50,0	61,0	60,9	+22	57,0	57,0	+14	58,0	57,7	+15	58,5	+17

[a]I, Moyenne des 3 valeurs expérimentales trouvées ($\mu g\ l^{-1}$). II, Ajout trouvé (moyenne par laboratoire) en $\mu g\ l^{-1}$. III, Ecart (%), ajout moyen trouvé par rapport à l'ajout théorique. IV, Ajout moyen trouvé sur l'ensemble des déterminations ($\mu g\ l^{-1}$).

TABLEAU 5

Comparaison entre les résultats de l'exercice intercalibration R.N.O. et nos essais pour Cd

Echantillons	Nos essais			Essais intercalibration R.N.O.		
	A	B	C	1	2	3
Teneur moyenne trouvée ($\bar{X}$) ($\mu g\ l^{-1}$)	0,01	0,76	5,49	0,10	0,78	5,68
Ecart type (σ)	0,015	0,110	0,655	0,029	0,135	0,670
Nombre de déterminations	8	9	9	105	128	140
Ajout théorique ($\mu g\ l^{-1}$)	0,00	0,75	5,00	0,00	0,65	5,70
Ajout trouvé (moyenne) ($\mu g\ l^{-1}$)		0,73	5,45		0,68	5,58
Coefficient de variation (%)		14,5	12		17,3	12
Précision (%) pour $P = 95\%$[a]		33	27		34	23

[a]$100\ \sigma\ t/\bar{X}$.

Si l'on compare (Tableau 5) ces résultats à ceux trouvés lors de l'essai d'intercalibration R.N.O., par les laboratoires de haute précision [2], on constate que les précisions sont du même ordre de grandeur. Bien que cette comparaison ne porte pas sur un nombre de déterminations identiques, il nous paraît justifié de considérer que les résultats sont équivalents, ce qui

confirme la validité de la méthode de séparation sur résine Chelex-100 (forme Ca^{2+}).

Pour le cuivre, les résultats obtenus par les trois laboratoires sont un peu plus dispersés mais sont dans l'ensemble acceptables. Pour le plomb, toutes les valeurs moyennes d'ajouts sont très sensiblement supérieures aux valeurs théoriques pour les deux niveaux étudiés et les erreurs relatives sont plus importantes pour cet élément que pour le cuivre et le cadmium. Le manque de précision du dosage du plomb par s.a.a. sans flamme est très certainement à l'origine de ces résultats très dispersés.

En effet, lors d'un essai d'intercalibration que nous avons réalisé en 1979 avec 13 laboratoires équipés de matériels différents, nous avons pu constater que le plomb donnait également les résultats les plus dispersés alors même que les déterminations portaient sur des solutions monoélément dans l'eau distillée [3].

Conclusion

Cet essai d'intercalibration exécuté par trois laboratoires montre que la méthode d'extraction sur résine Chelex-100 (forme Ca^{2+}), avec dosage des métaux par spectrométrie d'absorption atomique électrothermique, donne des résultats équivalents à ceux trouvés par les autres techniques couramment employées pour le dosage du cadmium dans l'eau de mer. Cette méthode donne aussi des résultats très acceptables pour le cuivre. Par contre, pour le plomb, il semble que la méthode de mesure (s.a.a. électrothermique) soit à l'origine d'une plus grande dispersion des résultats sans que la sélectivité de la méthode de séparation soit en cause.

Les auteurs remercient Melle Largeaud, M. Barrais du L. R. d'Angers et M. Touzé du L. R. de St-Brieuc pour leur participation à ces travaux.

BIBLIOGRAPHIE

1 J. Lamathe, Anal. Chim. Acta, 104 (1979) 307.
2 Y. Thibaud, Reports on I.C.E.S. intercalibrations of mercury and cadmium in seawater, No. 110, International Council for the Exploration of the Sea, Copenhagen, Denmark, 1981.
3 J. Ranchet, F. Menissier, J. Lamathe et I. Voinovitch, Analusis, 10 (1982) 71.

Analytica Chimica Acta, 142 (1982) 189—195
Elsevier Scientific Publishing Company, Amsterdam — Printed in The Netherlands

DETERMINATION OF TRACE METALS IN SODIUM BY ELECTRO-THERMAL ATOMIC ABSORPTION SPECTROMETRY

T. R. MAHALINGAM, R. GEETHA, A. THIRUVENGADASAMI and C. K. MATHEWS*
Radiochemistry Programme, Reactor Research Centre, Kalpakkam-603102, Tamil Nadu (India)

(Received 6th April 1982)

SUMMARY

Graphite-furnace atomic absorption spectrometry is used to analyze sodium metal after conversion to sodium nitrate. Chromium, Ni, Co, Cd and Pb have detection limits in sodium of 0.18, 0.48, 0.11, 0.02 and 0.48 $\mu g\ g^{-1}$; these are similar to the concentrations in nuclear-grade sodium, except for lead, which is below the detection limit. The behaviour of sodium nitrate, chloride and sulphate as matrices is compared.

The determination of traces of metallic impurities in the primary and secondary loops of a sodium-cooled fast reactor is important for monitoring and understanding corrosion and mass-transfer processes. Various methods have been developed for the determination of trace metals in nuclear-grade sodium [1—3]. A method that is widely used involves removal of sodium by distillation under vacuum and analysis of the residue by flame atomic absorption spectrometry [2]. One disadvantage of the distillation technique is that it cannot be used for the determination of volatile impurities such as cadmium and zinc which are partially or wholly lost during the distillation process. Moreover, the use of small samples is preferable for analysis of the radioactive primary sodium. Hence a direct method for analysing sodium by means of graphite-furnace atomic absorption spectrometry (a.a.s.) was developed in this laboratory [4]. Garbett et al. [5] have used the graphite rod atomiser for determination of iron, nickel and chromium in sodium by a.a.s., after converting the sample to sodium chloride. In the present work, conversion of sodium to sodium nitrate was preferred, as it was found to be a superior matrix to sodium chloride, especially for the determination of volatile impurities such as cadmium and lead.

In this paper the determination of chromium, nickel, cobalt, cadmium and lead in sodium nitrate solution (0.2% Na, w/v) is described. Sodium nitrate, sodium chloride and sodium sulphate were compared with respect to their contribution to non-specific absorption. By suitably selecting the charring temperature, it was possible to minimise matrix interference.

EXPERIMENTAL

Apparatus and reagents

A Model IL751 atomic absorption spectrometer (Instrumentation Laboratories, U.S.A.) fitted with a Model CTF 555 controlled-temperature furnace atomiser was used. The temperature calibration was checked in the temperature range 200—1000° C by placing a chromel—alumel thermocouple inside the furnace tube and measuring its output. In the higher range (1000—2000° C) it was checked by optical pyrometry. The variation from the manufacturer's stated values was found to be ±50° C. The pyrolytically-coated and uncoated graphite tubes used were supplied by Instrumentation Laboratories.

All the laboratory ware used was thoroughly cleaned by soaking for 8 h in each of the following: (1 + 1) nitric acid, 10% EDTA solution and quartz-distilled water. The washings were checked for blank response before the apparatus was used.

Demineralised water, double-distilled from a quartz assembly was used. Electronic-grade nitric acid (B.D.H.) was double distilled in a quartz apparatus before use. Stock standard solutions containing 1 mg ml^{-1} of the elements of interest were prepared from pure metals (B.D.H., analytical reagent). Working standards were prepared freshly by dilution of these standards with 0.1 M nitric acid and were stored in perspex vials.

Procedures

Nuclear-grade sodium (Metaux Speciaux, France) was taken for analysis. Sodium samples were cut in a glove box under an inert atmosphere, with a clean knife made of high-purity copper. Sodium samples were taken in clean quartz vessels (170 mm tall, 20 mm diameter). For the dissolution of sodium, the procedure outlined by Silverman [1] was followed. The samples were dissolved by dropwise addition of quartz-distilled water from a polyethylene dropping bottle, under argon. The vessels were cooled externally by ice-cold water and the rate of addition of water was adjusted so that the vessels were never allowed to become very hot. The whole operation was carried out inside a well-ventilated fumehood; the glass-panelled shutter of the fumehood was almost fully closed during the dissolution. It took about 15 min to dissolve a 1-g sample. The solutions were neutralised by adding the required amount of nitric acid and diluted suitably to give a sodium concentration of 0.2% (w/v). These solutions were stored in clean polyethylene bottles. The experimental blank was found to be very low, i.e., of the order of a few pg/25 μl. To establish the sample weight, sodium was determined by flame emission spectrometry after suitable dilution.

In order to decide on a suitable matrix, solutions of sodium nitrate, chloride and sulphate were used for the initial studies. The sodium concentration was adjusted by dilution to be about 0.2% (w/v) in each solution, and 25 μl of each was injected into the furnace. A deuterium hollow-cathode lamp was used and the non-specific absorption of these solutions was studied

at the wavelengths of the analytes at the selected atomisation temperature given in Table 1.

The volatilisation behaviour of the trace metal nitrates in the graphite furnace was also studied as a function of charring temperature; 25 μl of metal nitrate solutions of the following concentrations were tested: nickel, 1×10^{-8} g ml^{-1}; cobalt, chromium and lead, 6×10^{-9} g ml^{-1}; cadmium, 6×10^{-10} g ml^{-1}. As most of these nitrates decompose readily to form their oxides at low temperatures, the results, may be taken to indicate the volatilisation behaviour of the respective oxides in the graphite furnace.

The dry, char and atomisation conditions were optimised to achieve the best sensitivities and the lowest non-specific absorption (these are given in Table 1). The instrument was operated in the "temperature ramp mode". Taking nickel as an example, the data in Table 1 can be explained as follows. In the drying stage, the furnace tube is heated first from room temperature to 80° C in 45 s and then to 125° C in another 45 s; thus the sample is dried smoothly without sputtering. In the charring stage, the furnace is heated to 950° C in 40 s and subsequently held at 950° C for 20 s. The next stage involves "step heating" to 2000° C, which temperature is held for 5 s to achieve atomisation.

For the determination of impurities, 25 μl aliquots of sodium nitrate solution (0.2% Na) were injected from Finn pipettes with disposable polythene tips. The purge gas used was argon. Deuterium arc background correction was employed. The peak absorbance was read off from the digital display of the instrument console, and compared with standards prepared from pure solutions.

RESULTS AND DISCUSSION

From the plots shown in Fig. 1(a—c), sodium nitrate was found to give the least non-specific absorption and to allow lower charring temperatures to

TABLE 1

Optimum program settings for the graphite furnace

Element		Dry		Char		Atomise	
Nickel	Temp. (° C)	80	125	950	950	2000	2000
	Ramp time (s)	45	45	40	20	0	5
Cobalt	Temp. (° C)	80	125	950	950	2200	2200
	Ramp time (s)	45	45	40	20	0	5
Chromium	Temp. (° C)	80	125	900	900	2000	2000
	Ramp time (s)	45	45	40	20	0	5
Cadmium	Temp. (° C)	80	125	450	450	1000	1000
	Ramp time (s)	45	45	40	20	0	5
Lead	Temp. (° C)	80	125	550	550	1800	1800
	Ramp time (s)	45	45	40	20	0	5

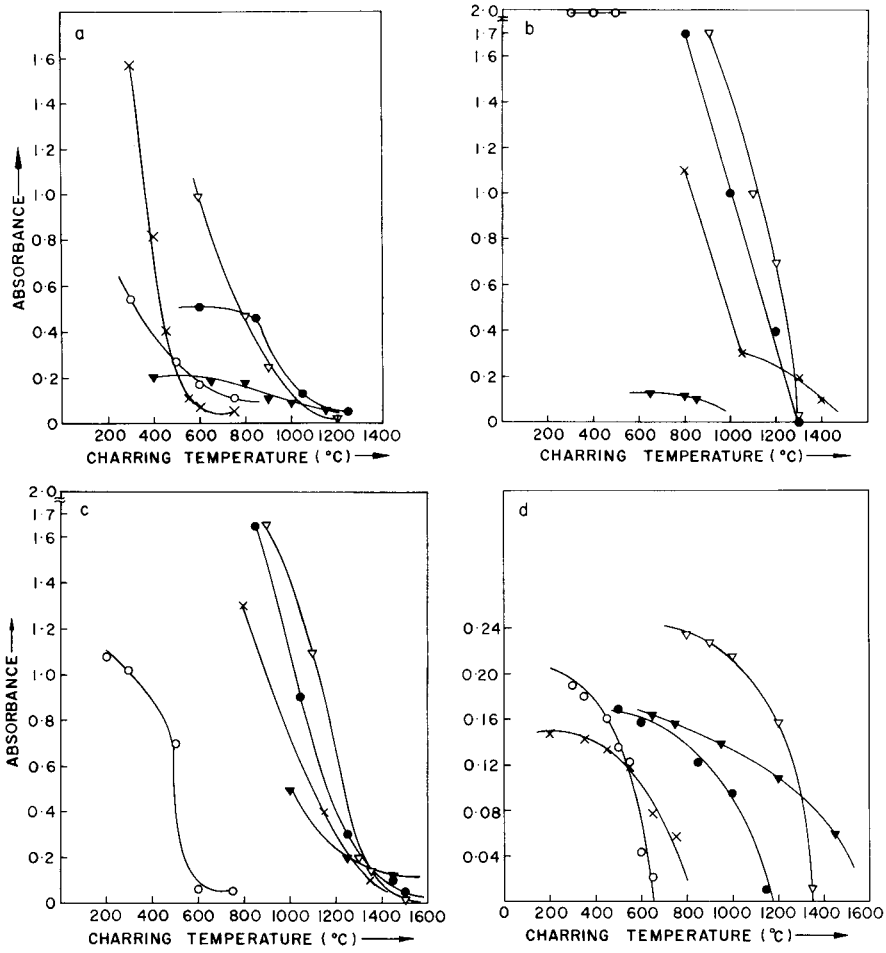

Fig. 1. Variation of non-specific absorption at the appropriate wavelength with charring temperature for: (a) sodium nitrate; (b) sodium chloride; (c) sodium sulphate. (d) Volatilisation behaviour of the trace metal nitrates. (○) Cadmium; (●) nickel; (▼) chromium; (▽) cobalt; (X) lead.

be used. The use of higher charring temperatures leading to sensitivity loss is thus avoided. Hence the sodium solution was neutralised with nitric acid. The effect of charring temperature on the behaviour of the trace metal nitrates is shown in Fig. 1(d). These results were used to establish the optimal conditions given in Table 1.

Matrix effects

Sodium nitrate decomposes at 380° C to sodium nitrite and finally to sodium oxide at about 800° C. Volatilisation of the resulting sodium oxide has been observed between 750 and 1350° C [6]. With the weight of sodium

used (ca. 50 μg) under the recommended conditions of charring and atomisation, the non-specific absorption was found to be between 0.1 and 0.3 absorbance at the analyte wavelengths used; this could be corrected by the simultaneous use of deuterium arc background correction.

Three sodium samples were analysed. They were all found to have the analytes considered at low levels. To evaluate the effect of the matrix, known amounts of the analytes were added to the sodium nitrate solution and the absorbances were measured. Three additions were done on each sample. These data were compared against calibrations obtained with pure standards (in 0.1 M nitric acid) under identical experimental conditions. These results are included in Table 2. The recoveries obtained were 95—99% indicating that there is no chemical interference from the sodium oxide resulting from the decomposition of the sodium nitrate, and that for the determination of these impurities in sodium calibration with pure standards is adequate.

The sensitivities and detection limits were also calculated from the standard addition data, and are presented in Table 2. The detection limits obtained are superior to those reported earlier by Garbett et al. [5].

Concentration of impurities in nuclear-grade sodium

Table 3 lists the measured values, the blank level and the net concentrations of the impurities. The Table shows, for example, that the concentration of nickel in nuclear-grade sodium is <1 μg g^{-1} and that the precision (67% confidence) is 74% at 0.27 μg g^{-1} and 26% at 0.75 μg g^{-1}.

For cobalt and chromium, the relative standard deviation (r.s.d.) is 25% at concentrations of 0.20 and 0.34 μg g^{-1}, respectively. Cadmium which is present in lower concentrations (0.02—0.04 μg g^{-1}) could be determined with somewhat better precision (r.s.d. = 19—35%). For lead, the measured concentrations were within the statistical fluctuations of the blank and so the

TABLE 2

Analytical characteristics

Element	Wavelength (nm)	Recovery[a] (%)	Sensitivity[b] (g)	Detection limit[c] (μg g^{-1})
Cadmium	228.8	99(6)	4.5×10^{-13}	0.02
Lead	283.3	95(8)	8.8×10^{-12}	0.48
Nickel	232.0	95(6)	8.8×10^{-12}	0.48
Chromium	357.9	96(8)	4.4×10^{-12}	0.18
Cobalt	240.8	95(8)	4.0×10^{-12}	0.11

[a]Mean of 9 determinations, with standard deviation for a single determination in parentheses. [b]The amount of analyte that gives an absorbance of 0.0044. [c]The amount equivalent to three times the standard deviation obtained while analysing sodium nitrate solutions containing the analytes at blank levels [7], expressed on the basis of the weight of sodium used.

TABLE 3

Concentration of impurities in nuclear-grade sodium

Impurity	Sample No.	Measured value[a] ($\mu g\ g^{-1}$)	Blank[a] ($\mu g\ g^{-1}$)	Conc. in sample[a,b] ($\mu g\ g^{-1}$)	Sample r.s.d. (%)
Ni	1	0.75 ± 0.17	0.48 ± 0.11	0.27 ± 0.20	74
	2	1.17 ± 0.17		0.69 ± 0.20	29
	3	1.23 ± 0.17		0.75 ± 0.20	26
Co	1	0.26 ± 0.04	0.17 ± 0.04	0.09 ± 0.05	55
	2	0.24 ± 0.04		0.07 ± 0.05	71
	3	0.37 ± 0.04		0.20 ± 0.05	25
Cr	1	0.40 ± 0.06	0.24 ± 0.06	0.16 ± 0.09	56
	2	0.44 ± 0.06		0.20 ± 0.09	45
	3	0.58 ± 0.06		0.34 ± 0.09	26
Cd	1	0.067 ± 0.006	0.044 ± 0.006	0.023 ± 0.008	35
	2	0.087 ± 0.006		0.043 ± 0.008	19
	3	0.078 ± 0.006		0.034 ± 0.008	24
Pb	1	1.12 ± 0.16	1.0 ± 0.2	0.1 ± 0.2	
	2	1.20 ± 0.16		0.2 ± 0.2	
	3	1.12 ± 0.16		0.1 ± 0.2	

[a]Mean ± standard deviation of 3 measurements. [b]Measured value minus blank. Standard deviation calculated from sum of variances of these two values.

concentration of lead in the samples is below the detection limit of this method. These results are expected from the detection limits found. Thus nickel, chromium, cobalt and cadmium can be determined at sub-$\mu g\ g^{-1}$ concentrations but with poor precision.

In these experiments, the nuclear-grade sodium used was highly pure. However, in samples of reactor coolant sodium, which is of prime interest here, the levels of these trace metals are expected to be higher because of the presence of corrosion products. Thus this technique should be adequate for the analysis of sodium coolant in fast reactor loops.

Furnace tube life

With the use of sodium nitrate, a furnace tube was found to last on average for about 120 heating cycles as against a normal life of about 200 cycles. For cadmium, where the atomisation temperature used was low (1000° C), the tube had to be freed from sodium matrix by taking it to 2000° C at the end of each cycle to restore sensitivity. Serious precision problems were encountered with the use of pyrolytically-coated graphite tubes for cadmium determination. The uncoated tubes were found to give satisfactory precision and so were preferred for cadmium determination.

REFERENCES

1 L. Silverman, The Determination of Impurities in Nuclear-Grade Sodium Metal, Pergamon, Oxford, 1971.
2 T. P. Ramachandran, Report ANL-7668, March 1970.
3 Interim Methods for the Analysis of Sodium and Cover Gas, Report ANL-ST-6, January 1971.
4 T. R. Mahalingam, R. Geetha, A. Thiruvengadasami and C. K. Mathews, Proceedings of the International Seminar on Material Behaviour and Physical Chemistry in Liquid Metal Systems, Karlsruhe, West Germany, March 1981, Plenum, New York, 1982, p. 329.
5 K. Garbett, G. I. Goodfellow and G. B. Marshall, Anal. Chim. Acta, 126 (1981) 147.
6 K. Garbett, G. I. Goodfellow and G. B. Marshall, Anal. Chim. Acta, 126 (1981) 135.
7 R. E. Sturgeon and C. L. Chakrabarti, Prog. Anal. At. Spectrosc., 1 (1978) 49.

Analytica Chimica Acta, 142 (1982) 197—205
Elsevier Scientific Publishing Company, Amsterdam — Printed in The Netherlands

DETERMINATION OF CADMIUM, INDIUM AND ZINC IN NICKEL—BASE ALLOYS BY ATOMIC ABSORPTION SPECTROMETRY WITH INTRODUCTION OF SOLID SAMPLES INTO FURNACES

I. S. BUSHEINA and J. B. HEADRIDGE*
Department of Chemistry, The University, Sheffield S3 7HF (Gt. Britain)
(Received 9th June 1982)

SUMMARY

Atomic absorption spectrometry with an induction furnace is used for the determination of cadmium (0.002—2 $\mu g\ g^{-1}$), indium (0.6—350 $\mu g\ g^{-1}$) and zinc (0.05—26 $\mu g\ g^{-1}$) in 0.8—35 mg samples of nickel—base alloys dropped into the furnace. A resistively-heated furnace is employed for the determination of lower concentrations of indium (<0.6 $\mu g\ g^{-1}$). Standardised alloys were used for calibration. Accuracy, precision and detection limits are described for numerous nickel—base alloys. With alloys containing zinc, >0.1 μg Cd g^{-1} and >0.6 μg In g^{-1}, the relative standard deviations are 12%, 8% and 7%, respectively. Calculated detection limits for cadmium, indium and zinc are 2 ng g^{-1}, 10 ng g^{-1} and 10 ng g^{-1}, respectively.

Many trace elements have deleterious effects on the mechanical properties of nickel—base alloys, and their concentrations must be carefully controlled [1—3]. Such control also applies to refined nickel used in the preparation of nickel—base alloys. For example, in British Standard 375:1977 it is stated that the maximum permitted concentrations (in $\mu g\ g^{-1}$) of certain trace elements in Grade R 99.95B refined nickel are: Ag 1, Al 5, As 1, Bi 0.2, C 150, Cd 1, Co 5, Cu 10, Fe 200, P 1, Pb 1, S 15, Sb 1, Se 1, Si 5, Sn 1, Te 0.5, Tl 0.2 and Zn 1. In addition, the Aerospace Materials Specification AMS 2280 (1975) states that the concentration of indium must not exceed 50 $\mu g\ g^{-1}$ in Classes 2 and 4 of trace element control. With the passage of time, these specifications are becoming more stringent and more convenient, accurate and sensitive methods for the determination of trace elements in nickel—base alloys are continually being sought. Atomic absorption spectrometry (a.a.s.) with the addition of solid samples to furnaces has been shown to be very useful for such determinations [4]. In this laboratory, work has already been completed on the determination of bismuth [5], silver and thallium [6], and arsenic, antimony, selenium and tellurium [7] in nickel—base alloys using such a method. In this paper, methods are described for the determination of cadmium (0.002—2 $\mu g\ g^{-1}$), indium (0.6—350 $\mu g\ g^{-1}$) and zinc (0.05—26 $\mu g\ g^{-1}$) in nickel—base alloys by using atomic absorption spectrometry with chips of alloy added directly to an induction furnace.

A more sensitive resistance furnace fitted with a background corrector has also been used to determine concentrations of indium as low as 30 ng g^{-1}.

EXPERIMENTAL

Materials

Analysed nickel—base alloys were supplied by Wiggin Alloys Ltd., Rolls-Royce Ltd. (Derby and Filton), Ross and Catherall Ltd., Materials Quality Assurance Directorate and the Bureau of Analysed Samples Ltd. Samples for analysis should preferably be millings or turnings so that no more than three pieces need to be added to the furnace at the same time. Millings and turnings should be degreased with a suitable solvent before use.

Procedures

Induction furnace and measurement procedure for a series of solid samples. These were identical to those previously described [8] except that the graphite core and side arms were made from AGTS-grade graphite (British Acheson Electrodes) and the flow rates of the purge and stir gas were as follows: for cadmium, purge gas 1.5 l min^{-1}, stir gas 100 ml min^{-1}; for indium, purge gas 2 l min^{-1}, stir gas 150 ml min^{-1}; for zinc, purge gas 2 l min^{-1}, stir gas 80 ml min^{-1} (at about 2540°C) and 450 ml min^{-1} (at about 1750°C). Graphite cores and side arms were baked under vacuum for 8 h (16 h for zinc) at ca. 1800°C before use. Absorbance measurements were made on a Perkin-Elmer 300S atomic absorption spectrometer using a cadmium (Juniper), indium (Pye Unicam) or zinc (Juniper) hollow-cathode lamp. A slit-width of 0.7 nm was used for all measurements and peak areas were calculated by multiplying the peak height (absorbance) by the width (s) at half height. The masses of samples added to both furnaces (see also below) were determined with a 5-place balance. The experimental conditions for the determination of cadmium, indium and zinc are shown in Table 1.

Resistively-heated furnace and measurement procedure for a series of solid samples. The furnace was an Instrumentation Laboratory 555 fitted with a square section graphite cuvette to accommodate graphite microboats. It was fitted within a Varian AA-6 atomic absorption spectrometer whose amplifier response had been speeded up as described by Lundberg [9]. Absorbance—time peaks were recorded on a JJ Instruments CR 552 recorder. The flow rate of argon within the furnace was always maintained at 20 standard cu. ft. h^{-1} (≈9.5 l min^{-1}).

A sample of degreased nickel—base alloy (2—15 mg) in the form of turnings, preferably a single turning, was placed on a graphite microboat (Instrumentation Laboratory, Part No. 44119) and inserted into the cuvette at room temperature. The cuvette was heated to a high temperature using the following programme: ramp from room temperature to 500°C over 5 s, ramp from 500°C to 1200°C over 5 s, step from 1200°C to 2800°C and hold for 5 s. The cuvette was allowed to cool to near room temperature before insertion

TABLE 1

Experimental conditions for the determination of cadmium, indium and zinc with the induction furnace

Metal	Concn. range ($\mu g\ g^{-1}$)	Sample mass range (mg)	Core temp. (°C)	Wavelength (nm)	Scale expansion
Cadmium	0.002—2	1—35	2100—2390	228.8	×1[a]
Indium	3—350	0.8—9	2320—2450	303.9	×1
	0.6—3	12—24	2450	303.9	×2
Zinc	5—26	4—20	2410—2500	307.6	×4[b]
	0.05—5	0.8—4	1670—1810	213.9	×1[c]

[a]Scale expansion of ×2 was frequently used for cadmium concentrations of $<0.4\ \mu g\ g^{-1}$. [b]Sometimes ×5. [c]Damping position 3 or 4 (time constants of 3 s and 10 s respectively) were employed to keep the apparent absorbances less than 1.0.

of the next sample. With the indium hollow-cathode lamp in position, a wavelength of 303.9 nm and a slit-width of 0.5 nm, recordings of absorbance vs. time were obtained for each sample. Peak areas were determined as above. Samples could be processed every 2—3 min.

The same furnace was used to determine the concentration of zinc in alloy R 3385 to be used as a standard for the determination of low concentrations of zinc ($<5\ \mu g\ g^{-1}$) in nickel—base alloys. The operating procedure was the same as for indium except that chips of nickel—base alloys within the range 3—18 mg, the 307.6-nm line of a zinc hollow-cathode lamp and a slit-width of 0.7 nm were employed with the following heating programme: ramp from room temperature to 100°C over 5 s, ramp from 100 to 300°C over 5 s, step from 300°C to 2800°C and hold for 5 s.

Calibration graphs. For each element, calibration graphs of peak area vs. mass were obtained by introducing increasing masses of suitable standardised alloys into the furnace under conditions capable of producing absorbances up to 1.0. Details of these alloys are shown in Table 2. To obtain characteristic masses and to determine indium concentrations $<0.08\ \mu g\ g^{-1}$, calibration graphs of peak height vs. mass were produced.

Determination of cadmium, indium and zinc in nickel—base alloys. When a series of nickel—base alloys was to be analysed, suitable masses were dropped into the graphite core over a period of 2 h or introduced on graphite microboats into an IL 555 cuvette over ca. 1.5 h. In a typical run, 33 samples were used, 9 for calibration and 6 for each of four samples to be analysed. When the run had been completed, the calibration graph was drawn and the mass of cadmium, indium or zinc in each sample was obtained from the graph.

RESULTS AND DISCUSSION

All calibration graphs were straight lines through the origin except where stated otherwise. The characteristic mass for cadmium decreased, as expected,

TABLE 2

Standardised alloys used for calibration

Metal	Concn. range ($\mu g\ g^{-1}$)	Alloy for calibration	Concn. ($\mu g\ g^{-1}$)	Standardisation method
Cd	0.1—2	R 3387	0.8	Square-wave polarog. after liquid—liquid extn.
	0.002—0.1	R 4751	0.19	Present method vs. R 3387 as standard
In	70—350	D1/3339	66	Furnace a.a.s. after dissolution
	0.6—70	D1/3340	14	Furnace a.a.s. after dissolution
	0.01—0.6[a]	R 3385	0.62	Present method vs. D1/3340 as standard
Zn	5—26	DTC	13	Flame a.a.s.
	0.2—5	R 3385	1.8[a]	Present method vs. DTC as standard
	0.01—0.2	BCS 345	0.27	Present method vs. R 3385 as standard

[a]With the IL 555 furnace.

from 18 pg at 2100°C to 13 pg at 2400°C. The characteristic mass for indium was 0.7 ng with the induction furnace and 31 pg with the IL 555. For zinc at the 307.6-nm line, the characteristic mass was 15 ng with the induction furnace and 2 ng with the IL 555.

Because there are only two useful resonance lines for zinc, and a.a.s. is rather insensitive at 306.7 nm, it was necessary with the induction furnace to use the 213.9-nm line to determine zinc in nickel—base alloys at $<5\ \mu g\ g^{-1}$. However, the 213.9-nm line is very sensitive, so that relatively low temperatures, a fast flow rate of argon through the furnace and appreciable damping had to be used to produce apparent absorbances less than 1.0. This in turn led to curved but usable calibration graphs. Characteristic masses were 7 pg and 11 pg for time constants of 3 s and 10 s, respectively.

Results for the determination of cadmium in 17 nickel—base alloys, of indium in 13 such alloys and of zinc in 16 such alloys are shown in Tables 3, 4 and 5, respectively. Because the induction furnace was used without a background corrector, checks for background absorption during the determination of cadmium, indium and zinc were made by substituting a hydrogen lamp for the appropriate hollow-cathode lamp. In no cases was background absorption detected.

Table 3 shows that the results for cadmium are accurate. This proves that R 3387 with a content of 0.8 μg Cd g^{-1} was a good choice for calibration. Because its cadmium content is only known to the nearest 0.1 $\mu g\ g^{-1}$, results are only quoted to one significant figure. For BCS 346, the cadmium content was actually found to be 0.36 $\mu g\ g^{-1}$ in this laboratory but obviously only limited reliance can be placed on the second figure after the decimal point. For cadmium contents in excess of 0.1 $\mu g\ g^{-1}$ the average relative standard deviation of the method (r.s.d., $n = 6$) was 8%.

The results for indium are also accurate for alloys D1/3338, D1/3339 and BCS 346 (Table 4), thus indicating that D1/3340 and D1/3339 with indium

TABLE 3

Results for the determination of cadmium in nickel—base alloys

Alloy	Supplier's result ($\mu g\ g^{-1}$)	Cd found ($\mu g\ g^{-1}$)	R.s.d. ($n = 6$) (%)
R 3385	0.5[a]	0.7	7
R 3386	0.4[a]	0.5	7
R 3388	0.7[a]	0.7	14
R 4742	0.1[a], <0.1[b]	0.05	12
R 4743	0.5[a], 0.4[b]	0.4	4
R 4746	<0.1[b]	0.017	20
R 4750	<0.1[a], <0.1[b]	0.03	24
R 4751	0.1[b]	0.19	10
DTA	<0.1[a]	0.006	33
DTB	0.9[a]	0.9	6
DTC	1.9[a]	1.8	11
DTD	2.0[a]	2.0	4
ST 1	<0.1[b]	0.002	18
ST 2	<0.1[b]	0.005	18
ST 3	<0.1[b]	0.005	31
BCS 345	<0.05[c]	0.005	12
BCS 346	0.34[c]	0.4	10

[a]Square-wave polarography after liquid—liquid extraction. [b]Hollow-cathode emission spectrometry. [c]Electrothermal a.a.s. after dissolution (IL report).

TABLE 4

Results for the determination of indium in nickel—base alloys

Alloy	Supplier's result ($\mu g\ g^{-1}$)	In found ($\mu g\ g^{-1}$)	R.s.d. ($n = 6$) (%)
R 3385	1[a]	0.62	6
R 3386	2[a]	1.5	9
R 3387	10[a]	7.5	3
R 3388	5[a]	4.5	6
D1/3338	350[b]	352	10
D1/3339	66[b]	65	9
D1/3341	<1[b]	0.09[e]	14
D1/3342	<1[b]	0.08[e]	15
D1/3343	<1[b]	0.03[e,f]	24
D1/3344	<1[b]	0.03[e,f]	22
D1/3345	<1[b]	0.04[e,f]	16
BCS 345	<0.05[c]	0.03[e,f]	14
BCS 346	20[d]	17	6

[a]Nominal value. [b]Electrothermal a.a.s. after dissolution. [c]Electrothermal a.a.s. after liquid—liquid extraction (IL report). [d]Flame a.a.s. after liquid—liquid extraction (IL report). [e]With the IL 555; other results from the induction furnace. [f]Peak-height measurements; other results are peak area measurements.

contents of 14 and 66 $\mu g\ g^{-1}$, respectively, are reliable standards. Exact agreement between the present results for R 3385—R 3388 and the supplier's values for these alloys cannot be expected because some indium is likely to be lost by volatilization during the preparation of the alloys. For indium contents in excess of 0.6 $\mu g\ g^{-1}$, the average r.s.d. (n = 6) of the method was 7%.

When the induction furnace was used, it was soon found that some of the nickel—base alloys had a very low indium content (e.g., D1/3341 was found to contain 0.08 $\mu g\ g^{-1}$ with r.s.d. of 17%). This corresponds to a limit of detection of 0.03 $\mu g\ g^{-1}$ and it was considered that a more sensitive method for indium would be helpful. Therefore six alloys including D1/3341 were analysed for indium by using the IL 555 furnace in place of the induction furnace. However, background noise was more noticeable with the IL 555 than with the induction furnace and, when the absorbances were less than 0.1, more precise results were obtained by measuring peak heights rather than peak areas. These results are clearly shown in Table 4. For the four alloys indicated with indium contents $\leqslant 0.04\ \mu g\ g^{-1}$, results based on peak area were identical to those based on peak height.

The results for zinc are also accurate (Table 5). Zinc is an awkward element to determine by this procedure because methods based on the use of the 213.9-nm resonance line are too sensitive, and this line could not be used for determining zinc in excess of 5 $\mu g\ g^{-1}$. However, the use of the other resonance line at 307.6 nm produced poor sensitivity and in order to maximize the concentration of zinc atoms in the light path, high furnace temperatures, high sample masses and absorbance scale expansion had to be employed. With the induction furnace and the 307.6-nm line, the calculated limit of detection (see below) was 2 μg Zn g^{-1}.

Because alloy R 3385 was to be used as a standard for determining zinc in nickel—base alloys within the range 0.2—5 $\mu g\ g^{-1}$, it was necessary to obtain a more accurate zinc content than that supplied with the alloy (2 $\mu g\ g^{-1}$). This was achieved by analysing the alloy in the IL 555 furnace at the 307.6-nm zinc line, with alloy DTC (13 μg Zn g^{-1}) as a standard. As shown in Table 5, a zinc content of 1.8 $\mu g\ g^{-1}$ was obtained with a standard deviation of 0.1 $\mu g\ g^{-1}$. For work with the induction furnace, the average r.s.d. (n = 6) was 10% at the 307.6-nm line and 15% at the 213.9-nm line.

Experimental limits of detection, taken as twice the standard deviation for determined trace element contents at the lowest levels, are shown in Table 6. From a previous study [7], a formula was devised for calculating the expected detection limit from characteristic masses: calculated detection limit = (characteristic mass × 0.2 × average r.s.d.)/sample mass. Detection limits calculated in this way are also shown in Table 6. Considering that the formula produces only approximate limits of detection, the agreement between experimental and calculated limits is remarkably good. With the induction furnace and the 213.9-nm zinc line, the calculated detection limit of 5 ng g^{-1} refers to a 4-mg sample. But the induction furnace can accommodate samples

TABLE 5

Results for the determination of zinc in nickel—base alloys

Alloy	Supplier's result ($\mu g\ g^{-1}$)	Zn found ($\mu g\ g^{-1}$)	R.s.d. ($n = 6$) (%)
R 3385	2[a]	1.8[d]	6
R 3386	3[a]	3.5	16
R 3387	9[a]	8	5
R 3388	6[a]	6	10
R 6285	7[a]	7	10
R 6286	11[a]	10	19
R 6287	6[a]	6	5
DTA	<5[a]	0.05	13
DTB	5[a]	6	9
DTD	13[a]	13	13
ST 1	<1[b]	0.10	15
ST 2	<1[b]	0.27	10
ST 3	<1[b]	0.33	19
RRF 2	20—40[c]	26	10
BCS 345	<0.5[a]	0.27	16
BCS 346	29[a]	26	8

[a]Flame a.a.s. [b]Hollow-cathode emission spectrometry. [c]D.c. arc emission spectrometry. [d]With the IL 555; other results from the induction furnace.

TABLE 6

Experimental and calculated limits of detection for cadmium, indium and zinc

Element	Experimental conditions	Detection limit ($ng\ g^{-1}$)	
		Experimental	Calculated
Cadmium	IF[a], 228.8 nm	2	1
Indium	IF, 303.9 nm	30	40
	IL 555, 303.9 nm	10	7
Zinc	IF, 213.9 nm	10	5
	IF, 307.6 nm	1000	2000
	IL 555, 307.6 nm	200	300

[a]Induction furnace.

of 40 mg if necessary, and these would produce a detection limit of about 0.5 ng Zn g^{-1}. Also the IL 555 furnace produces characteristic masses which are 2—20 times lower than those obtained with the induction furnace [10], a feature which has been confirmed in the present study. Undoubtedly the use of the IL 555 furnace for determining ultratrace concentrations of cadmium and zinc in nickel—base alloys would produce limits of detection below 0.5 ng g^{-1} for both elements.

The authors have now sufficient experience of analysing nickel—base alloys for trace elements by adding chips to the IL 555 furnace to compare the performance of this furnace with their induction furnace. The advantages of the induction furnace over the IL 555 are as follows. Five hundred alloy samples, in 15 complete runs, can be added to the induction furnace before the core has to be replaced, provided that there is no premature cracking of the silica sheath. However, no more than 33 samples, in one complete run, and often far fewer, can be added successively to one graphite microboat for insertion into the cuvette of the IL 555. This means that running costs are higher for the IL 555 furnace. The mode of operation of the induction furnace is simpler than that for the IL 555, and background noise is less with the induction furnace. Samples of up to 40 mg can be added to the induction furnace but the maximum mass of a sample for the IL 555 is 20 mg, and for some samples no more than 5 mg can be added at any one time because of unsuitable shape. For some elements, such as zinc, methods based on the IL 555 furnace and the usual resonance line are too sensitive for the concentration range normally encountered. The lower sensitivity of a.a.s. methods based on the induction furnace is then advantageous.

The advantages of the IL 555 furnace over the induction furnace are as follows. The IL 555 can be operated at a higher temperature. It has been used at 3200° C in this laboratory for the determination of arsenic in nickel—base alloys [7] but the maximum temperature that can be obtained with the induction furnace is 2600°C. Some elements, such as arsenic, antimony and selenium, are not released quickly enough from molten nickel—base alloys at 2600°C to be determined with the induction furnace. A whole run of 33 samples is completed faster on the IL 555 than on the induction furnace, mainly because the induction furnace must have its temperature raised slowly over about 30 min to a constant temperature to prevent cracking of the silica sheath. For the same reason the temperature of the induction furnace must be allowed to fall slowly to room temperature over about 30 min at the end of a run. Characteristic masses for the IL 555 furnace are lower than for the induction furnace because the internal volume of the IL 555 cuvette is much less than that of the graphite core and side arms of the induction furnace. However, the advantage of a lower characteristic mass is not fully reflected in a proportionately lower detection limit because the IL 555 microboat cannot accommodate sample masses as large as can be accommodated by the induction furnace. Background noise is somewhat larger with the IL 555. For certain trace elements, such as bismuth and lead, semiquantitative results can be obtained by calibration with aqueous solutions rather than with a solid metal standard [10]. Such aqueous standards are easily dispensed onto the graphite microboat for the IL 555 furnace but have to be dispensed on to small graphite discs for addition to the induction furnace. These discs have to be sucked out of the cold graphite core after approximately 20 have been added.

We thank the University of El-Fateh, Libya, for a studentship (for I.S.B.). We are indebted to the Science and Engineering Research Council and Rolls-Royce Ltd. (Derby) for financial assistance and to Wiggin Alloys Ltd., M.Q.A.D., Rolls-Royce Ltd. (Derby and Filton), Ross and Catherall Ltd. and the Bureau of Analysed Samples Ltd. for analysed samples.

REFERENCES

1 G. Mayer and C. A. Clark, Metall. Mater. Technol., 6 (1974) 491.
2 R. T. Holt and W. Wallace, Int. Metall. Rev., 21 (1976) 1.
3 K. M. Bills, Proc. of the 30th Chemists' Conference, British Steel Corporation, 1977, p. 101.
4 J. B. Headridge, Spectrochim. Acta, 35B (1980) 785.
5 J. B. Headridge and R. Thompson, Anal. Chim. Acta, 102 (1978) 33.
6 A. A. Baker, J. B. Headridge and R. A. Nicholson, Anal. Chim. Acta, 113 (1980) 47.
7 J. B. Headridge and R. A. Nicholson, Analyst, in press.
8 D. G. Andrews and J. B. Headridge, Analyst, 102 (1977) 436.
9 E. Lundberg, Chem. Instrum., 8 (1978) 197.
10 J. B. Headridge and I. M. Riddington, Mikrochim. Acta, in press.

Analytica Chimica Acta, 142 (1982) 207—216
Elsevier Scientific Publishing Company, Amsterdam — Printed in The Netherlands

BILAYER LIPID MEMBRANE ELECTROCHEMISTRY IN A FLOW INJECTION SYSTEM

MICHAEL THOMPSON* and U. J. KRULL

Department of Chemistry, University of Toronto, 80 St. George Street, Toronto, Ont. M5S 1A1 (Canada)

(Received 20th April 1982)

SUMMARY

The design and operation of a cell used to support bilayer lipid membranes in an electrolyte stream of flow rate up to 1.0 ml min^{-1} are described. Concentration—flow profiles and current—time response correlations are given for membrane interaction with dispersions of valinomycin. The results show that membranes provide reproducible responses and can be refreshed by on-line rinsing techniques. Further supporting evidence for the existence of a membrane surface perturbation effect has been obtained.

In recent years, flow injection analysis (f.i.a.) has attracted considerable interest as a method for fast repetitive analysis [1, 2]. The technique offers accurate reproducible results while allowing the sampling system to be regenerated between samplings in a non-disruptive manner. Such a methodology is ideally suited for the study of bilayer lipid membrane (BLM) electrochemistry, particularly with respect to membrane regeneration, to the kinetics of interaction with various electroactive species and the feasibility of using the BLM sensor as an on-line device. Consideration of structural integrity suggests that the optimum configuration for BLM formation in a flow-through experiment should involve membrane stabilization. This goal could be achieved by use of support structures such as the microfiltration filter membranes examined earlier in this laboratory [3]. However, the free BLM was chosen for this study in view of the fact that it offers the best definition of physical character together with elimination of a number of variables (such as the nature of the micro torus volume in the case of filters). Furthermore, the unsupported system was used for direct comparison with the batch-stirred interaction of BLM with valinomycin.

The current response of the BLM to the ion-carrier complex has been shown to be biphasic [4] and the possibility has been raised that the first maximum has its origins in a short-time signal caused by perturbation of membrane surface dipoles [5, 6]. The intra-membrane surface potential is relatively large [7, 8], and is believed to originate from the ester carbonyl oxygens, the headgroup region and preferential orientation of bound water [9]. In regard to the dominant role assumed by this potential, the concept

0003-2670/82/0000-0000/$02.75

of dipole alteration associated with chemoreception at excitable membranes, introduced by Lundström and Nylander [10], is particularly interesting. This model emphasizes the requirement for understanding of receptor physics if the potential of the BLM structure as a selective sensor is to be realized.

The present paper describes the design and operation of a configuration that allows the relatively delicate free BLM to be used in the flow injection mode. Additionally, work with macro-dispersions of valinomycin under various flow conditions provides a definitive distinction between localized concentration effects and the perturbing action of the ionophore on the membrane.

EXPERIMENTAL

Reagents and equipment

Phosphatidyl choline from egg yolk (Avanti Biochemicals, Birmingham, AL) was used exclusively for BLM formation. The cholesterol incorporated in membranes was of the partially oxidized variety and contained approximately 50% cholesterol as shown by control thin-layer chromatography [11]. Valinomycin (Sigma Chemical, St. Louis, MO) was used as the electroactive species in all experiments. All other chemicals were of reagent grade.

The flow-through cell for the BLM support is outlined in Fig. 1. The membrane housing was designed with one solution compartment open to facilitate introduction of lipid solution for BLM formation. It consisted of a teflon sheet (0.1 mm thick containing a 1.0-mm diameter aperture) clamped between two machined perspex solution cells. Small pressure transients with resultant periodicity in the membrane ion flux precluded the use of peristaltic pumping with the pumps available. Accordingly, the flow system (with teflon tubing of 1.6 mm internal diameter) consisted of a pressurized carrier solution reservoir, a rotary four-way valve system with a sampling loop utilizing a micropipette, a pinch valve for flow control, the membrane housing fitted with optics (for observation of membrane thinning and solution pressure effects) and a collection reservoir. A hydrostatic equilibrium with a solution level above the membrane-containing aperture could be maintained

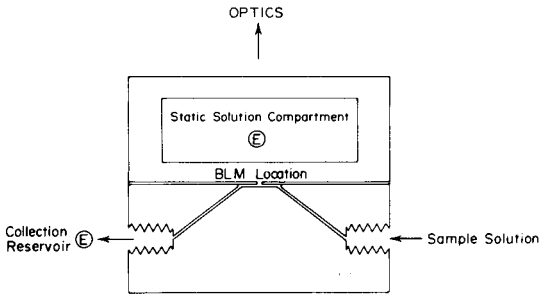

Fig. 1. Schematic diagram of flow-through cell for BLM support (E = reference electrode).

by adjusting the height of the collection reservoir. Transmembrane ion flux was monitored by using single-junction silver—silver chloride reference electrodes (Orion Research, Cambridge, MA) extended with salt bridges, in conjunction with a microcomputer-controlled digital electrometer 616B (Keithley, Cleveland, OH). All equipment was carefully shielded and a Faraday cage surrounded the measuring cell.

Procedures

For BLM formation, lipid solutions of 2% (w/v) phosphatidyl choline and 2% (w/v) oxidized cholesterol in dry decane were introduced into the teflon sheet aperture. The electrolyte carrier solution (0.1 M KCl) was maintained at a temperature of 21 ± 1°C. For experiments requiring minimal membrane disruption, samples of valinomycin (1.0×10^{-5} M in the carrier solution) spiked with methylene blue dye (ca. 0.01% w/v) were loaded into the sample loop before BLM formation. Injection volumes were generally in the range 100—400 μl. Because the flow of fresh carrier solution was temporarily interrupted on switching the rotary valve, a significant pressure transient was commonly produced. This transient was proportional to the flow rate and limited the useful flow rates to <1.0 ml min^{-1}. Sample concentration profiles were monitored via the optical absorption of the tracer dye just before entrance to the cell. Two types of study were conducted. The first involved investigation of the effects of short concentrated plugs of stimulant with respect to flow rate. Secondly, large volumes of sample solution were introduced to examine membrane loading processes.

RESULTS AND DISCUSSION

Transmembrane pressure

The flow design was based on the principles described by Růžička and Hansen [1]. Initially, a peristaltic pump with ten rollers which provided relatively smooth flow was incorporated in the system. It was found that such a pump was entirely incompatible with the fragile and flexible nature of the sensing membrane. Extremely small pressure differences across the membrane can cause substantial deformation. This type of distortion is characterized by a bulging effect which has previously been used as a direct measure of surface tension and strength [12, 13]. The effect tends to compress one side of the BLM while expanding the other, resulting in further thinning of the membrane. Furthermore, the stress alters the structure of the membrane/torus boundary and the torus/aperture surface contact area. Thus, the small pressure transients produced by the roller action of the peristaltic pump are sufficient to distort the membrane structure and the overall result of this weakening is reflected in the significant periodicity of ion permeability depicted in Fig. 2. Accordingly, these problems were eliminated by use of a flow system based on pressurization of the solution reservoir [14].

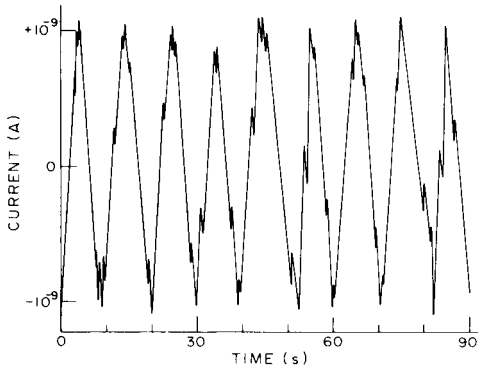

Fig. 2. Solution pressure fluctuation produced by peristaltic pumping results in periodicity of BLM residual current.

Signal magnitude

The velocity of solution passing by the membrane face determines the thickness of the unstirred layer which separates the bulk solution from the BLM [15]. This layer is a critical factor in determining membrane interaction with components in the bulk phase and is analogous in concept to the diffusion layer encountered in polarographic methods [16]. As the solution velocity increases, the diffusion layer may reduce in thickness by a factor of three or four resulting in a concomitant increase in membrane interaction.

The velocity of the solution in the flow-through system determines the residence time of the sample plug at the membrane interface. Because the signal generated by valinomycin interaction is based on membrane absorption, a greater signal must occur for a given sample plug volume at decreasing flow velocities. This integration effect results in increased contamination of the membrane and, therefore, much greater rinse times are required to return to the original background current. Variation of the sample volume also determines residence time, and at constant flow velocity, actually represents a method of introducing different "concentrations" of valinomycin to the sensor. The adjustments of flow rate and sample plug volume combine to produce concentration—flow profiles and current—time response curves as shown in Fig. 3. As previously described [5], an almost linear correlation exists between the BLM residual current and hydrocarbon zone thickness as illustrated by charging experiments. A similar relationship was observed between residual current and the second current maximum for valinomycin, as is expected if membrane thickness is a critical parameter. This latter fact was used to correlate data obtained from different experimental conditions. Series of three or more experiments for most of the flow conditions were done, and the data representing the current maxima were linearly interpolated for adjustment to a common arbitrary initial current value. Only current—time profiles exhibiting one maximum were employed for this analysis, because it was shown in separate experiments that this feature is related to

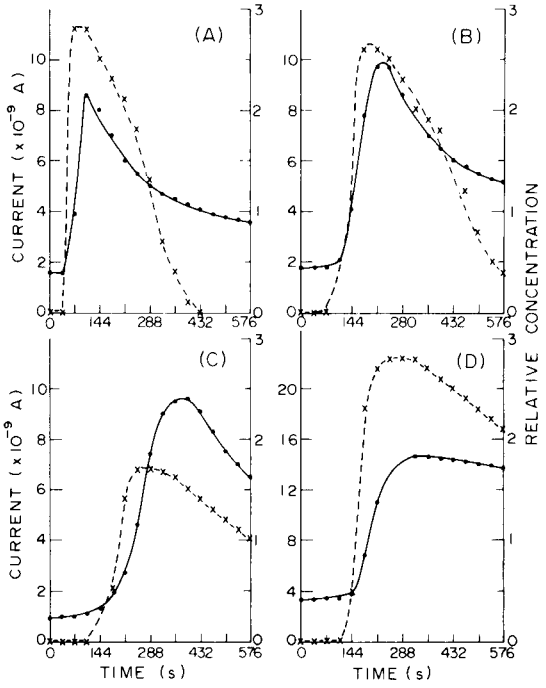

Fig. 3. Electrochemical signal (solid line) versus concentration profile (broken line) for BLM interaction with valinomycin dispersion. Sample volumes and flow rates: (A) 500 μl, 0.7 ml min^{-1}; (B) 200 μl, 0.4 ml min^{-1}; (C) 200 μl, 0.3 ml min^{-1}; (D) 400 μl, 0.2 ml min^{-1}.

the content of oxidized cholesterol in the BLM-forming solution. These methods of standardization allow the results to be correlated as shown in Fig. 4. For the BLM, rapid flow which reduces the unstirred layer thickness and the sample residence time must be compromised with the fact that the diffusion and incorporation effects are relatively slow, resulting in an optimum analytical sensitivity for a flow rate of 0.3—0.4 ml min^{-1}.

A semi-quantitative interpretation of the sensitivity of the sensing system to the various changing parameters was attempted. For each individual data point accumulated for each flow condition, a linear equation based on initial current, flow rate, plug length and the magnitude of the current maximum was developed. For the current maximum, I_M, the equation has the form $I_M = A\,I_R + BF + CV$, where I_R, F and V represent the experimental parameters of residual current, flow rate and injected volume, respectively, while A, B and C are the corresponding sensitivity factors. Because different flow rates change the physical state of the sensor, only equations based on similar flows were compared. The data derived from solution of these equations (Table 1) demonstrate that the initial current and sample volume sensitivities are maximized for a flow rate of 0.2—0.3 ml min^{-1}, though the dominating

flow-rate sensitivity results in maximum current generation at 0.3—0.4 ml min^{-1}, as illustrated by Fig. 4. These equations have some analytical significance even if the assumptions necessary in developing equations for such comparisons are false. They can be applied in concentration determinations for unknown samplings and commonly produce results within 20% of the actual concentration value for more than 80% of the experiments attempted. Figure 4 illustrates the signal versus concentration trends observed for the different flow rates investigated in this work. An alternative format for presenting these data is expressed in Fig. 5 to demonstrate clearly the logarithmic relationship of sample plug antibiotic content to the observed response. The trend is identical to that previously encountered in static solution (i.e., nonflowing) valinomycin experiments [17]. Because the membrane partition coefficient for valinomycin is a constant for a given membrane and the antibiotic is very soluble in the BLM hydrocarbon phase, there is no reason to suspect an exponential signal/concentration relationship. The explanation probably lies in a surface dipolar perturbation effect caused by the presence and ion-complexing action of valinomycin at the hydrocarbon/headgroup

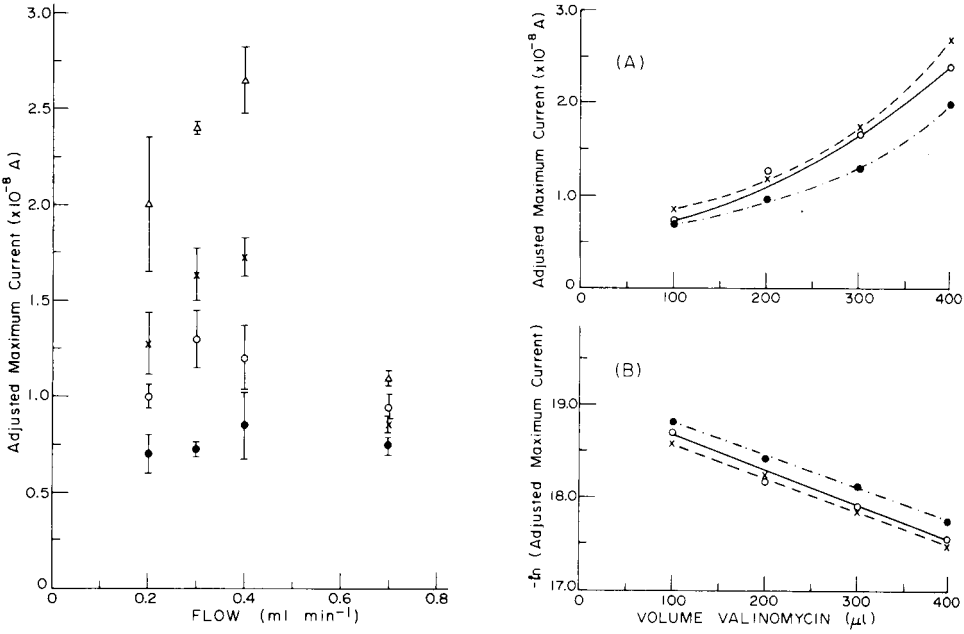

Fig. 4. Electrochemical signal for different flow rates and sample volumes: (•) 100 μl; (○) 200 μl; (×) 300 μl; (△) 400 μl. (Experimental conditions have been normalized to a common reference point, allowing appropriate adjustment of current.)

Fig. 5. A, Electrochemical signal versus valinomycin concentration at different solution flow rates: (•) 0.2 ml min^{-1}; (○) 0.3 ml min^{-1}; (×) 0.4 ml min^{-1}. B, Logarithmic relationship of signal to concentration.

TABLE 1

Variation in normalized BLM sensitivity with solution flow rate

Flow rate (ml min^{-1})	0.2	0.3	0.4	0.7
Initial current sensitivity	3.65	5.04	1.89	1.02
Sample volume sensitivity	4.09	6.11	3.23	2.05

zone interface. For linearly increasing antibiotic concentrations, an increasing membrane valinomycin content at current maximum should occur, resulting in a linear signal/concentration relationship. If a surface perturbation effect proportional to the membrane valinomycin content exists, then the net positive surface dipolar potential should decrease, increasing the valinomycin-ion complexation rate [18, 19] and the ion current. Such a situation would generate the observed signal/concentration trend.

Of prime importance in any analytical technique is the reproducibility of results. Figure 6 represents a series of signals generated by an individual BLM during on-line valinomycin sampling. The sampling time interval is limited by the kinetics of partitioning between the solution and membrane. The flowing carrier solution extracts valinomycin from the contaminated membrane between sample plugs allowing the membrane to resume its initial background current. An interesting feature of this extraction process is that the membrane does not always attain its original current on extensive rinsing. This indicates that either trapped valinomycin remains, that valinomycin transport through the membrane to the second solution compartment is great, or that a permanent change in the physical orientation of membrane lipid and cholesterol is induced.

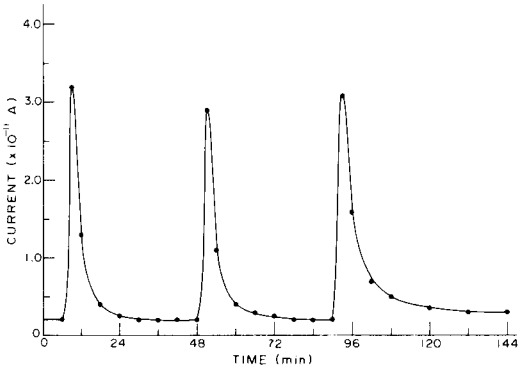

Fig. 6. Reproducibility of valinomycin response at a single BLM, for 50-μl sample volumes of 10^{-5} M valinomycin at a flow rate of 0.7 ml min^{-1}.

Membrane surface perturbation by valinomycin

It has been proposed that the first peak in the current—time profile of valinomycin action on BLM is related to membrane surface perturbation [5, 6]. However, arguments based on local concentration effects which may exist in static solution experiments may also provide viable mechanisms for generating the unusual signal. The f.i.a. system offers the unique advantage of allowing sample plugs of controlled concentration and duration to be applied to a free BLM in order to test the latter hypothesis. Results from this analysis are shown in Fig. 7, A—D. A comparison of the concentration profiles to the current—time response curves implies that a local concentration effect is not responsible for the first maximum observed in these experiments. Rather, as was shown in related work, the initial transient ion flux appears to be related to the membrane composition as determined by lipid and cholesterol oxidation.

If the first maximum is due to an enhancement of the complexation rate of valinomycin with ions, then it should also be possible to observe a "first peak" greater in magnitude than the second maximum, the latter occurring at a point in time where surface perturbation is greatly decreased. This effect was observed in both the flow-through and static solution experiments. A more definitive test of this phenomenon would involve the elimination of the perturbation effect upon saturation of the membrane with valinomycin. Because the effect is probably related to the process of incorporation of

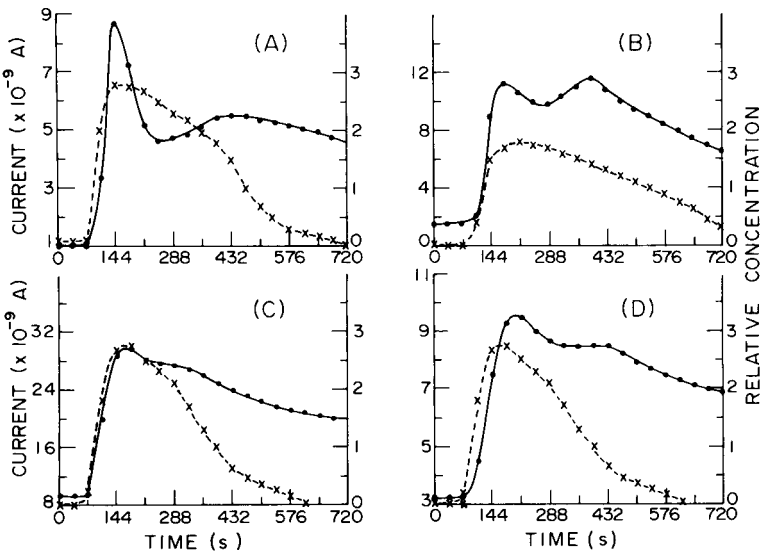

Fig. 7. Evolution of two current maxima (solid line) compared to the concentration profile (broken line) for BLM response to valinomycin dispersions. Sample volumes and flow rates: (A) 400 μl, 0.4 ml min^{-1}; (B) 300 μl, 0.3 ml min^{-1}; (C) 300 μl, 0.4 ml min^{-1}; (D) 300 μl, 0.4 ml min^{-1}.

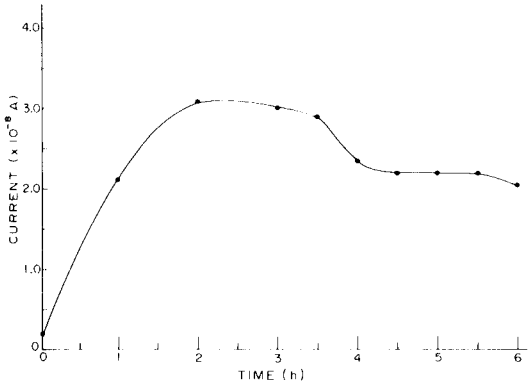

Fig. 8. Current—time profile for a BLM bathed with valinomycin-saturated electrolyte. Note the significant current decrease for steady antibiotic concentration between 3 and 4 h.

antibiotic into the membrane, the current should decrease as a concentration equilibrium between the solution and membrane develops. Should the effect not be present, then only a current increase which eventually attains a constant value is expected. Figure 8 illustrates that the concept of a surface dipolar perturbation is probably valid, because the flowing stream of antibiotic ensured a constant valinomycin concentration at the membrane surface.

We are indebted to the Natural Sciences and Engineering Research Council of Canada for support for this work and for provision of a Fellowship to U.J.K. Also, we are particularly appreciative of funds for equipment provision from the Atkinson Foundation of Toronto, Ontario.

REFERENCES

1 J. Růžička and E. H. Hansen, Flow Injection Analysis, Wiley, New York, 1981.
2 K. K. Stewart, Talanta, 28 (1981) 789.
3 M. Thompson, R. B. Lennox and R. A. McClelland, Anal. Chem., 54 (1982) 76.
4 M. Thompson, U. J. Krull and P. J. Worsfold, Anal. Chim. Acta, 117 (1980) 121.
5 M. Thompson and U. J. Krull, Anal. Chim. Acta, 141 (1982) 33.
6 M. Thompson and U. J. Krull, Anal. Chim. Acta, 141 (1982) 49.
7 G. Szabo, G. Eisenman, S. McLaughlin and S. Krasne, N.Y. Acad. Sci. Ann., 195 (1972) 273.
8 O. S. Andersen, in G. Giebisch, D. C. Tosteson and H. H. Ussing (Eds.), Membrane Transport in Biology, Vol. 1, Springer-Verlag, Berlin, 1978, p. 369.
9 W. F. Pickard, K. C. Sehgal and C. M. Jackson, Biochim. Biophys. Acta, 552 (1979) 1.
10 I. Lundström and C. Nylander, J. Theor. Biol., 88 (1981) 671.
11 L. L. Smith, W. S. Matthews, J. C. Price, R. C. Bachmann and B. Reynolds, J. Chromatogr., 27 (1967) 187.
12 H. Ti Tien, Bilayer Lipid Membranes, Dekker, New York, 1974.
13 M. K. Jain, The Bimolecular Lipid Membranes, Van Nostrand Reinhold, New York, 1972.

14 J. D. Frantz and P. E. Hare, Ann. Rep. Dir. Geophys. Lab., 1630 (1973) 704.
15 S. B. Hladky, Biochim. Biophys. Acta, 307 (1973) 261.
16 A. J. Bard and L. R. Faulkner, Electrochemical Methods, Wiley, New York, 1980.
17 P. J. Worsfold, Analytical Potential of Bilayer Lipid Membranes, Ph.D. Thesis, University of Toronto, 1980.
18 G. Stark and R. Benz, J. Membr. Biol., 5 (1971) 133.
19 R. Benz and D. Cros, Biochim. Biophys. Acta, 506 (1978) 265.

Analytica Chimica Acta, 142 (1982) 217—230
Elsevier Scientific Publishing Company, Amsterdam — Printed in The Netherlands

CHLORIDE INTERFERENCE WITH NON-STOICHIOMETRIC COPPER SULPHIDE COPPER(II)-SELECTIVE ELECTRODES
Part 3. New Equation for the Electrode Response

TADEUSZ HEPEL*
Institute of Chemistry, Jagiellonian University, 30-060 Krakow (Poland)
(Received 2nd April 1981)

SUMMARY

A general equation for the electrode potential response under metastable equilibrium conditions is derived for the non-stoichiometric copper sulphide electrodes immersed in solutions containing Cu(II) and Cu(I) and the interfering chloride ions. The theoretically predicted "anomalous" slopes $S_{II} = \delta E/\delta \log C_{Cu(II)}$ of the calibration curves, greater than 29.6 mV at 25°C, were confirmed experimentally in concentrated chloride solutions. The inapplicability of the Nicolsky equation for the electrodes at equilibrium is discussed on the basis of the theory presented. The new relationship (Eqn. 13) can be adapted for other ion-selective electrodes for which the exchange reactions with the solution species are fast enough and mass transport is not inhibited.

The mechanism of the corrosion process of the copper sulphide electrode proceeding in chloride solutions of copper(II) has been described in Part 1 of this series [1]. The domain of chloride ion interference has been determined in Part 2 [2] in terms of the chloride function λ and the relative error in copper(II) determination ϵ_0 by means of the equation

$$\log \lambda - \log [C_{II}^{in}] \geqslant + 11.35 + \log (f_{\pm}^2/f_{2+}) - \log (100\epsilon_0^{-2} + \epsilon_0^{-1}) + \log \beta \qquad (1)$$

where $\lambda([Cl^-], \mu) = \alpha_I^2/\alpha_{II}$ and $\beta = a_{CuS(n-s)}/a_{Cu_2S(n-s)}$

the α's being the side-reaction coefficients for Cu(I) and Cu(II), respectively.

The relation (1) concerns the metastable equilibrium state at the end of the corrosion process. In such a way, copper(II) ions may be determined at low concentrations even when the electrode is initially subject to corrosion. An exact description of the electrode behaviour during the course of a stationary corrosion process will be given in a later paper. The electrode response at the end of the corrosion process in the case when the solution contains initially Cu(II) and Cu(I) ions is the subject of the present work. If copper(I) ion is considered as an interferent, the copper sulphide electrode

---

*Present address: Department of Chemistry, State University of New York at Buffalo, Buffalo, NY 14214, U.S.A.

0003-2670/82/0000-0000/$02.75

potential may be expressed by using the approximated Nicolsky equation [3–5]

$$E = E^0_{ISE} + RT(2F)^{-1} \ln (a^{in}_{II} + K^{pot}_{II/I}(a^{in}_{I})^2) \quad (2)$$

where $K^{pot}_{II/I}$ is the selectivity coefficient, and a_I and a_{II} are the activities of the Cu^+ and Cu^{2+} ions; superscript "in" indicates the initial activities. However, this equation correctly describes the electrode potential only in the case when one of the terms: a^{in}_{II} or $K^{pot}_{II/I}(a^{in}_{I})^2$ may be neglected [4, 6]. In earlier work [3, 4] Eqn. (2) was constructed by using the isolated solution method [7, 8]. But a problem arises when the equilibrium of the electrode with both species in the solution is considered. In this paper, it is shown that under some conditions the fixed interference method [8, 9] of determining the selectivity coefficient may give quite different results than the isolated solution method. An exact equation describing the potential of a copper sulphide single-crystal electrode immersed in a solution of Cu(II) and Cu(I) (or one of them) will be derived. The deviations from the Nernstian slope will be also discussed on the basis of the present theory.

THEORY

The Nicolsky equation for the non-stoichiometric copper sulphide electrode

Because in this work only the metastable equilibria of the copper sulphide electrode with the solution of Cu(II) and Cu(I) ions at the end of the corrosion process are considered, transport phenomena in the membrane are not taken into account (that problem has been discussed [10–12]). The problems concerning the adsorption of some electroactive species at the electrode/solution interface are also neglected. The equilibrium of the reaction

$$Cu^{2+}(aq) + Cu_2S(n-s) \rightleftharpoons 2Cu^+(aq) + CuS(n-s) \quad (3)$$

may be described by means of the thermodynamic equilibrium constant K^0, $K^0 = K^0_{n-s}\beta$, where $K^0_{n-s} = a^2_I/a_{II}$ and β is the ratio of the activities of the $CuS(n-s)$ and $Cu_2S(n-s)$ species. The value of K^0_{n-s} may be changed as the activity ratio β in the solid changes. The net changes in the concentrations of species $CuS(n-s)$ and $Cu_2S(n-s)$ in a two-phase electrode with net composition $Cu_{2-x}S$ do not change the activities of these species if the same two phases are always present in the solid. By assuming the constancy of the factor β (instead of the sum of the concentrations of the $CuS(n-s)$ and $Cu_2S(n-s)$ species as in the classical derivation of the Nicolsky equation [5, 13], then from the expression $K^0 = K^0_{n-s}\beta$

$$a_{II} = (1 + \beta^{-1})^{-1}(a_{II} + a^2_I/K^0) \quad (4)$$

According to earlier work [4, 14], the electrode potential may be expressed as

$$E^{(ms)} = {}^2E^{0(ms)}_{n-s} + RT(2F)^{-1} \ln a_{II} \quad (5)$$

(ms indicating metastable equilibrium conditions) which corresponds to the electrode reaction

$$Cu^{2+}(aq) + CuS(n-s) + 2e^- = Cu_2S(n-s) \quad (6)$$

Joining Eqns. (4) and (5) yields the equation

$$E^{(ms)} = {}^2E^{0'} + RT(2F)^{-1} \ln (a_{II} + K_{II/I}a_I^2) \quad (7)$$

in which the terms a_I and a_{II} are the equilibrium activities and $K_{II/I} = (K^0_{n-s})^{-1}$. The value of the constant ${}^2E^{0'}$ is here defined as ${}^2E^{0'} = {}^2E^{0(ms)} + RT(2F)^{-1} \ln (\beta/2)$. It may be noted that Eqn. (7) may be constructed for different values $K_{II/I} = A(K^0_{n-s})^{-1}$ where A is a constant; $\beta/2$ is then replaced by $\beta/(1+A)$.

Because the equilibrium activities of copper(II) and copper(I) may differ from the initial activities, it is of interest to develop an equation describing the electrode potential in terms of a_{II}^{in} and a_I^{in}. As will be shown below, such an equation provides more information about the electrode behaviour and can be used to explain the anomalous phenomena observed in chloride solutions.

General treatment

When the copper sulphide electrode is immersed in a solution of Cu(II) or Cu(I) ions, the total concentration of copper in the solution changes until the metastable equilibria of all the copper(I) generation—disproportionation reactions

$$Cu^{II}L_p + Cu_2S(n-s) \rightleftharpoons 2Cu^{I}L_q + (p-2q)L + CuS(n-s) \quad (8)$$

are attained. [1—4, 15]. The respective formal (or conditional) equilibrium constant for reaction (8) may be expressed in general as

$$K^f_{n-s} = (K^0/\beta)(\alpha_I^2/\alpha_{II})(f_{2+}/f_+^2) = (C_I^{eq})^2/C_{II}^{eq} \quad (9)$$

where C_I^{eq} and C_{II}^{eq} are the total concentrations of copper(I) and copper(II) at equilibrium, f_+ and f_{2+} are the single ion activity coefficients of the aquo-copper(I) and aquo-copper(II) ions and α_I, α_{II} are the side-reaction coefficients $\alpha_M = 1 + \Sigma_{n,L}\beta_{ML_n}[L]^n$ for M = Cu(I), Cu(II). The value of K^f_{n-s} may change and it is treated as a parameter. Explicit determination of the equilibrium state to be attained (at a fixed value of K^f_{n-s}) gives the copper concentration function Y defined as

$$Y = Y^0 + Y^{in} = Y^0 + C_{II}^{in} + \tfrac{1}{2}C_I^{in} = C_{II}^{eq} + \tfrac{1}{2}C_I^{eq} \quad (10)$$

where Y^0 characterizes the spontaneous solubility of the electrode material; the value of Y^0 is important when the copper "concentration" introduced, Y^{in}, is very low. Under metastable equilibrium conditions the Nernst equations (5) and

$$E^{(ms)} = {}^1E^{0(ms)} + (RT/F) \ln (\beta a_I) \quad (11)$$

are fulfilled. Equation (11) corresponds to the electrode reaction

$$Cu^{+}(aq) + CuS(n-s) + e^{-} = Cu_2S(n-s) \tag{12}$$

By introducing an expression for the equilibrium activity of Cu^{2+} and Cu^{+} ions, obtained from Eqns. (9) and (10), into the Nernst equation (5 or 11), a general relation describing the electrode behaviour in solutions of Cu(II) and Cu(I) may be obtained. A detailed derivation of this relationship is presented in Appendix A. The equation obtained is of the form

$$E^{(ms)} = {}^{2}E^{\theta} - RT(2F)^{-1} \ln \alpha_{II} - RT(2F)^{-1} \ln \{[Y^{in} + Y^{0}]^{-1} + [K_{II/I}(2Y^{in} + 2Y^{0})^{2}]^{-1} + \kappa_{II/I}\} \tag{13}$$

$$\text{where } K_{II/I} = (1/K^{f}_{n-s}) = (f_{+}^{2}/f_{2+})(\alpha_{II}/\alpha_{I}^{2})(\beta/K^{0}) \tag{14}$$

and the function $\kappa_{II/I}$ is defined as

$$\kappa_{II/I} = 2Y^{-1}[1 + (1 + 16K_{II/I}Y)^{\frac{1}{2}}]^{-1} \tag{15}$$

The meaning of the particular terms in Eqn. (13) is as follows. ${}^{2}E^{\theta}$ represents the formal standard electrode potential written for reaction (6) and is related to an electrode of given phase composition (i.e., for a constant value of β); the second term in Eqn. (13) stands for the shift of the electrode potential caused by complexation of copper(II) ions in the solution; the expression under the logarithm of the third addend presents the reciprocal of the equilibrium concentration of copper(II) ions written in terms of the initial (introduced) concentration of copper(II) and copper(I) (total concentrations) and of the ratio $\alpha_{II}/\alpha_{I}^{2}$ (cf. Eqn. 14) which describes the competition between complexation of Cu^{2+} and Cu^{+} ions. The mathematical analysis of Eqn. (13) given in the Appendix shows under which conditions this equation can be simplified. If complexation of copper(II) ions predominates in the solution so that the total equilibrium concentration of Cu(II) is much greater than that of Cu(I) (the "cupric" conditions), and if the inequality $C_{II}^{in} \gg C_{I}^{in}$ is fulfilled, the electrode-potential response to the logarithm of the introduced Cu(II) concentration log C_{II}^{in}, is linear with a theoretical slope 29.58 mV (at 25° C)

$$E = {}^{2}E^{\theta} - 29.58 \log \alpha_{II} + 29.58 \log (C_{II}^{in} + Y^{0}) \tag{16}$$

This is for the normal operation range of the Cu(II)-selective electrode. Equation (16) follows from Eqn. (13) if the second and third terms in the sum under logarithm are neglected.

If in a given solution (e.g., in concentrated chloride media) copper(I) ions are stabilized and the equilibrium constant for the exchange reaction favours generation of Cu(I) ions at the electrode surface (the "cuprous" conditions), the second term in the sum under the logarithm in Eqn. (13) becomes the most important and the remaining terms may be neglected. If $C_{I}^{in} \gg C_{II}^{in}$, Eqn. (13) after little transformation can be expressed in the form (for 25° C)

$$E = {}^{1}E^{\theta} - 59.16 \log \alpha_{I} + 59.16 \log (C_{I}^{in} + 2Y^{0}) \tag{17}$$

This equation corresponds to the operation range where the electrode is a Cu(I)-selective electrode and the Nernstian slope (59.16 mV) as well as the formal standard potential ${}^1E^\theta$ are the same as those resulting from reaction (12).

In the two above limiting cases, the correction function $\kappa_{II/I}$ can be neglected.

From the analysis of the slopes $S_{II} = (\partial E/\partial \log C_{II}^{in})_{C_I^{in}}$ and $S_I = (\partial E/\partial \log C_I^{in})_{C_{II}^{in}}$, it follows that there are two additional limiting cases for Eqn. (13). The first of them appears under the "cupric" conditions, as described when introducing Eqn. (16), but now the assumption $C_{II}^{in} \gg C_I^{in}$ is replaced by C_{II}^{in}, $\gg C_{II}^{in}$. Equation (13) then simplifies to

$$E = {}^2E^\theta - 29.58 \log (\alpha_{II} 2) + 29.58 \log (C_I^{in} + 2Y^0) \qquad (18)$$

This equation corresponds to a case where the introduced copper(I) ions exchange with copper(II) at the electrode surface (compare the above remarks about the constancy of factor β). The slope S_I is now only 29.58 mV, i.e. half the value expected from reaction (12). Besides, the formal standard electrode potential ${}^2E^\theta$ and α_{II} concern copper(II) and not copper(I).

The remaining limiting case of Eqn. (13) is similar to that described for Eqn. (17) (the "cuprous" conditions), but with the condition $C_{II}^{in} \gg C_I^{in}$ instead of $C_I^{in} \gg C_{II}^{in}$. The electrode potential responds now linearly to log C_{II}^{in}, but with the abnormal slope of 59.16 mV (at 25° C)

$$E = {}^1E^\theta - 59.16 \log (\alpha_I/2) + 59.16 \log (C_{II}^{in} + Y^0) \qquad (19)$$

This is a limiting case of the anomalous chloride interference with the Cu(II)-selective electrode operation discussed extensively in the last decade. In this region almost the whole amount of copper(II) introduced is transformed to copper(I) via the exchange reaction with the electrode material. Again the factor β must maintain its constant value during this exchange reaction. In other cases, a new value of ${}^1E^\theta$ corresponding to the changed value of β ${}^1E^\theta = {}^1E^0 + 59.16 \log (\beta f_+)$, should be used.

Under the conditions of Eqns. (18) and (19), as in the case of Eqns. (16) and (17), the correction function $\kappa_{II/I}$ in Eqn. (13) can be neglected. Its value must be taken into account only in the intermediate regions of electrode operation, when the values of the first and second terms under the logarithm in Eqn. (13) are comparable, i.e., when the slope is greater than 29.58 and lower than 59.16 mV per tenfold change in the sum of initial total concentrations $C_{II}^{in} + \frac{1}{2}C_I^{in}$. This sum of initial concentrations was written here instead of concentrations C_{II}^{in}, C_I^{in} alone, because under "cupric" conditions (i.e., when the value of the exchange-reaction constant favours the exchange Cu(I) → Cu(II)), Eqns. (16) and (18) can be replaced, more generally, by

$$E = {}^2E^\theta - 29.58 \log \alpha_{II} + 29.58 \log (C_{II}^{in} + \tfrac{1}{2}C_I^{in} + Y^0) \qquad (20)$$

Similarly for "cuprous" conditions (i.e., for high values of K_{n-s}^f favouring

the exchange Cu(II) → Cu(I)) the limiting equations (17) and (19) can be replaced by the more general one

$$E = {}^{1}E^{\theta} - 59.16 \log \alpha_{I} + 59.16 \log (C_{I}^{in} + 2C_{II}^{in} + 2Y^{0}) \quad (21)$$

Both Eqns. (20) and (21) result directly from Eqn. (13). The forms of these equations are similar to the Nicolsky equation, but not identical. They do not contain selectivity coefficients and the concentrations are to the same power. Kinetic parameters are not involved in any of these equations because all the discussion in this paper is based on attainment of an equilibrium between the electrode material and the solution components.

The role of the exchange-reaction constant must be mentioned. From the analysis presented above and in the Appendix, the value of the equilibrium constant K^{f}_{n-s} (compared to the copper concentration function Y) decides whether the copper sulphide electrode operates as a Cu^{2+}-selective electrode or as a Cu^{+}-selective electrode, and decides the value of the slope, 29.58 or 59.16 mV, applicable in a given solution composition.

The general equation (13) describes the behaviour of the non-stoichiometric copper sulphide electrode as a Cu^{2+}-selective electrode and as a Cu^{+}-selective electrode, as well as the various anomalous effects relating to chloride interference. This equation should allow copper concentrations to be determined in solutions containing "interfering" ions, e.g., seawater. Equation (13) takes into account the electrode material composition and defines exactly the value of the formal standard electrode potential that is usually treated simply as an unknown constant E^{θ}_{ISE}.

Some experimental results that prove the applicability of Eqn. (13) for the non-stoichiometric copper sulphide electrode are presented below.

EXPERIMENTAL

The method of measurements was described earlier [2]. The electromotive force of the chemical cell

$$\begin{aligned} &Cu|Ag, AgCl(s), 0.1\ M\ NaCl, 10^{-3}\ M\ HClO_4, 4.899\ M\ NaClO_4|10^{-3}\ M\ HClO_4, \\ &4.999\ M\ NaClO_4|10^{-3}\ M\ HClO_4, w\ M\ NaCl, y\ M\ Cu(II), z\ M\ Cu(I), \mu = 5\ M \\ &(NaClO_4)|Cu_{2-x}S|Au|Cu \end{aligned} \quad (22)$$

was measured using some of the apparatus described before [16]. Non-stoichiometric copper sulphide electrodes were prepared as described previously [1].

RESULTS AND DISCUSSION

To check whether Eqn. (13) describes well the copper sulphide electrode response to copper(I) and copper(II), measurements were done in solutions of various chloride-ion concentration. In this manner, the value of the formal

equilibrium constant K^{f}_{n-s} may be changed within the wide range 10^{-12} to 10^{+1} mol dm^{-3}. For all the free chloride concentrations, the dependence of the electrode response on the copper(II) and copper(I) activities was investigated. The results obtained are presented in Figs.1—5. The electrode potential function ϵ is expressed as follows

$$\epsilon = E^{(ms)} - {}^{2}E^{0(ms)} - RT(2F)^{-1} \ln (\beta f_{2+}) + E_d$$
$$= \Phi - {}^{2}E^{0(ms)} - RT(2F)^{-1} \ln (\beta f_{2+}) + E_{Ref} \quad (23)$$

Here E_{Ref} stands for the potential of the reference electrode Ag/AgCl in 0.1 mol dm^{-3} chloride solution at μ = 5 mol dm^{-3}; Φ is the electromotive force of the electrochemical cell (22) and the term E_d contains the two junction potentials in the cell. The value of the constant: ${}^{2}E^{0(ms)} + RT(2F)^{-1} \ln (f_{2+})$ was assumed at such a level that the value of ϵ was

$$\epsilon = -RT(2F)^{-1} \ln [(C^{in}_{II})^{-1} + 0.25\, K^{-1}_{II/I}(C^{in}_{II})^{-2} + \kappa_{II/I}] \quad (24)$$

at the standardizing point: $[Cl^-] = 0$, $C^{in}_{I} = 0$ and $C^{in}_{II} = 10^{-3}$ mol dm^{-3} at

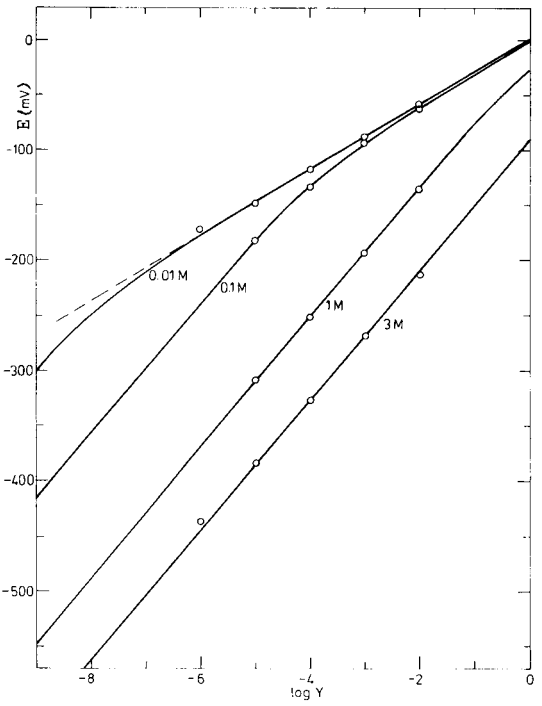

Fig. 1. The electrode potential function E vs. the logarithm of the copper function Y for the copper sulphide ion-selective electrode under metastable equilibrium conditions at the chloride concentrations shown on the curves. For further explanation, see text.

μ = 5 mol dm^{-3}. All the solid lines in Figs. 1—5 were computed on the basis of Eqn. (13) and the circles are the experimental results.

In Fig. 1 the dependence of the electrode potential ϵ on the copper concentration function Y is presented for different concentrations of chloride ion in the solution. The slope of the dashed extrapolated line is 29.6 mV per tenfold change in Y, which corresponds to operation as a Cu^{2+}-selective electrode. The slope of the curve for 3 mol dm^{-3} chloride solution is twice as great (59.2 mV). In the region of this curve the electrode operates as Cu^{+}-selective electrode. In Figs. 2—4, the calibration curves, E vs. log C_{II}^{in}, are presented for different constant levels of the initial total Cu(I) concentrations, C_I^{in}. The calibration curves shown in Fig. 2 were obtained for low chloride concentrations in the solution; the equilibrium constant of the exchange reaction (3), $K_{n-s}^{f} = 1/K_{II/I}$, was 4.76 × 10^{-8} mol dm^{-3}. The lower the level of the initial Cu(I) concentration in the solution, the wider becomes the range for the Cu(II) determination. The theoretical lower limit of detection, Y^0, was neglected in calculations in order to show more clearly that all the C_{II}^{in}-independent portions of these calibration curves are connected with the presence of the copper(I) ions in the solution. The condition $Y^0 = 0$ was held for all solid lines in Figs. 1—5.

The calibration curves presented in Fig. 3 were obtained in chloride solutions of moderate concentration, for which the value of the equilibrium

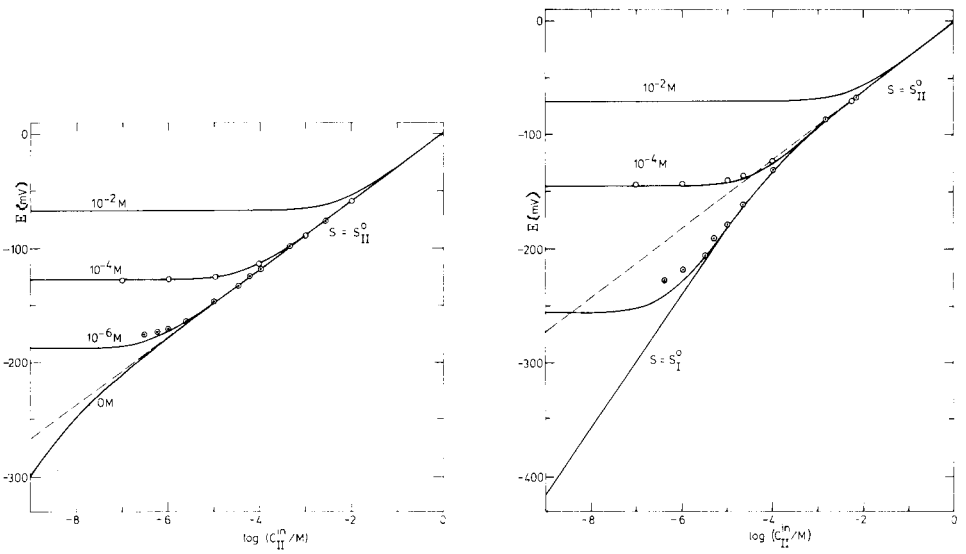

Fig. 2. Dependence of the electrode potential function on the logarithm of the initial (introduced) copper (II) concentration in 0.01 M Cl^- solution at μ = 5 M ($NaClO_4$) and 25° C, for the various C_I^{in} concentrations given on the curves. $K_{II/I}$ = 2.1 × 10^7 dm^3 mol^{-1}.

Fig. 3. The relation E vs. log C_{II}^{in} obtained for the non-stoichiometric copper sulphide electrode in 0.1 M chloride solution at μ = 5 M and 25°C, for the various C_I^{in} concentrations given on the curves. $K_{II/I}$ = 2.3 × 10^3 dm^3 mol^{-1}.

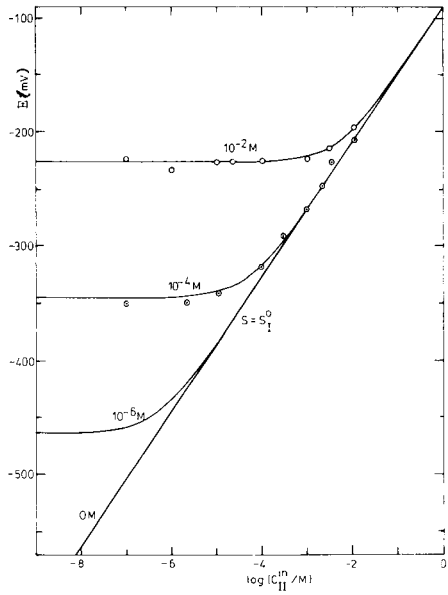

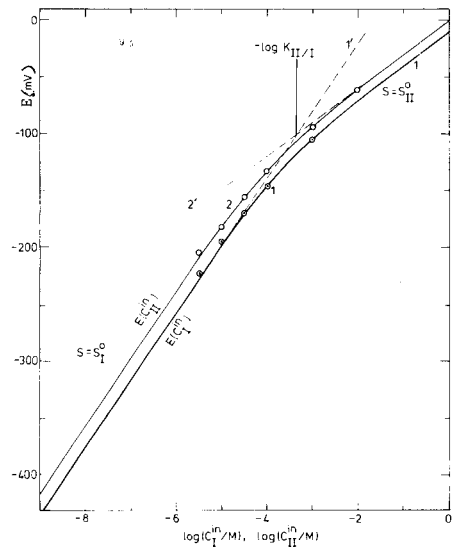

Fig. 4. The relation E vs. log C^{in}_{II} for 3 M chloride solution. Other conditions as for Fig. 3. Solid lines correspond to Eqn. (13) $K_{II/I} = 2.9 \times 10^{-3}$ dm^3 mol^{-1}.

Fig. 5. Determination of the value of $K_{II/I}$ using the separate solutions method. Chloride concentration, 0.1 M. Other conditions as for Fig. 3. Solid lines correspond to Eqn. (13). For further explanation, see text.

constant for the exchange reaction (3) was 4.35×10^{-4} mol dm^{-3}. At higher Cu(II) concentrations, the slope was S^0_{II}, i.e. 29.6 mV at 25° C. At lower Cu(II) concentrations, the slope of calibration curve for low initial Cu(I) concentration (10^{-6} mol dm^{-3}) increased in accordance with the predictions resulting from Eqn. (13) (S^0_I = 59.2 mV at 25°C). The experimental points obtained at $C^{in}_I = 10^{-6}$ mol dm^{-3} depart slightly from the theoretical curve in the range of the lowest Cu(II) concentration. This effect is due to the finite value of the lower limit of detection D that (as mentioned by other authors [3, 17, 18]) is higher than the theoretically expected $D = Y^0$.

The calibration curves E vs. log C^{in}_{II} shown in Fig. 4 concern concentrated chloride solutions where the copper sulphide electrode operates as a Cu^+-selective electrode. The value of the equilibrium constant of the exchange reaction (3) is 3.45×10^2 mol dm^{-3}, which requires that the Cu(II) ions react with the electrode material to form Cu(I) ions. The slope S_{II} is then $S_{II} = (\delta E/\delta \log C^{in}_{II})_{C^{in}_I} = S^0_I$, i.e., 59.2 mV at 25° C.

In Fig. 5 the calibration curves for changing initial Cu(I) concentrations at $C^{in}_{II} = 0$ (curve 1) and for changing initial Cu(II) concentrations at $C^{in}_I = 0$ (curve 2) are presented. The curves correspond to the value $K^f_{n-s} = 4.35 \times 10^{-4}$ mol dm^{-3}, i.e., $K_{II/I} = 2.3 \times 10^3$ dm^3 mol^{-1}. The way of evaluating the

value of log $K_{II/I}$ based on Eqn. (13) and the separate solutions method is shown by using extrapolation lines 1′ and 2′ whose intersection determines log $K_{II/I}$ = −log C_{II}^{in} (or −log C_I^{in} because of the same scale for C_I^{in} and C_{II}^{in}). This method was used in an earlier paper [4], but at that time the intermediate region near log C_{II}^{in} = −log $K_{II/I}$ could not be explained.

In Fig. 6, theoretical curves resulting from the Nicolsky equation are plotted for two cases, the first corresponding to the application of the separate solutions method of determining selectivity coefficients [8] (curves 1) and the second corresponding to the fixed interference method [8] (curve 1′). The different results obtained for certain conditions by means of these two methods (Fig. 6a) create the situation in which the experimental values of the selectivity coefficients $k_{II/I}^{pot}$ cannot be determined precisely. The inconstancy of the slope S_{II} (or S_I) as the ratio C_{II}^{in}/C_I^{in} changes makes it impossible to adopt any arbitrary procedure for the determination of the selectivity coefficient (Fig. 6b). It is also easy to prove that the experimental value of the selectivity coefficient $k_{II/I}^{pot}$, determined by a given method based on the Nicolsky equation (e.g., under the conditions where the copper sulphide electrode operates as a Cu^{2+}-selective electrode), changes as the value of C_I^{in}

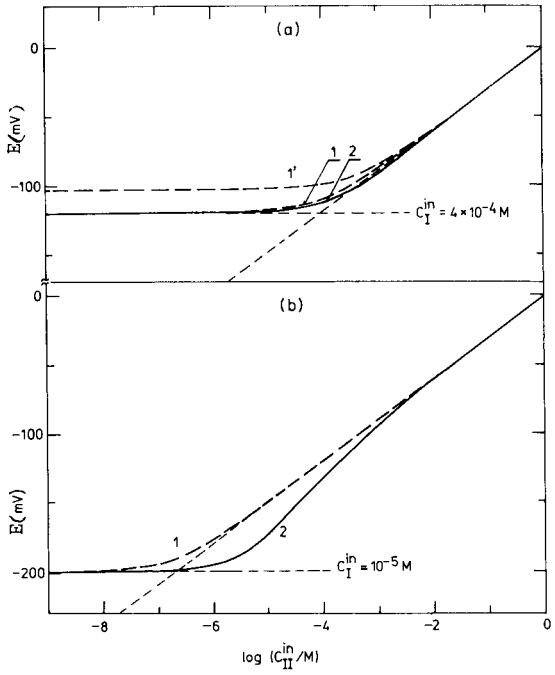

Fig. 6. Determination of the formal selectivity coefficient $k_{II/I}^{pot}$ (curves 1) using the fixed interference method and the Nicolsky equation. Curve 1′ corresponds to the Nicolsky equation with the value of $k_{II/I}^{pot}$ determined by the separate solutions method (curves 1′ and 2 at E = −103 mV, Fig. 5). Curves 2 are computed from Eqn. (13). All conditions as for Fig. 5.

changes. This happens because in the Nicolsky equation C_I^{in} is to the power two, whereas in Eqn. (20) it is to the power one, so that $k_{II/I}^{pot} = 0.5/C_I^{in}$, which is adequate for the electrode response in the "cupric" region.

Thus it follows from Eqn. (13) and the simplified equations (20, 21), as well as from the experimental results which agree very well with the theoretical predictions, that any selectivity towards the copper(I) or copper(II) introduced does not exist under the metastable equilibrium conditions after the end of the copper(I) disproportionation-generation process. As has been shown above, the coefficient $K_{II/I}$ in Eqn. (13) selects the slope of the electrode response to Cu(II) or Cu(I) ions and divides the operation mode of the copper sulphide electrode onto the "cupric" and "cuprous" ranges. The selectivity appears when there are some kinetic or diffusion inhibitions of the electrode processes. However, in this case the full metastable equilibrium between the electrode material and the species in the bulk solution is not reached. This problem will be elaborated later.

CONCLUSIONS

The approximate Nicolsky equation cannot be used to describe the selectivity of the non-stoichiometric copper sulphide electrode towards Cu(II) and Cu(I) ions when the electrode response is analyzed under (metastable) equilibrium conditions. An exact equation was derived for such conditions. This equation shows that the electrode operational mode can be exactly divided between the range of the Cu^{2+}-selective electrode (limiting Eqn. 20) and the range of the Cu^{+}-selective electrode (limiting Eqn. 21). In the first range, the electrode responds to both the Cu(II) and Cu(I) ions in solution but the slope of the calibration curve is always 29.58 mV per tenfold change in their concentration (at 25° C). The same applies to the second (Cu^{+}) range but the slope is now 59.16 mV for Cu(II) as well as Cu(I) ions. No significant changes in the electrode material composition are expected when the electrode operating in the "cupric" region is used for the determination of Cu(II) in absence of Cu(I) or when the electrode operating in the "cuprous" region is used in the solutions of Cu(I) not containing Cu(II). In other cases, some changes in the formal standard electrode potential may occur, especially at higher copper concentrations. The general equation (13) describes not only limiting cases of the "cupric" or "cuprous" operation but also all the intermediate ranges. On the basis of this equation, it is possible to predict the shape of the calibration curve and the exact slope, e.g., for such conditions as the chloride interference causing deviations from the "normal" electrode response. Determinations in solutions of bromides, chlorides (e.g., in seawater) or cyanides may be considered taking into account all the conclusions from the theory presented. Though this theory reported above was developed only for the non-stoichiometric copper sulphide ion-selective electrode and checked experimentally only for chloride solutions, it should be applicable to many other ion-selective electrodes. The theory does not take into account any

kinetic and diffusion effects. However, this is justified by the fact that with many metal sulphide electrodes, electrode reactions involving the electroactive species contained in the electrode material (e.g., reactions 3, 6 and 12) are very fast [1, 16, 18] and attainment of an equilibrium state is often observed.

APPENDIX A

Derivation of the metastable-equilibrium equation for the non-stoichiometric copper sulphide electrode (Eqn. 13)

As follows from Eqn. (9) defining the formal equilibrium constant K^{f}_{n-s} for exchange reaction (8), the total concentration of copper(II) at equilibrium, C^{eq}_{II}, is given by

$$C^{eq}_{II} = (\beta/K^{o})(\alpha_{II}/\alpha^{2}_{I})(f^{2}_{+}/f_{2+})(C^{eq}_{I})^{2} = (C^{eq}_{I})^{2}/K^{f}_{n-s} \quad \text{(A-1)}$$

The total concentration of Cu(I) at equilibrium may be evaluated from Eqn. (10): $C^{eq}_{I} = 2Y - 2C^{eq}_{II}$. (For brevity, K is used below instead of K^{f}_{n-s}.) Combining this equation with A-1 gives $C^{eq}_{II} = 4(Y - C^{eq}_{II})^{2}/K$, and rearrangement gives

$$(C^{eq}_{II})^{2} - (2Y + K/4)C^{eq}_{II} + Y^{2} = 0 \quad \text{(A-2)}$$

Solution of this quadratic equation leads to the equation for C^{eq}_{II}

$$C^{eq}_{II} = Y + (K/8) - (K^{2} + 16KY)^{\frac{1}{2}}/8 \quad \text{(A-3)}$$

The other solution of Eqn. A-2 is rejected because the difference $C^{eq}_{II} - Y$ must always be less than zero. Multiplying and dividing the right-hand side of Eqn. A-3 by the expression $Y + (K/8) + (K^{2} + 16KY)^{\frac{1}{2}}/8$, and rearrangement yields

$$C^{eq}_{II} = Y^{2}[Y + (K/8) + (K^{2} + 16KY)^{\frac{1}{2}}/8]^{-1} \quad \text{(A-4)}$$

$$\text{and } (C^{eq}_{II})^{-1} = Y^{-1} + K(8Y^{2})^{-1} + (8Y^{2})^{-1}(K^{2} + 16KY)^{\frac{1}{2}} \quad \text{(A-5)}$$

Adding and subtracting the term $K(8Y^{2})^{-1}$ from Eqn. A-5 gives

$$(C^{eq}_{II})^{-1} = Y^{-1} + K(4Y^{2})^{-1} + (8Y^{2})^{-1}[(K^{2} + 16KY)^{\frac{1}{2}} - K] \quad \text{(A-6)}$$

Multiplying and dividing the last term in Eqn. A-6 by the expression $(K^{2} + 16KY)^{\frac{1}{2}} + K$ and rearrangement yields

$$(C^{eq}_{II})^{-1} = Y^{-1} + K(4Y^{2})^{-1} + 2Y^{-1}[(1 + 16Y/K)^{\frac{1}{2}} + 1]^{-1} \quad \text{(A-7)}$$

The Nernst equation (5) may be written in the form

$$E^{(ms)}_{eq} = {}^{2}E^{\ominus} - RT(2F)^{-1} \ln \alpha_{II} + RT(2F)^{-1} \ln C^{eq}_{II} \quad \text{(A-8)}$$

where ${}^{2}E^{\ominus} = {}^{2}E^{o(ms)} + RT(2F)^{-1} \ln (\beta f_{2+})$. Combination of Eqns. A-7 and A-8 finally yields

$$E^{(ms)}_{eq} = {}^{2}E^{\ominus} - RT(2F)^{-1} \ln \alpha_{II} - RT(2F)^{-1} \ln [Y^{-1} + (4K_{II/I}Y^{2})^{-1} + \kappa_{II/I}] \quad \text{(A-9)}$$

where $K_{II/I} = K^{-1} = (K^{f}_{n-s})^{-1}$ and $\kappa_{II/I} = 2Y^{-1}[(1 + 16Y/K)^{\frac{1}{2}} + 1]^{-1}$.

APPENDIX B

Slope of the calibration curve

In the nomenclature recommendations [8] for ion-selective electrodes, the theoretical slope $S_i = S^{o}_{i} = RT(n_iF)^{-1}$ is used, but in practice some deviations are often observed. In general, for the slope S_{II}

$$S_{II} = (\delta E/\delta \ln C_{II}^{in})_{C_I^{in},\mu,\alpha_I,\alpha_{II}} \quad \text{(B-1)}$$

the Nicolsky equation (2) gives

$$S_{II} = RT(2F)^{-1}[1 + k_{II/I}^{pot}(C_I^{in})^2/(C_{II}^{in})]^{-1} \quad \text{(B-2)}$$

so that the maximum slope is S_{II}^0 (i.e., 29.58 mV at 25°C in decimal logarithmic scale). In contrast, from Eqn. (13) for the copper sulphide electrodes, slope S_{II} may be even twice as large under certain conditions. In order to calculate the derivative $(\delta E/\delta \ln C_{II}^{in})$, an equation resulting from combination of Eqns. A-3 and A-8 can be used.

$$E = {}^2E^0 - RT(2F)^{-1} \ln \alpha_{II} + RT(2F)^{-1} \ln [Y + K/8 - (K^2 + 16KY)^{\frac{1}{2}}/8] \quad \text{(B-3)}$$

This equation is equivalent to Eqn. A-9 and Eqn. (13) and is used here to avoid more complex algebra. First, the derivative $\delta E/\delta C_{II}^{in}$ is calculated

$$(\delta E/\delta C_{II}^{in})_{C_I^{in},\ldots} = RT(2F)^{-1}[1 - K(K^2 + 16KY)^{\frac{1}{2}}][Y + K/8 - (K^2 + 16KY)^{\frac{1}{2}}/8]^{-1} \quad \text{(B-4)}$$

After some algebra this gives

$$(\delta E/\delta C_{II}^{in})_{C_I^{in},\ldots} = RT(2F)^{-1} Y^{-1}[1 + (1 + 16Y/K)^{-\frac{1}{2}}] \quad \text{(B-5)}$$

Because $\delta C_{II}^{in} = C_{II}^{in}\, \delta \ln C_{II}^{in}$, Eqn. B-5 yields

$$S_{II} = (\delta E/\delta \ln C_{II}^{in})_{C_I^{in},\ldots} = RT(2F)^{-1}(C_{II}^{in}/Y)[1 + (1 + 16K_{II/I}Y)^{-\frac{1}{2}}] \quad \text{(B-6)}$$

where $K_{II/I} = K^{-1}$.

Analysis of Eqn. B-6 shows the following three ranges.

(a) Under the "cupric" conditions, i.e., when $Y \gg (16K_{II/I})^{-1}$, the slope S_{II} is

$$S_{II} = RT(2F)^{-1}(C_{II}^{in}/Y) \quad \text{(B-7)}$$

and if additionally $C_{II}^{in} \approx Y$, i.e., $C_{II}^{in} \gg Y^0 + \frac{1}{2}C_I^{in}$, then $S_{II} = RT(2F)^{-1}$, i.e. 29.58 mV at 25°C in decimal scale.

(b) Under the "cuprous" conditions, i.e., when $Y \ll (16K_{II/I})^{-1}$, slope S_{II} is given by

$$S_{II} = RTF^{-1}(C_{II}^{in}/Y) \quad \text{(B-8)}$$

and if additionally $C_{II}^{in} \approx Y$, then $S_{II} = RT/F$, i.e. 59.16 mV at 25°C in decimal scale.

(c) If $C_{II}^{in} \ll Y^0 + \frac{1}{2}C_I^{in}$, then $S_{II} = 0$ (this is the region below the lower limit of detection $D = Y^0 + \frac{1}{2}C_I^{in}$).

The analysis of the slope S_I

$$S_I = (\delta E/\delta \ln C_I^{in})_{C_{II}^{in},\mu,\alpha_I,\alpha_{II}} = RT(2F)^{-1} C_I^{in}(2Y)^{-1}[1 + (1 + 16K_{II/I}Y)^{-\frac{1}{2}}] \quad \text{(B-9)}$$

may be done similarly, again giving three ranges:

(a) $S_I = RT(2F)^{-1} C_I^{in}(2Y)^{-1}$ for $Y \gg (16K_{II/I})^{-1}$ (B-10)

and $S_I = RT(2F)^{-1}$, when additionally $C_I^{in} \gg 2(Y^0 + C_{II}^{in})$;

(b) $S_I = (RT/F)C_I^{in}/(2Y)$ for $Y \ll (16K_{II/I})^{-1}$ (B-11)

and $S_I = RT/F$, when additionally $C_I^{in} \gg 2(Y^0 + C_{II}^{in})$;

(c) $S_I = 0$ for $C_I^{in} \ll 2(Y^0 + C_{II}^{in})$.

REFERENCES

1 T. Hepel, Anal. Chim. Acta, 123 (1981) 151.
2 T. Hepel, Anal. Chim. Acta, 123 (1981) 161.
3 A. Hulanicki, M. Trojanowicz and M. Cichy, Talanta, 23 (1976) 47.
4 T. Hepel, M. Hepel and M. Leszko, Analyst (London), 102 (1977) 132.
5 B. P. Nicolsky, Zh. Fiz. Khim., 10 (1937) 495.
6 M. Hepel and A. Pomianowski, Zesz. Nauk. Uniw. Jagiellon., Pr. Chem., 18 (1973) 237.

7 G. Eisenman, D. O. Rudin and J. U. Casby, Science, 126 (1957) 831.
8 Recommendations for Nomenclature of Ion-Selective Electrodes, Inf. Bull. No. 43, IUPAC, 1975.
9 E. Pungor and K. Toth, Anal. Chim. Acta, 47 (1969) 291.
10 G. Eisenman, in R. A. Durst (Ed.), Ion-Selective Electrodes, Natl. Bur. Stand. (U.S.), Spec. Publ. 314, U.S. Government Printing Office, 1969, Ch. 1.
11 R. P. Buck, F. S. Stover and D. E. Mathis, J. Electroanal. Chem., 82 (1977) 345; T. R. Brumleve and R. P. Buck, J. Electroanal. Chem., 90 (1978) 1.
12 J. B. Lesourd, J. Electroanal. Chem., 86 (1978) 81.
13 A. Covington, in R. A. Durst (Ed.), Ion-Selective Electrodes, Natl. Bur. Stand. (U.S.), Spec. Publ. 314, U.S. Government Printing Office, 1969, Ch. 3.
14 T. Hepel and M. Hepel, Electrochim. Acta, 22 (1977) 295.
15 A. Hulanicki and A. Lewenstam, Talanta, 23 (1976) 661.
16 M. Hepel, J. Electroanal. Chem., 74 (1976) 37.
17 G. J. M. Heijne and W. E. van der Linden, Anal. Chim. Acta, 96 (1978) 13.
18 E. H. Hansen, C. G. Lamm and J. Růžička, Anal. Chim. Acta, 59 (1972) 403.

Analytica Chimica Acta, 142 (1982) 231—238
Elsevier Scientific Publishing Company, Amsterdam — Printed in The Netherlands

DIFFERENTIAL PULSE POLAROGRAPHY OF GERMANIUM(IV), TIN(IV), ARSENIC(V), ANTIMONY(V), SELENIUM(IV) AND TELLURIUM(VI) AT THE STATIC MERCURY DROP ELECTRODE IN CATECHOL—PERCHLORATE MEDIA

C. McCRORY-JOY* and J. M. ROSAMILIA

Analytical Chemistry Research Department, Bell Telephone Laboratories, Murray Hill, NJ 07974 (U.S.A.)

(Received 14th April 1982)

SUMMARY

The differential pulse polarography of Ge(IV), Sn(IV), As(V), Sb(V), Se(IV) and Te(VI) has been investigated in perchlorate media containing catechol using a static mercury drop electrode. Under optimum conditions, Ge(IV), Sn(IV), As(V), and Sb(V) undergo reduction to yield well-defined peaks; detection limits of 82 ppb, 28 ppb, 4 ppm, and 25 ppb, respectively, have been calculated. Few electrolytes are known for which these ions exhibit a quantitatively useful polarographic response. While Se(IV) and Te(VI) may be detected at levels of 115 ppb and 17 ppb, respectively, addition of catechol does not enhance the peak current relative to that observed in simple perchlorate solutions, as was the case for the other ions studied. The determination of germanium, arsenic and antimony in samples is described.

Studies of electrolytes and complexing agents are important in establishing suitable electrolyte compositions for electroanalytical procedures. Situations arise in which the limited choice of useful media or the capability of detecting only one of two or more oxidation states is a serious inconvenience. Polyphenols have been the subject of several investigations as components of electrolytes for polarographic measurements [1—12]. Direct current polarographic (d.c.p.) investigations of perchlorate electrolytes containing pyrogallol or 1,2,3-trihydroxybenzene have shown that tin(IV) [1—3] and arsenic(V) [4] are electroactive in these media. Increasing the concentration increases the wave height up to a point, beyond which higher concentrations of pyrogallol depress the wave height in either case [3, 4]. A more recent report describes the determination of arsenic(V) in ground waters by differential pulse polarography (d.p.p.) in a pyrogallol—perchlorate electrolyte [5]. Cyclic voltammograms of germanium(IV) in pyrogallol—perchloric acid media exhibit a single sharp peak for the reduction of Ge(IV) to Ge(0) [6]. In an investigation of Ge(IV) in the presence of catechol (1,2-dihydroxybenzene) a well-defined d.c.p. wave was obtained [7].

Pyrogallol and catechol are both known to form inner complexes or condensation products in strongly acidic media, with solubilities depending on

0003-2670/82/0000-0000/$02.75

the metal or non-metal involved and the specific conditions employed [13]. Several d.c.p. and cyclic voltammetry investigations have established that pyrogallol and 1,2-diphenols are adsorbed on the surface of mercury electrodes [3, 9–12], and in the case of tin(IV) and germanium(IV) have shown that the enhancement of peak currents and improved efficiency of the electrochemical reduction process is associated with the adsorption of pyrogallol or catechol. The importance of tin plating processes and the use of germanium, arsenic, antimony, selenium, and tellurium in the production of electronic devices led to an investigation of their electroanalytical chemistry in catechol—perchlorate media. The determination of Sn(IV), Ge(IV), As(V), and Sb(V) simplifies the sample treatment procedure because dissolution conditions can be chosen to produce these ions and chemical reduction to the lower oxidation states can be avoided.

EXPERIMENTAL

Apparatus and reagents

All polarographic measurements were made with a Princeton Applied Research Model 174 Polarographic Analyzer, a Model 303 Static Mercury Drop Electrode (SMDE) with a Ag/AgCl reference electrode, and a Hewlett-Packard 7046A or Houston Series 2000 X—Y recorder. The medium drop size of the SMDE was selected. A platinum wire was used as an auxiliary electrode for all electrochemical experiments. A drop time of 0.5 s and a modulation amplitude of 25 mV were employed for differential pulse polarographic (d.p.p.) measurements. The sweep rate was 10 mV s^{-1} in all d.p.p. experiments.

Except where specified, all chemicals were of analytical-reagent grade. Sodium arsenate, which was used to prepare the arsenic(V) stock solution, was assayed titrimetrically by addition of excess of iodide to an acidic solution of the salt and subsequent titration of the liberated iodine; the average assay for three samples was 99.97%. Hydrofluoric acid (J. T. Baker Ultrex) was used for the dissolution of silica soot samples. The following standard atomic absorption samples (Alfa Products) were used: germanium(IV) (1000 μg Ge ml^{-1}) prepared by dissolving H_2GeF_6 in deionized water containing 7% (v/v) HNO_3 and 1.2% (v/v) HF; a tin(IV) standard prepared by dissolving tin(IV) chloride in 7.4% (v/v) HCl to make a solution containing 1000 μg Sn ml^{-1}; selenous acid (1000 μg Se ml^{-1}) in deionized water; and tellurium(VI) (1025 μg ml^{-1}) prepared by dissolving sodium tellurate in deionized water containing 1.9% (v/v) HCl. The antimony(V) standard (12 μg Sb ml^{-1}) was prepared under a nitrogen atmosphere by diluting 500 μl of antimony(V) chloride (Alfa Products Puratronic grade) to a volume of 100 ml with 1.0 M $HClO_4$—0.1 M $NaClO_4$. The solution must be prepared fresh because antimony(V) hydrolyzes on standing for long periods of time.

Procedure

The d.p.p. behavior of all the ions investigated was examined in perchloric acid solutions (0.1—2.0 M), in solutions containing only sodium perchlorate (0.1—1.0 M), and in media combining the two in various proportions, to determine the behavior of the ions in the absence of catechol. A suitable electrolyte composition was chosen for the ions investigated; all except germanium(IV) gave a polarographic response, although not well-defined, in perchlorate media without catechol. The effect of varying the concentration of catechol was studied at constant pH, and the effect of varying pH at constant concentration of catechol was determined in each case. Calibration plots were prepared for each ion studied. Detection limits (d.l.) were calculated from the relationship d.l. = $(S_{yx})t/k$ where S_{yx} is the standard error, k is the slope, and t is the appropriate constant at the 99% confidence level for $(n - 2)$ degrees of freedom.

Samples

Samples of silica soot containing germanium oxide were obtained after formation during vapor deposition preparation of SiO_2—GeO_2 using a stationary torch. The GeO_2 content had been previously determined to be 11% by atomic emission spectrography. Samples were dissolved by adding 1 ml of hydrofluoric acid (J. T. Baker Ultrex) and 500 μl of concentrated nitric acid to 80 mg of sample in a 30-ml low-density polyethylene jar with a screw cap. The cap was tightened and dissolution was achieved within 2 h, the contents of the jar being allowed to react at room temperature. The sample was further diluted by adding a 100-μl aliquot to 10 ml of the catechol—perchlorate medium.

Gallium arsenide (99.99%) and indium arsenide (99.99%), were obtained from Alfa Products. Samples weighing 0.10 g were dissolved in 5 ml of concentrated nitric acid, after which the resulting solution was evaporated to dryness. The residue was dissolved in 3 ml of concentrated hydrochloric acid and diluted to a total volume of 25 ml with 0.1 M $NaClO_4$—0.1 M $HClO_4$. A 100-μl aliquot was added to a 10-ml volume of the appropriate catechol—perchlorate medium followed by polarographic measurement. Gallium antimonide and indium antimonide samples (99.99%) were dissolved by the same procedure.

Antimony in doped silicon wafers was determined after the wafers had been cut into small pieces, and each sample had been dissolved in a teflon beaker containing 10 ml of hydrofluoric acid to which an equal volume of nitric acid was added slowly during the dissolution. The resulting solution was evaporated to dryness, the residue was dissolved in 500 μl of concentrated hydrochloric acid and the solution was diluted to 25 ml with a solution containing 0.1 M catechol, 0.1 M $NaClO_4$, and 0.1 M $HClO_4$.

Two sets of samples were processed, the first consisting of six 3-in. diameter ⟨100⟩ silicon wafers from a lot with a maximum resistivity of 0.0030 Ωm cm and a minimum doping of 100 ppm antimony (100 mg Sb/1000 g wafer).

The second set, consisting of three ⟨111⟩ silicon wafers, came from a lot with a maximum resistivity of 0.0015 Ωm. The antimony content of the two sets of wafers was calculated as milligrams of antimony per 1000 g of silicon and as atoms of antimony per 10^{23} atoms of silicon.

RESULTS AND DISCUSSION

Polarography and cyclic voltammetry

The d.p.p. peak potentials at optimum electrolyte compositions, and detection limits for the ions studied are summarized in Table 1. The table includes regression parameters, the standard error of estimate, the number of data points, and the concentration range examined in each case.

Germanium. No d.p.p. response was detected for germanium(IV) in simple perchlorate media but the addition of catechol resulted in the appearance of a peak at −0.50 V vs. Ag/AgCl (Fig. 1). The peak current increases markedly with increasing catechol concentration up to a point beyond which a decrease in peak current is observed (Table 2). This decrease might be due to an adsorptive blocking of the electrode process. The result obtained for three samples of silica soot, 10.4 ± 0.2%, compares reasonably well with the atomic emission results for which a result of 11% Ge by weight was obtained.

Tin. A cyclic voltammogram obtained for a sample of tin(IV) standard in 0.1 M $HClO_4$–0.1 M $NaClO_4$—0.1 M catechol was identical to that reported by other workers [12]. Two well-defined peaks corresponding to the reduction of Sn(IV) and Sn(II) were observed. The enhancement of the cathodic peak currents relative to those observed in the absence of catechol is significant, as well as the improvement in the definition of the Sn(IV) reduction peak.

The differential pulse polarogram obtained for Sn(IV) exhibits two peaks corresponding to the reduction of Sn(IV) to Sn(II) and the reduction of Sn(II) to Sn(0) at −0.12 V and −0.40 V vs. Ag/AgCl, respectively. The catechol—perchlorate medium is being investigated for the purpose of determining Sn(IV) and Sn(II) simultaneously by current-sampled d.c.p. at the SMDE.

Arsenic. Arsenite is reduced in two steps in 1 M HCl, the first being the reduction of As(III) to As(0) and the second corresponding to the reduction of As(0) to AsH_3 [14]. This is not an ideally reversible process as reflected by the relatively broad d.p.p. peak obtained. The results of the assay of gallium arsenide and indium arsenide compared favorably with the calculated arsenic contents of 51.8% and 39.5% arsenic, respectively, with a value of 51.2 ± 0.5% obtained for four samples of gallium arsenide and a value of 39.5% ± 0.5% for four samples of indium arsenide.

Antimony. Antimony(III) is generally reducible under polarographic conditions but the reduction of the pentavalent state is observed only in strong hydrochloric acid or acidic halide solutions [15]. Antimony(V) reduces in two steps at the DME under these conditions, possibly with electrocatalysis by adsorbed halides, first to Sb(III) ion and then to Sb(0).

TABLE 1

D.p.p. peak potentials, detection limits and regression parameters for ions studied

Ion	E_p (V vs. Ag/AgCl)	Electrolyte composition	Detection limit	Slope ± s.d. (μA/ppm)	Intercept ± s.d. (μA)	Standard error (μA)	Range (ppm)	No. of data points
Ge(IV)	—0.51	0.1 M catechol 0.1 M $NaClO_4$ 0.1 M $HClO_4$	82 ppb	0.91 ± 0.01	0.17 ± 0.01	0.02	1—10	9
Sn(IV)	—0.12	0.1 M catechol 0.1 M $NaClO_4$ 0.1 M $HClO_4$	28 ppb	1.25 ± 0.01	—0.00 ± 0.00	0.01	1—10	10
As(V)	—0.23	0.5 M catechol 2.0 M $HClO_4$ 0.1 M $NaClO_4$	4 ppm	0.01 ± 0.00	0.03 ± 0.00	0.01	20—170	9
Sb(V)	—0.33	0.1 M catechol 0.1 M $HClO_4$ 0.1 M $NaClO_4$ 0.01 M HCl	25 ppb	3.24 ± 0.06	—0.11 ± 0.02	0.02	0.5—5.0	10
Se(IV)	—0.56	0.1 M catechol 0.1 M $HClO_4$ 0.1 M $NaClO_4$	115 ppb	0.70 ± 0.00	—0.13 ± 0.01	0.02	0.5—3.7	8
Te(VI)	—0.87	0.1 M catechol 0.1 M $HClO_4$ 0.1 M $NaClO_4$	17 ppb	2.38 ± 0.00	—0.01 ± 0.00	0.01	0.5—3.7	8

The presence of chloride or other halide ions and the suppression of hydrolysis were both found to be necessary for the reduction of Sb(V) to Sb(III). Attempts to study the polarographic behavior of Sb(III) in perchlorate media containing pyrogallol were complicated by precipitation [4].

The presence of chloride ion was necessary to avoid precipitation of Sb(V) in the systems studied here, so all media investigated contained a small concentration of chloride as well as perchlorate ion. Antimony(V) yields a d.p.p. response in a chloride–perchlorate medium (Fig. 2, curve a) which consists of two closely spaced peaks. Antimony(V) is known to undergo stepwise reduction to Sb(III) and then to Sb(0), and the reduction peak potentials for these reactions are quite close in most media [15]. When catechol is present, the two d.p.p. peaks observed merge to form a single symmetrical peak (Fig. 2, curve b) which increases in magnitude with further addition of catechol. Calibration plots were prepared for Sb(V) from data obtained in a medium containing 0.1 M catechol, 0.1 M $NaClO_4$, 0.1 M $HClO_4$ and 0.01 M HCl. The antimony content of gallium antimonide was determined to be 63.7 ± 0.3% for three samples of gallium antimonide, and the antimony content of indium antimonide was found to be 51.4 ± 0.4% for four samples. These results compare favorably with the theoretical compositions of 63.5% and 51.5%, respectively. The results for doped silicon samples, summarized in Table 3, show a reasonable correlation between the specified antimony content and the resistivity values for the samples given in the Experimental section.

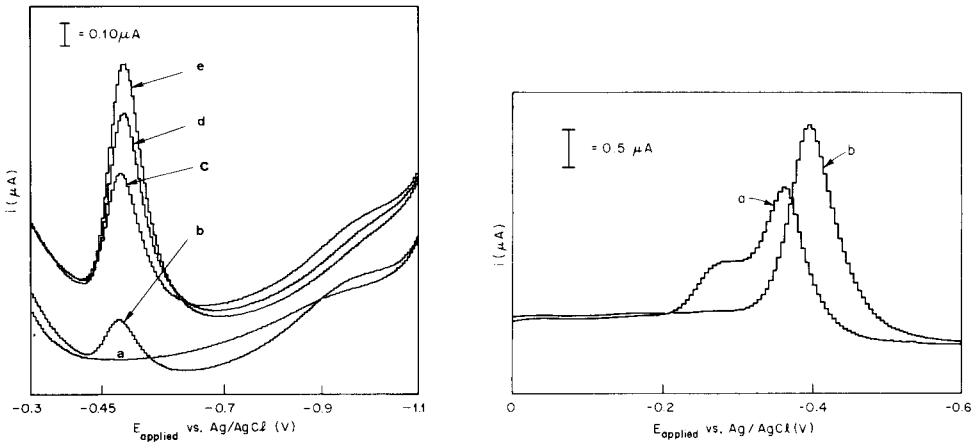

Fig. 1. Effect of addition of catechol on the differential pulse polarography of Ge(IV) (2 ppm Ge(IV) 1.0 M $HClO_4$, 0.1 M $NaClO_4$, 10 mV s^{-1}, modulation amplitude 25 mV). (a) Blank; (b) 10^{-3} M; (c) 10^{-2} M; (d) 5×10^{-2} M; (e) 10^{-1} M catechol.

Fig. 2. Differential pulse polarograms of antimony(V) in a chloride–perchlorate medium (5 ppm Sb(V) 0.1 M $HClO_4$, 0.1 M $NaClO_4$, 0.01 M HCl, 10 mV s^{-1}, modulation amplitude 25 mV). (a) Without catechol; (b) with 0.1 M catechol.

TABLE 2

Dependence of d.p.p. peak current for Ge(IV) on catechol concentration

log [Catechol]	−2.0	−1.7	−1.3	−1.1	−1.0	0.5	0.3	0.0
i_p (μA)	4.0	10.2	19.0	25.1	36.4	25.3	16.5	12.2

TABLE 3

Determination of antimony in doped silicon

Sample	Wt. of sample (g)	ppm Sb	(atoms Sb/10^{23} atoms Si)
First set			
1	5.05174	135	3.11×10^{18}
2	4.79169	188	4.33×10^{18}
3	4.96995	302	6.98×10^{18}
4	5.12970	342	8.68×10^{18}
5	4.98841	250	5.78×10^{18}
6	4.94453	288	6.71×10^{18}
Second set			
1	1.20979	814	1.88×10^{19}
2	1.21637	452	1.04×10^{19}
3	1.24680	519	1.20×10^{19}

Selenium. An attempt to characterize the reduction of Se(IV) in 1 M $HClO_4$ solution by d.c.p. yielded two ill-defined waves [4]. The addition of pyrogallol to the perchlorate medium depressed the wave heights about 33%. Depression of the d.p.p. peak was observed upon addition of catechol in this study. The results of the d.p.p. experiments suggest a complex reduction process for Se(IV) in the presence of catechol with no simplification in the polarographic behavior relative to that already reported [16]. The d.p.p. peak at −0.52 V vs. Ag/AgCl was used to prepare a calibration plot, but further investigation would be required to provide a detailed explanation for the peaks observed. A pronounced post-peak baseline depression is associated with polarographic maxima observed in d.c.p. experiments.

Tellurium. Tellurium(VI) was studied in this investigation rather than Te(IV) because of its greater solubility. In perchlorate media, two major peaks are observed for the otherwise complex reduction at −0.15 and −0.86 V vs. Ag/AgCl, respectively. The second reduction exhibits a pronounced maximum under conditions of d.c.p., a characteristic usually associated with the four-electron reduction of Te(IV) to the metal [16]. Both peaks show a linear dependence of peak current on the Te(VI) concentration. As observed for Se(IV), the addition of catechol depresses the peak currents arising from both the reactions observed, so no analytical advantage is realized. An investigation [17] of the formation of various chelates with catechol

showed that Te(VI) is reduced by catechol and that a small amount of a 1:2 Te(IV) chelate is precipitated upon standing, which may partially explain the behavior observed. The previously suggested association of the adsorption of catechol and other polyphenols with the enhanced efficiency of electrochemical reduction of Sn(IV) [10] and Ge(IV) [12] is supported by the results reported here. Addition of catechol results in a peak current enhancement in both cases. The effects of adsorbed polyphenols appear to be quite specific and vary with the phenol structure [11], and could also act in a specific manner toward various analyte ions.

Conclusion

Differential pulse polarography of Ge(IV), As(V), and Sb(V) in catechol—perchlorate electrolytes is a useful method for quantifying these species in practical samples. The calculated detection limits show that both trace and major level constituents can be determined by the procedures described.

The effects of catechol suggest adsorption of catechol on the surface of mercury and catalysis of the electrochemical reduction of Ge(IV), Sn(IV), As(V) and Sb(V). No advantage of the catechol—perchlorate media is observed for Se(IV) and Te(VI).

REFERENCES

1 C. L. Schmitt, E. F. Eiven and S. P. Dood, Bibliography of Polarographic Literature, 1922—1967, Sargent-Welch Scientific, Skokie, IN, 1969.
2 S. L. Phillips and E. Morgan, Anal. Chem., 34 (1961) 1192.
3 A. J. Bard, Anal. Chem., 34 (1962) 266.
4 S. M. C. White and A. J. Bard, Anal. Chem., 38 (1966) 61.
5 G. C. Whitnack, Anal. Chem., 47 (1975) 618.
6 Z. J. Karpinski, A. Polosak and Z. Kublik, Anal. Chim. Acta, 120 (1980) 55.
7 N. Konopik, Monatsh. Chem., 91 (1969) 717.
8 S. Glodowski and Z. Kublik, Anal. Chim. Acta, 104 (1979) 55.
9 Ya. I. Turyan, L. F. Ilina and P. I. Kudinov, Elektrokhimiya, 9 (1973) 1219.
10 S. K. Sharma and R. N. Soni, Chem. Anal., 19 (1974) 1131.
11 S. K. Sharma and R. N. Soni, Chem. Anal., 20 (1975) 27.
12 S. Glodowski and Z. Kublik, Anal. Chim. Acta, 115 (1980) 51.
13 F. Feigl, Specific, Selective and Sensitive Reactions, Academic Press, New York, 1949, pp. 177—179, 354—366.
14 D. J. Myers and J. Osteryoung, Anal. Chem., 45 (1973) 267.
15 V. Past, in A. J. Bard (Ed.), Encyclopedia of Electrochemistry of the Elements, Dekker, New York, Ch. IV-1.
16 I. M. Kolthoff and J. J. Lingane, Polarography, Vol. II, Interscience, New York, 1952, pp. 564—572.
17 J. Halmekoski, Ann. Acad. Sci. Fenn., 16A (1959) 4.

Analytica Chimica Acta, 142 (1982) 239—247
Elsevier Scientific Publishing Company, Amsterdam — Printed in The Netherlands

CONCENTRATION-MODULATED VOLTAMMETRY

JOSEPH WANG* and HOWARD D. DEWALD
Department of Chemistry, New Mexico State University, Las Cruces, NM 88003 (U.S.A.)
(Received 16th March 1982)

SUMMARY

A differential voltammetric technique based on measurements of the differences between currents with the sample and blank solutions flowing alternately through an electrochemical cell while the applied potential is scanned linearly, is described. In this way, the current of interest can be separated from unwanted currents, such as those from double-layer charging, surface transient, and oxygen reduction background components. The effective isolation of the desired current allows a detection limit of 2×10^{-8} M dopamine. A flow cell with a wall-jet glassy carbon disk working electrode was employed for these studies. Well defined current—potential curves are obtained for dopamine, ascorbic acid, homovanillic acid, chlorpromazine, and hexacyanoferrate(II) and (III) at the micromolar and submicromolar concentration levels. The modulated response was evaluated with respect to reproducibility, concentration dependence, detection limit, and other variables. The method is simple and suitable for automated on-line monitoring.

One of the most important applications of faradaic electrochemistry is its use for sensitive measurements in flowing streams. A wide range of flow-through electrochemical cells, based mainly on various solid electrodes, has been created for this purpose [1]. A limitation of most electrochemical flow detectors is the restriction of monitoring a single potential at a time. In many cases, such operation does not furnish the selectivity required even when a chromatographic separation is incorporated [2]. The redox potential selectivity of voltammetry has not been exploited effectively for measurements in flowing streams; the suggestions of using a dual-electrode detector (with each electrode held at a different potential) [3], or successive potential pulses [4], offer only partial and cumbersome solutions to the selectivity problem. The selectivity should be improved dramatically by using a scanning potential technique. Scanning potential pulse procedures, which are effective when applied at dropping mercury electrode flow cells [5], do not have adequate detection limits with solid electrode flow cells (because of the additional surface transient background components). Recently, linear potential scans have been incorporated with the pulsed-flow or stopped-flow operation of solid electrode flow cells to obtain current—potential curves for low concentrations of electroactive substances [6, 7].

This paper describes a new differential approach for obtaining sensitive voltammograms in flowing streams identified as concentration-modulated

0003-2670/82/0000-0000/$02.75

voltammetry. In this approach, sample and blank solutions alternately flow through the electrochemical cell while the working electrode potential is scanned linearly. The resulting modulated voltammogram has a sigmoidal (wave) shape with the limiting (mass-transfer controlled) current amplitude proportional to the concentration sought. The concentration-modulated current amplitudes are free from most background current components (e.g., double layer charging, surface transients and redox reactions of electroactive species). An advantage of the present approach over hydrodynamic modulation procedures [6, 7] is its ability to produce useful voltammograms in the presence of dissolved oxygen.

Differential measurement, well-established for the compensation of background signals in a variety of techniques (e.g., gas chromatography), has been proposed earlier for batch voltammetric measurements and flow amperometric detection employing dual-cell systems [8, 9]; problems incurred in matching two working electrodes limited its exploitation. By employing the concentration-modulated procedure, similar data can be obtained with a single working electrode. A sensitive amperometric (constant potential) detection of hexacyanoferrate(III) based on an alternate solution procedure was described as early as 1963 [10]. However, such solution switching has not been incorporated with a scanning potential procedure. The characterization and advantages of such incorporation are discussed in this paper.

EXPERIMENTAL

Apparatus and reagents

The flow cell, based on the "wall-jet" principle, has been described in detail previously [7]. The working electrode was a glassy carbon disk (0.25-cm diameter) onto which a solution stream is directed from a solution inlet nozzle (0.34-mm diameter). The distance between the nozzle tip and the surface of the electrode was 0.025 cm. The reference electrode (Ag/AgCl) was introduced to the cell downstream from the working electrode.

The blank and sample solutions were stored in two nalgene beakers, with similar hydraulic heads to provide equal flow rates upon exchanging the solution flowing through the cell. These reservoirs were connected, through teflon tubing (1.0-mm i.d., 2.0-mm o.d.), to a three-way teflon stopcock located 13 cm from the cell inlet. The stopcock permitted alternation between the sample and blank solutions. Connection between the stopcock and the cell was made via 7-cm long, 1.0-mm i.d. teflon tubing. All measurements were made with a Sargent-Welch Model 4001 polarograph.

Chemicals and reagents used have been described in detail previously [11] except as noted. Millimolar and submillimolar stock solutions of homovanillic acid and chlorpromazine (Sigma Chemical Co.), respectively, were prepared fresh each day. Aliquots of the stock solution were added to the supporting electrolyte to give the desired concentration.

Procedure

The working electrode was pretreated at the beginning of each day by cycling the applied potential between +0.9 V and −0.9 V for 8 min, allowing 2 min at each potential, while the supporting electrolyte solution was passed slowly through the cell. Following this, the electrode was held at the potential for the start of the scan for about 30 s. A linear potential scan (of 0.1 or 0.2 V min^{-1}) was then initiated. During the scan period, a concentration-modulated procedure was provided by manual switching of the stopcock, i.e., introducing periodically (every few seconds) the sample and blank streams. Except for about a 0.2-s shut-off time during the exchange, the solution flow was maintained at the rate governed by the hydraulic height.

RESULTS AND DISCUSSION

Concentration-modulated current amplitudes were evaluated first under conditions of constant potential at the mass-transfer controlled region. Figure 1 illustrates current—time responses for potassium hexacyanoferrate(II)

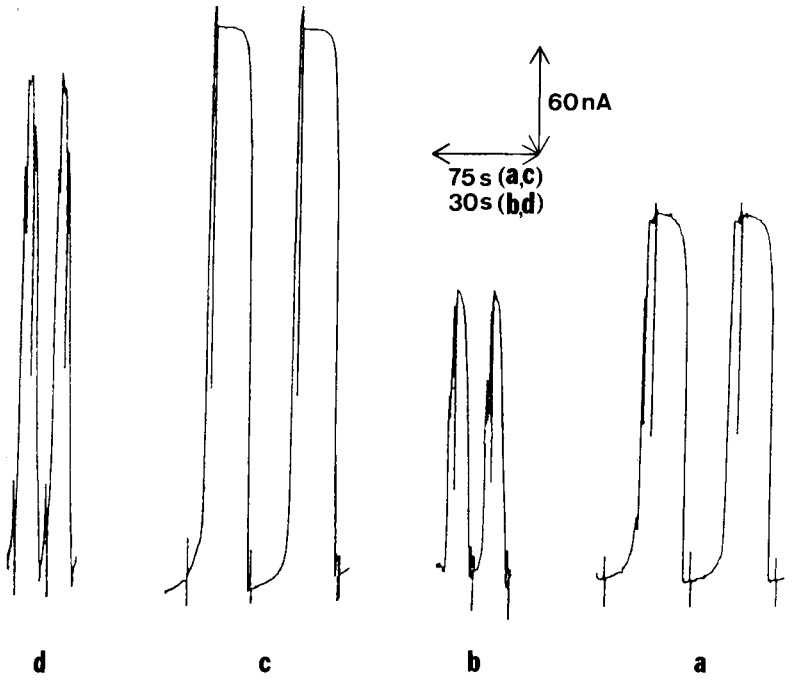

Fig. 1. Concentration-modulated current amplitudes for the oxidation of 12 μM $K_4Fe(CN)_6$ in 0.1 M phosphate buffer (pH 7.4). Applied potential, +0.9 V. Flow rates: 1.0 ml min^{-1} (a, b) and 3.0 ml min^{-1} (c, d). Cycling times: (a, c) 30 s sample and 30 s blank, (b, d) 5 s sample and 5 s blank. (The current spikes, before and near the end of the current amplitude, are due to the short shut-off times during the solution exchange.)

recorded under different experimental conditions. Response times for achieving the "sample" and "blank" current steady-states are about 12 s (sample) and 25 s (blank) at a flow rate of 1.0 ml min^{-1} (Fig. 1a) and 8 s (sample) and 27 s (blank) at 3.0 ml min^{-1} (Fig. 1c). By increasing the flow rate from 1.0 to 3.0 ml min^{-1}, a 46% increase in the concentration-modulated current amplitude is observed. An 83% reduction of the cycling period (from 30/30 s to 5/5 s) results in current reductions of 22% and 9% for the 1.0 and 3.0 ml min^{-1} operations, respectively (curves a and c vs. b and d). As is shown later in this paper, these non-steady-state current amplitudes are proportional to the bulk concentration of the analyte as is the case with flow injection systems [12]. The concentration-modulated procedure can be treated as a flow injection experiment with equal timing for the sample and blank solutions. It is well-established by flow injection theory that any point on the rising portion of the signal is as good a measure of the analyte concentration as the steady-state signal. Based on the similarity to flow injection systems, the shortest possible "dead volume" between the switching valve and the working electrode is desirable for getting maximum non-steady-state response for a given time. The large current amplitude and low noise level (e.g., Fig. 1c) illustrate the potential of this approach for performing useful amperometric measurements at relatively extreme anodic potentials (e.g., +0.9 V used in Fig. 1), because the modulated response has reduced dependency on solvent decomposition reactions.

Similar considerations are applied to the incorporation of alternate-solution and potential scanning procedures. Figure 2 shows representative linear scan concentration-modulated voltammograms for the oxidation of dopamine (b), ascorbic acid (c), and hexacyanoferrate(II) (d) at the micromolar concentration level, along with the corresponding background current (a) (the latter was obtained with the blank solution in both reservoirs). A sigmoidal modulated response is observed for these three species. The half-wave potentials for dopamine, ascorbic acid, and hexacyanoferrate(II) by concentration-modulated voltammetry are at +0.04, −0.04, and +0.18 V, respectively; the plateau regions start at +0.10, +0.19, and +0.41 V, respectively. These potential regions are similar to those reported for these species at various carbon electrodes (e.g., ref. 11); however, as is discussed below, the shape and half-wave potentials of concentration-modulated voltammograms should not be compared directly with those obtained in conventional voltammetry, because of the different nature of the measurement. The background voltammogram (a) shows the absence of differences between the blank solution in the two reservoirs.

The effect of the potential scan rate on the concentration-modulated current–potential response is shown in Fig. 3. Increased alternation frequency was incorporated with the increased scan rate (8, 5, and 4 s cycles for 0.1, 0.2, and 0.5 V min^{-1}, respectively). While the 0.1 and 0.2 V min^{-1} rates yield well-defined voltammograms, this is not the case at 0.5 V min^{-1}, at which the alternation frequency is not rapid enough to follow the rela-

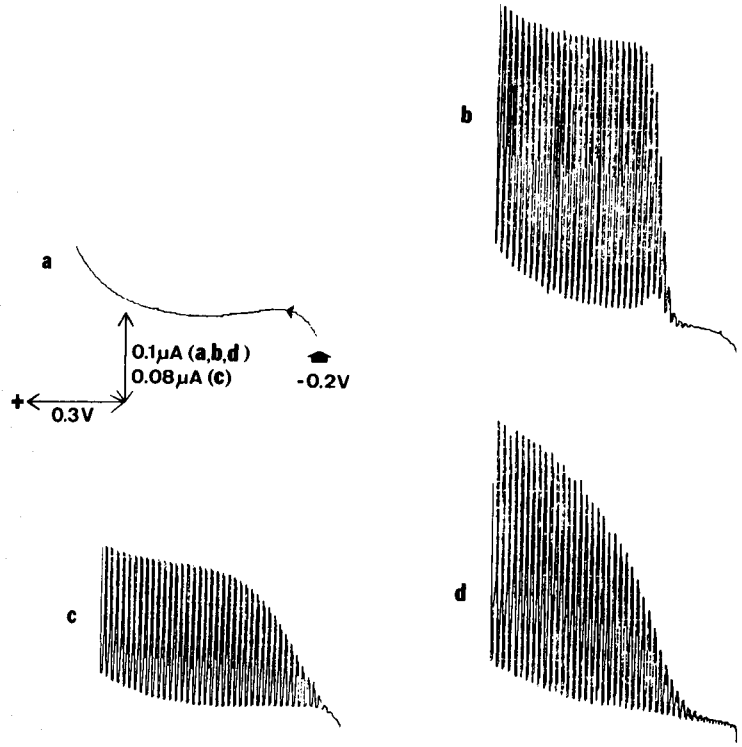

Fig. 2. Linear scan concentration-modulated voltammograms for 5 μM dopamine (b), 4 μM ascorbic acid (c), and 10 μM $K_4Fe(CN)_6$ (d), along with the corresponding background current (a). 0.1 M phosphate buffer (pH 7.4). Scan rate, 0.1 V min^{-1}; flow rate, 3.0 ml min^{-1}; cycling time, 5 s sample, 5 s blank. Scan starts at −0.2 V (a, b, c) and −0.1 V (d).

tively fast change in the potential (at 0.5 V min^{-1} a current amplitude is recorded every 50 mV, compared to around 25 mV at 0.1 and 0.2 V min^{-1}). For the same reason, the error in locating the half-wave potential depends on the closeness of the current oscillations, i.e., on the scan rate and switching frequency. The incorporation of an automated rapid switching circuit [13] would permit the achievement of subsecond cycling times, and thus the use of much faster scan rates.

The dopamine response, shown in Fig. 2(b), is part of a series of six 5-μM concentration increments that were used to evaluate the linearity and the sensitivity of the response. The 5, 10, 15, 20, 25, and 30-μM dopamine solutions yielded well-defined plateau regions, with current amplitudes (measured at +0.30 V) of 299, 602, 929, 1140, 1510, and 1760 nA, respectively. These data yielded a highly linear calibration plot over the entire range, the slope of which corresponds to a sensitivity of 58.5 nA μM^{-1}. Such linearity is expected because the concentration profile in the detector is dependent of the concentration level.

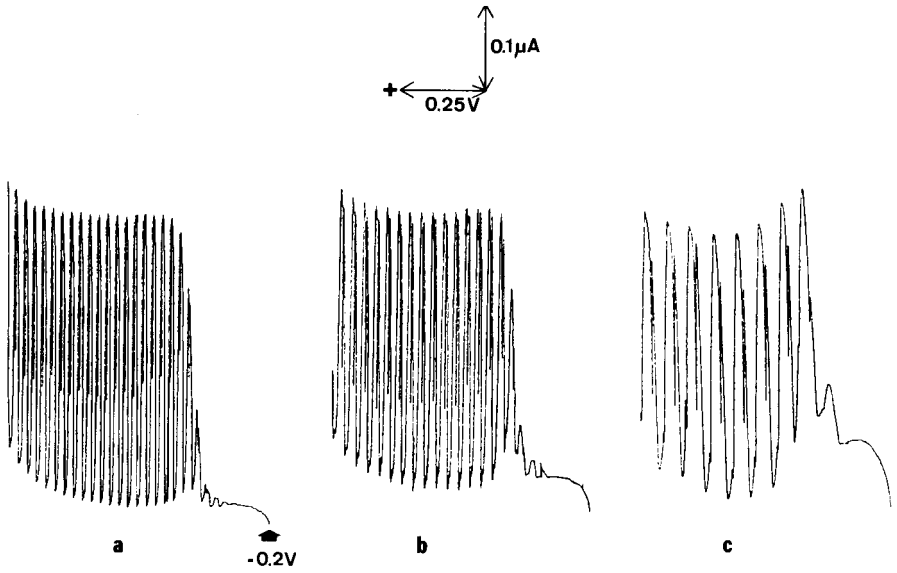

Fig. 3. Concentration-modulated voltammograms of 5 μM dopamine for different potential scan rates: (a) 0.1 V min^{-1}; (b) 0.2 V min^{-1}; (c) 0.5 V min^{-1}. Cycling times: (a) 8 s; (b) 5 s; (c) 4 s. Flow rate, 3.0 ml min^{-1}; 0.1 M phosphate buffer (pH 7.4).

Because the two solutions flowing alternately through the detector have similar oxygen concentrations, concentration-modulated voltammetry is capable of measuring low concentrations of reducible species in the presence of dissolved oxygen. The continuous removal of oxygen from flowing streams is fairly complicated [14], and is the principal time-consuming step in the measurement when it is replaced by a batch removal. Figure 4 demonstrates the utility of concentration-modulated voltammetry for cathodic measurements in the presence of dissolved oxygen. It shows characteristic voltammograms for different concentrations of hexacyanoferrate(III), along with the corresponding background current. Although dissolved oxygen is present at the 10^{-4} M concentration level, the background current is very low. The current amplitudes at −0.3 V for the reduction of hexacyanoferrate(III) are 54, 101, 174 and 252 nA for the 5, 10, 15, and 20 μM solutions, respectively. Because the solubility of oxygen is a function of the ionic strength, an effort must be made to match the ionic strengths of blank and sample solutions.

Figure 5 demonstrates the utility of concentration-modulated voltammetry for obtaining defined voltammograms at the submicromolar concentration level. Examination of the data for 7.5×10^{-7} M dopamine (b) and its corresponding background current (a) shows that the mass-transfer limited current amplitude is about 44 nA, whereas the noise level is only 0.6 nA. Hence, using the criterion of a signal-to-noise ratio of 2, the limit of detection for dopamine would be about 2×10^{-8} M. This value is better than the value of 1×10^{-7} M dopamine reported recently for stopped-flow voltammetry using

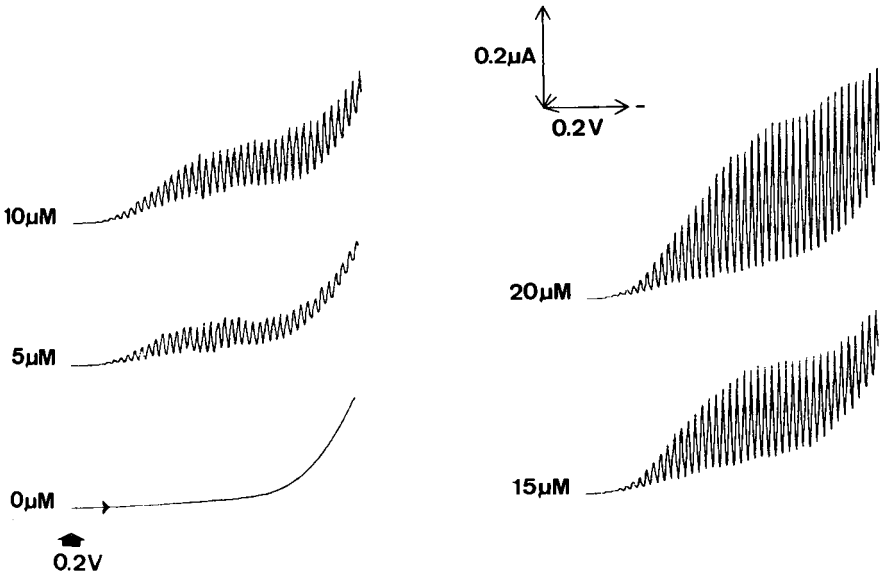

Fig. 4. Linear scan concentration-modulated voltammograms for $K_3Fe(CN)_6$ at micromolar concentrations. Conditions as in Fig. 2, except: flow rate, 2.0 ml min^{-1}; cycling time, 4 s sample, 6 s blank; all scans start at +0.2 V.

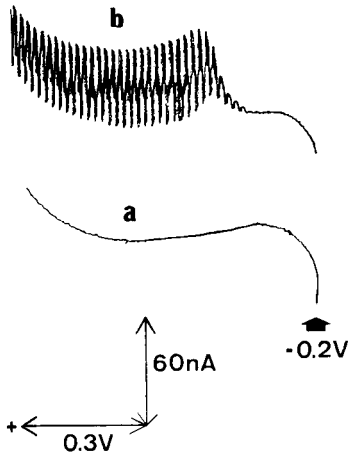

Fig. 5. Concentration-modulated voltammograms for 0.75 μM dopamine (b) and the supporting electrolyte (phosphate buffer, pH 7.4) solution (a). Conditions as in Fig. 2.

the same detector [7]. The detectability obtained with concentration-modulated voltammetry is similar to that of differential pulse polarography at the dropping mercury electrode. The sensitivity (44 nA for 0.75 μM dopamine), is in good agreement with the slope of the calibration curve (58.5 nA μM^{-1}) discussed earlier.

A series of seven successive concentration-modulated voltammetric measurements of 5 μM dopamine, performed over a total time of about 30 min, was used to evaluate the precision of the technique (conditions as in Fig. 3b). Reproducible waves, with similar potential regions, were obtained. The mean limiting current amplitude found was 324 nA with a range of 318—329 nA. The relative standard deviation was 1.4%.

Figure 6 illustrates a typical concentration-modulated voltammogram for a mixture of 5 μM ascorbic acid and homovanillic acid (b), along with the corresponding background current (a), and the differential pulse voltammetric response (c) recorded with continuous flow of the analyte solution. The response for concentration-modulated voltammetry shows two well-defined and reproducible waves, with half-wave potentials of +0.03 V (ascorbic acid) and +0.32 V (homovanillic acid). The ascorbic acid wave is about 70 mV more anodic than that shown in Fig. 2(c); this shift can be attributed to the aging

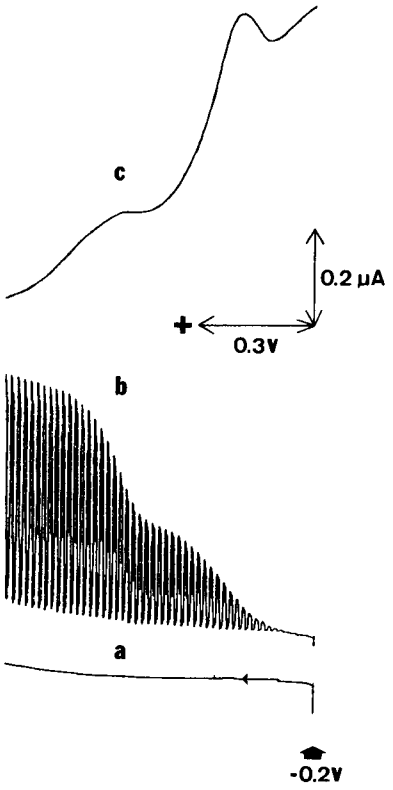

Fig. 6. Concentration-modulated (b) and differential pulse (c) voltammograms for a mixture of 5 μM ascorbic acid and homovanillic acid in 0.1 M phosphate buffer (pH 7.4). Voltammogram (a) shows the concentration-modulated background current. Scan rate, 0.1 V min^{-1}; flow rate, 2.5 ml min^{-1}; alternate-solution switching frequency, 5 s; potential pulse amplitude, 50 mV.

effect of the electrode via the participation of surface functional groups in the oxidation of ascorbic acid [15]. The mixture data were obtained on a fresh, polished surface, while those of Fig. 2(c) were obtained after two weeks of operation. The differential pulse voltammogram yields poorly defined peaks which cannot be quantified conveniently. Another mixture of 15 μM chlorpromazine and 10 μM dopamine gave two defined and separated waves by concentration-modulated voltammetry, with half-wave potentials of +0.04 V (dopamine) and +0.65 V (chlorpromazine). These data are a good example of the advantages of concentration-modulated voltammetry for measuring mixtures of electroactive species at very low concentration levels.

This work was supported by the Society for Analytical Chemists of Pittsburgh and by the Research Center of the College of Arts and Sciences, New Mexico State University.

REFERENCES

1 R. J. Rucki, Talanta, 27 (1980) 147.
2 D. A. Roston and P. T. Kissinger, Anal. Chem., 53 (1981) 1695.
3 C. L. Blank, J. Chromatogr., 117 (1976) 35.
4 P. T. Kissinger, Anal. Chem., 49 (1977) 447A.
5 J. Wang, E. Ouziel, C. Yarnitzky and M. Ariel, Anal. Chim. Acta, 102 (1978) 99.
6 W. J. Blaedel and Z. Yim, Anal. Chem., 52 (1980) 564.
7 J. Wang and H. D. Dewald, Anal. Chim. Acta, 136 (1982) 77.
8 I. Shain and K. J. Martin, Anal. Chem., 30 (1958) 1808.
9 K. Brunt and C. H. P. Bruins, J. Chromatogr., 161 (1978) 310.
10 W. J. Blaedel, C. L. Olson and L. R. Sharma, Anal. Chem., 35 (1963) 2100.
11 J. Wang, Anal. Chem., 53 (1981) 2280.
12 J. Ruzicka and E. H. Hansen, Anal. Chim. Acta, 99 (1978) 37.
13 J. S. Craven and D. E. Clouser, Paper 408, 30th Pittsburgh Conference on Analytical and Applied Spectroscopy, Cleveland, OH, 1979.
14 C. Yarnitzky and E. Ouziel, Anal. Chem., 48 (1976) 2024.
15 F. G. Gonon, C. M. Fombarlet, M. J. Buda and J. F. Pujol, Anal. Chem., 53 (1981) 1386.

Analytica Chimica Acta, 142 (1982) 249—257
Elsevier Scientific Publishing Company, Amsterdam — Printed in The Netherlands

SIMULTANEOUS DETERMINATIONS OF A MONOFLUORINATED IMIDAZO[1, 5-a][1, 4]BENZODIAZEPINE AND THE CORRESPONDING BENZOPHENONE AS A FUNCTION OF pH AND IN AQUEOUS FORMULATIONS BY ^{19}F NUCLEAR MAGNETIC RESONANCE SPECTROMETRY

PRANAB K. BHATTACHARYYA* and ANNE GRANT

Hoffmann-La Roche Inc., Pharmaceutical Research Products Section, Quality Control Department, Nutley, NJ 07110 (U.S.A.)

(Received 9th April 1982)

SUMMARY

8-Chloro-6-(2-fluorophenyl)-1-methyl-4H-imidazo[1, 5-a][1, 4]benzodiazepine (called "midazolam") exists in equilibrium with the corresponding benzophenone (the "open-Mng form"). The two compounds were determined simultaneously as a function of pH with ^{19}F-n.m.r. spectrometry. In a unique application of ^{19}F-n.m.r. spectrometry, the compounds are determined simultaneously in aqueous dosage forms without the need for sample preparation. The optimum signal-to-noise ratio for the major compound for the lowest concentration of sample used ($\approx$ 1 mg ml^{-1}) was 200:1 for 3000 scans. This was obtained by partial proton decoupling and exponential multiplication of the free induction decay with a line-broadening parameter of 12 Hz. Quantitative results are presented with a standard deviation of $< 2.0\%$ in the mean ratio of the two compounds. The results are also compared with those obtained by the spectrophotometric fluorescamine method. Advantages of the ^{19}F-n.m.r. technique in this determination are discussed.

In certain analytical applications, ^{19}F-n.m.r. spectroscopy possesses several advantages over proton n.m.r. spectroscopy. Its chemical shift scale is much larger and the magnitude of chemical shifts is determined almost entirely by the behavior of valence electrons. Because most compounds contain only a few fluorine atoms, there are fewer lines in the ^{19}F-n.m.r. spectrum than in the ^{1}H-n.m.r. spectrum. Consequently, the ^{19}F-n.m.r. technique is ideally suitable for analytical investigation of reactions involving fluorinated compounds in aqueous media and protonated solvents which lack fluorine resonances. This technique can also be applied to the determination of fluorinated compounds in formulated dosage forms. The liquid formulations can practically be scanned without prior treatment. In the case of solid dosage forms, the fluorinated ingredients of interest need only to be dissolved in appropriate solvents without concern for interfering components from the matrix which normally lack resonances in ^{19}F-n.m.r.

The ^{19}F-n.m.r. technique is applied here to quantify 8-chloro-6-(2-fluorophenyl)-1-methyl-4H-imidazo[1, 5-a][1, 4]benzodiazepine (I), called mid-

0003-2670/82/0000-0000/$02.75

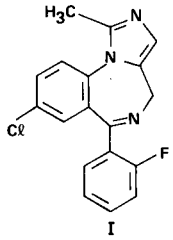

I

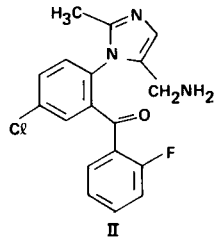

II

azolam and the corresponding benzophenone (II) in the reversible reaction I⇌II in aqueous media as a function of pH and in aqueous formulations. Only a few previous studies [1—8] have dealt with quantitative ^{19}F-n.m.r. Even in these few cases, compounds in the bulk form only were determined. The present investigation seems to be the first quantitative application of ^{19}F-n.m.r. spectrometry [9] in which compounds are measured in formulated samples without prior sample preparation such as extraction of the compounds.

EXPERIMENTAL

Instrumentation and methods

A Varian XL-100/Nicolet TT-100 n.m.r. spectrometer with deuterium lock was used. For quantitative work, each sample was put in a 12-mm o.d. tube, in which a 5-mm o.d. tube (longer than the 12-mm o.d. tube) containing D_2O for magnet lock was placed concentrically by means of a teflon plug. A 1.0-mm o.d. tube (longer than the 5-mm o.d. tube) containing 0.5% trifluoroacetic acid in water for external referencing of chemical shifts was also positioned concentrically within the 5-mm tube by means of a teflon plug of appropriate dimension.

The following experimental parameters were selected: the pulse width was 2 μs (flip angle $\approx 30°$); acquisition times were 0.82 s for determination of chemical shifts and ^{19}F—^{1}H coupling constants where scans of 5000 Hz sweep width acquired in 8K blocks of computer memory were zero-filled to 32K, and 0.51 s for quantitative studies where scans of 2000 Hz sweep width acquired in 2K blocks were zero-filled to 8K. Quadrature phase detection was employed throughout. To quantify the smallest concentrations of sample ($\approx$1 mg ml^{-1}), 3000 scans were acquired. The fluorine atoms in compounds I and II occupy the same position in the aromatic system; consequently, the spin-lattice relaxation times (T_1) of the fluorine nuclei in both compounds will be similar in magnitude. This was also proved indirectly by means of slower acquisitions in larger (up to 8K) blocks, when the ratio of the signal-to-noise ratios of I and II still maintained its proportionality to the square root of the number of scans. Partial proton decoupling was used to obtain higher sensitivity which mainly resulted from the partial collapse of the spin—spin multiplets. The theoretical maximum nuclear Overhauser enhancement [10] ($\approx 1 + \gamma_F/2\gamma_H$ where γ_F and γ_H are the fluorine and proton gyromagnetic ratios) is 1.5. For practical reasons,

higher decoupling power for complete saturation of proton resonances was not feasible. Partial proton decoupling resulted in a nuclear Overhauser enhancement of about 1.2. Optimum sensitivity was found when partial proton decoupling (119 dB at the decoupler offset 59535 Hz) and exponential multiplication of the free induction decay with a line broadening parameter of 12 Hz were employed. The signal-to-noise ratio of the smallest concentration of sample used ($\approx$1 mg ml^{-1}) after 3000 acquisitions and exponential multiplication of the free induction decay with 12 Hz was 160:1 without partial proton decoupling, and 200:1 with partial proton decoupling. The operational technique of resolution and sensitivity enhancement necessary in characterization and quantitative determination is illustrated in Fig. 1. It is shown that, when resolution enhancement is done, the multiplet patterns for I and II are graphically distinguishable.

Characterization

The chemical shifts and fluorine—proton spin—spin coupling constants in various solvents are listed in Table 1. The coupling constants were obtained by fitting spectra with the Nicolet 1180 ITRCAL simulation program (which

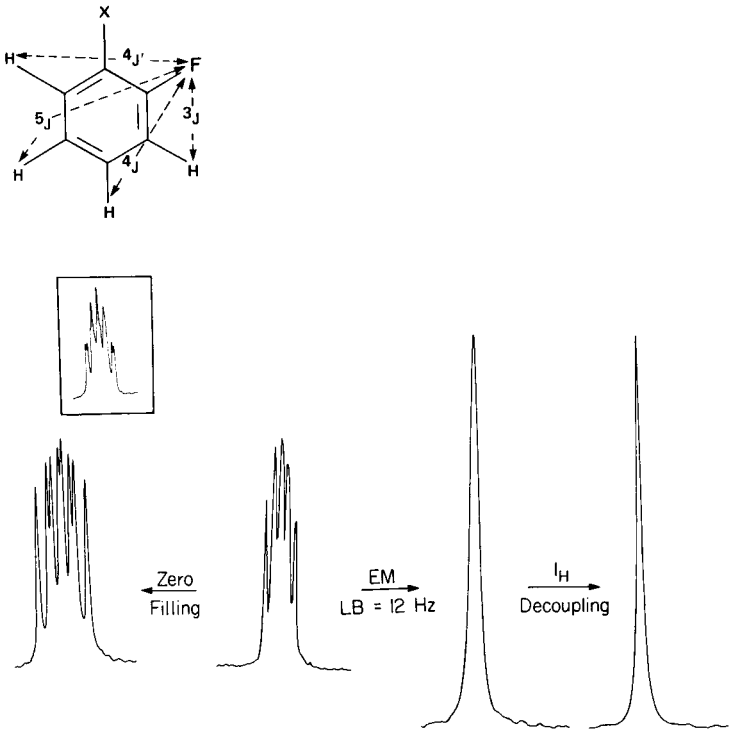

Fig. 1. Typical experimental operations for resolution and sensitivity enhancements on the resonance from compound I. The distinguishable multiplet pattern for compound II is shown at the top.

TABLE 1

The ^{19}F-n.m.r chemical shifts and coupling constants[a]

Solvent	Compound	δ (ppm)	Coupling constants (Hz)			
			^3J	$^4J'$	^4J	^5J
Chloroform-d	I[b]	−36.90	10.4	7.3	5.2	0
Methanol-d_4	I	−40.48	10.7	7.3	5.4	0
	IA	−39.90	10.8	7.3	5.3	0
	IIB	−35.59	10.8	7.0	5.5	−1.5
Methyl sulfoxide-d_6	I	−38.67	10.7	6.5	5.5	0
	IA	−36.98	10.3	7.5	5.9	0
	IIB	−34.88	11.1	6.7	5.8	−0.9
D_2O	IA	−38.98	11.1	7.3	5.3	0
	IIB	−35.06	11.3	6.6	5.9	−0.7

[a]The compounds IA and IIB are the maleate salt of I and the dihydrochloride salt of II, respectively. The chemical shifts are referenced to 0.5% trifluoracetic acid in water in an external capillary and uncorrected for bulk magnetic susceptibility differences, and are more accurate than ±0.01 ppm. The coupling constants are accurate to ±0.3 Hz or better. Their relative signs are derived from results given in ref. 11. The pD's (uncorrected) of samples IA and IIB dissolved in D_2O were 3.6 and 1.5, respectively. The free base II was not available and, therefore, the experiments were performed with IIB. 1 ppm = 94.1 Hz. Negative chemical shifts refer to more positive shieldings. [b]Compounds IA and IIB were insoluble in chloroform-d, as was I in D_2O.

is an adaptation of the LAOCN3 n.m.r. spin simulation program). The following symbols were used for the coupling constants.

In addition to the different chemical shifts which probably arise from substantially different paramagnetic contributions to the ^{19}F shielding constants, the ^{19}F-n.m.r. resonances of the benzodiazepine (I) and the benzophenone (II) are characterized by unique multiplet patterns caused by unique fluorine—proton spin—spin couplings. Analyses of these patterns (see Fig. 1) reveal a number of interesting and analytically useful features. In I, the electronic effects influence the magnetic interaction between the fluorine nucleus and the *o*-, *m*-, and *p*-protons in such a manner that three different spin—spin coupling constants are observed, with the para coupling being negligible ($|5_J| < 0.4$ Hz). In II, the pattern is drastically different and four different spin—spin coupling constants appear, the para coupling being quite appreciable ($5_J \approx -1$ Hz). The values of 3_J are ca. 11 Hz in these cases, which are in agreement with the values reported [11] for unsubstituted and substituted monofluorobenzenes. The difference between the two meta-coupling constants in the case of compound I ($\Delta^4J \approx 2$ Hz) is almost twice the difference in the case of compound II ($\Delta^4J \approx 1$ Hz). The larger of the two meta-coupling constants is assigned to $4_{J'}$, based on a comparison of the magnitudes of the meta-coupling constants with that in monofluorobenzene [11] and the consideration of the effect of greater electron densities caused by substituents other than H at position X. Thus, the multiplet patterns serve

as an additional internal check on the identification of these compounds from their chemical shifts alone in analytical studies.

pH profile of equilibrium

One of the main objectives of this study was to determine the equilibrium, I⇌II, at different pH values. This is basically a reaction of type A in which the compounds containing carbon–nitrogen double bonds are hydrolyzed to the corresponding ketones via initial addition of water and elimination of a nitrogen moiety which may proceed through a number of steps [12], the order of which depends on acid or base catalysis.

The relative concentrations of compound II, which are obtained from ^{19}F-n.m.r. (58, 21, 10, and 5.5% at pH 2.3, 2.9, 3.2, and 3.6, respectively) and ^{1}H-n.m.r. (94.5, 70, 56, 45.5, and 21% at pD 1.2, 2.1, 2.3, 2.4, and 2.7, respectively), are plotted in Fig. 2 as a function of pH. The standard deviation of these results is less than 2%. The experimental results, which were obtained in mole % (as maleates), are expressed in weight % (as free bases) by calculation. For the sake of comparison, the pH profiles obtained spectrophotometrically by means of the fluorescamine reaction [13, 14] (in which only the primary amines are measured) are also shown. This technique is based on the reaction of fluorescamine with primary amines to form pyrrolinones which absorb strongly at 380—410 nm; in this range, fluorescamine

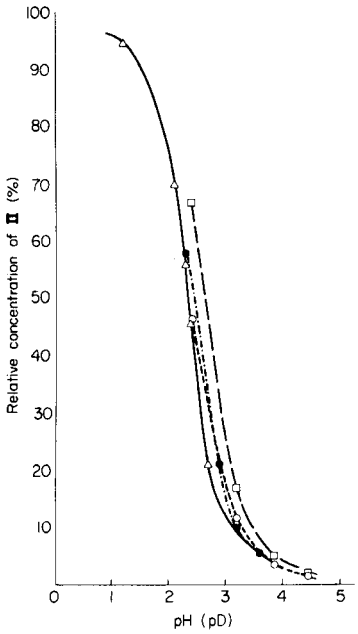

Fig. 2. The pH profiles of the equilibrium I⇌II, obtained by different methods. pD values are pH meter readings (uncorrected for deuterium). (•) ^{19}F-n.m.r.; (△) ^{1}H-n.m.r. (pD); (□) fluorescamine method, (○) fluorescamine method with a synthesized standard.

itself has practically no absorption and so does not interfere. The direct u.v. method was unsuitable because the spectra were influenced by the different degrees of protonation of the compounds in addition to the different chromophores. For the ^{19}F-n.m.r. and spectrophotometric fluorescamine determinations, ca. 10 mg of compound I as its maleate was dissolved in 1 ml of isopropanol and the solution was made up to 10 ml with an aqueous buffer of the desired pH. For the ^{1}H-n.m.r. determination, ca. 10 mg of the compound was dissolved in 5 ml of buffer prepared in D_2O, following procedures for aqueous buffers listed in the U.S.P. XX-NF XV (1980).

Figure 2 shows that, while the relative amounts of compound II obtained by ^{19}F-n.m.r. and ^{1}H-n.m.r. are similar, they are both lower than those measured in the spectrophotometric method (67, 17, 5, and 2% at pH 2.38, 3.18, 3.85, and 4.45, respectively). In this method, the sample, which contained both I and II, at the desired pH was treated with fluorescamine, and the absorbance at 382 nm was recorded. From Beer's Law, the percentage of compound II was obtained from the absorbance data of the chromophore formed, in situ, by reacting compound II with fluorescamine at pH 8. When the spectrophotometric measurements were repeated later with the newly-synthesized chromophore that formed in the fluorescamine reaction, the results (46, 11.5, 3.5, and 1.5% at pH 2.4, 3.2, 3.85, and 4.45, respectively) were in good agreement with the n.m.r. data (Fig. 2). The ^{1}H-n.m.r. measurements were made in D_2O. The spectrophotometric method involves complex formation between fluorescamine and compound II only at pH 8. Therefore, only the ^{19}F-n.m.r. technique provides an intact non-destructive determination of both compounds I and II simultaneously in aqueous medium at the desired pH.

^{19}F-n.m.r. technique for quantitative analysis of formulated solutions

The formulated samples (dosage forms) of interest all contained no more than a few mg ml^{-1} of compounds I and II in aqueous solution at a pH of ca. 3.2 (details of the various formulations are given in Table 2). Therefore, the practical impossibility of determining I and II in such a formulation by ^{1}H-n.m.r. is easy to realize because the tremendously strong signals originating from water and other protonated ingredients will totally override the peaks from I and II. In contrast, ^{19}F-n.m.r. spectrometry of such a sample shows the presence of midazolam or the benzodiazepine (I) and the open-ring or benzophenone form (II) in a quantitative manner (Fig. 3). Values of the relative amounts of I and II obtained by this technique in several formulated samples are listed in Table 2, in which the standard deviations of the results are also presented. The results obtained by the spectrophotometric method are also listed. In the latter method, the sample (at pH $\approx$3.2) is mixed rapidly with phosphate buffer pH 8.0 and treated immediately with fluorescamine reagent; the spectrum is recorded between 300 and 450 nm without delay, and the absorbance at 382 nm is measured to give the concentration of II. An examination of Table 2 shows that the

TABLE 2

^{19}F-n.m.r. determination of the I:II ratio in formulations

Lot number[a]	Base equiv. as I (mg ml^{-1})	pH	I:II (% w/w)	
			^{19}F-n.m.r.[b]	SFM[c]
C-100756	2.5	3.2	85.8:14.2	74.4:25.6
C-110690	5	3.2	84.5:15.5	78.4:21.6
C-110700	5	3.2	84.3:15.7	78.8:21.2
C-110710	1	3.35	88.7:11.3	81.6:18.4

[a]Lot C-100756, which was prepared from the maleate salt of I, also contained the following ingredients in ca. 1 ml of water: benzyl alcohol, benzyl chloride, disodium—edetate, sodium chloride, tartaric acid, and sodium hydroxide solution (for pH adjustment). The ingredients for the remaining three lots in ca. 1 ml of water were: free base I, benzyl alcohol, disodium—edetate, sodium chloride and HCl solution (for pH adjustment). [b]The standard deviation obtained from four measurements of the mean ratio was $<2\%$, which leads to a standard deviation of <0.3 in the numbers listed for both I and II (or, expressed otherwise, $<0.3\%$ for I and $<1.8\%$ for II). [c]The spectrophotometric fluorescamine method which can determine II only. These results are quoted from the Certificates of Analyses for these lots.

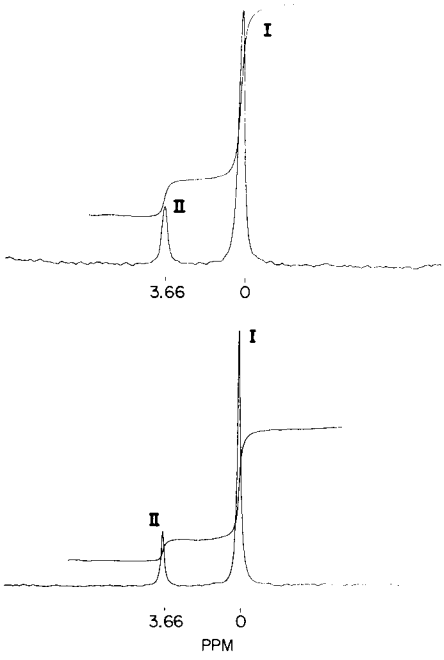

Fig. 3. Typical ^{19}F-n.m.r. resonances of compounds I and II in the formulated dosage forms (Lot C-110700), employing sensitivity enhancement operations, with a line-broadening parameter of 12 Hz. The position of I is arbitrarily marked as "0" ppm to show the relative chemical shift difference. The lower spectra are also partially ^{1}H-decoupled.

spectrophotometric values for the relative amounts of II are consistently lower than the ^{19}F-n.m.r. results. In their work with different experimental formulations at pH 3.3 which were prepared with the maleate salt of I, Toome and Manhart (unpublished results) obtained a value of 15.4% for II, using the synthesized chromophore as a reference standard for calibration. This is fairly close to the expected n.m.r. result for similar formulations (see Table 2, Lot C-100756).

DISCUSSION

It is important to point out the advantages of the ^{19}F-n.m.r. technique in this investigation in which fluorinated compounds in bulk form and formulations were determined. In this method, both midazolam and the open-ring form (I and II) are observed simultaneously on the spectrum in contrast to the spectrophotometric method, by which only the open-ring form II is detected while the main compound of interest, I, is totally undetected because the fluorescamine reaction takes place only with primary amines. Because the half-life of II→I is ca. 10 min, the spectrophotometric determinations must be done quickly at pH ≈ 8 (i.e., not at the sample pH) because that is the optimum pH for the fluorescamine reaction [13, 14]. The equilibrium between I and II makes high-performance liquid chromatography and thin-layer chromatography unsuitable for intact determination of these compounds. Polarographic procedures were found to be unsuccessful by Toome and Manhart (unpublished work) at pH 3.3, because the half-wave reduction potentials of the C=N and C=O groups overlap. In contrast the ^{19}F-n.m.r. measurements are suitable for any medium, protic or aprotic, and at any sample pH. The n.m.r. method is both specific and non-destructive, and compounds in pure form are not required for use as reference standards in such determinations.

The ^{19}F-n.m.r. determination is simple and straightforward. One of its unusual features is that the n.m.r. results can be employed to calculate calibration factors for results obtained by another technique which is non-specific for the major compound of interest (such as the spectrophotometric fluorescamine method which cannot detect compound I directly). From Table 2, for example, the calibration factors for II are calculated to be 0.555, 0.718, 0.741, and 0.614, respectively, for the four lots listed therein. Such calibration factors can be used for subsequent routine spectrophotometric determinations in similar samples. As indicated by the results of essentially the two different kinds of formulations in Table 2, the presence of different compounds or solvents (organic or inorganic, protic or aprotic) in the matrix may affect the equilibrium between I and II through a variety of solute–solvent interactions. This emphasizes the necessity for a quantitative technique, such as the ^{19}F-n.m.r. method, which possesses the required stringent characteristics outlined above. The spectral resolution and the sensitivity of the technique permit accurate quantitation with a relative

standard deviation of less than 2% in the mean value of the ratio I:II, without sample preparation or extraction.

The authors are grateful to Dr. V. Toome and K. Manhart of the Chemical Research Department for permission to quote spectrophotometric results from their unpublished work.

REFERENCES

1 R. E. Naylor and S. W. Lasoski, J. Polym. Sci., 44 (1960) 1.
2 C. W. Wilson, J. Polym. Sci., A1 (1963) 1305.
3 C. W. Wilson and E. R. Santee, J. Polym. Sci., [C] 8 (1965) 97.
4 G. R. Leader, Anal. Chem., 42 (1970) 17.
5 F. F.-L. Ho, Anal. Chem., 45 (1973) 603; 46 (1974) 496.
6 M. V. Buchanan, D. F. Hillenbrand and J. W. Taylor, Anal. Chem., 49 (1977) 2146.
7 R. J. Warren, A. D. Bender, D. B. Staiger and J. E. Zerembo, Anal. Chem., 50 (1978) 426.
8 M.Ranganathan and P. Balaram, Org. Magn. Reson., 13 (1980) 220.
9 P. K. Bhattacharyya and A. Grant, Abstracts, Vol. 10, No. 2, p. 127, 29th National Meeting, APhA Academy of Pharmaceutical Sciences, San Antonio, TX, November 1980.
10 J. H. Noggle and R. E. Schirmer, The Nuclear Overhauser Effect, Chemical Applications, Academic Press, New York, 1971.
11 J. W. Emsley, L. Phillips and V. Wray, Fluorine Coupling Constants, Pergamon Press, New York, 1977.
12 J. March, Advanced Organic Chemistry, McGraw-Hill, New York, 1977.
13 V. Toome, S. Bernardo, K. Manhart and M. Weigele, Anal. Lett., 7 (1974) 437.
14 S. Bernardo, M. Weigele, V. Toome, K. Manhart, W. Leimgruber, P. Böhlen, S. Stein and S. Udenfriend, Arch. Biochem. Biophys., 163 (1974) 390.

Analytica Chimica Acta, 142 (1982) 259—268
Elsevier Scientific Publishing Company, Amsterdam — Printed in The Netherlands

A TOTAL DISSOLUTION METHOD FOR DETERMINATION OF THE α-EMITTING ISOTOPES OF URANIUM AND THORIUM IN DEEP-SEA SEDIMENTS

JOHN THOMSON

Institute of Oceanographic Sciences, Wormley, Godalming, Surrey GU8 5UB (Gt. Britain)

(Received 27th March 1982)

SUMMARY

A method is described for the determination of specific activities of the natural α-emitting isotopes of uranium and thorium in deep-sea marine sediments. Such information is needed primarily for estimation of sediment accumulation rates. The method is based on total dissolution of sample after fusion with potassium fluoride (to dissolve silicates) and with sodium/potassium pyrosulphate (to dissolve other refractory minerals and convert to the sulphate system). Uranium and thorium fractions are purified for electroplating by anion exchange, with elements naturally present used as carriers. Final determinations are made by α-spectrometry by means of isotopic tracers added at the outset of processing. Experience gained with different types of deep-sea sediment is discussed.

Methods based on the natural radionuclide ^{230}Th are important for determining sediment accumulation rates in the deep sea [1, 2]. This results from the production of ^{230}Th [termed authigenic ^{230}Th or ^{230}Th(excess)] from ^{234}U in the oceanic water column, subsequent removal from the water column by settling material, and incorporation into the sediments. Mean accumulation rates are generally estimated from the decrease of ^{230}Th(excess) specific activity with depth; the half-life is known (75 200 years) and depth is treated as directly proportional to time. In the sediments, the ^{230}Th(excess) is diluted to an extent dependent on the accumulation rate and sediment composition by ^{230}Th contained primarily in terrigenous detrital material. The unequivocal method for determining ^{230}Th(excess) is by α-spectrometry; the analytical procedure involves spiking with yield tracers, dissolution of the sediment sample, separation of uranium and thorium fractions and mounting the purified fractions for α-spectrometry.

On the practical side, a decision must be made whether to leach samples to obtain ^{230}Th(excess), with the assumption that detrital ^{230}Th is bound in mineral lattices and resistant to dissolution, or to dissolve samples completely, when the detrital ^{230}Th is assumed to be in radioactive equilibrium with its immediate progenitor ^{234}U. Both approaches have been employed, but leaching methods, as used for example by Goldberg and coworkers

0003-2670/82/0000-0000/$02.75

[3—6], have uncertainties of various kinds [7—9]. If the total dissolution method is chosen, a common technique is to decompose the sediment sample progressively with various acids, successively removing the residual refractory component for further more severe acid treatment. An example of this method is that described by Ku [10, 11]. Two drawbacks of this procedure are that, first, the tracer will be removed essentially quantitatively from the solid sample in the first liquid fraction separated, so that care must be taken not to lose material in subsequent steps before the sample has been dissolved completely and all liquid fractions recombined. Secondly, some silica can be released to solution (unless hydrofluoric acid is used at the earliest stage) and can cause later problems by precipitation.

A method has been reported for complete dissolution of soil and other environmental samples for α-emitter measurements, based on potassium fluoride and sodium/potassium pyrosulphate fusions, by Sill and coworkers [12, 13]. The principal advantage of this method is that it ensures that all the radionuclides are in solution and will behave subsequently according to their characteristic solution chemistries. This paper presents an adaptation of that fusion method for deep-sea sediments and couples it with a conventional separation scheme based on anion exchange followed by electroplating. Experience with the method gained on various types of marine samples encountered and variations for other purposes are discussed.

In the method developed, tracers (spikes) are added to the sample at the earliest possible stage, and the total sample and tracer are brought into solution simultaneously, after silicates have been destroyed by potassium fluoride fusion and the sample has been converted to a sulphate system by alkali pyrosulphate fusion. The iron and aluminium naturally present are used as carriers for uranium and thorium, first in a mixed hydroxide precipitate and subsequently in preparing uranium and thorium for final purification by anion exchange for electroplating. The purified fractions are never heated to dryness as they are essentially carrier-free.

EXPERIMENTAL

The fusion steps below must be done with care in an efficient fume hood. All glassware is recycled between uses by soaking in a warm surfactant solution for at least 8 h, followed by soaking in warm (1 + 1) nitric acid for a similar period, and finally rinsed with distilled water. Analytical-grade reagents and double-distilled water are used throughout. The calibrated $^{232}U/^{228}Th$ spike is an aged solution originally obtained from the Radiochemical Centre, Amersham.

Fusion and dissolution steps

Sediment samples are usually prepared here as dried powders by grinding in an agate swing mill. Around 1.5—2 g of sample is weighed accurately and transferred to a platinum crucible; a 40-ml crucible is most convenient but

a 25-ml size can be used. After the sample has been moistened with water, 10 ml of 7 M nitric acid is added, dropwise at first to control effervescence if the sediment contains carbonate. When reaction has ceased, an accurately measured aliquot of a calibrated $^{232}U/^{228}Th$ spike is added, sufficient to give about twice as much spike activity as the natural ^{238}U or ^{232}Th activities in the sample. The mixture is then heated to dryness, usually overnight, at a temperature low enough to prevent spattering. Potassium fluoride (7.5 g) is added, mixed in and crushed with the dried sediment by means of a glass rod. The platinum crucible is then heated with a high-temperature air blast burner to fuse silicates, the contents being swirled occasionally to include all the sediment in the fusion. If pieces of sediment cake are not attacked, the cooled fluoride cake is broken up and the fusion repeated.

After complete fusion, the cooled cake is converted to a sulphate system by addition of 10 ml of concentrated sulphuric acid with evolution of hydrogen fluoride and silicon tetrafluoride, all the precautions and gradual increase of temperature prescribed by Sill et al. [12] being observed. When the fluoride has reacted completely with the sulphuric acid, 7.5 g of sodium sulphate is added to the crucible and mixed in by swirling. The temperature is gradually increased over an air blast burner until a pyrosulphate fusion is achieved. This fusion mixture is usually dark red because of the iron present, but when fusion has been done properly the melt is transparent. During cooling, the crucible is rotated to quench the melt over the surface.

The cooled cake is broken up after adding water and added to a mixture of 20 ml of concentrated hydrochloric acid, 130 ml of water and 5 ml of 30% (w/v) hydrogen peroxide. The mixture is heated (to accelerate calcium sulphate dissolution) until it becomes clear. At this stage, the golden colour of the titanium/hydrogen peroxide complex disappears, and any carbon dioxide present is removed. The hydrated oxides (mainly iron and aluminium) are then precipitated from the hot solution by adding concentrated ammonia liquor to a final pH of 7—8. The solution is cooled and the precipitate centrifuged off; the supernatant liquid is decanted, and 25 ml of concentrated hydrochloric acid is added to dissolve the precipitate. This solution is transferred quantitatively, with 6 M hydrochloric acid washes, to an anion-exchange column (column I; BioRad AG 1-X8, 100—200 mesh; 8 cm × 1 cm preconditioned with 50 ml of 6 M hydrochloric acid), which is further washed with two 50-ml portions and one 25-ml portion of 6 M hydrochloric acid. Iron and uranium are retained [14] while aluminium and thorium pass through in the effluent. Uranium and iron are eluted with two 35-ml portions of 1 M hydrochloric acid.

Uranium purification

After evaporation to dryness, the column I eluate is redissolved in 25 ml of 8 M hydrochloric acid. Iron is then extracted into an equal volume of di-isopropyl ether. The acid phase is again heated to dryness and converted to the nitrate form by evaporation to dryness with two 5-ml aliquots of con-

centrated nitric acid. This residue is dissolved in 6 ml of 7 M nitric acid and added to a second anion-exchange column (column II; BioRad AG 1-X8, 100—200 mesh; 12 cm × 1 cm preconditioned with 50 ml of 7 M nitric acid). Residual iron is removed in the effluent when the column is washed with 20 ml of 7 M nitric acid added dropwise. The purified uranium fraction is eluted from the column with two 35-ml volumes of 1 M hydrochloric acid.

Thorium purification

The effluent from column I is evaporated to dryness, redissolved in 10 ml of concentrated nitric acid and again heated to dryness. This step is repeated with a second 10-ml portion of the acid. A 50-ml portion of 7 M nitric acid/0.25 M oxalic acid mixture is added and the mixture is stirred overnight to achieve dissolution [15]. The solution is passed through a third column (column III; BioRad AG 1-X8, 100—200 mesh; 8 cm × 1 cm, preconditioned with 50 ml of 7 M nitric acid), which is washed with a further 50 ml of 7 M nitric acid/0.25 M oxalic acid and then 50-ml and 25-ml portions of 7 M nitric acid [15]. The purified thorium fraction is eluted with two 35-ml portions of 6 M hydrochloric acid.

Electroplating of sources for α-spectrometry

The procedure is the same for both uranium and thorium fractions and is based on the work of Talvitie [16]. The cell with water-cooled holder was similar in design to that of Puphal and Olsen [17] except that it was made from PTFE (10 cm high, 1.5-cm i.d.) and was used with a non-rotating platinum anode rod (15 cm × 1.5 mm, with the end 4 cm bent into a flat spiral) fixed through the PTFE plug cap. Polished stainless steel planchettes (2.5-cm diameter; Type BS 25 FS, Nuclear Supplies, Mirfield, Gt. Britain) are employed, the deposit being localised to a 1.5-cm diameter by the cell holder collar forcing a seal between the planchette and the smooth base face of the cell. Plating is done at a constant current of 1 A for 3 h from a regulated power supply (Model LT 30/2, Farnell Instruments, Wetherby, Gt. Britain), at a temperature of 60 ± 5°C. Between uses the cells and anodes are cleaned by boiling in concentrated nitric acid [13], and then rinsed, reassembled and stored full of distilled water.

An aliquot (1 ml) of sulphuric acid (1 + 1) is added to the eluate from columns II or III, and the solution is evaporated until sulphur trioxide fumes are evolved. Concentrated nitric acid (3 ml) is then added to destroy any organic residues from the ion-exchange resin, and the mixture is again heated to sulphur trioxide fumes. Water (6 ml) is added to the cooled residue and the sample is stored in this condition until just before electroplating. Then, bromothymol blue indicator is added, and the pH is adjusted to 2.2 by blowing ammonia over the surface (from the headspace over ammonia liquor in a polyethylene wash bottle). The solution is transferred immediately to the electroplating cell with about four 1-ml washes of water. The anode is inserted in the cell and the current switched on, the temperature being main-

tained around 60° C. After 3 h, 1.5 ml of ammonia liquor is added and the current is maintained for a further 2 min. The anode is then removed with the current still flowing, the cell assembly cooled, the plating solution discarded, and then the planchette is removed, thoroughly rinsed with water and acetone, and finally heated for 5 min on a hotplate at 250° C to fix the deposited radionuclides [16, 18].

Total tracer yields for both uranium and thorium through the entire chemical process are 60—80%, and are generally similar for both elements in a single analysis.

α-Spectrometry

The 4-channel spectrometer used was an Ortec system (E.G. & G. Instruments) comprising 450-mm^2 silicon surface barrier detectors, 142B preamplifiers and 471 amplifiers fed through a 577S mixer router to the quarters of a 1024-channel 6240B multichannel analyser. Electroplated sources are generally counted for 1—2 days, to collect at least 1000 counts in each peak of interest. The resolution over this period is 60—80 keV at f.w.h.m., adequate for separation of the peaks (^{238}U, ^{234}U and ^{232}U in the uranium mounts; ^{232}Th, ^{230}Th, ^{228}Th and ingrown ^{224}Ra in the thorium mounts) with a minimum source-to-detector clearance. The ultimate resolution obtainable from the sources is better if a larger source-to-detector distance is used, but at the cost of detection efficiency [19].

RESULTS AND DISCUSSION

Most experience with the above method has been gained with Atlantic red clay sediments, and for such material the method is satisfactory. Table 1 lists data obtained for one red clay box core, and the derived sediment ^{230}Th-(excess) accumulation rate is illustrated on Fig. 1. From start to completion, the data for each section were obtained in six working days, but sets of samples can be processed simultaneously. In practice, the limiting factor is counter availability.

Other sediment types, rich in carbonate and organic matter, require small variations of the procedure, as discussed below, together with variations for determination of ^{231}Pa by a proxy method, and for phosphorite samples.

Sediments of high carbonate content or high organic content

While the presence of about 40% of calcium carbonate does not interfere seriously with the method, when the calcium carbonate content exceeds 50% ('calcareous ooze' samples), the high proportion of calcium sulphate at the pyrosulphate step makes it difficult to achieve a clear pyrosulphate fusion. For such samples, the solution in dilute hydrochloric acid was generally opalescent. Satisfactory results were obtained by repeating the mixed hydrated oxide precipitation; opalescence was not found in the second dilute hydrochloric acid solution. Subsequent steps remained unaltered.

TABLE 1

Data from a red clay box core and from NBS SRM 120b[a]

Depth (cm)	U (ppm)	Th (ppm)	Th/U	$\frac{^{234}U^{b}}{^{238}U}$	$\frac{^{230}Th^{b}}{^{232}Th}$	^{230}Th (dpm g^{-1})	^{234}U (dpm g^{-1})	^{230}Th(excess) (dpm g^{-1})	^{231}Pa(excess) (dpm g^{-1})
10164/5BX									
0—1	2.59 ± 0.09	17.6 ± 0.6	6.8 ± 0.3	0.90 ± 0.04	6.66 ± 0.13	28.4 ± 0.8	1.73 ± 0.06	26.7 ± 0.8	1.07 ± 0.11
10—12	2.54 ± 0.07	14.6 ± 0.8	5.7 ± 0.4	0.97 ± 0.03	6.61 ± 0.21	23.5 ± 1.1	1.84 ± 0.05	21.7 ± 1.1	0.76 ± 0.08
20—22	2.37 ± 0.07	14.8 ± 0.8	6.2 ± 0.4	0.93 ± 0.03	5.05 ± 0.16	18.2 ± 0.9	1.65 ± 0.05	16.6 ± 0.9	0.44 ± 0.06
30—32	2.60 ± 0.06	17.1 ± 0.4	6.6 ± 0.2	0.88 ± 0.03	3.95 ± 0.07	16.4 ± 0.4	1.71 ± 0.04	14.7 ± 0.4	0.36 ± 0.08
36—38	2.57 ± 0.07	18.4 ± 0.6	7.2 ± 0.3	0.91 ± 0.03	3.42 ± 0.06	15.3 ± 0.5	1.76 ± 0.05	13.5 ± 0.5	0.14 ± 0.05
NBS 120b			U/Th					$\frac{^{230}Th^{b}}{^{234}U}$	$\frac{^{231}Pa^{b}}{^{235}U}$
—	132 ± 2	8.8 ± 0.4	15.1 ± 0.7	1.04 ± 0.01	48 ± 2	101 ± 1	102 ± 2	0.99 ± 0.02	0.99 ± 0.05
—	132 ± 2	9.3 ± 0.4	14.2 ± 0.6	1.05 ± 0.01	46 ± 2	102 ± 1	103 ± 2	0.99 ± 0.02	0.93 ± 0.07

[a]Quoted uncertainties are based on 1σ counting uncertainties only. [b]Activity ratio.

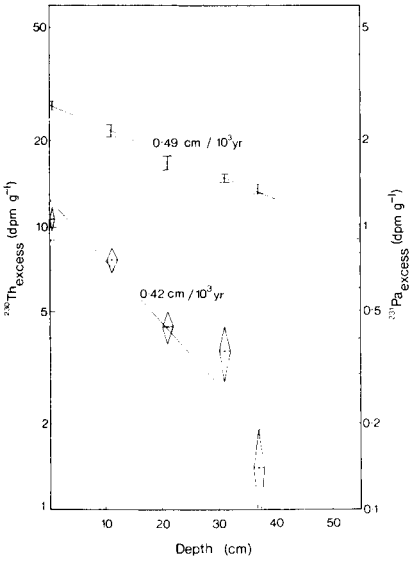

Fig. 1. Plot of the ^{230}Th(excess) (top line, data represented by bars) and ^{231}Pa(excess) (bottom line, data represented by diamonds) data listed on Table 1, together with derived sediment accumulation rates. The sample (10164/5BX) is a red clay box core taken from the Nares Abyssal Plain (western Atlantic Ocean) at 26° 05'N 60° 21'W, 5550 m depth.

A high organic content (e.g., sapropels with >2% organic carbon) is generally associated with a reduced sediment, which can attack platinum ware. This potential problem was overcome by oxidising the dried sediment (following treatment with nitric acid and spike addition) at 450° C in a muffle furnace for 15 min. The oxidised sediment was then re-introduced to the routine scheme at the sodium fluoride fusion step. Data from Eastern Mediterranean cores containing sapropel sections have been reported which were obtained by this technique [20].

Variation for determination of ^{231}Pa via ^{227}Th

In the (4 + 3) natural series, a geochemical situation occurs similar to that for ^{230}Th in the (4 + 2) series. In this case, ^{231}Pa is produced in the water column from its parent ^{235}U, and is subsequently removed from seawater to the sediments on a short timescale [1, 2, 21]. Thus ^{231}Pa may be used analogously to ^{230}Th(excess) to determine accumulation rates, but with the practical drawback that it is present at lower levels of activity. The theoretical activity ratio ^{230}Th/^{231}Pa from production by uranium in the water column is 10.6, although higher values are usual in core tops for various reasons [1, 2, 21]. Although the ^{231}Pa(excess) method has been demonstrated to provide useful corrobration to ^{230}Th(excess) accumulation rates in important cases [22], its use has been restricted by the greater technical demands of ^{231}Pa measurements. Recently, it has been shown that ^{227}Th is a

satisfactory proxy indicator of ^{231}Pa [23, 24], and the present method may be adapted readily to provide such data.

^{227}Th has a complex α-spectrum with energies between 5.03 and 6.04 MeV [25]. In this energy range, the ^{228}Th daughters ^{224}Ra and ^{212}Bi have distinct peaks, so that there is advantage in the use of unspiked samples to minimise counting uncertainties from contributions of ^{228}Th daughters in the α-spectra. An absolute measure for ^{227}Th may be derived from the ^{230}Th value determined in the parallel spiked sample run in the usual manner.

The unspiked sample is fused as previously described, but the hydrated oxide precipitate formed from the sample solution is dissolved to 50 ml of 7 M nitric acid/0.25 M oxalic acid solution. This solution is immediately presented to Column III, which is washed, eluted and electroplated as previously described. This procedure is effective in removing all α-emitting contaminants except ^{210}Po (5.30-MeV α-particle), some evidence of which is seen in the final spectrum. Counting is started immediately after electroplating, and continued for not more than 10^5 s (27.8 h) to minimise the effects of ingrowth of ^{228}Th daughters.

Only the higher energy peak (5.89—6.04 MeV, 57% total emissions) is integrated, and corrected for background, a ^{212}Bi contribution [23, 24] and decay from the start of the anion column separation. This allows calculation of the ^{227}Th/^{230}Th activity ratio in the spectrum, and hence the ^{227}Th specific activity from the ^{230}Th specific activity obtained from the complementary spiked analysis of the same sample. With the assumption that ^{227}Th and ^{231}Pa are at secular equilibrium [23, 24], ^{231}Pa(excess) is then calculated by subtraction of the ^{235}U specific activity (which is 0.046 times the ^{238}U specific activity).

Table 1 lists ^{231}Pa(excess) data for core 10164/5BX obtained in this way. These are plotted on Fig. 1 to derive an accumulation rate corroborating the ^{230}Th(excess) data.

Variation for phosphorites

Although not strictly marine sediments themselves, phosphorite concretions are believed to be forming at present in the shelf sediments of a few areas of the world ocean. These areas underlie the highly productive waters of upwelling areas [26]. Because phosphorites (strictly, carbonate fluorapatite) incorporate uranium at relatively high levels (50—200 ppm with an average of 60—80 ppm [27]), an estimate of age up to a few hundred thousand years may be made from ingrowth of ^{230}Th towards radioactive equilibrium with this uranium over time. Such a procedure was first introduced for phosphorites by Burnett and Veeh [28] and work to date has been reviewed recently [29]. Despite the geological youth of some phosphorites, they can be considerably indurated and resistant to complete dissolution. A variant of the present method was developed to achieve total dissolution.

Around 0.5 g of powdered sample is generally sufficient for such material, and may be fused in the usual fashion with a flux—sample ratio of 10:1; 5 g

of potassium fluoride, 7.5 ml of sulphuric acid and 5 g of sodium sulphate are used through the fusion procedures. Since complexation with phosphate can interfere with the anion-exchange procedures for thorium, a hydroxide precipitation is made at pH 3.5 from the solution in dilute hydrochloric acid to leave the bulk of phosphate in solution [30]. This precipitate contains most of the thorium, but only a small fraction of the uranium: the supernatant liquid is therefore retained. The precipitate is dissolved to 6 M hydrochloric acid solution and passed through Column I with a single 50-ml wash of 6 M hydrochloric acid, and the effluent is processed in the normal way for further purification of the thorium fraction.

The fraction of uranium (and iron) included in the first precipitation at pH 3.5 is eluted from Column I and recombined with the original supernatant solution. A second hydroxide precipitation is made in this solution at pH 7, and this second precipitate is processed in the normal way through Columns I and II for purification of the uranium fraction.

Table 1 illustrates data for the NBS SRM 120b (Phosphate Rock, Florida) obtained with this method. The quoted $^{231}Pa/^{235}U$ data were obtained from unspiked duplicates by a combination of this fusion procedure and the proxy ^{231}Pa method described above.

The author thanks Dr. C. W. Sill for valuable observations on the draft manuscript.

REFERENCES

1 E. D. Goldberg and K. W. Bruland, in E. D. Goldberg (Ed.), The Sea, Vol. 5, Wiley—Interscience, New York, 1974, pp. 451—489.
2 T. L. Ku, Ann. Rev. Earth Planet. Sci., 4 (1976) 347.
3 E. D. Goldberg and M. Koide, Science, 128 (1958) 1003.
4 E. D. Goldberg and M. Koide, Geochim. Cosmochim. Acta, 26 (1962) 417.
5 E. D. Goldberg, M. Koide and J. J. Griffin, in H. Craig, S. L. Miller and G. J. Wasserburg (Eds.), Isotopic and Cosmic Chemistry, North-Holland, Amsterdam, 1964, pp. 211—232.
6 E. D. Goldberg, Earth Planet. Sci. Lett., 4 (1968) 17.
7 T. L. Ku, W. S. Broecker and N. Opdyke, Earth Planet. Sci. Lett., 4 (1968) 1.
8 P. S. Antal, Limnol. Oceanogr., 11 (1966) 278.
9 M. Bernat and C. J. Allegre, Earth Planet. Sci. Lett., 21 (1974) 310.
10 T. L. Ku, J. Geophys. Res., 70 (1965) 3457.
11 T. L. Ku, Ph.D. Thesis, Columbia University, New York, 1966.
12 C. W. Sill, K. W. Puphal and F. D. Hindman, Anal. Chem., 46 (1974) 1725.
13 C. W. Sill, Accuracy in trace analysis: sampling, sample handling and analysis, Natl. Bur. Stand. (U.S.), Spec. Publ., 422 (1976) 463; Anal. Chem., 49 (1977) 618 and 50 (1978) 1559.
14 K. A. Kraus, G. E. Moore and F. Nelson, J. Am. Chem. Soc., 78 (1956) 2692.
15 J. Korkisch, I. Steffan, G. Arrhenius, M. Fisk and J. Frazer, Anal. Chim. Acta, 90 (1977) 151.
16 N. A. Talvitie, Anal. Chem., 44 (1972) 280.
17 K. W. Puphal and D. R. Olsen, Anal. Chem., 44 (1972) 284.
18 C. W. Sill and D. G. Olson, Anal. Chem., 42 (1970) 1596.
19 D. R. Mann, H. D. Livingston and A. G. Gordon, Woods Hole Oceanogr. Inst. Tech. Rep. WHOI-75-26 (1975), 17 pp.

20 J. Thomson, Sediment. Geol., 32 (1982) 99.
21 R. F. Anderson, Ph.D. Thesis, Woods Hole Oceanogr. Inst., Woods Hole, 1981.
22 W. S. Broecker and J. van Donk, Rev. Geophys. Space Phys., 8 (1970) 169.
23 A. Mangini and C. Sonntag, Earth Planet. Sci. Lett., 37 (1977) 251.
24 D. J. DeMaster, Ph.D. Thesis, Yale University, New Haven, 1979.
25 C. M. Lederer and V. S. Shirley (Eds.), Table of Isotopes, 7th edn., Wiley—Interscience, New York, 1978.
26 G. N. Baturin and P. L. Bezrukov, Mar. Geol., 31 (1979) 317.
27 J. B. Cathcart, U.S. Geol. Surv. Prof. Pap. 988-A, B (1978) A1—A6.
28 W. C. Burnett and H. H. Veeh, Geochim. Cosmochim. Acta, 41 (1977) 755.
29 H. H. Veeh and W. C. Burnett, in M. Ivanovich and R. S. Harmon (Eds.), Uranium-series Disequilibrium: Application to Environmental Problems in the Earth Sciences, Oxford University Press, 1982.
30 T. Y. Toribara and L. Koval, Talanta, 14 (1967) 403.

Analytica Chimica Acta, 142 (1982) 269—275
Elsevier Scientific Publishing Company, Amsterdam — Printed in The Netherlands

DETERMINATION OF ARSENIC AND ANTIMONY IN GEOLOGICAL MATERIALS AND NATURAL WATERS BY COPRECIPITATION WITH SELENIUM AND NEUTRON ACTIVATION—γ-SPECTROMETRY

C. M. ELSON*, J. MILLEY and A. CHATT

Trace Analysis Research Centre, Department of Chemistry, Dalhousie University, Halifax, N.S. B3H 4J1 (Canada)

(Received 1st June 1982)

SUMMARY

A simple, quantitative method for collecting arsenic and antimony from the digests of geological materials and from salt and fresh waters is described. The procedure involves the addition of selenium(IV) to an acidified sample followed by precipitation of selenium by tin(II) chloride. The precipitate is collected, dried, and irradiated. Arsenic and antimony are quantified directly from the activities of ^{76}As and ^{122}Sb, respectively. The method has detection limits of 9 ng As and 12 ng Sb per gram of rock or 500 g of water, and has been applied to eight new reference standards from the U.S. Geological Survey. Gold is quantitatively collected by the same procedure.

The levels of arsenic and antimony in geological materials vary from several micrograms per gram to less than 0.1 $\mu g\ g^{-1}$ [1]. In seawater, these same elements are present at or below a few nanograms per gram [2]. Antimony can be determined in rocks by instrumental or epithermal neutron activation methods at levels as low as 0.1 $\mu g\ g^{-1}$ [3, 4]. Arsenic, however, cannot be determined at comparable concentrations by these techniques because of interferences from nuclides such as ^{24}Na [5]. Hence, separations based on precipitation [5], distillation [6], or hydride generation [7] are often used. In the case of seawater, arsenic and antimony must be separated from the sample matrix prior to irradiation to minimize interferences from ^{24}Na, ^{82}Br, etc. Arsenic and antimony are also determined routinely by a combination of hydride generation or solvent extraction and atomic absorption spectrometry [8, 9]. A recent review lists detection limits for arsenic by various techniques including atomic absorption spectrometry and neutron activation [10]. At present, hydride generation appears to provide the most effective means of separating arsenic and antimony from sample matrices and, thereby, minimizing interferences.

---

*On sabbatical leave from Department of Chemistry, Saint Mary's University, Halifax, N.S. B3H 3C3, Canada.

A simple, quantitative, and selective procedure for separating and preconcentrating arsenic and antimony from complex matrices is described below. The method is based on coprecipitation of the two elements with selenium from strongly acidic solutions; it can be applied to rocks and natural waters. Tin(II) chloride is used to precipitate selenium, and arsenic and antimony are quantified directly in the precipitation. Gold is also collected quantitatively by this procedure.

EXPERIMENTAL

Reagents

All chemicals were reagent-grade unless otherwise specified. Glassware and teflon-ware were cleaned with warm (1+1) nitric acid. The rock reference standards were obtained from the United States Geological Survey; the River Sediment (SRM 1645) came from the U.S. National Bureau of Standards. Atomic absorption standard solutions (Ventron Corporation) containing 1000 ppm of the elements were used to prepare tracers, in the method of standard additions, and as comparators for quantitation. In the case of arsenic and gold, the standard solutions were checked against solutions prepared from weighed amounts of arsenic(III) oxide and gold wire, respectively. Tracers were prepared by evaporating aliquots of standard solution in 2/5-dram polyethylene vials under an infrared (i.r.) lamp, irradiating for 4 h, cooling for 24 h, redissolving in either $NaOH/HNO_3$ for arsenic and antimony or aqua regia for gold, and diluting to 100 ml. The addition of 1 ml of tracer solution to a sample yielded a tracer concentration comparable to the concentration of the analyte.

Solutions containing 0.5 mg Se ml^{-1} were prepared by dissolving 0.408 g of selenous acid in 500 ml of 9% hydrochloric acid. The reducing agent, tin(II) chloride, was prepared by dissolving 20 g of $SnCl_2 \cdot 2H_2O$ in 25 ml of warm hydrochloric acid and diluting to 100 ml.

Irradiation and counting

All irradiations were done in the Dalhousie University SLOWPOKE-2 reactor at a flux of 5×10^{11} n cm^{-2} s^{-1}. The composition, homogeneity, and reproducibility of the SLOWPOKE flux have been described [11]. Arsenic and antimony were determined as the nuclides ^{76}As ($t_{1/2}$ = 1.10 d, E_γ = 559.1 keV) and ^{122}Sb ($t_{1/2}$ = 2.74 d, E_γ = 564.0 keV) following 15—90-min irradiation and 20-h cooling periods. Gold was measured using the nuclide ^{198}Au ($t_{1/2}$ = 2.70 d, E_γ = 412 keV), after 4—6 h irradiation and 50—60 h cooling time. Sample activities were counted using a 60-cm^3 Canberra Ge(Li) detector with a full width at half maximum of 1.9 keV, a peak-to-Compton ratio of 35:1, and an efficiency of 9.5% (all measured at the 1332-keV photopeak of ^{60}Co) coupled to a Tracor Northern TN-11 pulse-height analyzer. The samples were counted at a distance of 5 mm from the top of the detector for 10—15 min. The nuclides were identified from their γ-ray spectra

and half-lives and were quantified by comparing net photopeak areas with those of standards.

Procedures

Sample preparation. Weigh 0.3—1.0-g samples of rocks and river sediment into teflon beakers and gently heat with 10 ml of concentrated nitric acid and 10 ml of 72% perchloric acid until the volume is reduced to 2—3 ml. Add a further 3 ml of perchloric acid and 10 ml of 40% hydrofluoric acid and continue heating until the volume again reaches 2—3 ml. Dissolve these residues in (1 + 3) hydrochloric acid with heating and transfer to 250-ml beakers. The final volume should be ca. 100 ml.

Acidify samples of fresh and salt waters on collection with 5 ml of Ultrex hydrochloric acid (Baker Chemicals) per 500 ml. Filter through 0.4-μm filters (Nuclepore) and store in polyethylene bottles. Weigh 0.2—0.5 kg of water sample into 600-ml or 1-l beakers and add 20—50 g of Ultrex hydrochloric acid. Carry reagent blanks through the same procedure.

Selenium collection. Add 10 ml of 500 ppm selenium solution to rock digests or acidified water samples and heat to near boiling. If the method of standard additions is to be used, spike the sample prior to adding the selenium. Add 5 ml of tin(II) solution followed by a further 2—3 ml. Reduce the heat and allow the precipitate to coagulate for 20—30 min. Collect the precipitate by careful filtration through the central portion of a 47-mm, 0.3-μm filter (Nuclepore). Wash with warm (1 + 3) hydrochloric acid and water. Fold the filter and dry at 60°C for 15—30 min. Heat-seal the filter in a polyethylene bag (5—6 mm square) and place in a polyethylene vial ready for irradiation.

Prepare comparator standards by evaporating aliquots of standard solutions on Nuclepore filters under an i.r. lamp; then fold the filters and place in polyethylene bags along with 8 mg of selenous acid.

RESULTS AND DISCUSSION

When tin(II) chloride was added to the samples, iron(III) was reduced at the same time that selenium began to precipitate. A second portion of the reducing agent was added to ensure the complete precipitation of selenium. The precipitate had a red colour characteristic of elemental selenium. Because selenium, arsenic, and antimony are dissolved by oxidizing acids such as nitric acid, care was taken to minimize the final volume of rock digests without taking the samples to dryness. Arsenic and antimony were presumed to be coprecipitated in the elemental form. There was, however, a dependence of the collection efficiency upon the agent used; collection on selenium was quantitative while tellurium recovered less than 12% of these elements from pure solutions. The coprecipitation step may involve isomorphous inclusion as opposed to compound formation, as has been suggested by Sandell [12] for the coprecipitation of platinum by tellurium.

Initially, there was some concern that the reducing agent might be co-precipitated by selenium; hence, some other agents were tested. Neither sodium nitrite nor sodium sulfite was effective and, in warm (1 + 3) hydrochloric acid, the precipitate formed by hydrazine hydrate or ascorbic acid changed to a grey-red form on digestion. Tin(II) chloride was chosen and the only nuclide of tin that was observed under the present cooling and irradiation conditions was ^{117m}Sn ($t_{1/2}$ = 14 d, E_γ = 158 keV) which did not interfere because it had a very low activity.

In the following discussion, all uncertainties are reported as ± 1 standard deviation unit.

Arsenic and antimony determinations

The recoveries of radioactive tracers added to digested samples of NBS River Sediment averaged 95 ± 3% for arsenic and 102 ± 2% for antimony. When the method of standard additions was applied to the same digested material, the spikes were completely recovered (103% As and 98% Sb). The average recoveries of arsenic and antimony tracers from seawater samples were 99 ± 4% and 96 ± 6%, respectively. The selenium collection procedure was therefore considered to be quantitative.

During preliminary experiments, samples of NBS River Sediment were digested with a mixture of nitric, perchloric and hydrofluoric acids, and then evaporated to dryness. The levels of arsenic and antimony found in the sediment under these conditions were 35.5 ± 0.7 μg As g^{-1} and 34.3 ± 0.8 μg Sb g^{-1}. The antimony content was in good agreement with recently published values (see Table 1) but quite different from the NBS suggested value of 51 μg g^{-1}. The arsenic level was approximately half of both the NBS suggested value (66 μg g^{-1}) and recent literature values (Table 1). The recovery of an arsenic spike, added prior to digestion, was also very low. But when samples of the sediment were digested with warm aqua regia and bromine and filtered before the selenium collection step, the concentrations of arsenic and antimony were within 10% of published values (60.9 ± 0.7 μg As g^{-1} and 30.2 ± 0.2 μg Sb g^{-1}). These findings confirmed the work of Bajo [13] who reported that substantial losses of arsenic but not antimony were observed when samples containing As(III) and Sb(III) were heated with perchloric and hydrofluoric acids. The adopted digestion procedure involved heating samples with a mixture of nitric and perchloric acids to convert As(III) to As(V) prior to the addition of hydrofluoric acid.

Results for the eight new USGS Standards plus three older standards, the NBS River Sediment, and three water samples appear in Table 1 together with published values. The results for the USGS and NBS standards are in agreement with published values except for the arsenic contents of RGM-1 and BHVO-1. Water samples from the domestic well in Waverley, N.S., have been found [17] to contain 30 ng As ml^{-1}. The seawater sample has also been shown [18] to contain 1.33 ± 0.88 μg As kg^{-1} and 0.28 ± 0.02 μg Sb kg^{-1}. The present findings for the water samples are in reasonable agreement with these results.

TABLE 1

Concentration of arsenic and antimony in geological materials and water samples[a]

Sample		Arsenic conc.		Antimony conc.	
		This work	Published work	This work	Published work
NBS river sediment (1645)		62.6 ± 2.1	66[b], 71 [7]	33.6 ± 2.2	51[b], 33.2, 36 [7]
USGS	SCO-1	12.2 ± 0.1	10.8 [14], 12.4 [7], 54.3 [15]	2.49 ± 0.06	2.51 [3], 2.27 [7], 2.6 [15], 2.7 [16]
	SGR-1	66.7 ± 0.4	74.5 [14], 71 [7], 66.2 [15]	4.05 ± 0.33	3.70 [3], 3.46 [7], 3.4 [15], 3.5 [17]
	AGV-1	0.76 ± 0.05	0.8 [1]	3.96 ± 0.04	4.17 [3], 4.8 [15]
	QLO-1	1.84 ± 0.08	2.11 [7]	2.18 ± 0.37	2.03 [3], 1.26 [7], 2.5 [15], 2.0 [16]
	MAG-1	8.78 ± 0.36	9.6 [7], 6.0 [15]	1.29 ± 0.13	0.88 [3], 1.02 [7], 0.97 [16]
	STM-1	4.53 ± 0.36	5.2 [7]	1.78 ± 0.12	1.67 [3], 1.65 [7], 1.6 [15], 1.8 [16]
	RGM-1	1.08 ± 0.26	2.75 [7], 2.9 [15]	1.27 ± 0.07	1.30 [3], 1.15 [7], 2.2 [15], 1.29 [16]
	GSP-1	0.13 ± 0.02	0.09 [1]	3.22 ± 0.02	3.22 [3], 3.4 [15]
	G-2	0.24 ± 0.01	0.25 [1]	0.08 ± 0.02	0.08 [3]
	BHVO-1	0.24 ± 0.06	0.46 [7], 1.5 [15]	0.17 ± 0.01	0.16 [3], 0.12 [7], 0.15 [16]
	SDC-1	0.23 ± 0.04	0.23 [7]	0.53 ± 0.01	0.53 [3], 0.47 [7], 0.56 [16]
Muddy pond, Waverley, N.S.		108 ± 6	—	5.13 ± 0.22	—
Domestic well, Waverley, N.S.		26.1 ± 0.1	—	1.07 ± 0.01	—
Northwest Arm, Halifax Harbour		0.95 ± 0.03	—	0.38 ± 0.12	—

[a]Geological materials ($\mu g\ g^{-1}$); water samples ($\mu g\ kg^{-1}$). [b]NBS suggested value.

The consistency among the present results and literature or other values for both the rock and water samples indicated that the selenium collection procedure was relatively free from interference. In fact, a typical γ-ray spectrum of the selenium precipitate from a digested rock demonstrated photopeaks for only ^{75}Se, ^{82}Br, ^{24}Na and ^{117m}Sn in addition to those of arsenic and antimony. The sources of the selenium and tin are obvious; sodium must have been coprecipitated from the sample but the precipitate washing procedure kept the activity of this nuclide very low. The bromine nuclide originated from the Nuclepore membranes and washing them with warm nitric acid did not reduce the bromine content significantly. The amount of bromine varied greatly from batch to batch and some filters with smaller amounts of bromine were used. Hence, the 559-keV photopeak of ^{76}As was free of interference from the 554-keV peak of ^{82}Br. The background activity was due almost entirely to ^{75}Se which produced dead times of ca. 8% following a 90-min irradiation and 20-h decay. The selectivity of the collection procedure resulted, in part, from the irradiation and cooling periods employed, and some other elements, particularly the platinum metals, were probably also coprecipitated; gold has been quantitatively

collected (see below) and tellurium has been reported to recover several platinum metals [12].

The detection limits based on counting statistics, twice the square root of the background, 90-min irradiation, 20-h decay and 15-min counting were 9 ng As g^{-1} and 12 ng Sb g^{-1} for geological materials and 18 ng As kg^{-1} and 24 ng Sb kg^{-1} for water samples.

Gold determinations

Results for gold in the South African Reference Material, SARM-7, were 0.27 ± 0.01 $\mu g\ g^{-1}$ compared to the certified value of 0.31 ± 0.01 $\mu g\ g^{-1}$ [19]. Spikes of gold added to digested samples of SARM-7 were completely recovered (97 ± 2%). Further, the recoveries of gold radiotracers from seawater samples at the level of 50 ng kg^{-1} were also quantitative (99 ± 3%).

Samples of seawater collected from the Northwest Arm of Halifax Harbour failed to display the 412-keV photopeak of ^{198}Au above the detection limit of 1.5 ng Au kg^{-1} following a 6-h irradiation, 62-h cooling period and 30-min counting time. It has been reported [20] that the concentration of dissolved gold in seawater is variable and lies in the range 1—50 ng l^{-1}.

The detection limit for gold in SARM-7 was 1.6 ng g^{-1} based on a 4-h irradiation, 53-h decay and 10-min counting period. The longer irradiations needed to determine gold increased the activities of ^{75}Se, ^{82}Br (from the filters), and ^{24}Na (from seawater). The γ-ray spectrum of the selenium precipitates collected during the analysis of SARM-7 also demonstrated a photopeak characteristic of ^{64}Cu plus a strong annihilation peak arising from the β-decay mode of ^{64}Cu. Copper is present at a relatively high level (0.09%) in SARM-7 which explained its coprecipitation.

The selenium collection procedure is, therefore, capable of quantitatively collecting arsenic, antimony and gold from digested geological materials and natural waters.

The authors (C. M. E. and A. C.) acknowledge the financial support of the Natural Sciences and Engineering Research Council of Canada and the cooperation of the SLOWPOKE-2 Operations Group, Dalhousie University, in particular, Dr. J. Holzbecher.

REFERENCES

1 F. J. Flanagan, Geochim. Cosmochim. Acta, 37 (1973) 1189.
2 J. P. Riley and G. Skirrow, Chemical Oceanography, 2nd. edn., Academic Press, London, 1975, Vol. I, p. 418.
3 L. J. Schwarz and J. J. Rowe, U.S. Geol. Surv., Prof. Pap. 840 (1976) 67.
4 W. D. Ehmann, J. Bruckner and D. M. McKown, J. Radioanal. Chem., 57 (1980) 491.
5 E. Steinnes, Analyst, 97 (1972) 241.
6 K. Terada, K. Okuda and T. Kiba, J. Radioanal. Chem., 36 (1977) 47.
7 H. A. van der Sloot, D. Hoede, T. J. L. Klinkers and H. A. Das, J. Radioanal. Chem., 71 (1982) 463.

8 R. G. Godden and D. R. Thomerson, Analyst, 105 (1980) 1137.
9 K. S. Subramanian and J. C. Meranger, Anal. Chim. Acta, 124 (1981) 131.
10 R. R. Brooks, D. E. Ryan and H. Zhang, Anal. Chim. Acta, 131 (1981) 1.
11 D. E. Ryan, D. C. Stuart and A. Chattopadhyay, Anal. Chim. Acta, 100 (1978) 87.
12 E. B. Sandell, Colorimetric Determination of Traces of Metals, 3rd edn., Interscience, New York, 1959, p. 721.
13 S. Bajo, Anal. Chem., 50 (1978) 649.
14 B. P. Fabbi and L. F. Espos, U.S. Geol. Surv., Prof. Pap. 840 (1976) 89.
15 H. A. van der Sloot and J. Zonderhius, Geostandards Newsl., 3 (1979) 185.
16 R. J. Rosenberg and R. Zilliacus, Geostandards Newsl., 4 (1980) 191.
17 R. McCurdy, Victoria General Hospital, Halifax, personal communication (1982).
18 S. K. Nyarku and A. Chatt, to be published.
19 T. W. Steele, J. Levin and I. Copelowitz, National Institute for Metallurgy, Johannesburg, 1975, Rep. No. 1696.
20 J. P. Riley and G. Skirrow, Chemical Oceanography, 2nd. edn., Academic Press, London, 1975, Vol. III, p. 358.

Analytica Chimica Acta, 142 (1982) 277—279
Elsevier Scientific Publishing Company, Amsterdam — Printed in The Netherlands

Short Communication

RETICULATED VITREOUS CARBON ELECTRODE MATERIALS CHEMICALLY MODIFIED WITH IMMOBILIZED ENZYME

H. J. WIECK, CATHERINE SHEA and A. M. YACYNYCH*

Department of Chemistry, Rutgers, the State University of New Jersey, New Brunswick, NJ 08903 (U.S.A.)

(Received 19th April 1982)

Summary. The direct covalent attachment of glucose oxidase to the surface of reticulated vitreous carbon (RVC), a honeycomb carbonaceous material, is reported. The activity of the bound enzyme on different types of RVC, and the activity of adsorbed blanks are presented.

A recent paper by Wang [1] has reviewed the electroanalytical uses of reticulated vitreous carbon (RVC). This interesting honeycomb carbonaceous material has properties which make it quite attractive for use as an electrochemical detector in flowing systems [2]. Work in this laboratory has involved investigating the electrochemical characteristics and the practical applications of enzymes covalently attached to carbonaceous surfaces. Attachment of glucose oxidase (E.C. 1.1.3.4) to various carbonaceous surfaces has been reported by a number of workers [3—6]. Hydrogen peroxide produced by glucose oxidase-catalyzed oxidation of glucose can be measured amperometrically by its oxidation at an electrode surface. A chemically modified electrode with immobilized enzyme which utilizes this method for quantifying glucose has been reported [5]. A flow-through electrochemical cell consisting of a Sepharose-bound enzyme, which had been packed into the pores of an RVC disk, has been described by Blaedel and Wang [7].

The direct covalent attachment of an enzyme to RVC should prove to be quite interesting and useful. Two types of RVC (RVC-80S and RVC-80A) were examined. The surface areas of these materials, as measured by the BET (nitrogen) technique, were 0.17 $m^2\ g^{-1}$ and 159 $m^2\ g^{-1}$, respectively. Covalent attachment and adsorption of the enzyme on both of these surfaces were investigated. The activities of the covalently attached and adsorbed enzyme were then compared.

Experimental

Cylinders of RVC (Normar Industries, Anaheim, CA) were cut using a number two cork borer. Each was ca. 4 cm long and 0.5 cm in diameter. After overnight extraction with anhydrous methanol in a Soxhlet extractor, the rods

were oven-dried (110°C). The entire RVC rod and a connector fashioned from the tip of a glass medicine dropper were covered with heat-shrinkable teflon tubing, and connected to a peristaltic pump. A solution containing ca. 3 mg ml^{-1} of a water soluble carbodiimide (*i*-cyclohexyl-3-(2-morpholino-ethyl)-carbodiimide-metho-*p*-toluene sulfonate) in pH 4.6 potassium hydrogenphthalate buffer was pumped through the RVC cylinder at 7.3 ml min^{-1} for 1 h. The cylinder and tubing were then rinsed with only a buffer solution. A solution containing 2 mg ml^{-1} of glucose oxidase (Sigma G6125) in pH 5.6 potassium hydrogenphthalate buffer was prepared and pumped through the RVC. The solution was allowed to circulate through the RVC for 3 h (flow rate 7.3 ml min^{-1}). The RVC was then rinsed with and stored in pH 5.6 potassium hydrogenphthalate buffer. This procedure parallels the one used by Bourdillon et al. [4] after oxidative pretreatment.

For comparison, samples of RVC-80S and RVC-80A which had not been reacted with the carbodiimide, were also treated with the glucose oxidase solution, and then were washed in a manner similar to that used for the attached samples. These samples were designated as the adsorbed blanks. The activity of the enzyme on each sample was determined by the conventional spectrophotometric assay with *o*-dianisidine.

Results

The results for triplicate samples are presented in Table 1. Three conclusions can be drawn from these data. First, for both the RVC-80S and RVC-80A, covalent attachment of the enzyme leads to a sample which has higher activity than its adsorbed counterpart. Second, the enzyme on RVC-80S apparently has a higher activity than the enzyme on RVC-80A. Finally, the materials which were subjected to the carbodiimide attachment have activities which are more reproducible from sample to sample.

While the covalent attachment of an electrochemically active moiety to RVC has been accomplished by Anderson and Lung [8], this represents the first direct covalent attachment of an enzyme to RVC. An electrode which utilizes this attachment scheme is being constructed and tested. A manuscript describing its electrochemical characteristics, and its application in a flow injection system is forthcoming.

TABLE 1

Glucose oxidase activities[a] on various RVC samples

	RVC-80S	RVC-80A
Carbodiimide attached	5.75 ± 0.5	2.25 ± 0.3
Adsorbed blank	1.75 ± 0.75	1.13 ± 0.88

[a]Activity (units/g RVC) of triplicate samples.

Thanks are extended to Dr. Arnold Norris and Normar Industries for providing samples of RVC. A. M. Y. thanks Biomedical Research Support Grants, the National Science Foundation (grant number CHE 8022237), the National Institutes of Health (grant number GM 28125-01) for research support, and Rutgers University for a Junior Faculty Fellowship.

REFERENCES

1 J. Wang, Electrochim. Acta, 26 (1981) 1721.
2 A. N. Strohl and D. J. Curran, Anal. Chem., 51 (1979) 353.
3 Y. K. Cho and J. E. Bailey, Biotechnol. Bioeng., 20 (1978) 1651.
4 C. Bourdillon, J. P. Bourgeois and D. Thomas, J. Am. Chem. Soc., 102 (1980) 4231.
5 R. M. Ianniello and A. M. Yacynych, Anal. Chem., 53 (1981) 2090.
6 J. A. Osborn, R. M. Ianniello, H. J. Wieck, T. F. Decker, S. L. Gordon and A. M. Yacynych, Biotechnol. Bioeng., 24 (1982) 1653.
7 W. J. Blaedel and J. Wang, Anal. Chem., 52 (1980) 1426.
8 C. W. Anderson and K. R. Lung, private communication.

Analytica Chimica Acta, 142 (1982) 281—284
Elsevier Scientific Publishing Company, Amsterdam — Printed in The Netherlands

Short Communication

FREQUENCY SHIFTS OF PIEZOELECTRIC QUARTZ CRYSTALS IMMERSED IN ORGANIC LIQUIDS

T. NOMURA* and M. OKUHARA

Department of Chemistry, Faculty of Science, Shinshu University, Asahi, Matsumoto 390 (Japan)

(Received 12th May 1982)

Summary. A piezoelectric quartz crystal oscillates in organic liquids. The frequency change (ΔF) depends on the density (d) and viscosity (η) according to $\Delta F = ad^{1/2} + b\eta^{1/2} - c$, where a, b and c, are constants depending on the crystal.

A piezoelectric quartz crystal usually oscillates only when dry. Thus determinations of components in solution using the crystal can be done by reaction of the component in solution with the crystal, after which the latter is washed and dried before the frequency change is measured [1]. A crystal which has the electrode on one side in contact with an aqueous solution oscillates. The frequency depends on the density and conductivity of the solution [2]. Konash and Bastiaans [3] reported that a crystal with one electrode in contact with an organic solvent also oscillates. The frequency again depends on the density, and the arrangement may be used as a detector for liquid chromatography [3]. For such measurements, the crystal must be fixed with a liquid-tight seal to avoid leakage of liquid to the electrode on the other side. This sometimes caused the crystal to break under the stress of the fixture.

It has recently been established that a crystal completely immersed in an organic solution oscillates [4]; the frequency is dependent on the viscosity, density and conductivity of the solution. In this communication, it is shown that the frequency of a crystal immersed in an organic solvent containing no electrolyte is influenced only by the density and viscosity.

Experimental

Apparatus and chemicals. A 9-MHz AT-cut quartz crystal, having gold electrodes plated with platinum (Toyo Craft Ltd.), was used and was connected by a holder plated with gold. The crystal, held vertically with the crystal below the holder, was connected to an oscillator (Amtron International Kits) modified with a condenser as shown in Fig. 1. The frequency of the crystal was measured with a digital counter (Takeda Riken, TR-5143G). The

0003-2670/82/0000-0000/$02.75

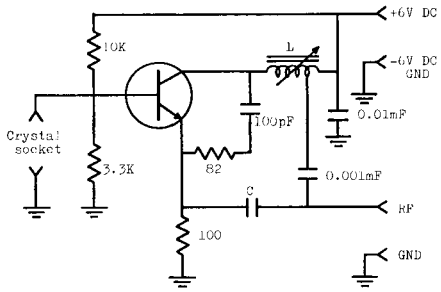

Fig. 1. Oscillator circuit: (L) tunable inductance; (C) condenser inserted.

crystal and the oscillator were contained in an air bath thermostated at 25 ± 0.5°C.

All organic solvents were special grade chemicals (Wako Pure Chemicals).

Procedure. The frequency of the crystal, previously washed with acetone and dried in the air bath, was measured (F_1). The whole crystal (up to the holder) was immersed in an organic solvent thermostated in a water bath at 25 ± 0.1°C. The frequency of the crystal was measured 30 and 60 s later and the mean value (F_2) calculated. The frequency difference ($\Delta F = F_1 - F_2$) was measured several times and the mean value calculated to give the frequency shift caused by the organic solvent.

Results and discussion

The frequency shifts of the crystal immersed in various organic solvents are shown in Table 1. It was found that the frequency shifts depended on the density and viscosity. For example, although acetone, ethanol and methanol have almost the same density, the frequency shifts were proportional to their viscosities. In contrast, methanol and chloroform, or acetonitrile and carbon disulfide, have similar viscosities, and their different frequency shifts depended on their densities. The crystal did not oscillate in liquids of high density and viscosity (1-butanol, nitrobenzene and carbon tetrachloride).

From these results, it was assumed that the shifts between the frequency of the dry crystal and that immersed in an organic liquid depended on the density and viscosity, and not the dielectric constant of the solvents: $\Delta F = \Delta F_d + \Delta F_\eta$, where ΔF_d and ΔF_η are the frequency shifts dependent on the density and viscosity, respectively.

When mixed liquids having almost the same density but significantly different viscosities were used, the frequency shifts depended on the viscosity, as shown in Table 2. The frequency shifts were linearly dependent on the square root of the viscosity. From such a linear plot, the frequency shifts corresponding to zero viscosity gave the density contribution at $d = 0.78$ g ml^{-1}. After deduction of this contribution, the equation for the viscosity

TABLE 1

Frequency shifts of the crystal between air and organic liquids

Liquid	Density[a] (d^{25}, g ml^{-1})	Viscosity[a] (η^{25}, cP)	Dielectric constant[a] (ϵ^{25})	Frequency shift (ΔF, Hz)	
				Measured	Calc.[b]
Hexane	0.6547	0.305	1.83	3404	3394
Cyclohexane	0.7739	0.930(22°C)	2.02	5943	
Acetonitrile	0.7768	0.344	36.0	4170	4186
Acetone	0.7845	0.302	20.7	4019	4042
Ethanol	0.7851	1.078	24.3	6385	6434
Methanol	0.7866	0.542	32.6	4981	4965
4-Methyl-2-pentanone	0.7961	0.542		5020	5011
2-Butanone	0.7998	0.370	18.4	4423	4403
1-Butanol	0.8057	2.46	17.1	c	
Toluene [6]	0.8625	0.552	2.37	5404	5359
Benzene	0.8737	0.596	2.27	5600	5553
Dioxane	1.0280	1.255	1.83	7940	7939
Nitrobenzene	1.1986	1.811	34.8	c	
1,2-Dichloroethane	1.2453	0.800(19.4°C)	10.7	7615	
Carbon disulfide [6]	1.2560	0.349		6233	6274
Chloroform [6]	1.4985	0.538	4.27	7870	7861
Carbon tetrachloride [6]	1.5848	0.903		c	

[a]From [5]. [b]Calculated from $\Delta F = 8629\, d^{1/2} + 4891\, \eta^{1/2} - 6289$. [c]Does not oscillate in the solvent.

dependence of the frequency shifts was calculated to be $\Delta F_\eta = 4763\, \eta^{1/2} - 143$. Likewise the density effect was calculated to be $\Delta F_d = 8655\, d^{1/2} - 6077$. Thus the total frequency shift (ΔF) was given by

$$\Delta F = (4.76\, \eta^{1/2} + 8.66\, d^{1/2} - 6.22) \times 10^3 \text{ Hz} \quad (1)$$

The frequency shifts calculated from this equation by using the densities and viscosities given in Table 1 agreed with the measured frequency shifts in Table 1 to within 60 Hz. The best fit to the results in Table 1 is given by

$$\Delta F = 8629\, d^{1/2} + 4891\, \eta^{1/2} - 6289 \text{ Hz}$$

The frequency shifts calculated from this equation are shown in Table 1. The corresponding equation derived by the same procedure when another quartz crystal was used, was $\Delta F = 8708 d^{1/2} + 4769 \eta^{1/2} - 6606$ Hz.

TABLE 2

Frequency shifts of the crystal between air and mixed organic liquids

Solvents	Viscosity[a] (η^{25}, cP)	Specific gravity[a] (d^{25}, g ml^{-1})	Frequency shifts measured (ΔF, Hz)
Ethanol—methanol			
(Methanol, wt. %)			
0	1.078	0.7851	6385
18.8	0.924		6009
40.7	0.793		5694
59.5	0.700		5445
77.9	0.620		5220
99.7	0.552	0.7866	5019
Acetonitrile—ethanol			
(Acetonitrile, wt. %)			
0	1.101	0.7851	6401
8.47	0.885	0.7850	5881
29.82	0.591	0.7844	5118
50.32	0.453	0.7827	4649
70.48	0.382	0.7806	4397
89.79	0.351	0.7768	4246
100	0.344	0.7768	4157
Acetonitrile—methanol			
(Acetonitrile, wt. %)			
0	0.544	0.7867	4981
5.83	0.513	0.7869	4892
19.87	0.450	0.7869	4673
40.82	0.390	0.7831	4415
62.79	0.347	0.7768	4235
81.40	0.333	0.7821	4134
100	0.345	0.7808	4170

[a]Obtained from [5].

REFERENCES

1 J. L. Jones and J. F. Mieure, Anal. Chem., 41 (1969) 484.
2 T. Nomura and A. Minemura, Nippon Kagaku Kaishi, 1980 (1980) 1621.
3 P. L. Konash and G. J. Bastiaans, Anal. Chem., 59 (1981) 1921.
4 T. Nomura, M. Okuhara, K. Murata and O. Hattori, Bunseki Kagaku, 30 (1981) 417.
5 G. J. Janz and R. P. T. Tomkins (Eds.), Non-aqueous Electrolytes Handbook, Academic Press, New York, 1972.
6 Kagaku Binran, Kisohen, II, The Chemical Society of Japan, Maruzen, Tokyo, 1975.

Analytica Chimica Acta, 142 (1982) 285—287
Elsevier Scientific Publishing Company, Amsterdam — Printed in The Netherlands

Short Communication

POTENTIOMETRIC TITRATION OF TELLURIUM WITH A FLUORIDE-SELECTIVE ELECTRODE

R. PARDO*, J. L. BERNAL and E. BARRADO

Departamento de Química Analítica, Facultad de Ciencias, Universidad de Valladolid, Valladolid (Spain)

(Received 19th October 1981)

Summary. Tellurium, as tellurite, can be determined with a fluoride-selective electrode by means of an indirect procedure based on precipitation of tellurite with excess of lanthanum(III), followed by back-titration with standard fluoride. The end-point is located by using the Gran method, and the titrations are suitable for tellurite concentrations above 1 mM.

Several anions can be determined potentiometrically with the fluoride-selective electrode [1]. All the procedures described, except the oxalate titration with lanthanum(III) proposed by Cedergren and Sundin [2], are based on the titration of the anion with a suitable cation that also precipitates with fluoride. The titration is monitored with the fluoride electrode. In this form, Efstathiou and Hadjiioannou [3] have proposed the use of the complex cation $PbCl^+$ to titrate various anions (sulphate, chromate, etc.). Selig [4] suggested lanthanum(III) for arsenate and phosphate. In a previous paper [5], two methods were proposed for the determination of selenite with lanthanum(III) and fluoride. This same procedure can be applied to tellurite, and a method for its determination is described in the present communication. The method is based on back-titration and the end-points are located by using the Gran method [6] in its mathematical form and with Gran plot paper.

Experimental

Equipment. Potentials were measured with a Philips PW9414 digital ion-activity meter, in combination with an Orion 9409 fluoride-selective electrode and a Philips R44/2-SD/1 double-junction saturated calomel reference electrode with its outer chamber filled with saturated KCl solution. pH was measured with a Radiometer 29 pH meter and a Radiometer GK2401C glass electrode.

Reagents. For the stock fluoride solution (0.10 M), 4.199 g of sodium fluoride was dissolved in 1 l of deionized water. Stock lanthanum(III) solution (0.033 M) was prepared by dissolving 14.43 g of lanthanum(III) nitrate hexahydrate in 1 l of deionized water. For the stock tellurite solution

(0.05 M), 12.69 g of anhydrous potassium tellurite was dissolved in 1 l of deionized water.

All reagents used were of analytical grade.

Recommended procedure. For determination of the blank, dilute 5 ml of lanthanum(III) solution to 50 ml with deionized water. Place the reference and selective electrodes in this solution, add 7 ml of standard fluoride solution and then add up to 10 ml in 1-ml increments with continuous stirring. The e.m.f. values must be read 30 s after each addition. For the samples, add 5 ml of lanthanum(III) to the sample, dilute to 50 ml with deionized water and proceed as before.

When the Gran method is used to locate the end-point, the e.m.f. readings (in mV) are plotted against the volume of fluoride solution added on special Gran paper. Straight lines are drawn through the points corresponding to each determination and extrapolated to zero ordinate. The distance between the intercepts ($V_{zero} - V_{sample}$) is the volume of standard fluoride equivalent to the tellurite present in the sample.

In the mathematical mode, the Gran function of each titration point is calculated. The volumes for the blank and the samples are determined by means of a least-squares fit of the values of the Gran function corresponding to each titration. The equivalence volume is determined as before.

Results and discussion

Because pH strongly affects the precipitation of $La_2(TeO_3)_3$, its influence was studied. Similarly to the selenite determinations [5], the pH changes during the titration. To establish the optimum value, the pH of several solutions containing 19 mg of tellurium (0.15 mmol of tellurite) was adjusted to different values with appropriate buffer solutions. When these solutions were titrated as in the recommended procedure, the results obtained were very poor: above pH 7, the amount of tellurite found was higher than the 0.15 mmol added, whereas below pH 7 the results were very low. Good results were obtained only when the titration was done in neutral unbuffered medium. Therefore, the use of buffered media must be avoided when samples of tellurite are prepared for this titration. This conclusion was also reached in the case of the selenite titrations [5].

The Gran plot paper used was designed for a slope of 57 mV/decade and for a volume correction of 20%. The results obtained when the plot was applied, are shown in Table 1. The mean recovery of tellurium was 102.5%, with a standard deviation of 2.6%. The mathematical procedure for locating the end-points is slower than the manual Gran plot (unless a programmable calculator is used). The results obtained (Table 1) are similar to those derived from the graphical procedure but the standard deviations are smaller. This may be due to the small equivalence volumes obtained when less than 10 mg of tellurite was determined. The mean recovery, by the mathematical method, was 101.9% with a standard deviation of 0.6%.

The use of more dilute standard solutions of lanthanum(III) and fluoride

TABLE 1

Potentiometric titrations of tellurite

Te added (mg)	Te found (mg)[a]			
	Graphical method		Mathematical method	
	$\bar{x}$	s_r(%)	$\bar{x}$	s_r(%)
50.30	50.25	0.70	49.25	0.24
30.18	30.39	0.61	30.45	0.26
20.12	20.32	0.73	20.11	0.23
15.09	15.72	0.83	15.34	0.27
10.06	10.19	1.70	10.21	0.28
7.54	7.85	1.90	7.88	0.40
5.03	5.36	2.15	5.37	0.45

[a]All the results are mean ($\bar{x}$) of 4 determinations with relative standard deviation (s_r).

and the utilization of water—ethanol mixtures, do not allow the determination threshold to be lowered significantly.

In conclusion, the method proposed enables 5.0—50 mg of tellurium as tellurite to be determined. Tellurite and tellurate can be distinguished because lanthanum(III) tellurate is more soluble than lanthanum(III) fluoride, and the back-titration is then impossible.

REFERENCES

1 M. S. Frant and J. W. Ross, Science (N.Y.), 154 (1966) 3756.
2 A. Cedergren and G. Sundin, Anal. Chim. Acta, 94 (1977) 467.
3 C. E. Efstathiou and T. P. Hadjiioannou, Anal. Chim. Acta, 109 (1979) 319.
4 W. Selig, Mikrochim. Acta, (1973) 349; (1974) 315.
5 J. L. Bernal, E. Barrado and R. Pardo, Anal. Chim. Acta, 111 (1979) 71.
6 G. Gran, Analyst, 77 (1952) 661.

Analytica Chimica Acta, 142 (1982) 289—292
Elsevier Scientific Publishing Company, Amsterdam — Printed in The Netherlands

Short Communication

STUDIES ON ANALYTICAL METHODS BY AMPEROMETRIC TITRATION USING A ROTATING PLATINUM ELECTRODE
Part 47. Successive Determination of L-Cysteine and L-Cystine by Amperometric Titration

SANAE IKEDA* and HIROMU SATAKE

Department of Applied Chemistry, Tokushima University, Minamijosanjima-cho, Tokushima 770 (Japan)

(Received 24th February 1982)

Summary. The successive determination of L-cysteine and L-cystine (2—5 μmol of each) in mixtures is achieved by amperometric titration with standard potassium iodate solution using a rotating platinum wire electrode at + 0.6 V vs. SCE. L-Cysteine is titrated in acidic bromide-containing solution; sodium chloride (15 g) is then added and the titration is continued to determine L-cystine.

L-Cysteine (RSH) and L-cystine (RSSR) are important biologically active substances. As L-cysteine is readily oxidized to L-cystine in air, and L-cystine is hydrolyzed to L-cysteine in water, they often occur together (e.g., in hair, horn and liver). Various methods are available for determining L-cysteine and L-cystine separately [1—15], but few methods are available for their successive determination. The present communication reports a simple, rapid amperometric titration which is suitable for determining the two compounds in successive steps. Titrations are done with potassium iodate [16] using a rotating platinum electrode at + 0.6 V vs. SCE, and are based on the difference in reaction rates. In a base electrolyte containing potassium bromide and sulfuric acid, L-cysteine reacts rapidly with potassium iodate whereas L-cystine reacts very slowly; the addition of sodium chloride makes L-cystine react rapidly with iodate.

Experimental

Apparatus. An automatic amperometric titrator [17] was used. The platinum electrode was rotated at 2000 rpm and was held at + 0.6 V vs. SCE.

Reagents. All reagents were of analytical-reagent grade (Wako Pure Chemical Industries); doubly-distilled water was used. L-Cysteine solution (10^{-3} M) was prepared by dissolving L-cysteine monohydrochloride monohydrate in oxygen-free water under an atmosphere of nitrogen. L-Cystine solution (5×10^{-4} M) was prepared by dissolving L-cystine in oxygen-free 10^{-1} M hydrochloric acid. Both solutions were standardized by titration with bromate [18]. Working solutions were prepared by suitable dilution of the stock solutions with oxygen-free water.

Recommended procedure. Measure 5 ml of 4 M potassium bromide, 5 ml of 5 M sulfuric acid and 30 ml of water into a 100-ml titration cell, and heat it to about 45°C, maintaining this temperature as far as possible in subsequent steps. Then add exactly 10 ml of an aqueous solution containing L-cysteine and L-cystine (2—5 μmol of each). Immediately titrate the resultant mixture with 0.025-ml portions of standard 5×10^{-3} M potassium iodate solution at intervals of 5 s until the end-point for L-cysteine is reached, as indicated by point (a) in Fig. 1. Then, add 15 g of sodium chloride at point (b) and dissolve it. Continue the titration with 0.05-ml portions of the titrant at intervals of 10 s to give the end-point (c) for L-cystine. The titration time is about 10 min (1 ml of 5×10^{-3} M $KIO_3 \equiv 0.5855$ mg of L-cysteine monohydrochloride monohydrate or 0.4806 mg of L-cystine).

Results and discussion

Figure 1 shows a typical titration curve. It was found that two moles of L-cysteine react with three moles of potassium iodate in the potassium bromide—sulfuric acid solution. The overall reaction is $2\,RSH + 3\,IO_3^- + 6\,HBr \rightarrow 2\,RSO_3H + 3\,IBr_2^- + 3\,H_2O$ though the intermediate steps are undoubtedly complex. Then two moles of L-cystine react with five moles of potassium iodate in the potassium bromide—sulfuric acid—sodium chloride solution, the overall reaction being $2\,RSSR + 5\,IO_3^- + 10\,HCl \rightarrow 4\,RSO_3H + 5\,ICl_2^- + 3\,H_2O$. A suitable concentration range for potassium bromide in the L-cysteine determination in 0.5 M sulfuric acid was 0.2—2 M. The optimum amount of sodium chloride added for the L-cystine determination was ca. 15 g. Titrations were done at about 45°C to achieve good end-points.

Table 1 shows the results obtained by the recommended procedure for

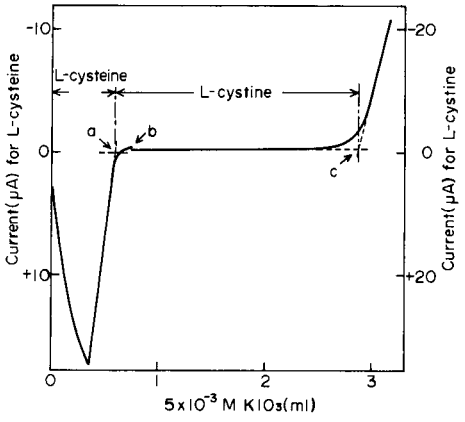

Fig. 1. Successive titration of L-cysteine and L-cystine. Sample solution (50 ml) contained 5×10^{-5} M L-cysteine, 10^{-4} M L-cystine, 0.4 M KBr and 0.5 M H_2SO_4. Titration conditions as in text. (a) End-point for L-cysteine; (b) addition of 15 g of NaCl; (c) end-point for L-cystine.

TABLE 1

Successive titration of L-cysteine and L-cystine in mixtures

Mixture	Taken (μmol)	Found[a] (μmol)	Relative error (%)	Coefficient of variation (%)	Titrant KIO_3 (M)
L-Cysteine	9.981	9.946	−0.3	0.3	5×10^{-3}
L-Cystine	2.320	2.370	+2.2	0.2	
L-Cysteine	6.918	6.918	0.0	0.1	5×10^{-3}
L-Cystine	0.928	0.998	+7.5	0.7	
L-Cysteine	4.990	4.993	+0.1	0.2	5×10^{-3}
L-Cystine	4.640	4.636	−0.1	0.1	
L-Cysteine	4.990	4.991	$+0.0_2$	0.1	5×10^{-3}
L-Cystine	2.320	2.321	$+0.0_4$	0.2	
L-Cysteine	1.967	1.969	+0.1	0.3	5×10^{-3}
L-Cystine	4.640	4.636	−0.1	0.1	
L-Cysteine	1.000	1.003[b]	+0.3	0.1	10^{-3}
L-Cystine	0.232	0.271[b]	+17	0.6	
L-Cysteine	0.5000	0.4993[b]	−0.1	0.2	10^{-3}
L-Cystine	0.236	0.266[b]	+13	1.4	
L-Cysteine	0.5000	0.4994[b]	−0.1	0.3	10^{-3}
L-Cystine	0.464	0.490[b]	+5.6	0.3	

[a]Mean of 5 titrations. [b]Titrations under nitrogen atmosphere.

five replicate titrations of mixtures containing the two species at various concentrations. It can be seen that L-cysteine (2—5 μmol) and L-cystine (2—5 μmol) in the mixtures could be determined successively with good accuracy and reproducibility.

The presence of L-histidine, L-phenylalanine, ammonium chloride, lead(II) nitrate, iron(III) chloride and sodium sulfate did not interfere with the determinations of L-cysteine (5 μmol) and L-cystine (2.5 μmol). However, L-methionine, L-tyrosine and iron(II) sulfate interfered because these compounds were also oxidized by iodate.

REFERENCES

1 M. R. F. Ashworth, The Determination of Sulfur-containing Groups, Academic Press, London, 1976, Vol. 2.
2 J. T. Stock and L. M. Doane, Anal. Chim. Acta, 86 (1976) 317.
3 L. M. Doane and J. T. Stock, Anal. Chem., 50 (1978) 1891.
4 R. Eggli and R. Asper, Anal. Chim. Acta, 101 (1978) 253.
5 E. Sobrova, Chem. Listy, 70 (1976) 747.
6 I. Stoian and R. Craciuneanu, Rev. Chim. (Bucharest), 30 (1979) 383.
7 K. K. Verma, Curr. Sci., 47 (1978) 82.
8 K. K. Verma, A. Srivastava, J. Ahmed and S. Bose, Talanta, 25 (1979) 469.

9 K. K. Verma, Talanta, 26 (1979) 277.
10 N. Ivanov, Scr. Sci. Med., 16 (1979) 14.
11 R. J. Thibert, M. Sarwar and J. E. Carroll, Mikrochem. Acta, 1969, 619.
12 I. M. Kolthoff and W. Stricks, Anal. Chem., 23 (1958) 763.
13 A. A. Inkin and V. T. Kharlamov, Zh. Anal. Khim., 28 (1973) 2037.
14 H. Satake, S. Ikeda and M. Tanaka, Nippon Kagaku Kaishi, 1981, 1726.
15 S. Ikeda and H. Satake, Bunseki Kagaku, 31 (1982) 37.
16 S. Ikeda and H. Satake, Anal. Lett., A11 (1978) 403.
17 H. Satake and S. Ikeda, Bunseki Kagaku, 28 (1979) 468.
18 Y. Okuda, J. Biochem., (Tokyo), 5 (1925) 201.

Analytica Chimica Acta, 142 (1982) 293—297
Elsevier Scientific Publishing Company, Amsterdam — Printed in The Netherlands

Short Communication

DETERMINATION OF ALIPHATIC ALDEHYDES IN AQUEOUS SOLUTION BY CHEMILUMINESCENCE MEASUREMENTS

B. VOGIN and F. BARONNET*

Laboratoire de Physico-Chimie des Hydrocarbures, L.A. 328 du CNRS, ENSIC (INPL), 1, rue Grandville, 54042 Nancy Cedex (France)

J. C. ANDRE

Groupe Recherche et Applications en Photophysique et Photochimie, L.A. 328 du CNRS, ENSIC (INPL), 1, rue Grandville, 54042 Nancy Cedex (France)

(Received 13th October 1981)

Summary. The determination of aliphatic aldehydes (5×10^{-6} — 2.5×10^{-4} mol) in aqueous solution was achieved by inhibition of the luminol chemiluminescence induced by hydrogen peroxide in the presence of potassium hexacyanoferrate(III).

In the oxidation reactions of hydrocarbons which are dispersed in an aqueous phase (suspension or micelles), alcohols and then aldehydes may be produced [1, 2]. The concentration of aliphatic aldehydes can readily be determined by various techniques such as chromatography or absorption spectrophotometry when the aldehyde is not dissolved in an aqueous phase, but the problem is more complicated when the aldehyde is dissolved in water because of solvation effects. Table 1 outlines some techniques used to determine aldehydes in solution. When the solvent is water, most of the various existing techniques seem to be either not sensitive enough or too complicated. Aldehydes are able to form addition complexes with hydrogen peroxide [3, 4]; this is the basis of a technique for aldehyde determination which is easy to implement and rapid (10 min), based on the chemiluminescence of luminol when oxidized by hydrogen peroxide. Shaw [13] recently used this reaction to determine hydrogen peroxide. The method described here is based on that of Shaw.

Experimental

Reagents. Luminol solution (9×10^{-3} M) was prepared from 1.6 g of luminol, 61.8 g of boric acid and 73 g of sodium hydroxide per litre of distilled water, adjusted to pH 10.5 by addition of hydrochloric acid. Potassium hexacyanoferrate(III) solution (10^{-2} M) was 3.293 g l^{-1} with pH adjusted to 10.5 with sodium hydroxide. Dilute hydrogen peroxide solutions were prepared from a titrimetrically standardized 70% solution.

Apparatus. The photomultiplier of a Jobin-Yvon JY 3C spectrofluorimeter

0003-2670/82/0000-0000/$02.75

TABLE 1

Methods of determination of aldehydes in solution

Method	Measurable lower conc. limit (mol l^{-1})	Time required	Solvent	Ref.
Chemical RCHO → hydrazone	ca. 3×10^{-6}	2 h	hydrocarbon	5
Chemical RCHO → hydrazone	5×10^{-5}	20 min	alcohol	6
Distillation[a]	5×10^{-4}	—	water	7
U.v. spectrophotometry	ca. 5×10^{-3}	<10 min	water	8
D.c. polarography	ca. 10^{-5}	10 min	alcohol	9
			water	10
Radioactivity	10^{-12} mol	>1 h	—	11
Enzymatic[b]	10^{-5}	10 min	water	12
Chemiluminescence (present work)	5×10^{-6} mol	10 min	water	

[a]Needs sophisticated equipment; aldehyde measured by fluorescence after distillation.
[b]Uses alcohol dehydrogenase or aldehyde dehydrogenase, with spectrophotometric measurement of NADH.

was used for measurements of the chemiluminescence. The monochromators were used in the zero order; the source was switched off. The measurement cell was a standard fluorimeter cell (1 × 1 × 4 cm).

Procedure. In the optical cell, mix 0.9 ml of luminol solution and 0.9 ml of hexacyanoferrate(III) solution. After exactly 5 min, add rapidly 2 ml of hydrogen peroxide solution (or peroxide + aldehyde solution see below), and shake the cell. Place the cell into the temperature-controlled (35°C) sample holder and measure the emission intensity as a function of time.

Results

As shown in Fig. 1, the luminol—potassium hexacyanoferrate(III) mixture emits light; therefore it is necessary to wait for a few minutes until this emission decreases, in order to increase the signal-to-background ratio. After introduction of the peroxide solution, a signal which is a function of the concentration of free hydrogen peroxide is observed. The intensity of this signal decreases with time. In order to make a correct measurement of the signal S at time $t = 0$, equations were sought which described the signal decrease vs. time, so the value of S at $t = 0$ could be calculated. A plot of ln S vs. t is linear, which shows that it can be assumed, with reasonable accuracy, that S is an exponential function of time. Therefore, for each measurement, a value of $S(0)$ is calculated, which is considered as proportional to the initial concentration of hydrogen peroxide.

Figure 2 shows the variation of $S(0)$ with hydrogen peroxide concentration in the absence of aldehyde. The upper linear limit depends on the luminol concentration.

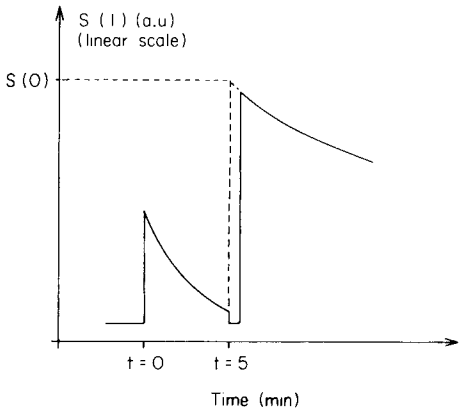

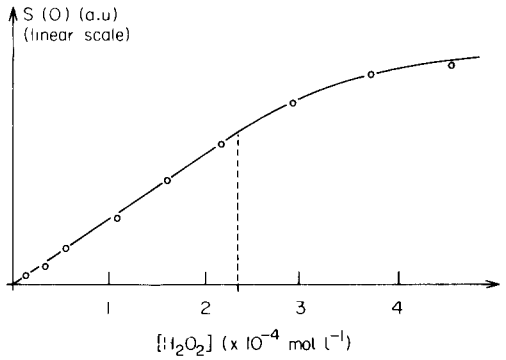

Fig. 1. Variation of chemiluminescence signal S vs. time. 0 min, mixing of luminol and hexacyanoferrate; 5 min, addition of H_2O_2 (or H_2O_2 + aldehyde).

Fig. 2. Intensity of chemiluminescence at t = 0 [S(0)] vs. H_2O_2 concentration in the optical cell.

Addition reaction between an aldehyde and hydrogen peroxide. Aldehydes form addition compounds with hydroperoxides [3, 4]. Two reactions can be put forward [3]

$$RCHO + H_2O_2 \overset{K_1}{\rightleftharpoons} RCH(OH)OOH \qquad (I)$$

$$2RCHO + H_2O_2 \overset{K_2}{\rightleftharpoons} RCH(OH)OOCH(OH)R \qquad (II)$$

The peroxides formed are generally unstable and may decompose to give various products, particularly acids [14]. For acetaldehyde at 0° C, Satterfield and Case [3] found K_1 = 48.1 l mol^{-1} and K_2 = 490 l^2 mol^{-2}. Under the present experimental conditions, $[H_2O_2] \ll [RCHO]$, $[RCHO] \leqslant 10^{-1}$ mol l^{-1} and $[H_2O_2] \leqslant 6 \times 10^{-5}$ mol l^{-1}. If x denotes the concentration of RCH(OH)OOH and y that of RCH(OH)OOCH(OH)R, then $y/x = K_2[RCHO]/K_1 = (490/48.1) \times 10^{-1} \approx 1$. Therefore, under the present conditions, the two addition peroxides are formed and, at high aldehyde concentrations, the two equilibria described above are largely displaced to the right. However, in such experimental conditions, $S(0)$ is still negligible. Therefore, it seems logical to assume that the two addition peroxides are not reactive towards luminol. At lower aldehyde concentrations, $[RCHO] < 10^{-2}$ mol l^{-1}, it is chiefly the peroxide (I) which is formed; thus $y/x = K_2[RCHO]/K_1 = (490/48.1) \times 10^{-2} \approx 0.1$.

The aldehyde concentration can be determined either by calculations based on the equilibrium between hydrogen peroxide and the aldehyde, or

more easily by using a calibration graph such as that shown in Fig. 3. For concentrations of hydrogen peroxide within the linear calibration range, the effect of increasing acetaldehyde concentration is shown in Fig. 3. For the various concentrations of hydrogen peroxide present initially, the signal $S(0)$ can be expressed by $S(0) = A[H_2O_2]_0/(1 + K_1[RCHO] + K_2[RCHO]^2)$, where A is a proportionality constant. The curve derived from this theoretical model fits well with that obtained by least-squares fit of the experimental results. For four aldehydes (acetaldehyde, formaldehyde, propionaldehyde and isobutyraldehyde), the value of K_1 was 170 mol^{-1} l and those of K_2 were, respectively, 3700, 24 500, 3700 and 8000 mol^{-2} l^2; the plots of $S(0)$ vs. $[RCHO]^{1/2}$ were very similar to acetaldehyde in each instance.

Aldehyde determinations. Twenty measurements of the concentration of 5×10^{-6} M hydrogen peroxide, gave a 90% confidence interval of ±7%. The relative error of measurements of acetaldehyde at various concentrations is plotted in Fig. 4. The error curve tends to rise at lower concentrations ($>10^{-1}$ mol l^{-1}) in the case of formaldehyde (Fig. 4). The curve shows that the aldehyde can be determined with reasonable precision between 5×10^{-3} and 0.25 mol l^{-1}. At high aldehyde concentrations, the signal is relatively small compared to the background noise and therefore the relative error tends to rise. Determinations can be carried out on samples of 1 ml; therefore the measurement range is approximately 5×10^{-6}—2.5×10^{-4} mol.

The effect of other substances on the aldehyde determination was investigated. Cyclohexane (saturated aqueous solution, ca. 5×10^{-2} mol l^{-1}), 2-methyl-2-butene (saturated aqueous solution, ca. 5×10^{-2} mol l^{-1}), acetic acid (5×10^{-4} mol l^{-1}), ethanol (5×10^{-2} mol l^{-1}), a saturated solution of carbon dioxide diluted 50 times, and a preliminary bubbling of carbon

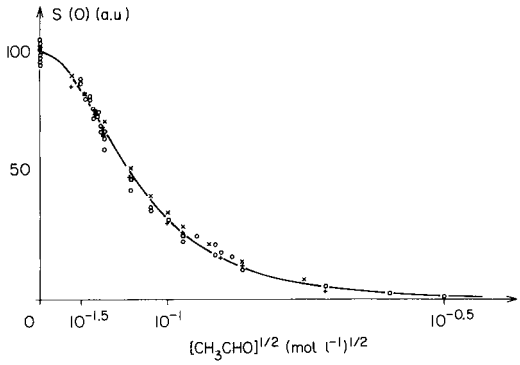

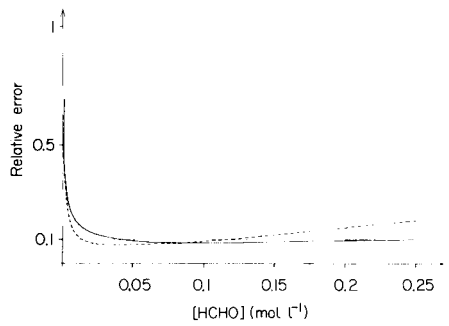

Fig. 3. Intensity of chemiluminescence signal $S(0)$ vs. acetaldehyde concentration for various initial concentrations of H_2O_2. (+) $[H_2O_2]_{0,1} = 5 \times 10^{-6}$ mol l^{-1}, scale factor = 1; (×) $[H_2O_2]_{0,2} = 1.5 \times 10^{-5}$ mol l^{-1}, $S(0)$ multiplied by 3; (○) $[H_2O_2]_{0,3} = 5 \times 10^{-5}$ mol l^{-1}, $S(0)$ multiplied by 10. Solid line obtained by least-squares fitting of data.

Fig. 4. Relative error of measurements of aldehyde concentration: (—) acetaldehyde; (---) formaldehyde.

monoxide in the measuring cell had no effect on the chemiluminescence, in the absence or presence of aldehyde (0.5×10^{-3} mol l^{-1} acetaldehyde). These results indicate that interferences are limited and that the technique is suitable for determining aldehydes in mixtures formed in oxidation reactions.

B. V. thanks Produits Chimiques Ugine Kuhlmann for financial support during this work and the authors gratefully acknowledge the assistance of B. Lescure in performing some of the measurements.

REFERENCES

1 K. Nakao and Y. Suzuki, Japan Kokai 78, 10 387, 1978.
2 C. Rousseau and R. Martin, unpublished work.
3 C. N. Satterfield and L. C. Case, Ind. Eng. Chem., 46 (1954) 998.
4 B. L. Dunicz, D. D. Perrin and D. W. G. Style, Trans. Faraday Soc., 47 (1951) 1210.
5 E. V. Kuznetsova, S. A. Taranenko, T. Mil'kina and O. E. Batalin, Zh. Anal. Khim., 32 (1977) 1185.
6 S. Tagami, T. Nakamura, T. Nakano and D. Shiho, Chem. Pharm. Bull., 23 (1975) 891.
7 A. R. Stowell, K. E. Crow, R. M. Greenway and R. D. Batt, Anal. Biochem., 84 (1978) 384.
8 D. I. Belkin, G. V. Kravchenko and M. Ya. Rozkin, Zh. Anal. Khim., 31 (1976) 1022.
9 V. E. Strukova, Yu. E. Falkovich, Ya. I. Tur'yan, V. I. Grinfel'd and Z. A. Lisetskaya, Izv. Vyssh. Uchebn. Zaved., Pishch. Tekhnol., (1976) 170.
10 J. D. McLean and J. F. Holland, U.S. Patent No. 3 922 205, 1975.
11 M. Guarnieri, U.S. Patent No. 4 172 706, 1977.
12 T. Matsuda and T. Hirai, Japan Kokai Tokkyo Koho 79, 155 890, 1979.
13 F. Shaw, Analyst (London), 105 (1980) 11.
14 C. N. Satterfield, R. E. Wilson, R. M. Leclair and R. C. Reid, Anal. Chem., 26 (1954) 1792.

Analytica Chimica Acta, 142 (1982) 299—304
Elsevier Scientific Publishing Company, Amsterdam — Printed in The Netherlands

Short Communication

DETERMINATION OF TOTAL PRIMARY AMINES IN SEAWATER AND PLANT NECTAR WITH FLOW INJECTION SAMPLE PROCESSING AND FLUORESCENCE DETECTION

ROBERT L. PETTY*, WILLIAM C. MICHEL, JEFFREY P. SNOW and KENNETH S. JOHNSON

Marine Science Institute, University of California at Santa Barbara, Santa Barbara, CA 93106 (U.S.A.)

(Received 4th February 1982)

Summary. Flow injection sample processing is used with fluorescence detection for the determination of total primary amines in seawater and nectar. The effects of carrier stream flow rate and dispersion tube length on sensitivity and sampling rates were studied. Relative responses of several amino acids and other primary amines were determined using two dispersion tube lengths. Linear calibration curves were obtained over the ranges $0—10^{-6}$ M and $0—10^{-5}$ M glycine. Precisions of better than 2% at 10^{-6} M and a detection limit of 1×10^{-8} M glycine were obtained. Applications to the analysis of seawater from the vicinity of a baited lobster trap and diluted nectar samples from *Erythrina sp.* are described.

Determination of the amino acid composition of natural substances is frequently of great importance. In this laboratory, it has been necessary to determine amino acids in various types of samples, such as animal tissues, plant fluids, and seawater. These determinations have been done by both resin and reversed-phase high-performance liquid chromatography, using either post- or pre-column derivatization with *o*-phthalaldehyde (OPA) and fluorescence detection [1, 2]. Because the chromatographic procedures are time-consuming and tedious, samples must be carefully selected before being submitted to this procedure.

The flow injection technique [3], with a carrier stream of OPA reagent and a fluorimeter, offers a rapid and precise method for screening large numbers of samples for total primary amines. An appropriate flow injection system for performing such a determination includes a carrier stream containing the reagent, an injection valve for reproducibly introducing the sample into the carrier stream, a reaction coil (dispersion tube) providing a medium degree of dispersion (D = 3—10) [3], and a fluorimeter equipped with a micro flow cell. Addition of an automatic sample introduction system [4] allows unattended operation. Such a system was assembled in this laboratory, using components available from an h.p.l.c. system.

Only three reports have thus far been published regarding applications of

0003-2670/82/0000-0000/$02.75

flow injection methods to the determination of amino acids. One was concerned mainly with the demonstration of general flow injection concepts and theory [3], one covered only the determination of glycine [5], and the third, utilizing amperometric detection, did not have adequate sensitivity for our purposes [6]. This communication reports the development and optimization of a flow injection procedure for total primary amines, and applications of this procedure to the determination of in situ primary amine release in seawater, and of amines in diluted nectar samples for the purpose of interspecific comparisons. The advantages of this method over a segmented flow procedure [7] are also discussed.

Experimental

Apparatus. The apparatus used is shown schematically in Fig. 1, and consisted of the following components: Beckman-Altex Model 110A metering pump for reagent delivery; Fluid Metering, Inc., Model RPSY pump for pumping samples from the autosampler to the injector; Rheodyne Model 7010 loop injector valve with a 20- or 100-μl sample loop; Varian-Techtron Model 51 automatic sample changer (50 sample capacity); Turner Model 111 filter fluorimeter with h.p.l.c. type flow-through door and 20-μl cell volume, equipped with a 360 nm narrow-pass excitation filter (Kodak 7-60) and a 550 nm cut-off emission filter (Kodak 2A-12); Houston Instrument Omniscribe recorder; and 0.5-mm i.d. teflon or stainless-steel tubing.

Reagents and standards. All reagents were analytical reagent grade, unless otherwise specified. Water was deionized, distilled, and filtered through a Milli-Q (Millipore Corp.) water purification apparatus. The OPA reagent was prepared as follows [8]. A 25-g sample of boric acid was dissolved in 950 ml of water and the pH was adjusted to 10.4 with 45% (w/v) potassium hydroxide solution. A portion (3 ml) of a 30% solution of Brij 35 (polyoxyethylene lauryl ether, Atlas Chemical) was added, followed by 2 ml of mercaptoethanol (Sigma). A solution of 650 mg of *o*-phthalaldehyde (Fluoropa, Dionex) in 10 ml of anhydrous methanol was then added with gentle stirring.

Standards were prepared by dissolving appropriate amounts of the amines (Sigma) in water to make 0.010 M stock solutions, and diluting these to appropriate working concentrations.

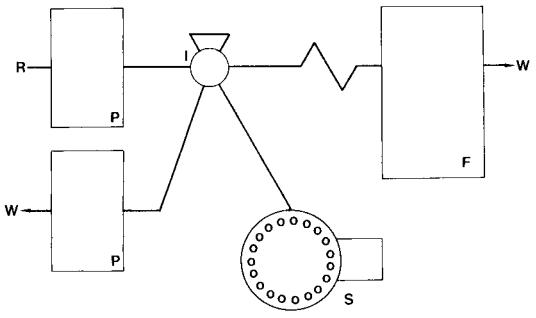

Fig. 1. Schematic diagram of flow injection apparatus. R is the OPA reagent, W is waste, P is a pump, I is the loop injector, S is the sample changer, and F is the fluorimeter.

Samples. Seawater samples were obtained simultaneously from benthic sampling ports positioned equidistant from the bait source (180 g of ground abalone mantel and epipodium tissue) in a polyethylene lobster trap, located in 5 m of water at the More Mesa reef near Santa Barbara, CA. Each sample was drawn through microbore tubing (Tygon, 0.03 in. i.d.) into a 40 ml glass syringe, filtered (0.45-μm membrane), preserved with 1 drop of pentachlorophenol solution (5 mg ml^{-1} in aqueous 95% ethanol), and stored at $<4°$ C. If less than 10 ml of seawater was collected during the 10-min sampling period, sample tube clogging was indicated and a notation was made. Amines were quantified within 4 days of sample acquisition.

Nectar samples were obtained from the coral trees *Erythrina caffra* and *Erythrina corralloides*, located at the University of California at Santa Barbara campus. Three inflorescences from each species were collected and nectar was drawn from eight flowers per inflorescence, for a total of 24 samples from each species. Samples were taken between 1300 and 1400 h on a partly cloudy day. The individual flowers were carefully removed from the inflorescence and subsequently emasculated. Nectars were collected using a blunt end 250-μl luer lock syringe. Individual samples were frozen immediately and amine determinations were completed within 24 h. Prior to quantitation, the samples were diluted 100-fold with water.

Results and discussion

A systematic investigation of flow-injection parameters was needed to determine the optimum conditions for amine determinations. The parameters of carrier stream pumping rate and dispersion tube length were examined for a glycine solution (4×10^{-7} M in water) as the test sample. The fluorescence signal (peak height) was plotted against both tube length and pumping rate to give the three-dimensional representation of product formation curves [3] shown in Fig. 2. Sampling rate was proportional to pumping rate for a given dispersion tube length, with 120 samples per hour being determined with a 110-cm tube at 1.0 ml min^{-1} flow, and 150 samples per hour with a 50-cm tube. The optimum conditions for a particular application can be determined by examination of these results. Thus, for highest sensitivity, a short tube length and slow pumping rate give the best results. Sensitivity decreases with increased pumping rates (sampling rates), but relatively more slowly with longer dispersion tubes. The best overall compromise for sampling rate and sensitivity appears to be in the range of 1.0—1.5 ml min^{-1} carrier flow rate with a 100—125-cm dispersion tube. This will provide sensitivities of about 80% of the maximum while still allowing about 150 samples per hour to be processed.

The sensitivity of this method is dependent on the particular amines present in the sample, on their rates of reaction with the OPA reagent, and upon the rate of decay of their reaction products [2, 3, 7]. The relative sensitivities of several amino acids, plus a tripeptide, ammonia, and glutathione, are presented in Table 1. The responses were determined with two

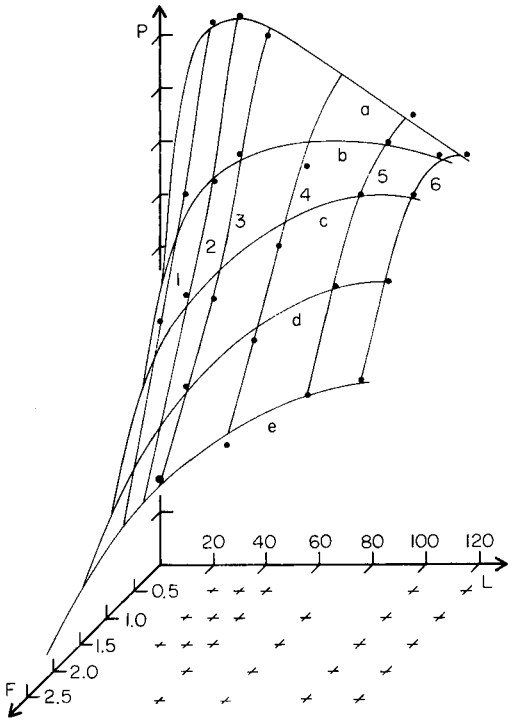

Fig. 2. Three-dimensional product formation curve for glycine in OPA solution. Tube lengths (L in cm): (1) 30; (2) 40; (3) 50; (4) 75; (5) 105; (6) 125. Flow rates (F in ml min^{-1}): (a) 0.5; (b) 1.0; (c) 1.5; (d) 2.0; (e) 2.5. P is peak height (arbitrary units).

different diffusion tube lengths, in order to give an idea of the contribution of reaction rate and product decay to sensitivity for each of the compounds. Most of the compounds gave an increased response, relative to glycine, when the longer tube was used (longer reaction time). Three were the same as glycine and one was less responsive. The overall average for the amino acids was a 15% increase in relative response, providing a fairly uniform response for all those tested. However, the absolute response for the 200-cm tube was an average of 54% of that obtained with the 100-cm tube.

Calibration curves were obtained for glycine in distilled water. Two sets of conditions were used for different concentration ranges. For low concentrations, ($C < 10^{-6}$ M) a 100-μl sample loop was used, and reagent was pumped at 1.0 ml min^{-1}. The curve fitted the following equation: $F = (70.21 \pm 0.79)C_G^\circ - (8.61 \pm 0.48)$, with a standard error of 1.39 and correlation coefficient of 0.9968 (F is fluorescence, in arbitrary units, and C_G° is glycine concentration). The negative intercept (negative peaks for $<10^{-7}$ M glycine samples) was due to dilution of the reagent, which had an inherent low level of fluorescence, by the sample solvent (water). This could be alleviated by use of an inert carrier stream, into which the sample is injected, and which

TABLE 1

Relative responses of amino acids and other primary amines[a]

Compound	Relative response[b]		Compound	Relative response[b]	
	100-cm tube	200-cm tube		100-cm tube	200-cm tube
Arginine	87	109	Ornithine	93	77
Asparagine	44	92	Phenylalanine	66	90
Cysteine[c]	29×10^{-2}	97×10^{-2}	Serine	100	108
Glutamic acid	79	99	Taurine	103	95
Glycine	100	100[d]	Threonine	68	100
Isoleucine	76	100	Tryptophane	68	79
Leucine	90	88	Valine	73	100
Lysine	118	116			
Methionine	85	101	Average[e]	83	96
Ammonium chloride	6	19			
Glutathione	50	98			
Glycylglycyl-glycylglycine	10	19			

[a]Amines of 10^{-4} M concentration in 20-μl sample loops injected into OPA reagent stream pumped at 1.5 ml min^{-1}. Fluorimeter equipped with 20% plus 1% neutral density filters.
[b]Relative responses were calculated separately for each dispersion tube.
[c]Cysteine concentration was 10^{-2} M.
[d]Peak height of glycine sample run through the 200-cm tube was 47% of that run through the 100-cm tube.
[e]Average for amino acids, not including cysteine.

subsequently merges with the reagent stream [3]. A detection limit of about 0.01 μM glycine, corresponding to an injected amount of only 1×10^{-12} mol, was observed.

For more concentrated samples, a 20-μl sample loop was used, with a 1.5-ml min^{-1} flow rate. A calibration curve with slope 15.49 ± 0.04, intercept 0.25 ± 0.30, correlation coefficient 0.9999, and standard error 0.50, was obtained for the range of $1-20 \times 10^{-6}$ M glycine. At concentrations above ca. 4×10^{-5} M, the curve began to deviate from linearity. The linear range could be extended, however, by one or more of the following alterations: (a) smaller sample loop volume; (b) faster pumping rate; (c) higher reagent concentration. Any of these changes would, of course, require re-calibration.

Replicate injections of the same sample typically showed precision of better than 2% at concentrations greater than 5×10^{-7} M, and 5% at 5×10^{-8} M.

This method was used for such diverse samples as seawater and diluted nectar. The seawater samples were collected near a bait source in a lobster trap which was situated in a sub-tidal reef area. The average concentration for 50 samples taken from 9 sampling ports over 48 h was $(4.6 \pm 3.6) \times 10^{-7}$ M (based on glycine calibration). For seven samples taken from a

control area (unbaited trap) over the same time period, the average concentration was $(2.9 \pm 1.3) \times 10^{-7}$ M. Use of this technique in the field for much smaller, higher time-resolved samples is planned.

Nectar samples were collected in order to compare total primary amine (and subsequently individual amino acids) concentrations in two species of the genus *Erythrina* (coral trees). Prior to quantitation, samples were diluted with water to ensure peak height readings within the linearity of the calibration curve. The averaged concentrations found for the two species examined were $(3.29 \pm 0.26) \times 10^{-3}$ M (*Erythrina caffra*) and $(1.72 \pm 0.13) \times 10^{-3}$ M (*Erythrina corraloides*). The demonstrated ease and rapidity of this technique make future large-scale interspecific comparisons quite likely.

The present procedure has several advantages over the previously reported automated total primary amine procedure [7]. It is faster (more than 150 samples per hour vs. 30), has lower detection limits (1×10^{-8} M vs. 5×10^{-8} M), more precise (2% at 10^{-6} M vs. 6% at 10^{-5} M), and probably more accurate (a calculated calibration correction factor was necessary in the previous procedure). Reagent consumption, although greater per unit time than the previous method, is much lower on a per sample basis. In addition, the simplicity and robustness of the flow injection apparatus makes this technique well suited to shipboard or similar field-type analytical work.

This work was supported by the Marine Science Institute, U.C.S.B. The generous cooperation of Professors James Case and Dale Smith is also acknowledged.

REFERENCES

1 J. R. Benson and P. E. Hare, Proc. Natl. Acad. Sci. U.S.A., 72 (1975) 619.
2 P. Lindroth and K. Mopper, Anal. Chem., 51 (1979) 1667.
3 J. Ruzicka and E. H. Hansen, Flow Injection Analysis, Wiley, New York, 1981, 207 pp.
4 K. K. Stewart, J. F. Brown and B. M. Golden, Anal. Chim. Acta, 114 (1980) 119.
5 J. I. Braithwaite and J. N. Miller, Anal. Chim. Acta, 106 (1979) 395.
6 B. S. Hui and C. O. Huber, Anal. Chim. Acta, 134 (1982) 211.
7 B. Josefsson, P. Lindroth and G. Ostling, Anal. Chim. Acta, 89 (1977) 21.
8 Pierce Technical Bulletin, Preparation of Fluoropa Reagent Solution for Detection of Amino Acids and Peptides, Pierce, Rockford, IL, 1975.

Analytica Chimica Acta, 142 (1982) 305—311
Elsevier Scientific Publishing Company, Amsterdam — Printed in The Netherlands

Short Communication

FLUORESCENCE STUDY OF AN IMMOBILIZED LIGAND—METAL ION COMPLEX

MAURI A. DITZLER*, GERARD DOHERTY, STEVEN SIEBER and RICHARD ALLSTON

Department of Chemistry, College of the Holy Cross, Worcester, MA 01610 (U.S.A.)

(Received 29th March 1982)

Summary. A ligand known to form a fluorescent complex with aluminum ion was immobilized on silica gel. The immobilization sequence was verified by cross-polarization magic-angle spinning n.m.r. spectroscopy and diffuse reflectance u.v. spectroscopy. The solid-state fluorescence of the immobilized ligand complexed with aluminum ion was similar to the fluorescence of a solvated complex of a model ligand. The potential to eliminate possible interfering species by isolating the complex from solution was demonstrated.

This communication presents results which suggest that significant advantages may accrue to molecular fluorescence detection of metal ions by immobilizing the fluorogenic ligand on silica gel. Ligands immobilized on silica gel have previously been shown to be useful in preconcentrating ions prior to direct detection by x-ray fluorescence [1—3]. Immobilized ligands have also been used as chromatographic stationary phases [4]. This report describes the application of front surface molecular fluorescence [5—10] to the detection of immobilized ligand—metal complexes. Unlike the earlier studies based on x-ray fluorescence, the principal advantage does not result from the preconcentration of the analyte, but rather a diminution of the effects of potentially interfering species. Because the ligand is immobilized on an insoluble substrate (silica gel) it should be possible to wash away any interfering species after the ion of interest has been complexed. This is a particularly important consideration with respect to molecular fluorescence which is subject to a wide range of interferences. Two types of interference are examined, that from other fluorescing species and that from strongly absorbing species present in the sample.

Immobilized fluorescent reagents have previously been used to study interactions between bonded phases and solvents [11], as a monitor for pH [12], and as a scintillator for the detection of radioactive and non-fluorescent substrates in liquid chromatography [13].

Experimental

Reagents. The solid substrate was Type-H silica gel (Sigma Chemical Company). The 2,2′,4-trihydroxyazobenzene was prepared as described by

0003-2670/82/0000-0000/$02.75

Diehl and Ellingboe [14]. Aluminum solutions were prepared by dilution of a stock solution prepared from $KAl(SO_4)_2 \cdot 12H_2O$. 4,6-Dichloro-2-ethylaminotriazine and 2,4-di(ethylamino)-6-chlorotriazine were prepared by the procedure of Thurston et al. [15].

Spectroscopic equipment and procedures. Fluorescence spectra were obtained with a Perkin-Elmer Model 204 spectrofluorimeter using the associated front surface accessory which allows excitation at an angle of 60°. Powder sample holders with quartz covers were used. Diffuse reflectance spectra were obtained on a Perkin-Elmer Model 559 u.v.-visible spectrophotometer with an internal reflectance sphere lined with barium sulfate. Samples were prepared for reflectance analysis by pressing into pellets at 5000 psi for 4 min. The absolute reflectance values were obtained by referencing relative reflectance measurements to barium sulfate as described elsewhere [16]. The ^{13}C (22.63 MHz) cross-polarization magic-angle spinning n.m.r. spectrum was obtained using a Bruker SXP20/100 spectrometer equipped with a BDR proton decoupler and magic-angle probe. A single-contact pulse sequence with a contact time of 3 ms and a recycle time of 4 s was used. The sample was spun at 3 kHz in a Kel-F rotor. Each spectrum was the average of 20 000 scans.

Preparation of ligand. n-Propylamine was bonded to the silica gel surface as described by Leyden et al. [1]. The resulting aminated silica gel (10 g) was dispersed in 200 ml of water containing 10 g of sodium hydrogencarbonate and cooled to 0—5°C in an ice bath; 2 g of 2,4,6-trichlorotriazine in 125 ml of acetone was slowly added to this mixture with the temperature held below 10°C throughout the reaction. After 1 h, the mixture was subjected to vacuum to ensure penetration of the solution into the pores of the gel. The resulting modified silica gel was collected by filtration and thoroughly washed with water, acetone, methanol, and diethyl ether. A portion (10 g) of this modified silica gel and 5 g of sodium carbonate were dispersed in 225 ml of toluene; 2 g of 2,2′,4-trihydroxyazobenzene was added and the resulting slurry was stirred and refluxed for 2.5 h. The resulting silica gel was isolated by filtration and washed thoroughly with toluene, water, ethanol, and diethyl ether. The gel was then exhaustively washed with acetone in a Soxhlet extractor.

Aluminum complexation methods. In these studies, 0.25 g of the immobilized ligand—substrate system was equilibrated by mixing with 1 l of the appropriate solution. The solutions were buffered at pH 4.5 with an acetic acid—acetate buffer. In addition to the appropriate volume of stock aluminum solution, some samples contained 10 ml of a 0.05% solution of either disodium fluorescein in water or rosolic acid in ethanol. All systems were allowed to equilibrate for 1 h and were then filtered and washed with 50 ml of water buffered at pH 4.5 with an acetic acid—acetate buffer. The solution containing rosolic acid was washed with ethanol (≈100 ml) until the effluent was colorless and then with buffer. All samples were allowed to air-dry overnight.

The model compound was equilibrated with aluminum ions in (2 + 3) ethanol—water. The mixture contained 1 ml of dye solution (0.2 g of 2,2′,4-trihydroxyazobenzene in 100 ml of ethanol), 3 ml of buffer (pH 4.5 from 500 g of ammonium acetate and 60 ml of glacial acetic acid in 1.0 l), the appropriate amount of aluminum stock solution, and any foreign species being investigated in a total volume of 100 ml. Fluorescence was measured after a reaction time of 2 h.

Results and discussion

The proposed structure of the substrate—linkage—ligand system is shown below. Several recent advances in the spectroscopic analysis of immobilized systems were useful in monitoring the immobilization sequence [16, 17]. The first step, immobilization of the alkylamine chains, was verified by cross-polarization magic-angle spinning n.m.r. The solid-state ^{13}C—n.m.r.

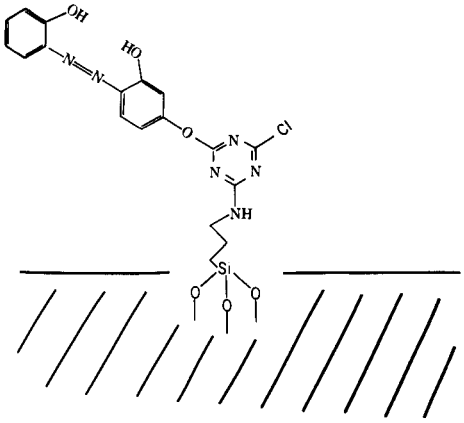

spectrum of the modified silica gel was consistent with the solution spectrum of a model compound, 3-aminopropyltriethoxysiliane. The system resulting from the reaction of the immobilized alkylamine with 2,4,6-trichlorotriazine was not amenable to this type of ^{13}C—n.m.r., as the triazine ring does not contain carbon atoms bonded directly to a hydrogen atom. This condition precludes efficient cross-polarization. Instead, the system was studied by diffuse reflectance ultraviolet spectroscopy. It has been shown that diffuse reflectance spectra of immobilized systems, presented as the Kubelka—Munk function, are similar to transmission spectra of soluble model compounds presented as the absorbance function [16]. The primary concern here was to ascertain the number of surface bonded sites per molecule of the triazine. Past studies suggest that the low temperature and mildly basic conditions should result in reaction of a single site [15]. 4,6-Dichloro-2-ethylaminotriazine and 2,4-di(ethylamino)-6-chlorotriazine were prepared to model the mono- and di-linked possibilities, respectively. The spectral properties of hexane solutions of these compounds are given in Table 1 along with those from the reflectance study of the immobilized system. As expected, the

TABLE 1

Spectral features of immobilized systems and model compounds

System	Peak wavelengths (nm)	
	Major peak	Minor peak
Immobilized at low temperature	236	264
Immobilized at high temperature	<230	255
4,6-Dichloro-2-ethylaminotriazine	233	266
2,4-Di(ethylamine)-6-chlorotriazine	220	261

immobilized system, prepared at low temperature, is most similar to the model compound with only one ethylamine substituted for a chlorine atom. When the triazine was immobilized at higher temperature (refluxing), which should favor disubstitution, the product gave a reflectance spectrum (see Table 1) which corresponded more closely to the model compound with two chlorines replaced by ethylamine molecules. Thus it appears that reaction at low temperature minimizes multiple linkage of the triazine to the gel. The final step involved immobilization of the ligand by reacting 2,2′,4-trihydroxyazobenzene with the immobilized dichlorotriazine. Two factors are of concern here, the number of ligands reacting with each dichlorotriazine and the position of linkage to the ligand. The presence of chlorine atoms in the final system, as shown by a positive sodium fusion test, suggests that only one of the available positions on the triazine ring reacts with a ligand molecule. This is consistent with the low reactivity of the third position. It is important that the ligand couples at the 4-hydroxy position instead of one of the potentially chelating hydroxy groups. It was anticipated that these chelating hydroxy groups would be less acidic because of internal hydrogen bonding and thus less likely to form the reactive anion than the 4-hydroxy group. Apparently, the chelating portion of the ligand was not altered in the reaction for at least some of the molecules, because the fluorescence spectra of the complex between the immobilized system and aluminum ions are similar to spectra of the corresponding complex of 2,2′,4-trihydroxyazobenzene in solution.

Figure 1(a) represents the excitation and emission spectra of the immobilized system complexed with aluminum(III). The solution spectra of the model system described above are included for comparison as Fig. 1(b). The similarities are apparent. The peak wavelengths in the emission spectra are almost identical for the immobilized (564 nm) and solvated systems (562 nm). The apparent minimal effect of linkage to the ligand at a position para to the chelating azo moiety is consistent with a report on the effect of substituent groups on the fluorescence of aluminum complexes with dihydroxyazomethines [18]. It has been reported that a fluorescent molecule immobilized on silica gel experiences an environment that is somewhat less polar than that represented by water or methanol [11]. The similarities in emission spectra observed here between the immobilized and solvated systems suggest

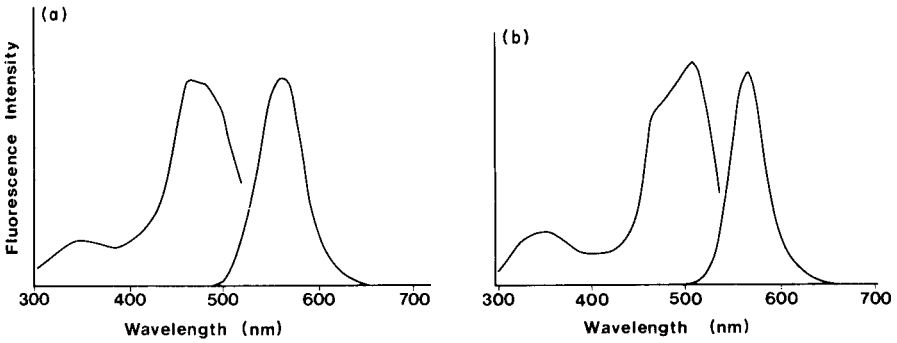

Fig. 1. (a) Excitation and emission spectra of immobilized ligand—aluminum complex; 0.25 g of substrate—ligand equilibrated with and isolated from 1 l of 1.5 ppm aluminum solution. (b) Corresponding spectra of an excess of model ligand in equilibrium with 1.5 ppm aluminum solution. Excitation spectra obtained with emission measured at 565 nm. Emission spectra obtained with excitation at 465 nm. Neither system exhibits significant fluorescence in absence of aluminum.

that the complex is relatively insensitive to its environment. Indeed, a shift in the solvent for the model system from a (2 + 3) ethanol—water mixture to a (4 + 1) mixture brought about a minimal shift in peak wavelength from 562 to 563 nm. The most noticeable difference between the emission spectra is the greater peak width which characterizes the spectrum of the immobilized system. This is consistent with the nonuniform environment experienced by the immobilized ligand on the heterogeneous substrate. The only noteworthy difference between the excitation spectra of the two systems is the dominance in solution of what appears as a shoulder on the long wavelength side of the spectrum for the immobilized system. This difference can be attributed to a skewing of the spectrum due to absorption by the excess of uncomplexed ligand present in the solution system. It is absent if an excess of aluminum is used.

Quantitative utility. The primary quantitative advantage expected for this system was an elimination of interferences. This type of aluminum complex is reported to have a high formation constant and is also relatively slow to dissociate. Both of these factors suggest that it should be possible to isolate the system from the solution in which it was formed and remove any adsorbed foreign materials by thorough washing without danger of losing the aluminum ion.

This potential was tested for solutions containing either disodium fluorescein or rosolic acid. Fluorescein should interfere with the solution determination of aluminum(III) because its peak wavelengths for excitation and emission are similar to those of the aluminum complex. Rosolic acid should interfere by absorption of exciting radiation (λ_{max} = 460 nm at pH 4.5).

Table 2 summarizes the results of the interference studies of these species for the solution system and the immobilized system after isolation and

TABLE 2

Comparison of the effects of potential interferences on the immobilized and solvated complex

System	Interferent[a]	Response ratio[b]
Solvated	Rosolic acid	0.80
Immobilized	Rosolic acid	1.0
Solvated	Fluorescein	1.6
Immobilized	Fluorescein	1.0

[a]Interferent present at 5×10^{-4}%, Al^{3+} present at 1.5 ppm except in the solution study of fluorescein in which both interferent and Al^{3+} were diluted by 10. [b]Ratio of responses with and without interferent.

washing. The effects in solution were as predicted; the fluorescein substantially increased the fluorescence at the wavelength monitored while rosolic acid decreased the observed fluorescence. For the immobilized system, the interference from fluorescein was eliminated by washing with the same acetate buffer used as the solvent in the solution studies. The effects of the rosolic acid were eliminated by washing with 95% ethanol until the effluent was colorless followed by rinsing with the acetate buffer to insure that the appropriate protonation existed and that the associated anions were consistent with the control.

It is difficult to compare the sensitivities of the immobilized and model systems. While the response in the solution procedure is dependent only on the concentration of aluminum, the response of the immobilized system is dependent on the volume of solution equilibrated with the system as well as the amount of ligand—substrate employed. It is, however, apparent that for this particular immobilized system, its utility is not in increased sensitivity. For a given concentration, the free ligand system gave a response which was roughly five times as great as that obtained when 0.25 g of the immobilized system was equilibrated with 1 l of solution.

Several equations are available which describe the relationship between fluorescence intensity and concentration for front surface fluorescence of solid materials [5]. For this system, the applicable form must take into account the fact that the substrate is highly scattering and capable of absorbing the exciting radiation and to a lesser extent, the emitted radiation. Although the silica gel itself is nonabsorbing in the visible region, the presence of an excess of the immobilized ligand will, in effect, provide an absorbing substrate. It has been predicted that, for these conditions, the response will be linearly related to concentration at low levels of fluorescence [19]. This is consistent with present observations on the immobilized ligand—aluminum complex. The responses from 0.25-g samples of the ligand—substrate, equilibrated with 1 l of solutions containing 0.1, 0.2, 0.3, 0.4, 0.5, 1.0 and 1.5 ppm aluminum fit a linear relationship (linear correlation coefficient = 0.998).

The authors acknowledge assistance in the n.m.r. study from Paul Inglefield. Financial support to R. Allston through the National Science Foundation Minority Graduate Fellowship program is also acknowledged. This research was also supported in part by a National Science Foundation Equipment Grant No. CHE 77-09059.

REFERENCES

1 D. E. Leyden, G. H. Luttrell and T. A. Patterson, Anal. Lett., 8 (1975) 51.
2 D. E. Leyden and G. H. Luttrell, Anal. Chem., 47 (1975) 1612.
3 D. E. Leyden, W. K. Nonidez and P. W. Carr, Anal. Chem., 47 (1975) 1449.
4 J. R. Jezorek and H. Freiser, Anal. Chem., 51 (1979) 366.
5 R. J. Hurtubise, Solid Surface Luminescence Analysis, Dekker, New York, 1981.
6 Z. Skuric, F. Vlic and J. Prpic-Marecic, Anal. Chim. Acta, 73 (1974) 213.
7 N. Turina, J. Chromatogr., 93 (1974) 211.
8 D. E. Ryan, J. Holzbecher and H. Rollier, Anal. Chim. Acta, 73 (1974) 49.
9 H. Rollier and D. E. Ryan, Anal. Chim. Acta, 74 (1975) 23.
10 R. G. Delumyea and G. H. Schenk, Anal. Chem., 48 (1976) 95.
11 C. H. Lochmüller, D. B. Marshall and D. R. Wilder, Anal. Chim. Acta, 130 (1981) 31.
12 L. A. Saari and W. R. Sietz, Anal. Chem., 54 (1982) 821.
13 S. R. Abbott, German Patent 2,942,370 (1980); US Appl. 953,380 (1978); Chem. Abstr. 93: 125162f.
14 H. Diehl and J. L. Ellingboe, Anal. Chem., 32 (1960) 1120.
15 J. T. Thurston, J. R. Dudley, D. W. Kaiser, I. Hechenbleikner, F. C. Schaefer and D. Holm-Hansen, J. Am. Chem. Soc., 73 (1951) 2981.
16 R. T. Allston, M.Sc. Thesis, College of the Holy Cross, MA, 1982.
17 D. E. Leyden, D. S. Kendall and T. G. Waddell, Anal. Chim. Acta, 126 (1981) 207.
18 R. J. Argauer and C. E. White, Anal. Chem., 36 (1964) 2141.
19 J. Goldman, J. Chromatogr., 78 (1973) 7.

Analytica Chimica Acta, 142 (1982) 313—318
Elsevier Scientific Publishing Company, Amsterdam — Printed in The Netherlands

Short Communication

FLUORIMETRIC DETERMINATION OF PYRENE:PROTEIN ASSOCIATION RATIOS

LINDA B. McGOWN* and DAVID I. UEDA

Department of Chemistry, California State University Long Beach, Long Beach, CA 90840 (U.S.A.)

(Received 26th April 1982)

Summary. Two fluorimetric methods for determining pyrene:protein association ratios are described. The methods are useful for measuring the uptake by proteins of small, fluorescent molecules with limited aqueous solubility (10^{-6} M or less). The association ratios (moles pyrene per mole protein) determined by the two methods were found to be: bovine β-lactoglobulin (0.32, 0.33), human serum albumin (0.44, 0.42), bovine γ-globulin (0.23, 0.20), and human γ-globulin (0.04, 0.00).

Interactions between proteins and a variety of biologically-active molecules, such as drugs and carcinogens, have been widely studied. The use of fluorescent molecules as probes of biological microenvironments is a related area in which these interactions are important. Frequently, these studies require the determination of the extent of uptake of relatively small molecules by proteins or other macromolecules. Among the most frequently used techniques for quantifying such uptake are radioanalytical methods [1—5], which often require long incubation and separation steps. Fluorimetric methods have also been used. For example, the binding of thyroxine by serum albumin was studied by measuring the quenching of the protein fluorescence by bound thyroxine [6]. Fluorescence was also used to study the interaction of 1-anilino-8-naphthalene sulphonate with yeast alcohol dehydrogenase [7] and to determine the particle-mediated membrane uptake of carcinogens [8].

This communication describes the use of fluorescence measurements to quantify the uptake of pyrene by four proteins. Two different methods are used to determine the pyrene:protein association ratios in aqueous solution. The techniques are applicable to protein interactions with any molecule which fluoresces, and which has a low aqueous solubility. This latter is required because in both methods, calculation of the association ratios depends on solubilization of the small molecule by uptake on the protein. The methods can be used for molecules with solubilities such that fluorescence increases

*Present address: Department of Chemistry, Oklahoma State University, Stillwater, OK 74078, U.S.A.

linearly with increasing concentration (by solubilization) of the molecule (i.e., solubilities up to $\sim 10^{-6}$ M).

Experimental

Fluorescence emission spectra were recorded using an Aminco-Bowman Ratio II spectrofluorimeter in the conventional, single-beam mode, in conjunction with an x—y recorder. Single-wavelength fluorescence measurements were made in the ratio mode, in which the ratio of the sample excitation beam to a portion of the beam directed to a reference detector is taken electronically, to compensate for source output fluctuations.

All fluorescence intensity measurements were corrected for blank fluorescence, and corrected intensities were used in all calculations. In cases in which the proteins contributed a significant fluorescence, their contributions were also included in the blank corrections, so that all fluorescence referred to is due to pyrene only.

Two methods for determining pyrene:protein association ratios were evaluated. In Method 1, increments of pyrene were added to fixed amounts of protein. In Method 2, increments of protein were added to fixed amounts of pyrene. Both methods were performed directly in the fluorescence cuvet, readings being taken after each addition of protein or pyrene upon reaching a stable value (generally less than 3 min per addition). The cuvet initially contained 2 ml of buffer (0.1 M phosphate, pH 7.0, 0.15 M NaCl), and protein (Method 1) or pyrene (Method 2) (10—250 μl). Aliquots (1 μl, usually equivalent to 1 nmol) of pyrene (Method 1) or protein (Method 2) were added, from a fixed volume, 1-μl micropipet, so that dilution factors were negligible.

Aqueous solutions of pyrene (Aldrich Chemical; 99%+) were prepared from a 1.00×10^{-2} mol l^{-1} solution of pyrene in ethanol (100%, reagent grade). Thus, solutions in the cuvet contained up to 0.15% ethanol for Method 1 and up to 0.05% ethanol for Method 2.

All proteins were from United States Biochemical Corp. The following molecular weights were used in calculations: human serum albumin (crystallized, m.w. = 66 000), bovine serum albumin (crystallized, m.w. = 66 000), β-lactoglobulin (bovine milk, m.w. = 36 800), bovine γ-globulin (fraction II, m.w. = 157 000), and human γ-globulin (fraction II, m.w. = 160 000).

Mathematical description and calculation of pyrene:protein association ratios. In this description, all volumes are expressed in milliliters and all concentrations are in μmol l^{-1}. In Method 1, 1-nmol increments of pyrene were added to three different concentrations of the protein. To calculate the association ratio, n, it is assumed that the blank-corrected fluorescence intensity, I_F, can be expressed as: $I_F = \overline{I_F}P + \overline{I'_F}P'$, where $\overline{I_F}$ is the fluorescence intensity per μmol l^{-1} pyrene, P is the concentration of free pyrene monomer in solution, and I'_F and P' are the same quantities for pyrene associated with the protein. The maximum fluorescence intensity reached, $I_{F,max}$, is then expressed as the sum of the maximum, solubility-limited concentration

of free pyrene in solution and the maximum amount taken up by the protein: $I_{F,max} = \overline{I_F} P_{max} + \overline{I_F'} P'_{max}$. The last term, P'_{max}, is the one sought, namely, the maximum concentration of pyrene associated with a given amount of protein, from which n is calculated. P'_{max} is calculated from the preceding equation, and the n values are then calculated from $n = P'_{max}/C^0_{protein}$, where $C^0_{protein}$ is the total protein concentration.

The quantity, $\overline{I_F} P_{max}$, is found from a blank run with zero protein concentration. It should have a constant value, dependent on the aqueous solubility of pyrene. However, variations may occur when runs are done on different days and in different cuvets. All runs for a given protein were done on a single day in a single cuvet to minimize this variability.

To determine $\overline{I_F'}$, fluorescence of a sub-solubility concentration of pyrene (9×10^{-7} mol l^{-1}) was measured in the presence of a 50-fold excess of the protein. If no association occurs, the $\overline{I_F'}$ value measured will simply be that for free pyrene ($\overline{I_F}$). If uptake occurs into a site which completely quenches the pyrene fluorescence, $\overline{I_F'}$ will be zero and n cannot be calculated by either method.

In Method 2, 1-nmol increments of protein were added to solutions containing a fixed amount of pyrene (equivalent to 7.5×10^{-6} mol l^{-1}, well above the aqueous solubility of pyrene). The initial intensity, $\overline{I_F} P_{max}$, corresponds to the aqueous solubility of pyrene. As protein is added, additional pyrene monomer enters the solution in amounts determined by the uptake ability of the protein. The slope of the curve of I_F vs. volume of protein solution, taken from the steepest portion of the curve, is expressed as slope $= \Delta I_F/\Delta$ volume. Using the values for $\overline{I_F'}$ determined as for Method 1, cuvet volume V and these slopes, n can be calculated from

$$n = (\Delta I_F/\Delta V)(1\overline{I_F'})(V/C^0_{protein}) \quad (1)$$

Results and discussion

Pyrene emission spectra. Figure 1 shows the fluorescence emission spectra (λ_{ex} = 334 nm) for pyrene alone and in the presence of bovine β-lactoglobulin. The total pyrene content in the cuvet is well above the aqueous solubility of pyrene monomer ($\approx 1 \times 10^{-6}$ M). The pyrene monomer emission peaks occur at 370 nm and 390 nm. The large, broad emission peak at 460 nm is due to pyrene excimer formation [9]: $P + h\nu = P^*$ and $P^* + P = PP^*$ (excimer). Any change in the pyrene emission spectrum on addition of protein is attributed to pyrene–protein interactions. In most cases, the proteins themselves were found to contribute negligible fluorescence at the wavelengths used, and in all cases the contribution was less than 10% of the total fluorescence. Increases in pyrene monomer emission are most likely due to "solubilization" of pyrene, i.e., increases in the total monomer concentration of the solution (pyrene in aqueous solution plus pyrene associated with the protein). All of the proteins studied caused substantial increases in pyrene monomer emission except for human γ-globulin, which caused only a slight increase (Fig. 1).

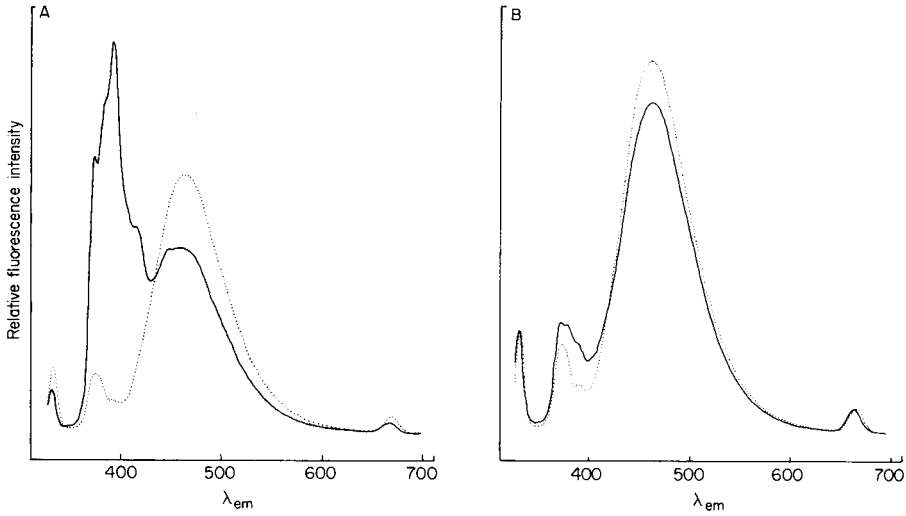

Fig. 1. Pyrene fluorescence emission spectra (λ_{ex} = 334 nm): (· · ·) alone; (——) in the presence of (A) 264 μM bovine β-lactoglobulin and (B) 110 μM human γ-globulin. Solutions are saturated with pyrene, with excess of pyrene at the bottom of the cuvet, and contain 0.1 M phosphate buffer, pH 7.0, 0.15 M NaCl.

Pyrene:protein association ratios. Figure 2 shows the curves obtained for bovine β-lactoglobulin by Method 1. Three different protein concentrations were run. Curves obtained for the other proteins were similar to those in Fig. 2, differing only in the relative spacing between the curves which reflects the different solubilization abilities of the proteins. The $\overline{I}_F P_{max}$ values found for each protein are shown in Table 1, along with the association ratios calculated for each run as well as average values for each protein. The precision for Method 1 was excellent, with a standard deviation of 8×10^{-3}.

Curves obtained for each of the four proteins by Method 2 are shown in Fig. 3. The corresponding association ratios are shown in Table 1.

The values for the association ratios by the two methods are in good agreement for all the proteins. The use of multiple runs in Method 1 should eliminate possible concentration effects and improve accuracy. Method 2 is faster because only a single run is required per protein, and the calculations are simpler. Results for both methods are obtained within 20—30 min per run.

Interpretation of the results for the association ratios on a molecular scale is beyond the scope of this investigation. The methods used will only allow determination of overall association ratios and do not take into account the possibility of the existence of more than one form of a protein or the dynamic nature of proteins in solution. All of the proteins investigated showed definite pyrene uptake except for human γ-globulin. The very low but nonzero values found for this protein by Method 1 may be due to impurities in the protein preparation (no uptake was measured by Method 2).

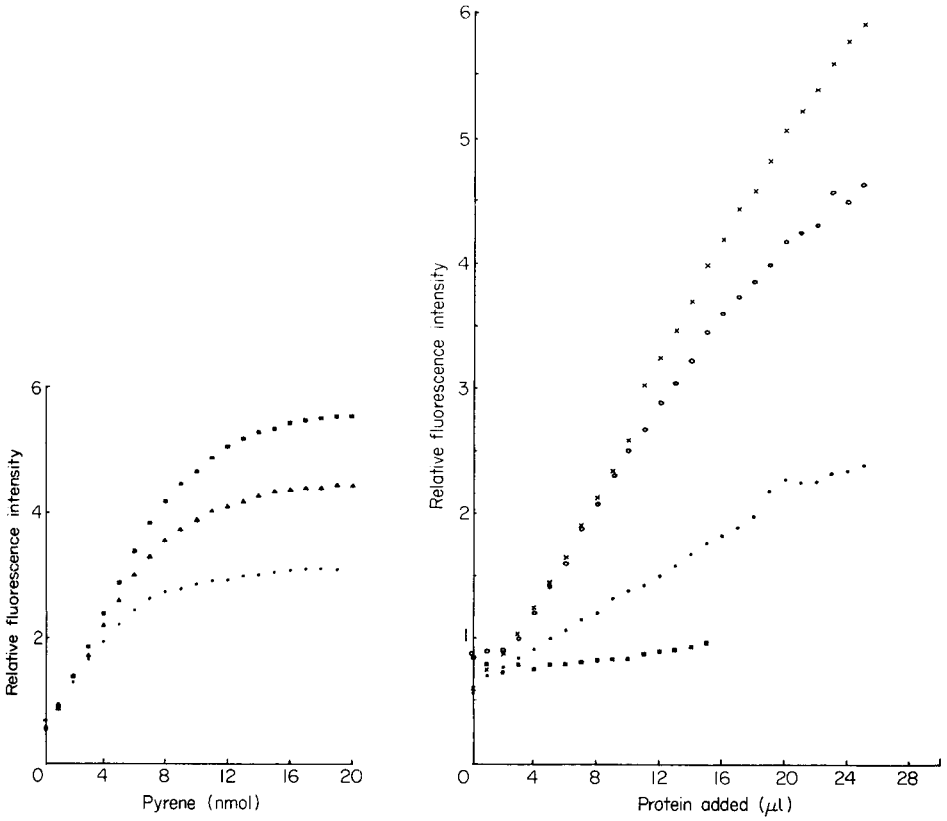

Fig. 2. Method 1 curves for addition of 1-nmol (1-μl) increments of pyrene to bovine β-lactoglobulin: (•) 4.06, (▲) 8.11, (■) 12.1 μmol l^{-1} protein; 0.1 M phosphate buffer, pH 7.0, 0.15 M NaCl.

Fig. 3. Method 2 curves for addition of 1-μl increments of protein to a cuvet containing a saturated pyrene solution with excess of pyrene in 0.1 M phosphate buffer, pH 7.0, 0.15 M NaCl. (■) Human γ-globulin, 1.0 × 10^{-3} mol l^{-1}; (•) bovine γ-globulin, 1.0 × 10^{-3} mol l^{-1}; (○) human serum albumin, 1.0 × 10^{-3} mol l^{-1}; (×) bovine β-lactoglobulin, 2.4 × 10^{-3} mol l^{-1}.

Conclusions

Measurement of overall association ratios is useful for comparing the uptake of small, fluorescent molecules by various proteins, as shown above. Such determinations are also valuable for measuring the effects of environmental factors, such as pH, the presence of other molecules, and solvent effects, on the association ratios. Finally, by developing methods which can be used for relatively insoluble molecules, the uptake of molecules not normally found in aqueous biological environments can be studied (e.g., polynuclear aromatic classes of environmental pollutants and drugs) and the information can be used to help predict the mechanisms of their transport and distribution via proteins in these systems.

TABLE 1

Results for association ratios, n, by Methods 1 and 2

	Method 1				Method 2
	Protein (μmol l^{-1})	$\overline{I_F}P_{max}$	n	n_{av} ± s.d.	n
Human serum albumin	0	2.40	—		
	2.54		0.44	0.44 ± 0.00	0.42
	7.59		0.44		
Bovine β-lactoglobulin	0	1.08	—		
	4.06		0.32	0.32 ± 0.01	0.33
	8.11		0.33		
	12.1		0.32		
Bovine γ-globulin	0	1.00	—		
	2.49		0.23	0.23 ± 0.01	0.20
	4.98		0.23		
	9.90		0.22		
Human γ-globulin	0	1.69	—		
	2.49		0.04	0.04 ± 0.01	0.00
	4.98		0.03		
	9.90		0.05		

REFERENCES

1 D. H. Phillips, P. L. Grover and P. Sims, Int. J. Cancer, 22 (1978) 487.
2 K. Hemminki and H. Vainio, Cancer Lett., 6 (1979) 167.
3 H. P. Shu and A. V. Nichols, Cancer Res., 39 (1979) 1224.
4 T. H. Zytkovicz, H. L. Moses and T. C. Spelsberg, Cancer Res., 38 (1978) 2307.
5 M. McKenzie, T. McLemore, P. Rankin, R. R. Martin, N. Wray, E. Cantrell and D. Busbee, Cancer, 42 (1978) 2733.
6 R. F. Steiner, J. Roth and J. Robbins, J. Biol. Chem., 241 (1966) 560.
7 F. M. Dickinson, FEBS Lett., 15 (1971) 17.
8 J. R. Lakowicz, M. McNamara and L. Steenson, Science, 199 (1978) 305.
9 C. A. Parker and C. G. Hatchard, Nature, 190 (1961) 165.

Analytica Chimica Acta, 142 (1982) 319—324
Elsevier Scientific Publishing Company, Amsterdam —Printed in The Netherlands

Short Communication

SPECTROPHOTOMETRIC DETERMINATION OF SULFATE BY SOLVENT EXTRACTION WITH THE NON-IONIC SURFACTANT SPAN 20 AND CRYSTAL VIOLET

SHIGEYA SATO

Faculty of Education, Kumamoto University, 2-40-1 Kurokami, Kumamoto 860 (Japan)

(Received 2nd March 1982)

Summary. The sulfate ion is extracted into toluene with Span 20 (sorbitan monolaurate) and crystal violet. The calibration graph is linear over the range 2.5×10^{-5}—2.5×10^{-4} mol l^{-1} sulfate (2.4—24 mg l^{-1}) in the aqueous phase when the extracted crystal violet is measured at 600 nm. The method is applied to natural waters.

Sensitive spectrophotometric determinations of anions by ion-pair extraction with colored large cations are well known [1—3]. The sulfate ion is difficult to extract into organic solvents because of its hydrophilic nature. Indirect methods have been reported for sulfate determinations based on the extraction of chromogenic agents released by reaction with sulfate; the barium chloranilate method [4] is the best known of these and has been modified in various ways [5—7]. New reagents for sulfate have been synthesized and applied to nephelometric and spectrophotometric determinations of sulfate [8—11].

Non-ionic surfactants such as polyethylene glycol ethers form complexes with diammonium tetrathioisocyanatocobaltate(II) which can be extracted into some organic solvents [12]. Such extractions have been used for determinations of non-ionic surfactants [13] and of the central metal ions of chelate complexes [14, 15], but have not been reported for anions. In recent work on the extraction—spectrophotometric determination of hydrophilic anions with non-ionic surfactants, it was found that sulfate was extracted into toluene with the non-ionic surfactant Span 20 (sorbitan monolaurate) and crystal violet (chloride) [16]. This communication describes a more extensive study of the procedure and its application to natural waters.

Experimental

Apparatus. A Hitachi Perkin-Elmer Model 139 spectrophotometer was used for absorbance measurements and a Hitachi 624 digital spectrophotometer for the spectra, with glass cells of 10-mm path length. An Iwaki Model KM-Shaker, a Hitachi centrifuge 03P and a Hitachi-Horiba M-3 pH meter were also used.

0003-2670/82/0000-0000/$02.75

Reagents. A 1.0×10^{-3} mol l^{-1} crystal violet solution was prepared by dissolving guaranteed-grade crystal violet in deionized water. A stock standard sodium sulfate solution (1.0×10^{-2} mol l^{-1}) was prepared in deionized water and diluted as required. Reagent-grade toluene was used as received. The extraction solvent was toluene containing 0.1% (w/v) Span 20 (Katayama Co.). Deionized water was used throughout. All other reagents were of analytical-reagent grade.

Calibration procedure. Transfer an aliquot (0.1—1.0 ml) of the standard sulfate solution to a stoppered 10-ml brown test tube and mix in 1 ml of crystal violet solution and 1 ml of 0.05 M succinic acid. Dilute to 4 ml with deionized water. Shake with 4 ml of the toluene—Span 20 solution for 15 min. Centrifuge for 5 min at 2000 rpm, transfer the organic phase to a 10-mm glass cell, and measure the absorbance at 600 nm, using toluene alone as reference.

Results and discussion

Absorption spectra. The absorption spectra of a blank and a sulfate extract in toluene—Span 20 obtained by the standard procedure are shown in Fig. 1. These spectra can be ascribed to crystal violet, the wavelength of maximum absorption being 600 nm in each case. The ion-pair formed between crystal violet and sulfate was not extracted into toluene when Span 20 was absent.

Effect of pH on the extraction. Various buffer solutions were investigated (succinate, citrate, tartrate, borate, phosphate, acetate and carbonate solutions). It was confirmed that the pH value remained constant throughout the experimental period; the initial pH values were adjusted with the relevant acid and sodium hydroxide, as required. For all buffer solutions, the absorbance (the difference between sample and the reagent blank) decreased over the pH range 2.8—5.5 (Table 1), i.e., the percentage extraction of sulfate decreased. The apparent molar absorptivity at pH 4.5 without buffer solution was high, but sulfate was not extracted at pH 4.5 when phosphate

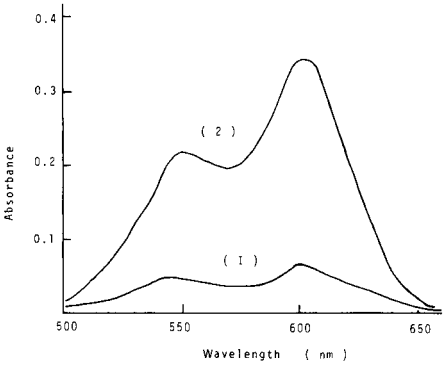

Fig. 1. Absorption spectra of the organic phase: (1) reagent blank; (2) 1.25×10^{-4} mol l^{-1} sulfate. Crystal violet, 2.5×10^{-4} mol l^{-1}; toluene reference.

TABLE 1

Effect of pH on the extraction

Buffer solution		pH				
		2.8	3.2	3.9	4.5	5.5
0.05 M succinate	Blank[a]	0.07	0.08	0.10	0.13	0.15
	ϵ[b]	2200	1800	1500	250	170
0.05 M citrate	Blank	0.07			0.18	
	ϵ	750			500	
0.05 M tartrate	Blank	0.08			0.10	
	ϵ	690			310	
0.05 M phosphate	Blank				0.09	
	ϵ				0	
Water[c]	Blank				0.07	
	ϵ				2200	

[a]Absorbance. [b]Apparent molar absorptivity (l mol^{-1} cm^{-1}). [c]Without buffer solution.

buffer was used and the extraction of sulfate at constant pH in the presence of non-ionic surfactant was greatly affected by the aliphatic acid anion present (Table 1). In the proposed method, 1 ml of 0.05 M succinic acid solution is recommended.

Effects of other variables. At a constant concentration of sulfate (1.25×10^{-4} mol l^{-1}) the effect of changing the concentration of crystal violet was examined; provided that the crystal violet was in excess of a 1:1 mole ratio to sulfate, constant extraction was obtained when a reagent blank was used as a reference. The reagent blank remained constant for the range $0.1—5.0 \times 10^{-4}$ mol l^{-1} crystal violet.

Increasing the Span 20 concentration led to an increase in absorbance of both the reagent blank and sulfate extracts (Fig. 2). The concentration of

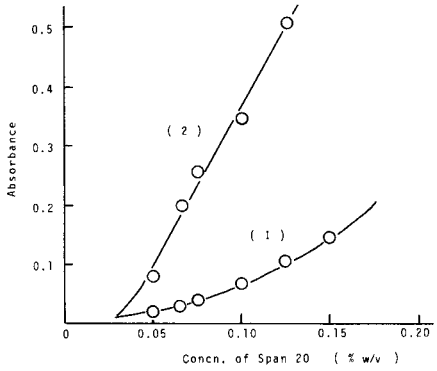

Fig. 2. Effect of Span 20 concentration in toluene: (1) reagent blank; (2) 1.25×10^{-4} mol l^{-1} sulfate. Crystal violet, 2.5×10^{-4} mol l^{-1}; toluene reference.

Span 20 in toluene, therefore, was fixed at 0.1% (w/v). Maximum extraction of the sulfate required a shaking time longer than 10 min; for safety, shaking times were fixed at 15 min, but this could be extended to 25 min without affecting the results.

Tests of other organic solvents showed that crystal violet was readily extracted without Span 20 into dichloromethane, chloroform and 4-methyl-2-pentanone, or with Span 20 into chlorobenzene, cyclohexane and carbon tetrachloride. Crystal violet was also extracted into toluene (absorbance 0.070) and benzene (absorbance 0.100), toluene being preferable because of the lower reagent blank. Other surfactants were tested but, as shown in Table 2, Span 20 provides optimal extraction of sulfate.

Calibration graph. The calibration graph obtained by the standard procedure was linear over the range 2.5×10^{-5}—2.5×10^{-4} mol l^{-1} sulfate (2.4—24 mg l^{-1}) in the aqueous phase. The apparent molar absorptivity (related to the sulfate concentration in the aqueous phase) calculated from the slope was 2200 l mol^{-1} cm^{-1}. The reagent blank was 0.070 against a toluene reference and the coefficient of variation was 5% for ten runs at 1.5×10^{-4} mol l^{-1} sulfate.

Effect of diverse ions. Table 3 shows the apparent molar absorptivities obtained for sulfate and various ions. Most of the anions were extracted to some extent with Span 20, but phosphate was not extracted at all. Hydrogencarbonate was not extracted when succinic acid was added. The apparent molar absorptivities obtained for cations are actually due to the chloride in the salts added. Table 4 shows the effects of ions usually present in river and seawater. Chloride and nitrate at the same molar concentrations as sulfate did not interfere, but ten-fold concentrations of chloride gave positive errors.

Applications. The proposed method was applied to the determination of sulfate in river and seawater. Samples of these waters were filtered through a 0.45-μm membrane filter. The chloride ion in seawater (diluted to 10-fold) was removed by shaking with silver oxide and filtering; 0.5 ml of the resulting seawater was taken. River waters (1 ml) were treated directly. The results obtained are shown in Table 5, together with data obtained by the barium chloranilate method [4]. These results are in good agreement.

This extraction system with non-ionic surfactants may be useful for the extraction of other hydrophilic anions which are difficult to extract by the usual systems.

TABLE 2

Effect of the other non-ionic surfactants[a]

	Span 20	Span 40	Span 60	Span 80	Tween 20
Blank[b]	0.070	0.063	0.046	0.038	0.0
ϵ[c]	2200	1100	460	0	0

[a] 2.5×10^{-4} mol l^{-1} crystal violet with 0.1% (w/v) surfactant in toluene. [b] Blank absorbance. [c] Apparent molar absorptivity (l mol^{-1} cm^{-1}).

TABLE 3

Apparent molar absorptivities for different ions

Ion	Added as	With Span 20	Without Span 20	Ion	Added as	With Span 20[b]
SO_4^{2-}	Na_2SO_4	2200	0	K^+	KCl	50
Cl^-	NaCl	50	0	Na^+	NaCl	50
Br^-	NaBr	140	5	Ca^{2+}	$CaCl_2$	100
I^-	NaI	2800	200	Mg^{2+}	$MgCl_2$	90
NO_3^-	$NaNO_3$	280	15	Fe^{3+}	$FeCl_3$	170
HCO_3^-	$NaHCO_3$	0	0	Al^{3+}	$AlCl_3$	170
		2300[a]	25[a]			
$H_2PO_4^-$	NaH_2PO_4	0	0			
		0[a]	0[a]			

[a]In the absence of 1.25×10^{-2} mol l^{-1} succinic acid. [b]There was no extraction in the absence of Span 20.

TABLE 4

Effect of diverse anions on the results for 1.25×10^{-4} mol l^{-1} sulfate

Anion	Added as	Concentration ($\times 1.25 \times 10^{-4}$ M)	Absorbance at 600 nm[a]	Relative error (%)
None	—	—	0.345	—
Cl^-	NaCl	1	0.347	+0.6
		10	0.408	+18.3
NO_3^-	$NaNO_3$	1	0.334	−3.2
HCO_3^-	$NaHCO_3$	10	0.348	+0.9

[a]Toluene reference.

TABLE 5

Application to sea and river waters in Kumamoto Prefecture

Sample	Barium chloranilate method		This method
	SO_4^{2-} (ppm)	Recovery (%)[a]	SO_4^{2-} (ppm)[b]
Seawater near shore			
at Ushibuka	1500	101	1510 ± 60
at Misumi	2130	100	2220 ± 50
at Oda	2150	98	2090 ± 80
River water			
Shirakawa	49		48 ± 2
Kurokawa	51		48 ± 2

[a]3.8 mg of sulfate was added. [b]Mean of five determinations with standard deviation.

The author thanks Professor Y. Yamamoto and Dr. E. Iwamoto of Hiroshima University for their kind guidance and helpful discussions, and Professor S. Uchikawa of Kumamoto University for helpful suggestions and warm encouragement.

REFERENCES

1 Y. Tamamoto and S. Kinuwaki, Bull. Chem. Soc. Jpn., 37 (1964) 434.
2 S. Uchikawa, Bull. Chem. Soc. Jpn., 40 (1967) 798.
3 Y. Yamamoto, T. Kumamaru, Y. Hayashi and M. Yamamoto, Anal. Chim. Acta, 69 (1974) 321.
4 R. J. Bertolacini and J. E. Barney, II, Anal. Chem., 29 (1957) 281.
5 H. N. S. Schafer, Anal. Chem., 14 (1967) 1719.
6 Y. Yamamoto, K. Hiiro and T. Tanaka, Jpn. Analyst, 17 (1968) 206.
7 T. Murakami, M. Kamaya and T. Akazawa, Jpn. Analyst, 29 (1980) 483.
8 W. I. Stephen, Anal. Chim. Acta, 50 (1970) 413.
9 K. Tôei, H. Miyata and Y. Yamawaki, Anal. Chim. Acta, 94 (1977) 485.
10 P. K. Dasgupta, L. G. Hanley, Jr. and P. W. West, Anal. Chem., 50 (1978) 1793.
11 T. Koita, H. Miyata and K. Tôei, Jpn. Analyst, 29 (1980) 176.
12 E. G. Brown and T. J. Hayes, Analyst, 80 (1955) 755.
13 C. Calzolari, L. Favretto and F. Tunis, Analyst, 99 (1974) 171.
14 T. Sotobayashi, T. Suzuki and K. Yamada, Chem. Lett., (1976) 77.
15 T. Suzuki, N. Murakami and T. Sotobayashi, Bull. Chem. Soc. Jpn., 53 (1980) 1453.
16 S. Sato, E. Iwamoto and Y. Yamamoto, Anal. Lett., 14 (1981) 531.

Analytica Chimica Acta, 142 (1982) 325—328
Elsevier Scientific Publishing Company, Amsterdam — Printed in The Netherlands

Short Communication

SPECTROPHOTOMETRIC DETERMINATION OF CHROMIUM(VI) THROUGH ION-PAIR FORMATION WITH PHENYLFLUORONE

R. IZQUIERDO-HORNILLOS, J. L. PERAL-FERNANDEZ* and R. GALLEGO-ANDREU

Departamento de Química Analítica, Facultad de Ciencias Químicas, Universidad Complutense de Madrid, Ciudad Universitaria, Madrid-3 (Spain)

(Received 5th January 1982)

Summary. Two successive outer sphere complexes with mole ratios of 1:1 and 1:2 are formed between chromium(VI) and phenylfluorone at pH 1.5 in 40% ethanol. These have absorption maxima at 490 and 470 nm, respectively. The 1:1 complex obeys Beer's law at 500 nm ($\epsilon = 2.1 \times 10^4$ l mol^{-1} cm^{-1}) in the range 13—1700 ng l^{-1} chromium(VI).

Phenylfluorone is a widely employed analytical reagent for the spectrophotometric determination of anions such as W(VI) [1], Mo(VI) [2], Sn(IV) [3, 4], Ge(IV) [5], and several cations, e.g., U(VI) [6], Pb(II) [7] and Bi(III) [8]. Its analytical use is based on the presence in its molecule of *o*-OH groups on the same aromatic ring. The acid—base conjugated species can be represented (L being the phenylfluorone ligand) as

$$H_4L^+ \overset{K_0}{\rightleftharpoons} H_3L \overset{K_1}{\rightleftharpoons} H_2L^- \overset{K_2}{\rightleftharpoons} HL^{2-} \overset{K_3}{\rightleftharpoons} L^{3-}$$

with pK values of pK_0 = 2.11, pK_1 = 6.28, pK_2 = 10.21 and pK_3 = 11.7, calculated for 10% ethanol in water with ionic strength 0.1 M [9].

In the papers published on the analytical applications of phenylfluorone, it is assumed that chromium(VI) is a very serious interference in the determination of several anions. Thus, Cr(VI) must be absent for the spectrophotometric determination of germanium(IV), because of the strongly oxidizing properties of Cr(VI) [5]. In this communication, the experimental conditions for formation of an outer sphere complex between phenylfluorone and Cr(VI) are established in ethanol—water media, whose dielectric constant is lower than that of water. This stabilizes the ion-pair and hinders the oxidation of phenylfluorone, because the oxidizing ability of Cr(VI) is diminished in such solutions.

Experimental

Reagents. Analytical reagent-grade chemicals were used without further purification. A 1.0×10^{-4} M stock solution of phenylfluorone (Merck) was prepared in ethanol containing 5.0 ml of 12 M hydrochloric acid per litre. The solution was stable after 7 days. It was standardized against a standard

germanium(IV) solution spectrophotometrically at 510 nm. Potassium dichromate was dried at 110°C for 2 h and dissolved in distilled water to give a 5.0×10^{-3} M solution. Working solutions were prepared daily by dilution with distilled water.

Dichloroacetic acid (aqueous 2.0 M solution) was used to prepare (daily) the buffer solution by adding appropriate amounts of 2.0 M sodium hydroxide.

Instruments. A Pye-Unicam SP8-200 spectrophotometer was used.

Procedure. Solutions containing chromium(VI) were mixed with 10.0 ml of 1.0×10^{-4} M phenylfluorone solution and 10.0 ml of dichloroacetic acid buffer pH 1.3 and diluted to 25.0 ml with distilled water. The absorbance was measured at 500 nm in 1.00-cm glass cells against a reagent blank prepared under the same conditions.

Results and discussion

Absorption spectra. It can be seen in Fig. 1 that whereas the 1:1 Cr(VI): phenylfluorone system shows one absorption maximum at 490 nm, this maximum appears at 474 nm for the 1:2 system; 470 nm is the wavelength of maximum absorption of a phenylfluorone solution at the same pH.

Effect of pH and time. Figure 2 shows the effect of pH on "complex" formation at 470, 490 and 500 nm (this last wavelength gives the greatest sensitivity for Cr(VI)). The complex is formed at ca. zero pH and is destroyed at ⩾pH 3. Maximum colour development occurs at an apparent pH of 1.5 in the final water—ethanol solution. As the complex is formed at pH 1.5, a dichloro-

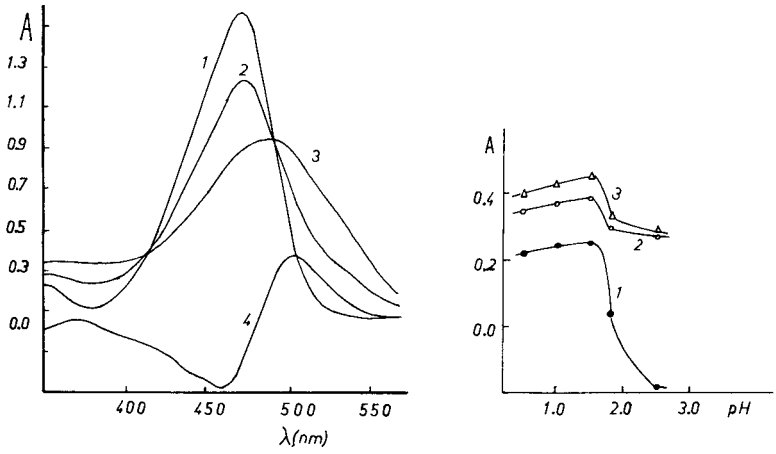

Fig. 1. Absorption spectra at pH 1.5: (1) phenylfluorone; (2) Cr(VI):phenylfluorone = 1:2; (3) Cr(VI):phenylfluorone = 1:1; (4) difference between curves 3 and 1. (4.0×10^{-5} M phenylfluorone.)

Fig. 2. Effect of pH on Cr(VI)/phenylfluorone solutions: (1) 470 nm; (2) 490 nm; (3) 500 nm. (4.0×10^{-5} M Cr(VI) and phenylfluorone.)

acetate buffer was chosen. This buffer slightly diminished the absorbance at 490 and 500 nm, whereas at 470 nm it caused an increase. The absorbance remained constant above a buffer concentration of 0.32 M. Thus, a buffer concentration of 0.80 M was chosen to ensure sufficient buffering capacity. All experiments indicated that 500 nm is the most suitable wavelength for analytical measurements.

The solutions should be allowed to stand for 10—30 min at room temperature. After 30 min, a slight decrease in the absorbance of the complex was observed. The absorbance was not affected by direct exposure to sunlight.

Composition and formation constant of the complexes. The stoichiometric composition of the complex was studied by application of the mole ratio and continuous variations methods. At 470 and 500 nm, the stoichiometry found was Cr(VI):phenylfluorone = 1:1. However, at 490 nm, two complexes (1:1 and 1:2) were detected by application of the mole ratio method (the existence of both complexes can be proved from the spectra shown in Fig. 1). Only the 1:1 complex was detected when the method of continuous variations was applied at 490 nm.

The value of the formation constant of the 1:1 complex, calculated from the method of continuous variations (at 500 nm) was 1.1×10^6 l mol^{-1} (μ = 0.1 M). The formation constant for the 1:2 complex was not calculated because dissociation severely limited the accuracy when the mole ratio method was applied.

Mechanism of the reaction. At pH 1.5 the predominant species of phenylfluorone (L) is H_4L^+, whose dissociation equilibrium is little affected by the dielectric constant (E) of the medium. However, for the Cr(VI) system, the predominant species under these conditions is $HCrO_4^-$; its dissociation equilibria are affected by the dielectric constant of the medium (in 40% ethanol at μ = 0.1 M, E = 58 and pK_1 = 1.2). Thus, the formation of an ion-pair can be considered, according to the theory of Bjerrum and Fuoss.

Because 1:1 and 1:2 complexes are formed, the reaction can follow two successive steps. To prove experimentally if proton interchange with the medium is possible, the method of Kirby et al. [10] was applied to the chromium(VI)—phenylfluorone reaction to establish the number of protons (n) released. Values of n near unity were obtained, which implies an exchange of only one proton, which obviously must come from $HCrO_4^-$. The reaction between Cr(VI) and phenylfluorone is therefore likely to be

$$H_4L^+ + HCrO_4^- \rightleftharpoons [(H_4L^+)\,(CrO_4^{2-})]^- \quad (\text{for } \lambda = 490 \text{ nm})$$

$$[(H_4L^+)\,(CrO_4^{2-})]^- + H_4L^+ \rightleftharpoons [(H_4L^+)_2\,(CrO_4^{2-})] \quad (\text{for } \lambda = 474 \text{ nm})$$

In the case of the 1:1 complex, a stable 7-membered ring may be formed, as well as some hydrogen bonding.

Analytical parameters. Beer's Law is obeyed at 500 nm at pH 1.5 in the range 0.013—1.7 ppm chromium (VI). The molar absorptivity is 1.6×10^4 l mol^{-1} cm^{-1}. According to the method of Ringbom and Ayres, the optimal measurement range is 0.77—1.7 ppm chromium (VI). The statistical

parameters for a mean Cr(VI) concentration of 1.2 ppm are: standard deviation = 0.013 ppm Cr(VI) (1.1%), standard deviation of the mean = 0.016 ppm; confidence limit = 1.2 ± 0.030 ppm (n = 16, t = 2.13 for a probability level of 95%).

Interferences. The interferences of other substances were studied by mixing Cr(VI), possible interfering ion (at concentrations 0.01, 0.1, 1, 10 and 100 times that of chromium), reagent and buffer, in that order, and diluting with water.

The following ions showed no interference at concentrations 100 times that of Cr(VI): Pb(II), Hg(II), Tl(I), Cu(II), Cd, La, Ce(III), V(VI), Ni(II), Co(II), Zn, Ca, Sr, Mg, Na, Rb, Li, K, NH_4^+, BO_2^-, F^-, SO_4^{2-}, $H_2PO_4^-$, $H_2AsO_4^-$ tartrate, citrate, $Fe(CN)_6^{4-}$, SCN^-, Br^-, ClO_3^-, NO_3^-, acetate, EDTA and ClO_4^-. The following did not interfere in 10-fold amounts: Cr(III), Al and Th. Equal concentrations of Bi, Fe(III), V(IV), Mn(II), Ba and oxalate did not interfere. At 0.1-fold concentrations, Hg(I), Ag, Fe(II), Be, Au(III), ZrO^{2+}, $Fe(CN)_6^{3-}$ and I^- and at 0.01 fold, Sn(II), Sn(IV) and Mo(VI) were without effect. Tungsten(VI) and MnO_4^- interfered at all concentrations tested. There was no effect of ionic strength shown by sodium perchlorate up to 0.2 M. Interference was considered to be any variation in the absorbance value greater than the confidence limit given above.

REFERENCES

1 O. A. Tataev, K. N. Bagdasanov and Kh. G. Buganov, Sb. Statei Molodykh Uch. Dagestan Fil. Akad. Nauk, (1969) 198; Chem. Abstr., 75 (1971) 104784y.
2 O. A. Tataev, K. N. Bagdasanov and Kh. G. Buganov, Sb. Statei Molodykh Uch. Dagestan Fil. Akad. Nauk, (1969) 203; Chem. Abstr., 75 (1971) 104785z.
3 O. A. Tataev and A. Sh. Schakhabudinov, Zh. Anal. Khim., 27 (1972) 2385.
4 V. H. Kulkarni and M. L. Good, Anal. Chem., 50 (1978) 973.
5 J. Gillis, J. Hoste and A. Claeys, Anal. Chim. Acta, 1 (1947) 302.
6 G. G. Shchemeleva and P. N. Kovalenko, Peredovye Metody Khim. Tekhnol. Kontrolya Proizvd., (1964) 237; Chem. Abstr., 63 (1965) 10679d.
7 Kh. A. Osmanov and M. N. Magaranov, Fiz. Khim. Metody Anal. Kontrolya Proizvd., 2 (1976) 95; Chem. Abstr., 88 (1978) 57911u.
8 O. A. Tataev and A. Sh. Shakhabudinov, Zh. Anal. Khim., 28 (1973) 170.
9 V. A. Nazarenko, N. V. Lebedeva and E. A. Biryuk, Zh. Usev. Khim. Ova. im D. T. Mendeleeva, 9 (1964) 589; Chem. Abstr., 62 (1965) 2695f.
10 J. R. Kirby, R. M. Milburn and J. H. Taylor, Anal. Chim. Acta, 26 (1962) 458.

Analytica Chimica Acta, 142 (1982) 329—332
Elsevier Scientific Publishing Company, Amsterdam — Printed in The Netherlands

Short Communication

DETERMINATION OF TRACES OF SULFUR IN SELENIUM BY MOLECULAR EMISSION CAVITY ANALYSIS

TH. A. KOUIMTZIS

Laboratory of Analytical Chemistry, University of Thessaloniki, Thessaloniki (Greece)

(Received 6th April 1982)

Summary. The selenium sample (ca. 1 mg) containing 40—90 $\mu g\ g^{-1}$ sulfur is decomposed in a combustion apparatus and the evolved sulfur dioxide is adsorbed on about 30 mg of silica gel. The silica gel is deposited in a cavity and the sulfur is determined by molecular emission cavity analysis. Incomplete sulfur recoveries (86 ± 4%) caused by incomplete conversion to sulfur dioxide necessitate a correction factor.

Sulfur is an important impurity in high-purity selenium, but few methods for determining traces of sulfur in selenium have been described. Usually the procedures recommended are based on the separation of sulfur as barium sulfate which is determined gravimetrically or turbidimetrically. In both cases the presence of large amounts of selenious acid affects the results because of some coprecipitation of barium selenite. An alternative method [1] is to determine sulfur as methylene blue after separation of selenium as selenium tetrabromide and reduction of sulfate to sulfide by hydriodic and hypophosphorous acids in acetic acid solution. The application of the above methods to the determination of sulfur in selenium always involves the preliminary complete volatilization of selenium by repeated treatment with hydrobromic acid. This procedure is time-consuming and requires sulfur-free reagents.

Acs and Barabas [2] reported a method of determining traces of sulfur in selenium based on the separation of the dioxides of sulfur and selenium which are produced by burning the sample. The method involves igniting selenium samples in a stream of oxygen at 800° C, capturing the selenium dioxide in suitable traps, and absorbing the sulfur dioxide in a solution of sodium tetrachloromercurate. The sulfur dioxide is determined spectrophotometrically with pararosaniline. The proportion of sulfur converted to sulfur dioxide was reported to be 80—90% [2]. The method seems rapid but is not applicable for samples that contain very small concentrations of sulfur and $\geqslant$ 0.7-g samples are required. The determination of sulfur in selenium by neutron activation analysis has also been proposed [3, 4].

A method for sulfur dioxide determination by molecular emission cavity analysis (m.e.c.a.) has been described [5]. It is based on the absorption of sulfur dioxide by a little silica gel which then is deposited into a small cavity. The cavity is introduced into a suitable hydrogen—nitrogen—air flame and

the resulting S_2 emission is monitored. Under optimal conditions, the intensity of the emission varies linearly with the square of the amount of sulfur over the range 5—120 ng of SO_2. The high sensitivity of this method makes it well suited to the determination of traces of sulfur in various samples [6].

In the present communication, this method is used for the determination of traces of sulfur in selenium. For this purpose a modification of the combustion apparatus described by Acs and Barabas [2] is used for the combustion of the selenium samples. The sulfur dioxide evolved is absorbed by silical gel and is determined by measuring the intensity of the S_2 emission produced when the silica gel is introduced via the m.e.c.a. cavity into the hydrogen flame.

Experimental

Reagents. Liquid sulfur dioxide (B.D.H.) was supplied in aluminum canisters. The absorption train used to prepare sulfur dioxide samples for calibration has been described [5]. The silica gel used (60—120 mesh, for chromatography, B.D.H.) was dried for 4 h at 200°C before use, to remove any absorbed water vapor.

Three selenium samples containing 43, 59 and 89 ppm sulfur were used. Their sulfur concentration was established nephelometrically as barium sulfate after complete volatilization of the selenium as selenium tetrabromide. A standard addition technique was also used to confirm the results obtained. The results given above are the average values of three determinations. Nitric and hydrochloric acids were Merck Suprapur. Hydrobromic acid (Merck pro analyse) was distilled before use. These acids were used to dissolve the standard selenium samples and volatilize selenium prior to the nephelometric determination of sulfate. All other reagents used were of analytical grade.

Apparatus. A Unicam SP90 atomic absorption spectrometer, connected to a Perkin-Elmer model-165 recorder, was used to measure the S_2 emission intensity. All the modifications needed for this purpose, including the specially-shaped cavity, as well as the optimal composition of the flame, have been described [5].

The apparatus used for the combustion of the selenium samples was as follows. The quartz combustion tube (75 cm long, 9-mm i.d., 12-mm o.d.) had a conventional ground stopper and side-arm, and was drawn out to a beak end. About 40 cm of the tube was heated by an electric furnace. Platinum sample boats on a push rod were used to introduce the sample into the heated part of the combustion tube. Immediately after the combustion tube was the first selenium trap, which was a glass tube (10 cm long, 6-mm i.d.) packed with glass wool. Next to this trap was an empty glass U-tube, slightly widened on the exit side, which was placed in a bath of cold water so that the gases were cooled before entering a second selenium trap. This second trap (10 cm long, 6-mm i.d.) was two-thirds packed with glass wool, the

remaining third being packed with glass-fiber filter paper; this trap was attached to the glass absorption tube for sulfur dioxide (10 cm long, 1.5-mm i.d.) which was packed with 20—40 mg of silica gel. The flow rate of the oxygen through the system was controlled by means of a needle valve situated between the oxygen supply and the rheometer, before entry to the combustion tube.

Procedure. The furnace temperature was set at 800 ± 10° C. The appropriate amount of selenium sample (containing 2.5—60 ng of sulfur) was weighed into a platinum boat. The boat was placed on the push rod and introduced into the cool part of the combustion tube. The oxygen flow rate was set at 3—5 l h^{-1}. The push rod with the sample boat was then introduced into the hot zone with the aid of a magnet. The boat was ignited for 10 min and the sulfur dioxide produced was collected in the absorption tube. The absorption tube was disconnected and the silica gel was deposited into the cavity. The cavity was introduced into the flame and the S_2 emission, produced by the absorbed sulfur dioxide, was recorded. With the aid of a S_2 emission calibration graph prepared with sulfur dioxide, the amount of SO_2 was found and the concentration of sulfur in the selenium sample was calculated, assuming an 86% conversion to sulfur dioxide (see below).

To avoid possible losses of sulfur dioxide (by adsorption on glass or on the materials used to remove selenium dioxide), the combustion apparatus was conditioned by treating it with sulfur dioxide, which was then removed by passing through large amounts of oxygen.

Results and discussion

The combustion of the selenium samples and the absorption of the sulfur dioxide produced were done with great care. To release all the sulfur as sulfur dioxide, the oxidation of selenium to selenium dioxide must be complete. This depends on a careful balance between the size of the sample, the oxygen flow rate and the furnace temperature [2]. As previously mentioned, the method of determining sulfur dioxide is very sensitive (5—120 ng of SO_2), thus the size of the selenium sample needed is much smaller than that in the method of Acs and Barabas [2] where 3—300 μg of sulfur was required. As a result, the oxygen demand for complete oxidation of the selenium is very small. An oxygen flow rate of 3 l h^{-1} was sufficient. The temperature of the furnace was about 800° C, as used by Acs and Barabas [2].

An important factor is the removal of selenium dioxide carried by the oxygen stream before it reaches the absorption tube. Absorption of any selenium dioxide by the silica gel would result in a positive interference from Se_2 emission which would be measured in addition to the S_2 emission. The removal of selenium dioxide was easily accomplished because of the low oxygen flow rate, by using the two traps described above.

The conditions described in the procedure were found to be optimum. Under these conditions three selenium samples were analysed; the results are summarised in Table 1. The results indicate that the reproducibility of the

TABLE 1

Determination of sulphur in some typical selenium samples

Sample	S conc. ($\mu g\ g^{-1}$)	Sample mass (mg)	Found	
			SO_2 (ng)	Corrected[a] S ($\mu g\ g^{-1}$)
I	43	0.675	50	43
		0.960	74	45
		1.184	86	42
		1.416	104	43
		1.608	122	44
II	59	0.528	56	62
		0.604	64	62
		0.804	82	59
		1.061	104	57
		1.137	116	59
III	89	0.432	64	86
		0.573	86	87
		0.631	98	90
		0.679	106	91
		0.747	112	87

[a]Assuming an 86% yield of SO_2.

method is good. The recovery of sulfur was found to be 86 ± 4%. After correction by this factor, acceptable accuracy for the three samples was achieved.

The ultimate sensitivity of the method was not examined because of the lack of standard selenium samples with sufficiently low sulfur concentrations. It should be possible to determine 1 ppm sulfur by using 20—30-mg selenium samples, with adjustment of the conditions for combustion and selenium dioxide removal.

REFERENCES

1 B. Sjöborg, Talanta, 14 (1967) 693.
2 L. Acs and S. Barabas, Anal. Chem., 36 (1964) 1825.
3 J. Hoste and D. Solte, Fresenius, Z. Anal. Chem., 221 (1969) 245.
4 C. Ballaux, R. Dams and J. Hoste, Anal. Chim. Acta, 43 (1968) 1.
5 Th. A. Kouimtzis, Anal. Chim. Acta, 88 (1977) 303.
6 A. Calokerinos and A. Townshend, Prog. Anal. At. Spectrosc., 5 (1982) 63.

Analytica Chimica Acta, 142 (1982) 333—338
Elsevier Scientific Publishing Company, Amsterdam — Printed in The Netherlands

Short Communication

DETERMINATION OF ALUMINIUM IN SILICON BY ELECTRO-THERMAL ATOMIC ABSORPTION SPECTROMETRY

M. TADDIA

"G. Ciamician" Chemical Institute of the University, I-40126 Bologna (Italy)

(Received 13th May 1982)

Summary. The sample is decomposed with hydrofluoric and nitric acids and the diluted solution is injected into the graphite furnace. For a 100-mg sample, the detection limit (3σ) is 1.2 μg Al g^{-1}. The coefficient of variation is 3—13% for 9—7000 μg Al g^{-1} in silicon.

Solar-grade silicon may be produced from metallurgical-grade silicon by different refining processes [1]. Because aluminium is an impurity commonly found in the silicon starting material and is known to degrade the performance of devices composed of high-purity silicon, the impurity concentration must be measured and controlled. The advantages inherent in the application of atomic absorption spectrometry (a.a.s.) to the analysis of high-purity materials (high selectivity, sensitivity, speed and relatively low cost) are well recognized. Electrothermal atomization with direct injection of the sample avoids preliminary separation of the analyte from the matrix, thus simplifying the procedure and decreasing contamination. Theoretical [2] and experimental [3] studies of factors influencing the determination of aluminium by means of a graphite furnace have been published. Several workers [4—6] have recently employed the technique for the determination of aluminium in a variety of matrices. The literature records few methods for the analysis of silicon by graphite furnace a.a.s. High-purity silica has been analyzed for copper and iron [7], and more recently the determination of arsenic, thallium and antimony in semiconductor silicon films was reported [8]. The aim of the present study was to develop a graphite-furnace a.a.s. method for the determination of aluminium in silicon.

Experimental

Apparatus. The Perkin-Elmer 372 atomic absorption spectrometer used was equipped with a HGA-500 graphite furnace or a nitrous oxide—acetylene burner. An Intensitron aluminium hollow-cathode lamp (25 mA, 309.3 nm) was used, at a spectral bandwidth of 0.7 nm. Argon provided the inert atmosphere within the furnace. Samples (10 μl) were injected manually with Brand micropipettes. The operating parameters used are given in Table 1. Deuterium background correction was found to be unnecessary. An

0003-2670/82/0000-0000/$02.75

TABLE 1

Operating parameters for the graphite furnace

Step	Temp. (°C)	Ramp (s)	Hold (s)	Internal argon flow (ml min^{-1})
1	120	8	20	300
2	250	2	8	300
3	1450	10	60	300
4	2700	1	8	50

integration time of 7 s was used. Peak absorbances were registered on a Leeds—Northrup 681A chart recorder. Plastic ware was used for all solutions containing fluoride.

Reagents. A stock solution of 1000 mg Al l^{-1} (aluminium chloride, Merck standard solution) was used. More dilute standards in 0.2% (w/v) nitric acid were prepared daily. All other solutions were made from electronic or analytical-grade materials.

Procedure. Introduce 100 mg of the sample into a polymethylpentene test tube, add 5 ml of 5 M hydrofluoric acid and 1 ml of 65% nitric acid, and mix thoroughly. Place the covered tube for 60 min on a bath at 120°C to complete dissolution. Allow to cool, centrifuge to collect all drops condensed on the walls, quantitatively transfer to a 100-ml flask and make up to volume with water.

Aluminium is determined by using a standard addition technique. To a series of four calibrated flasks add successively 20 ml of the decomposed sample solution and exactly 0, 2, 4 or 6 ml of a standard containing 1 μg Al ml^{-1}. Dilute to 50.0 ml and inject 10 μl into the furnace. Read the absorbance in the peak-height mode. By weighing different quantities of silicon and by taking appropriate aliquots of the main solution, the procedure is applicable to 9—7000 μg Al g^{-1} of silicon in the samples studied.

For flame a.a.s. measurements, separation of the matrix is required and can be done by using a method previously described [9]. Dissolve the residue in the appropriate amount of hot 0.2% nitric acid, add potassium (1000 mg l^{-1}) as ionization buffer and nebulize the solution into a nitrous oxide—acetylene flame. Optimize the instrumental parameters according to the manufacturer's instructions. Use a standard addition procedure to complete the determination.

Results and discussion

When elemental silicon is dissolved in a mixture of hydrofluoric and nitric acids, the resulting solution may exhibit a rather complicated and variable composition. Besides silicon tetrafluoride, hexafluorosilicic acid may also be present and the presence of hexafluorosiloxane and polymeric substances has also to be considered [10]. The thermal behaviour of such a mixture and the effect on aluminium are not easily predictable. As the object was to

develop a method for the determination of aluminium in the untreated sample solution, the effects of different instrumental parameters on the signals obtained from such a solution were tested.

Choice of furnace program. A four-step program (Table 1) was found to be suitable. The drying and pre-ashing temperatures and ramp times were chosen to dry the sample without sputtering. This avoids losses, prevents damage to the quartz windows by hydrofluoric acid and promotes better reproducibility of the signal. The matrix is probably partially removed during the first and second steps, as the azeotrope $HF—H_2O—H_2SiF_6$, b.p. 116°C [9]. Optimization of ashing temperature and time was directed at volatilizing most of the silicon matrix whilst minimizing aluminium losses. Various ashing temperatures and times were tested with the atomization conditions reported in Table 1. The effect of ashing temperature on the aluminium signal in the presence of 2.0 mg Si ml^{-1} is shown in Fig. 1. The optimum temperature is 1400—1500°C; above 1500°C aluminium is probably lost by volatilization.

The effect of the ashing time at various temperatures is shown in Fig. 2. It can be seen that ashing for 60 s at 1400—1500°C provides the maximum signal. The experimental conditions cited above must be partly modified for the determination of aluminium in the absence of silicon. When aluminium standards in 0.2% nitric acid have to be measured, the maximum allowable ashing temperature is 1200°C (Fig. 1).

The aluminium signal was found to increase with the atomization temperature, but to extend the lifetime of the graphite tube, a temperature not exceeding 2700°C was used. To minimize memory effects a clean-out step

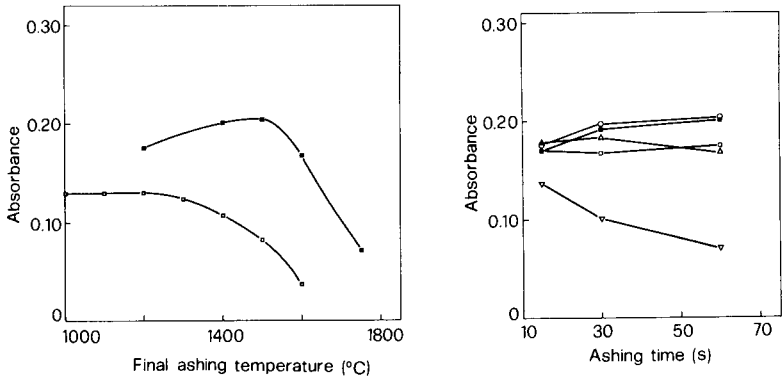

Fig. 1. Peak absorbance for aluminium as a function of final ashing temperature for: (▪) 0.2 μg Al ml^{-1} in the presence of 2.0 mg Si ml^{-1}; (▫) 0.1 μg Al ml^{-1} in 0.2% nitric acid. Other conditions as in Table 1.

Fig. 2. Peak absorbance for 0.2 μg Al ml^{-1} in the presence of 2.0 mg Si ml^{-1} as a function of the ashing time at: (▽) 1750°C; (△) 1600°C; (○) 1500°C; (▪) 1400°C; (▫) 1200°C.

(5 s at 2700°C) is recommended before each series of samples is processed. These conditions agree very well with those chosen by Yudelevich et al. [8] to determine aluminium impurities in rhenium.

Calibration. Calibration graphs were obtained by adding known amounts of aluminium(III) to silicon solutions prepared from high-purity samples. They were first checked to establish that they contained an aluminium level below the detection limit of the method. A linear calibration graph was obtained up to 0.3—0.4 μg Al ml^{-1} in the silicon solution tested. Evidence of a depressive matrix effect on the aluminium sensitivity is shown in Table 2. A marked change in peak shape at the highest silicon concentration was also noted. The peak became broader, indicating more difficult atomization. There may be several reasons for the matrix effect. For instance, the effect of silicon carbide (formed above 1700°C [11]) on the kinetics of the reduction process should be considered. The information given above led to the preference for a standard addition procedure. The use of background correction was unnecessary because no signal was obtained from aluminium-free silicon samples. A compromise between matrix effects and analyte dilution was achieved by diluting to 50 ml a solution of $\leqslant$100 mg of sample. For the conditions described above, the detection limit (3 σ) was 1.2 μg Al g^{-1} of silicon and the sensitivity (1% absorption) was 2.0 μg Al g^{-1}. These values may be improved by removing the matrix. When nitrous oxide flame atomization was used, the sensitivity was only 17 μg Al g^{-1} of silicon.

Interferences. Because iron, nickel and titanium are also commonly present in metallurgical-grade silicon, their effect on the aluminium signal was investigated. To take into account mutual interactions, all tests were done in silicon solutions (0.6 mg Si ml^{-1}) containing 0.1 μg Al ml^{-1}. Interference levels (expressed as % change in the peak height absorption signal with respect to that obtained in the absence of the interferent) are reported in Table 3. At the dilution normally used to determine aluminium by the recommended procedure, the ions tested would not influence the signal.

Analytical results. To estimate the reliability of the method, silicon samples from different manufacturers were analyzed. A comparison was made by using the alternative flame a.a.s. procedure given above. The results are shown in Table 4. The coefficient of variation lies in the range 3—13% depending on the aluminium level. An additional test was done for samples having an aluminium concentration for which the flame a.a.s. method was

TABLE 2

Effect of silicon matrix on the aluminium sensitivity relative to 0.2% (w/v) nitric acid

Silicon (mg ml^{-1})	0.49	2.0	3.0	17.7
Sensitivity ratio[a]	1.00	0.84	0.51	0.18

[a]Ratio between slope of sample calibration graph and that for 0.2% nitric acid.

TABLE 3

Effect of possible interfering ions on the aluminium signal in the presence of silicon (for conditions, see text)

Ion	Concentration ($mg\ l^{-1}$)	Interference (%)	Ion	Concentration ($mg\ l^{-1}$)	Interference (%)
Fe^{3+}	20	+16	Ti^{4+}	20	+8
	80	+12		80	+8
	400	−31		400	−19
Ni^{2+}	120	−9			

TABLE 4

Comparison between graphite furnace and flame a.a.s. for the determination of aluminium in silicon samples

Sample	Al found ($\mu g\ g^{-1}$)[a]			
	Graphite furnace	No. of results	Flame	No. of results
Merck 12497	9.6 ± 1.3	6	—	—
Schuchardt SI 172	177 ± 8	9	178 ± 14	4
Alfa Ventron	200 ± 6	7	205 ± 25	5
BDH 30066	7180 ± 220	5	7290	2

[a]Mean and standard deviation.

inadequate. Known amounts of analyte were added to the silicon before acid attack. The mean recovery for 1—5 μg of aluminium added to 100 mg of silicon was 98% ± 6%. These results are considered to be satisfactory. The great advantage of the furnace procedure is that it avoids the tedious removal of the silicon matrix. The method might be improved from the standpoint of precision and sensitivity by protecting the graphite with a suitable coating.

The author thanks Professor P. Lanza for valuable discussions. This work was supported by the National Research Council (C.N.R.), under a contract related to the "Progetto Finalizzato per la Chimica Fine e Secondaria".

REFERENCES

1 F. Gazzarrini, Chim. Ind., 61 (1979) 919.
2 J. Å. Persson, W. Frech and A. Cedergren, Anal. Chim. Acta, 92 (1977) 85.
3 J. Å. Persson, W. Frech and A. Cedergren, Anal. Chim. Acta, 92 (1977) 95.
4 P. E. Gardiner, J. M. Ottaway, G. S. Fell and D. J. Halls, Anal. Chim. Acta, 128 (1981) 57.
5 J. Å. Persson, W. Frech, G. Pohl and K. Lundgren, Analyst, 105 (1980) 1163.
6 W. Toda, J. Lux and J. C. van Loon, Anal. Lett. B13 (1980) 1105.
7 C. W. Fuller, Anal. Chim. Acta, 62 (1972) 261.

8 I. G. Yudelevich, L. V. Zelentsova, N. F. Beisel, T. A. Chanysheva and L. Vechernish, Anal. Chim. Acta, 108 (1979) 45.
9 M. Taddia, Microchem. J., 22 (1977) 369.
10 J. L. Margrave, K. G. Sharp and P. W. Wilson, J. Am. Chem. Soc., 92 (1970) 1530.
11 G. Müller-Vogt and W. Wendl, Anal. Chem., 53 (1981) 651.

Analytica Chimica Acta, 142 (1982) 339—343
Elsevier Scientific Publishing Company, Amsterdam — Printed in The Netherlands

Short Communication

EFFECTS OF COOLING OF A NITROUS OXIDE—ACETYLENE BURNER IN ATOMIC ABSORPTION SPECTROMETRY

K. IKRÉNYI* and A. BARTHA

Hungarian Geological Survey, Geochemical Department, P.O. Box 106, 1442 Budapest (Hungary)

(Received 26 April 1982)

Summary. A water-cooled burner is used for the determination of silicon, aluminium and calcium geological samples by a.a.s. The cooling modifies and stabilizes the nitrous oxide—acetylene flame so that sensitivity increases and the relative standard deviation decreases significantly in comparison with measurements in which traditional burners are used.

The determination of silicon, aluminium and calcium oxides is a routine requirement in geological analysis because of their abundance in rocks. The determination of silicon and aluminium by atomic absorption spectrometry (a.a.s.) requires a very reductive nitrous oxide—acetylene flame for atomization [1]. The elimination of the interferences of silicon and aluminium (and certain anions) on the determination of calcium by a.a.s. also requires the use of this flame. Unfortunately, the atomic absorption responses of these elements in the nitrous oxide—acetylene flame are not stable with time, and the consequent non-linear decrease of the absorbance hinders the attainment of the 1% relative standard deviation (r.s.d.) which is expected for total silicate analysis.

The parallel between decreasing sensitivity and the heating of the burner seemed to be so significant that tests were made with a commercial burner head equipped with a water-cooling device. As a result, the r.s.d. proved to be as good as with the air—acetylene flame. Thus the major and minor constituents of rocks and minerals could be determined sequentially by a.a.s. in the same stock solution. The application of water cooling for burners for a.a.s. is based on experience in the use of thermostatted electrodes in arc emission spectrometry. Rousselet [2] described a water-cooled air—acetylene burner for analysing biological materials because heating prevented occlusion of the burner slot. He mentioned that cooling the burner stabilized the shape of the flame and minimized the danger of the flash-back. Neybon and Caqualis [3] equipped a nitrous oxide—acetylene burner with a cooling covering but, because of the low efficiency of cooling, they did not mention any analytical improvement. Goguel [4] described a thermostatted plain-slot

0003-2670/82/0000-0000/$02.75

nitrous oxide—acetylene burner and studied the changes in flame characteristics during the warm-up period of the uncooled burner. Widmer [5] has applied water cooling to Pye Unicam-type burners, but, in spite of evident advantages, the water-cooled burner has not become commercially available. The manufacturers prefer burners equipped with cooling fins. Because the warm-up of the burner causes significant changes in the structure of a nitrous oxide—acetylene flame, cooled and uncooled burners were investigated in studying the optimum conditions for use of this flame.

Water-cooled burner

The Pye-Unicam 50-mm ridge-slot titanium burner made for the SP190 series atomic absorption spectrometers, was used. It is similar to the nitrous oxide—acetylene burners of other firms (Instrumentation Laboratory, Varian-Techtron, Karl Zeiss etc.). Figure 1 shows how the water-cooling was achieved. Two channels were drilled into the body of the burner near the slot; the distance between the surface of the channels and the top of the ridge slot was 7 mm. Goguel [4] thermostatted his plain-slot burner at 55° C. However, it was found here that even a water flow-rate of 0.4—0.5 l min^{-1} provides the required cooling effect; the temperature of the outflowing water does not exceed the ambient temperature. The loss of heat is only 0.4 J min^{-1}, so that the cooling effect on the flame is negligible.

Results and discussion

With a conventional uncooled burner, the flame heats the burner head and other connected components and the hot surface radiates heat to the surroundings. Eventually, equilibrium is established between heat radiation and

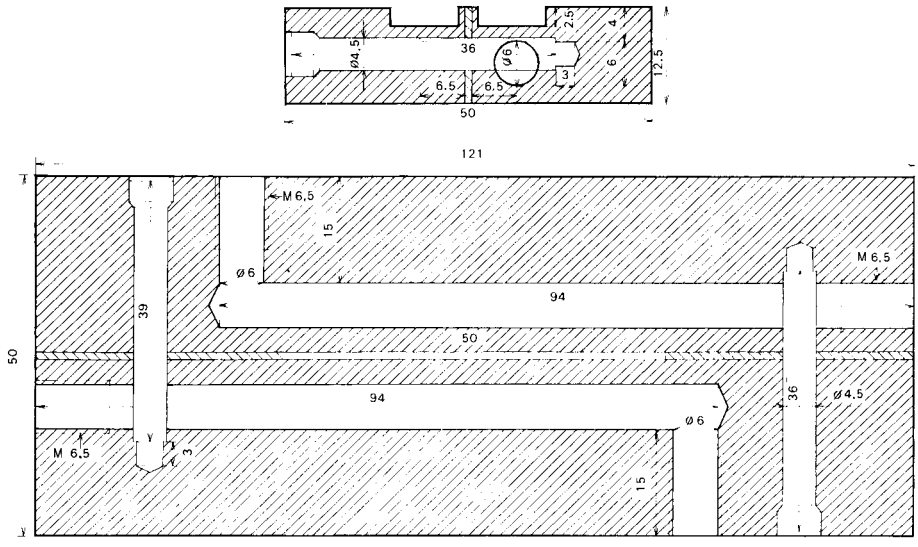

Fig. 1. Cross-section of the water-cooled burner head. All dimensions are given in mm.

absorption, after which the temperature of the burner does not change. Figure 2 shows the type of relative absorbance change for aluminium that can occur during the warming period, which can be 20 min for the traditional nitrous oxide—acetylene burner but is only 8 min when the radiation surface is enlarged with cooling fins (Pye-Unicam SP9 burner). The temperature of the burner head was measured in the channel near to the slot (see Fig. 1) by a thermocouple. The heating periods can be seen in Fig. 3 for various nitrous oxide—and air—acetylene flames. Before thermal equilibrium is achieved, the temperature of the uncooled burner exceeds the boiling point of water, so that the sample enters the flame not as droplets but as solid particles.

Relation between the absorbance and the temperature of the burner. Evaporation of solvent in the carrier gas is slower than in the flame, allowing some chemical reactions to take place (e.g., conversion of chlorides to oxides or silicates) before the sample enters the flame; this can influence the efficiency of atomization. The decrease in the relative absorbance of silicon, calcium and aluminium with burner temperature is shown in Fig. 4. The responses for silicic acid, calcium chloride and aluminium chloride are linearly dependent on the burner temperature. There is a break point at 360—370 K (i.e., where the inner surface of the burner near to the slot approaches 373 K) at which droplet evaporation to solid particles becomes highly probable. In the analysis of rock samples (G-1 granite and W-1 diabase, Fig. 4), the relationship is also linear below the evaporation temperature but curves off significantly at higher temperatures.

The flame gas mixture reaches the temperature of the burner and expands, therefore the velocity of gas passing laminarly through the slot increases in proportion to the temperature. The acceleration of the input gases causes an expansion of the flame, including the analytically-important atomization

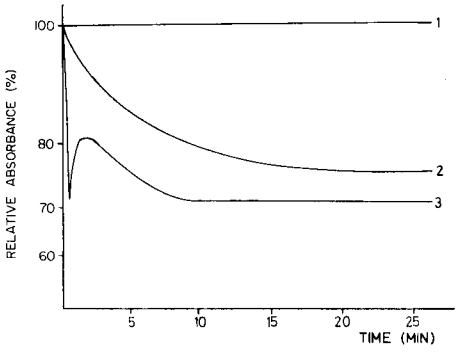

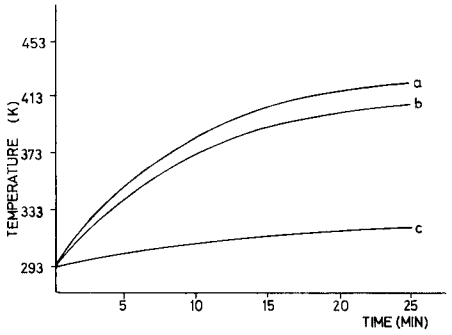

Fig. 2. Relative absorbance changes for aluminium with time using the following burner heads: (1) water-cooled SP190; (2) uncooled SP190; (3) uncooled SP9.

Fig. 3. Temperature change of the SP190 burner head with time for the following flames: (a) fuel-lean N_2O—C_2H_2; (b) fuel-rich N_2O—C_2H_2; (c) stoichiometric air—C_2H_2.

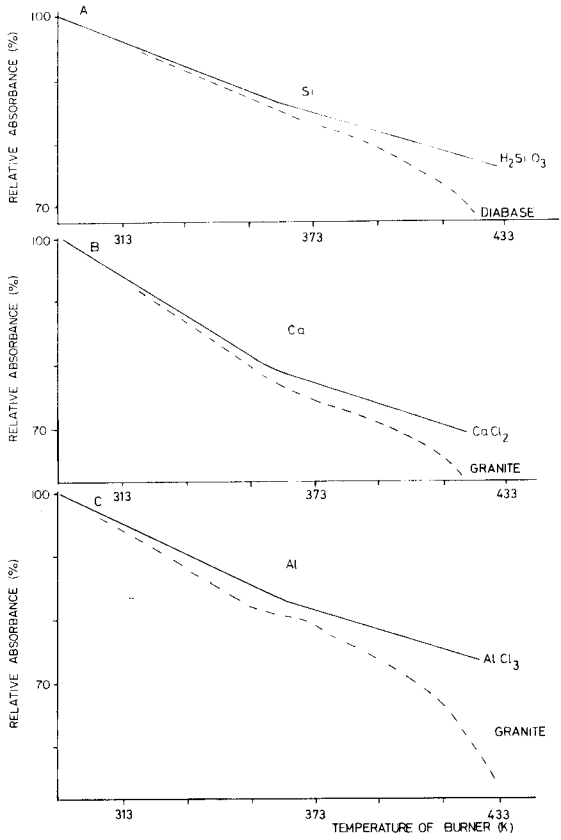

Fig. 4. Relative absorbance as a function of burner temperature for pure solutions and solutions of some rock samples. A, silicon in silicic acid and diabase; B, calcium in calcium chloride and granite; C, aluminium in aluminium chloride and granite.

zone, thus the absorbance is decreased in proportion to the decrease in atom concentration owing to the volume increase and to the decreased residence time in the light path. Chemical reactions occurring during evaporation vary the slope in Fig. 4; a "pre-flame" matrix effect is superimposed on the direct proportionality between absorbance and temperature. This part of the matrix effect can be eliminated by water cooling of the burner.

Effects of composition of gas mixture and of flame position. As can be seen in Fig. 5, the absorbances of magnesium, manganese, silicon and aluminium have a single peak dependence on acetylene flow while that for calcium has two peaks, when the burner is cooled by water. With the uncooled burner there is no absorbance maximum for magnesium, manganese and calcium in the fuel-lean flames, and the absorbance is always less than that achieved when the water-cooled burner is used.

The cooling of the burner head near the slot by circulating water therefore eliminates the undesirable effects mentioned above on the atomic absorption

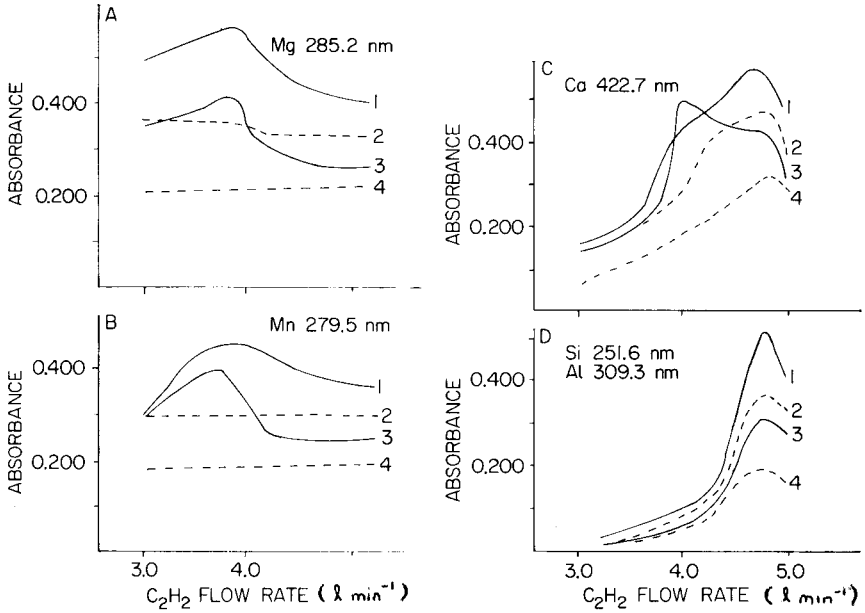

Fig. 5. Changes in the absorbance of several elements as a function of acetylene flow rate. Continuous curves refer to the water-cooled burner; dotted curves refer to the uncooled burner after burning the flame for 15 min. (1, 2) Burner slot parallel; (3, 4) burner slot perpendicular to optical axis. N_2O = 4.9 l min^{-1}. Burner height adjusted to the maximum sensitivity. A, Magnesium 285.2-nm line; B, manganese 279.5-nm line; C, calcium 422.7-nm line; D, silicon 251.6-nm line and aluminium 309.3-nm line.

response signal. Also the r.s.d. for the determination of silicon, aluminium and calcium in geological materials is 1.0% as a consequence of the stabilization of the nitrous oxide—acetylene flame parameters. In addition, the cold burner head is easy to change, contamination of the slot is negligible, and the sensitivity is higher than when the commercial burner is used.

REFERENCES

1 J. B. Willis, Nature, 207 (1965) 715.
2 F. Rousselet, At. Absorpt. Newsl., 5 (1966) 46.
3 R. Neybon and B. R. Caqualis, At. Absorpt. Newsl., 6 (1967) 92.
4 R. Goguel, Spectrochim. Acta, 26 (1971) 313.
5 D. S. Widmer, Pye-Unicam Ltd., Cambridge, U.K., personal communication, 1980.

Analytica Chimica Acta, 142 (1982) 345—347
Elsevier Scientific Publishing Company, Amsterdam — Printed in The Netherlands

Short Communication

DETERMINATION OF CARBONATE/HYDROGENCARBONATE RATIOS BY CARBON-13 NUCLEAR MAGNETIC RESONANCE SPECTROMETRY

RAPHAEL BAR* and YOEL SASSON

Casali Institute of Applied Chemistry, The Hebrew University of Jerusalem, 91904 Jerusalem (Israel)

(Received 5th May 1982)

Summary. A linear relationship between the carbonate/hydrogencarbonate mole fraction in an aqueous solution and the chemical shift of the ^{13}C-n.m.r. peak has been established, and applied for the determination of the carbonate/hydrogencarbonate ratio, in solutions where the overall carbonate concentration is known and exceeds 0.05 M.

The determination of carbonate and hydrogencarbonate has been widely investigated and documented. A non-destructive method for the determination of the carbonate/hydrogencarbonate ratio in an aqueous solution by ^{13}C-n.m.r. spectrometry is described in this communication. Lauterbur [1] reported that concentrated aqueous sodium hydrogencarbonate and saturated aqueous potassium carbonate have different ^{13}C-n.m.r. peaks, whereas Patterson and Ettinger [2] found that the spectrum of a solution of carbonic acid, hydrogencarbonate and carbonate consists of a single average resonance peak. A study of the relationship between the chemical shift of this peak and the different proportions of the carbonate species yielded a quantitative procedure.

Experimental

Aqueous solutions for spectrometry were prepared by accurately weighing (± 10 μg) mixtures of sodium hydrogencarbonate and sodium carbonate of different mole ratios, while keeping the total concentration constant at 0.5 M. The exact equilibrium mole fractions (with respect to carbonate species only) were determined by potentiometric titrations. The spectra of the solution were recorded with a CFT-20 Varian n.m.r. spectrometer after 600 pulses, with an acquisition time of 0.511 s and a pulse delay of 20 s. The probe temperature was 31°C (± 0.5). The chemical shifts were measured with respect to an external reference, deuterated acetone.

Results and discussion

A thorough analysis of aqueous carbonate solutions indicates the existence of five carbon species in equilibrium: CO_2(gas), CO_2(dissolved), H_2CO_3,

0003-2670/82/0000-0000/$02.75

HCO_3^- and CO_3^{2-}. However, the very small amounts of dissolved carbon dioxide and carbonic acid can be neglected and the system can be regarded as an equilibrium: $CO_3^{2-} + H_2O \rightleftharpoons HCO_3^- + OH^-$. Thus, the observed chemical shift would be $\delta_{ob} = X_{CO_3^{2-}}\,\delta^\circ_{CO_3^{2-}} + (1 - X_{CO_3^{2-}})\,\delta^\circ_{HCO_3^-}$, where $X_{CO_3^{2-}}$ is the mole fraction of carbonate and $\delta^\circ_{CO_3^{2-}}$ and $\delta^\circ_{HCO_3^-}$ are the corresponding chemical shifts of pure carbonate and hydrogencarbonate. Consequently, a plot of $(\delta_{obs} - \delta^\circ_{HCO_3^-})$ vs. $X_{CO_3^{2-}}$ should be a straight line with a slope of $(\delta^\circ_{CO_3^{2-}} - \delta^\circ_{HCO_3^-})$.

Figure 1 shows such a plot of the results obtained, where $\delta^\circ_{CO_3^{2-}}$ and $\delta^\circ_{HCO_3^-}$ were assumed to be the chemical shifts of 0.5 M carbonate and 0.5 M hydrogencarbonate solutions, respectively. Regression analysis [3] of the results forcing the intercept to vanish, showed a standard deviation of 1 Hz, a slope of 147.8 with a standard error of 0.9, a correlation coefficient of 0.998 and an average error in $X_{CO_3^{2-}}$ determination of 1.8%. Because the chemical shift is influenced by the concentration and the medium, the total carbonate concentration was kept constant (0.5 M). The characteristic low sensitivity of a ^{13}C-n.m.r. probe [4] sets a minimum carbon limit to which this method is applicable. In the n.m.r. system used here, this minimum was found to be 0.05 M. As seen in Fig. 1, a plot of pH vs. chemical shift gives a sigmoidal curve, which reflects its equivalence to a titration curve.

Linear interpolation between the chemical shifts of carbonate and hydrogencarbonate solutions enables an unknown carbonate mole fraction to be determined and consequently the carbonate/hydrogencarbonate mole ratio to be measured. Thus, after the total concentration of carbonate species in the sample has been measured, the chemical shifts of identical concentrations of carbonate and hydrogencarbonate must be recorded separately in the same medium. In this manner, the carbonate mole fraction of 1:1 carbonate/hydrogencarbonate solutions (0.25 M) in 2.5 M sodium formate, 2 M potassium nitrate or 1 M sodium chloride were determined with errors of 2.3%, 2.8% and 2.5%, respectively.

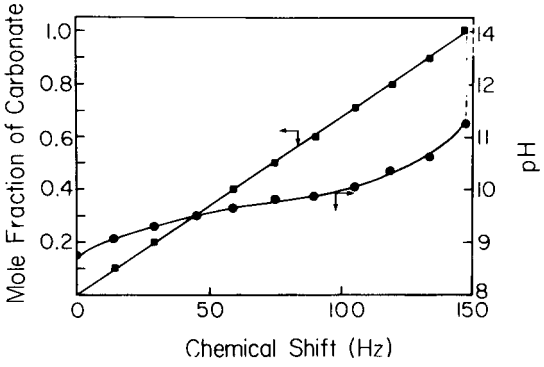

Fig. 1. Mole fraction of carbonate and pH of aqueous solutions of hydrogencarbonate—carbonate mixtures vs. chemical shift, defined as the separation of the n.m.r. peak of the mixture from that of pure hydrogencarbonate.

Experimental errors could be significantly reduced by use of a more sophisticated n.m.r. system such as a Brucker CWM 300 in which the range of chemical shifts observed would be 480 Hz (rather than 150 Hz) and the instrumental accuracy higher.

The authors are grateful to Professor J. Blum for his most constructive advice and to Mrs. Liliana Karpuj-Bar for her technical help.

REFERENCES

1 P. C. Lauterbur, Ann. N.Y. Acad. Sci., 70 (1957) 841.
2 A. Patterson, Jr. and R. Ettinger, Z. Electrochem., 64 (1960) 98.
3 C. A. Bennett and N. L. Franklin, Statistical Analysis in Chemistry and the Chemical Industry, Wiley, New York, 1954.
4 J. B. Stothers, Carbon-13 NMR Spectroscopy, Academic Press, New York, 1972, p. 13.

Analytica Chimica Acta, 142 (1982) 349—354
Elsevier Scientific Publishing Company, Amsterdam — Printed in The Netherlands

Short Communication

FAST NEUTRON ACTIVATION ANALYSIS OF BULK COAL SAMPLES FOR ALUMINA, SILICA AND ASH

M. BORSARU* and P. J. MATHEW

CSIRO Division of Mineral Physics, P.O. Box 124, Port Melbourne, Vic. 3207 (Australia)

(Received 6th April 1982)

Summary. The fast neutron activation technique was applied to bulk samples (≈11 kg) of Australian black coal. The determination of alumina is based on the reaction $^{27}Al(n,p)^{27}Mg$ by counting the 0.844-MeV peak ($t_{1/2}$ = 9.4 min). Silica is determined by means of the reaction $^{28}Si(n,p)^{28}Al$; the 1.78-MeV peak ($t_{1/2}$ = 2.3 min) is counted and a correction for the interference from alumina is applied. The ash content is based on the correlation between ash and the sum of alumina and silica. The accuracies (1 SD) for the determination of alumina, silica and ash were 0.52% Al_2O_3, 0.79% SiO_2 and 1.02% ash, respectively. The ash, alumina and silica contents of the samples were in the ranges 8.8—37.5%, 1.3—10.3% and 6.4—22%, respectively.

Considerable research has been done in the last two decades to develop nuclear techniques and instrumentation for the measurement of ash and ash components in coal. The techniques developed include β-ray back-scatter, bremsstrahlung, x-ray and low-energy γ-ray back-scatter, γ-ray transmission, neutron inelastic scattering, capture or activation methods. Many of the x-ray, low-energy γ-ray and β-ray methods have shortcomings such as shallow penetration, sensitivity to variations in ash composition, particle size, moisture and surface texture, and the need for sampling and sample preparation. These disadvantages make them unsuitable for bulk analysis in coal preparation and utilisation plants. A few commerical instruments based on these techniques are currently available although the coal mining industry seems reluctant to use them on a wide basis.

Bulk analysis for ash is desirable in the coal industry [1] and, because of their penetrating power, high-energy γ-rays and neutrons are most suited for bulk analysis. Sowerby [2] employed a combined neutron inelastic scattering and γ-ray method to measure the specific energy, ash and moisture in bulk coal samples. Sowerby and Ngo [3] described recently the determination of ash in bulk coal samples, using annihilation γ-rays after irradiation by ^{60}Co γ-rays. A prompt neutron γ-ray method was described by Stewart and Hall [4] for monitoring the major ash elements in coal moving on a conveyor belt. Brown et al. [5] described a continuous nuclear analyser for coal based on prompt neutron activation. The 14-MeV neutrons produced by neutron generators have been employed also for coal analysis [6—8]. Instrumental

0003-2670/82/0000-0000/$02.75

neutron activation analysis with a Ge(Li) γ-ray detector has been used to determine many elements in coal [9—10]. Thermal neutron activation has been employed to measure alumina in bulk coal samples [1, 11]. Wormald et al. [11] have developed a method for measuring ash in coal in moving wagons; the method is based on the correlation between alumina and ash. In general, this method is not applicable to Australian coals because of the poor correlation between ash and alumina content.

In the present work, fast neutron activation analysis was employed for the determination of alumina, silica and ash in bulk (≈11 kg) coal samples. The attraction of neutron activation is that the peaks in the γ-ray spectra recorded are well separated so that the method is less sensitive to drifts in the electronic equipment than most of the methods mentioned above.

Experimental

A selection of 47 samples of black coal was used. Thirty-four of the samples were collected during a span of six months from a mine working on the Wongawilli seam in southern N.S.W. The samples included fresh coal samples from mine faces in different parts of the mine, grab samples collected from the conveyor to the washery, output of the heavy media cyclone, filter cakes and blended samples from the stockpile. The other 13 samples came from different locations on the eastern coast of Australia. The ash composition in the dried samples is given in Table 1. The free moisture content was in the range 0.5—2.5% by weight for the 34 samples collected from the same area and from 0.7—6% by weight for the other 13 samples. In the samples as received, the particle size varied between powder and —60 mm.

The bulk samples were irradiated in two separate brass boxes of sizes (40 × 30 × 8 cm) and (40 × 33 × 14 cm). The 20-Ci ^{241}Am-Be neutron source and the experimental rig employed have been described [12]. The weights of coal in the two boxes were in the range 9—12 kg and 13—20 kg, respectively. Alumina concentration was determined from the 0.844-MeV γ-ray counts following the decay of ^{27}Mg ($t_{1/2}$ = 9.4 min) produced by the reaction ^{27}Al(n,p)^{27}Mg. Silica concentration was determined from the intensity of the 1.78-MeV γ-rays following the decay of ^{28}Al ($t_{1/2}$ = 2.3 min)

TABLE 1

The ash composition in the samples

	34 samples		All samples	
	Range	Mean[a]	Range	Mean[a]
Ash (wt %)	8.8—37.5	19.86 ± 7.96	7—37.5	19.70 ± 8.26
Al_2O_3 (wt % in coal)	1.4—9.75	3.75 ± 2.17	1.3—10.15	4.15 ± 2.3
SiO_2 (wt % in coal)	6.4—22	13.69 ± 4.59	4.7—22	12.97 ± 4.99
Fe_2O_3 (wt % in coal)	0.2—3.15	1.22 ± 0.81	0.06—3.15	1.22 ± 0.82

[a]With standard deviation.

produced by the fast neutron reaction $^{28}Si(n,p)^{28}Al$. The 1.78-MeV γ-ray counts must be corrected for the contribution from ^{28}Al produced by the thermal neutron reaction $^{27}Al(n,\gamma)^{28}Al$. This correction was achieved by monitoring the thermal neutron flux underneath the bulk sample during irradiation. This technique had been successfully used for the simultaneous determination of alumina and silica in bulk bauxite samples [12]. The determination of ash in coal is based on the correlation between the ash and "alumina plus silica" content of coal.

The concentrations of alumina and silica in coal were determined as described earlier [12] by employing the stepwise multiple regression technique [13].

Results and discussion

Determination of alumina concentrations in coal. Two independent sets of measurements were done. The bulk coal samples were contained in the smaller box for the first set of measurements and in the bigger box for the second set of measurements. Table 2 gives the standard deviations for the alumina determination in each run; it can be seen that the standard deviation is slightly smaller when the smaller sample ($\approx$11 kg) is employed, possibly because the ratio between the number of fast neutron and thermal neutrons is greater in the smaller sample than in the larger sample, owing to the big thermalising power of coal. The standard deviation is not significantly affected whether samples from different areas or the same area are considered. Figure 1A shows a plot of assayed (on a dry basis) alumina grades versus predicted grades for the first run when all 47 samples are considered (σ = 0.48% Al_2O_3).

Determination of silica concentrations in coal. Table 2 shows the standard deviations for the silica determination in each run; the standard deviations obtained without the correction for alumina interference are also given. It is

TABLE 2

Precision of the alumina, silica and ash determinations in coal

Constituent	Run[a]	Standard deviations (σ)	
		For 34 samples from one area	For all 47 samples from different areas
Alumina	1	0.52	0.48
	2	0.59	0.61
Silica	1	0.79 (0.92)[b]	1.16
	2	1.07 (1.37)[b]	1.53
Ash	1	1.02	1.26
	2	1.28	1.50

[a]Run 1, $\approx$11 kg samples; run 2, $\approx$16 kg samples. [b]The values in parentheses were obtained when no correction for alumina was applied.

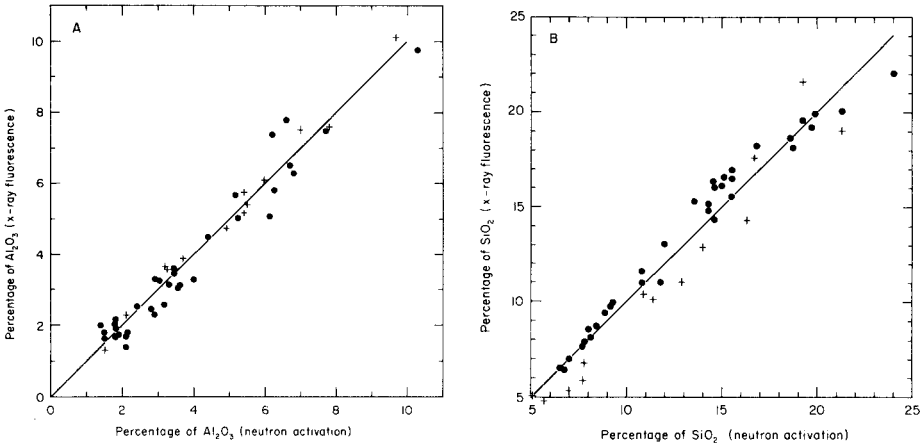

Fig. 1. Comparison of neutron activation and x-ray fluorescence assays for (A) Al_2O_3 and (B) SiO_2 in coal. (•) Samples from one mine only; (+) samples from other mines in Eastern Australia.

evident that the standard deviation is about 40% larger for samples collected from different coal deposits than for samples from the same area. This is in contrast to the case of alumina (see above). Further, the standard deviation is improved by about 11% when the correction for alumina interference is applied. The improvement was bigger (≈28%) when the larger box was employed; more neutrons are thermalised in the larger sample and therefore the interference from the $^{27}Al(n,\gamma)^{28}Al$ reaction is bigger. The significance of correcting for the alumina interference is obvious, though it does not improve the precision by the same amount reported for the determination of silica in bulk bauxite samples [12]. In that case the standard deviation was improved by more than 100%. Figure 1B shows a plot of assayed (on a dry basis) silica grades versus predicted grades for the first run when all the 47 samples are considered (σ = 1.16% SiO_2).

Determinations of ash contents in coal samples. The ash and ash composition of a good cross-section of Australian black coals [14] were studied in this work to examine the correlation between ash content in coal and major components of ash. This study showed that the ash content of these coals could be predicted from "alumina + silica" content with a precision (1σ) of 0.73% ash, mainly because an average of 87% of the ash in Australian coals is composed of these two elements. The correlation between "alumina + silica" and ash content in coal became even stronger for coal samples collected from the same mine. Thus the simultaneous measurement of alumina and silica in coal provides a convenient method of determining the ash content of coal.

The linear regression equation used for the prediction of percentage ash in coal has the form

$$\% \text{ ash} = C_0 + C_1(\text{Al} + \text{Si})_{\text{n.a.}}$$

where $(Al + Si)_{n.a.}$ is calculated by the proposed method. Table 2 gives the standard deviation for the prediction of ash in each run.

Figure 2 shows a plot of assayed ash content (by ignition) versus predicted ash by neutron activation when all the 47 samples were considered (σ = 1.26% ash).

The influence of the free moisture in the determination of alumina and silica. The effect of free moisture on the determination of alumina and silica was investigated by adding up to 11% (w/w) water to three samples in steps of 1% water. The alumina and silica concentrations in the samples were measured after each incremental addition. The measurements were done by using the regression coefficients determined from the analysis of the 34 samples collected from the same area. It was found that the variation of free moisture in the samples affected the predicted assays of the measurement; an increase in free moisture produced a decrease in the predicted activation assays on a dry basis for both alumina and silica. In order to obtain good accuracy for the determination of alumina and silica, the variation in free moisture should be small (<2% in the present work for the 34 samples collected from one area), otherwise the coal samples should be dried before the measurement.

Possible interferences from manganese, iron, phosphorus and ^{30}Si were shown to be negligible.

Conclusions

The alumina, silica and ash content in bulk samples (≈11 kg) of Australian coal were successfully determined by fast neutron activation; the standard

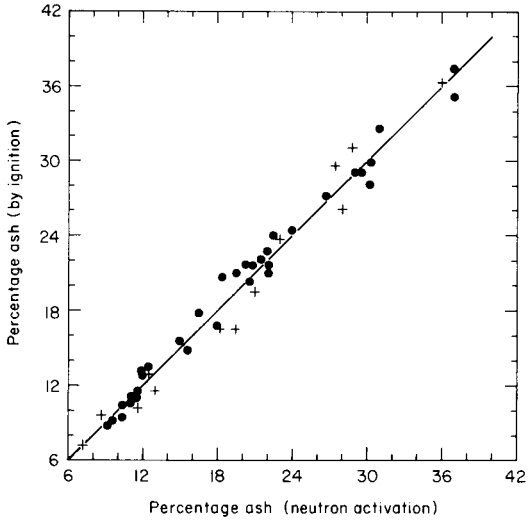

Fig. 2. Comparison of neutron activation and conventional ignition methods for ash assays in coal. (•) Samples from one mine only; (+) samples from other mines in Eastern Australia.

deviations determined for samples collected from only one area were 0.52%, 0.79% and 1.02%, respectively. These standard deviations do not take into account errors in the sampling and chemical analysis of the coal samples analysed. For example, in the case of ash, when such errors are considered ($\sigma \approx 0.5\%$ ash), the standard deviation arising from the activation determination becomes less than 1% ash. The variation of the free moisture in the samples must be less than 2% by weight in order to achieve the accuracies indicated. The standard deviation for the alumina determination in this work was 0.52% Al_2O_3. If better precision for the alumina determination in bulk coal samples is required, then thermal neutron activation is recommended [1].

The proposed method does not require any sample preparation and the time of analysis is 12 min per sample. However, 9 samples can be analysed per hour by using two identical boxes and counting one sample while the other one is irradiated.

The authors thank H. L. Maltman and M. Pretor for providing coal samples, and M. Vogel for valuable help. Support was provided under the National Energy Research, Development and Demonstration Program administered by the Commonwealth Department of National Development.

REFERENCES

1 M. Borsaru and P. J. Mathew, Anal. Chim. Acta, 118 (1980) 109.
2 B. D. Sowerby, Nucl. Instrum. Methods, 160 (1979) 173.
3 B. D. Sowerby and V. N. Ngo, Nucl. Instrum. Methods, 188 (1981) 429.
4 R. F. Stewart and A. W. Hall, Proceedings of the 13th Intersociety Energy Conversion Engineering Conference, San Diego, California, August 1978, Vol. 1, p. 586.
5 D. R. Brown, H. Bozargmanesh and T. Gozani, Coal Min. Process., 17 (1980) 88.
6 T. C. Martin, S. C. Mathur and I. L. Morgan, Int. J. Appl. Radiat. Isot., 15 (1964) 331.
7 L. Loska and L. Gorski, Radiochem. Radioanal. Lett., 10 (1972) 315.
8 R. Kurosawa, Nippon Kogyo Kaishi, 84 (1968) 101.
9 C. Block and R. Dams, Anal. Chim. Acta, 71 (1974) 53.
10 J. J. Rowe and E. Steinnes, Talanta, 24 (1977) 433.
11 M. R. Wormald, C. G. Clayton, I. S. Boyce and D. Mortimer, Int. J. Appl. Radiat. Isot., 30 (1979) 297.
12 M. Borsaru and P. L. Eisler, Anal. Chem., 53 (1981) 1751.
13 N. R. Draper and H. Smith, Applied Regression Analysis, Wiley, New York, 1968, pp. 171, 172 and 178—195.
14 Joint Coal Board and Queensland Coal Board, Report on Australian Black Coals, 1976.

Analytica Chimica Acta, 142 (1982) 355—359
Elsevier Scientific Publishing Company, Amsterdam — Printed in The Netherlands

Short Communication

A MOBILE MASS SPECTROMETRY LABORATORY FOR ISOTOPIC RATIO MEASUREMENTS OF URANIUM AND PLUTONIUM

DAVID H. SMITH*, J. R. WALTON, H. S. McKOWN, R. L. WALKER and J. A. CARTER

Analytical Chemistry Division, Oak Ridge National Laboratory, Oak Ridge, TN 37830 (U.S.A.)

(Received 27th May 1982)

Summary. A modified quadrupole mass spectrometer is housed in a van that serves as a mobile laboratory to provide on-site determinations of isotopic ratios and concentrations of uranium and plutonium. Each element can be determined at 1—3 ng levels with precisions of 1—2%.

Safeguards programs are charged with the responsibility of establishing a material balance for all fissionable isotopes. Among their needs is an analytical instrument that provides on-site isotopic determinations of uranium and plutonium. Mass spectrometry is the method of choice for such measurements; in addition, isotopic dilution can be used for quantitative assays.

Because it was necessary that the system be mobile, severe weight constraints were imposed (total weight <250 kg). It was decided to investigate the possibility of using a quadrupole mass spectrometer. Such an instrument combines light weight and compact size with comparative ease of operation and thus was virtually ideal from the portability point of view. However, its ability to measure isotopic ratios from a thermal ionization source was unknown; bias correction might not be reproducible enough from sample to sample to yield the desired precision. It was necessary to use very small samples, particularly of plutonium, and the sensitivity of the instrument in this regard was also unknown. The potential advantages were so great, however, that it seemed worthwhile to acquire an instrument to evaluate.

Instrumentation

The instrument, from a vendor specializing in custom-designed instrumentation (Pernicka Corporation, Mountain View, CA), was modified to meet particular specifications. The mass spectrometer is a Balzers QMC311 quadrupole, which is known for its high sensitivity. High vacuum is provided by a Pfeiffer turbomolecular pump; base pressure of the instrument is $<10^{-6}$ Pa. Operation of the instrument is controlled by a Tektronix 31 calculator specially programmed. The instrument is shock-mounted in two cabinets in the van. Each module weighs less than 80 kg; the total weight is well under the maximum specified.

0003-2670/82/0000-0000/$02.75

A sample-insertion probe developed for this instrument is shown in Fig. 1. It was found that conventional filament construction, with each end of the V-shaped rhenium canoe spot-welded on the same side of the supports, could not be orientated on the optical axis of the mass spectrometer. The simple expedient of spot welding the ends of the filament on opposite sides of the supports (see insert in Fig. 1) resolved this problem and yielded an increase of about a factor of five in ion current at the detector.

A recreational vehicle was acquired and modified to provide a mobile laboratory to house the instrument. Modifications included replacement of the original carpet with a vinyl floor covering, both to give a cleaner environment and to reduce problems in the event of an acid spill. A 130-A alternator was installed to allow operation of the pumping system while underway.

The quadrupole mass spectrometer was mounted on the right side of the van and ancillary equipment required for sample preparation was mounted on the left side; the ancillary equipment included two microscopes, a vortex mixer, and a centrifuge. A stainless-steel hood was installed over the original cook-top in the right rear for use in sample preparation. The bath tub (at the rear) was used for secondary containment of chemicals while the van was underway. The mobile laboratory is thus a self-sufficient entity, housing all the equipment required for obtaining, preparing, and making measurements on any samples but those radioactive enough to require containment.

Instrumental performance

All samples were prepared by the resin bead method developed earlier [1—3] or some variant of the bead method. This technique offers significant advantages over other sample preparation techniques. If the material to be assayed is radioactive, such as spent nuclear fuel dissolver solutions, the beads serve for separation, isolating uranium and plutonium from fission products

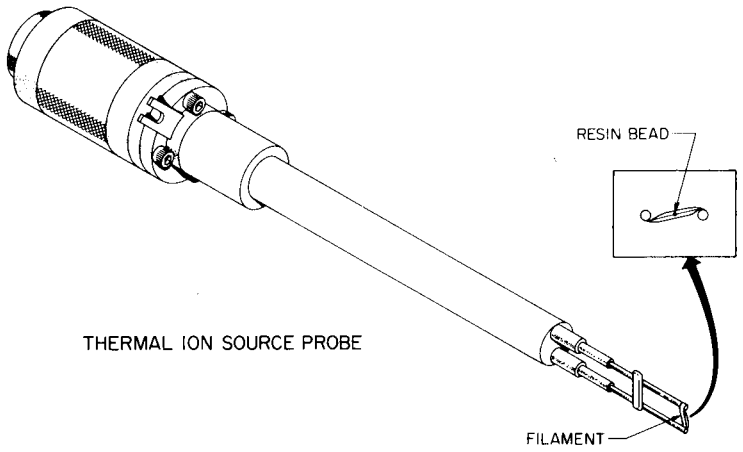

Fig. 1. Sample insertion probe.

and other actinides [4]. Under appropriate conditions of acid and uranium concentration, 1—3 ng each of uranium and plutonium will adsorb on each bead. A single bead serves as a sample for mass spectrometry and approximates a point source of ions. By providing a reducing medium, it also reduces loss of sample as oxide species. In addition, it seems to act as a reservoir of sample, delivering it to the ionization region in a relatively controlled manner [5]. All of these properties lead to an improvement of about a factor of ten in ionization efficiency when compared to solution loadings. Efficiencies of 0.5% (ions detected/atoms loaded) have been obtained for uranium [6]. The ability to separate uranium and plutonium and the enhancement of ionization efficiency give the resin bead technique two powerful advantages over other methods; it offers simplified sample preparation chemistry and smaller sample requirements.

If elements other than uranium or plutonium are to be determined, or if the solution to be sampled is not radioactive, the benefits accruing from resin bead loading can still be exploited. An aliquot (1 μl) of solution is placed in the filament "canoe" and a resin bead is added. The bead absorbs the solution and, upon drying, the sample is left on it. No difference in behavior was observed when samples were loaded in this manner as opposed to being adsorbed from solutions onto beads.

Initial laboratory evaluation of the mass spectrometer showed that it had ample resolution and sensitivity. Examples of spectra for uranium and plutonium are shown in the oscilloscope traces in Fig. 2. Resin-bead loaded samples gave 5—8 V signals of U^+ that lasted an hour or more. A resolution of 300 was readily obtained, sufficient for satisfactory plutonium determinations. A series of standards was run to assess the precision of the instrument. Results are listed in Table 1 with uncertainties quoted at ±1 standard deviation.

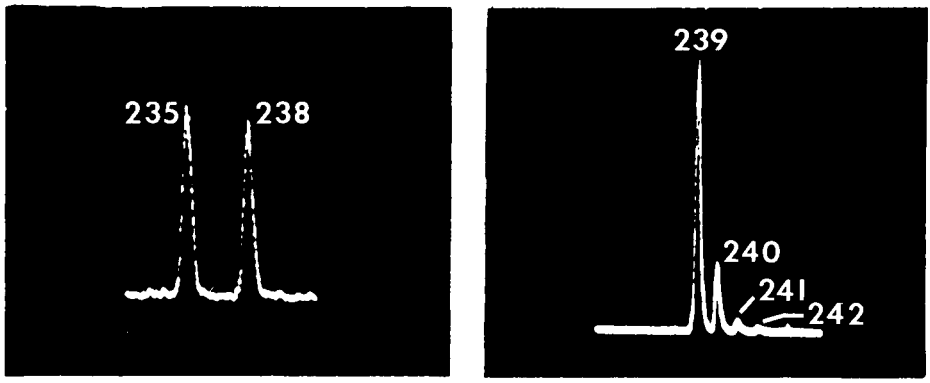

Fig. 2. Oscilloscope traces of uranium and plutonium quadrupole mass spectra.

TABLE 1

Results from NBS Standards

NBS Number	Ratio ($^{235}U/^{238}U$)	
	Certified	Measured
U-500	0.9997	0.9993 ± 0.0053
U-750	3.166	3.2013 ± 0.0090
U-930	17.35	17.63 ± 0.270
U-200	0.251	0.247 ± 0.003
U-100	0.1136	0.11430 ± 0.0015
U-030	0.0314	0.03191 ± 0.00064
U-010	0.01014	0.01025 ± 0.00019
U-950a (natural)	0.007253	0.007240 ± 0.00021

A sample typical of those encountered in the nuclear fuel cycle was processed on both the quadrupole and two-stage isotope ratio mass spectrometers [7]. Results are given in Table 2; highly enriched ^{233}U and ^{242}Pu were used as spikes for isotope dilution purposes. The two elements were determined sequentially from the same filament loading [1].

Precision and accuracy in these and other experiments done in the laboratory demonstrated that the instrument was capable of providing satisfactory results (imprecisions of ±1—2%), and the mass spectrometer was mounted in the van.

The instrument in the van has made a number of field trips, and has been used to determine uranium in ground waters and process streams in or near various nuclear facilities. Uranium concentrations in ground waters ranged from <0.5 to 2 $\mu g\ l^{-1}$, which is normal uranium background in U.S. streams. Samples with 1 $\mu g\ l^{-1}$ or more were processed satisfactorily without chemical separation of uranium; the raw sample was acidified, spiked, and loaded directly on the filament. Contaminant species were burned away before uranium was measured; this process took ca. 1 h. Samples with less than 1 $\mu g\ l^{-1}$ uranium were concentrated by an extraction step. Samples in process streams ranged from 30 to 750 $\mu g\ l^{-1}$ and were processed without chemical separation. In all cases, good agreement was obtained with results obtained by other techniques. On one trip, uranium and plutonium were determined at the Savannah River Plant, and good agreement was obtained with results obtained by titration.

Elements other than uranium and plutonium that have been determined include lutetium and boron. The instrument thus seems capable of quantifying all elements amenable to thermal ionization.

Conclusions

A mobile facility capable of providing timely on-site isotopic ratio measurements for uranium and plutonium has been developed; the isotope dilution

TABLE 2

Results obtained for an ORNL field sample of U + Pu + (spike ^{242}Pu + ^{233}U)

Pu	Quadrupole	2-stage	U	Quadrupole	2-stage
238/242	0.0220	0.0210	235/233	0.0108	0.01074
239/242	0.8661	0.8648	238/233	0.8847	0.8991
240/242	0.4815	0.4649	Concn. (g l^{-1})	161.0	163.6
241/242	0.1754	0.1619			
Concn. (g l^{-1})	1.493	1.491			

technique enables concentrations to be measured. Imprecisions for measurements of ratios between 0.01 and 100 are 1—2%. Areas of potential future application include helping to establish material balance in the nuclear fuel cycle and in environmental monitoring. In each case, the ability of the investigator to obtain prompt determinations will be of great value in selecting subsequent samples.

The authors thank Hoy Smith and Hosie Simmons for their help in sample preparation. This research was sponsored by the U.S. Department of Energy, Office of Safeguards and Security, under Contract W-7405-eng-26 with the Union Carbide Corporation.

REFERENCES

1 R. L. Walker, R. E. Eby, C. A. Pritchard and J. A. Carter, Anal. Lett., 7 (1974) 563.
2 D. H. Smith, R. L. Walker and J. A. Carter, J. Inst. Nucl. Mater. Manage., 8 (1980) 66.
3 R. L. Walker, J. A. Carter and D. H. Smith, Anal. Lett., 14 (1982) 1603.
4 J. P. Faris and R. F. Buchanan, Anal. Chem., 36 (1964) 1157.
5 D. H. Smith, W. H. Christie and R. E. Eby, Int. J. Mass Spectrom. Ion Phys., 36 (1980) 301.
6 D. H. Smith and J. A. Carter, Int. J. Mass Spectrom. Ion Phys., 40 (1981) 211.
7 D. H. Smith, W. H. Christie, H. S. McKown, R. L. Walker and G. R. Hertel, Int. J. Mass Spectrom. Ion Phys., 10 (1972—73) 343.

ANALYTICA CHIMICA ACTA, VOL. 142 (1982)

AUTHOR INDEX

Allston, R., see Ditzler, M. A. 305
Al-Zamil, I. Z.
— and Townshend, A.
Molecular emission cavity analysis. Part 23. Determination of nitrite and nitrate after conversion to nitrogen monoxide 151
Andre, J. C., see Vogin, B. 293

Bar, R.
— and Sasson, Y.
Determination of carbonate/hydrogencarbonate ratios by carbon-13 nuclear magnetic resonance spectrometry 345
Baronnet, F., see Vogin, B. 293
Barrado, E., see Pardo, R. 285
Bartha, A., see Ikrényi, K. 339
Bergmark, B., see Lundberg, E. 129
Bernal, J. L., see Pardo, R. 285
Bhattacharyya, P. K.
— and Grant, A.
Simultaneous determinations of a monofluorinated[1,4]benzodiazepine and the corresponding benzophenone as a function of pH and in aqueous formulations by ^{19}F nuclear magnetic resonance spectrometry 249
Bischoff, R.
— and Schwedt, G.
Differenzierung der Bindungsformen von Kupferspuren in pflanzlichen Lebensmitteln Mittels Ionenaustausch an Cellulose-Materialien und Gel-Filtration 109
Bodnar, W. B., see Ellis, A. T. 73
Bodnar, W. B., see Ellis, A. T. 89
Borsaru, M.
— and Mathew, P. J.
Fast neutron activation analysis of bulk coal samples for alumina, silica and ash 349
Bos, P., see Kok, W. Th. 31
Busheina, I. S.
— and Headridge, J. B.
Determination of cadmium, indium and zinc in nickel-base alloys by atomic absorption spectrometry with introduction of solid samples into furnaces 197

Carr, P. W., see Shih, Y.-T. 55
Carter, J. A., see Smith, D. H. 355
Chatt, A., see Elson, C. M. 269
Compton, B. J.
— and Purdy, W. C.
The high-performance liquid chromatography and detection of phospholipids and triglycerides. Part 2. Comparison of an ultraviolet absorption and post-column reactor detector 13

De Galan, L., see van Dalen, H. P. J. 159
Dewald, H. D., see Wang, J. 239
Ditzler, M. A.
—, Doherty, G., Sieber, S. and Allston, R.
Fluorescence study of an immobilized ligand—metal ion complex 305
Doherty, G., see Ditzler, M. A. 305
D'Silva, A. P., see Rice, G. W. 47

Ellis, A. T.
—, Leyden, D. E., Wegscheider, W., Jablonski, B. B. and Bodnar, W. B.
Preconcentration methods for the determination of trace elements in water by x-ray fluorescence spectrometry. Part 1. Response characteristics 73
Ellis, A. T.
—, Leyden, D. E., Wegscheider, W., Jablonski, B. B. and Bodnar, W. B.
Preconcentration methods for the determination of trace elements in water by x-ray fluorescence spectrometry. Part 2. Interference studies 89
Elson, C. M.
—, Milley, J. and Chatt, A.
Determination of arsenic and antimony in geological materials and natural waters by coprecipitation with selenium and neutron activation—γ-spectrometry 269
Equel, J.-C., see Lamathe, J. 183

Fassel, V. A., see Rice, G. W. 47
Frei, R. W., see Kok, W. Th. 31
Fujishiro, Y.
—, Kubota, M. and Ishida, R.
Some analytical characteristics of an argon—nitrogen d.c. plasma arc for emission spectrometry 173

Frech, W., see Lundberg, E. 129

Gallego-Andreu, R., see Izquierdo-Hornillos, R. 325
Geetha, R., see Mahalingam, T. R. 189
Grant, A., see Bhattacharyya, P. K. 249

Hanekamp, H. B., see Kok, W. Th. 31
Headridge, J. B., see Busheina, I. S. 197
Hepel, T.
Chloride interference with non-stoichiometric copper sulphide copper(II)-selective electrodes. Part 3. New equation for the electrode response 217
Hiraoka, S., see Yoshimura, K. 101

Ikeda, S.
— and Satake, H.
Studies on analytical methods by amperometric titration using a rotating platinum electrode. Part 47. Successive determination of L-cysteine and L-cystine by amperometric titration 289
Ikrényi, K.
— and Bartha, A.
Effects of cooling of a nitrous oxide—actylene burner in atomic absorption spectrometry 339
Imasaka, T.
—, Ishibashi, K. and Ishibashi, N.
Time-resolved fluorimetry with a subnanosecond dye laser source for the determination of polynuclear aromatic hydrocarbons after separation by high-performance liquid chromatography 1
Ishibashi, K., see Imasaka, T. 1
Ishibashi, N., see Imasaka, T. 1
Ishida, R., see Fujishiro, Y. 173
Izquierdo-Hornillos, R.
—, Peral-Fernandez, J. L. and Gallego-Andreu, R.
Spectrophotometric determination of chromium(IV) through ion-pair formation with phenylfluorene 323

Jablonski, B. B., see Ellis, A. T. 73
Jablonski, B. B., see Ellis, A. T. 89
Johnson, K. S., see Petty, R. L. 299

Kok, W. Th.
—, Hanekamp, H. B., Bos, P. and Frei, R. W.
Amperometric detection of amino acids with a passivated copper electrode 31
Krull, U. J., see Thompson, M. 207
Kouimtzis, Th. A.
Determination of traces of sulfur in selenium by molecular emission cavity analysis 329
Koupparis, M. A.
—, Walczak, K. M. and Malmstadt, H. V.
Automated determination of nitrate in waters with a reduction column in a microcomputer-based stopped-flow sample processing system 119
Kubota, M., see Fujishiro, Y. 173
Kwee, B. G., see van Dalen, H. P. J. 159

Lamathe, J.
—, Magurno, C. and Equel, J.-C.
Essais interlaboratoires: dosage du cadmium, du cuivre et du plomb dans l'eau de mer par spectrométrie d'absorption atomique électrothermique 183
Leyden, D. E., see Ellis, A. T. 73
Leyden, D. E., see Ellis, A. T. 89
Lochmüller, C. H.
— and Marshall, D. B.
The effect of end-capping reagent on liquid chromatographic performance 63
Lundberg, E.
—, Bergmark, B. and Frech, W.
Investigations of reactions involved in electrothermal atomic absorption procedures. Part 11. A theoretical and experimental investigation of factors influencing the determination of tin 129

Magurno, C., see Lamathe, J. 183
Mahalingam, T. R.
—, Geetha, R., Thiruvengadasami, A. and Mathews, C. K.
Determination of trace metals in sodium by electrothermal atomic absorption spectrometry 189
Malmstadt, H. V., see Koupparis, M. A. 119
Marshall, D. B., see Lochmüller, C. H. 63
Mathew, P. J., see Borsaru, M. 349
Mathews, C. K., see Mahalingam, T. R. 189
McCrory-Joy, C.
— and Rosamilia, J. M.
Differential pulse polarography of germanium(IV), tin(IV), arsenic(V), antimony(V), selenium(IV) and tellurium(VI) at the static mercury drop electrode in catechol—perchlorate media 231

McGown, L. B.
— and Ueda, D. I.
Fluorimetric determination of pyrene: protein association ratios 313
McKown, H. S., see Smith, D. H. 355
Michel, W. C., see Petty, R. L. 299
Milley, J., see Elson, C. M. 269

Nomura, T.
— and Okuhara, M.
Frequency shifts of piezoelectric quartz crystals immersed in organic liquids 281

Okuhara, M., see Nomura, T. 281

Pardo, R.
—, Bernal, J. L. and Barrado, E.
Potentiometric titration of tellurium with a fluoride-selective electrode 285
Peral-Fernandez, J. L., see Izquierdo-Hornillos, R. 325
Petty, R. L.
—, Michel, W. C., Snow, J. P. and Johnson, K. S.
Determination of total primary amines in seawater and plant nectar with flow injection sample processing and fluorescence detection 299
Purdy, W. C., see Compton, B. J. 13

Rice, G. W.
—, Richard, J. J., D'Silva, A. P. and Fassel, V. A.
Comparison of analytical figures of merit of an active nitrogen afterglow and a flame ionization detector for gas chromatography 47
Richard, J. J., see Rice, G. W. 47
Rosamilia, J. M., see McCrory-Joy, C. 231

Safavi, A.
— and Townshend, A.
Molecular emission cavity analysis. Part 22. Determination of selenium and tellurium by direct injection into the cavity 143
Sasson, Y., see Bar, R. 345
Satake, H., see Ikeda, S. 289
Sato, S.
Spectrophotometric determination of sulfate by solvent extraction with the non-ionic surfactant Span 20 and crystal violet 317
Schwedt, G., see Bischoff, R. 109
Shea, C., see Wieck, H. J. 277
Shih, Y.-T.
— and Carr, P. W.
Determination of metals at trace levels via pre-column derivatization and non-polar stationary-phase high-performance liquid chromatography with *n*-butyl-2-naphthylmethyldithiocarbamate complexes 55
Sieber, S., see Ditzler, M. A. 305
Smith, D. H.
—, Walton, J. R., McKown, H. S., Walker, R. L. and Carter, J. A.
A mobile mass spectrometry laboratory for isotopic ratio measurements of uranium and plutonium 355
Snow, J. P., see Petty, R. L. 299

Taddia, M.
Determination of aluminium in silicon by electrothermal atomic absorption spectrometry 333
Tarutani, T., see Yoshimura, K. 101
Thiruvengadasami, A., see Mahalingam, T. R. 189
Thomson, J.
A total dissolution method for determination of the α-emitting isotopes of uranium and thorium in deep-sea sediments 259
Thompson, M.
— and Krull, U. J.
Bilayer lipid membrane electrochemistry in a flow injection system 207
Townshend, A., see Al-Zamil, I. Z. 151
Townshend, A., see Safavi, A. 143

Ueda, D. I., see McGown, L. B. 313

van Dalen, H. P. J.
—, Kwee, B. G. and De Galan, L.
The selective determination of halogens and sulphur in solution by atmospheric-pressure helium microwave-induced plasma emission spectrometry coupled to an electrothermal introduction system 159
Vogin, B.
—, Baronnet, F. and Andre, J. C.
Determination of aliphatic aldehydes in aqueous solution by chemiluminescence measurements 293

Walczak, K. M., see Koupparis, M. A. 119
Walker, R. L., see Smith, D. H. 355
Walton, J. R., see Smith, D. H. 355
Wang, J.
— and Dewald, H. D.
Concentration-modulated voltammetry 239
Wegscheider, W., see Ellis, A. T. 73
Wegscheider, W., see Ellis, A. T. 89
Wieck, H. J.
—, Shea, C. and Yacynych, A. M.
Reticulated vitreous carbon electrode materials chemically modified with immobilized enzyme 277

Yacynych, A. M., see Wieck, H. J. 277
Yoshimura, K.
—, Hiraoka, S. and Tarutani, T.
Determination of molybdenum in natural waters after selective adsorption on Sephadex gel 101

ACA announcements

ANNOUNCEMENTS OF MEETINGS

29th INTERNATIONAL CONGRESS OF PURE AND APPLIED CHEMISTRY

The 29th IUPAC Congress will take place on June 5–10, 1983, in Cologne, G.F.R., at the invitation of the Deutscher Zentralausschuss für Chemie. The Gesellschaft Deutscher Chemiker will be responsible for the detailed organisation of the Congress. Prominent chemists from all over the world have been invited to present plenary and section main lectures. The scientific programme will embrace the following sections and topics: new advances in inorganic chemistry, organic chemistry and physical and theoretical chemistry; progress in the production of chemical basic materials; and education in chemistry. Plenary lectures on the removal of chemical wastes and on the removal of wastes of origin other than chemical industry will also be presented.

A joint symposium on Chemical Information Flow at Present and in the Future will be held during the congress week.

Congress circulars containing further details such as the titles and lecturers for the plenary and section main lectures, and forms for submitting discussion papers and for preliminary registration are available on request from: General Secretariat of the 29th IUPAC Congress, Dr. W. Fritsche, c/o Gesellschaft Deutscher Chemiker, P.O. Box 90 04 40, D-6000 Frankfurt/Main 90, G.F.R.

3rd SYMPOSIUM ON SEPARATION SCIENCE AND TECHNOLOGY FOR ENERGY APPLICATIONS

The above-mentioned symposium will be held on June 27–July 1, 1983, in Gatlinburg, TN, U.S.A. This symposium is a continuation of a series cosponsered by the U.S. Department of Energy, the Oak Ridge National Laboratory, and the American Chemical Society Division of Industrial and Engineering Chemistry.

Topics will include: liquid–liquid extraction methods; membrane processes; physical methods, which utilize high applied field gradients; photochemical methods; and hydrometallurgic processes for the recovery of metals from ores.

Further details may be obtained from: A.P. Malinauskas, Oak Ridge National Laboratory, P.O. Box X, Oak Ridge, TN 37830, U.S.A.

2nd INTERNATIONAL CONFERENCE ON CARBONACEOUS PARTICLES IN THE ATMOSPHERE

This conference, to be held on Sept. 11–14, 1983, in Linz, Austria, is being organised by the Österreichische Gesellschaft für Mikrochemie und Analytische Chemie and the Gesellschaft Österreichischer Chemiker and is intended to provide an international forum for reviewing current research on characterization, sources, transport, formation, transformation, and effects of carbonaceous particles in the atmosphere. In the context of this conference, the term "carbonaceous particles" is used to describe organic and inorganic carbon-containing species associated with suspended particles. During the last decade, there has been a dramatic resurgence of interest in such pollutants, as evidenced by the extent and diversity of research presented at the 1st Conference on Carbonaceous Particles in the Atmosphere held at the Lawrence Berkeley Laboratory, Berkeley, CA, U.S.A., in 1978.

Presentations for this conference should be focused on (but not limited to) the following topics: sources, transport and atmospheric chemistry; climate effects, visibility degradation and other physical effects; analytical chemistry and measurement techniques, including sampling; ecological, biological and human health effects and effects on materials. Abstracts of papers should be submitted as soon as possible.

For further information contact Doz. Dr. H. Puxbaum, Institute for Analytical Chemistry, Technical University of Vienna, Getreidemarkt 9, A-1060 Wien, Austria.

CALENDAR OF FORTHCOMING MEETINGS

Nov. 17–19, 1982
New York, NY, U.S.A.

Eastern Analytical Symposium
Contact: Ivor L. Simmons, M&T Chemicals, Inc., Research Lab, P.O. Box 1104, Rahway, NJ 07065, U.S.A.

Dec. 6–8, 1982
Baltimore, MD, U.S.A.

2nd International Symposium on HPLC of Proteins, Peptides and Polynucleotides
Contact: Shirley E. Schlessinger, Symposium Manager, 2nd International Symposium on HPLC of Proteins, Peptides and Polynucleotides, 400 East Randolph, Chicago, IL 60601, U.S.A. Tel.: (312) 527-2011.

Dec. 20–22, 1982
London, Great Britain

International Conference on the Detection and Measurement of Hazardous Substances in the Atmosphere
Contact: Dr. John F. Gibson, The Royal Society of Chemistry, Burlington House, London W1V 0BN, Great Britain.

March 7–12, 1983
Atlantic City, NJ, U.S.A.

1983 Pittsburgh Conference and Exhibition on Analytical Chemistry and Applied Spectroscopy
Contact: 1983 Pittsburgh Conference, 437 Donald Road, Dept. FP, Pittsburgh, PA 15235, U.S.A.

April 5–8, 1983
Cardiff, Great Britain

International Symposium in Electroanalysis in Biomedical, Environmental and Industrial Sciences
Contact: Short Courses Section, University of Wales Institute of Science and Technology (UWIST), Cardiff CF1 3NU, Wales, Great Britain. (Further details published in Vol. 138.)

April 26–28, 1983
Riva del Garda, Italy

5th International Symposium on Capillary Chromatography
Contact: Dr. P. Sandra, Laboratory of Organic Chemistry, University of Ghent, Krijgslaan 281 (S4), B-9000 Ghent, Belgium

May 2–6, 1983
Baden-Baden, G.F.R.

VIIth International Symposium on Column Liquid Chromatography
Contact: Gesellschaft Deutscher Chemiker, Abteilung Fachgruppen, Postfach 90 04 40, Varrentrappstrasse 40–42, D-6000 Frankfurt (Main) 90, G.F.R.

June 1–3, 1983
Budapest, Hungary

The Budapest Chromatography Conference
Contact: Dr. Tibor Devenyi, Institute of Enzymology, Hungarian Academy of Sciences, Budapest, Hungary, or Dr. Haleem J. Issaq, NCI-Frederick Cancer Research Facility, P.O. Box B, Frederick, MD 21701, U.S.A.

June 5–10, 1983
Cologne, G.F.R.

29th Congress of the International Union of Pure and Applied Chemistry (IUPAC)
Contact: General Secretariat of the 29th IUPAC Congress, Dr. W. Fritsche, c/o Gesellschaft Deutscher Chemiker, Postfach 90 04 40, D-6000 Frankfurt (Main) 90, G.F.R.

June 13–17, 1983
Annapolis, MD, U.S.A.

5th International Symposium on Affinity Chromatography and Biological Recognition
Contact: Fifth International Symposium Secretariat, 9650 Rockville Pike, Bethesda, MD 20814, U.S.A.

June 26–July 1, 1983
Amsterdam, The Netherlands

23rd Colloquium Spectroscopium Internationale
Contact: Conference Secretariat 23 CSI, c/o Organisatie Bureau Amsterdam BV, Europaplein, 1078 GZ Amsterdam, The Netherlands. Tel.: (020) 44 08 07. Telex: 13499 raico nl. (Further details published in Vol. 138.)

June 27–July 1, 1983 Gatlinburg, TN, U.S.A.	**3rd Symposium on Separation Science and Technology for Energy Applications** Contact: A.P. Malinauskas, Oak Ridge National Laboratory, P.O. Box X, Oak Ridge, TN 37830, U.S.A.
July 17–23, 1983 Edinburgh, Scotland, Great Britain	**SAC '83, 6th International Conference and Exhibition on Analytical Chemistry** Contact: Miss P.E. Hutchison, The Royal Society of Chemistry, Analytical Division, Burlington House, London W1V 0BN, Great Britain. Tel.: 01-734-9971. (Further details published in Vol. 132.)
Aug. 28–Sept. 2, 1983 Amsterdam, The Netherlands	**9th International Symposium on Microchemical Techniques** Contact: Symposium Secretariat, c/o Municipal Congress Bureau, Oudezijds Achterburgwal 199, 1012 DK Amsterdam, The Netherlands. Tel: (020) 552 3459. (Further details published in Vol. 135, No. 2.)
Aug. 29–Sept. 2, 1983 Bratislava, Czechoslovakia	**4th Danube Symposium on Chromatography and 7th International Symposium "Advances and Application of Chromatography in Industry"** Contact: Dr. Ján Remen, The Analytical Section of the Czechoslovak Scientific and Technical Society, Slovnaft, 823 00 Bratislava, Czechoslovakia.
Sept. 5–9, 1983 Bucharest, Romania	**MACRO '83: 29th IUPAC International Symposium on Macromolecules** Contact: IUPAC MACRO'83, Calea Plevnei 139, R-77131 Bucharest, Romania.
Sept. 11–14, 1983 Linz, Austria	**2nd International Conference on Carbonaceous Particles in the Atmosphere** Contact: Doz. Dr. H. Puxbaum, Institute for Analytical Chemistry, Technical University of Vienna, Getreidemarkt 9, A-1060 Wien, Austria.
Sept. 19–22, 1983 Fukuoka, Japan	**International Meeting on Chemical Sensors** Contact: Professor Noboru Yamazoe, Secretary, International Meeting on Chemical Sensors, Department of Materials Science and Technology, Graduate School of Engineering Sciences, Kyushu University, Kasuga, Kasuga-shi, Fukuoka 816, Japan.
Nov. 10–16, 1983 Düsseldorf, G.F.R.	**9th International Congress and Exhibition for Instrumentation and Automation (INTERKAMA 83)** Contact: INTERKAMA 83, Düsseldorfer Messegesellschaft mbH, NOWEA, Postfach 32 02 03, D-4000 Düsseldorf 30, G.F.R.
Dec. 7–10, 1983 Singapore, Singapore	**Chem Asia '83 Conference** Contact: Singapore Exhibition Services, Ltd., 601 Cathay Building, Singapore 0922, Singapore.
May 20–25, 1984 New York, NY, U.S.A.	**8th International Symposium on HPLC** Contact: Professor Cs. Horváth, Mason Laboratory, Yale University, P.O. Box 2159, Yale Station, New Haven, CT 06520, U.S.A.
Oct. 1–5, 1984 Nürnberg, G.F.R.	**15th International Symposium on Chromatography** Contact: Gesellschaft Deutscher Chemiker, Abteilung Fachgruppen, Postfach 90 04 40, Varrentrappstrasse 40–42, D-6000 Frankfurt (Main) 90, G.F.R.

SPOT TESTS IN INORGANIC ANALYSIS

Sixth English Edition, Completely Revised and Enlarged.

By FRITZ FEIGL in collaboration with VINZENZ ANGER.

This standard work investigates the application of specific, selective, and sensitive reactions to research problems in qualitative inorganic analysis. It examines all pertinent information relating to each of the 742 tests cited, including details of operation, interferences and limits of detection. The book is an easy-to-use research tool for laboratory workers and researchers in analytic inorganic chemistry and related fields.

CONTENTS: Chapters. 1. Development, present state and prospects of inorganic spot test analysis. 2. Methodology of spot test analysis (completely revised and enlarged by Dr. G. Skalos). 3. Preliminary orientational tests. 4. Tests for the elements, their ions and compounds. 5. Application of spot reactions in tests of purity, examination of technical materials, studies of minerals. 6. Tabular summary.

"... will doubtlessly remain the authoritative book on the subject for a long time."

- Journal of the Electrochemical Society

"The book should be in chemistry libraries at all levels."

- Choice

"The volume contains a wealth of useful information and belongs on the reference shelf of every chemist who has occasion to carry out simple, rapid and selective detection tests without resorting to the use of a $40,000 instrument.

- Journal of Chemical Education

1972 xxix + 698 pages
US $97.50/Dfl. 230.00
ISBN 0-444-40929-7

SPOT TESTS IN ORGANIC ANALYSIS

Seventh English Edition, Completely Revised and Enlarged.

by FRITZ FEIGL in collaboration with VINZENZ ANGER.

This volume deals with all theoretical and practical aspects of the applications of spot tests to organic analysis. Information is given on more than 900 tests. This book continues to be of great value to organic and analytical chemists in academic as well as industrial laboratories.

CONTENTS: Chapters: 1. Development, present state and prospects of organic spot test analysis. 2. Preliminary (exploratory) tests. 3. Detection of characteristic functional groups in organic compounds. 4. Detection of structures and certain types of organic compounds. 5. Identification of individual organic compounds. 6. Applications of spot tests in the differentiation of isomers and homologous compounds. Determination of constitutions. 7. Applications of spot reactions in the testing of materials, examination of purity, characterization of pharmaceutical products etc. Appendix. Individual compounds and products examined. Author index. Subject Index.

"Even in these days of physical instrumentation there is ample room for the techniques described in this book which were originated and largely developed by Prof. Feigl."

- Laboratory Practice

"It should be classified as a 'must' for every laboratory, regardless of its field of specialization."

- Talanta

1966 Second Reprint 1975
xxiii + 772 pages
US $97.50/Dfl. 230.00
ISBN 0-444-40209-8

ELSEVIER

P.O. Box 211, 1000 AE Amsterdam, The Netherlands

52 Vanderbilt Avenue, New York, N.Y. 10017

The Dutch guilder price is definitive. US $ prices are subject to exchange rate fluctuations.

(continued from outside back cover)

Bilayer lipid membrane electrochemistry in a flow injection system
M. Thompson and U. J. Krull (Toronto, Ontario, Canada) 207
Chloride interference with non-stoichiometric copper sulphide copper(II)-selective electrodes. Part 3. New equation for the electrode response
T. Hepel (Krakow, Poland) 217
Differential pulse polarography of germanium(IV), tin(IV), arsenic(V), antimony(V), selenium(IV) and tellurium(VI) at the static mercury drop electrode in catechol–perchlorate media
C. McCrory-Joy and J. M. Rosamilia (Murray Hill, NJ, U.S.A.) 231
Concentration-modulated voltammetry
J. Wang and H. D. Dewald (Las Cruces, NM, U.S.A.) 239
Simultaneous determinations of a monofluorinated [1,4]-benzodiazepine and the corresponding benzophenone as a function of pH and in aqueous formulations by ^{19}F nuclear magnetic resonance spectrometry
P. K. Bhattacharyya and A. Grant (Nutley, NJ, U.S.A.) 249
A total dissolution method for determination of the α-emitting isotopes of uranium and thorium in deep-sea sediments
J. Thompson (Godalming, Gt. Britain) 259
Determination of arsenic and antimony in geological materials and natural waters by coprecipitation with selenium and neutron activation–γ-spectrometry
C. M. Elson, J. Milley and A. Chatt (Halifax, N.S., Canada) 269

Short Communications

Reticulated vitreous carbon electrode materials chemically modified with immobilized enzyme
H. J. Wieck, C. Shea and A. M. Yacynych (New Brunswick, NJ, U.S.A.) 277
Frequency shifts of piezoelectric quartz crystals immersed in organic liquids
T. Nomura and M. Okuhara (Matsumoto, Japan) 281
Potentiometric titration of tellurium with a fluoride-selective electrode
R. Pardo, J. L. Bernal and E. Barrado (Valladolid, Spain) 285
Studies on analytical methods by amperometric titration using a rotating platinum electrode. Part 47. Successive determination of L-cysteine and L-cystine by amperometric titration
S. Ikeda and H. Satake (Tokushima, Japan) 289
Determination of aliphatic aldehydes in aqueous solution by chemiluminescence measurements
B. Vogin, F. Baronnet and J. C. Andre (Nancy, France) 293
Determination of total primary amines in seawater and plant nectar with flow injection sample processing and fluorescence detection
R. L. Petty, W. C. Michel, J. P. Snow and K. S. Johnson (Santa Barbara, CA, U.S.A.) 299
Fluorescence study of an immobilized ligand–metal ion complex
M. A. Ditzler, G. Doherty, S. Sieber and R. Allston (Worcester, MA, U.S.A.) 305
Fluorimetric determination of pyrene:protein association ratios
L. B. McGown and D. I. Ueda (Long Beach, CA, U.S.A.) 313
Spectrophotometric determination of sulfate by solvent extraction with the non-ionic surfactant Span 20 and crystal violet
S. Sato (Kumamoto, Japan) 319
Spectrophotometric determination of chromium(VI) through ion-pair formation with phenylfluorone
R. Izquierdo-Hornillos, J. L. Peral-Fernandez and R. Gallego-Andreu (Madrid, Spain) 325
Determination of traces of sulfur in selenium by molecular emission cavity analysis
Th. A. Kouimtzis (Thessaloniki, Greece) 329
Determination of aluminium in silicon by electrothermal atomic absorption spectrometry
M. Taddia (Bologna, Italy) 333
Effects of cooling of a nitrous oxide–acetylene burner in atomic absorption spectrometry
K. Ikrényi and A. Bartha (Budapest, Hungary) 339
Determination of carbonate/hydrogencarbonate ratios by carbon-13 nuclear magnetic resonance spectrometry
R. Bar and Y. Sasson (Jerusalem, Israel) 345
Fast neutron activation analysis of bulk coal samples for alumina, silica and ash
M. Borsaru and P. J. Mathew (Melbourne, Victoria, Australia) 349
A mobile mass spectrometry laboratory for isotopic ratio measurements of uranium and plutonium
D. H. Smith, J. R. Walton, H. S. McKown, R. L. Walker and J. A. Carter (Oak Ridge, TN, U.S.A.) . . . 355

Author Index 361

CONTENTS

(Abstracts/contents lists in: Anal. Abstr.; Biol. Abstr.; Chem. Abstr.; Curr. Contents Phys. Chem. Earth Sci.; Life S Index Med.; Mass Spectrom. Bull.; Sci. Citation Index; Excerpta Med.)

Time-resolved fluorimetry with a sub-nanosecond dye laser source for the determination of polynuclear aromatic hydrocarbons after separation by high-performance liquid chromatography
T. Imasaka, K. Ishibashi and N. Ishibashi (Hakozaki, Japan) . . . . . .
The high-performance liquid chromatography and detection of phospholipids and triglycerides. Part 2. Comparison of an ultraviolet absorption and post-column reactor detector
B. J. Compton and W. C. Purdy (Montreal, Quebec, Canada) . . . . . .
Amperometric detection of amino acids with a passivated copper electrode
W. Th. Kok, H. B. Hanekamp, P. Bos and R. W. Frei (Amsterdam, The Netherlands) . . . . . .
Comparison of analytical figures of merit of an active nitrogen afterglow and a flame ionization detector for gas chromatography
G. W. Rice, J. J. Richard, A. P. D'Silva and V. A. Fassel (Ames, IA, U.S.A.) . . . . . .
Determination of metals at trace levels via pre-column derivatization and nonpolar stationary-phase high-performance liquid chromatography with *n*-butyl-2-naphthylmethyldithiocarbamate complexes
Y.-T. Shih and P. W. Carr (Minneapolis, MN, U.S.A.) . . . . . .
The effect of end-capping reagent on liquid chromatographic performance
C. H. Lochmüller and D. B. Marshall (Durham, NC, U.S.A.) . . . . . .
Preconcentration methods for the determination of trace elements in water by x-ray fluorescence spectrometry. Part 1. Response characteristics
A. T. Ellis, D. E. Leyden (Fort Collins, CO, U.S.A.), W. Wegscheider (Graz, Austria), B. B. Jablonski (Houston, TX, U.S.A.) and W. B. Bodnar (Boulder, CO, U.S.A.) . . . . . .
Preconcentration methods for the determination of trace elements in water by x-ray fluorescence spectrometry. Part 2. Interference studies
A. T. Ellis, D. E. Leyden (Fort Collins, CO, U.S.A.), W. Wegscheider (Graz, Austria), B. B. Jablonski (Houston, TX, U.S.A.) and W. B. Bodnar (Boulder, CO, U.S.A.) . . . . . .
Determination of molybdenum in natural waters after selective adsorption on Sephadex gel
K. Yoshimura, S. Hiraoka and T. Tarutani (Hakozaki, Japan) 1
Differenzierung der Bindungsformen von Kupferspuren in pflanzlichen Lebensmitteln Mittels Ionenaustausch an Cellulose-Materialien und Gel-Filtration
R. Bischoff und G. Schwedt (Göttingen, B.R.D.) 1
Automated determination of nitrate in waters with a reduction column in a microcomputer-based stopped-flow sample processing system
M. A. Koupparis, K. M. Walczak and H. V. Malmstadt (Urbana, IL, U.S.A.) 1
Investigations of reactions involved in electrothermal atomic absorption procedures. Part 11. A theoretical and experimental investigation of factors influencing the determination of tin
E. Lundberg, B. Bergmark and W. Frech (Umeå, Sweden) 1
Molecular emission cavity analysis. Part 22. Determination of selenium and tellurium by direct injection into the cavity
A. Safavi (Birmingham, Gt. Britain) and A. Townshend (Hull, Gt. Britain) 1
Molecular emission cavity analysis. Part 23. Determination of nitrite and nitrate after conversion to nitrogen monoxide
I. Z. Al-Zamil (Birmingham, Gt. Britain) and A. Townshend (Hull, Gt. Britain) 1
The selective determination of halogens and sulphur in solution by atmospheric-pressure helium microwave-induced plasma emission spectrometry coupled to an electrothermal introduction system
H. P. J. van Dalen, B. G. Kwee and L. De Galan (Delft, The Netherlands) 1
Some analytical characteristics of an argon–nitrogen d.c. plasma arc for emission spectrometry
Y. Fujishiro, M. Kubota and R. Ishida (Yatabe, Japan) 1
Essais interlaboratoires: dosage du cadmium, du cuivre et du plomb dans l'eau de mer par spectrométrie d'absorption atomique électrothermique
J. Lamathe (Paris, France), C. Magurno et J.-C. Equel (Les Milles, France) 1
Determination of trace metals in sodium by electrothermal atomic absorption spectrometry
T. R. Mahalingam, R. Geetha, A. Thiruvengadasami and C. K. Mathews (Tamil Nadu, India) 1
Determination of cadmium, indium and zinc in nickel–base alloys by atomic absorption spectrometry with introduction of solid samples into furnaces
I. S. Busheina and J. B. Headridge (Sheffield, Gt. Britain) 1

(continued on inside back cov